AD-A188 513 LOW VELOCITY IMPACT OF COMPOSITE AEROSTRUCTURES(U) 1/3
VILLANOVA UNIV PA P V MCLAUGLIN SEP 86 NADC-87186-60
N62269-82-C-0704

UNCLASSIFIED F/G 1/3 NL

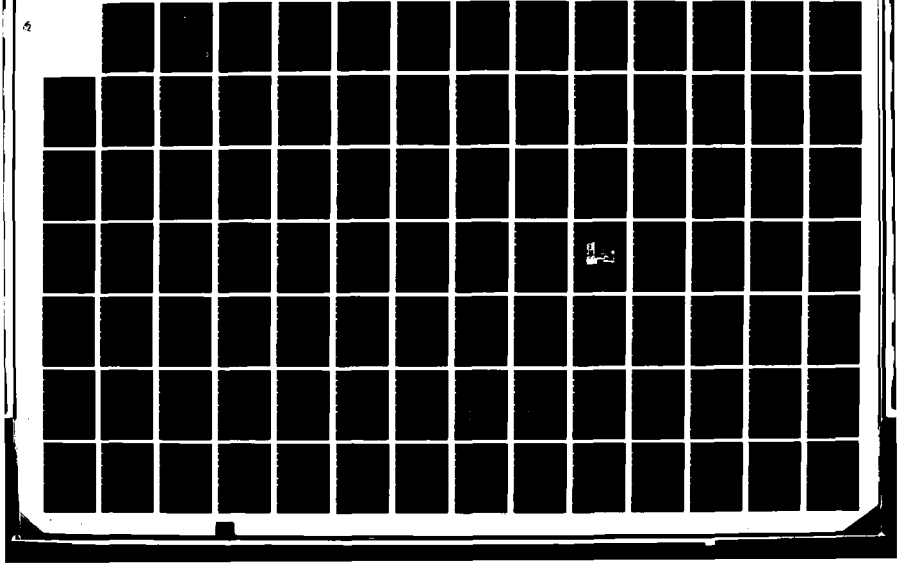

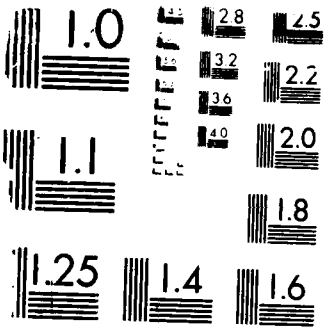

REPORT NO. NADC-87106-60

LOW VELOCITY IMPACT OF COMPOSITE AEROSTRUCTUES

Philip V. McLaughlin, Jr.

VILLANOVA UNIVERSITY
Villanova, PA 19085

SEPTEMBER 1986

FINAL REPORT
TASK NO. 2303001
Program Element No. 61153N
Work Unit No. 133126
Project No. WR02303
Contract No. N62269-82-C-0704
N62269-85-64-50534

Approved for Public Release; Distribution is Unlimited

Prepared for
Air Vehicle and Crew Systems Technology Department (Code 6043)
NAVAL AIR DEVELOPMENT CENTER
Warminster, PA 18974-5000

Unclassified

SECURITY CLASSIFICATION OF THIS PAGE

REPORT DOCUMENTATION PAGE

1a. REPORT SECURITY CLASSIFICATION Unclassified	1b. RESTRICTIVE MARKINGS
2a. SECURITY CLASSIFICATION AUTHORITY	3. DISTRIBUTION / AVAILABILITY OF REPORT Approved for Public Reslease; Distribution is Unlimited.
2b. DECLASSIFICATION / DOWNGRADING SCHEDULE	
4. PERFORMING ORGANIZATION REPORT NUMBER(S)	5. MONITORING ORGANIZATION REPORT NUMBER(S) NADC-87106-60
6a. NAME OF PERFORMING ORGANIZATION Villanova University 6b. OFFICE SYMBOL (If applicable)	7a. NAME OF MONITORING ORGANIZATION Air Vehicle and Crew Systems Technology Department (Code 6043)
6c. ADDRESS (City, State, and ZIP Code) Villanova, PA 19085	7b. ADDRESS (City, State, and ZIP Code) Naval Air Development Center Warminster, PA 18974-5000
8a. NAME OF FUNDING / SPONSORING ORGANIZATION 8b. OFFICE SYMBOL (If applicable)	9. PROCUREMENT INSTRUMENT IDENTIFICATION NUMBER N62269-82-C-0704 N62269-85-64-50534
8c. ADDRESS (City, State, and ZIP Code)	10. SOURCE OF FUNDING NUMBERS

PROGRAM ELEMENT NO.	PROJECT NO.	TASK NO.	WORK UNIT ACCESSION NO.
61153N	WR02303	2303001	133126

11. TITLE (Include Security Classification)

(U) Low Velocity Impact of Composite Aerostructures

12. PERSONAL AUTHOR(S) Philip V. McLaughlin, Jr.

13a. TYPE OF REPORT	13b. TIME COVERED	14. DATE OF REPORT (Year, Month, Day)	15. PAGE COUNT
FINAL	FROM Sept 83 TO Sep 85	1986 September	276

16. SUPPLEMENTARY NOTATION

Part of this work was performed during the author's tenure as a National Research Council Senior Research Associate at the Naval Air Development Center (6 Sep 83 to 9 Aug 84)

17. COSATI CODES			18. SUBJECT TERMS (Continue on reverse if necessary and identify by block number)
FIELD	GROUP	SUB-GROUP	Composite material, impact, graphite/epoxy finite element analysis, creep, viscoelasticity
01	03		
20	11		

19. ABSTRACT (Continue on reverse if necessary and identify by block number)

While considerable effort has been put into understanding the low-velocity impact of composite laminates, there is still considerable uncertainty concerning the analysis tools required to give accurate predictions of stresses and strains for design purposes. It has been determined that elastic bending solutions are inaccurate, and that several phenomena may explain the differences observed between elastic theory and experiment. These are:

1. Contact deformations
2. Transverse shear deformations
3. Viscoelasticity
4. Large deflections and membrane effects.

The objective of this project is to determine if and under what conditions each of the four phenomena must be modeled in analyses of low-velocity impact of fiber composite laminated structures. (continued on reverse)

20. DISTRIBUTION / AVAILABILITY OF ABSTRACT	21. ABSTRACT SECURITY CLASSIFICATION
☒ UNCLASSIFIED/UNLIMITED ☐ SAME AS RPT. ☐ OTIC USERS	Unclassified

22a. NAME OF RESPONSIBLE INDIVIDUAL	22b. TELEPHONE (Include Area Code)	22c. OFFICE SYMBOL
L.W. Gause	215-441-1330	NADC/6043

DD FORM 1473, 84 MAR 83 APR edition may be used until exhausted. All other editions are obsolete.

SECURITY CLASSIFICATION OF THIS PAGE

U.S. Government Printing Office: 1985—507-047

19. ABSTRACT (contd.)

FEAP74, a finite element code developed for USDOT to treat contact-impact problems, was secured for the analytical portion. Viscoelastic and large deflection elements in the code were defective, and analysis was limited to elastic impact. The program was used to analyze a considerable number of long, laminated plates clamped on two parallel edges. The analysis treated flexure, contact, and transverse shear deformations together and separately to obtain the relative orders of magnitude of each effect.

Tests were designed to duplicate the conditions of the analysis. AS-3501 graphite/epoxy plate samples were fabricated and tested using the *NAVAIRDEVCEN* impact tower with automated data storage and manipulation capabilities. Each test specimen was strain gaged so that time-histories of back-surface strain could be measured and compared with analysis.

The program has shown that flexural viscoelasticity is negligible, but that viscoelastic transverse shear and contact deformations are important for short composite plates. It appears that membrane effects may be important for longer plates where strains are significantly underpredicted by elastic small-deflection analysis. These results will give guidance to analysts who must predict strains and stresses in order to achieve safe, efficient, impact-resistant composite structures.

Since previous creep data on AS-3501 graphite/epoxy material was determined using minutes as data intervals, it was unsuitable for time frames of a fraction of a second which represent duration of impact loading. The determination under this program of an experimental viscoelastic creep compliance for AS-3501 graphite/epoxy material will provide analytical viscoelastic models with accurate property data with which to analyze laminates undergoing low-velocity impact.

ACKNOWLEDGEMENTS

The author gratefully acknowledges the support of the National Research Council and the Naval Air Development Center during this program. Special thanks are due to Mr. L. W. Gause for indispensible technical support with the NAVAIRDEVCEN Instrumented Impact Tower and data reduction software, and to Dr. J. Alper and Mr. V. Catone for professional assistance with viscoelastic property and impact tests.

The assistance of the following Villanova University students in experimental and analytical support tasks has been especially helpful to the project: Mr. E. N. Gianopulos, Mr. D. Krieger, Mr. P. E. McLaughlin, and Mr. E. F. Silvent.

TABLE OF CONTENTS

TABLE OF CONTENTS (CONCLUDED)

LIST OF TABLES

LIST OF FIGURES

LIST OF FIGURES (CONCLUDED)

I. INTRODUCTION

Laminated fiber composites, used extensively in military aircraft, can be damaged by impact of blunt, hard objects such as stones or dropped tools. It is necessary to be able to analyze these structures and design them to resist impact damage. For low velocity impact where wave propagation may not play a role, it has not been established under what conditions certain effects need to be included in analyses. The most important of these appear to be contact deformation between impactor and structure, transverse shear deformations, viscoelastic material behavior, and large deformation (membrane) effects. The research reported here was undertaken to determine the relative importance of these phenomena in predicting the impact response of laminated composites.

There are several types of blunt object impact damage which can occur in laminated composites [1-3]*:

- penetration caused by high-velocity impact;
- crushing of impacted surface material, delamination, and shattering of the back surface at moderate velocities which is caused by the interaction of elastic wave effects and quasistatic structural stresses; and
- a combination of flexural cracking and interply damage which can occur at low impactor velocities and may not involve wave propagation effects.

It is the incipient damage caused by low velocity, blunt object, transverse impact with which this report is concerned.

---

*Numbers in square brackets identify references.

Several investigators have researched the problem. Chou and Flis [4] have shown that analysis of beam and plate structures considering only flexure and static deflection shapes can give non-conservative predictions of structural strains. They also show [4, 5] that solving problems dynamically but still treating only flexure as was done by McQuillen, Llorens, and Gause [6] and Hayes and Rybicki [7] significantly overpredicts the strains. Llorens, McQuillen, and Gause [8, 9, 10] attempted to correct this overprediction using exact and approximate viscoelastic damping, but were only partially sucessful: non-conservative results were obtained in several cases. It was demonstrated [4] that treatment of Herzian contact deformation between impactor and structure as was done by Sun and Chattopadhyay [11], Bostaph and Elber [12], and Elber [13] also tends to correct the elastic flexural overpredictions, but direct comparison with experimental data was not available.

There is an uncertainty whether viscoelastic structural damping or Hertzian contact deformation is more important to achieving accurate predictions of structural strains in low-velocity impact of composite beams and plates. References [12] and [13] show that membrane force effects can also play an important role in obtaining accurate predictions of stresses and deformations in thin composite plates undergoing impact. It is also well-known that transverse shear deformations can be important for thick plates. Several researchers [10, 14-16 for example] have used finite element methods to analyze composite laminate impact problems, some including the effects of elastic contact stress [14, 15] , contact deformation [16] and transverse shear deformation [14-16]. Several

of the methods were semi-empirical or approximate and have not been substantiated by experimental evidence. None has investigated the relative importance of structural viscoelasticity, contact stresses, transverse shear deformations, and membrane effects.

A program of analysis and experiment was initiated to investigate under what conditions each of the four phenomena described above may be important to analyzing composite structures. The program consisted of:

1. An investigation into viscoelastic properties of composites to determine which were the most likely modes of viscoelastic dissipative mechanisms during impact and to determine the short-time viscoelastic properties of AS-3501 graphite/epoxy.

2. Finite element analysis of low-velocity impact of composite plates.

3. Impact tests of AS-3501 graphite/epoxy plates.

The original plan was to analyze AS 3501 graphite/epoxy composite beams using the FEAP74 finite element code [17-23]. The code was developed for the U. S. Department of Transportation for impact studies and contains 3-D, 2-D, shell (with transverse shear), and contact elements; viscoelasticity; orthotropy; and large displacements. When received, the program was found to be defective in the viscoelasticity and large deflection shell elements. Also, the viscoelastic element was not orthotropic. As a result, the analysis portion of the program was limited to elastic finite element analysis which treated elastic shear and contact deformations. The analyses were used to evaluate the relative importance of these effects on prediction of strains and to provide an analytical baseline for comparison with tests.

In order to evaluate the accuracy of elastic analysis predictions for behavior of laminated composites undergoing impact, tests were conducted on specially fabricated AS-3501 graphite/epoxy plates using the NAVAIRDEVCEN instrumented impact tower. Results of the tests were compared with the finite element analyses, and conclusions were drawn concerning the need for including transverse shear, contact, and other deformation phenomena in an impact analysis capability.

This report presents analysis and test work performed under the program, recommends a viscoelastic model of AS-3501 composite plates for use in impact analysis, and draws conclusions concerning the importance of elastic and viscoelastic behavior to impact analysis of composite laminates.

II. VISCOELASTIC BEHAVIOR OF COMPOSITE LAMINATES

A. DISSIPATIVE MECHANISMS DURING IMPACT

The work of Llorens, McQuillen, and Gause [8 - 10] has demonstrated that an energy absorption mechanism other than elastic flexure is active during low-velocity impact (less than 9 m/s or 30 ft/s). Their analysis and comparison with test data for impacted AS-3501 plates show that flexural viscoelastic analysis compares much better with experimental results than purely elastic flexural analysis. However, there are still large discrepancies for certain plate aspect ratios indicating that the energy absorption mechanism may not be flexural, and that perhaps a different viscoelastic model might improve accuracy of analytical predictions.

1. Flexural Viscoelasticity of AS-3501 Graphite/Epoxy

It is well-known [24-27, for example] that, for a unidirectional composite consisting of high-stiffness elastic fibers in a viscoelastic polymeric matrix, the effective viscoelastic composite behavior is most pronounced under transverse normal stress σ_{22}, transverse shear stress τ_{13} and τ_{23}, and axial shear stress τ_{12} (Figure 1). Viscoelastic behavior will be exhibited under axial normal stress, but, due to the dominance of the high-stiffness elastic fibers, it can be negligible compared to the other modes. In plate bending, however, the mode of deformation can be predominately flexure and it may be that axial normal viscoelasticity alone can be great enough to explain test results on impacted plates.

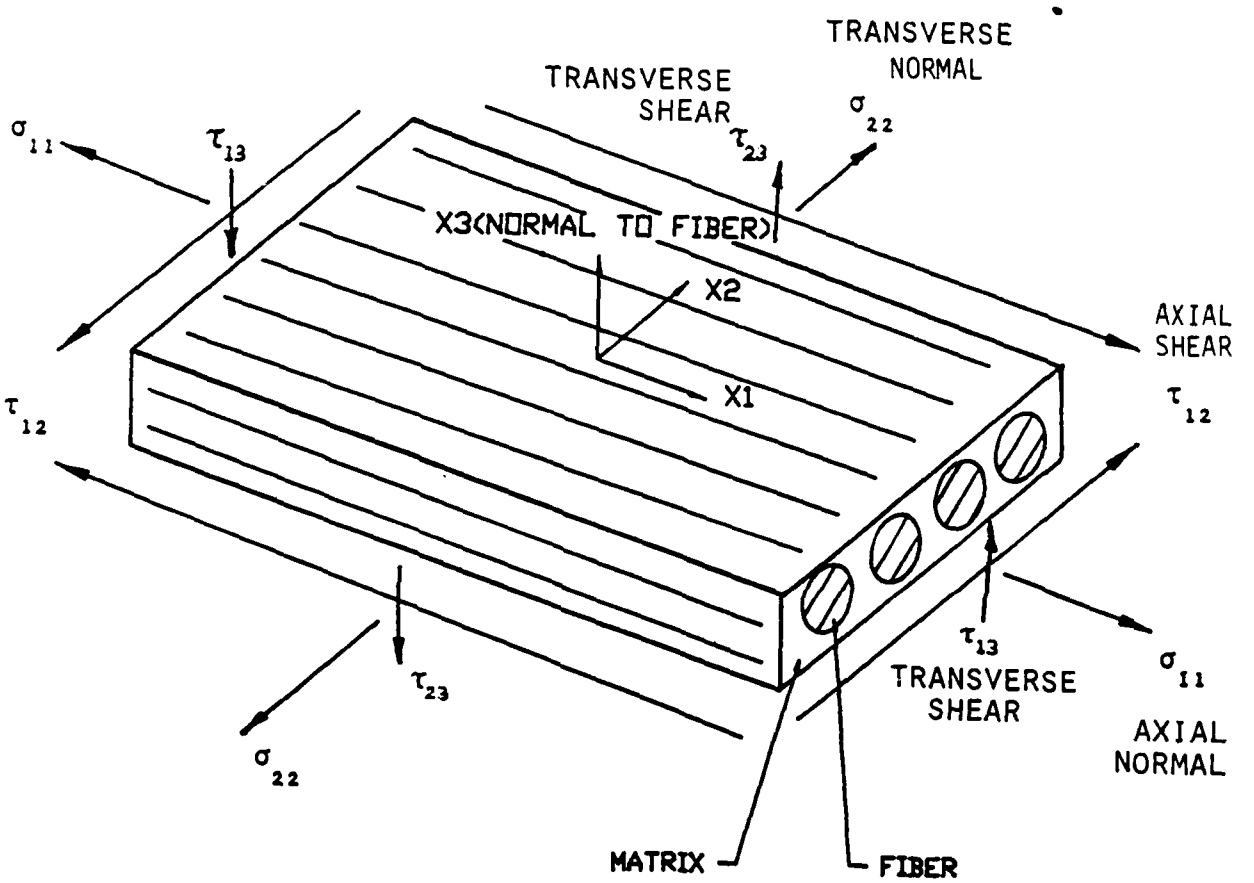

Figure 1. Unidirectional fiber composite stresses.

In order to see if viscoelastic behavior of AS-3501 graphite/epoxy under axial normal stress is great enough to give the flexural viscoelastic behavior required to correlate analysis with test data [8 - 10], viscoelastic properties of AS-3501 obtained from the tests of Renton and Ho [28] were analyzed and compared with the flexural viscoelastic properties used in references [8 - 10].

a. Matrix Shear Power Law Creep Compliance [28]. - Renton and Ho [28] have done tensile creep tests of $[\pm 45]_S$ laminates of AS-3501 and have used a power law creep compliance given by

$$e/s = D_0 + D_1 t^n \qquad (1)$$

where

e = tensile strain

s = tensile stress

t = time

D_0, D_1, and n = viscoelastic constants.

Under all environments, n = 0.18 gave good correlation with test data. The constants D_1 and D_0 for room temperature tests at 50% relative humidity were found to be

$$D_0 = 3.412(10^{-7}) \text{ in}^2/\text{lb } \{4.949(10^{-5}) \text{ MPa}^{-1}\}$$
$$D_1 = 0.108(10^{-7}) \text{ in}^2/\text{lb } \{0.155(10^{-5}) \text{ MPa}^{-1}\}$$

Using laminate analysis and assuming that the Halpin-Tsai equations relating constituent properties to composite properties are valid, Renton and Ho construct a nomogram by which the matrix

shear creep compliance, F_M, can be obtained from [±45] tensile creep compliance. Using the values of D_0 and D_1 given above and Figure 24 of Reference [28], the following relationship is obtained for room-temperature matrix shear creep compliance:

$$F_M = 9.30(10^{-6}) + 0.340(10^{-6})t^{0.18} \text{ in}^2/\text{lb} \qquad (2)$$
$$= 13.5(10^{-4}) + 0.493(10^{-4})t^{0.18} \text{ MPa}^{-1}$$

b. Matrix Extensional Power Law Creep Compliance. - Even if matrix isotropy is assumed, one must know the bulk creep compliance or the creep Poisson compliance to be able to determine the extensional creep compliance, D_M of the matrix [27]. However, for an order-of-magnitude estimate, it is assumed that Poisson's ratio ν_M remains constant with time at a value of 0.3. For isotropic behavior, this results in an extensional creep compliance for the matrix of

$$D_M = 0.5F_M/(1 + \nu_M)$$
$$= 3.58(10^{-6})(1 + 0.03656t^{0.18}) \text{ in}^2/\text{lb} \qquad (3)$$
$$= 5.19(10^{-4})(1 + 0.03656t^{0.18}) \text{ MPa}^{-1}$$

c. Unidirectional Composite Extensional Creep Compliance. - Assuming isotropic, linear elastic fibers with Poisson's ratio of 0.3, the effective axial creep compliance D* of a unidirectional composite with fiber volume fraction V_F is

$$D^* = [V_F/D_F + (1 - V_F)/D_M)]^{-1} \qquad (4)$$

For AS-3501, fiber volume fraction is $V_F = 0.62$. Fiber modulus can be calculated from equation (3) with t = 0 and equation (4) with composite initial modulus $1/D^* = 21.0$ Mlb/in^2 (145 GPa). The result is $1/D_F = 33.75$ Mlb/in^2 (232.7 GPa). For arbitrary time, (4) gives

$$D^* = 4.75(10^{-8})(1 + 0.03656t^{0.18})/(1 + 0.03637t^{0.18}) \text{ in}^2/\text{lb} \quad (5)$$
$$= 6.90(10^{-6})(1 + 0.03656t^{0.18})/(1 + 0.03637t^{0.18}) \text{ MPa}^{-1}$$

as the axial creep compliance of unidirectional AS-3501.

d. Laminate Extensional Creep Compliance Power Law Approximation. - In order to compare the viscoelastic properties of AS-3501 to those used for impacted plate experimental correlation in [8-10], it is noted that the extensional moduli of the multidirectional laminates used in [8-10] are approximately half that of the unidirectional composite. Assuming that equation (4) will approximate the shear creep compliance of the multidirectional plate if $2D_F$ is used in place of D_F, the following equation is obtained for an order-of- magnitude estimate of plate extensional creep compliance D_p^*:

$$D_p^* = 9.46(10^{-8})(1 + 0.03656t^{0.18})/(1 + 0.03619t^{0.18}) \text{ in}^2/\text{lb} \quad (6)$$
$$= 13.72(10^{-6})(1 + 0.03656t^{0.18})/(1 + 0.03619t^{0.18}) \text{ MPa}^{-1}$$

Another order-of-magnitude estimate would be to double the unidirectional axial creep compliance (5). This results in an approximation which is numerically very close to equation (6);

therefore, (6) will be used as the laminated plate extensional creep compliance.

e. Exponential Approximation of Laminate Extensional Creep Compliance. - Since the viscoelastic creep function assumed in the plate analysis of references [8-10] is an exponential law, it is desirable to take the power law creep compliance (6) obtained from Renton and Ho's data and fit it to an exponential three-parameter viscoelastic solid having a creep relaxation function of

$$D_p^*{}_{RH} = 1/q_1 + (p/q_2 - 1/q_1)\exp[-q_1 t/q_2] \qquad (7)$$

where q_1, q_2, and p are viscoelastic constants. Fitting (7) to (6) at t = 0 s, 1.0 s, and infinity gives the following values for the constants

$$q_1 = 10.46 \text{ Mlb/in}^2 \text{ (72.13 GPa)}$$
$$q_2 = 294. \text{ Mlb.s/in}^2 \text{ (2029. GPa.s)} \qquad (8a,b,c)$$
$$p = 27.85 \text{ s}$$

It is noted that these creep compliance calculations are approximate and are to be used for order-of-magnitude comparisons only!

2. Flexural Viscoelasticity Required to Correlate Impact Data

The flexural viscoelastic constitutive relation used by Llorens, McQuillen, and Gause[8-10] to correlate plate impact data is equivalent to a Kelvin solid having the following extensional creep compliance:

$$D_P{}^*_{LMG} = (1/q_3)(1 - \exp[-q_3 t/q_4]) \qquad (9)$$

which has the form of (7), but with p = 0. Their analysis of impacted plates correlates with tests of AS-3501 laminates when

$$q_4/q_3 = 25(10^{-6})s \text{ to } 100(10^{-6})s. \qquad (10a)$$

For an accurate comparison between (9) and (7), is necessary that

$$q_3 = q_1 \qquad (10b)$$

In order to compare the amount of extensional viscoelasticity required by Llorens, McQuillen, and Gause to correlate their test data with the extensional viscoelasticity available from AS-3501 as determined above from the tests of Renton and Ho, it is desirable to have a quantitative measure of damping which is not heavily dependent upon the form of the assumed viscoelastic constitutive relation. The amount of energy per unit volume dissipated in one cycle of sinusoidal loading, EDC, is one such convenient quantity which is calculated from the equation [29, 30]

$$EDC = T\, w(q_B - q_A p) s_0{}^2/(q_A{}^2 + q_B{}^2 w^2) \qquad (11)$$

where

w = loading frequency

q_A, q_B, p = viscoelastic constants (A = 1 or 3, B = 2 or 4)

s_0 = stress half-amplitude

The ratio of energy density dissipated per cycle using the material behavior required to correlate plate impact data (EDC_{LMG}) to that which has been calculated using known AS-3501 material behavior (EDC_{RH}) becomes

$$EDC_{LMG}/EDC_{RH} = \frac{q_4(q_1^2 + q_2^2 w^2)}{(q_3^2 + q_4^2 w^2)(q_2 - q_1 p)} \qquad (12)$$

and should tell if flexural viscoelasicity or some other energy absorption mechanism is dominating impact behavior.

The tests of Chou, Flis, and Miller [31] were used to correlate the analysis of [8-10]. These tests had typical impact event times of 5 ms which are equivalent to an oscillatory period of 10 ms and a cyclic frequency w of approximately 600 rad/s. Using this frequency and a representative value of $q_4/q_3 = 60$ s, equations (8), (10), and (12) give

$$EDC_{LMG}/EDC_{RH} = 6(10^4) \qquad (13)$$

Clearly, the degree of flexural viscoelastic behavior required to fit impact data is several orders of magnitude greater than that which exists in the material. It is concluded that the energy absorbing mechanism cannot be flexural viscoelasticity. The determination and modeling of the true cause(s) of the disparity between elastic impact analysis and test data may provide better correlation between analysis methods and tests and yield guidelines for more accurate design approaches to impact resistance.

3. Impact Energy Absorbing Mechanisms

Energy absorbed by composite plates during impact is not entirely due to elastic flexure, and Llorens, McQuillen, and Gause have shown that other mechanisms are operative. The preceeding analysis has shown that flexural viscoelasticity is negligible and that other energy absorptive phenomena must be treated in order to obtain good analytical predictions for design purposes. As presented in the introduction to this report, the following mechanisms are considered to be the strongest candidates:

1. Contact deformations between impactor and plate.
2. Transverse shear deformations.
3. Membrane forces.

Of these, the membrane force effects are known to be important whenever plate deflections exceed plate thickness (methods of treatment of large deflections of thin composite laminates during impact analysis have been described by Elber and Bostaph [12,13], for example). Shorter, thicker plates appear to require treatment of contact deformations and/or transverse shear deformations.

Both contact deformations and transverse shear deformations are matrix-dominated phenomena, i.e., the properties of the matrix material will control laminate behavior in these modes. Fiber-dominated laminates are therefore stiff in flexure (or any other in-plane deformation mode such as membrane stretching), but may be relatively flexible under transverse normal stress and transverse shear stress. Transverse normal stress effects will control contact deformations induced by hard impactors. For composites, transverse shear effects can be important for relatively thin plates. For example, it is well-known that the

deflection, u, of a cantilevered wide plate under a concentrated transverse load, P, at its tip can be approximated by strength-of-materials analysis as

$$u = (PL^3/3CI)(1 + 0.25Ch^2/GL^2)$$

where

L = plate length

h = plate thickness

$I = wh^3/12$, w = plate width

G = material transverse shear modulus

C = plate extensional modulus

The last term in the last parentheses represents the contribution of transverse shear deformation to deflection. For isotropic materials where E and G are the same order of magnitude, the transverse shear deflection will be no more than 3% of the total if length L is longer than 5h. For a typical graphite epoxy, L must be greater than 20h for the same relative magnitude of shear deflection.

In addition, since polymeric matrix behavior is viscoelastic, it is possible that treatment of elastic transverse normal and shear is insufficient: viscoelastic contact deformations and transverse shear deformations may need to be modeled in order to obtain reasonable analytical accuracy for design or analysis purposes.

B. VISCOELASTIC PROPERTIES OF AS-3501

1. Viscoelastic Material Modeling

It has been demonstrated here and elsewhere that in-plane stress-strain relations can be elastic without loss of accuracy for low-velocity plate impact analysis. In order that a plate exhibit contact deformation viscoelasticity and transverse shear viscoelasticity, it will be necessary to model transverse normal and shear stress-strain relations as viscoelastic. An elementary model which would take the major effects into account although it may not be thermodynamically correct is to assume that composite transverse normal and shear viscoelastic relations are uncoupled and have the following exponential relaxation functions:

$$G_T = G_0 + G_1 \exp(-t/b) \quad \text{(shear)} \tag{14}$$

$$C_T = C_0 + C_1 \exp(-t/a) \quad \text{(normal)} \tag{15}$$

where C_0, G_0, C_1, G_1, a, and b are constants. This would allow use of certain finite element codes which use this functional form ([17], for example, with appropriate code modification for orthotropy).

In order to obtain the three material constants required in each of equations (14) and (15), tests must be performed. The most efficient way to obtain shear properties for equation (14) is to perform a creep test of a $[\pm 45]_S$ laminate in tension as was done by Renton and Ho [28]. The creep compliance thus obtained can be inverted to give the relaxation modulus (14) by Laplace transform techniques using the correspondence principle of linear

viscoelasticity [27, for example]. Using relationships developed between matrix, fiber, and composite viscoelastic stress-strain relations [24, 27], one may determine matrix viscoelastic stress-strain relations from composite shear behavior and in turn use the matrix behavior to calculate the transverse normal viscoelastic relaxation modulus (15)(see reference [28] for one description of this process).

Experimentally, then, creep tests on $[\pm 45]_S$ tension specimens are sufficient to determine any viscoelastic properties that may be important to impact analysis of composite laminates. All multidirectional laminates of the same unidirectional material have approximately the same transverse normal and shear behavior since stacking sequence affects only in-plane constitutive relations.

The time from impact to rebound or fracture will depend upon material stiffness properties, structural geometry, and impactor mass. During low-velocity impact of aircraft skins by stones, tools, or other similar-size masses, this elapsed time is seldom greater than 0.05 s and can be considerably shorter. The viscoelastic test data for [±45] AS-3501 graphite/epoxy laminates generated by Renton and Ho [28] used creep data intervals of one minute (60 s). Since the impact events are taking three orders of magnitude less time than the first data point in [28], the use of Renton and Ho's data for accurate viscoelastic deformation calculations is questionable.

The following section describes tests performed to determine the shear relaxation modulus of AS-3501 graphite/epoxy for use during short time intervals typical of impact occurrences.

2. Test Program

In order to develop viscoelastic properties which might be valid over time intervals on the order of fractions of a second, a series of high-speed creep tests was performed on $[\pm 45]_{2S}$ AS-3501 using an Instron servohydraulic tensile test machine at the laboratories of the Naval Air Development Center.

Each specimen was 0.5 in (25.4mm) wide and 9.0 in (225 mm) long and was appropriately tabbed with glass end tabs. Each was instrumented with a 3-element rectangular strain gage rosette with the middle gage in the direction of loading and the other two at angles of $+45^{\circ}$ and -45° to the loading direction.

Load and axial strain were read into a Nicolet digital storage scope, and the 45° strain gages were monitored by a Tektronix fluorescent storage oscilloscope. Photographic records of 45 strains were made with a Polaroid camera fitted to the Tektronix scope.

Specimens were "instantaneously" ramp-loaded to a predetermined load (ranging from 125 lb [556 N] to 640 lb [2.85 kN]) and held at this constant load for approximately ten minutes. During the first twenty seconds, 2,000 data points were recorded by the Nicolet storage scope for both load and strain. This provided 10 data points in the first 0.1 s which is considerably better than one data point every 60 s. Twenty-second data records were also made after approximately five minutes and ten minutes, respectively, to obtain long-time creep information.

3. Test Results

Typical creep test data are presented in Figures 2, 3, and 4 which give axial load and strain for the first twenty seconds, the twenty second interval beginning after an elapsed time of five minutes, and the twenty second interval after an elapsed time of thirteen minutes, respectively.

It was found that during the initial loading, approximately two data intervals of 0.01 s were required for the test machine to reach the desired load, and another 28 data intervals for the hydraulics to stabilize the load (one or two "dips" of about 4% from the preset load typically occurred). The strain data was adjusted for the load variations by multiplying the strain at a given time by the ratio of actual load at that time to the stable load reached after 0.5 s. Also, as is evident in Figure 2, noise was superimposed on the strain signal. Data were assumed to lie midway between noise peaks. Figure 5 shows the results of adjusting and smoothing the data from Figure 2 (note the expanded time scale in Figure 5).

Adjusted extensional strain data in the 0°, $+45^{\circ}$, and -45° directions from the strain gage rosette were transformed using the common plane transformation equations to yield the axial shear strain (parallel to fiber directions). Load was divided by the [±45] specimen cross-sectional area to obtain tensile stress which was then transformed to axial shear stress (parallel to fiber direction - Figure 1). The resulting shear stress and time history of shear strain were analyzed to determine axial shear relaxation modulus as follows:

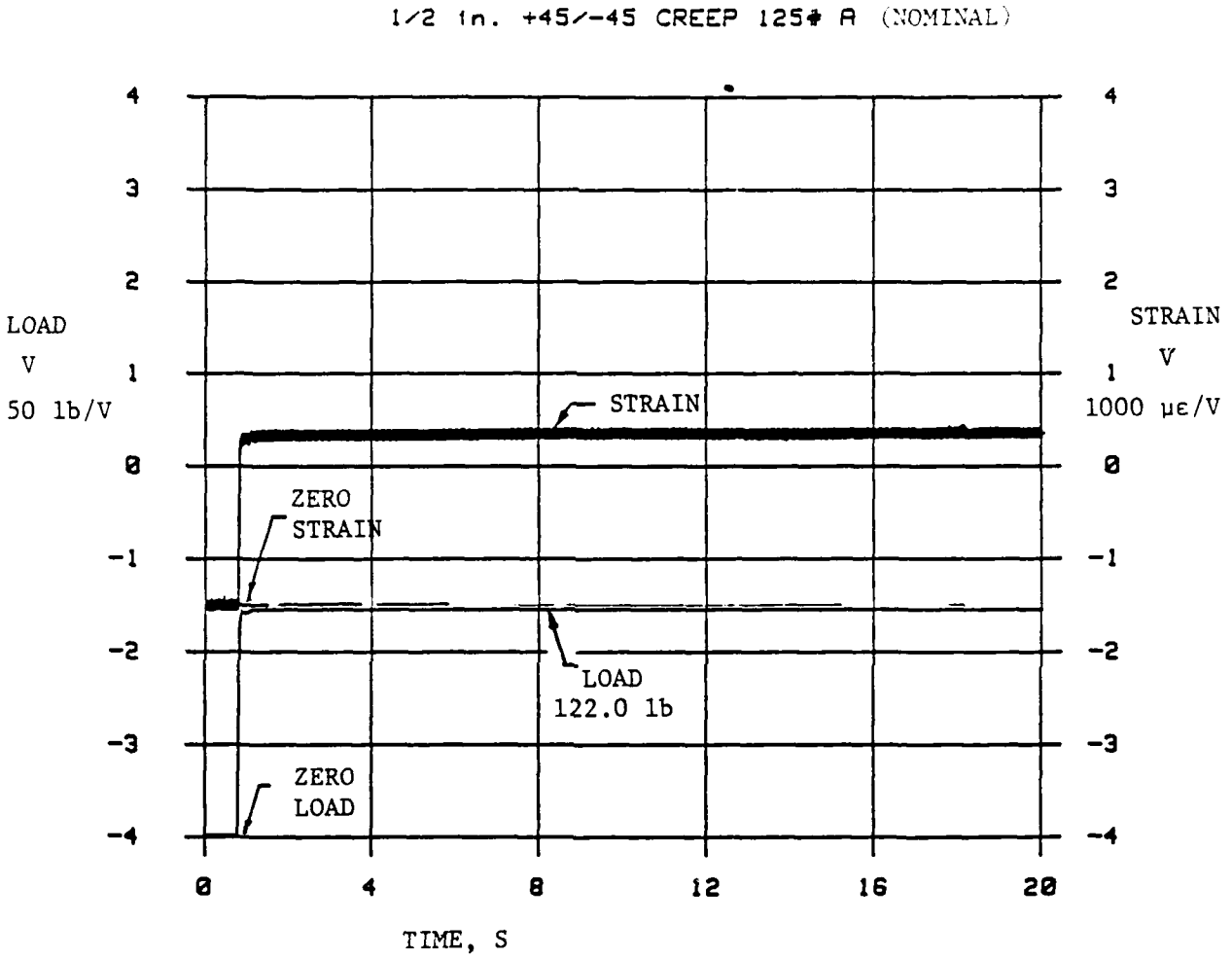

Figure 2. Load and axial strain vs. time during creep test of [±45] AS-3501 graphite/epoxy tension specimen under 122 lb (543 N) load. Time interval 0.0 s to 20 s.

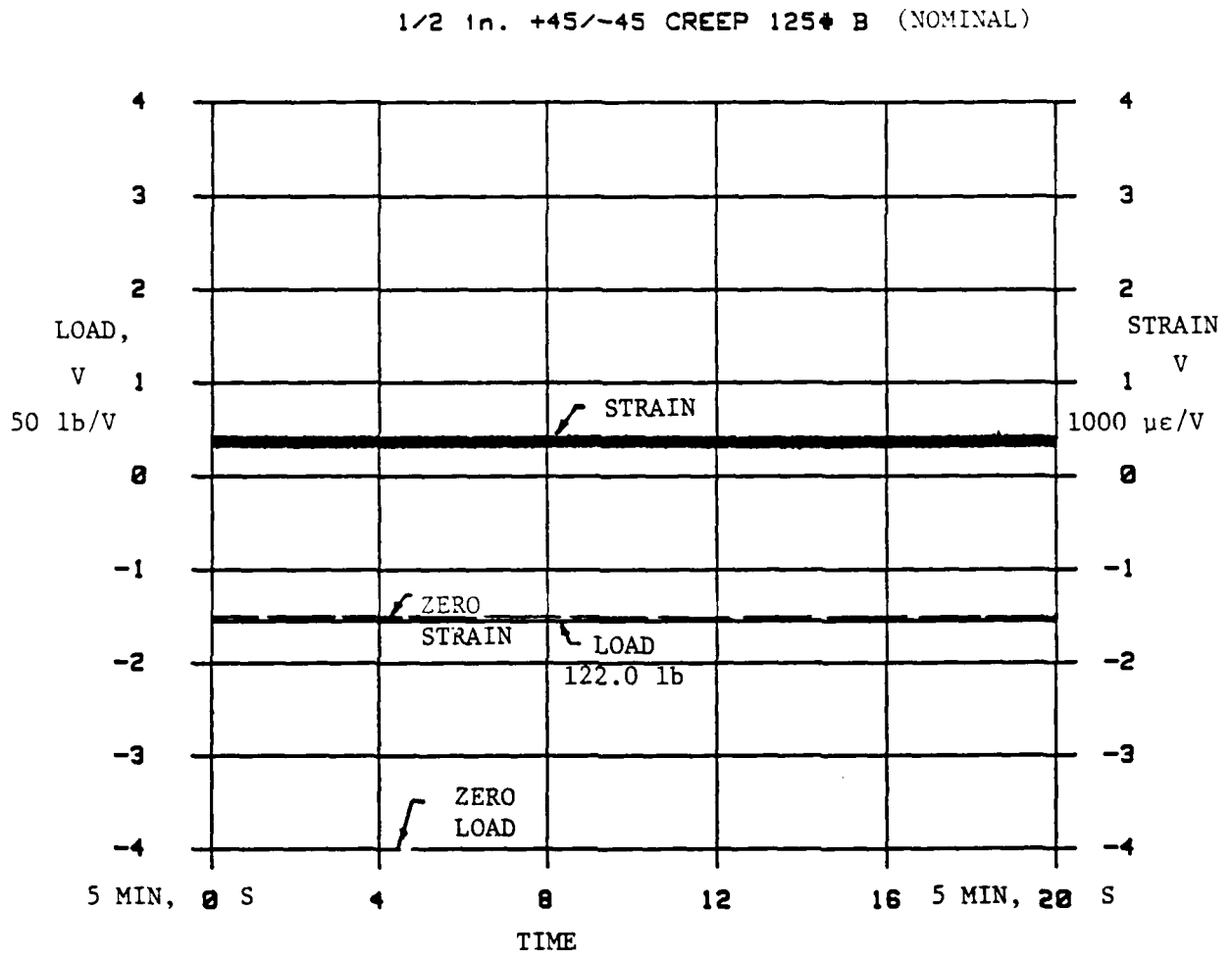

Figure 3. Load and axial strain vs. time during creep test of [±45] AS-3501 graphite/epoxy tension specimen under 122 lb (543 N) load. Time interval 300 s to 320 s.

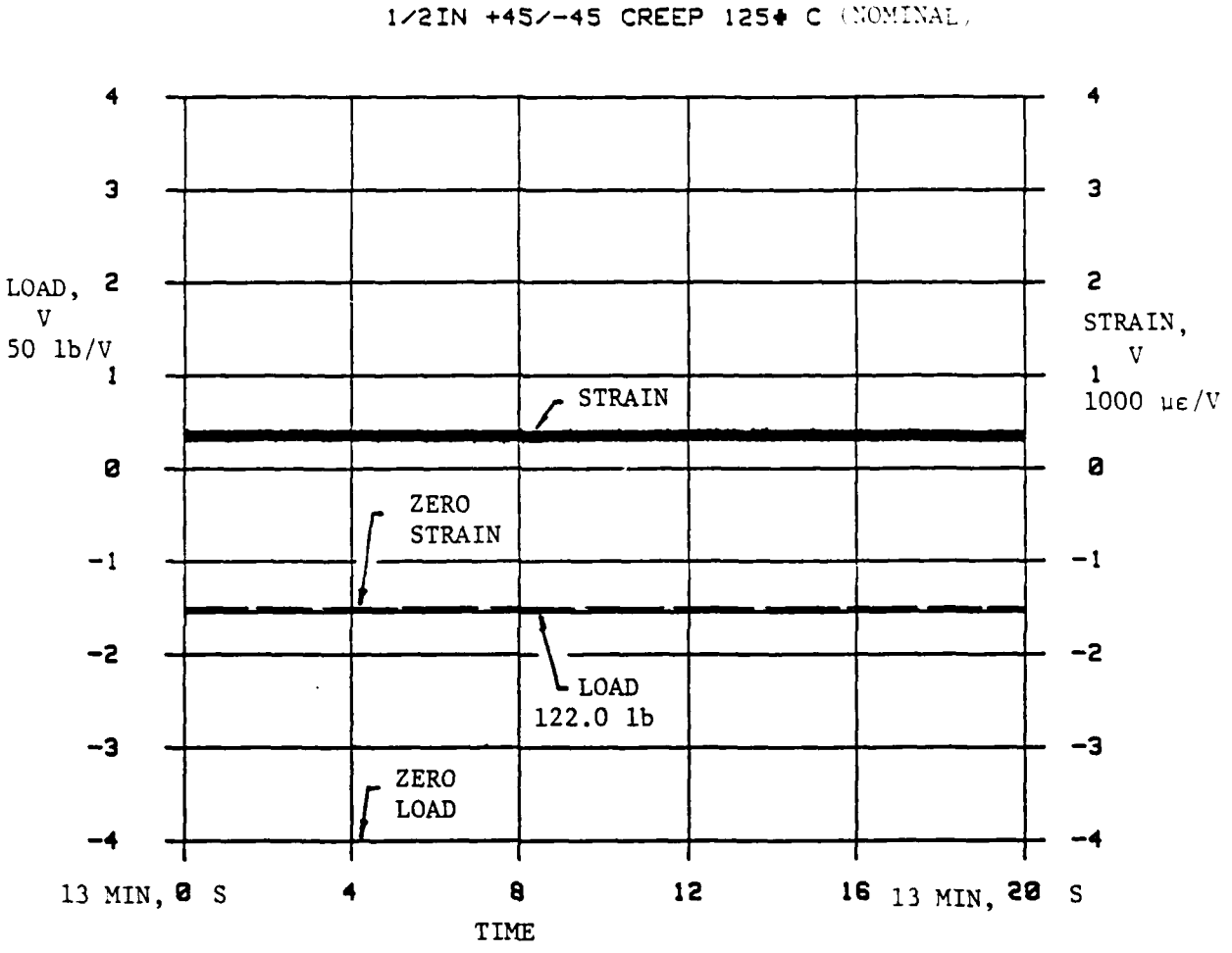

Figure 4. Load and axial strain vs. time during creep test of [±45] AS-3501 graphite/epoxy tension specimen under 122 lb (543 N) load. Time interval 780 s to 800 s.

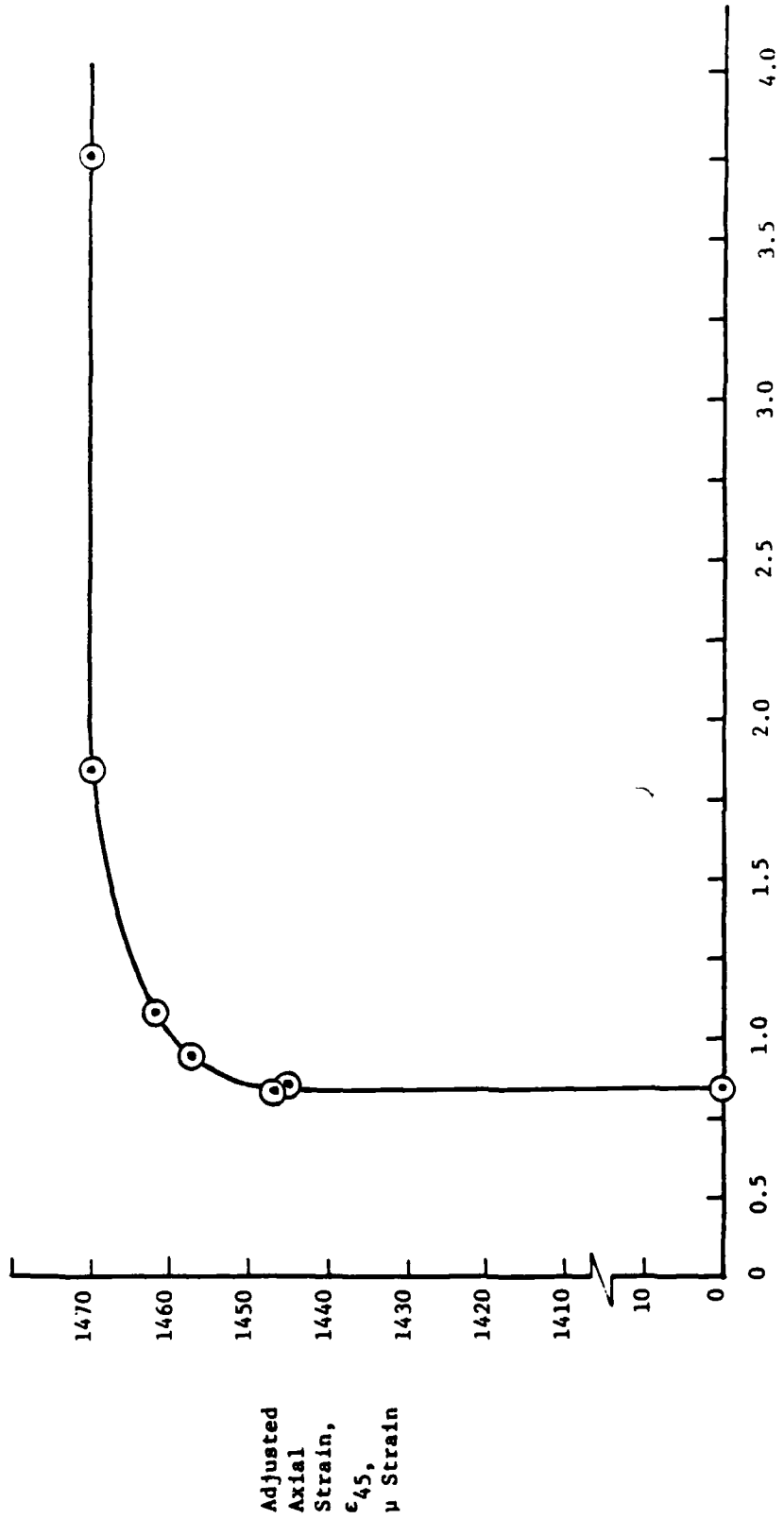

Figure 5. Adjusted axial strain vs. time for creep test of [±45] AS-3501 graphite/epoxy tension specimen under 125 lb (556 N) load. Time interval 0.0 s to 20 s.

The form of shear relaxation modulus chosen was that of equation (14) which has three viscoelastic constants - the static (slow load) shear modulus G_0, the viscous modulus G_1, and the exponential decay parameter, b:

$$G_{12} = G_0 + G_1\exp(-t/b) \tag{16}$$

It can be shown that the shear creep compliance corresponding to this relaxation modulus is

$$F_{12} = 1/G_0 - G_1[G_0(\ G_0 + G_1)]^{-1}\exp(-t/c) \tag{17a}$$

where

$$c = b(G_0 + G_1)/G_0 \tag{17b}$$

The static shear modulus G_0 was determined from slow-speed tension tests of specimens similar to those used for creep tests. The ratio of viscous modulus G_1 to shear modulus G_0 was calculated from the equation

$$G_1/G_0 = G_D/G_0 - 1 \tag{18}$$

where G_D is the dynamic shear modulus found from high-speed test data. In this case, G_D was determined from plots of stress versus strain obtained from the initial 0.05 s of creep data. With G_0 and G_1 known, the exponential creep decay parameter, c, was found by choosing one point on the adjusted extensional strain curve and solving for c from equation (17a). The exponential relaxation decay parameter b was then determined from equation (17b).

The parameter b was calculated from several points on the initial portion of the creep strain curve and was found to be affected by the point chosen for its determination. The most consistent results were obtained when data points were taken within the the first 0.3 s of creep data where the majority of the creep strain took place.

Computed relaxation modulus constants obtained from the viscoelastic creep tests are presented in Table 1. Appendix A contains computer-generated plots of the creep data from the tests.

Table 1. Relaxation Modulus Constants for AS-3501 in Axial Shear.

Relaxation Modulus Constant	Value $[G_{12} = G_0 + G_1 \exp(-t/b)]$
G_0	$0.941(10^6)$ lb/in^2 [6.49 MPa]
G_1/G_0	0.0313
b	$0.15 + 0.05$ s^{-1}

III. ELASTIC ANALYSIS OF IMPACTED COMPOSITE BEAMS

A. FINITE ELEMENT MODEL

1. Structural Configuration and Material Properties

Elastic analysis of AS-3501 graphite/epoxy composite plate structures was performed to determine the relative effects of contact deformations and transverse shear deformations, and to provide an analytical baseline for comparison of data from impact tests. For both analytical and experimental simplicity, a long plate clamped at both ends was chosen. Plates ranged in length from 2.56 in (65 mm) to 13.98 in (355 mm), but all plates were 1.57 in (40 mm) wide. Plates had thicknesses of 1/8 in (3 mm) or 1/4 in (6 mm) corresponding to 24- and 48-plies of AS-3501, respectively. Figure 6 illustrates plate configurations analyzed.

The actual stacking sequences used in impact tests which the finite element analysis was designed to model were $[(\pm 45/0_2)_2/\pm 45/0/90]_S$ and $[(\pm 45/0_2)_2/\pm 45/0/90]_{2S}$. For the model, each plate was assumed to have uniform orthotropic elastic constants corresponding to $[\pm 45/0_2]_{NS}$ stacking sequences of AS-3501 graphite/epoxy. Laminate analysis confirmed that axial strains in a plate contained less than 1% error with the uniform material assumption compared to individual ply modeling.

The major material axis was chosen to be oriented at either 0° or 90° to plate longitudinal axis for each of the four plate geometries, which gave a total of eight plates to be analyzed. Figure 6 presents geometry, material, and associated numbering system details.

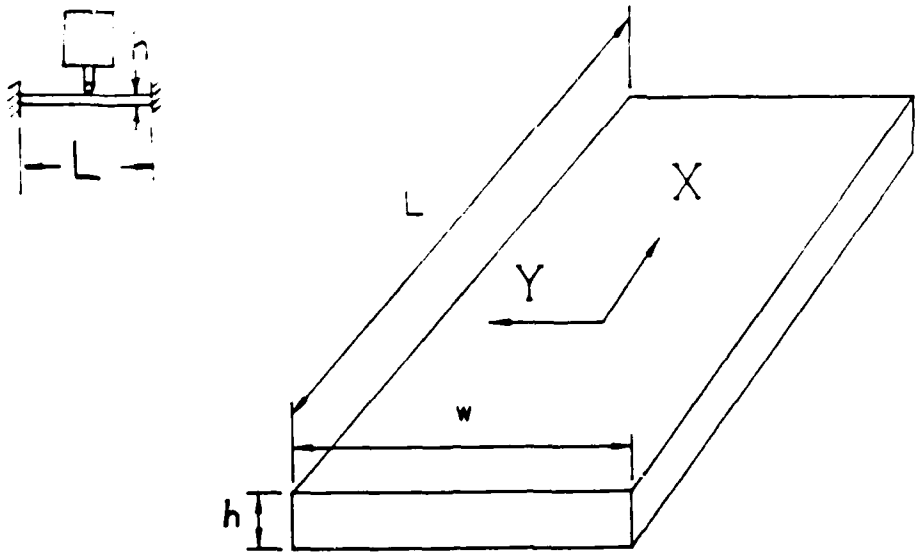

PLATE ID	LNGTH L in/mm	WIDTH W in/mm	THKNS h in/mm	STACKING SEQUENCE (X = 0°)	MATERIAL CODE
I1	14/355	1.57/40	.128/3.25	$[(\pm45/0_2)_2/\pm45/0/90]_S$	H
I2	"	"	"	$[(\pm45/90_2)_2/\pm45/90/0]_S$	L
I3	5.31/135	"	"	$[(\pm45/0_2)_2/\pm45/0/90]_S$	H
I4	"	"	"	$[(\pm45/90_2)_2/\pm45/90/0]_S$	L
I5	"	"	.256/6.5	$[(\pm45/0_2)_2/\pm45/0/90]_{2S}$	H
I6	"	"	"	$[(\pm45/90_2)_2/\pm45/90/0]_{2S}$	L
I7	2.56/65	"	"	$[(\pm45/0_2)_2/\pm45/0/90]_{2S}$	H
I8	"	"	"	$[(\pm45/90_2)_2/\pm45/90/0]_{2S}$	L

MATERIAL CODE	AVERAGE PLANE STRAIN ELASTIC CONSTANTS* Mpsi (GPa)			
	C_{XX}	C_{ZZ}	C_{XZ}	C_{SS}
H- High Stiffness in X Direction	11.2(75.4)	1.71(11.8)	0.86(5.91)	1.30(8.96)
L- Low Stiffness in X Direction	5.45(37.6)	1.71(11.8)	.712(4.91)	1.30(8.96)

* Normal Stress s and Strain e:

$$s_{XX} = C_{XX}\, e_{XX} + C_{XZ}\, e_{ZZ}$$

$$s_{ZZ} = C_{XZ}\, e_{XX} + C_{ZZ}\, e_{ZZ}$$

Shear Stress s_{XZ} and Strain e_{XZ}: $s_{XZ} = C_{SS}\, e_{XZ}$
(Note that e_{XZ} is tensorial shear strain)

Figure 6. Structural and material configurations analyzed by FEAP74 finite element code.

Since plates were an order of magnitude wider than they were thick, a two-dimensional plane strain analysis was appropriately selected for the impact analyses. In order to determine the effects of elastic contact deformations and transverse shear deformations on analysis results, transverse material properties were altered and finite element analyses were run in the following sequence:

a. full two-dimensional orthotropic elasticity which contained the effects of flexure, elastic contact deformations, and elastic transverse shear deformations.

b. transverse normal stiffness was increased by two orders of magnitude which eliminated contact deformations but maintained flexure and transverse shear effects.

c. both transverse normal and transverse shear stiffnesses were incraesed by two orders of magnitude which eliminated contact and transverse shear deformations but maintained flexural effects.

2. Finite Element Code

The finite element code chosen for the analysis was FEAP74, a program developed by University of California, Berkeley, for the U. S. Department of Transportation especially for contact-impact problem analysis. The code contains operational two- and three-dimensional orthotropic elastic elements, laminated orthotropic plate element, and contact elements. Dynamic impact problems can be analyzed using explicit or implicit finite difference formulations in the time domain. The implicit option was chosen since results thus obtained are always stable and convergent.

Unfortunately, large deflection plate and viscoelastic elements were inoperable in the version received from Cal-Berkeley. While these elements were not able to be made operational, several other errors were found in the code and corrected so that the other elements will run with the implicit dynamic analysis option. The version currently on tape storage at the NADC computer facility contains all corrections which were made.

3. Finite Element Mesh Construction

In order to prevent possible numerical instabilities during the finite element analyses, care was taken to construct elements having nearly equal stiffnesses in the principal directions. Plane strain meshes sized from 64 elements and 87 nodes to 383 elements and 462 nodes were analyzed for optimal accuracy and running time. It was found that less than 3% difference in pertinent stresses and strains was obtained between meshes having four elements through the beam thickness and six elements through the beam thickness. Accordingly, four-element-thick beam meshes were used for the finite element production runs.

The impactor from the NADC impact tower required less precision in modeling than did the plates. Force in the load cell of the impactor was the quantity of interest since time histories of the load could be obtained during tests. Care was taken to model the impactor tip so that accurate contact stresses would be obtained, but the remaining parts (load cell, tip connector, frame, and guides) were modeled as axial elements. A dynamic study of the impactor frame was made to determine how accurate a dynamic model of the frame was necessary. Strength-of-materials analysis showed

that natural frequencies of the frame and its parts could be on the same order of magnitude as those of the plates, and that careful attention needed to be paid to stiffnesses as well as masses of the frame parts. The resulting impactor mesh was therefore designed to be dynamically representative during impact.

Figure 7 illustrates the mesh developed for the I7 beam and the 8.4 lb (3.8 kg) impactor which has a 1/8-in- (3.2-mm-) radius cylindrical tip. The remaining beam meshes are similar.

B. RESULTS

Finite element analysis results were obtained for all eight plate configurations with (a) full elastic behavior, (b) flexure and transverse shear deformations only, and (c) flexure only. The longest plates, I1 and I2, with aspect ratios (length-to-thickness) of about 100, suffered numerical instability problems when both transverse shear and normal stiffnesses were artificially increased together. An attempt at resolving the problem by creating a finer mesh was thwarted by size limitations imposed by the FEAP74 code. All other runs were completed and results are available.

Runs were made at impactor initial velocities ranging from 42 in/s (500 mm/s) to 315 in/s (8 m/s). It was determined that impactor force and beam flexural strain results were proportional to velocity, and therefore only the 315 in/s (8 m/s) results are presented here.

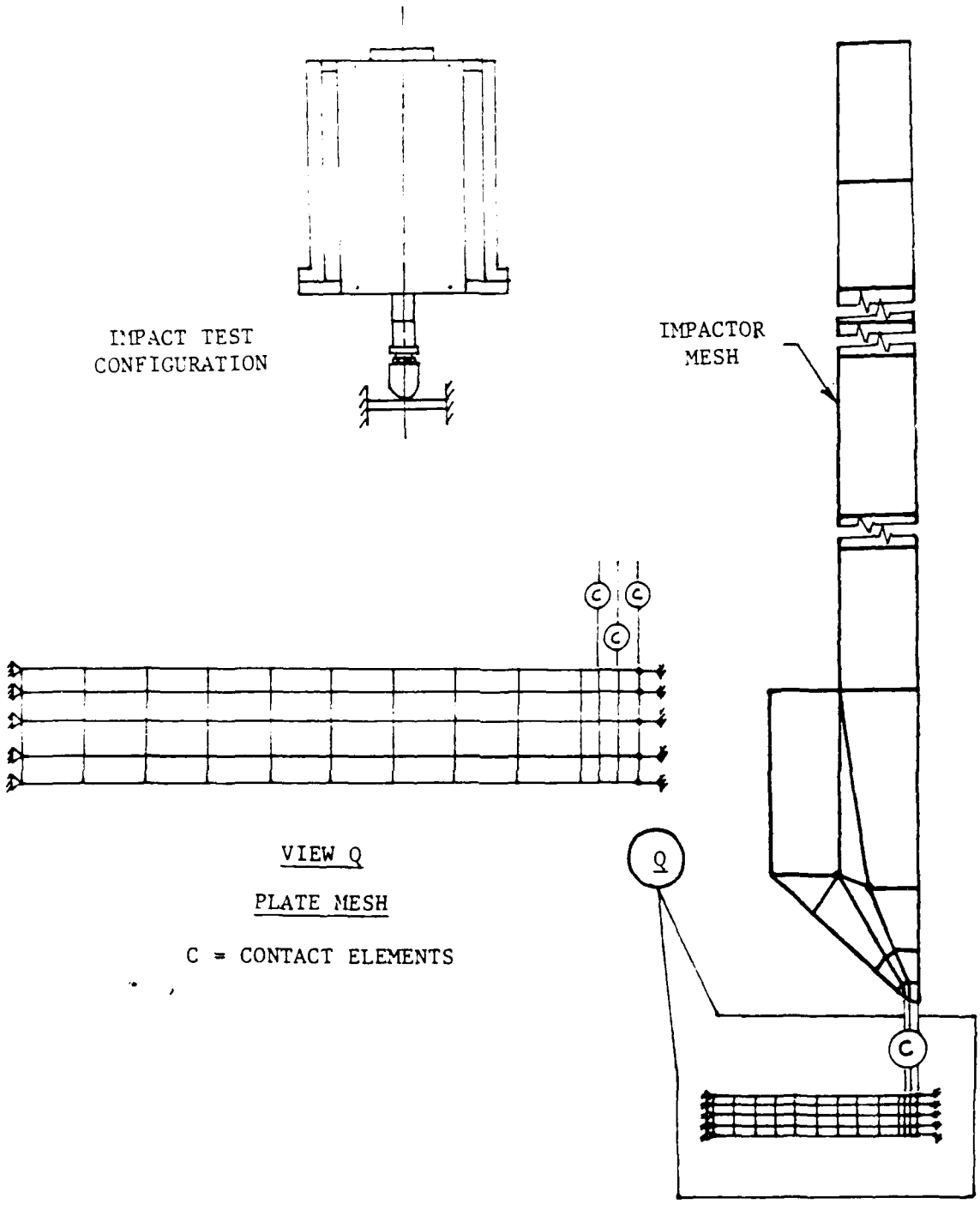

Figure 7. Finite element mesh for 2.56 in (65 mm) x 1.57 in (40 mm) x .25 in (6.5 mm) graphite/epoxy plate and impactor structure.

Figure 8 illustrates the time history of axial strain which occurs at midspan on the surface of the plate on the side immediately opposite the impact location. Note that the strain is lower when transverse shear and contact deformations are included as a result of the additional energy absorption mechanisms other than flexure. Table 2 presents maximum load cell force and maximum axial strain on the surface opposite the impact point for all plates and deformation mechanisms studied. As expected, the long plates show little effect of neglecting contact and transverse shear deformations.

As previously discussed, finite element analysis was performed for the most part under an impactor velocity of 315 in/s (8 m/s) and no gravity effects. Tests, however, were carried out under velocities which varied from 19 in/s (480 mm/s) to 170 in/s (4300 mm/s). In order to compare finite element analysis results with test results, a non-dimensionalization of analytical data from finite element runs was undertaken. Using a one-degree-of-freedom system model of a mass m impacting a massless spring of spring rate k with initial velocity v_0 in a gravity field (gravitational acceleration g) gives, for the contact force P between mass and spring

$$P = v_0(km)^{1/2}\sin(wt) + mg[1 - \cos(wt)] \qquad (19a)$$

where

$$w = (k/m)^{1/2} \qquad (19b)$$

and t is time. If the spring is a long plate of length L clamped at either end with thickness h, cross-sectional moment of inertia

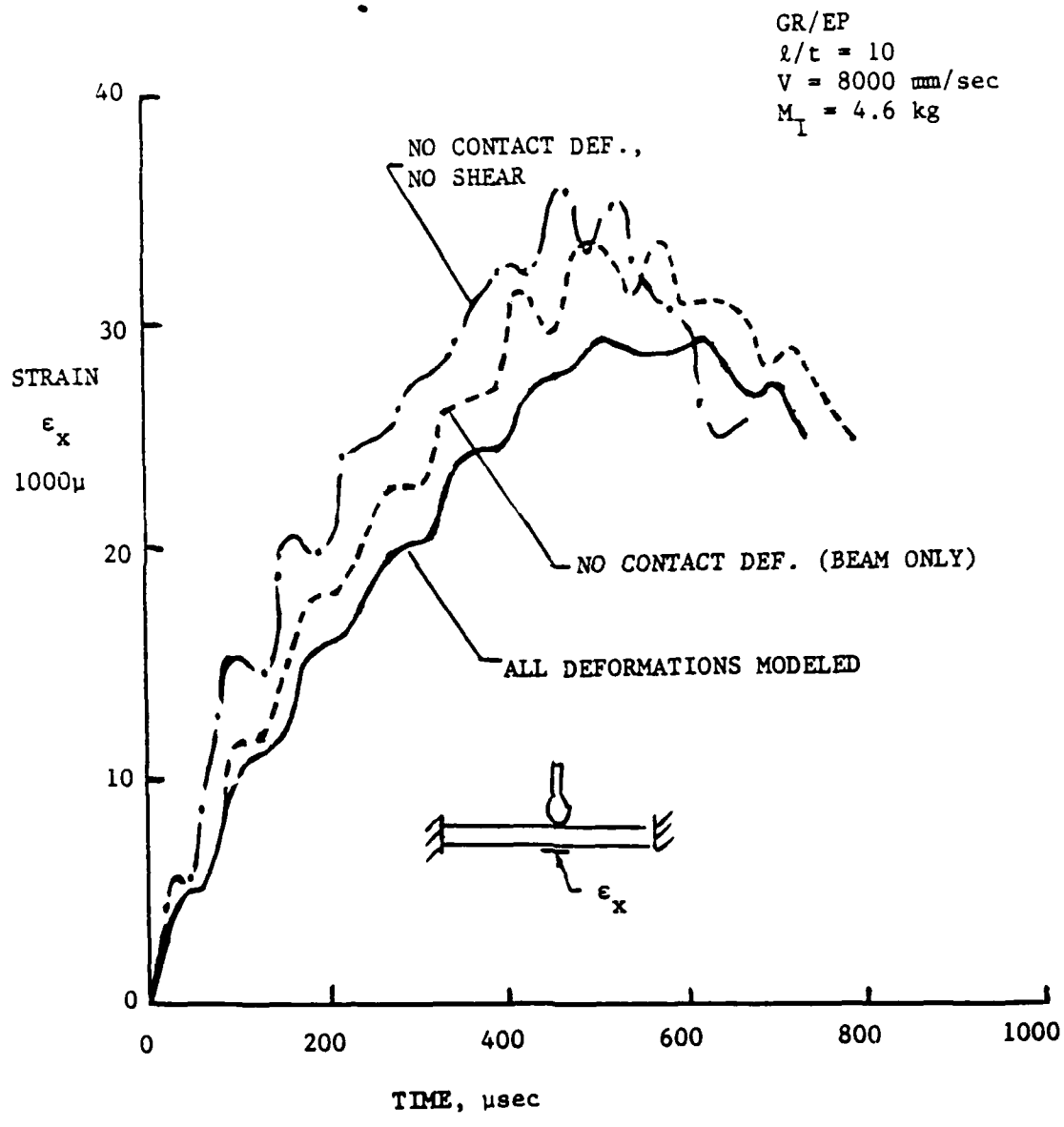

Figure 8. Predicted time history of midspan axial normal strain on I7 plate surface opposite impact site.

Table 2. Maximum impactor load cell force, P, and axial bottom-surface strain, e, predicted during impact of composite plates by 8.4 lb (3.8 kg) mass at 315 in/s (8.0 m/s).

			Load P, kN Deformation Modes Used			Strain e, 10^{-3}m/m Deformation Modes Used		
Plate ID	Aspect Ratio	Mtl. Angle (deg)	Flexure Contact & Shear	Flexure & Shear	Flexure Only	Flexure Contact & Shear	Flexure & Shear	Flexure Only
I1	112	0	4.35	4.40	NDG	30.5	30.6	NDG
I2	112	90	4.23	8.25*	NDG	60.0	81.0*	NDG
I3	42	0	9.9	10.0	10.1	42.0	42.5	43.0
I4	42	90	8.16	8.25	8.30	60.5	60.0	60.5
I5	21	0	26.25	28.7	31.5	30.2	37.0	38.0
I6	21	90	20.2	21.2	22.0	46.0	51.7	53.5
I7	10	0	67.5	70.0	72.0	30.0	33.7	37.0
I8	10	90	56.0	56.5	57.	49.5	54.0	58.0

NDG: identifies unacceptable finite element results.
*: probably incorrect due to numerical instability

I, and material plane strain extensional stiffness C_{XX}; and if it is further assumed that the static flexural deflection curve represents dynamic deflection, then

$$k = 192C_{XX}I/L^3 \qquad (19c)$$

The first term in equation (19a) is the force due to impactor initial velocity and the second term is the effect of gravity. A nondimensional load cell force p^*_{FE} is defined for finite element results which adds the gravitational force as follows:

$$P^*_{FE} = P_{FE}/[v_0(km)^{1/2}] + [g(km)^{1/2}/(v_0k)][1 - \cos(wt)] \qquad (20)$$

where P_{FE} is value of load cell force from finite element analysis at any given time t. The flexural strain e in a plate undergoing dynamic impact loading represented by equations (19) is found to be

$$e = (12h/L^3)\{(v_0/w)\sin(wt) + (mg/k)[1 - \cos(wt)]\} \quad (21)$$

In a manner similar to load nondimensionalization, a nondimensional strain e^*_{FE} which adds gravitational effects is defined as

$$e^*_{FE} = e_{FE}/[12v_0h/(L^2w)] + [mgL^2w/(12v_0hk)][1- \cos(wt)] \quad (22)$$

where e_{FE} is the axial normal strain obtained from the finite element analysis. Time is nondimensionalized by the time for which a mass remains in contact with a spring for a simple mass-spring system:

$$t^* = t/(\pi w) \quad (23)$$

Nondimensional load cell force, p^*_{FE}, and nondimensional strain e^*_{FE} opposite the impact location on the plate surface have been calculated for fully elastic finite element runs of all plates (I1 through I8). A complete set of graphs of nondimensional force and strain versus nondimensional time are presented in Appendix B.

C. COMPARISON OF FLEXURAL, CONTACT, AND SHEAR DEFORMATION EFFECTS

Table 2 presents load cell force and axial normal strain on the plate surface opposite the impact point obtained from finite element analysis with (a) all elastic deformations, (b) flexure and

transverse shear deformations but no contact deformations, and (c) flexure only with no transverse shear or contact deformations. As expected, plates with large aspect ratios (length-to-thickness) do not appear to be greatly affected by neglecting contact or transverse shear deformations. Results for plates with aspect ratios less than 40, however, show that both contact and transverse shear deformations can be important.

For quantitative comparison purposes, the data of Table 2 has been recast into Table 3 which shows the percent increase in predicted load or strain which occurs when (1) contact deformations are ignored and (2) when both contact and transverse shear deformations are ignored. Differences of three percent or less between analysis methods were not considered significant and are indicated by a dash in the table.

Table 3 shows some results which were unexpected. It was anticipated that the shorter plates (smaller aspect ratio) would show the greatest differences when contact and shear deformations were neglected. Instead, the shortest plate exhibits less difference from the fully elastic analysis than the next longer one. Time histories of the finite element results were examined, and it was found that the major reasons for the larger differences predicted in forces and strains for the longer I5 plate than for the shorter I7 plate was the superposition of higher order vibrational harmonics upon the first mode. It appears that artificially stiffening a structure by neglecting certain deformation modes can create natural frequencies which, if excited, may override the fundamental flexural deformation mode giving larger forces and strains than would ordinarily occur. This effect

Table 3. Percent increase in predicted load cell force and axial normal strain caused by neglecting contact and transverse shear deformations in elastic finite element analysis.

			Total % Increase, Load Cell Force — Deformation Mode Neglected		Total % Increase, Axial Normal Strain — Deformation Mode Neglected	
Plate	Aspect Ratio	Mtl. Angle (deg)	Contact Only	Contact & Shear	Contact Only	Contact & Shear
I1	112	0	-	NDG	-	NDG
I2	112	90	+95*	NDG	+35*	NDG
I3	42	0	-	-	-	-
I4	42	90	-	-	-	-
I5	21	0	+9	+20	+23	+26
I6	21	90	+5	+9	+12	+16
I7	10	0	+4	+12	+7	+23
I8	10	90	-	+9	-	+17

- indicates less than 3% difference from complete elastic analysis.

NDG: identifies unacceptable finite element results.

* probably incorrect due to numerical instability.

is not expected to occur for every plate since the excitation of higher order harmonics will depend upon plate stiffness (material, thickness, and length), the impactor mass and stiffness, and the initial impact velocity. Therefore, one set of impactor and velocity conditions may excite one structure and not another. This conclusion is important because it means that "rules of thumb" for deciding when to and when not to use a given analysis capability may be extremely difficult to generate since plate geometry, plate material stiffness, impactor geometry, impactor material stiffness, and impactor velocity all play a role.

However, it is clear from the data presented in Tables 2 and 3 that for AS-3501 graphite epoxy plates clamped on two opposite ends, elastic contact and transverse shear deformations play an important part in predicting accurate stresses and strains. Analyses of plates with length-to-thickness ratios greater than 40:1 do not require the inclusion of these effects to obtain accurate flexural strain predictions, while plates with 20:1 and smaller ratios will require these effects if less than 3% error is desired. It is apparent that each effect - contact and shear - accounts for anywhere between 5% and 20%, and they both appear to be equally important for the structures, materials, and impactor analyzed. It may be that these effects will be more important for plates restrained on all four sides and for spherical rather than cylindrical impactor tip geometry.

Further conclusions concerning the ability of elastic analysis to model impact of composite plates will be drawn from comparison between analysis and test results in the succeeding sections of this report.

IV. IMPACT TESTS OF AS-3501 GRAPHITE/EPOXY PLATES

A. EQUIPMENT AND TEST SETUP

1. Test Specimens

Tests were designed to duplicate the conditions of the analysis. AS-3501 graphite/epoxy laminated plates were fabricated at NAVAIRDEVCEN using two stacking sequences: 24-ply $[(\pm 45/0_2)_2/\pm 45/0/90]_S$ and 48-ply $[(\pm 45/0_2)_2/\pm 45/0/90]_{2S}$. Specimens I1 through I4 were cut from the 24-ply laminate and specimens I5 through I8 were cut from the 48-ply laminate. Odd numbered specimens had the high-stiffness direction along the plate's longitudinal axis, while even numbered specimens had the low-stiffness direction along the plate's axis. Figure 9 gives specimen dimensions.

2. Test Apparatus

Plate impact samples were clamped at either end using one of two clamping apparati. The shorter specimens (I3 through I8) were c-clamped between 3/8-in- (9.5-mm-) thick steel plates to a steel frame which was designed especially to fit the NAVAIRDEVCEN impact tower bed. The longest I1 and I2 plates were clamped in a modified rig normally used for plates supported on all four edges but which was modified for the two-edged support situation. The primary difference between the two clamping fixtures was the length of specimen clamped between two steel plates. Specimens I3 through I8 had clamp plates 2 in (51 mm) long on either end, while the I1 and I2 specimens were clamped 1/2 in (13 mm) on either end. Also,

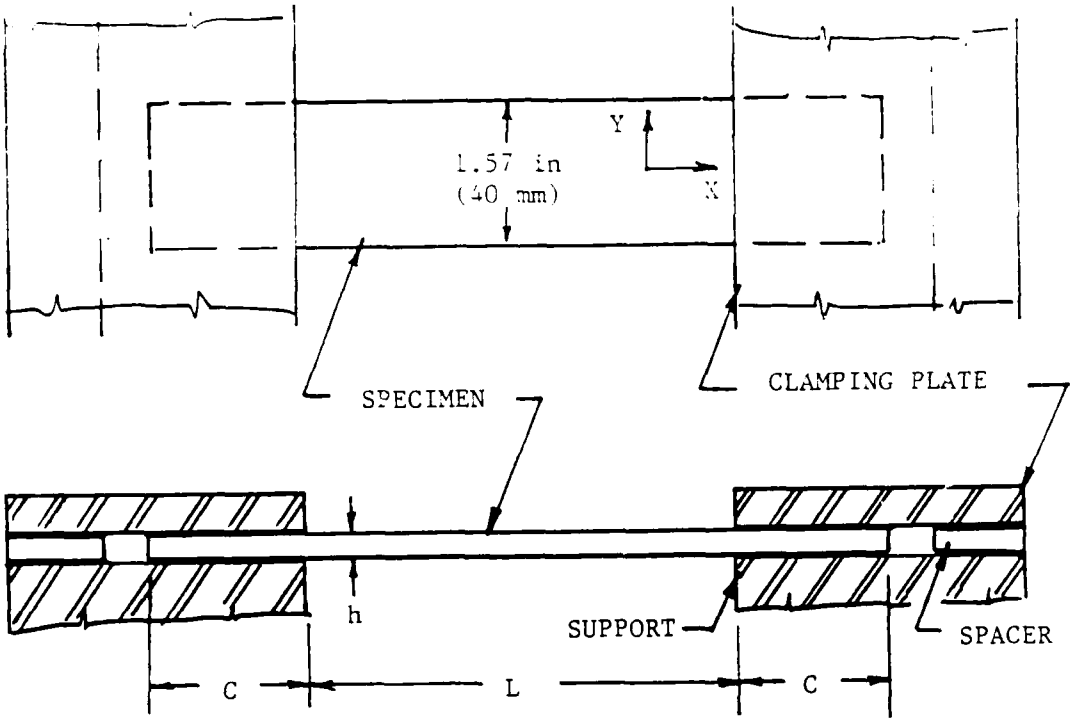

SPECIMEN	L in/mm	C in/mm	h in/mm	STACKING SEQUENCE
I1	14/355	0.5/13	.128/3.25	$[(\pm 45/0_2)_2/\pm 45/0/90]_S$
I3	5.31/135	2.0/51	"	"
I5	"	"	.256/6.5	"
I7	2.56/65	"	"	"
I2	14/355	0.5/13	.128/3.25	$[(\pm 45/0_2)_2/\pm 45/0/90]_{2S}$
I4	5.31/135	2.0/51	"	"
I6	"	"	.256/6.5	"
I8	2.56/65	"	"	"

Figure 9. Laminated graphite/epoxy impact test specimen geometry.

considerably greater clamping force could be exerted by the c-clamps on the shorter specimens than could be obtained with two eccentric 1/8 in bolts used by the rig for clamping specimens I1 and I2. As described below, the lesser clamping force on the I1 and I2 specimens allowed membrane forces to pull the specimens from the supports invalidating the tests.

Plates were impacted using the NAVAIRDEVCEN instrumented impact tower with automated data storage and reduction capabilities. The tower, shown in Figure 10, consists of two cylindrical impactor guides, the impactor which contains a load cell for measuring impact force, a mechanism for drop height control/impactor lift and automatic release, a test bed with specimen supports, and instrumentation for measuring velocity of impactor at the point of impact. A Nicolet two-channel digital storage scope is used to store more than 4,000 data points per timed event.

The main body of the impactor (see upper left inset, Figure 7) is fabricated from steel plate. It contains provisions for adding weights to control impactor mass. For the tests conducted here, no added weights were used, and the total impactor mass was either 8.4 lbm (3.8 kg) with a 2,000 lb (9 kN) load cell or 9.8 lbm (4.4 kg) with a 10,000 lb (44 kN) load cell. The impactor is designed to use interchangeable tips. For the tests conducted here, two special cylindrical impactor tips were designed and manufactured - one with a 2 in (51 mm) diameter impact surface and one with a 0.25 in (6.4 mm) diameter impact surface. Both were 1.625 in (41.3 mm) wide - slightly wider than the specimens. Nearly all of the tests were conducted with the 2,000 lb (9 kN) load cell and the 0.25 in (6.4 mm) impactor tip.

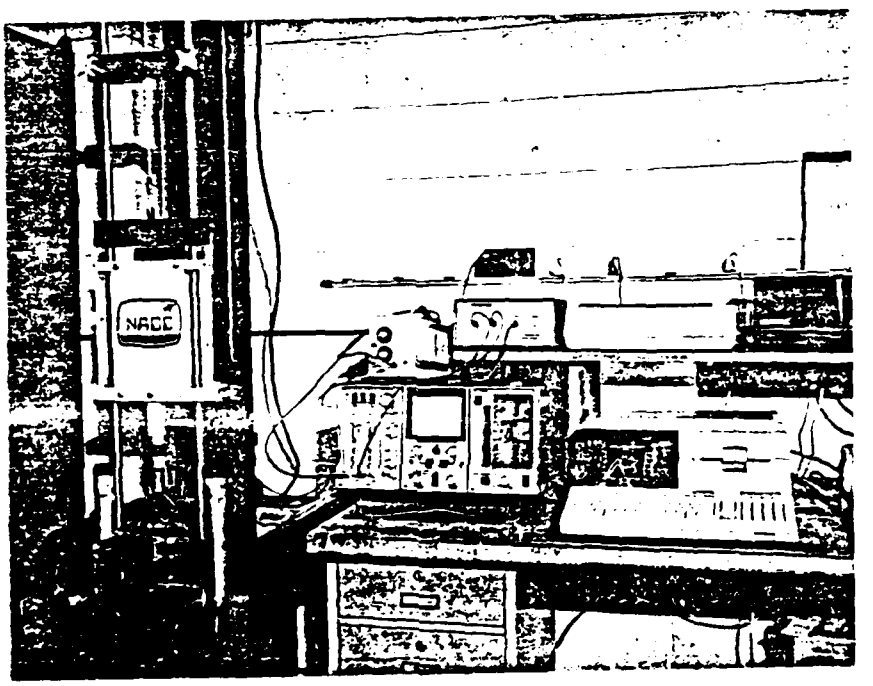

Figure 10. Naval Air Development Center Instrumented Impact Tower.

Data were analyzed using impact computer software and plotting routines developed especially for the NAVAIRDEVCEN instrumented impact tower facility by Mr. L. W. Gause. This software provides time plots of impact force, impactor displacement, specimen strain, and absorbed energy for the impact event, and plots of impact force and absorbed energy versus impactor displacement. It also calculates velocity at impact and maximum values of force, displacement, strain, and other quantities of interest.

B. TEST PROGRAM

Nondestructive impact tests of all eight configurations of AS-3501 graphite/epoxy plates were performed. Each test specimen was strain gaged so that time histories of axial strain at midspan on the back-surface (surface opposite the impact site) could be measured and compared with analysis. Both back-surface strain and impactor load cell force were recorded during the impact event on the Nicolet digital storage scope.

Drop heights varied between 1.0 in (25 mm) and 5.0 in (125 mm) resulting in impact velocities from about 2 ft/s (0.6 m/s) to 5 ft/s (1.5 m/s). Care was taken to maintain back-surface strain less than 0.005 to avoid structural cracks.

One specimen of each size and material orientation was subjected to three consecutive tests at the same drop height to demonstrate repeatability. Time histories of impact events were found to be nearly identical (impact loads and structural strains were virtually the same from test-to-test, varying less than 1% in magnitude and duplicating higher order harmonics as small as 0.02

of the total impact period). Due to the excellent repeatibility of test data, two impact tests were deemed sufficient for each test condition: the first to measure force and strain, and the second to measure impact velocity and to verify that the specimen had not been damaged (identical traces of impact force with time were considered to show that insignificant damage had occurred).

Appendix C lists the impact tests performed on specimen configurations I1 through I8.

C. RESULTS

Contact load and back surface strain histories for each test were stored on floppy diskettes by the Nicolet storage scope. The computerized data reduction system was utilized to obtain experimental verification of impact velocities; to calculate impactor head displacement and absorbed energy; and to generate time plots of impactor force, plate axial strain, displacement, and absorbed energy.

Figures 11 through 13 show the reduced data for the I7 specimen impacted at 3.6 ft/s (1.1 m/s). Similar plots have been obtained for all specimens and a complete set is provided in Appendix D.

It is noted that the longest plates (specimens I1 and I2 with aspect ratios 100:1) pulled loose from the supports due to large deflections creating significant membrane force effects, and the data may be invalid for comparison with analytical predictions.

For comparison with the analytical predictions, load cell force, plate axial normal strain, and contact impact duration were nondimensionalized in the manner used for the analytically

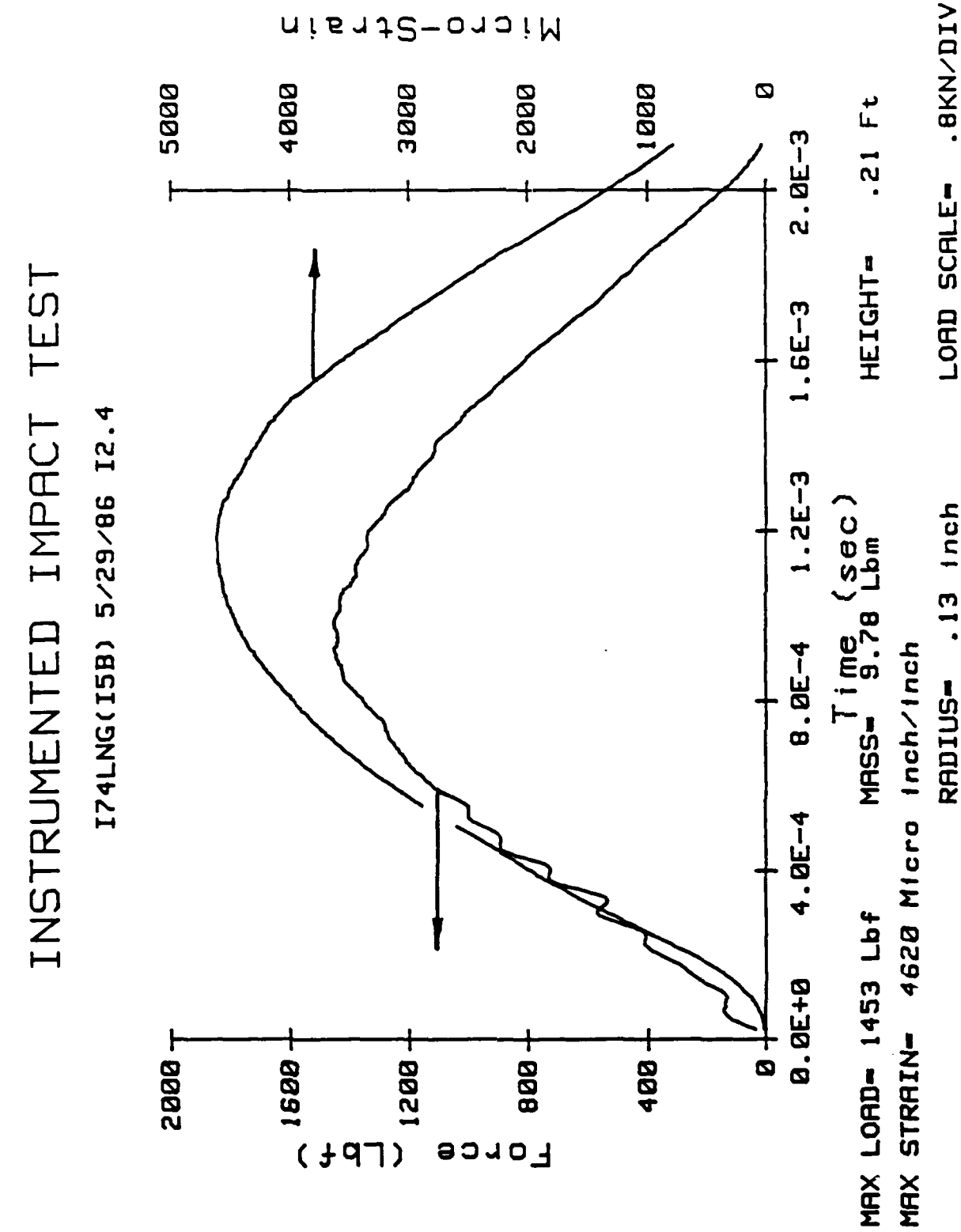

Figure 11. Impactor load cell force and axial normal plate strain versus time for specimen I7, impactor velocity 3.6 ft/s (1.1 m/s).

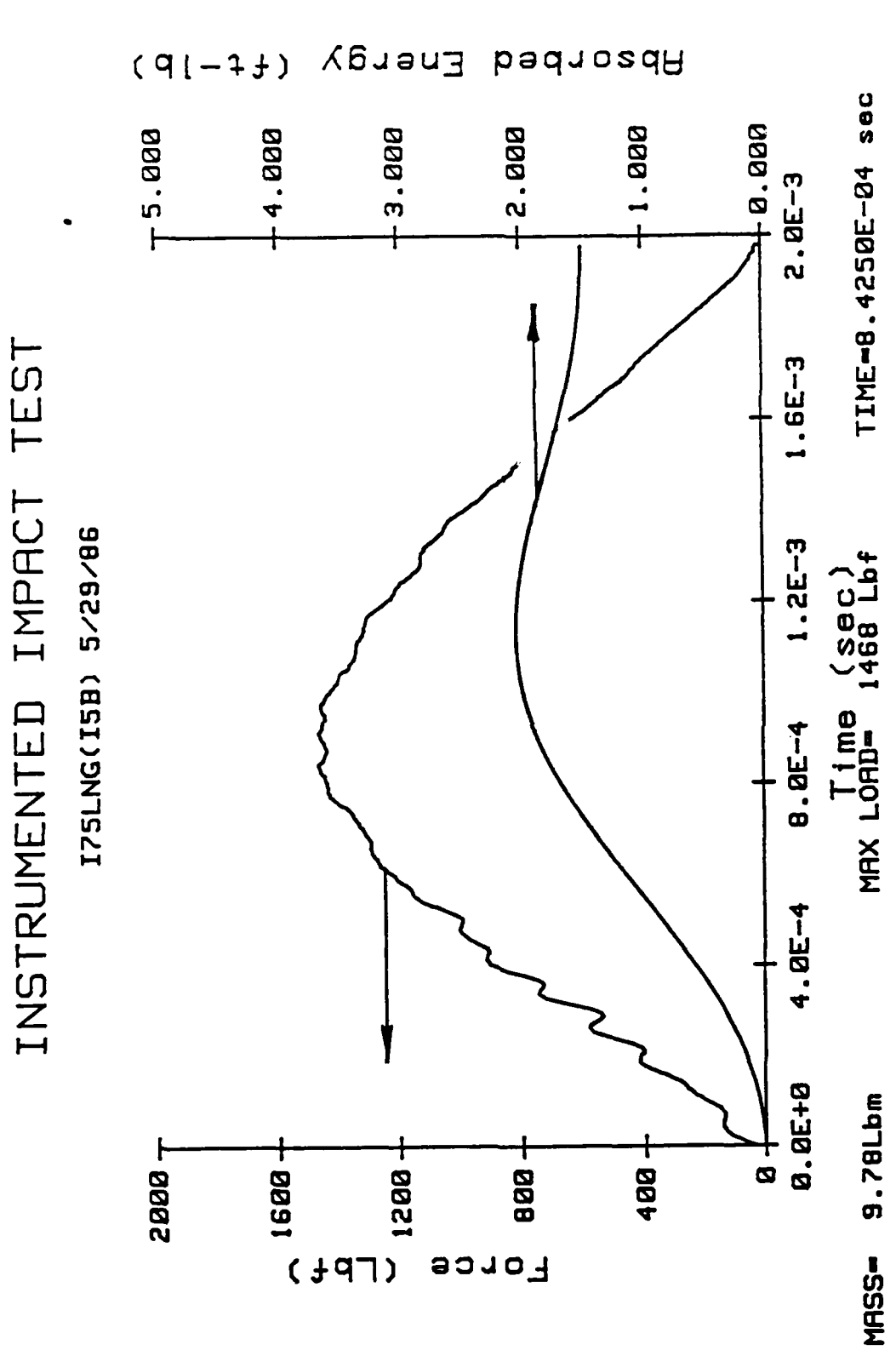

Figure 12. Impactor load cell force and absorbed energy versus time for specimen I7, impactor velocity 3.6 ft/s (1.1 m/s).

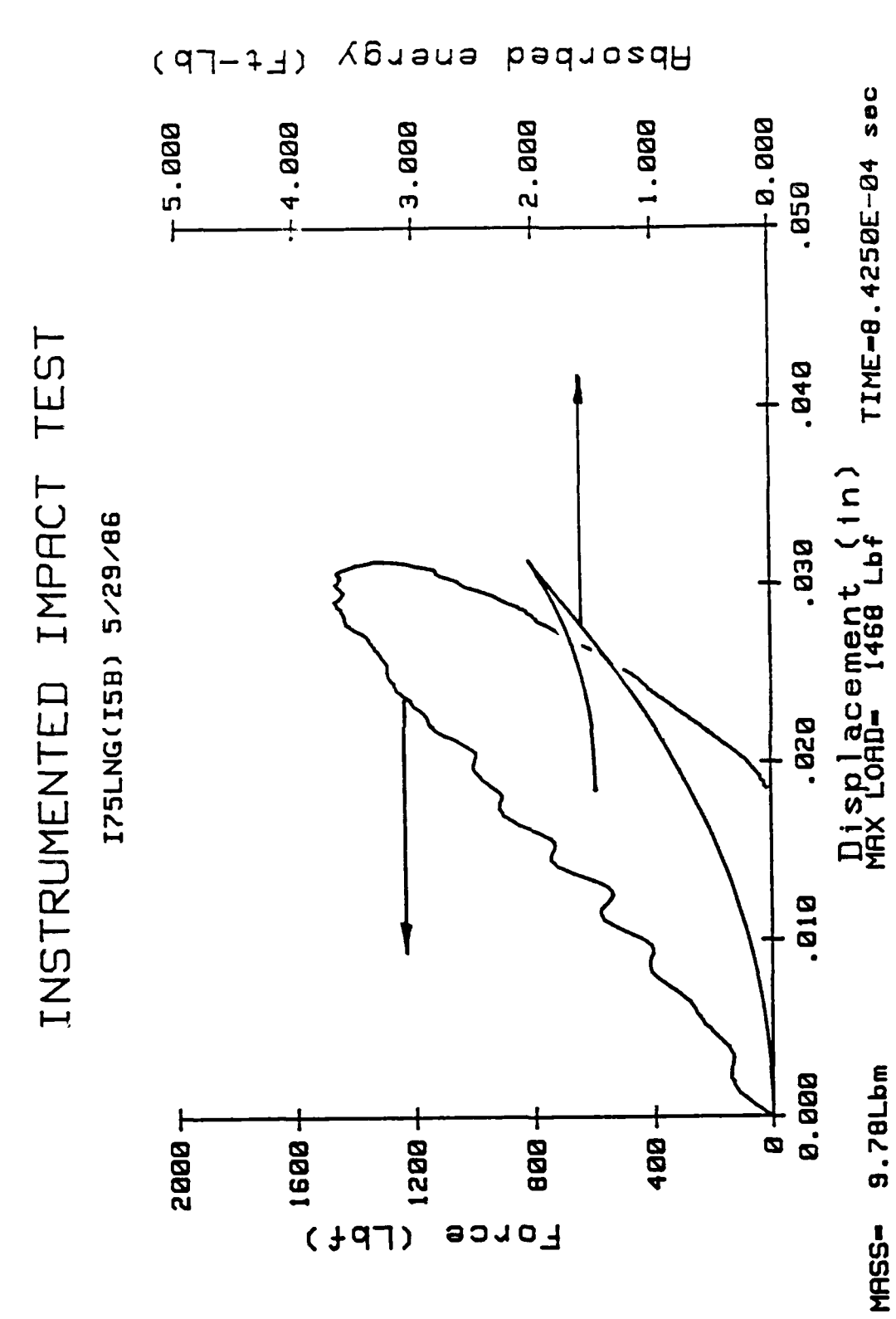

Figure 13. Impactor load cell force and absorbed energy versus impactor displacement for specimen I7, impactor velocity 3.6 ft/s (1.1 m/s).

determined quantities, but without the gravity term which is not needed for the test data:

nondimensional load cell force from test:

$$p^*_{EXP} = P_{EXP}/[v_0(km)^{1/2}] \quad (24)$$

nondimensional strain opposite impact location from test:

$$e^*_{EXP} = e_{EXP}/[12v_0h/(L^2w)] \quad (25)$$

where P_{EXP} and e_{EXP} are test impactor force and plate strain, respectively, k is plate stiffness given by equation (19b), v_0 is impact velocity, m is impactor mass, h is plate thickness, and L is plate length between supports. [Nondimensional time t* is given by equation (23).]

Nondimensional time histories of impactor force and plate axial normal strain are presented in Figures 14 and 15 for the I7 specimen impacted at 3.6 ft/s (1.1 m/s). Complete nondimensional results are presented in Appendix E.

Nondimensional test results are summarized with finite element results in Table 4. The first line of p* and e* data for each specimen are amplitudes of the first mode force and strain responses, respectively. The second line gives the maximum higher mode amplitudes. The maximum amplitude of force or strain may be found by adding first mode and higher mode amplitudes. The nondimensional contact impact duration t^*_{MAX} is the time for which the impactor remains in contact with the plate during the initial impact event nondimensionalized by equation (23). Data for the long plate I1 and I2 specimens are included for completeness even though they may be invalid as discussed above.

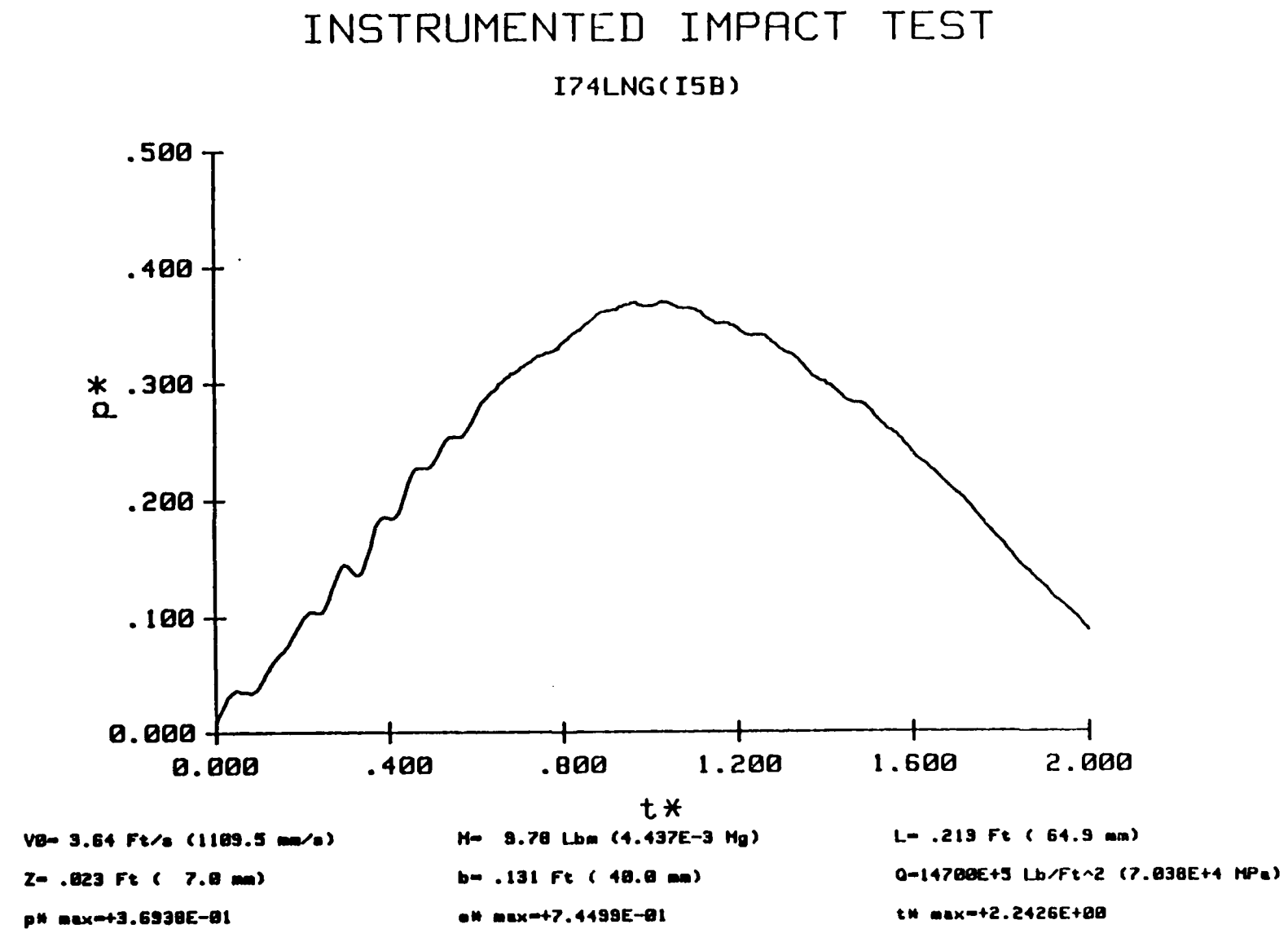

Figure 14. Nondimensional impactor load cell force, p*, versus nondimensional time for specimen I7, impactor velocity 3.6 ft/s (1.1 m/s).

NADC-87106-60

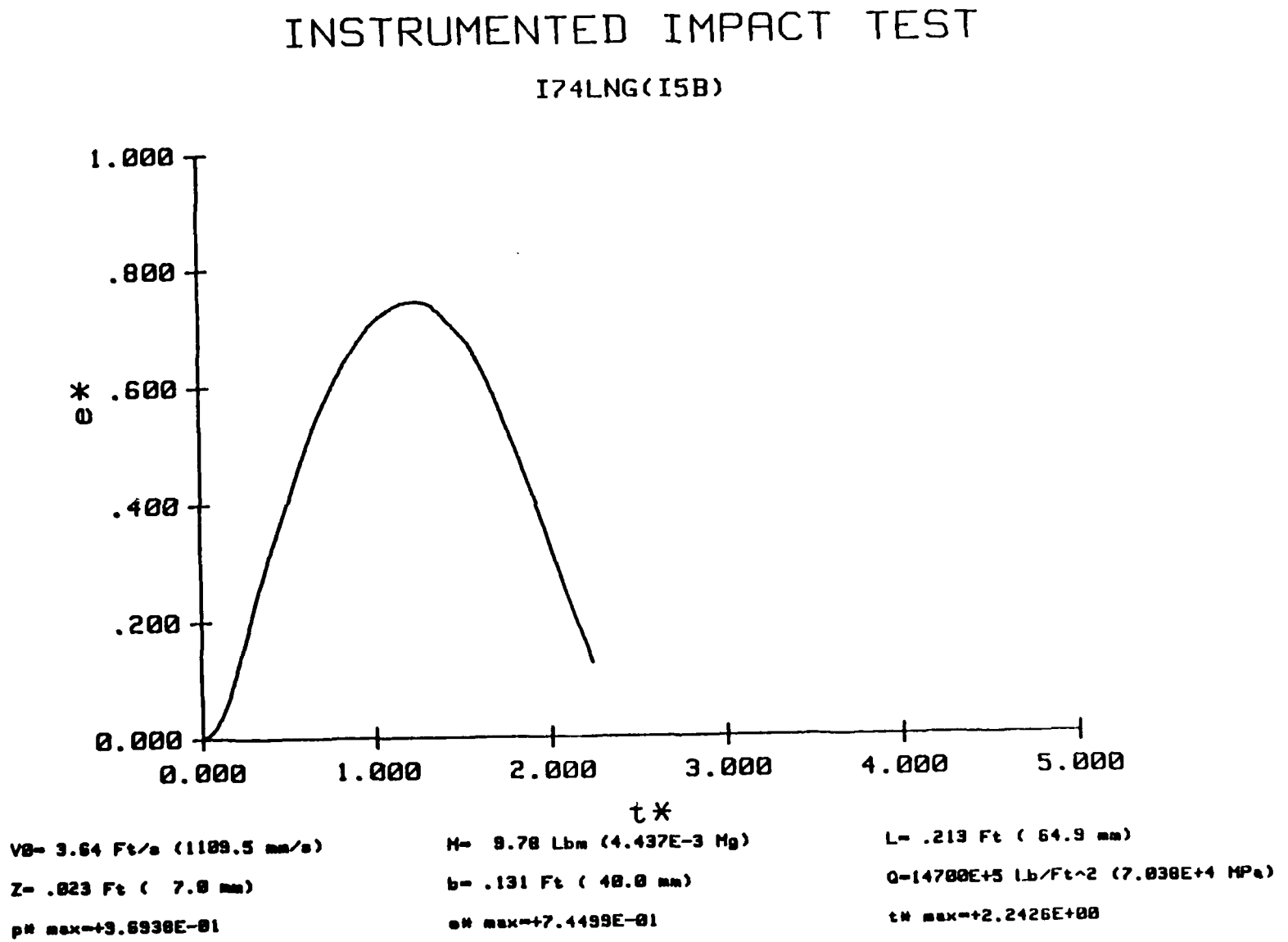

Figure 15. Nondimensional axial normal plate strain versus nondimensional time for specimen I7 , impactor velocity 3.6 ft/s (1.1 m/s).

Table 4. Nondimensional impactor force p*, plate axial normal strain e*, and contact impact duration t^*_{MAX} obtained by finite element analyses (FE) and tests (EXP).

	1 SPM NO.	2 L/h	1ST MODE FORCE AND STRAIN@ + HIGHER MODE RESPONSE				IMPACT DURATION		STRAIN RATIO#
			3 p^*_{EXP}	4 p^*_{FE}	5 e^*_{EXP}	6 e^*_{FE}	7 t^*_{MAXEXP}	8 t^*_{MAXFE}	9 $\frac{e^*_{EXP}}{e^*_{FE}}$
	[I1	112	0.85 +.1	0.90 +.5	1.11	1.1 +.2	1.05	0.85	1.01]$
HIGH MATL STIFFNESS	[I3	42	0.65	0.66	1.11	0.89	1.2	0.94	1.25]
	[I5	21	0.50	0.58 +.02	0.87	0.83 +.15	1.45	1.0	1.05]
	[I7	10	0.38	0.58	0.75	0.81	2.19	1.47	0.93]
	[I2	112	1.18 +.07	1.4 +.5	1.4 +.08	1.2 +.5	0.95	0.8	1.17]
LOW MATL STIFFNESS	[I4	42	0.60 +.07	0.68 +.14	1.3	0.88 +.06	1.24	0.86	1.48]
	[I6	21	0.53	0.62 +.06	0.99	0.85 +.16	1.43	1.0	1.16]
	[I8	10	0.39	0.69	0.75	0.89	1.86	1.28	0.84]

@ First mode: amplitude of fundamental frequency force and strain response.
Higher mode: amplitude of frequency response for second and higher mode frequencies combined.

Strain ratio: ratio of plate axial normal strain on the back surface obtained experimentally to that predicted by finite element analysis.

$ Experimental data for the long I1 and I2 plates are suspect due to support slippage during the test.

HIGH and LOW MATL STIFFNESS indicate that odd numbered specimens have approximately $[\pm 45/0_2]_S$ layup and even numbered specimens have approximately $[\pm 45/90_2]_S$ layup. Refer to Figure 9.

Recall that impact test results are nondimensionalized with respect to maximum values predicted by an elementary one degree of freedom strength of materials analysis: nondimensional quantities of 1.0 indicate that experimental results and one degree of freedom results coincide. As expected, test results (columns 3, 5, and 7) for the I3 through I8 specimen tests are generally closer to the one degree of freedom predictions for longer, thinner plates. It is not likely that tests should agree with the one degree of freedom predictions even for long plates, since the analysis ignores higher degree vibrational modes.

Contact and transverse shear deformations effectively add flexibility to a structure, and these effects are more important for shorter plates. Therefore, the decrease in nondimensional impactor force and plate axial normal strain with decrease in aspect ratio is expected, as is the increase in contact impact time with decrease in aspect ratio.

Except for the longest I1 and I2 specimens, the data appear to be consistent and in accord with fundamental principles.

V. COMPARISON OF IMPACT ANALYSIS WITH TESTS

Table 4 presents nondimensional impactor force, plate axial strain, and contact impact time for analytical elastic finite element results (columns 4, 6, and 8) in addition to experimentally measured values (columns 3, 5, and 7). Column 9 is the ratio of the experimentally measured plate axial normal strain to that predicted by the finite element analysis.

It is apparent from Table 4 that the small displacement elastic analysis, even with transverse shear and contact deformations, may be inadequate to predict structural strains for composite plates. Experimental strains were from 15% lower to 45% higher than predicted by the finite element elastic analysis.

The shortest plates (aspect ratio 10:1) exhibited smaller axial normal strains and impactor forces than predicted. Transverse shear and contact viscoelasticity may account for these differences. If so, the effects may be more pronounced for plates supported on all edges and for sharper impact indenter radii than the 1/8-in (3-mm) radius used for both test and analysis.

Experimental axial strains in the longer plates (aspect ratios greater than 20:1) were greater than predicted by analysis. It is doubtful that viscoelastic effects can account for this difference, since they would absorb more energy and reduce flexural strains. Membrane effects would stiffen the structure and reduce flexural strains. Although additional axial strains would be imparted by the membrane forces, it is not anticipated that they would increase total axial strains beyond those which would be predicted by small displacement flexural analysis.

VI. CONCLUSIONS

The major conclusions from this study are as follows:

1. Flexural viscoelasticity is not an important energy absorption mode during low-velocity impact of graphite/epoxy composite plates. The degree of flexural viscoelastic behavior required to fit experimental impact data of graphite/epoxy plates is several orders of magnitude larger than that available in the material.

2. Finite element analysis indicates that elastic contact and transverse shear deformations are important to accurate prediction of structural stresses and strains for plates clamped on opposing edges with length-to-thickness ratios of 20 and less. Results of purely flexural analysis of plates with aspect ratios of 40 and greater appears not to differ from results of analyses containing elastic contact and transverse shear deformation effects.

3. The neglect of contact and transverse shear effects can alter the structural response of an impacted plate by creating a higher order resonant response (or eliminating one) and may produce large errors in stress and strain predictions. It is therefore difficult to develop quantitative "rules of thumb" for errors resulting from analytical approximations, as the dynamic response will depend upon plate geometry, plate material, support conditions, impactor mass, and impactor structural geometry and stiffness. However, present analyses indicate that errors between 5% and 20% can result for short plates by neglecting either contact or shear deformations.

4. Membrane effects are definitely important for plates clamped on two opposing edges having aspect ratios of 100 or greater.

5. Comparison between analysis and test shows that elastic contact and shear deformation modeling still overpredicts strains in impacted graphite/epoxy plates with aspect ratios of 10 or less. Transverse normal and shear viscoelastic behavior might explain the difference. It is recommended that an analysis capability which includes these viscoelastic effects be developed and used to study stresses and strains in plates supported on all sides. It is probable that fully supported plates impacted with a spherical indenter will exhibit greater discrepancies than the plates used in this study which were supported on two opposing ends and impacted with a cylindrical indenter.

6. Experimental strains in long plates (aspect ratios of 20 and greater) can be as much as 48% higher than analytical elastic predictions. This might be due to two effects:

(a) membrane forces during large deflections, and/or

(b) significant structural natural frequency alteration due to improper material modeling.

This points to the need for inclusion of membrane force effects (e. g., references [12, 13] or [17]) in the analysis of plates, reinforces the desirability of modeling viscoelastic contact and shear behavior of the material, and shows the advisability of conducting a study which will evaluate these effects for plates supported on all edges.

7. It is well-known that the prediction of accurate deflections does not insure that stresses and strains are accurately predicted: since displacements are integrals of strains and integration is a "smoothing" process, there are many examples of analyses which may have only 3% error in displacement but as much as 20% error in strains and stresses. In a similar fashion, the existence of the well-known St. Venant effect, where self-equilibrating stress states decay rapidly with distance from the disturbance, generally indicates that high locally-generated stresses and strains will reduce rapidly with distance from the cause. Therefore, the errors in axial normal strain reported here are most likely indicative of much larger errors in stresses and strains in the immediate vicinity of the contact impact location.

8. Progress has been made to determine which analytical capabilities are necessary to accurately analyze the impact response of composite plates for design purposes. However, the program has raised new questions as well as answered old ones. Continued investigation into this problem is necessary until the answers are obtained. Only then can the composites community be satisfied that it can accurately and efficiently analyze not only structural stresses and strains (those not in the impact region and not directly affected by contact stresses), but also stresses in the immediate vicinity of the contact region.

VIII. REFERENCES

1. Gause, L. W., Rosenfeld, M. S., and Vining, R. E., "Effect of Impact Damage on the XVF-12A Composite Wing Box," Report No. NADC-79225-60, August, 1979.

2. Hertzberg, P. E., Smith, B. W., and Miller, A. G., "Effect of Matrix Resin on the Impact Fracture Characteristics of Graphite/Epoxy Laminates," NASA Contractor Report No. 165784, January, 1982.

3. Ramkumar, R. L., "Composite Impact Damage Succeptibility," Report No. NADC-79068-60, January, 1981.

4. Chou, P. C., and Flis, W. J., Design Curve for Beams under Impact Loading," AIAA Journal, Vol. 15, 1977, pp. 455-456.

5. Chou, P. C., and Flis, W. J., "Comparison of Solution Methods for Composite Material Beam Response Due to Impact," NADC-76093-30, December, 1975.

6. McQuillen, E. J., Gause, L. W., and Llorens, R. E., "Low Velocity Transverse Normal Impact of Graphite/Epoxy Composite Laminates," Journal of Composite Materials, Vol. 10, 1976, pp. 79-91

7. Hayes, S. V., and Rybicki, E. F., "The Development of a Low Velocity Impact Methodology for Hybrid Material Systems," ATC Report No. R-9200/TCR-63, Vought Corporation, July, 1981.

8. Llorens, R. E., and McQuillen, E. J., "Off-Center, Low-Velocity, Transverse Normal Impact of a Viscoelastic Beam," Report No. NADC-78237-60, September, 1978.

9. Llorens, R. E., and McQuillen, E. J., "Off-Center, Low-Velocity, Transverse Normal Impact of a Simply Supported Plate," Report No. NADC-79215-60, September, 1979.

10. Llorens, R. E., and Gause, L. W., "Low Velocity, Transverse Normal Impact of a Clamped Plate," Report No. NADC 81250-60, October, 1981.

11. Sun, C. T., and Chattopadhyay, S., "Dynamic Response of Anisotropic Laminated Plates under Initial Stress to Impact of a Mass," Journal of Applied Mechanics, Vol. 42, SEptember, 1975, pp. 693-698.

12. Bostaph, G. M., and Elber, W., "Static Indentation Tests on Composite Plates for Impact Succeptibility Evaluation," Proceedings of the Army Symposium on Solid Mechanics, 1982 - Critical Mechanics Problems in Systems Design, Report No. AMMRC MS 82-4, U. S. Army, September, 1982, pp. 288-317.

13. Elber, W., "Failure Mechanics in Low-Velocity Impacts on Thin Composite Plates," Report No. NASA TP-2152, NASA Langley Research Center, May, 1983.

14. Ramkumar, R. L., "A Finite Element (NASTRAN) Prediction of the Transient Failures in a Laminate Subjected to Low Velocity Normal Impact," Report No. NOR 80-161, Northrop Corporation, September, 1980.

15. Humphreys, E. A., and Goering, J., "Development of an Analytic Procedure to Calculate Damage Accumulation in Composites During Low Velocity Impact," NASA Contract Report No. 166086, February, 1983.

16. Stanton, E. L., and Crain, L. M., "An Analysis of Interlaminar Stress Gradients and Impact Damage in Graphite-Epoxy Laminates," Report No. NADC-80135-60, March, 1980.

17. Taylor, R. L., and Sackman, J., "Contact-Impact Problems: Volume 1 - Engineering Report and User's Manual," Report No. UC SESM 78-4-I, University of California-Berkeley, December, 1978.

18. Taylor, R. L., and Sackman, J., "Contact-Impact Problems: Volume 2 - Programmer's Manual," Report No. UC SESM 78-4-II, University of California-Berkeley, December, 1978.

19. Hughes, T. J. R., Taylor, R. L., and Sackman, J. L, "Finite Element Formulation and Solution of Contact-Impact Problems in Continuum Mechanics," Report No. UC SESM 74-8, University of California - Berkeley, 1974.

20. Hughes, T. J. R., Taylor, R. L., and Sackman, J. L, "Finite Element Formulation and Solution of Contact-Impact Problems in Continuum Mechanics - II," Report No. UC SESM 75-3, University of California - Berkeley, 1975.

21. Hughes, T. J. R., Taylor, R. L., and Sackman, J. L, "Finite Element Formulation and Solution of Contact-Impact Problems in Continuum Mechanics - III," Report No. UC SESM 75-7, University of California - Berkeley, July, 1975.

22. Hughes, T. J. R., Taylor, R. L., Sackman, J. L., and Kanoknukulchai, W, "Finite Element Formulation and Solution of Contact-Impact Problems in Continuum Mechanics-IV," Report No. UC SESM 76-4, July, 1976.

23. Kanoknukulchai, W., "A Large Deformation Formulation for Shell Analysis by the Finite Element Method," Ph. D. Dissertation, University of California, Berkeley, December, 1978.

24. Hashin, Z., "Viscoelastic Fiber Reinforced Materials," AIAA Journal, Vol. 4, 1966, pp. 1411-1417.

25. Schapery, R. A., "Stress Analysis of Viscoelastic Composite Materials," Journal of Composite Materials, Vol. 1, 1967, pp. 228-267.

26. Hashin, Z., "Complex Moduli of Viscoelastic Composites - II. Fiber Reinforced Materials," International Journal of Solids and Structures, Vol. 6, 1970, pp. 797-802.

27. Hashin, Z., "Theory of Fiber Reinforced Materials," NASA Contractor Report No. NASA CR-1974, March, 1972.

28. Renton, W. J., and Ho, T., "The Effect of Environment On the Mechanical Behavior of AS/3501-6 Graphite/Epoxy Material," ATC Report No. B-92100/8CR-105, Vought Corporation, August, 1978.

29. Flugge, W., Viscoelasticity, Blaisdell, 1967.

30. McLaughlin, P. V., Jr., "Aerostructure NDT by Thermal Field Techniques, Phase I: Fundamental Information and Basic Technique Development," Report No. NAEC-92-157, Naval Air Engineering Center, May, 1982.

31. Chou, P. C., Flis, W. J., and Miller, "Certification of Composite Aircraft Structures under Impact, Fatigue, and Environmental Conditions. Part I - Low Speed Impact of Plates of Composite Materials," Report No. NADC-78259-60, Naval Air Development Center, January, 1978.

APPENDIX A. CREEP TEST DATA FOR [45] AS-3501 GRAPHITE/EPOXY LAMINATES

MCL 2 TEK 1

0-20SEC

1/2 in. +45/-45 CREEP 125# A (NOMINAL)

LOAD : 10 V = 500 lb

STRAIN 10V = 10,000 μ ε

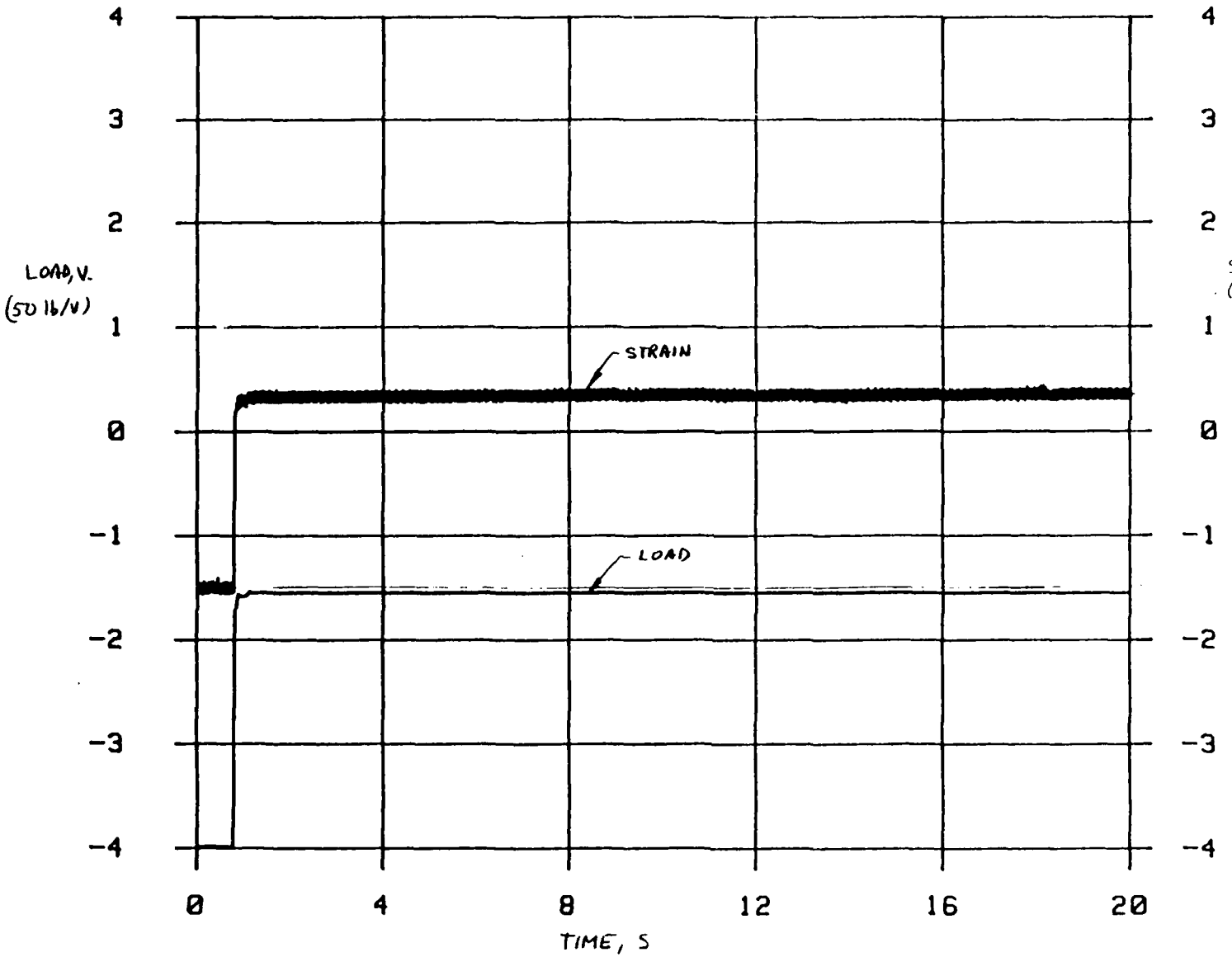

$\varepsilon_0 = \frac{6.5}{28.3} \times 8 \times 10^{-3}$

$= .001839$

$P_0 = \frac{10.36 \text{ div}}{35.96 \text{ div/V}} \times 500 \text{ lb/V}$

$= 122.03 \text{ lb}$

NADC-87106-60

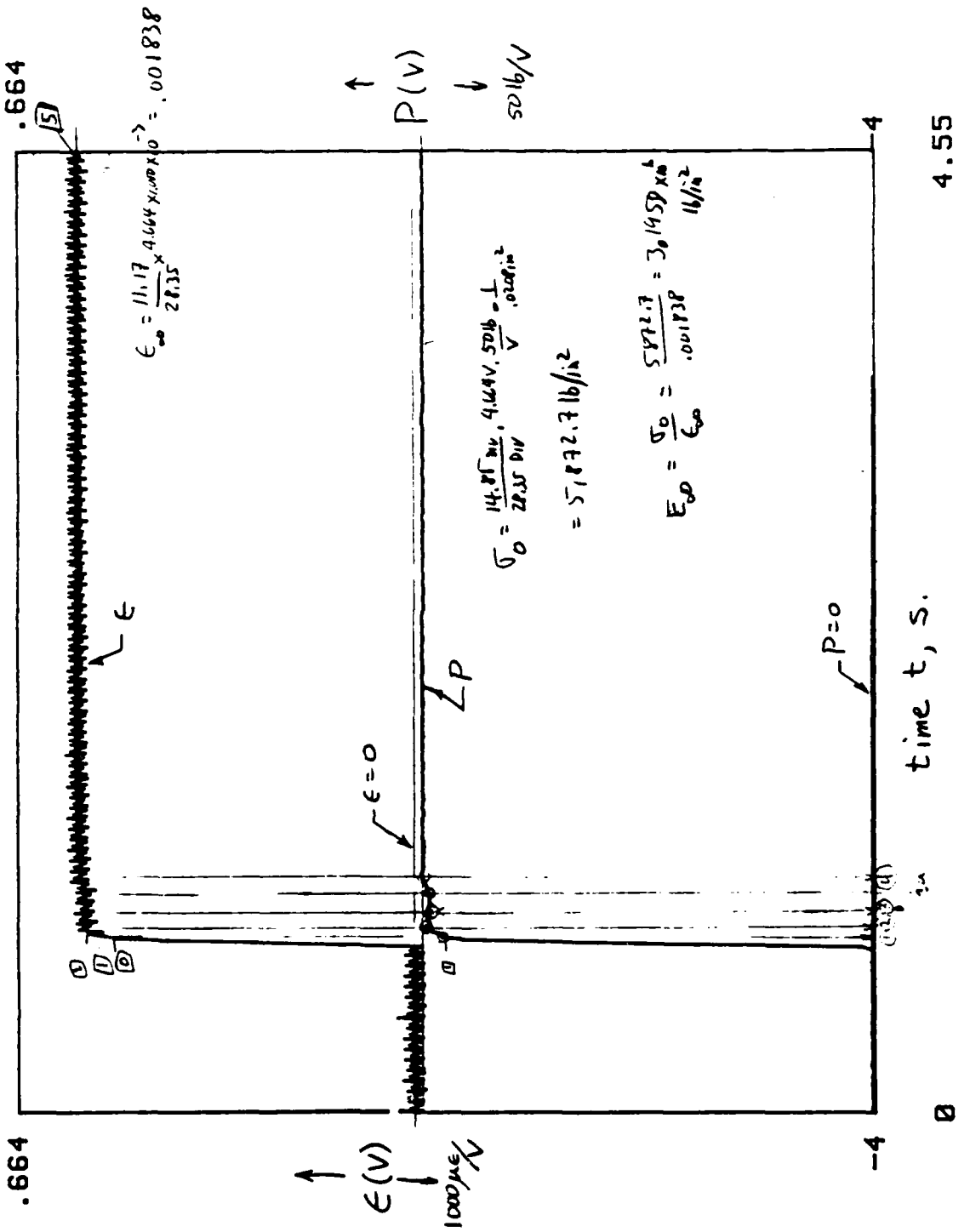
NOMINAL 125 lb CREEP TEST EXPANDED TIME SCALE
.664
P(V)
5016/V
4
4.55
ε
ε=0
P
P=0
time t, s.
0
-4
.664
ε(V)
1000 με/V

7/14/87
MCL 2 TK#2
5 min - 5:10
LOAD : 10V = 5016
STRAIN : 10V - 10,000 με

1/2 In. +45/-45 CREEP 125# B (NOMINAL)

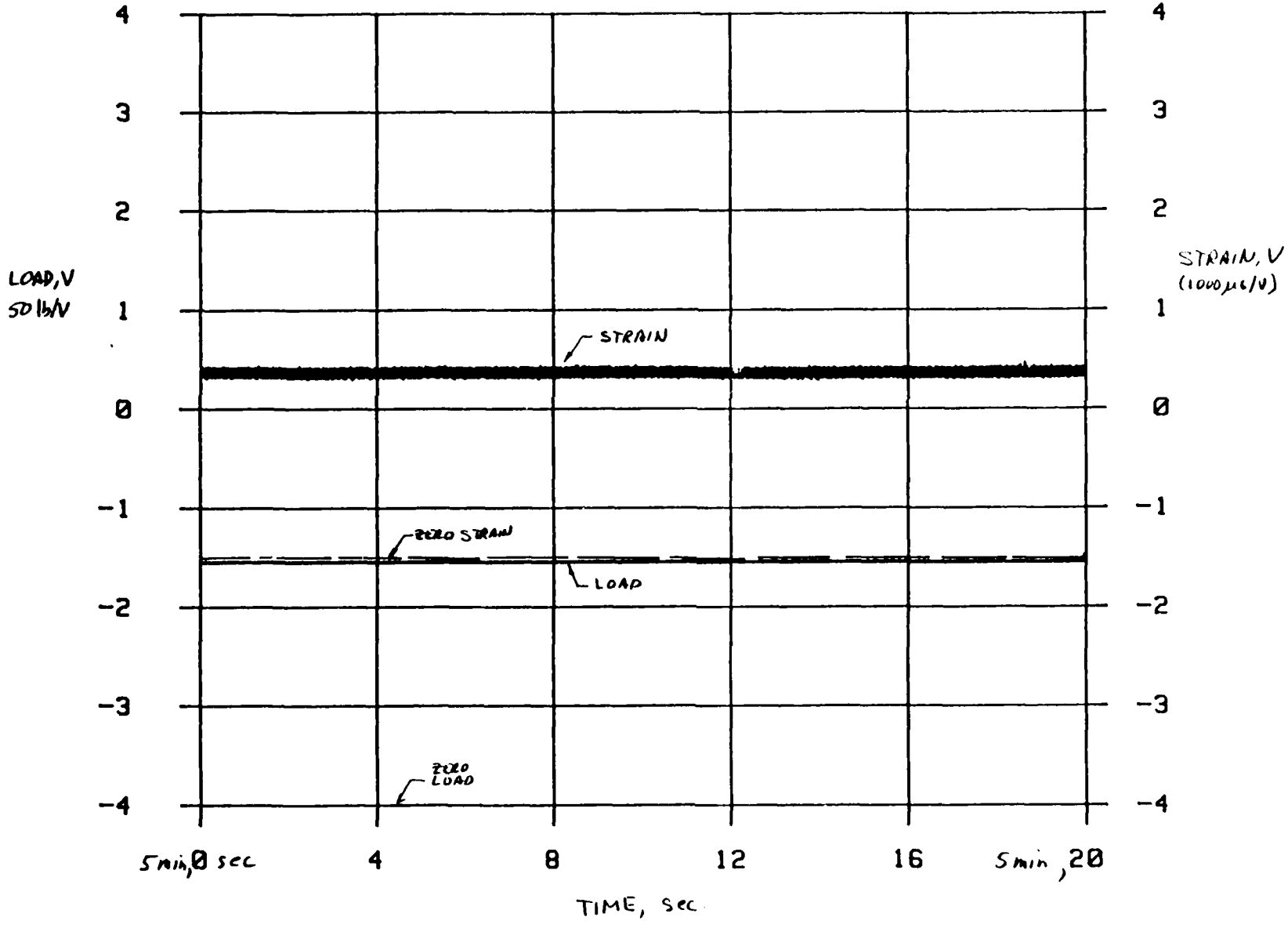

NADC-87106-60

R

MCL 2 TRK 3
13 min - 13:20
LOAD: 10V = 5016
STRAIN: 10V = 10,000 με

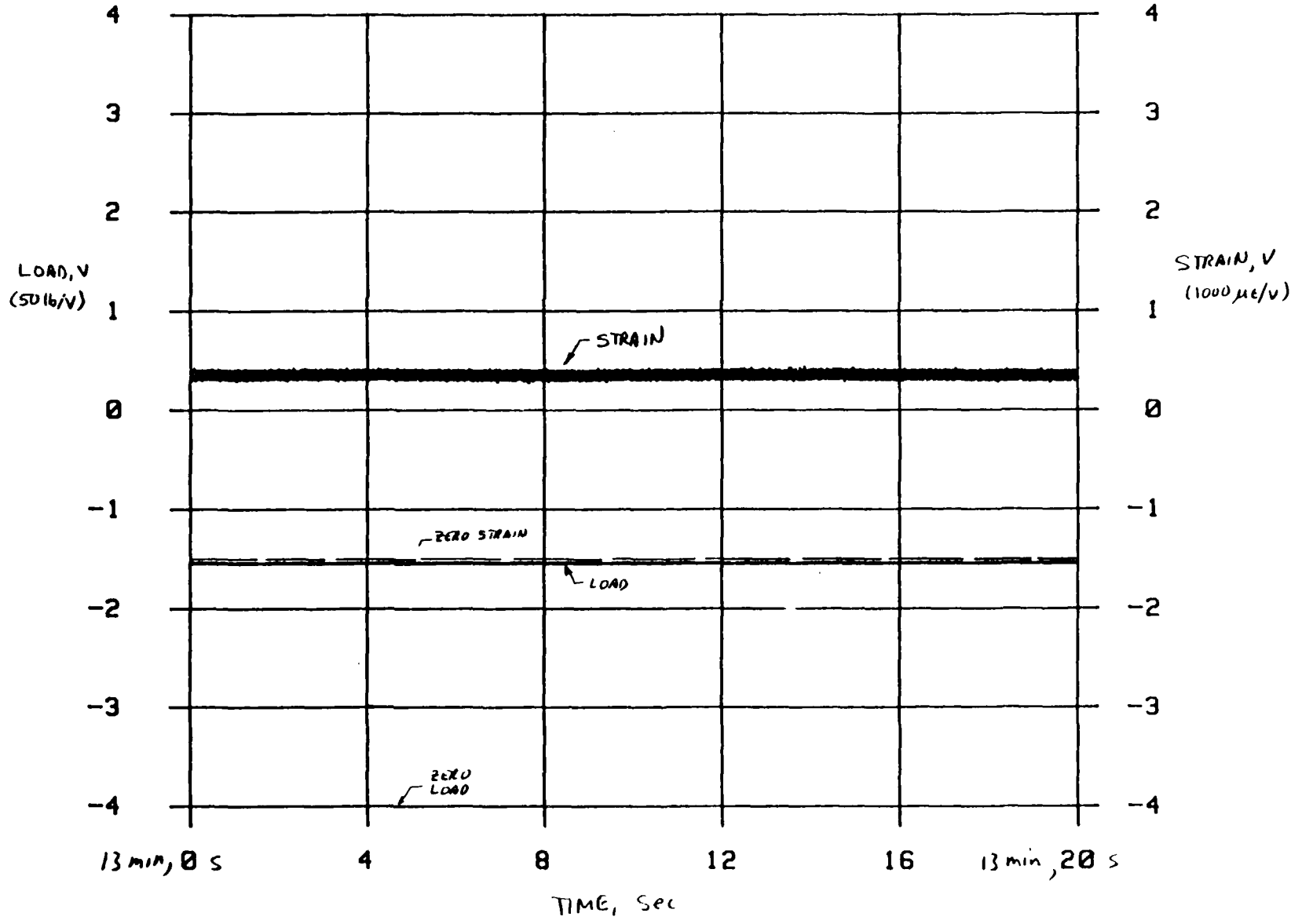

MCL 2 TRM 1

125 lb CREEP TEST

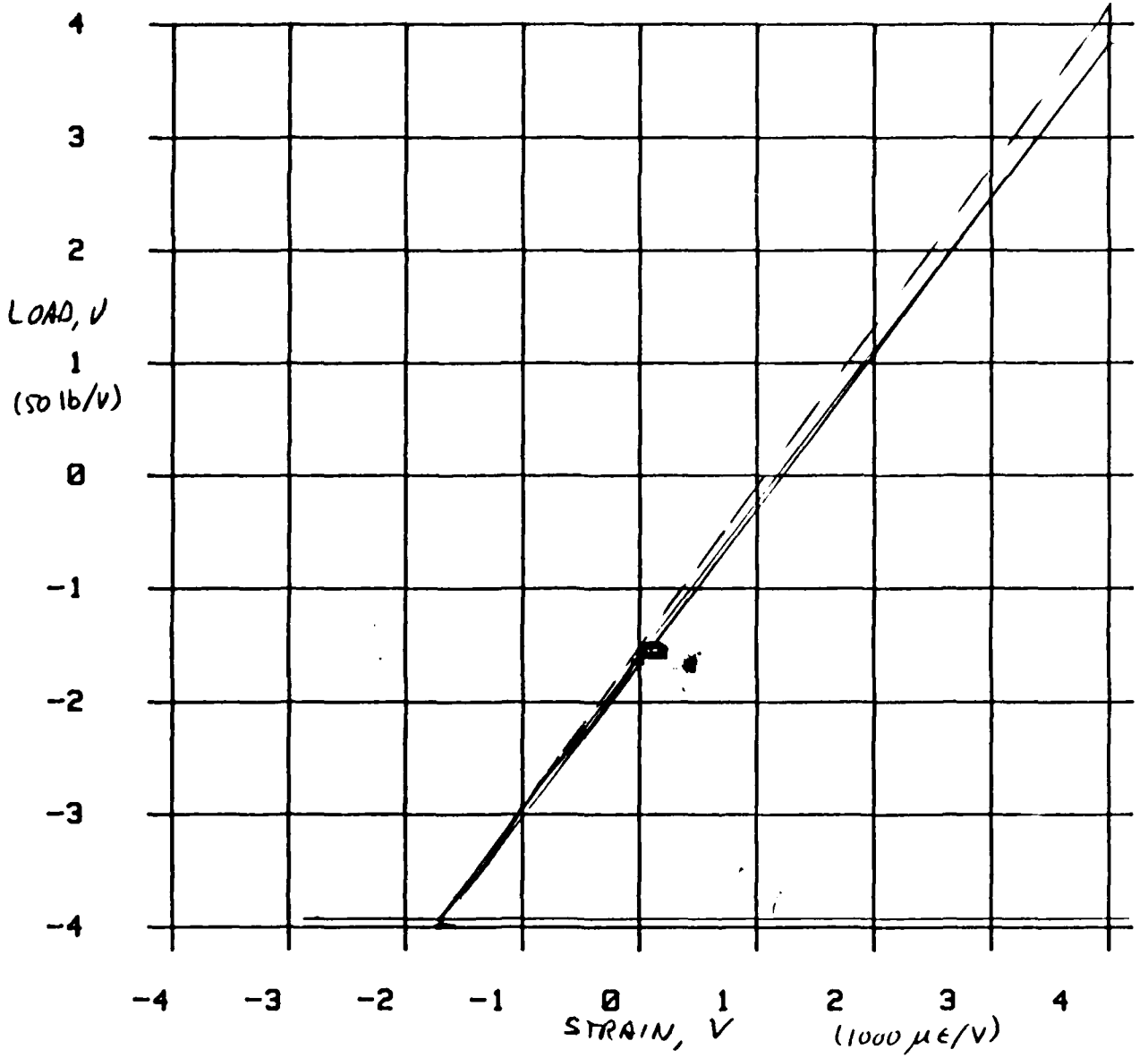

$\Delta\sigma = \frac{27.4\ \text{DIV}}{29.5\ \text{DIV}} \times \frac{4\text{W}16}{.01\text{W}in^2}$

$= 18,653.17\ lb/in^2$

$\Delta\varepsilon = \frac{21.1\ \text{DIV}}{29.5\ \text{DIV}} \times 8\times10^{-3} = .005722\ \omega$

$\therefore E_{\text{LW}} = 3.260\times10^6\ lb/in^2$

$E_{\text{M1}} = \frac{28.9}{29.5} \times \frac{4\omega}{.01\omega} \times \frac{29.5}{21.1} \times \frac{1}{8\times10^{-3}}$

$= 3.4023\times10^6\ lb/in^2$

$E_{\text{BEST}} \approx 3.30\times10^6\ lb/in^2$

7/19/84

MCL 2 TRACK
0 - 20 sec

LOAD 10V = 500lb
STRAIN 10V = 10,000 με

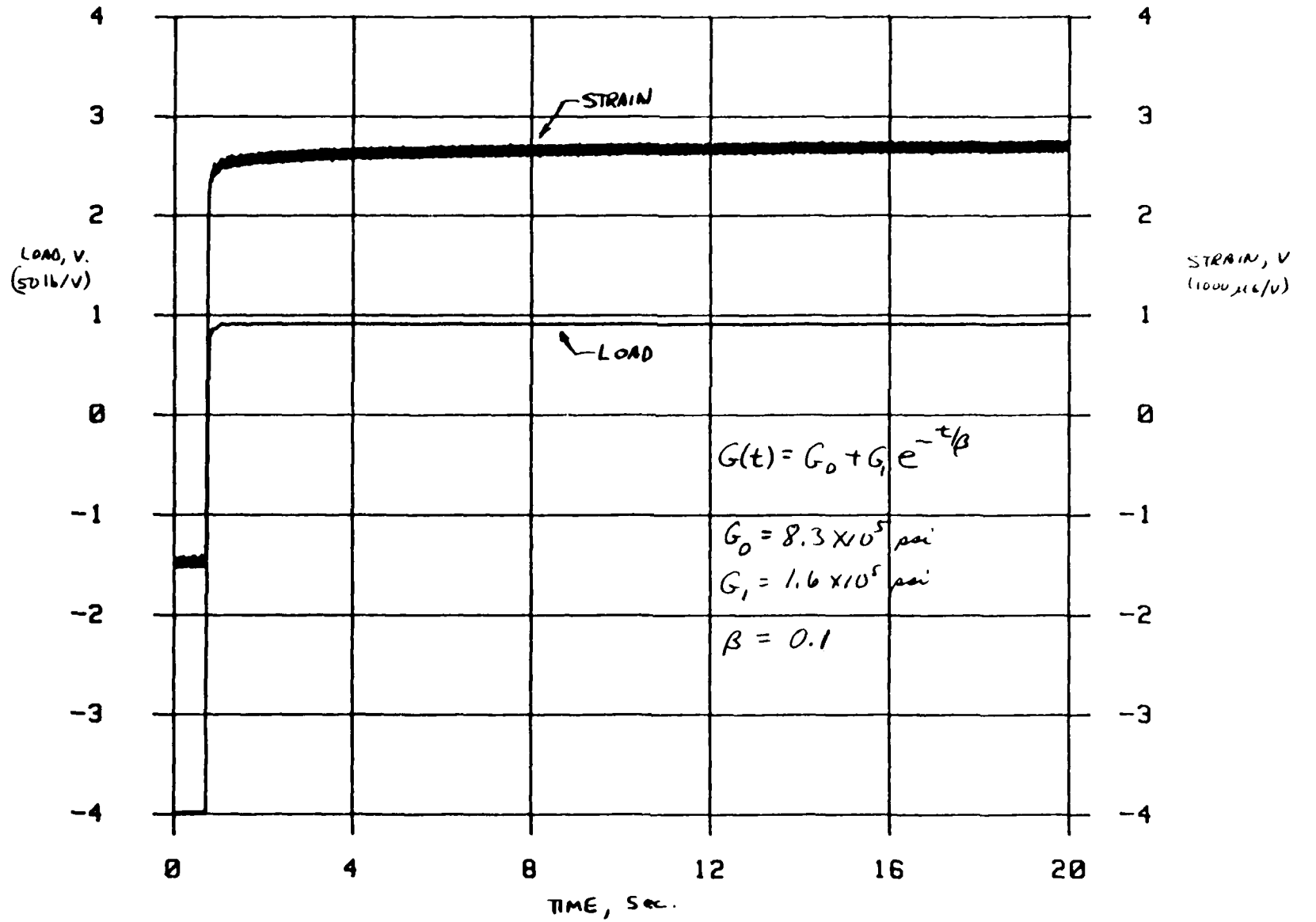

NADC-87106-60

R

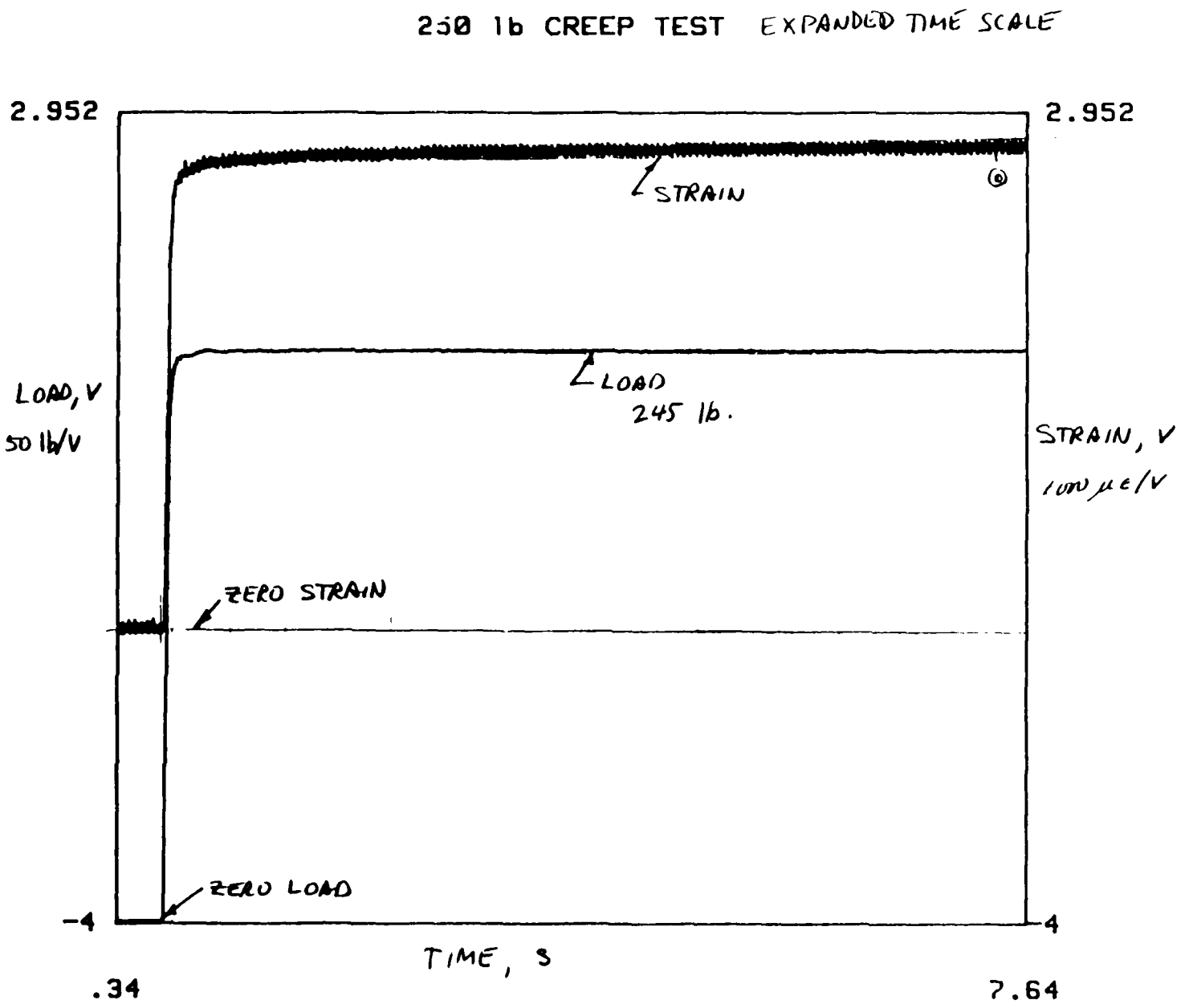

NADC-87106-60

R

MCL2 TRK 5
5min - 5:20
LOAD: 10V = 500 lb
STRAIN: 10V = 10,000 μ ε

1/2 in +45/-45 CREEP 250# B (NOMINAL)

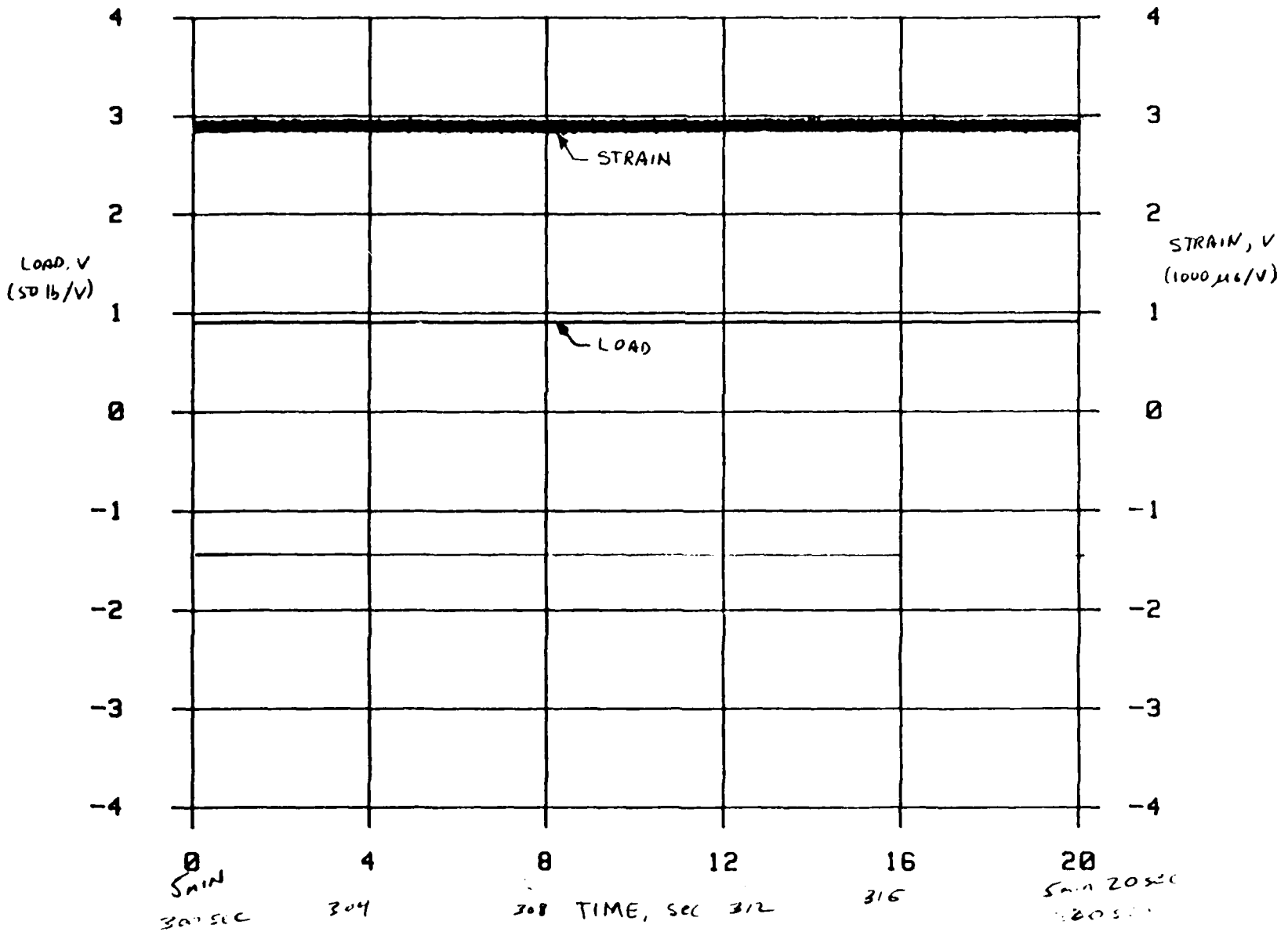

MCL 2 TRK 6

10 min - 10 IPS

LOAD 10V = 5000 lb

STRAIN 10V = 10,000 μ ε

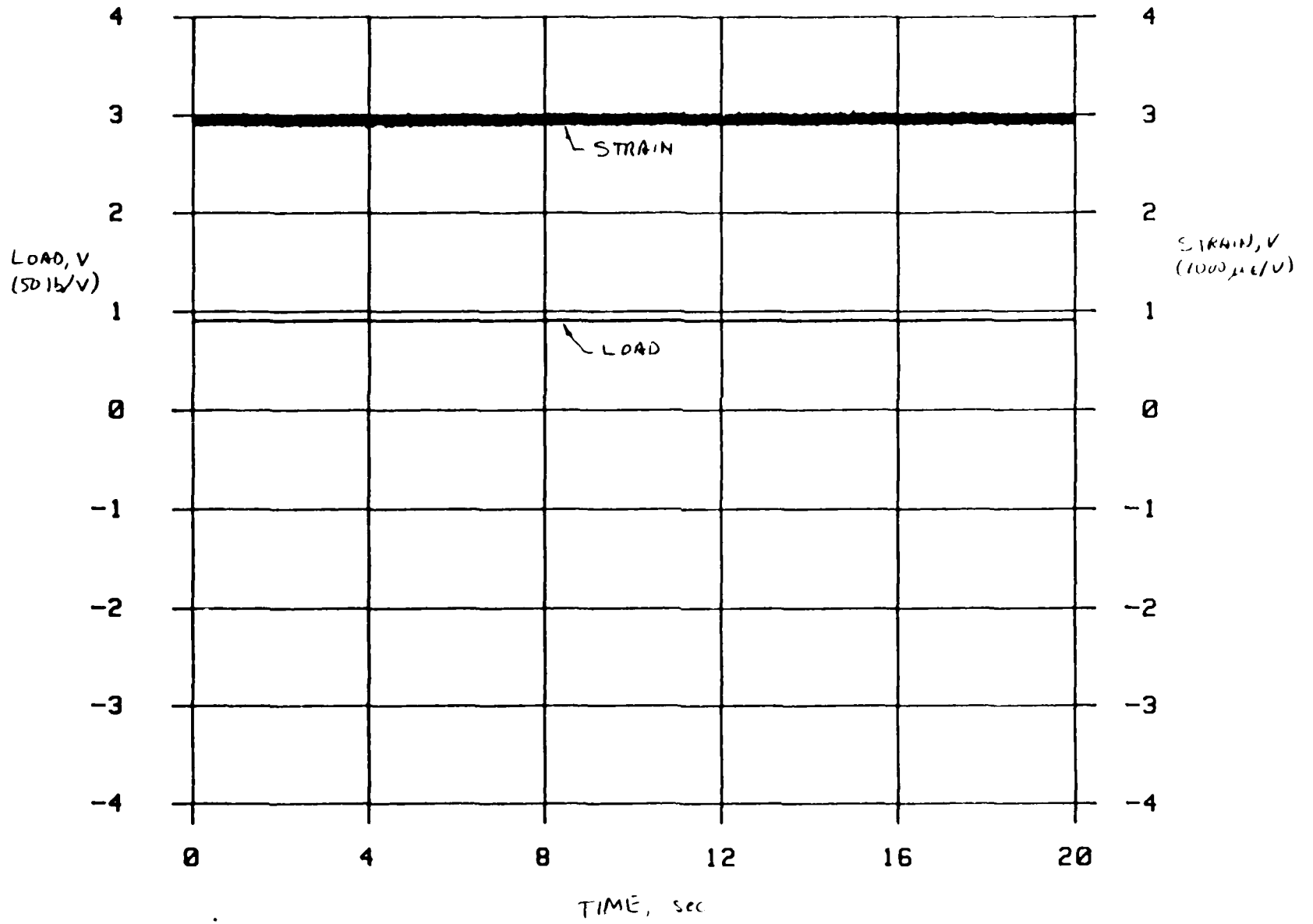

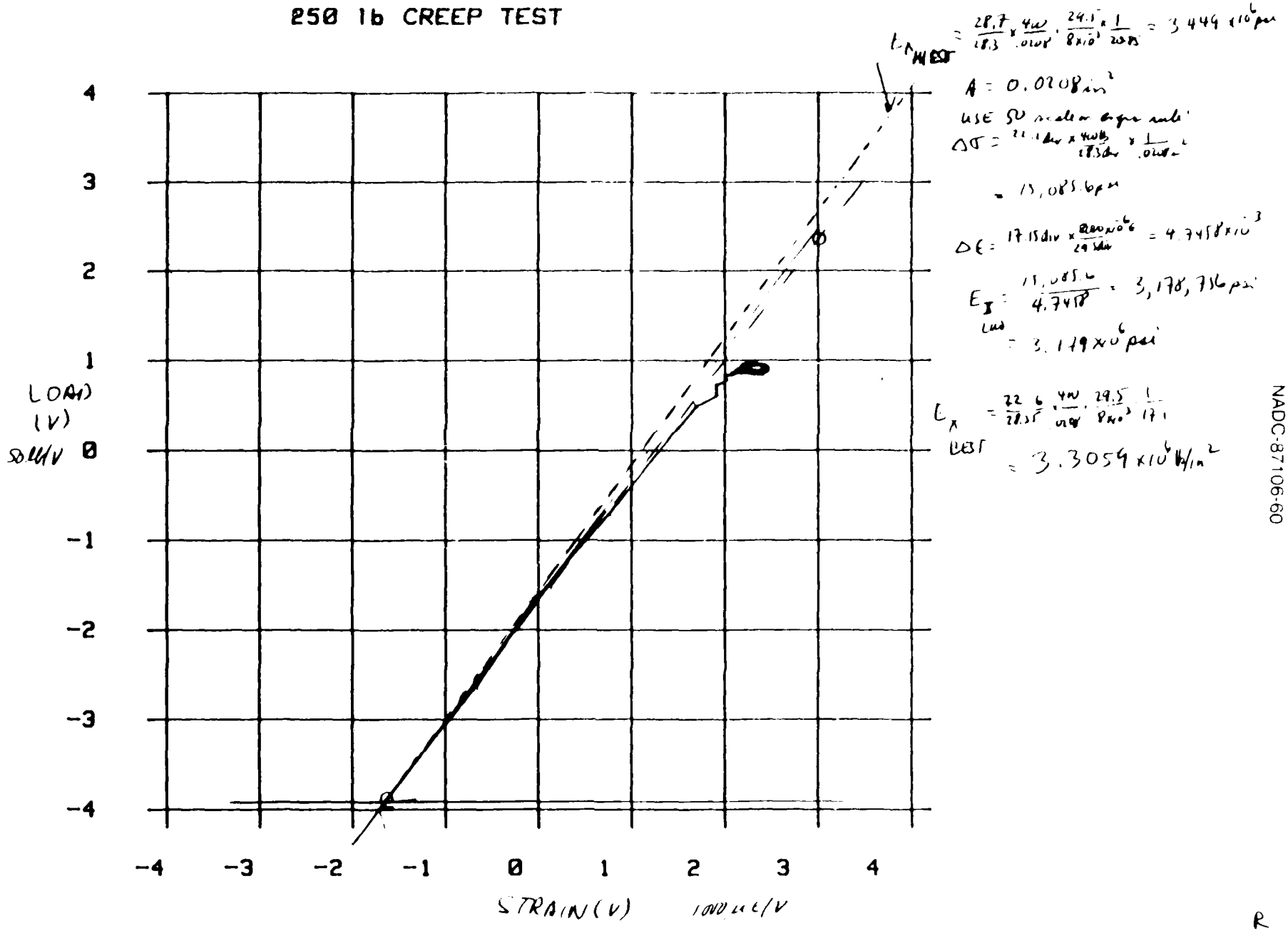

NADC-87106-60

-A11-

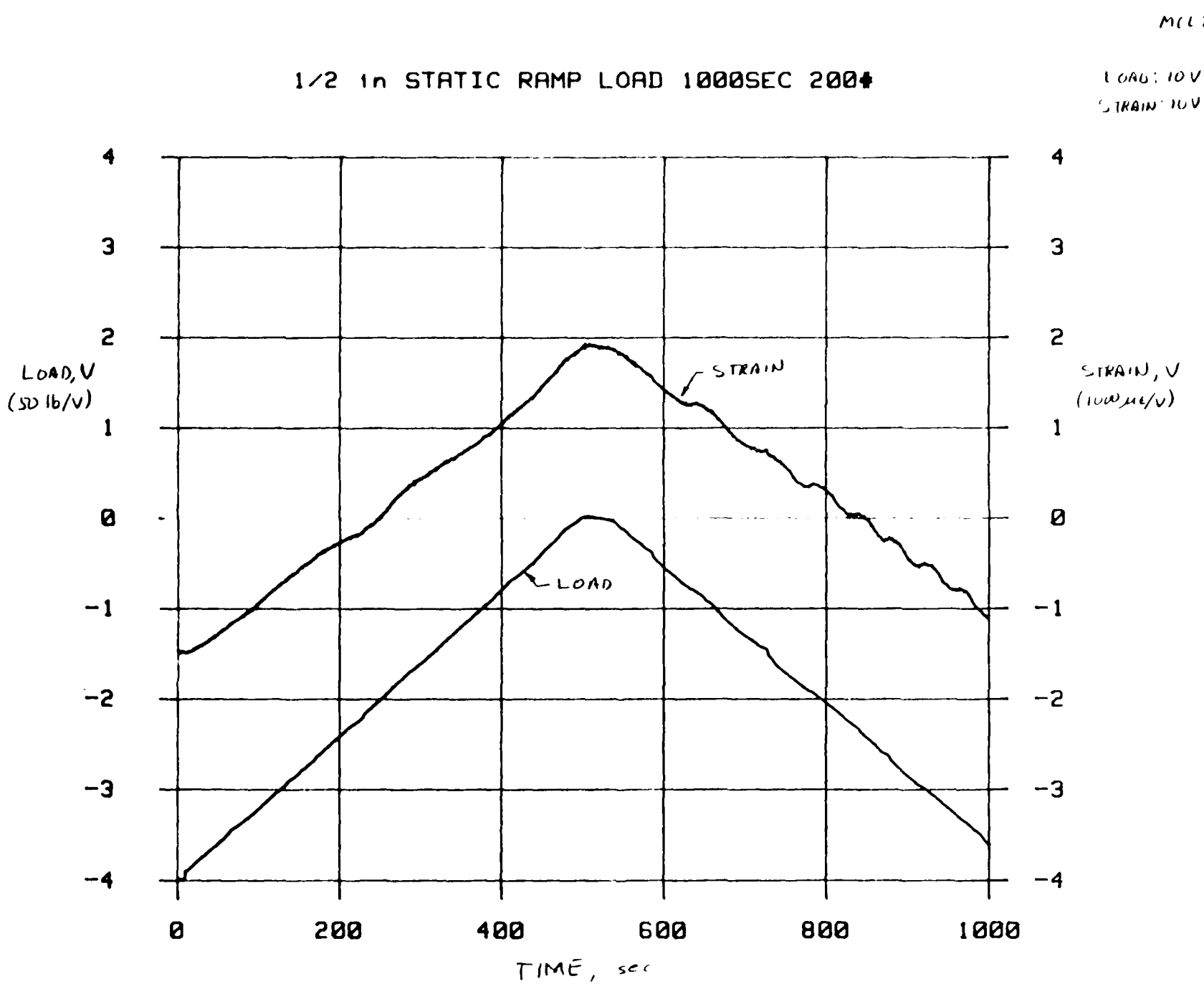
1/2 in STATIC RAMP LOAD 1000SEC 200#
LOAD: 10 V = 500 LB
STRAIN: 10 V = 10,000 με
LOAD, V
(50 lb/V)
STRAIN, V
(1000 με/V)
STRAIN
LOAD
4
3
2
1
0
-1
-2
-3
-4
0
200
400
600
800
1000
TIME, sec

MCL2 TRK 7

STATIC TEST #1

½ IN SPECIMEN

1000 sec/2 volt

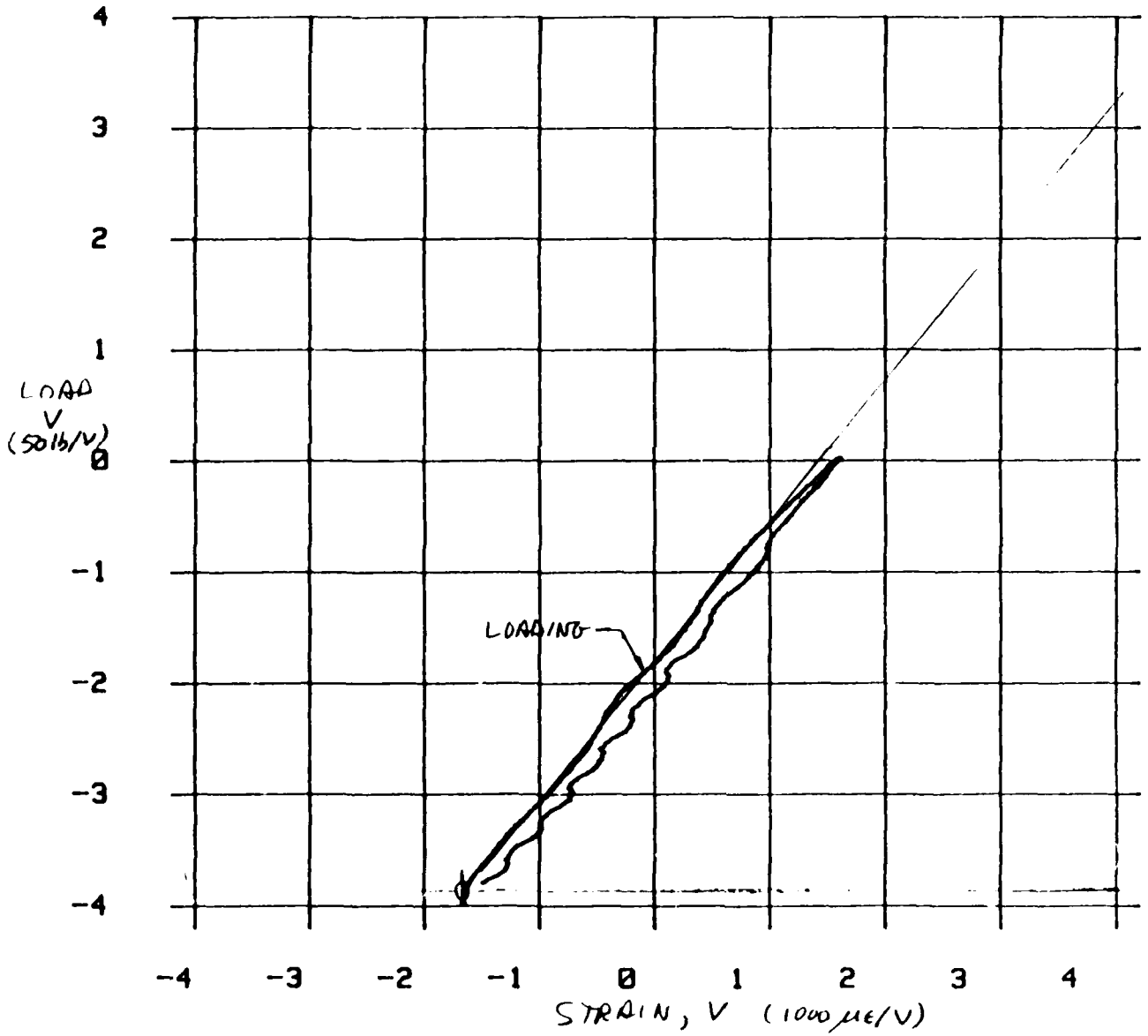

0.1, 50

= 60.2

$E = 2.3168 \times 10^4$

$\Delta\sigma = \frac{24.1\,DIV}{29.3\,DIV} \times \frac{40\,lb}{.020\,in^2} = 16.377 \times 10^3\ lb/in^2$

$\Delta\varepsilon = \frac{20A\,DIV}{29.5\,DIV} \times 8000 \times 10^{-6} = 566.78 \times 10^{-6}$

$E_I = 2.889 \times 10^6\ lb/in^2$

R

1/2 in STATIC RAMP LOAD, 4SEC, 200# MINIMAL MAX LOAD

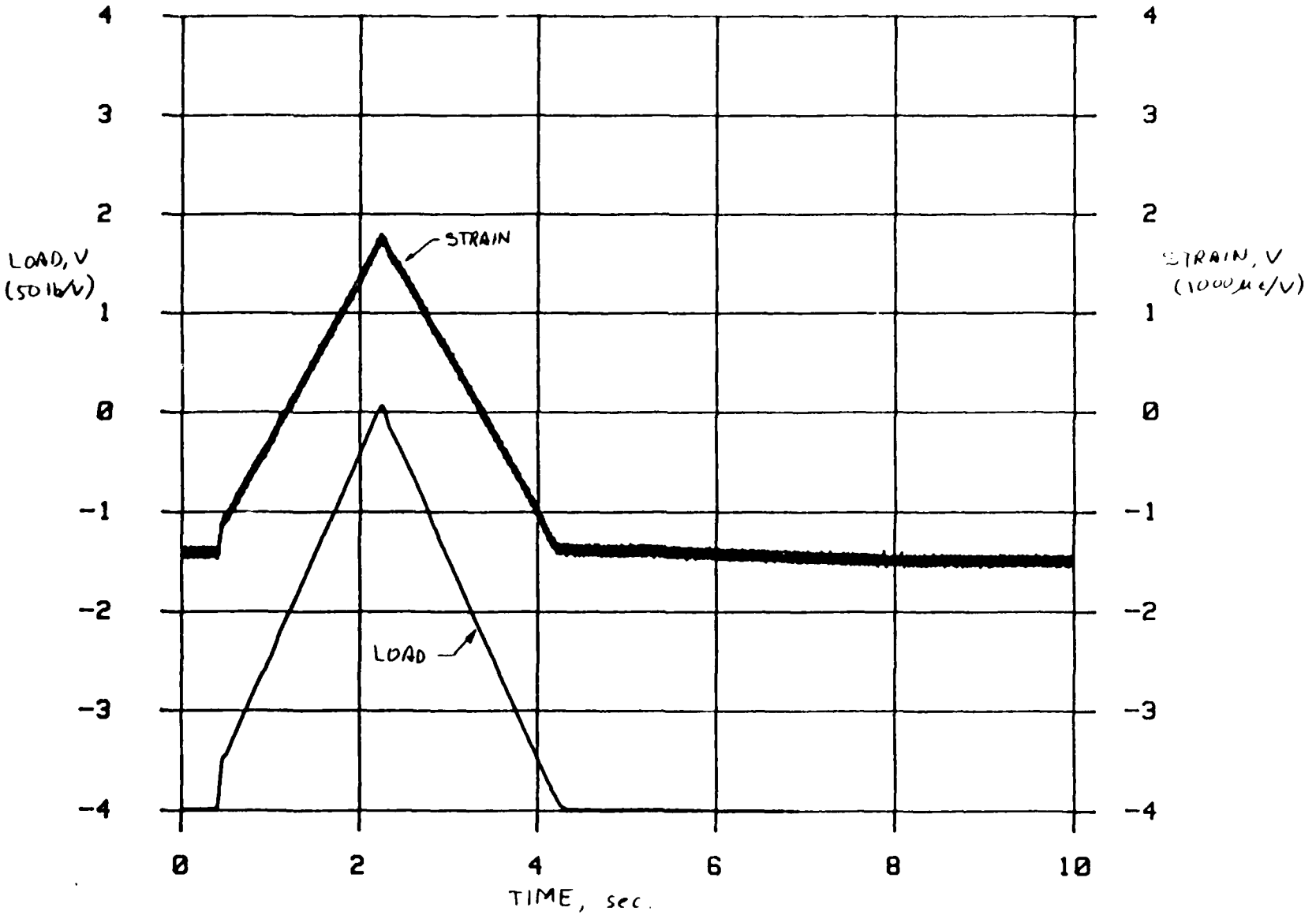

MCL2 TRK8

STATIC TEST #2

4 SEC LOAD & UNLOAD
200# NIMINAL MAX LOAD

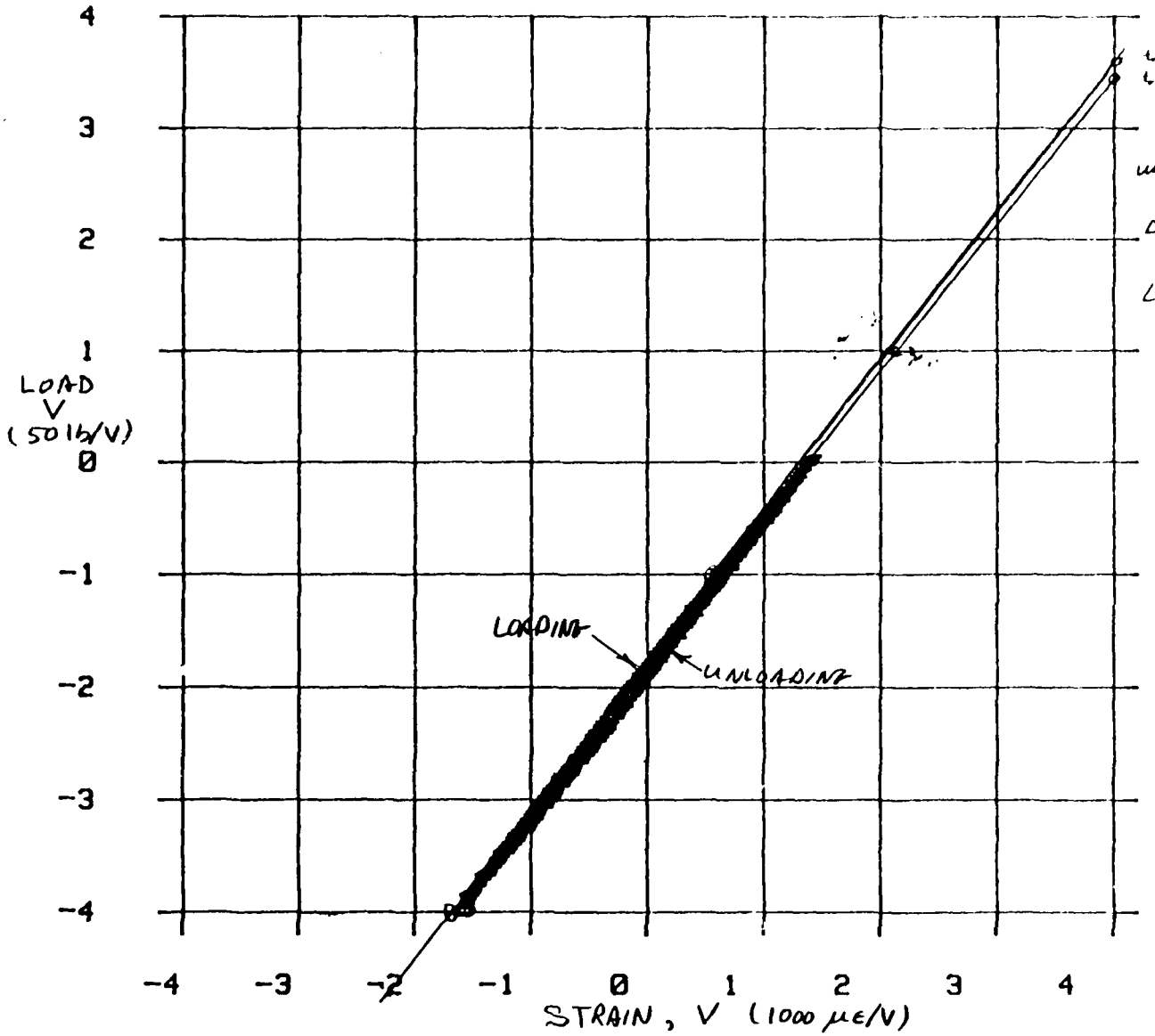

ε_{150}
ε_{200}

using SD scale on magic rule:

$\Delta\sigma_{2\omega} = \frac{26.4\ \text{DIV}}{29.3\ \text{DIV}} \times \frac{400\ \text{lb}}{.0208\ \text{in}^2} = 17{,}939.7\ \text{lb/in}^2$

$\Delta\varepsilon = \frac{20.95}{29.50\ \text{DIV}} \times 8000 \times 10^{-6} = .0056814$

$\therefore E_{\text{I}_{2\omega}} = \frac{17{,}939.7}{.0056814} = 3{,}1576 \times 10^6\ \text{psi}$

$\therefore E_{\text{I}_{2\omega}} = 3.156 \times 10^6\ \text{psi}$

$\Delta\sigma_{150} = \frac{27.0}{28.3} \times \frac{400}{.0208} = 18{,}347\ \text{lb/in}^2$

$\therefore E_{\text{I}_{150}} = \frac{18{,}347}{.0056814} = 3.229 \times 10^6\ \text{lb/in}^2$

R

MEASUREMENTS TAKE 1

LOAD: 10 V = 500 lb
STRAIN: 10 V = 10,000 με

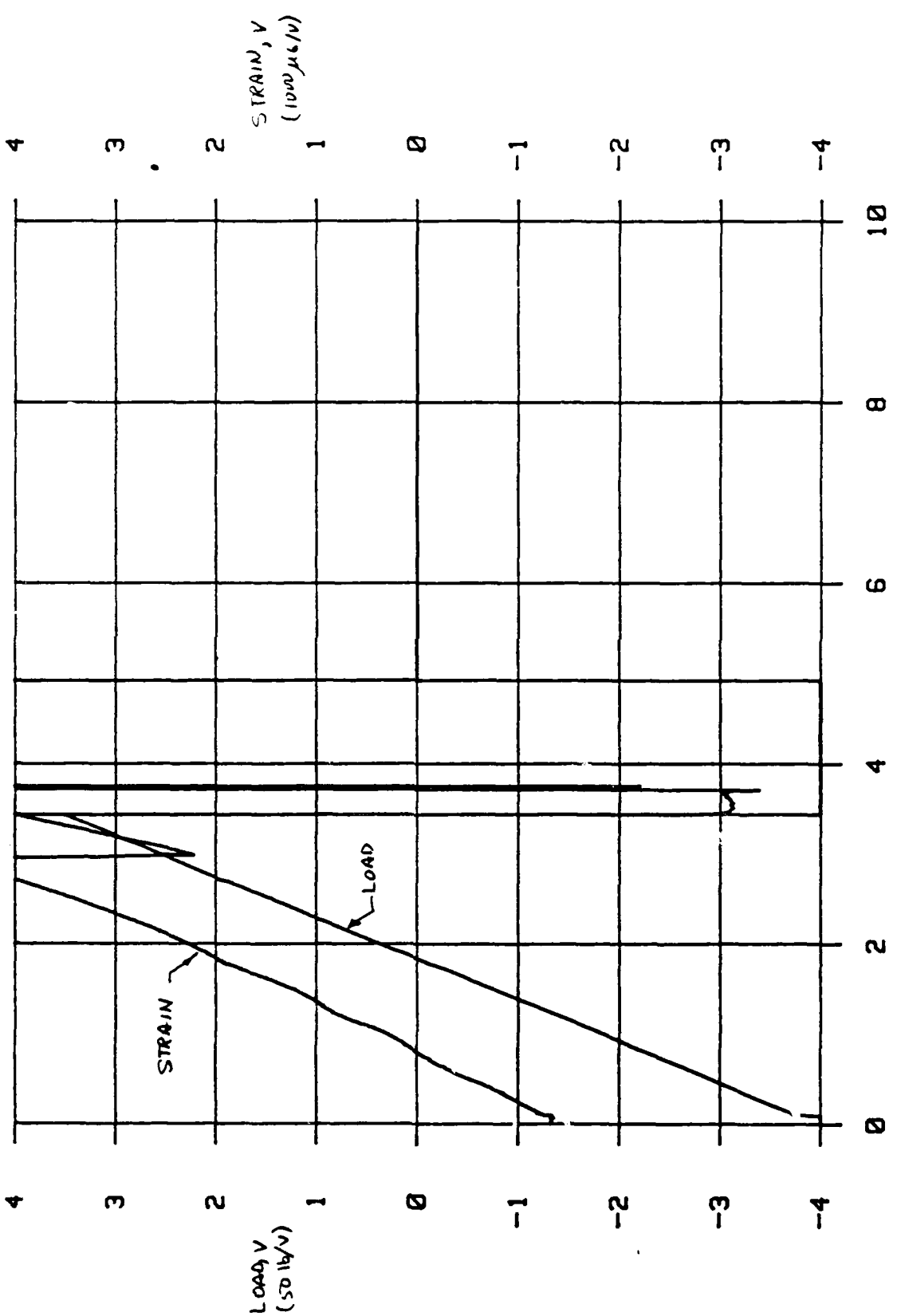

MICRONETICS 3, TRACK 1

STATIC TEST #3 ½ IN RAMP LOAD TO FAILURE

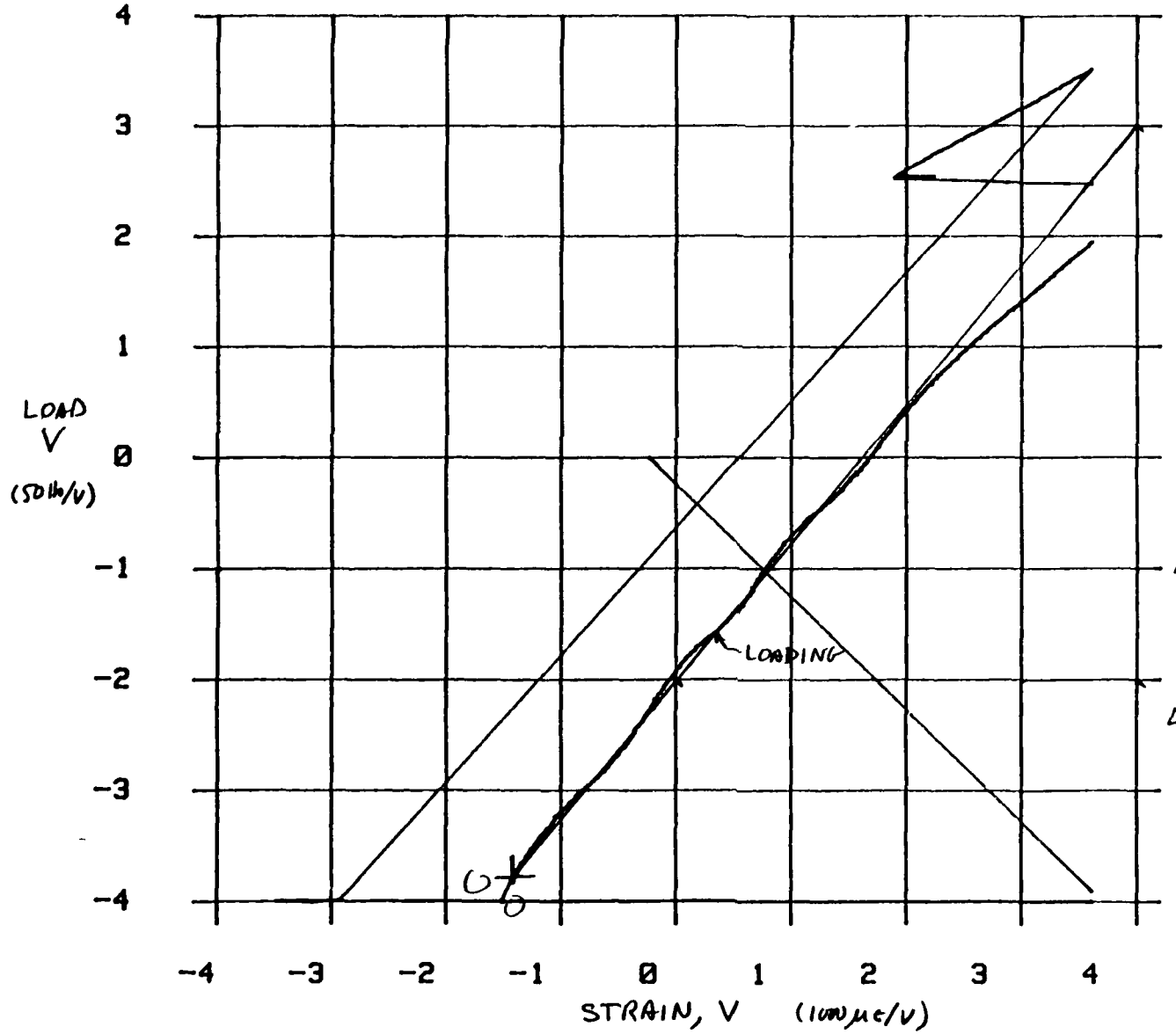

USE 50 scale on engis rule

$\Delta\sigma = \frac{24.0\,DIV}{28.3\,DIV} \times \frac{400\,lb}{1.02\,in^2} = 16,309 \times 10^3\,lb/in^2$

$\Delta\epsilon = \frac{20.0\,DIV}{29.5\,DIV} \times 8,000 \times 10^{-6} = 5.4237 \times 10^{-3}$

$\therefore E_{\Sigma} = 3.007 \times 10^6\,lb/in^2$

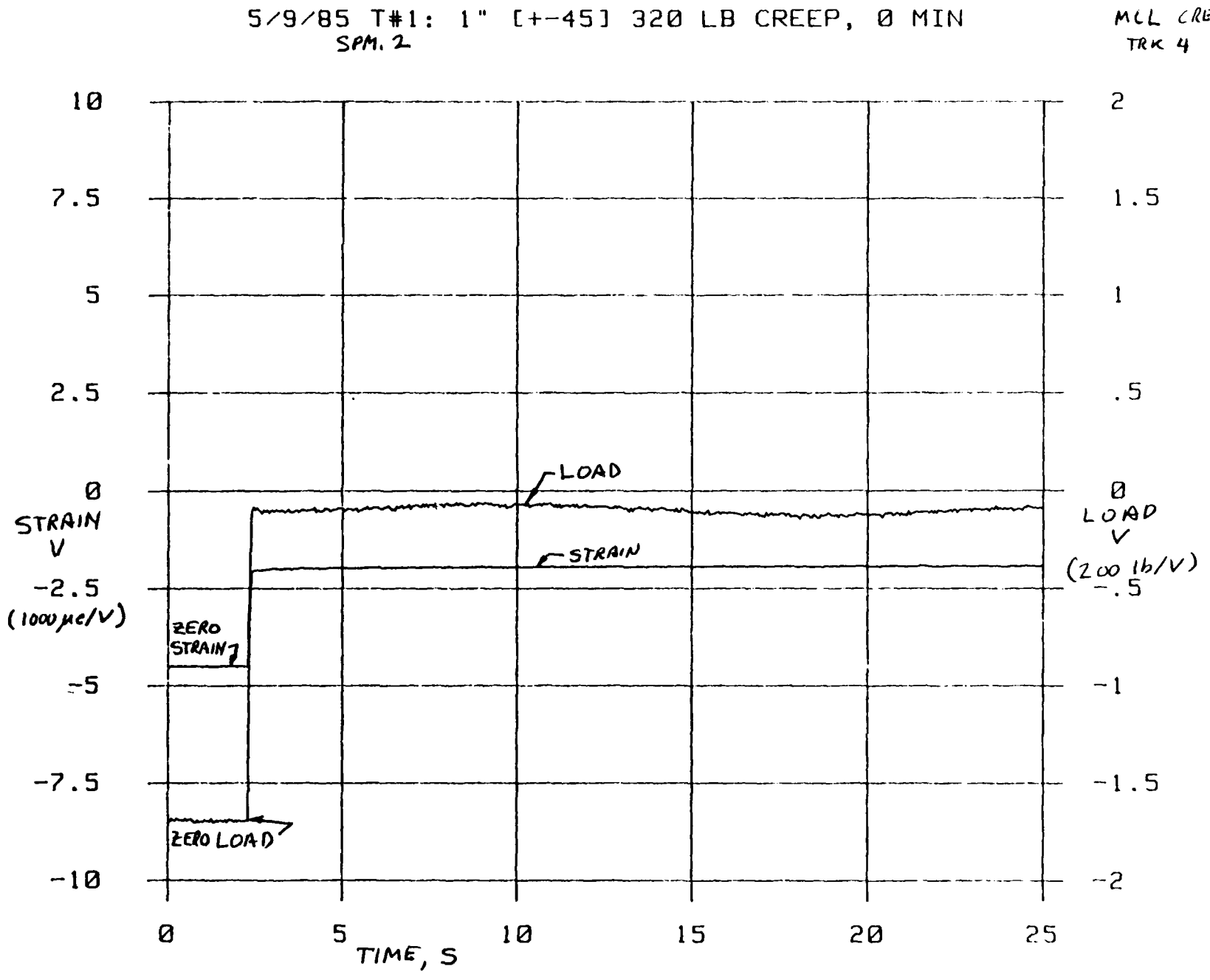
5/9/85 T#1: 1" [+-45] 320 LB CREEP, 0 MIN
SPM. 2
MCL CREEP 1
TRK 4
10
7.5
5
2.5
0
-2.5
-5
-7.5
-10
STRAIN
V
(1000 με/V)
2
1.5
1
.5
0
-.5
-1
-1.5
-2
LOAD
V
(200 lb/V)
LOAD
STRAIN
ZERO STRAIN
ZERO LOAD
0
5
10
15
20
25
TIME, S

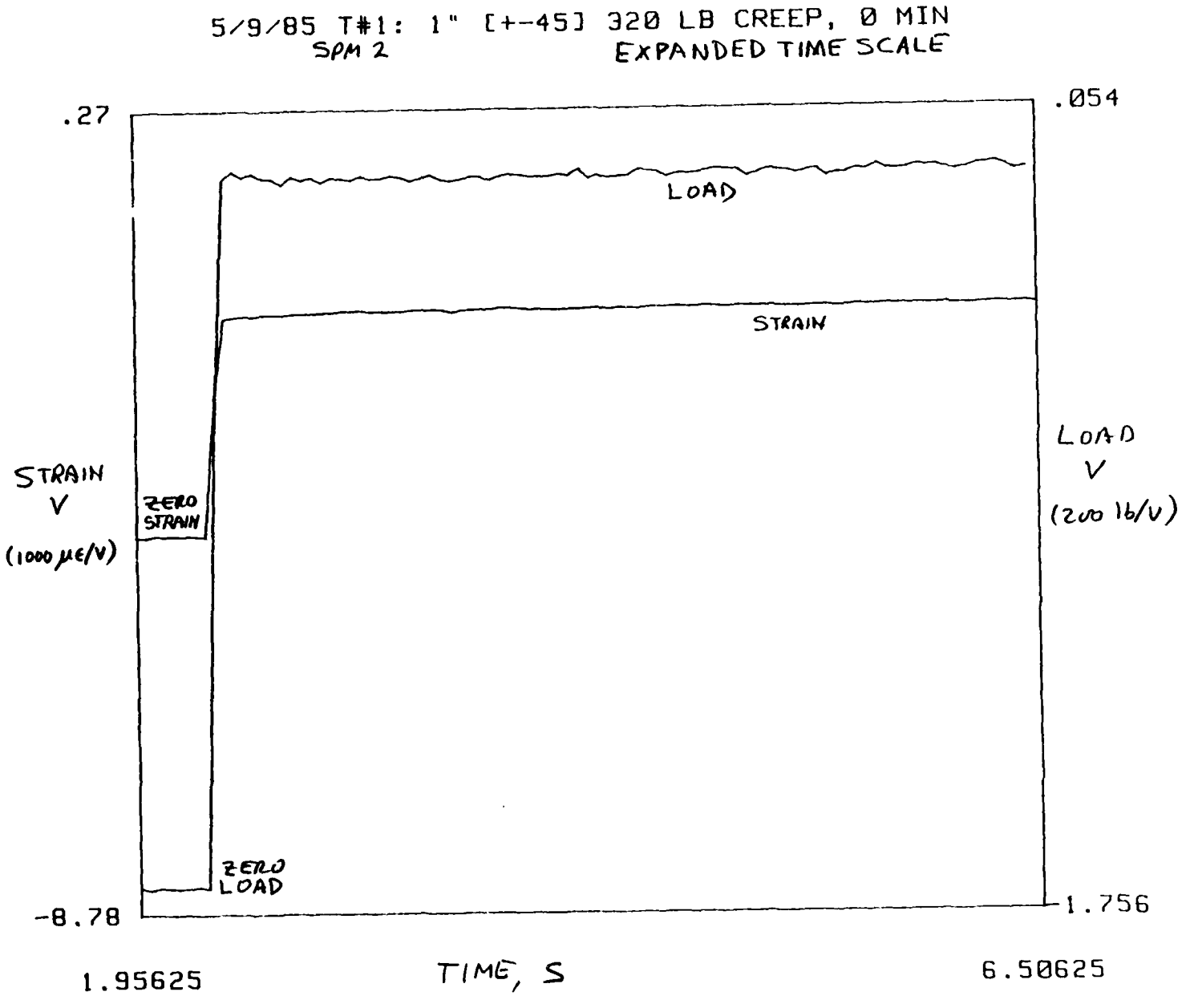
5/9/85 T#1: 1" [+-45] 320 LB CREEP, 0 MIN
SPM 2
EXPANDED TIME SCALE
.27
.054
LOAD
STRAIN
STRAIN
V
(1000 με/V)
ZERO STRAIN
LOAD
V
(200 lb/V)
ZERO LOAD
-8.78
1.756
1.95625
TIME, S
6.50625

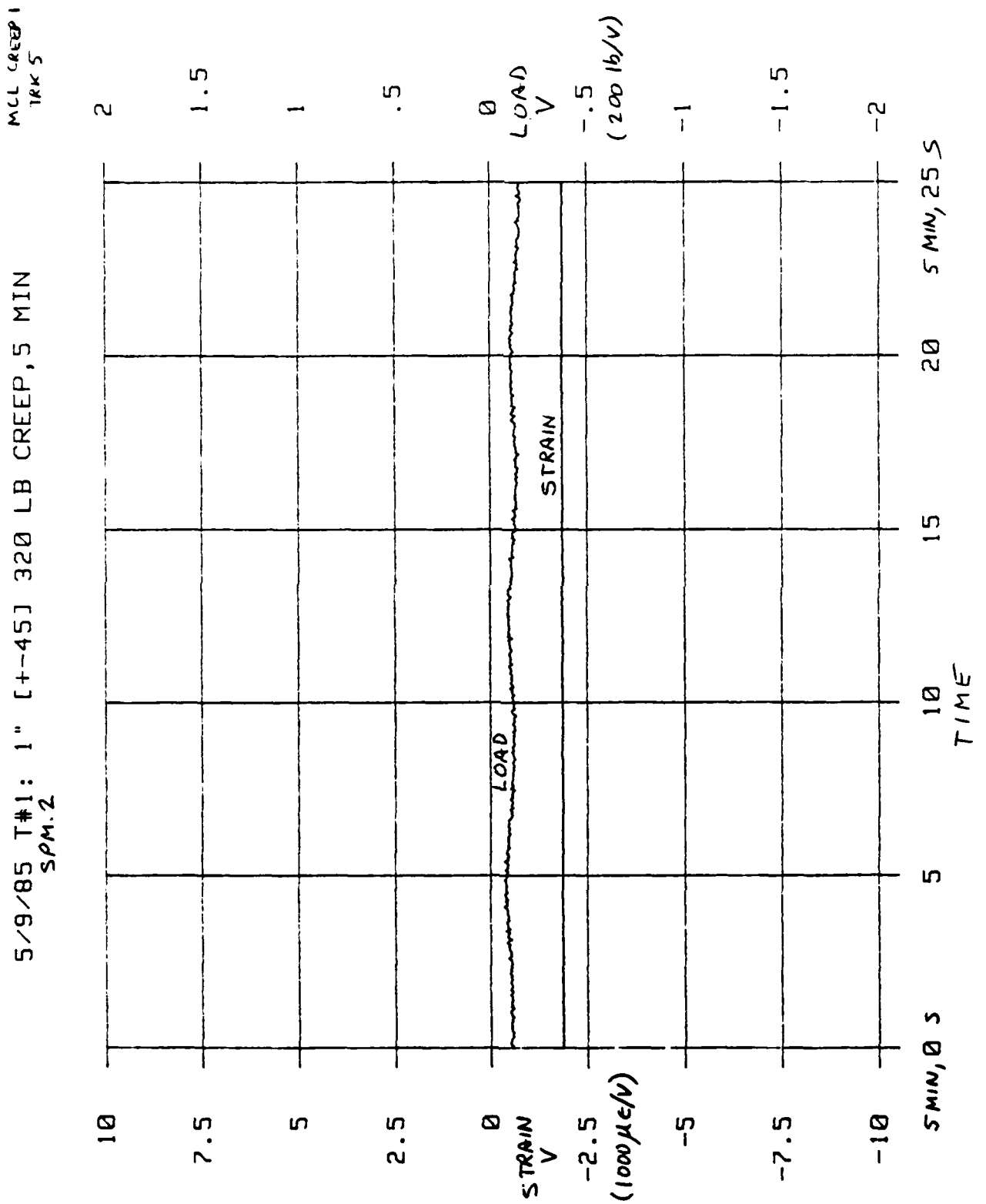
MCL CREEP 1
IRK 5
5/9/85 T#1: 1" [+-45] 320 LB CREEP, 5 MIN
SPM.2
LOAD
STRAIN
LOAD V
(200 lb/V)
STRAIN V
(1000 με/V)
TIME
5MIN, 0 S
5MIN, 25 S
2
1.5
1
.5
0
-.5
-1
-1.5
-2
10
7.5
5
2.5
0
-2.5
-5
-7.5
-10
5
10
15
20

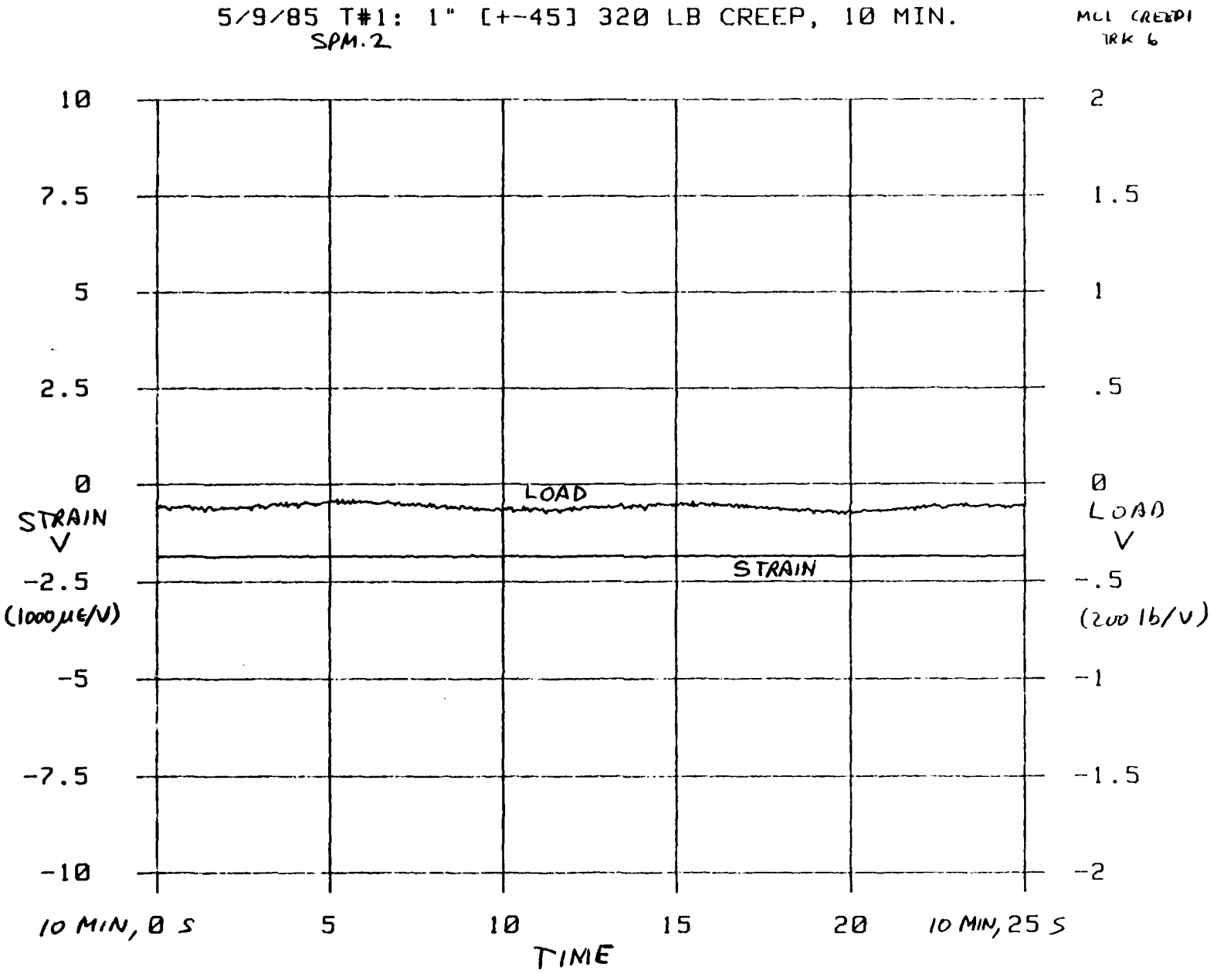
5/9/85 T#1: 1" [+-45] 320 LB CREEP, 10 MIN.
SPM.2
MCL CREEP1
TRK 6
10
7.5
5
2.5
0
-2.5
-5
-7.5
-10
STRAIN
V
(1000 μE/V)
LOAD
STRAIN
2
1.5
1
.5
0
-.5
-1
-1.5
-2
LOAD
V
(200 lb/V)
10 MIN, 0 S
5
10
15
20
10 MIN, 25 S
TIME

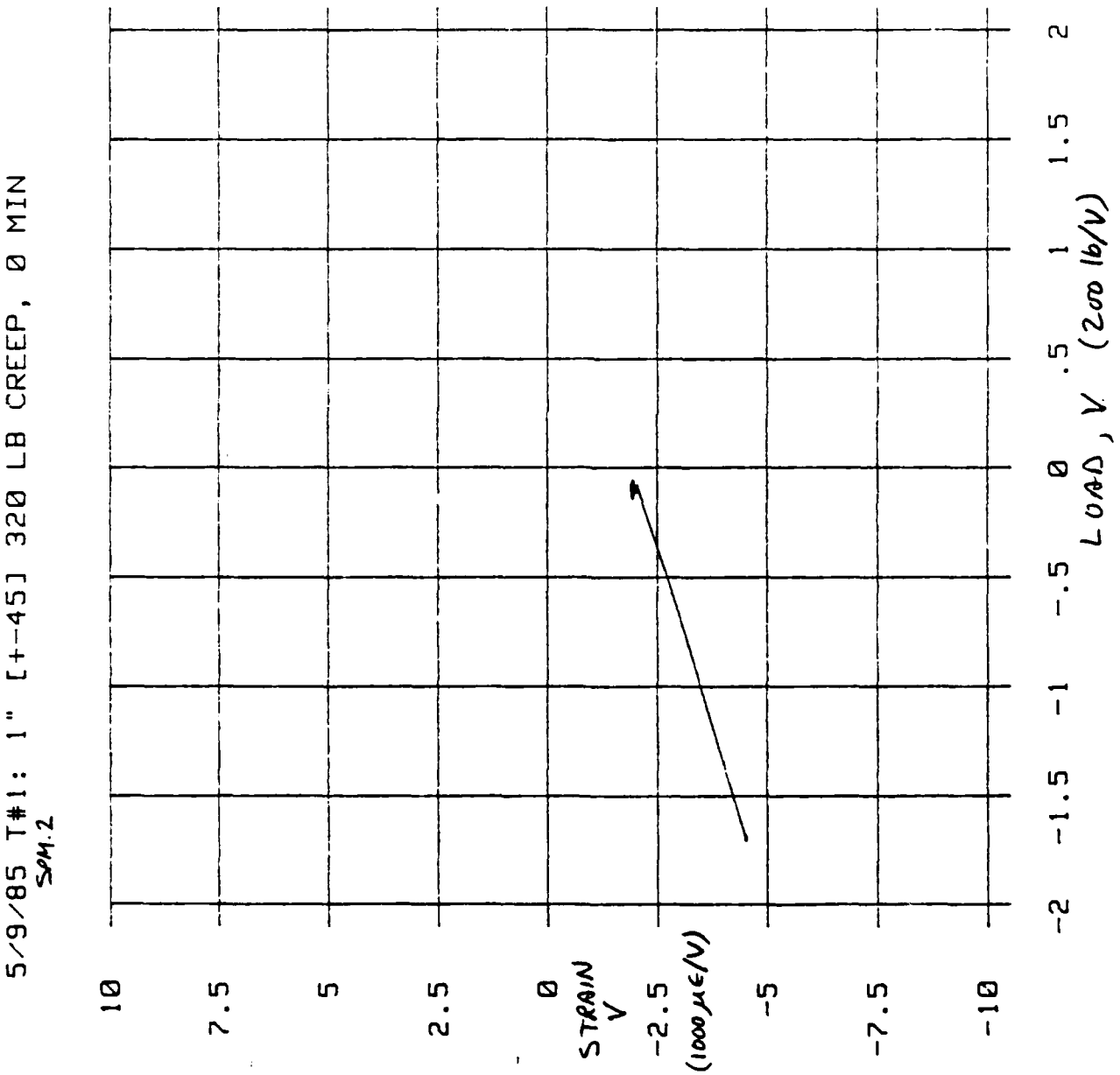
5/9/85 T#1: 1" [+-45] 320 LB CREEP, 0 MIN
SM.2
10
7.5
5
2.5
0
-2.5
-5
-7.5
-10
STRAIN
V
(1000 με/V)
-2
-1.5
-1
-.5
0
.5
1
1.5
2
LOAD, V (200 lb/V)

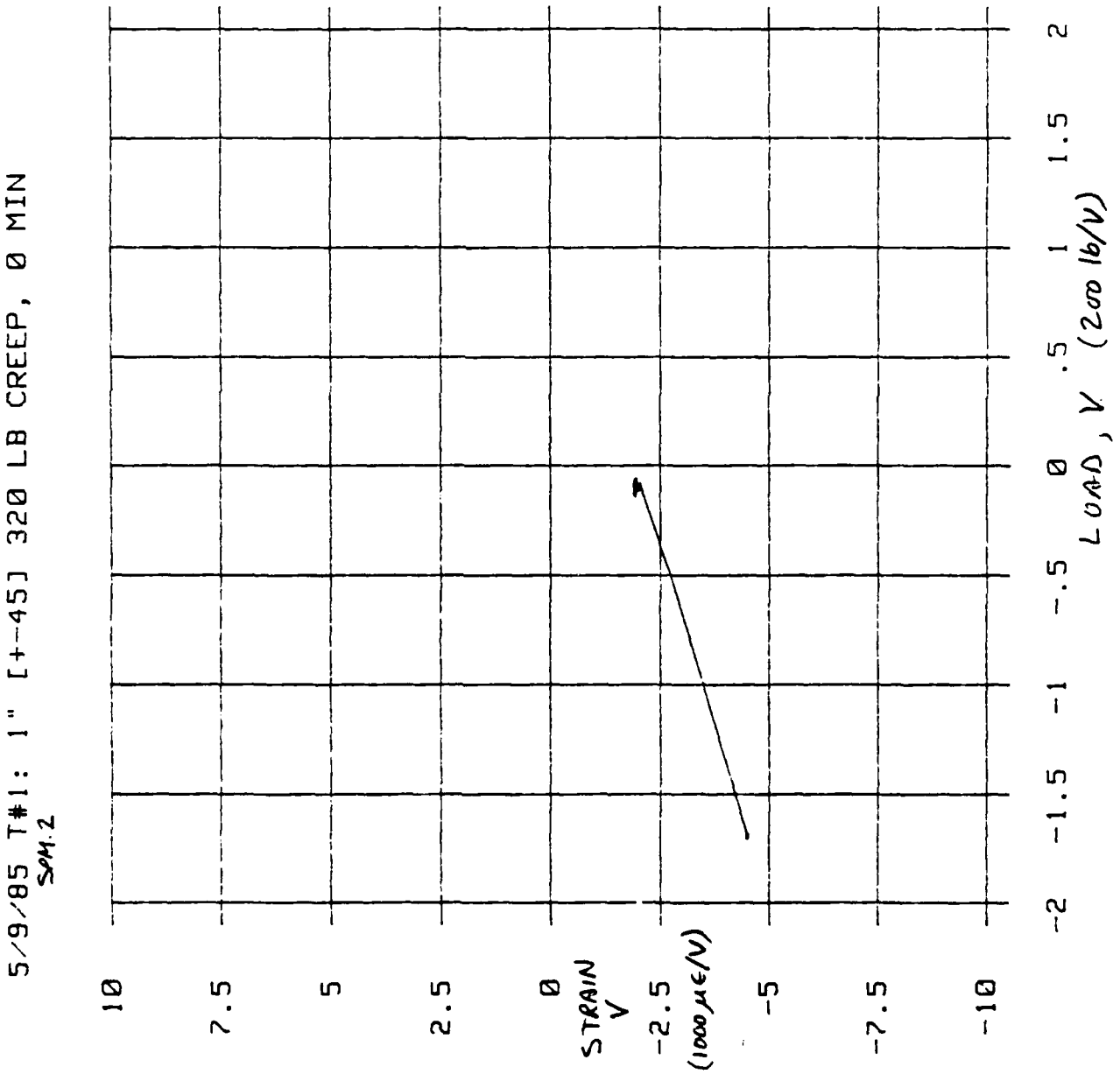
5/9/85 T#1: 1" [+-45] 320 LB CREEP, 0 MIN
SPM.2
10
7.5
5
2.5
0
-2.5
-5
-7.5
-10
STRAIN
V
(1000 με/V)
-2
-1.5
-1
-.5
0
.5
1
1.5
2
LOAD, V (200 lb/V)

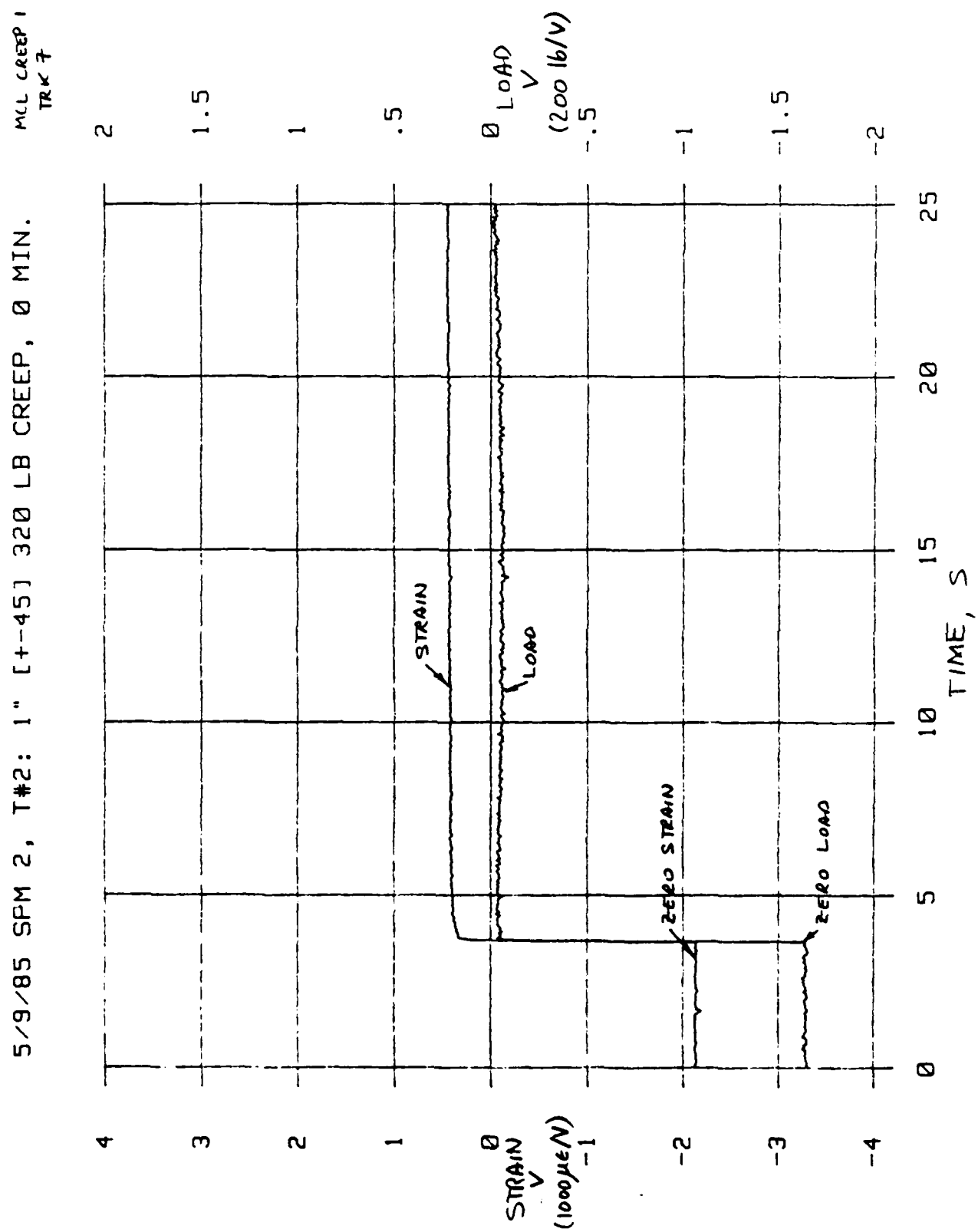
5/9/85 SPM 2, T#2: 1" [+-45] 320 LB CREEP, 0 MIN.
MCL CREEP 1
TRK 7
STRAIN
LOAD
ZERO STRAIN
ZERO LOAD
TIME, S
STRAIN V (1000με/V)
LOAD V (200 lb/V)

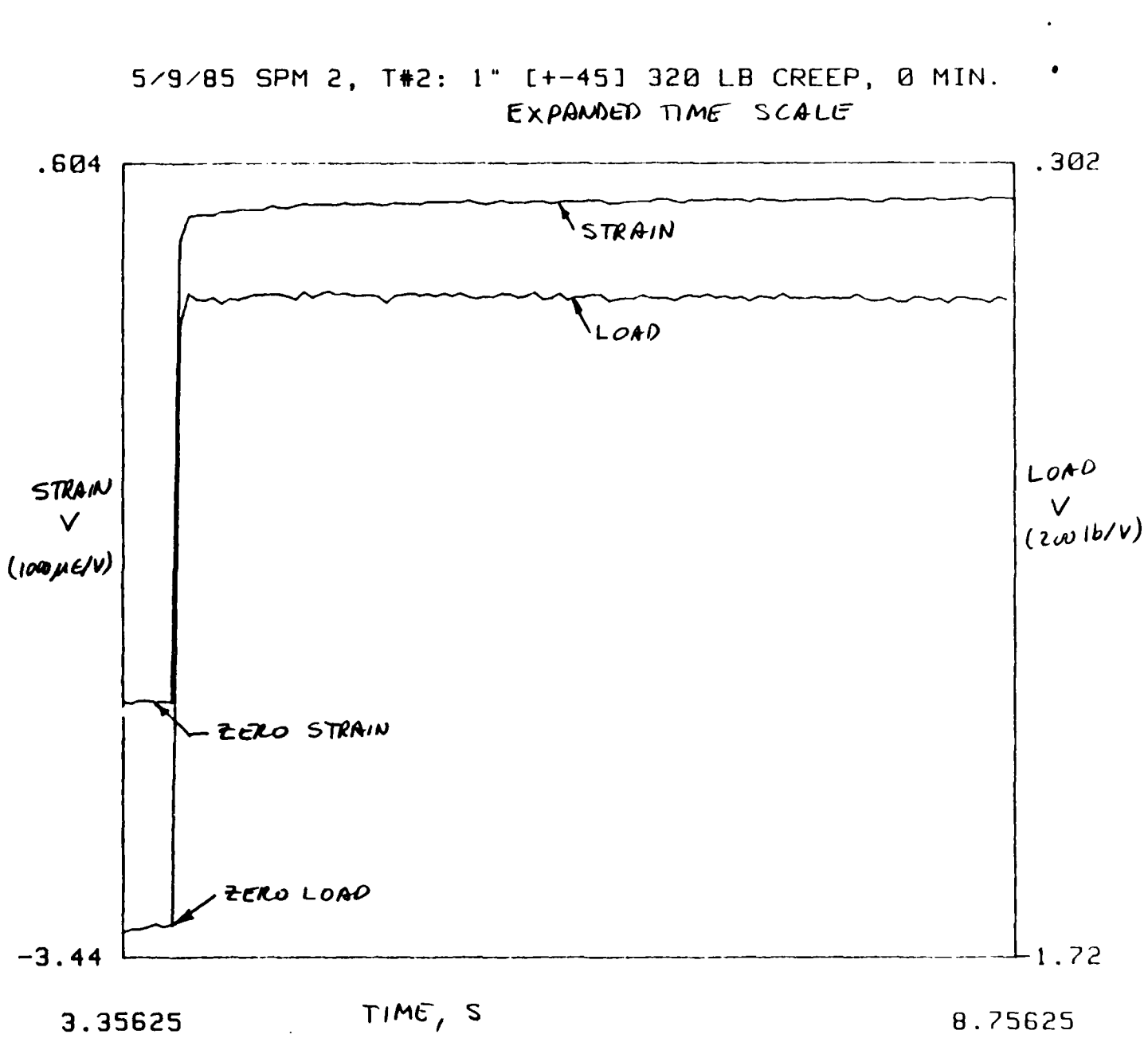
5/9/85 SPM 2, T#2: 1" [+-45] 320 LB CREEP, 0 MIN.
EXPANDED TIME SCALE
.604
.302
STRAIN
LOAD
STRAIN
V
(100με/V)
LOAD
V
(200 lb/V)
ZERO STRAIN
ZERO LOAD
-3.44
1.72
3.35625
TIME, S
8.75625

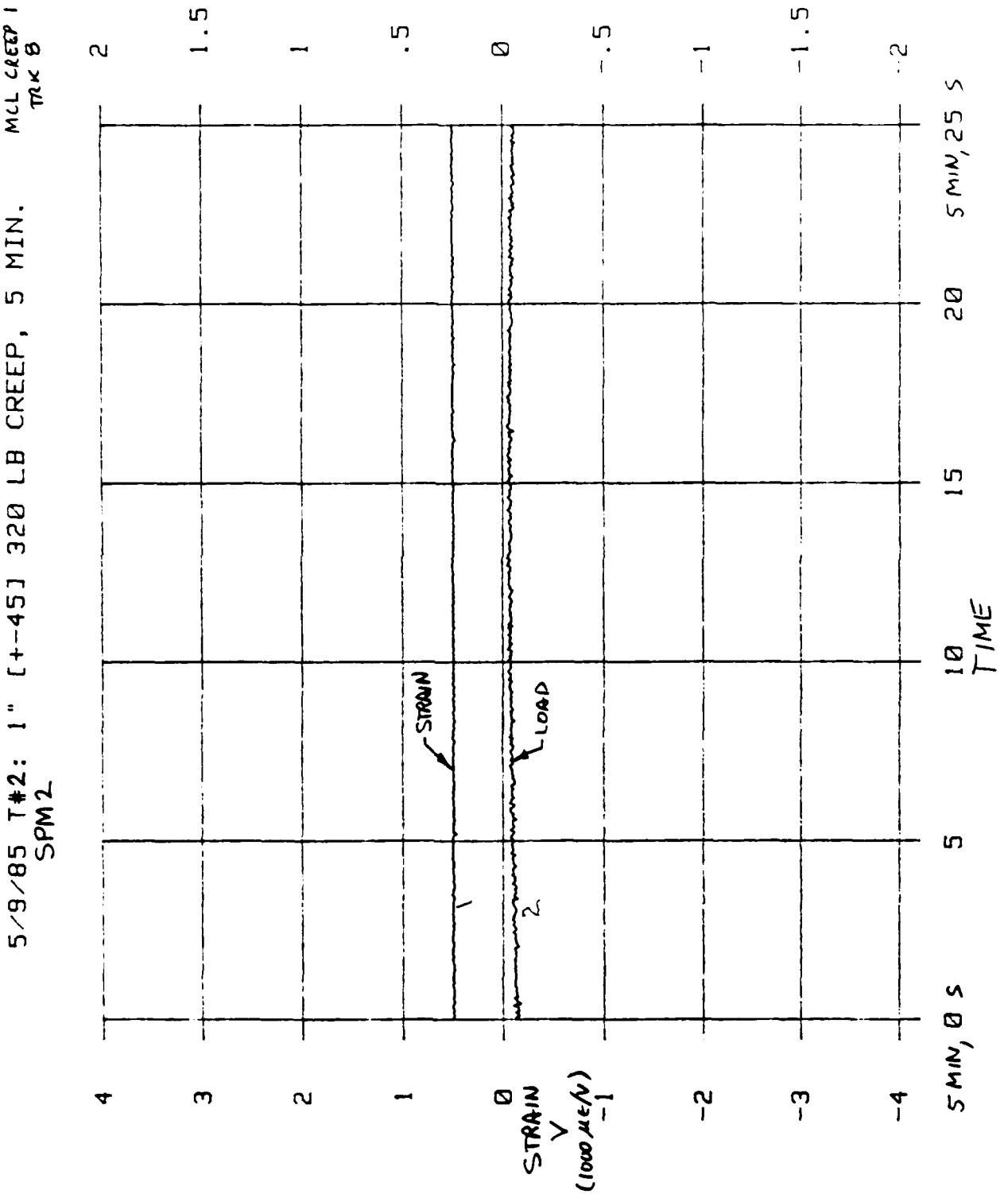
5/9/85 T#2: 1" [+-45] 320 LB CREEP, 5 MIN.
SPM2
MCL CREEP 1
MK 8
STRAIN
LOAD
1
2
STRAIN
V
(1000 με/V)
TIME
5MIN, 0 S
5MIN, 25 S
4
3
2
1
0
-1
-2
-3
-4
2
1.5
1
.5
0
-.5
-1
-1.5
-2
5
10
15
20

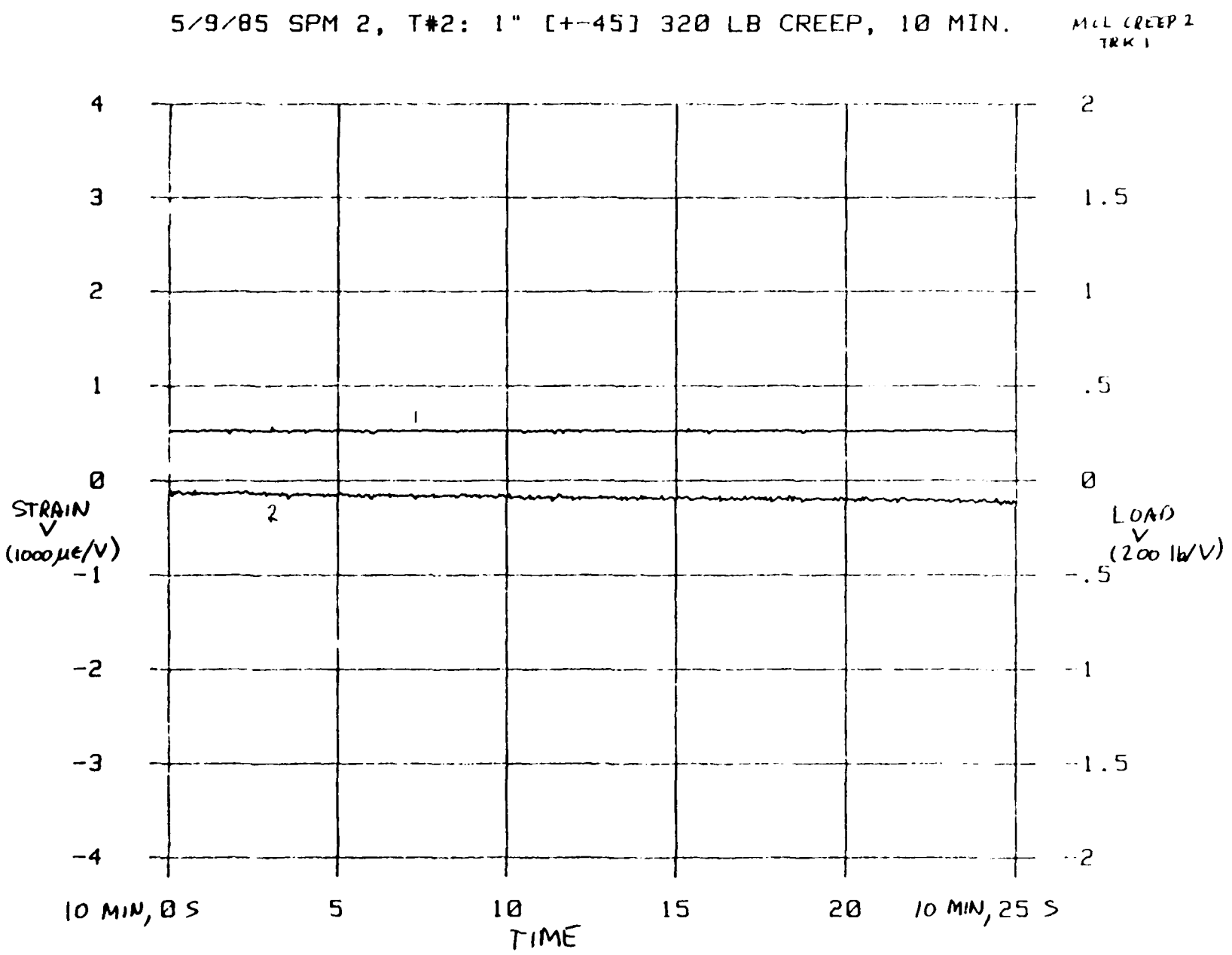
5/9/85 SPM 2, T#2: 1" [+-45] 320 LB CREEP, 10 MIN.
MCL CREEP 2
TRK 1
4
3
2
1
0
-1
-2
-3
-4
STRAIN
V
(1000με/V)
2
1
.5
0
-.5
-1
-1.5
-2
LOAD
V
(200 lb/V)
10 MIN, 0 S
5
10
15
20
10 MIN, 25 S
TIME

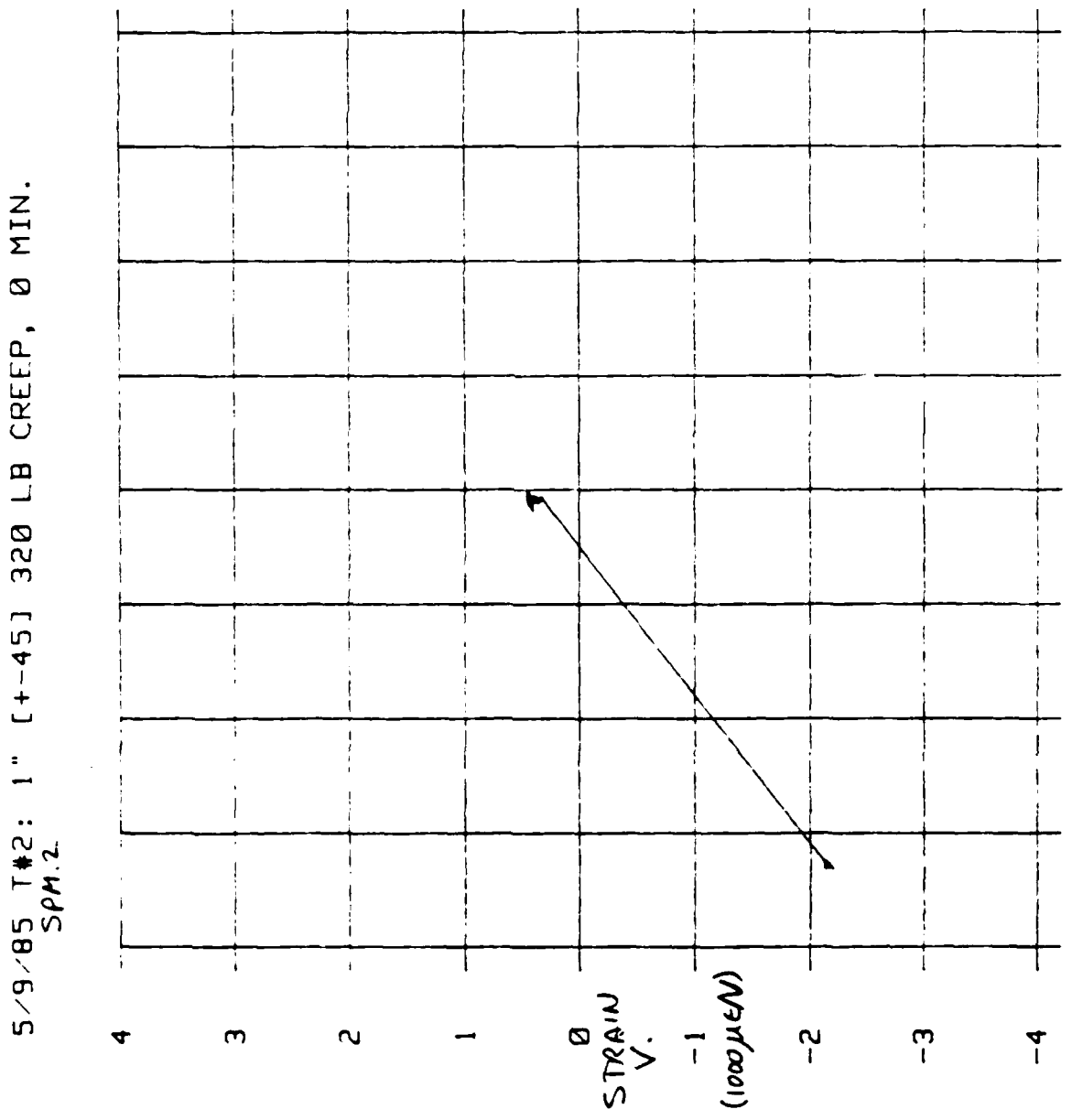
5/9/85 T#2: 1" [+-45] 320 LB CREEP, 0 MIN.
SPM.2
4
3
2
1
0
-1
-2
-3
-4
STRAIN
V.
(1000 μ in/in)
-2
-1.5
-1
-.5
0
.5
1
1.5
2
LOAD
V.
(200 lb/v)

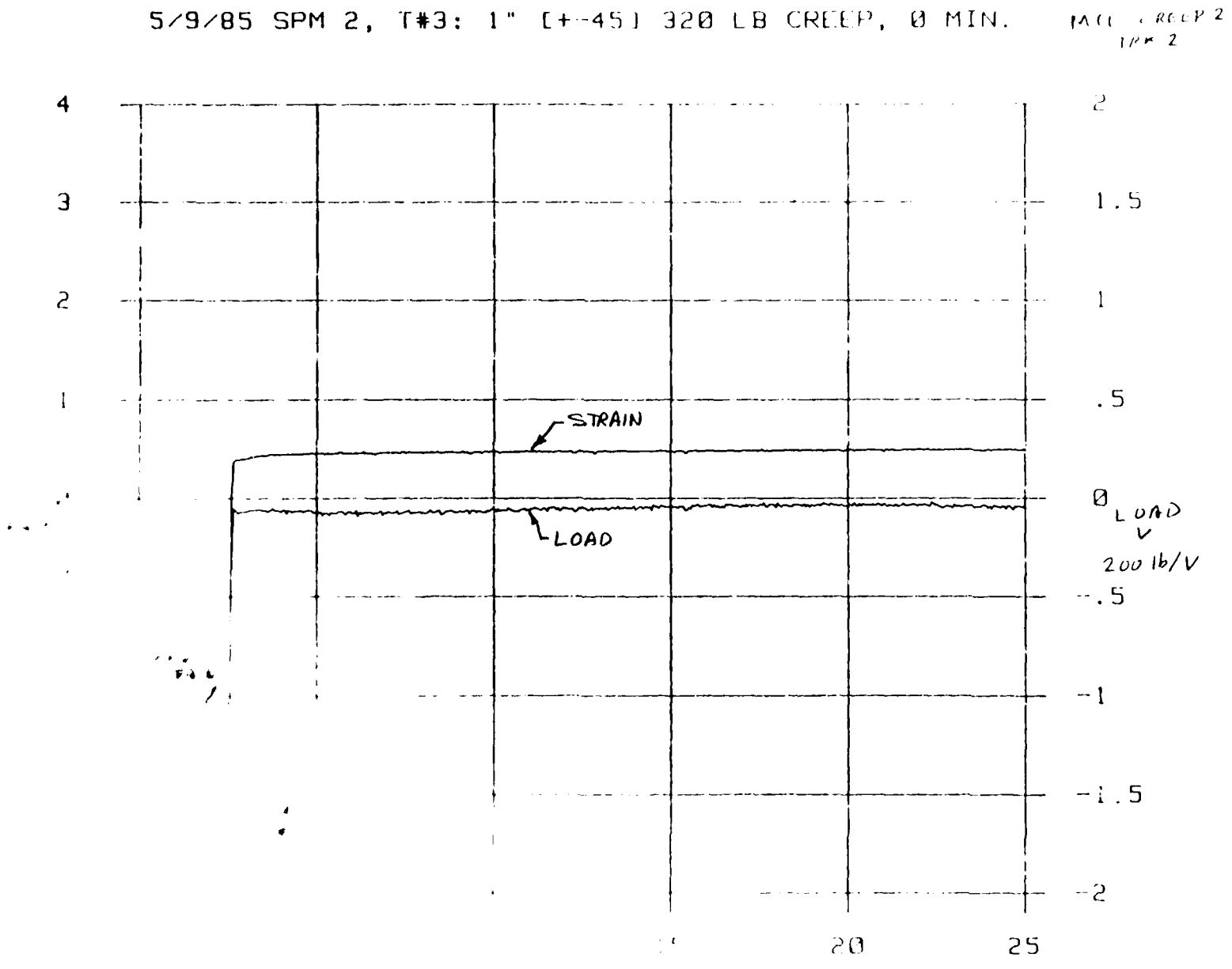
5/9/85 SPM 2, T#3: 1" [+-45] 320 LB CREEP, 0 MIN.
4
3
2
1
2
1.5
1
.5
STRAIN
0
LOAD
LOAD
V
200 lb/V
-.5
-1
-1.5
-2
20
25

AD-A188 513 LOW VELOCITY IMPACT OF COMPOSITE AEROSTRUCTURES(U) 2/4
VILLANOVA UNIV PA P V MCLAUGLIN SEP 86 NADC-87106-60
N62269-82-C-0704

UNCLASSIFIED F/G 1/3 NL

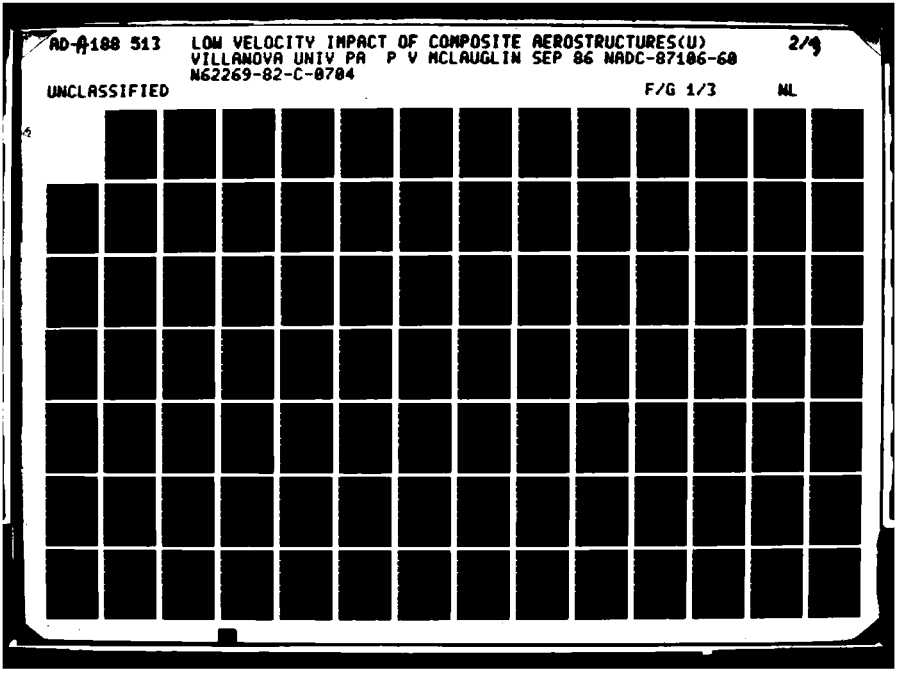

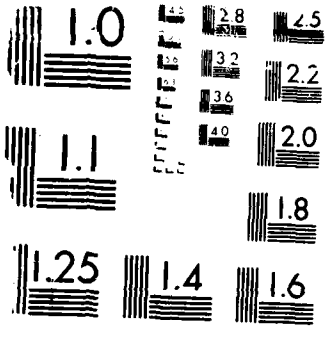

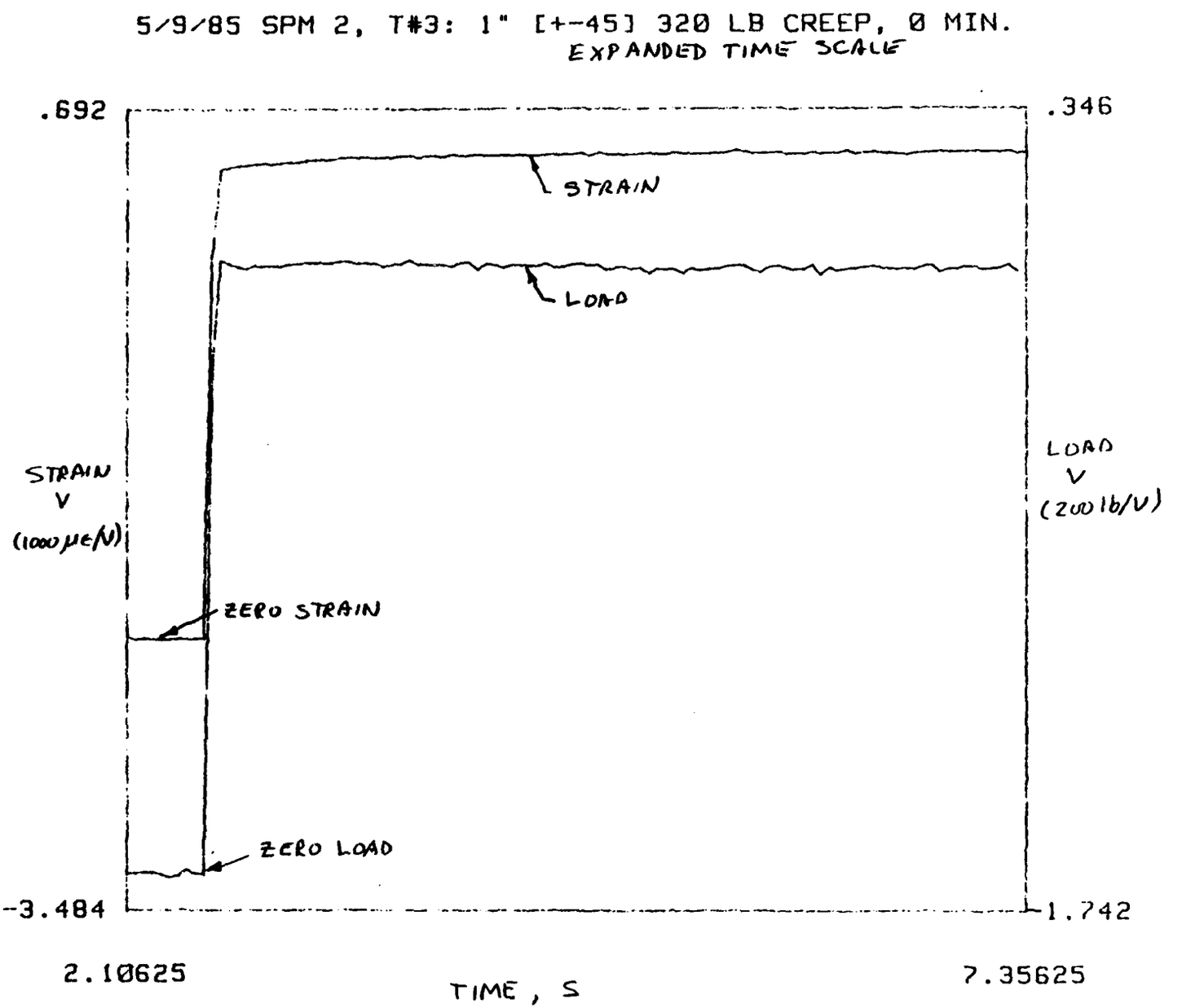
5/9/85 SPM 2, T#3: 1" [+-45] 320 LB CREEP, 0 MIN.
EXPANDED TIME SCALE
.692
.346
STRAIN
LOAD
STRAIN
V
(1000 με/V)
LOAD
V
(200 lb/V)
ZERO STRAIN
ZERO LOAD
-3.484
1.742
2.10625
TIME, S
7.35625

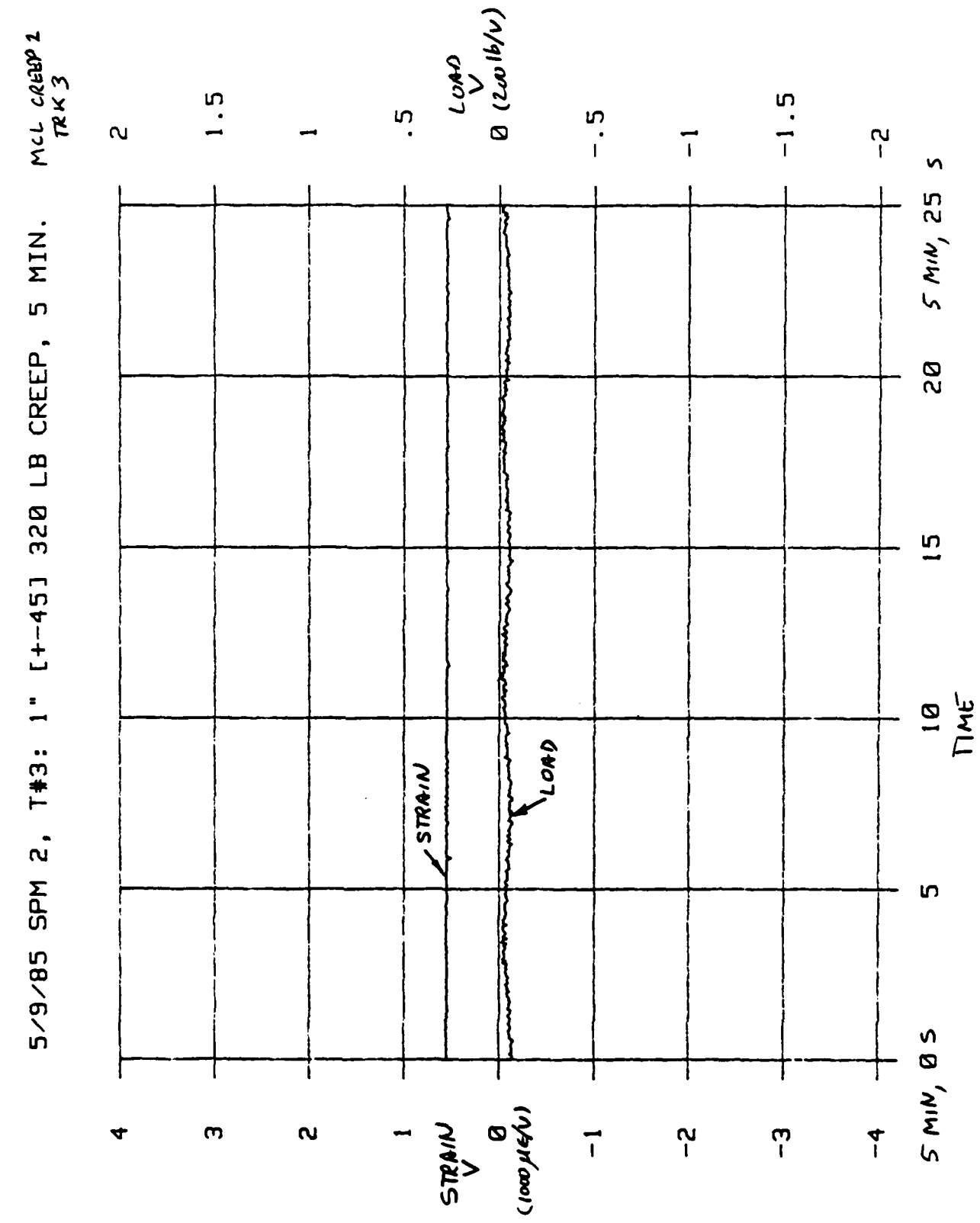
5/9/85 SPM 2, T#3: 1" [+-45] 320 LB CREEP, 5 MIN.
MCL CREEP 2
TRK 3
STRAIN
V
0
(1000 με/V)
LOAD
V
0 (200 lb/V)
STRAIN
LOAD
5 MIN, 0 S
5 MIN, 25 S
TIME

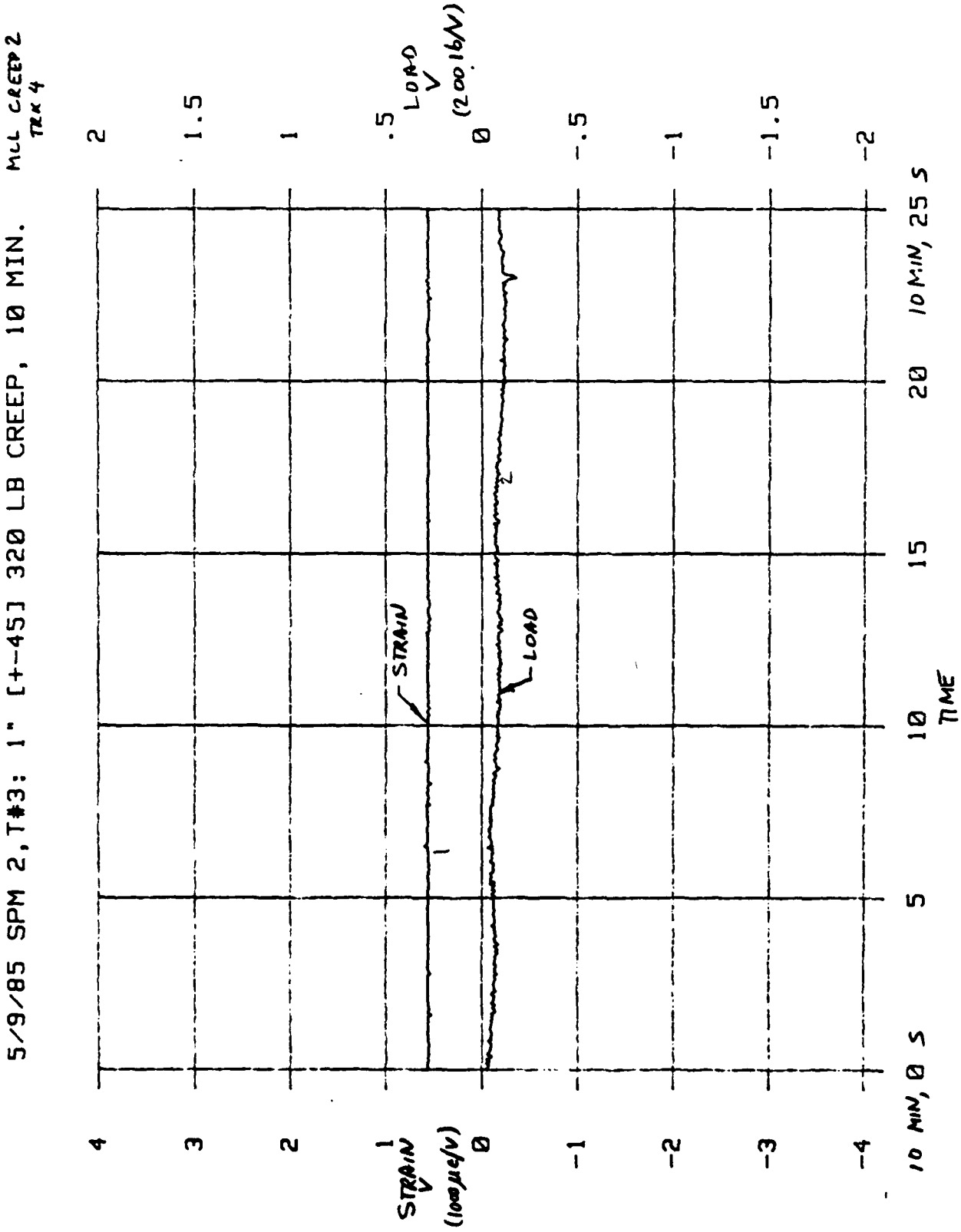
5/9/85 SPM 2, T#3: 1" [+-45] 320 LB CREEP, 10 MIN.
MUL CREEP 2
TRK 4
LOAD V (200 lb/V)
STRAIN V (100 με/V)
STRAIN
LOAD
TIME
10 MIN, 0 S
10 MIN, 25 S

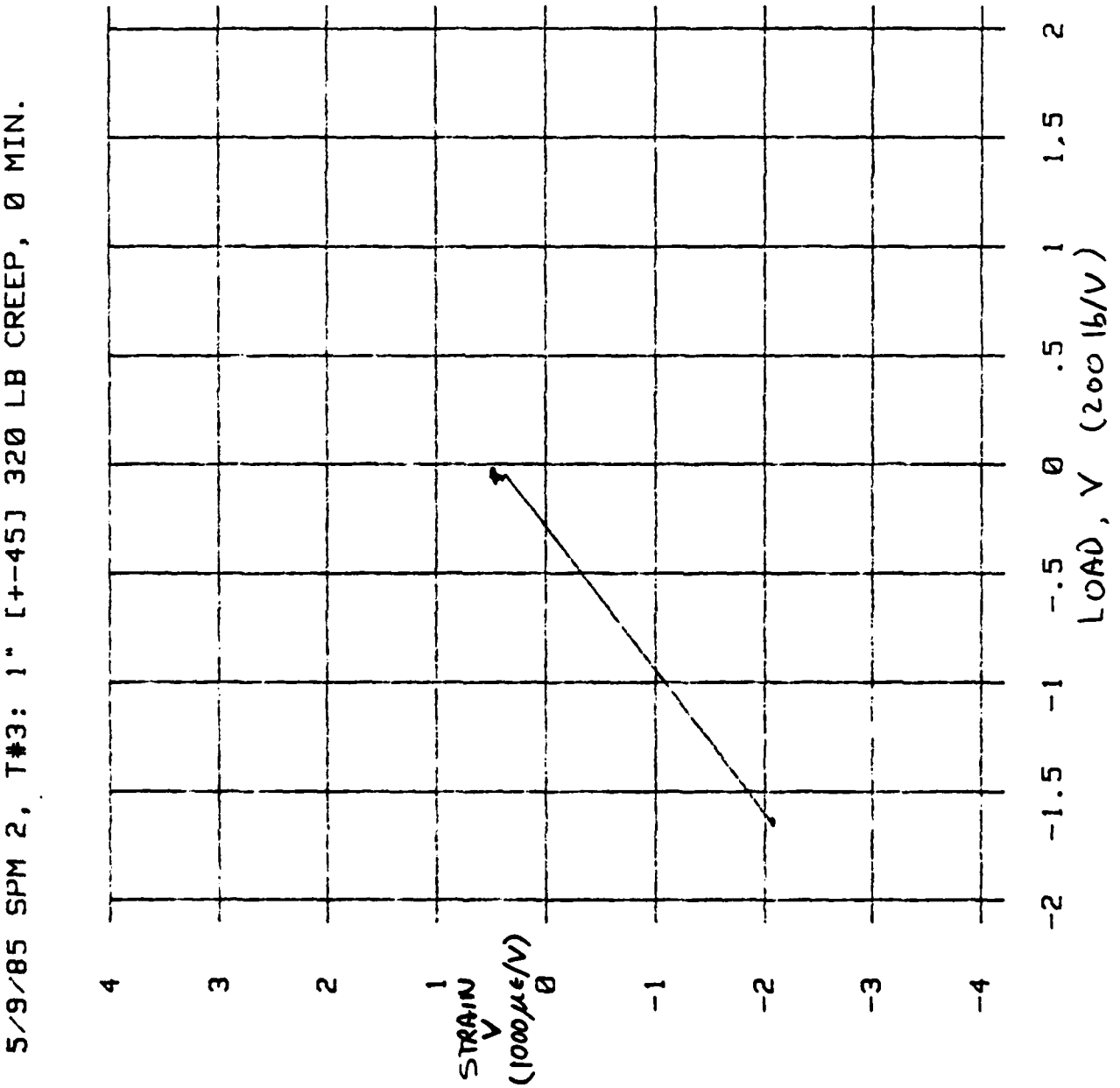
5/9/85 SPM 2, T#3: 1" [+-45] 320 LB CREEP, 0 MIN.
STRAIN V (1000με/V)
4
3
2
1
0
-1
-2
-3
-4
-2
-1.5
-1
-.5
0
.5
1
1.5
2
LOAD, V (200 lb/V)

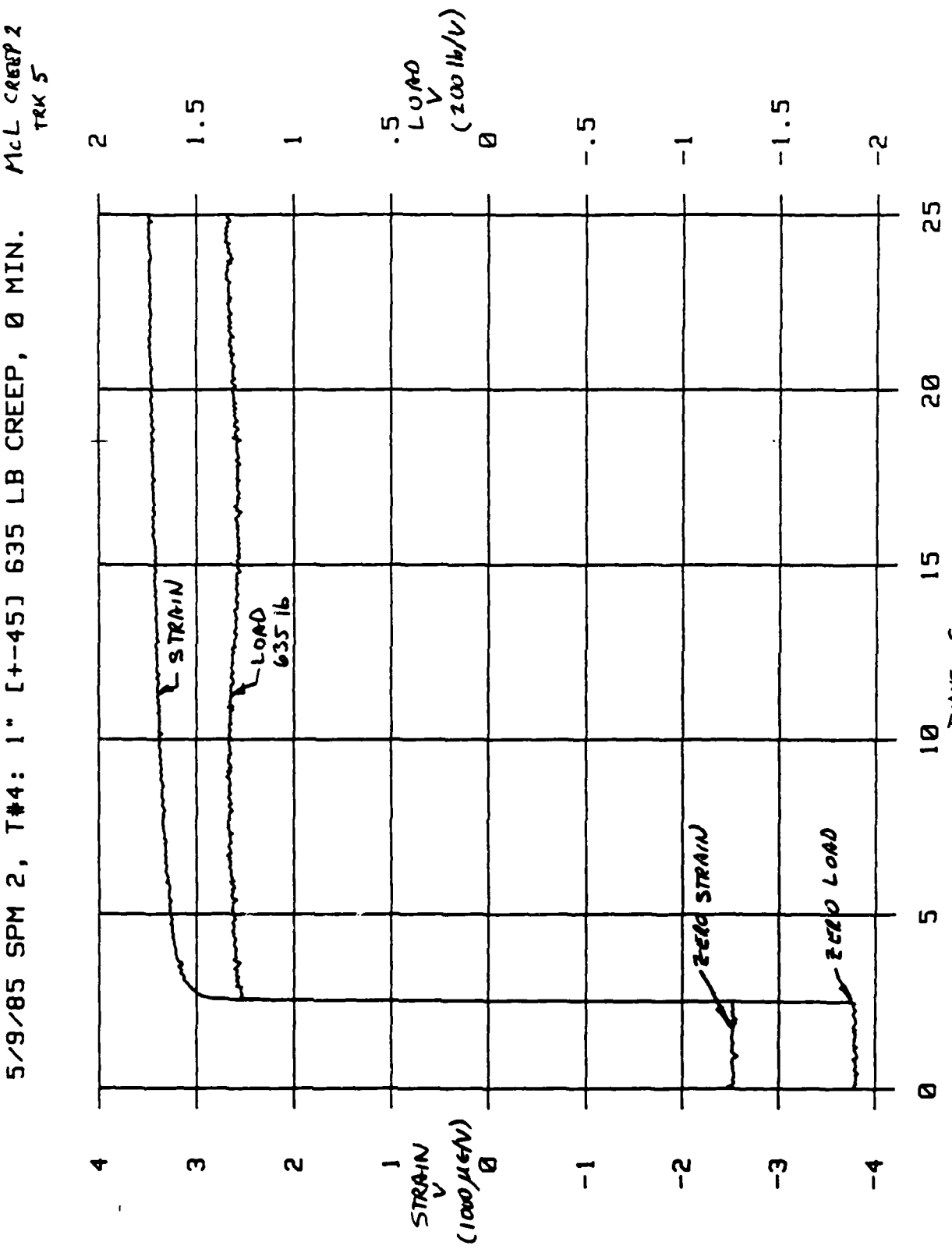
5/9/85 SPM 2, T#4: 1" [+-45] 635 LB CREEP, 0 MIN.
McL CREEP 2
TRK 5
STRAIN
LOAD
635 lb
ZERO STRAIN
ZERO LOAD
STRAIN V (1000 μεV)
LOAD V (200 lb/V)
TIME, S
4
3
2
1
0
-1
-2
-3
-4
2
1.5
1
.5
0
-.5
-1
-1.5
-2
0
5
10
15
20
25

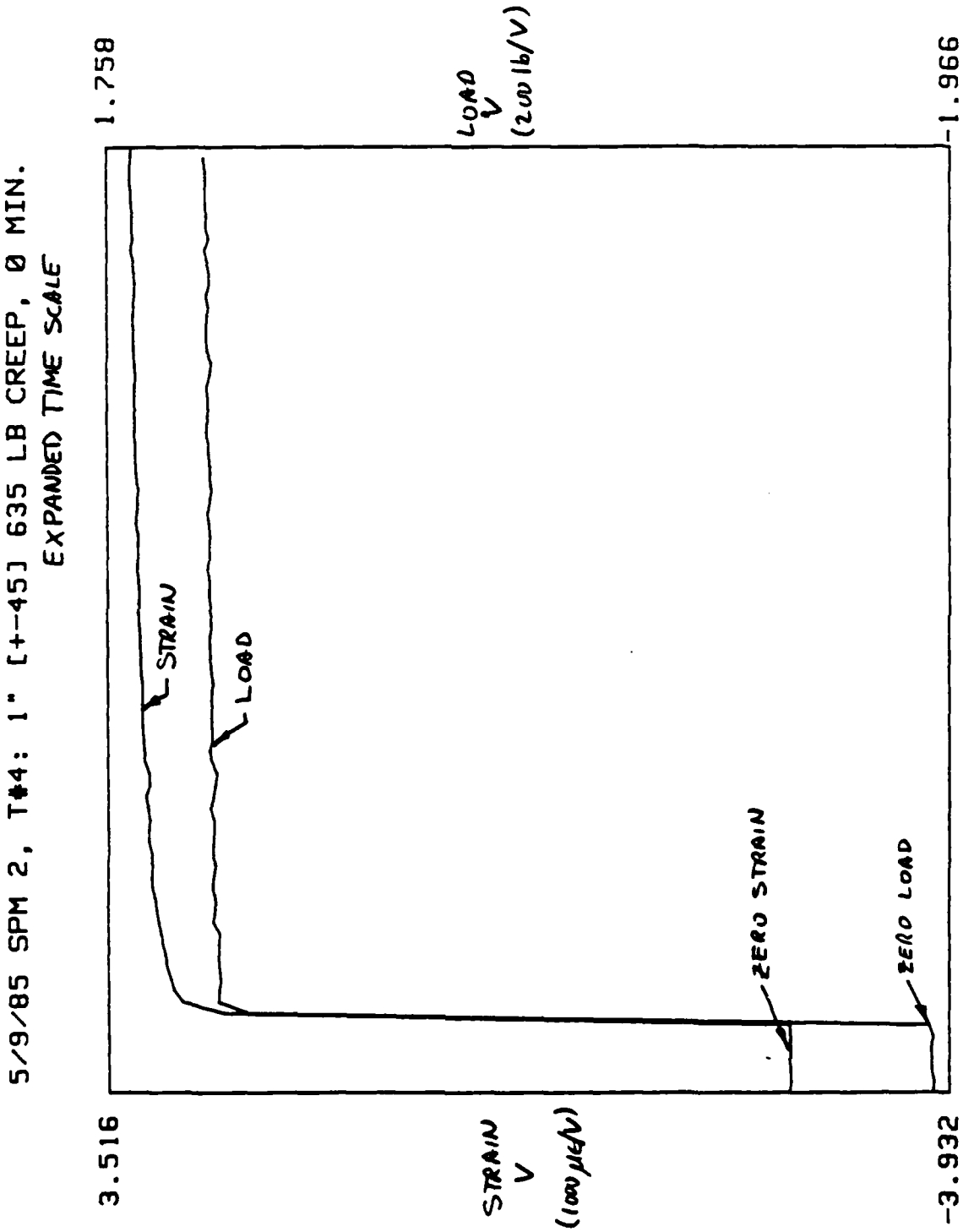
5/9/85 SPM 2, T#4: 1" [+-45] 635 LB CREEP, 0 MIN.
EXPANDED TIME SCALE
1.758
LOAD
V
(2000 lb/V)
-1.966
STRAIN
LOAD
ZERO STRAIN
ZERO LOAD
3.516
STRAIN
V
(1000 με/V)
-3.932
2.20625
TIME, S
6.35625

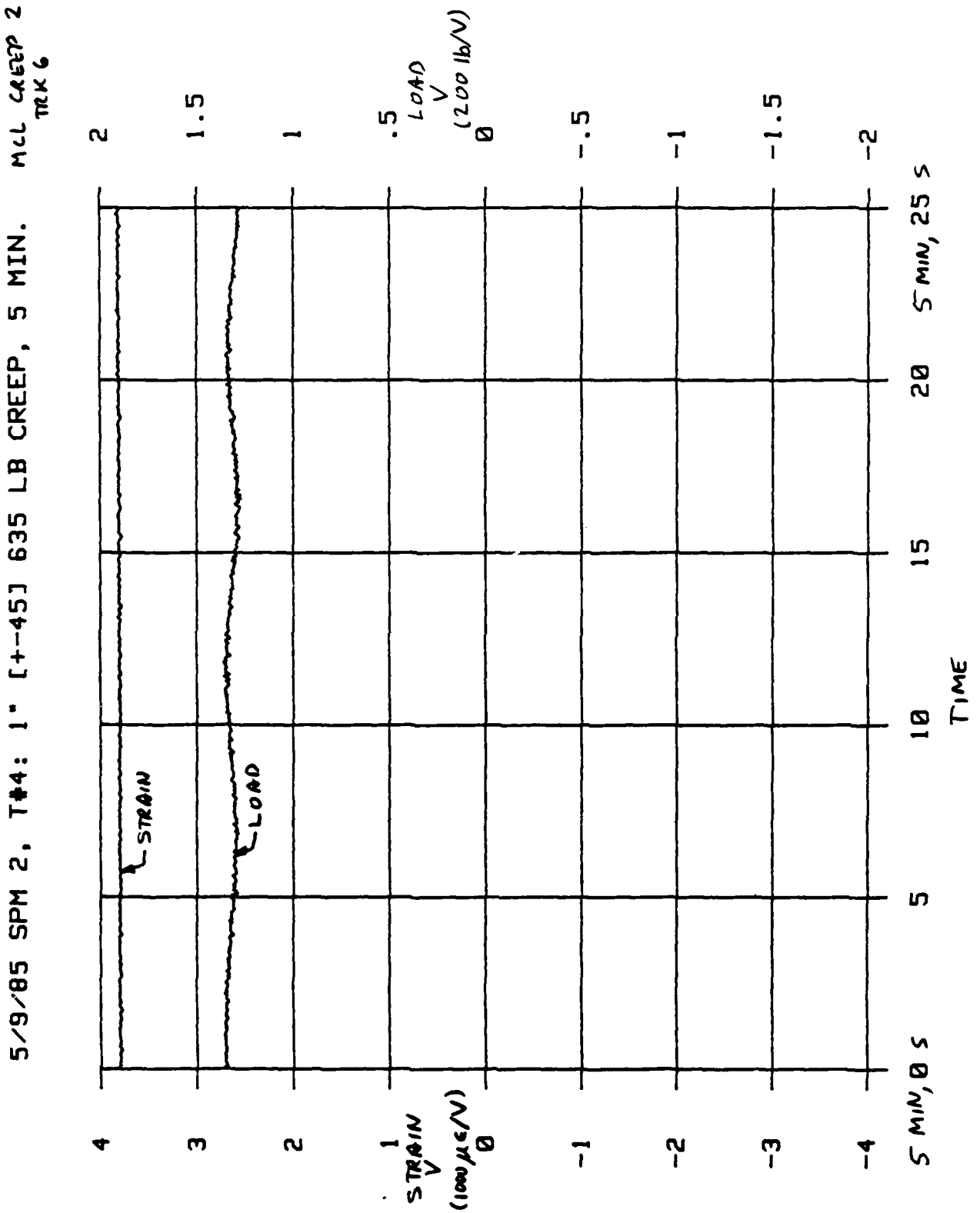
5/9/85 SPM 2, T#4: 1" [+-45] 635 LB CREEP, 5 MIN.
MCL CREEP 2
TRK 6
STRAIN
LOAD
STRAIN V (1000 με/V)
LOAD V (200 lb/V)
TIME
5 MIN, 0 S
5 MIN, 25 S

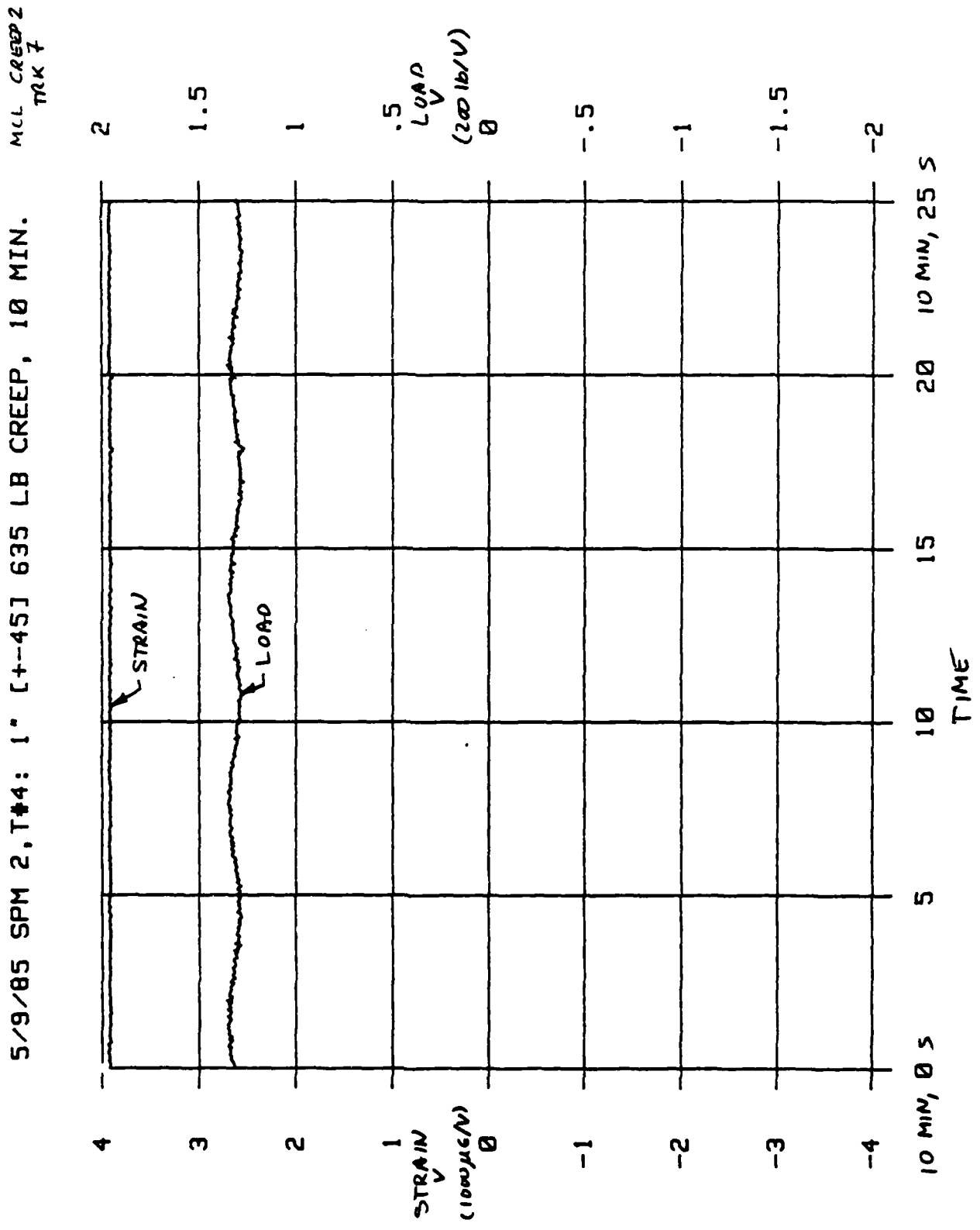
MCL CREEP 2
MK 7
5/9/85 SPM 2, T#4: 1" [+-45] 635 LB CREEP, 10 MIN.
STRAIN
LOAD
STRAIN V (100μE/V)
LOAD V (200 lb/V)
TIME
10 MIN, 0 S
5
10
15
20
10 MIN, 25 S

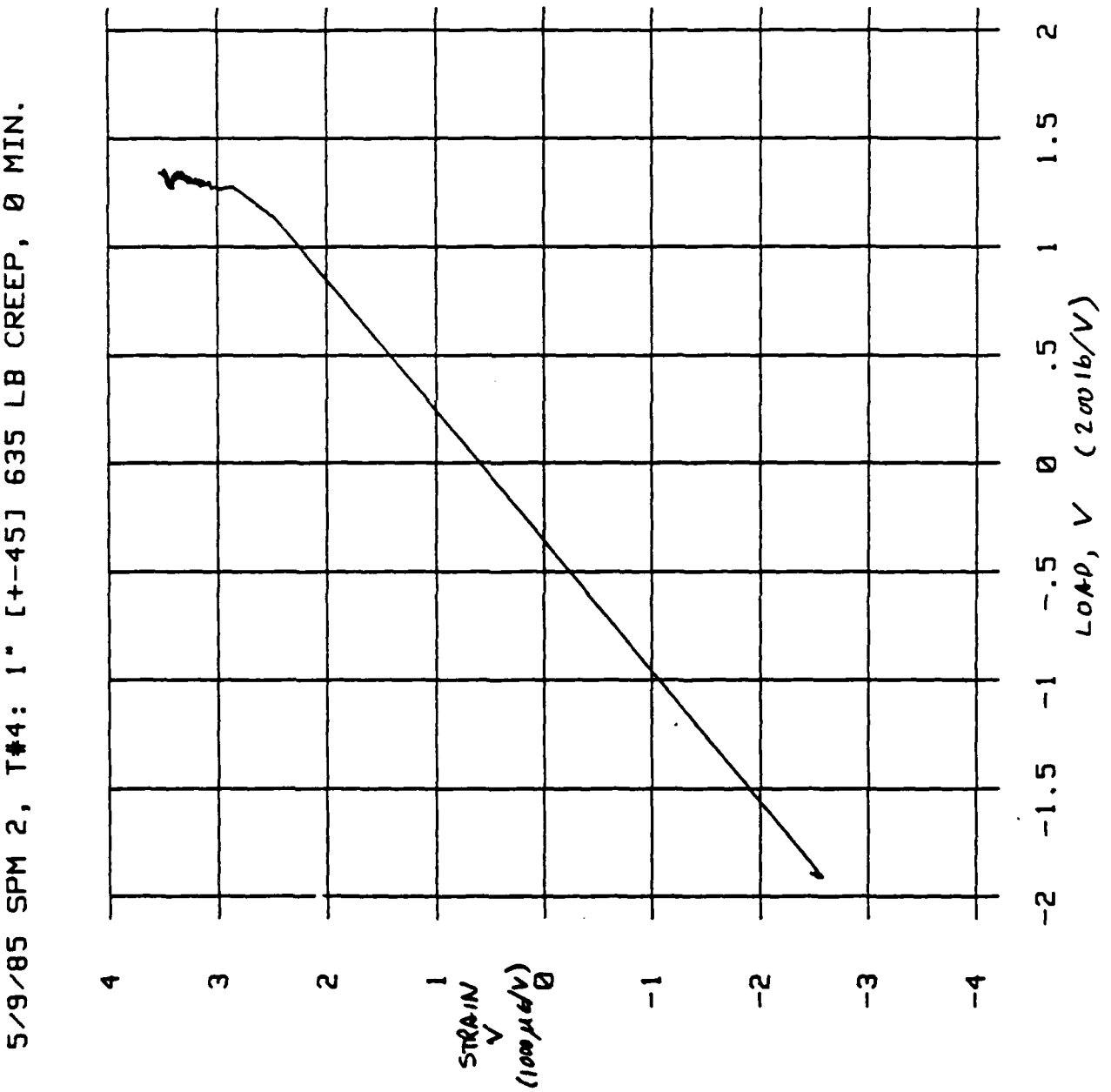
5/9/85 SPM 2, T#4: 1" [+-45] 635 LB CREEP, 0 MIN.
STRAIN V (1000 μin/in/V)
4
3
2
1
0
-1
-2
-3
-4
-2
-1.5
-1
-.5
0
.5
1
1.5
2
LOAD, V (2000 lb/V)

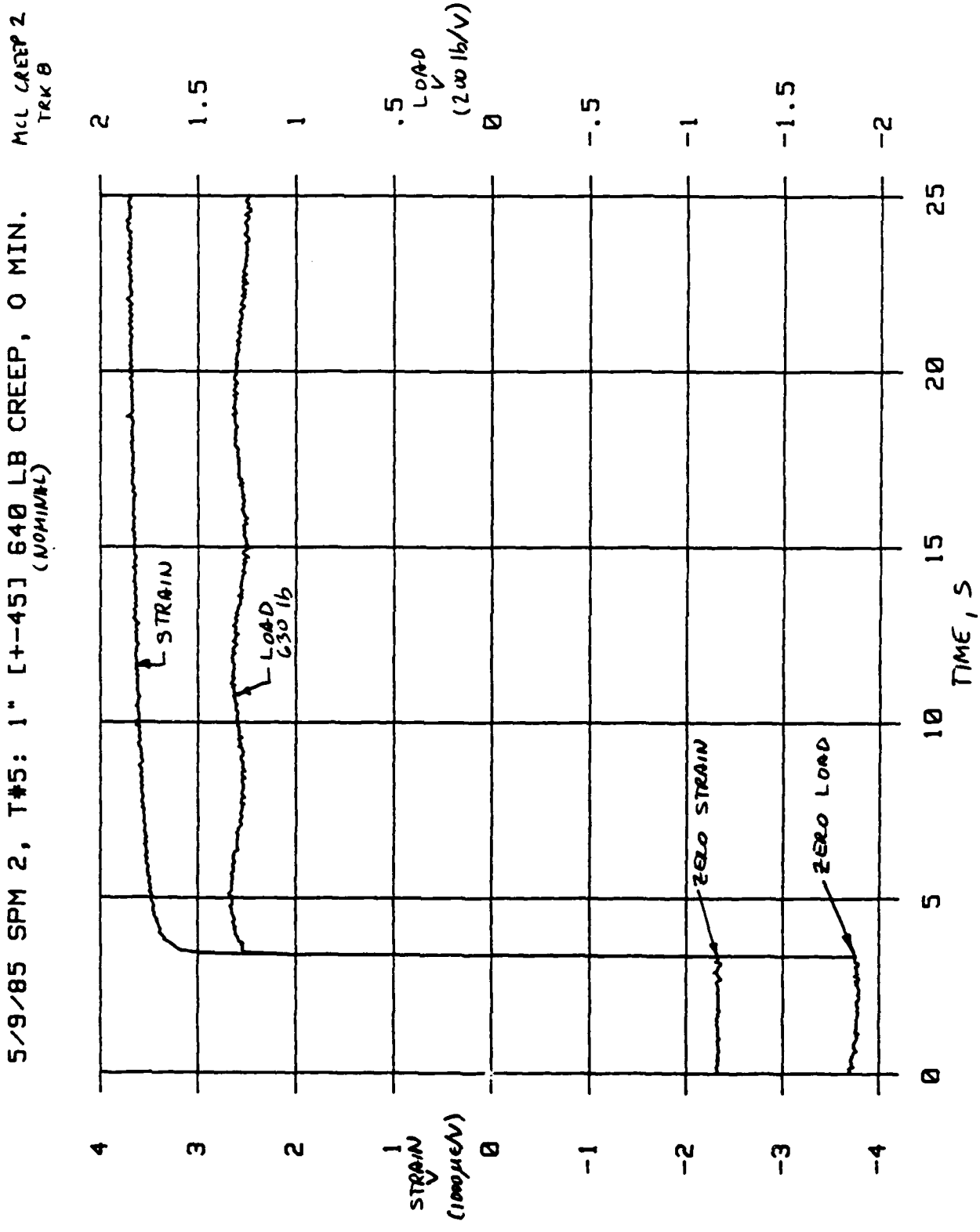
5/9/85 SPM 2, T#5: 1" [+-45] 640 LB CREEP, 0 MIN.
(NOMINAL)
MCL CREEP 2
TRK 8
STRAIN
LOAD
630 lb
ZERO STRAIN
ZERO LOAD
STRAIN
V
(1000 με/V)
LOAD
V
(2000 lb/V)
TIME, S
4
3
2
1
0
-1
-2
-3
-4
2
1.5
1
.5
0
-.5
-1
-1.5
-2
0
5
10
15
20
25

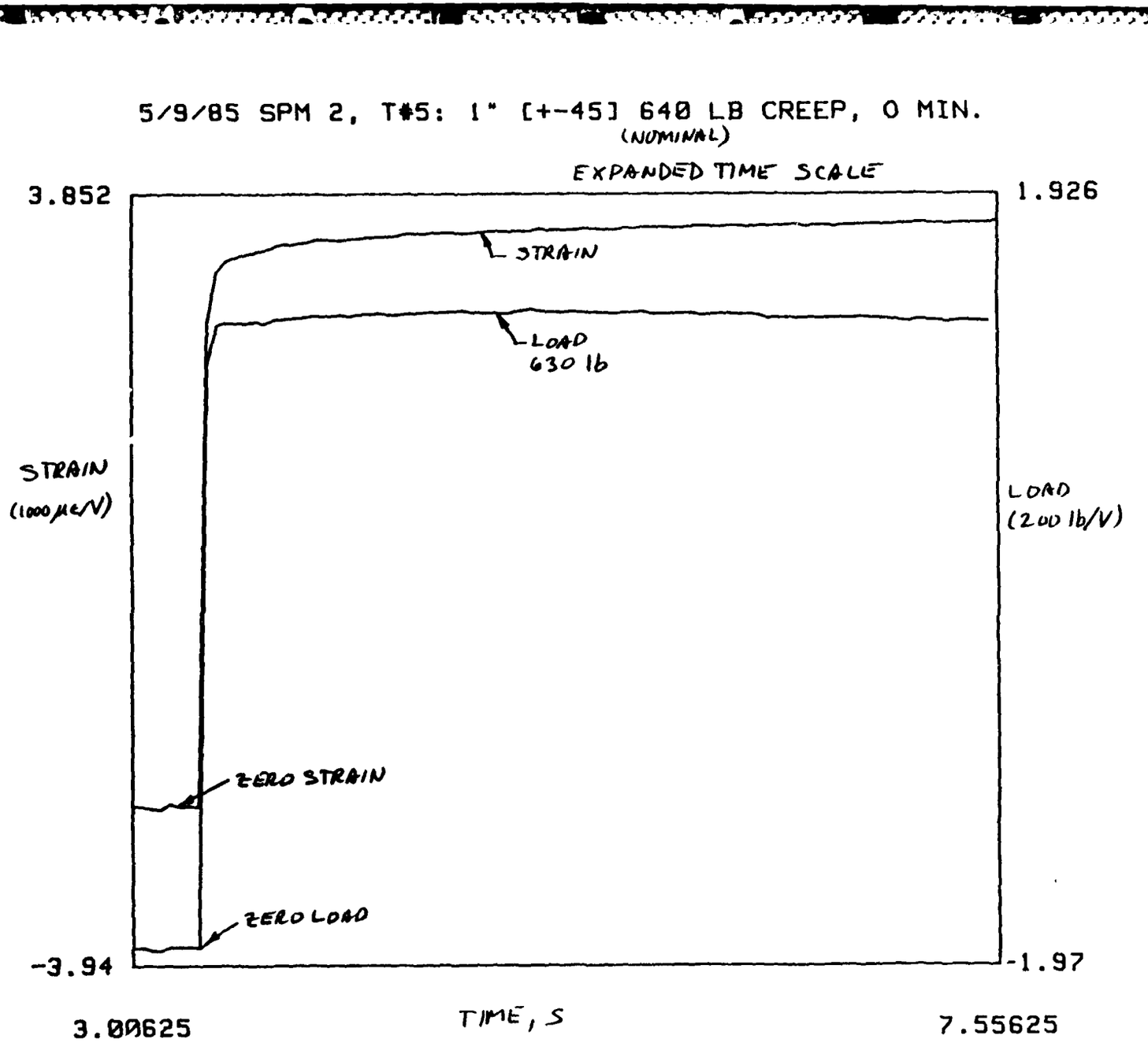
5/9/85 SPM 2, T#5: 1" [+-45] 640 LB CREEP, 0 MIN.
(NOMINAL)
EXPANDED TIME SCALE
3.852
1.926
STRAIN
LOAD
630 lb
STRAIN
(1000 με/V)
LOAD
(200 lb/V)
ZERO STRAIN
ZERO LOAD
-3.94
-1.97
3.00625
TIME, S
7.55625

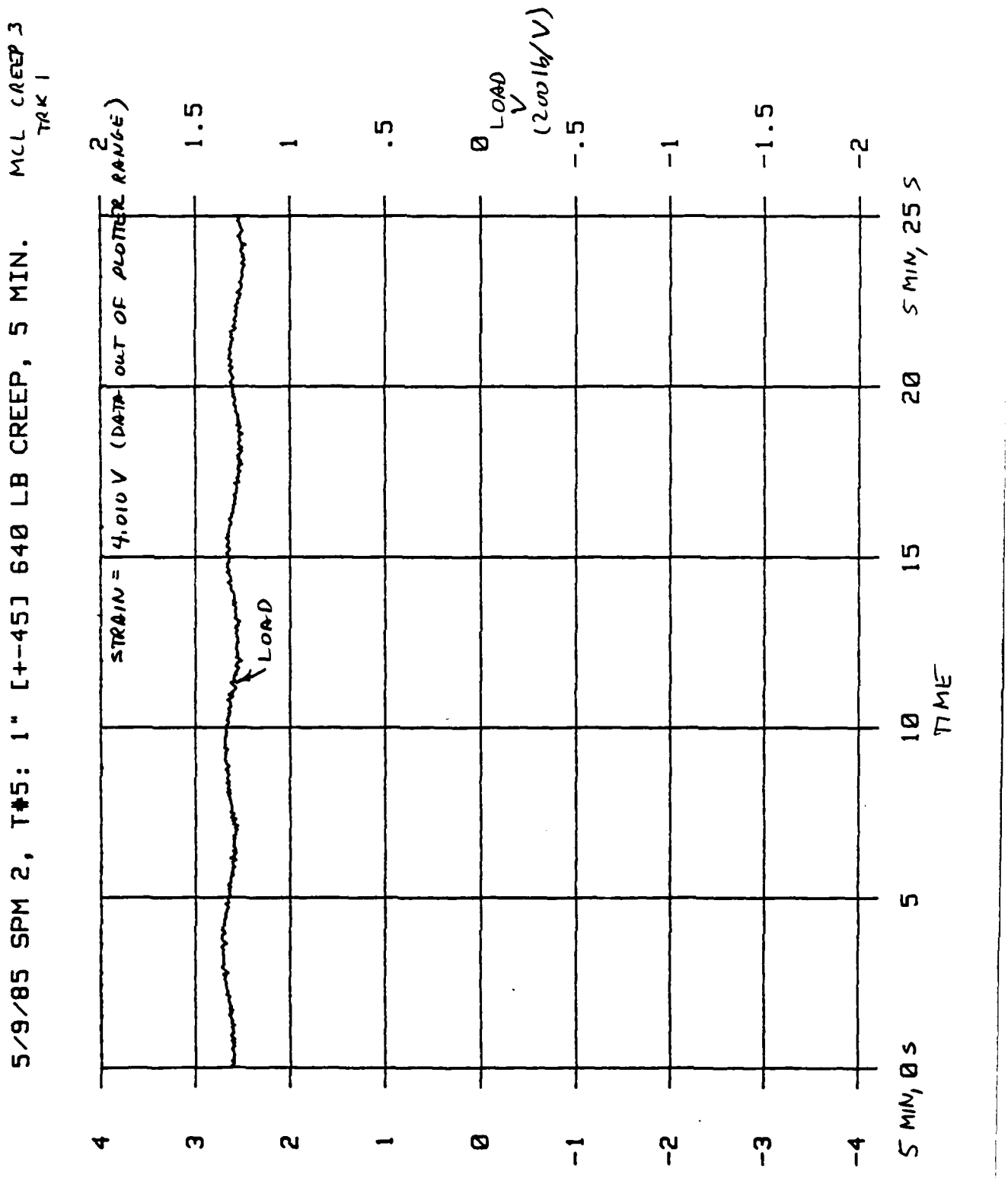
5/9/85 SPM 2, T#5: 1" [+-45] 640 LB CREEP, 5 MIN.
MCL CREEP 3
TAK 1
STRAIN = 4.010 V (DATA OUT OF PLOTTER RANGE)
LOAD
LOAD V (2001b/V)
TIME
5 MIN, 0 s
5 MIN, 25 s
4
3
2
1
0
-1
-2
-3
-4
1.5
1
.5
0
-.5
-1
-1.5
-2
5
10
15
20

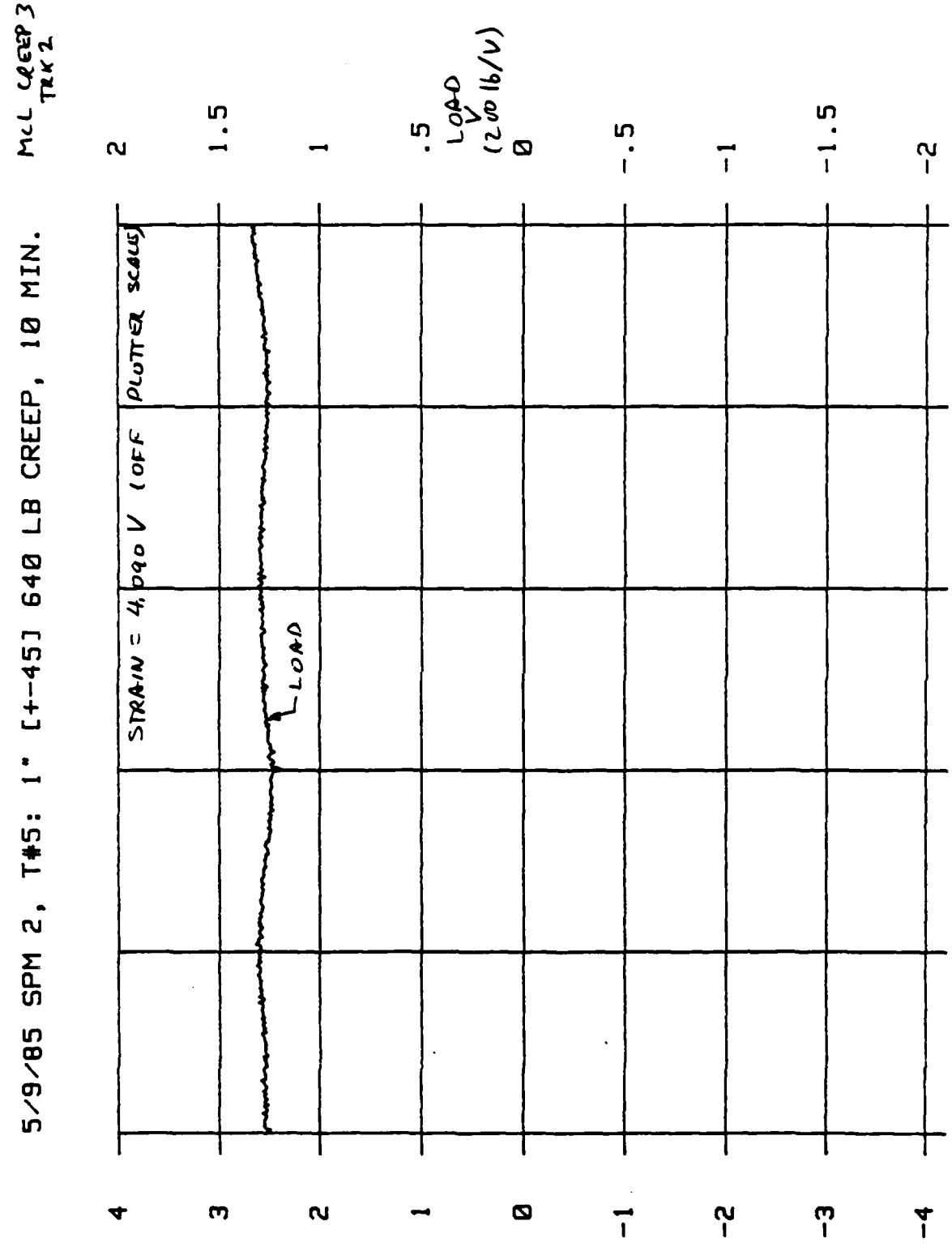
5/9/85 SPM 2, T#5: 1" [+-45] 640 LB CREEP, 10 MIN.
MCL CREEP 3
TRK 2
STRAIN = 4,000 V (OFF PLOTTER SCALE)
LOAD
LOAD V (200 lb/V)
TIME
10 MIN, 0 S
10 MIN, 25 S
4
3
2
1
0
-1
-2
-3
-4
2
1.5
1
.5
0
-.5
-1
-1.5
-2
5
10
15
20

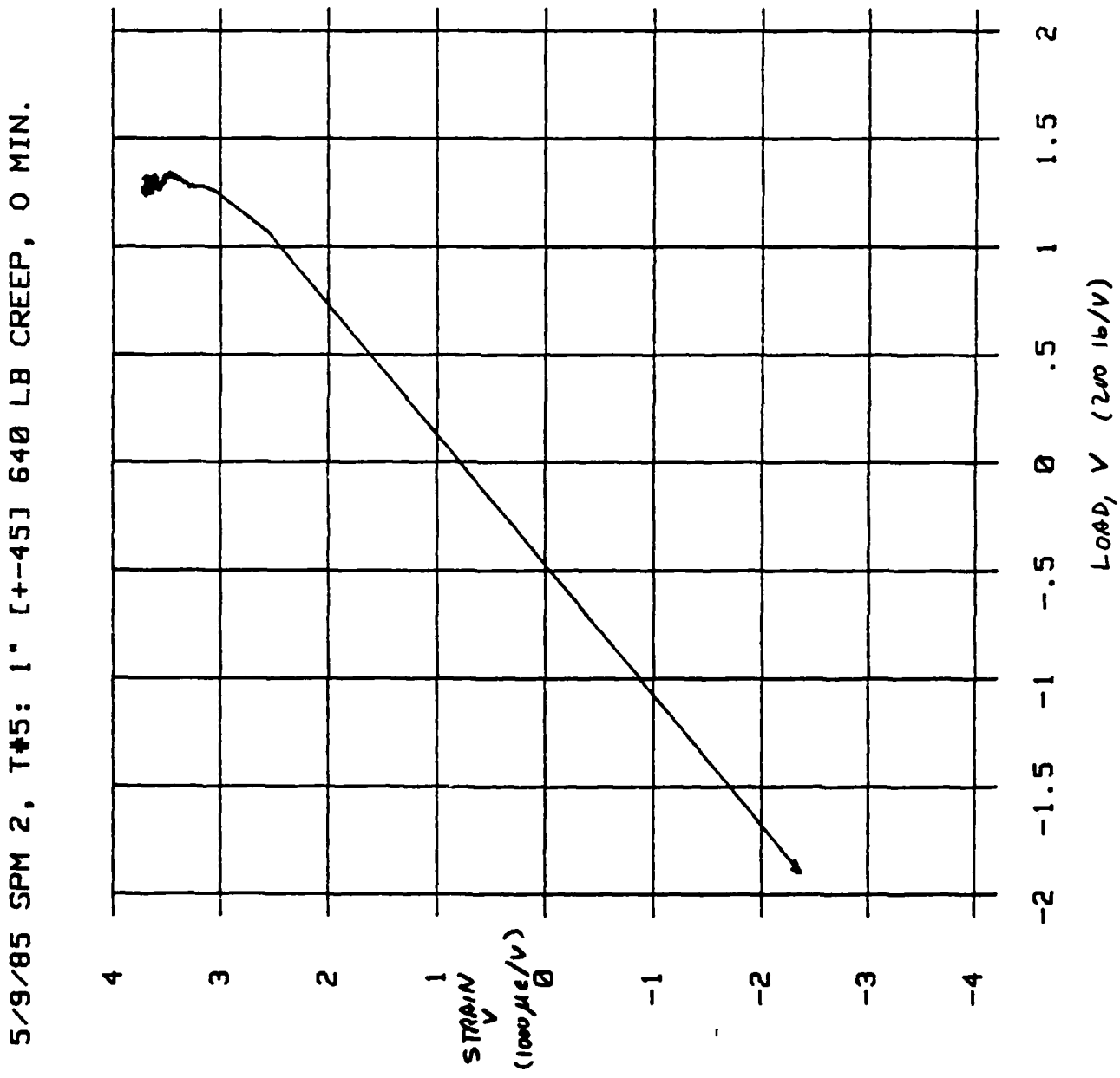
5/9/85 SPM 2, T#5: 1" [+-45] 640 LB CREEP, 0 MIN.
STRAIN V (1000 με/V)
4
3
2
1
0
-1
-2
-3
-4
-2
-1.5
-1
-.5
0
.5
1
1.5
2
LOAD, V (200 lb/V)

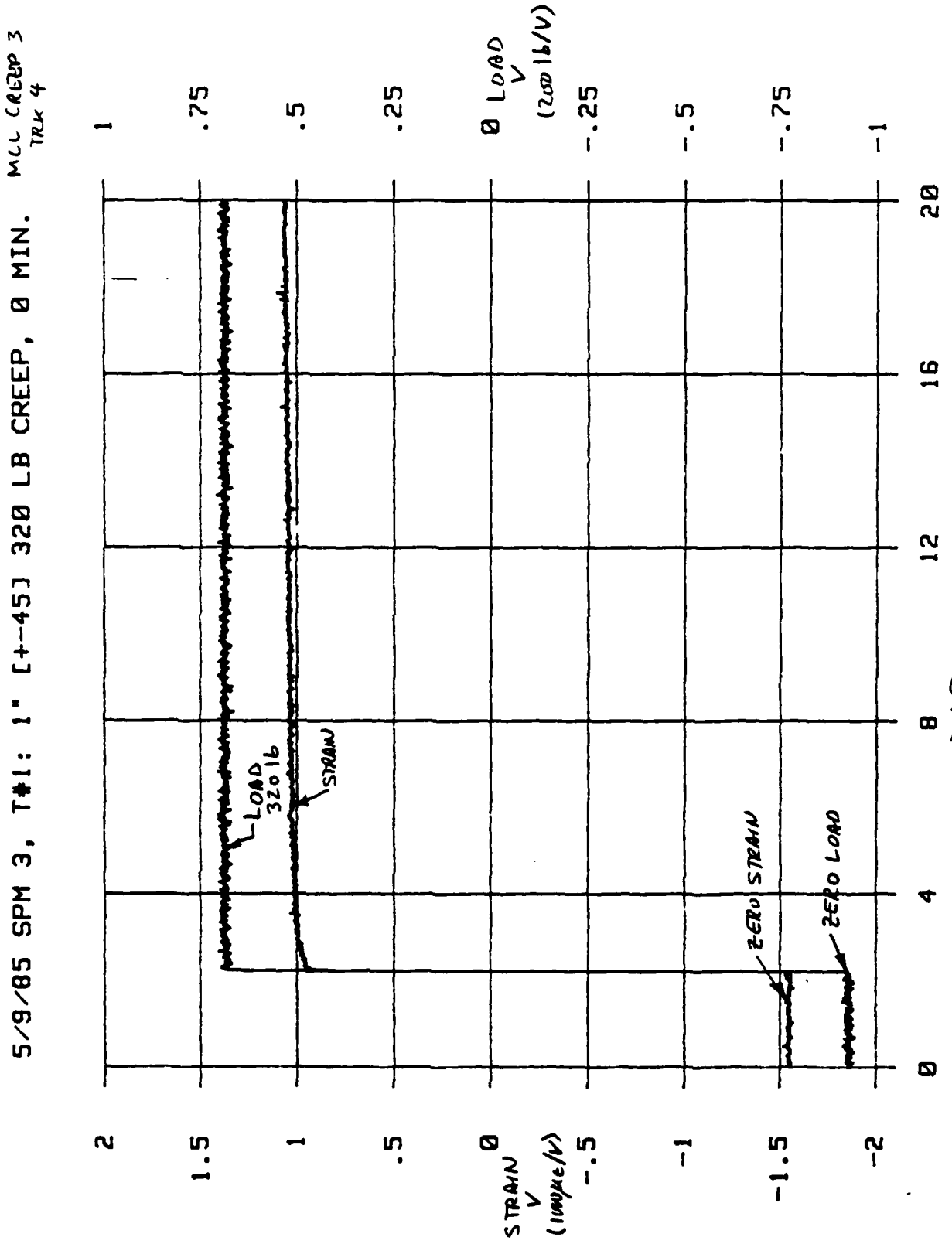
5/9/85 SPM 3, T#1: 1" [+-45] 320 LB CREEP, 0 MIN.
MCL CREEP 3
TRK 4
LOAD
320 lb
STRAIN
ZERO STRAIN
ZERO LOAD
STRAIN
V
(1000με/V)
LOAD
V
(200 lb/V)
TIME, S
2
1.5
1
.5
0
-.5
-1
-1.5
-2
1
.75
.5
.25
0
-.25
-.5
-.75
-1
0
4
8
12
16
20

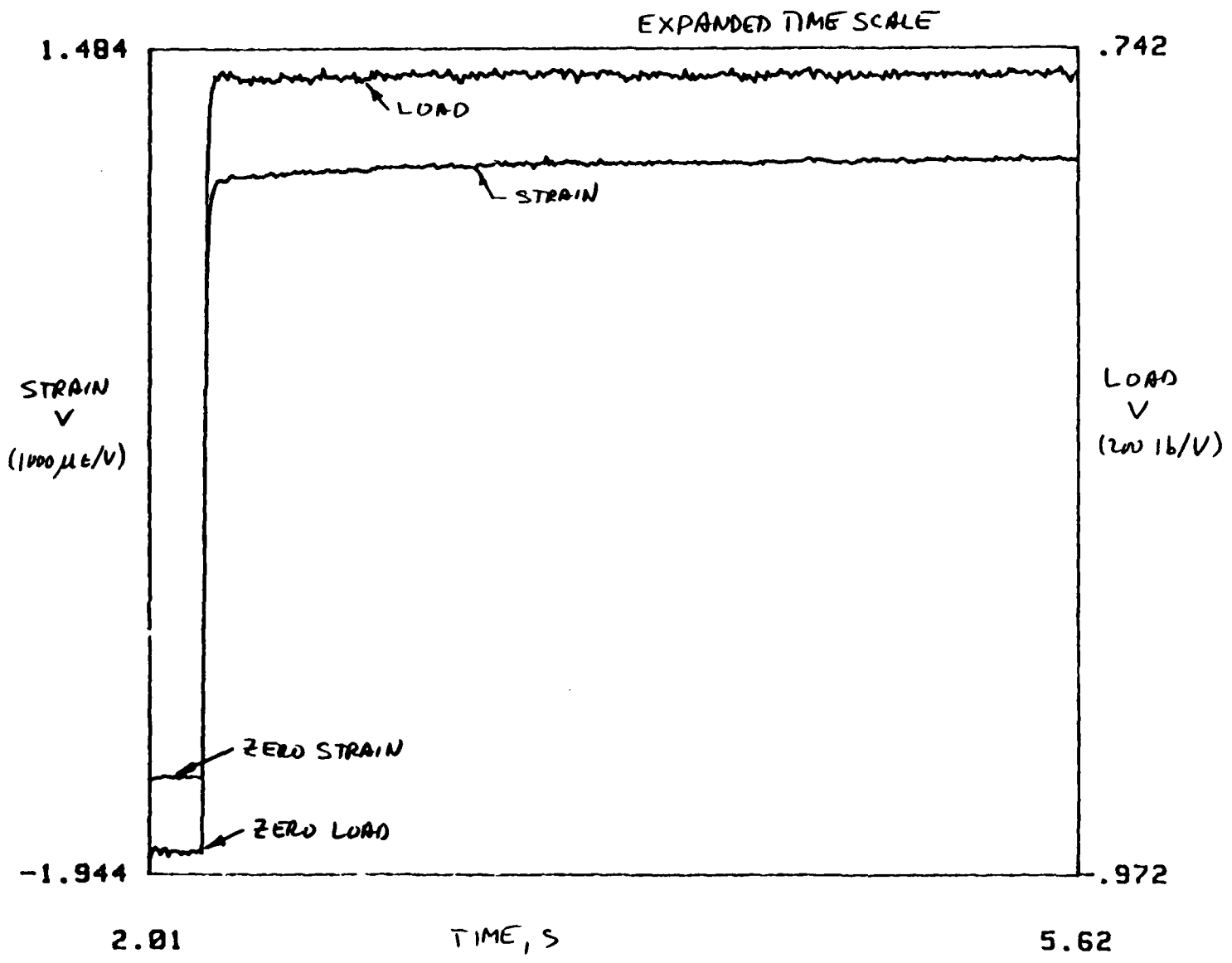
5/9/85 SPM 3, T#1: 1" [+-45] 320 LB CREEP, 0 MIN.
EXPANDED TIME SCALE
1.484
.742
LOAD
STRAIN
STRAIN
V
(1000 με/V)
LOAD
V
(200 lb/V)
ZERO STRAIN
ZERO LOAD
-1.944
.972
2.01
TIME, S
5.62

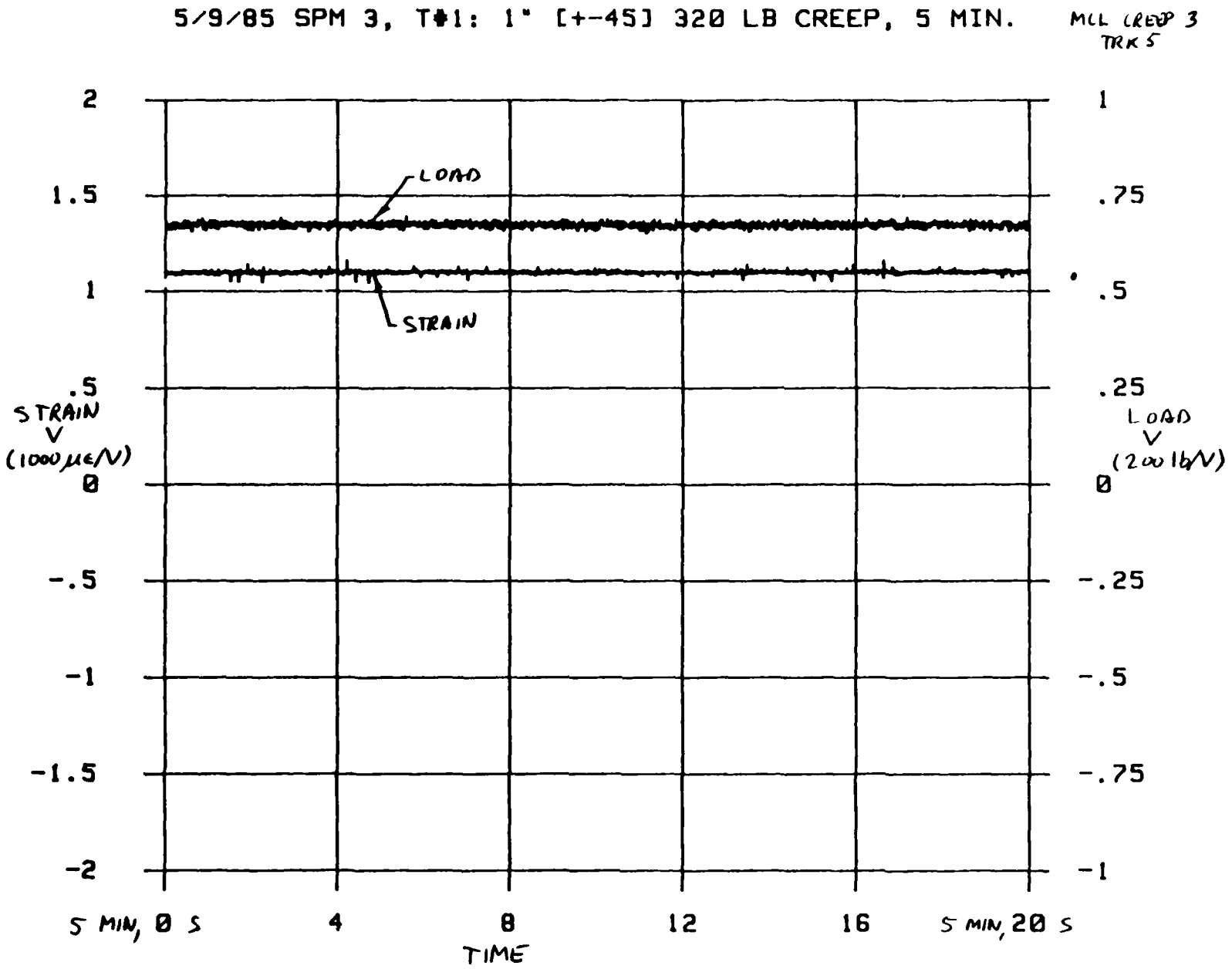
5/9/85 SPM 3, T#1: 1" [+-45] 320 LB CREEP, 5 MIN.
MCL CREEP 3
TRK 5
LOAD
STRAIN
2
1.5
1
.5
0
-.5
-1
-1.5
-2
STRAIN
V
(1000 με/V)
1
.75
.5
.25
0
-.25
-.5
-.75
-1
LOAD
V
(200 lb/V)
5 MIN, 0 S
4
8
12
16
5 MIN, 20 S
TIME

R

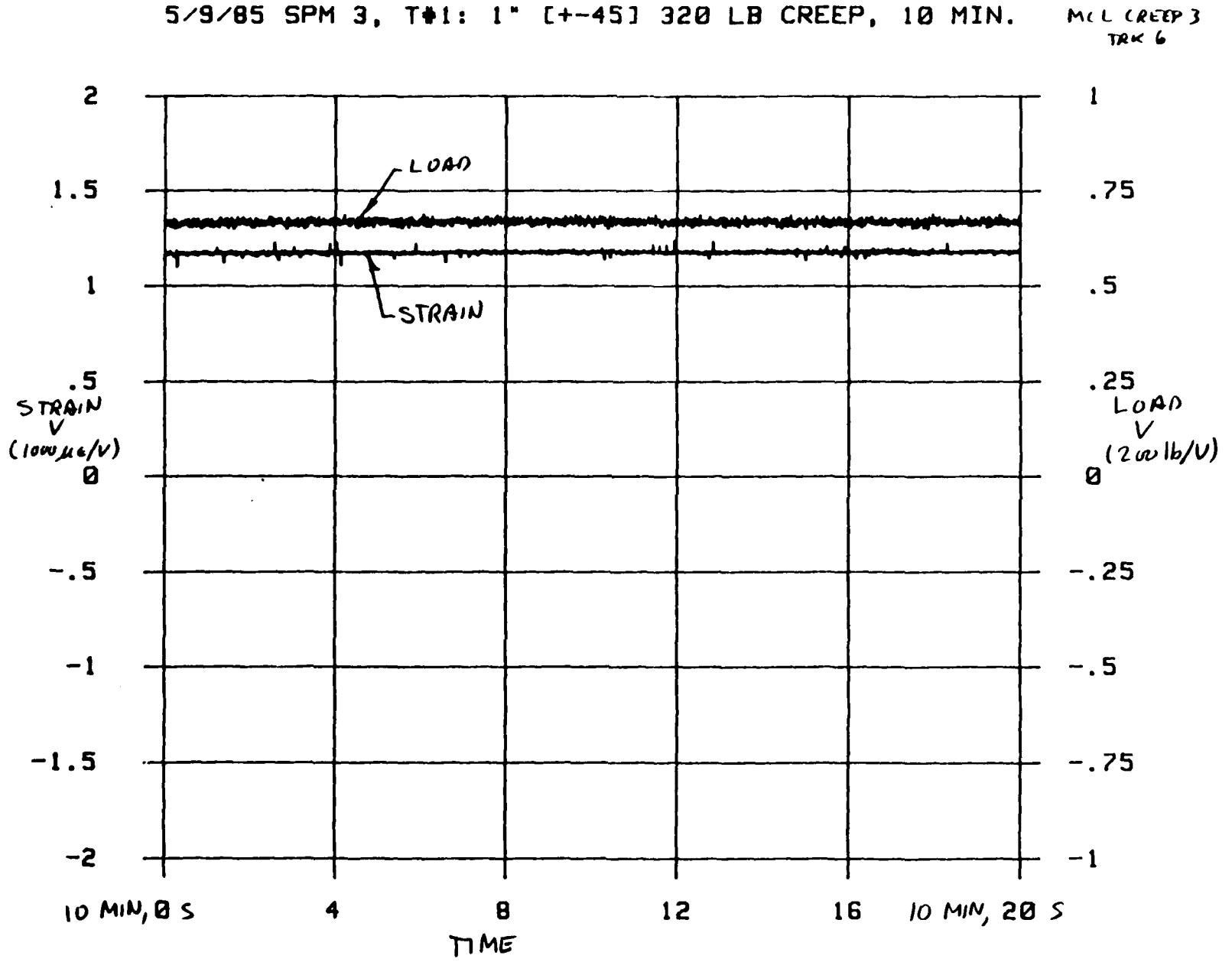
5/9/85 SPM 3, T#1: 1" [+-45] 320 LB CREEP, 10 MIN.
MCL CREEP 3
TRK 6
LOAD
STRAIN
2
1.5
1
.5
0
-.5
-1
-1.5
-2
STRAIN
V
(1000 με/V)
1
.75
.5
.25
0
-.25
-.5
-.75
-1
LOAD
V
(200 lb/V)
10 MIN, 0 S
4
8
12
16
10 MIN, 20 S
TIME

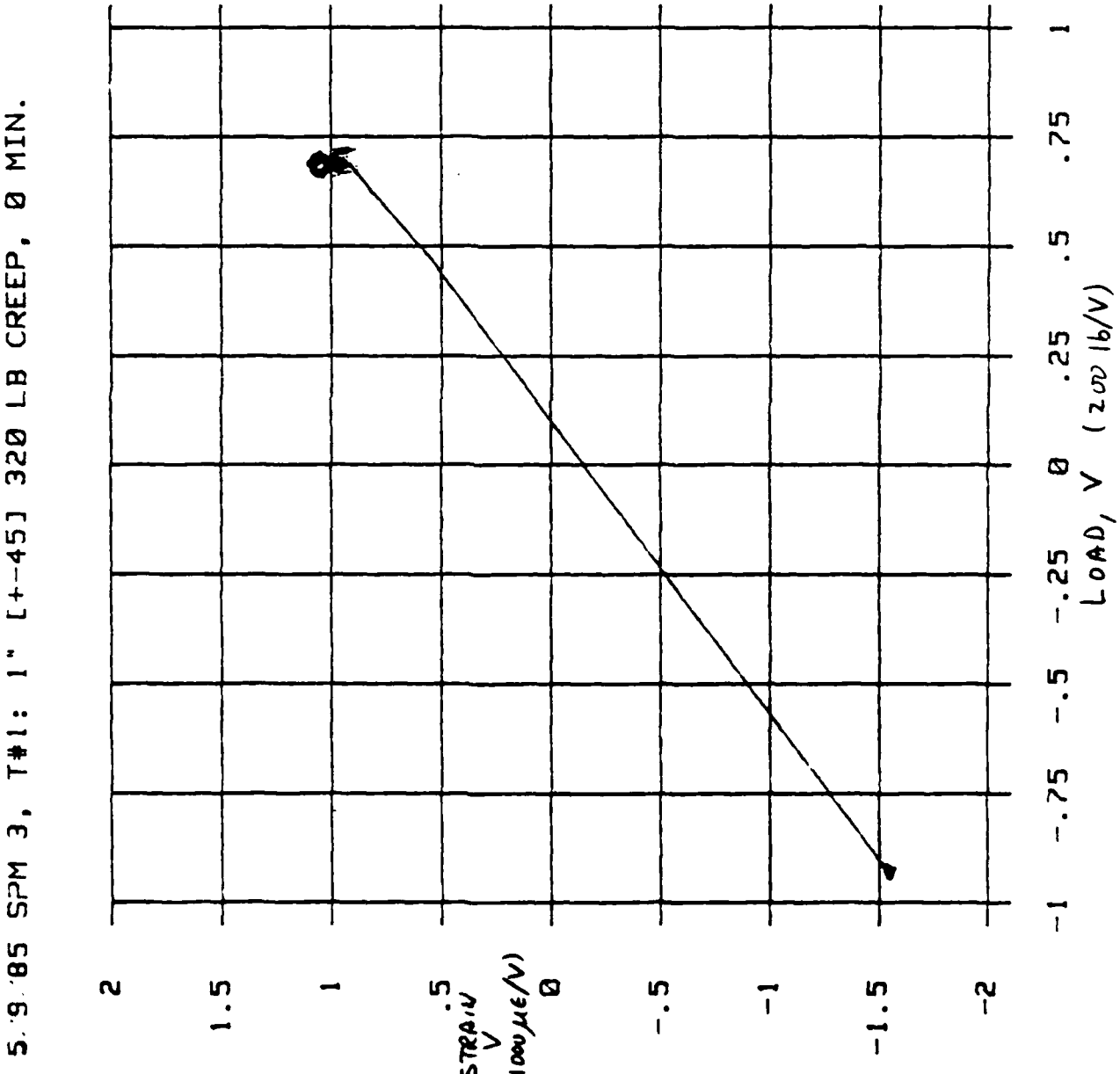
5.9.85 SPM 3, T#1: 1" [+-45] 320 LB CREEP, 0 MIN.
STRAIN V (100 με/V)
2
1.5
1
.5
0
-.5
-1
-1.5
-2
-1
-.75
-.5
-.25
0
.25
.5
.75
1
LOAD, V (200 lb/V)

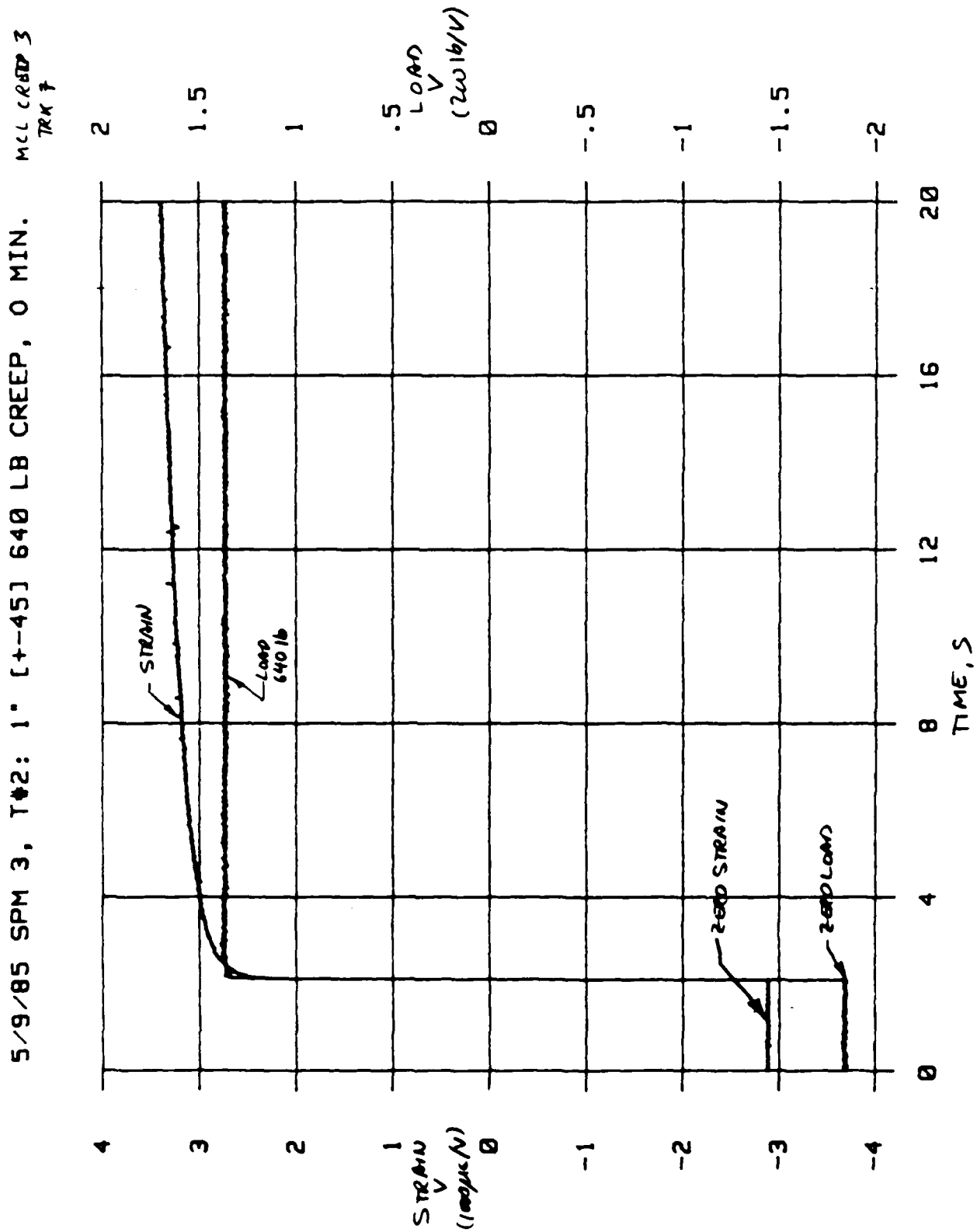
5/9/85 SPM 3, T#2: 1" [+-45] 640 LB CREEP, 0 MIN.
MCL CREEP 3
TRK #
STRAIN
LOAD 640 lb
ZERO STRAIN
ZERO LOAD
STRAIN V (microin/in)
LOAD V (2.5 lb/V)
TIME, S
4
3
2
1
0
-1
-2
-3
-4
2
1.5
1
.5
0
-.5
-1
-1.5
-2
0
4
8
12
16
20

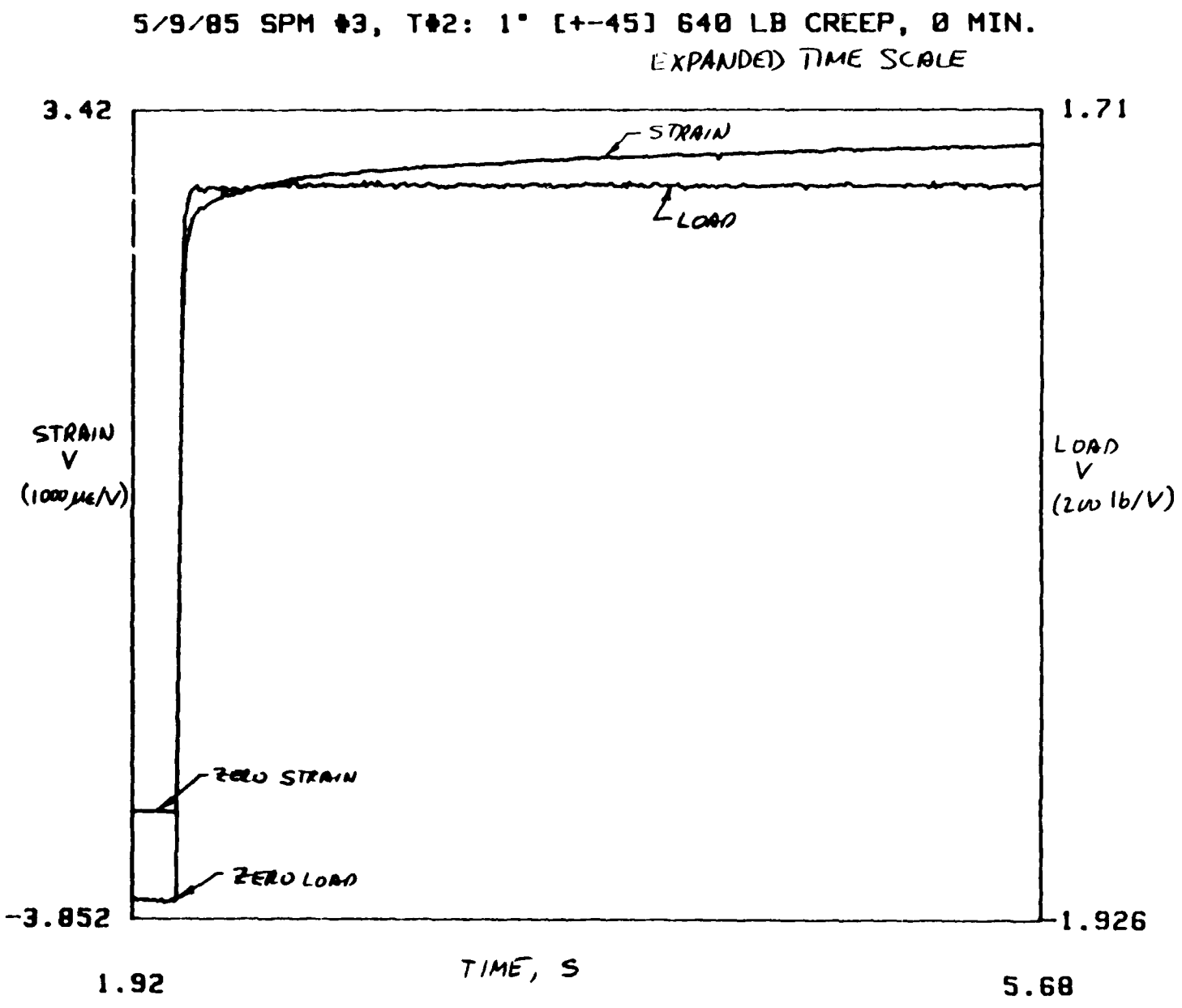
5/9/85 SPM #3, T#2: 1" [+-45] 640 LB CREEP, 0 MIN.
EXPANDED TIME SCALE
3.42
1.71
STRAIN
LOAD
STRAIN
V
(1000 με/V)
LOAD
V
(200 lb/V)
ZERO STRAIN
ZERO LOAD
-3.852
1.926
TIME, S
1.92
5.68

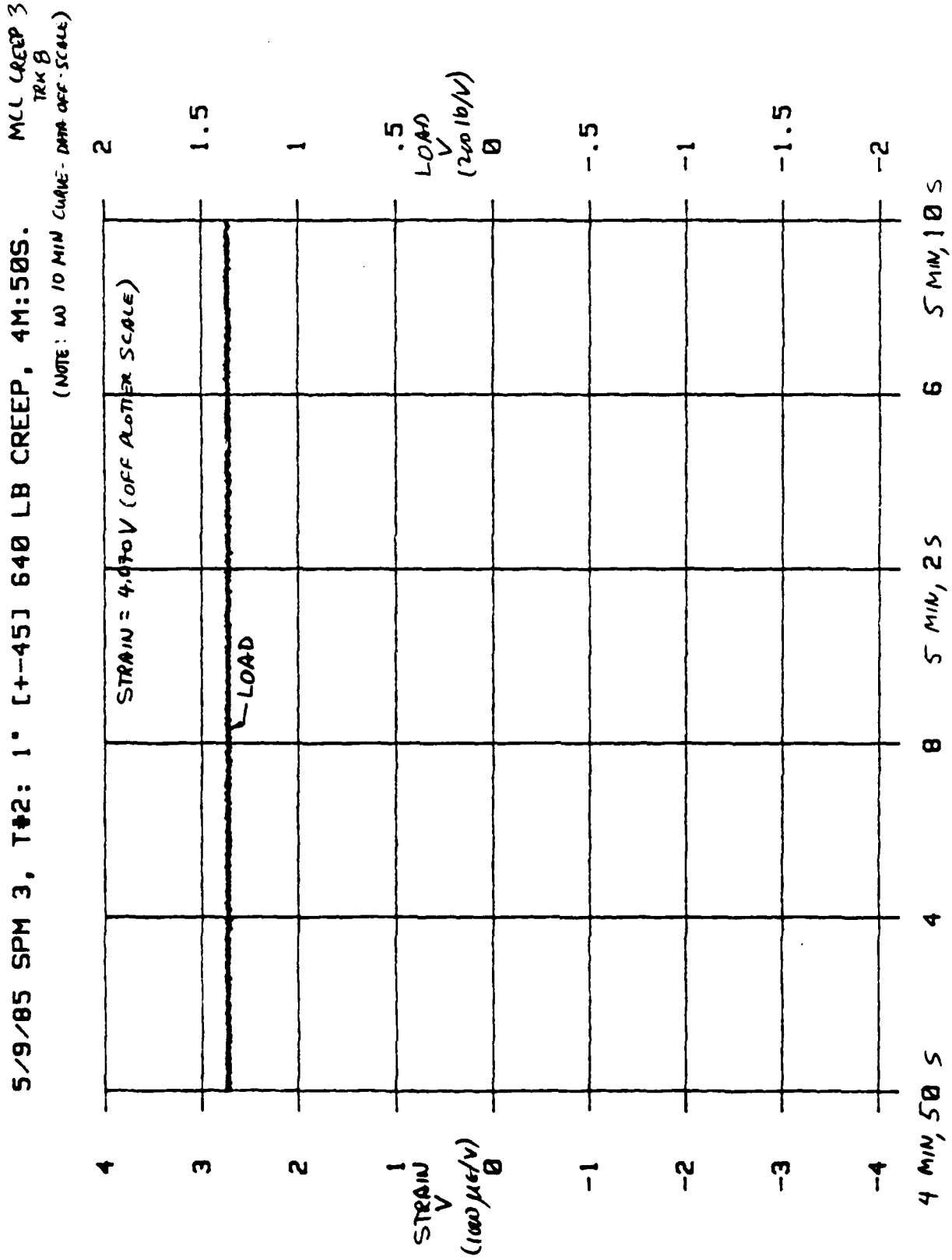
5/9/85 SPM 3, T#2: 1° [+-45] 640 LB CREEP, 4M:50S.
MCL CREEP 3
TRK B
(NOTE: W/ 10 MIN CURVE - DATA OFF-SCALE)
STRAIN = 4.070 V (OFF PLOTTER SCALE)
LOAD
STRAIN V (1000 με/V)
LOAD V (240 lb/V)
4 MIN, 50 S
5 MIN, 2 S
5 MIN, 10 S

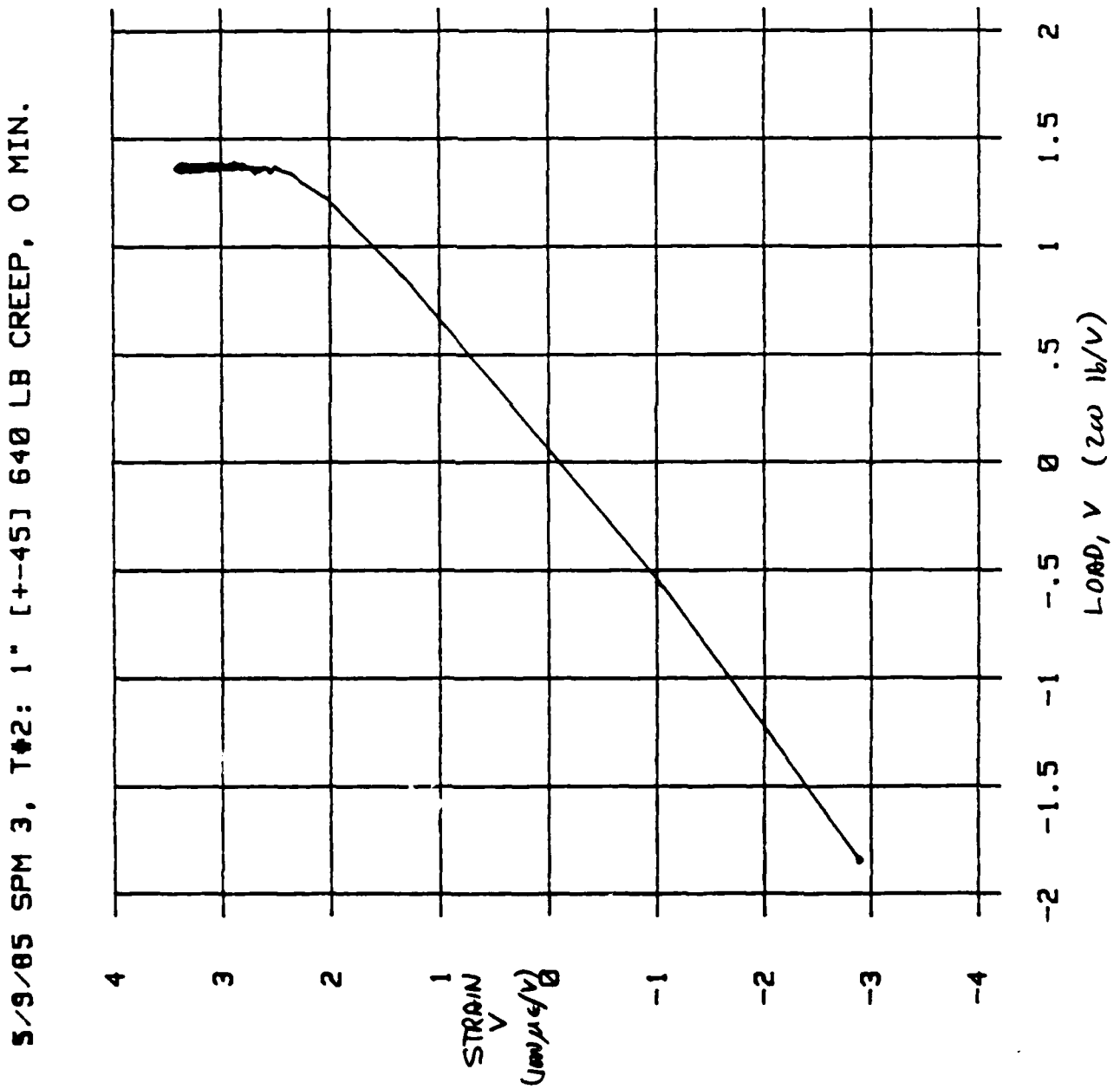
5/9/85 SPM 3, T#2: 1" [+-45] 640 LB CREEP, 0 MIN.
STRAIN V (μm/μ/V)
4
3
2
1
0
-1
-2
-3
-4
-2
-1.5
-1
-.5
0
.5
1
1.5
2
LOAD, V (2ω lb/V)

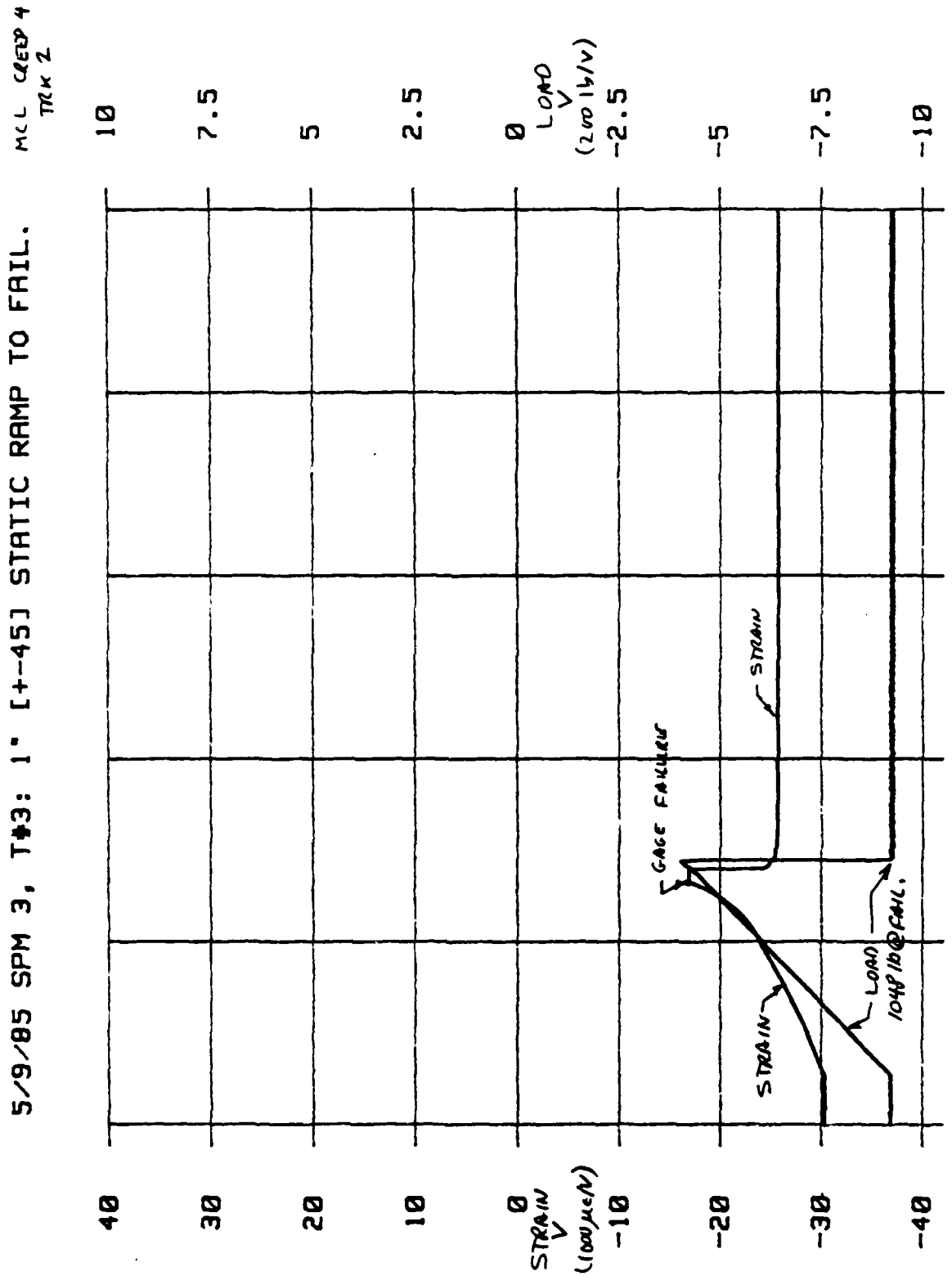
5/9/85 SPM 3, T#3: 1" [+-45] STATIC RAMP TO FAIL.
MCL CREP 4
TRK 2
STRAIN (1000 μ in/in)
LOAD (2000 lb/in)
TIME, 100 S
GAGE FAILURE
STRAIN
STRAIN
LOAD 10HP 10@FAIL.

5/9/85 SPM 3, T#3: 1° [+-45] STATIC RAMP TO FAIL.

EXPANDED SCALES

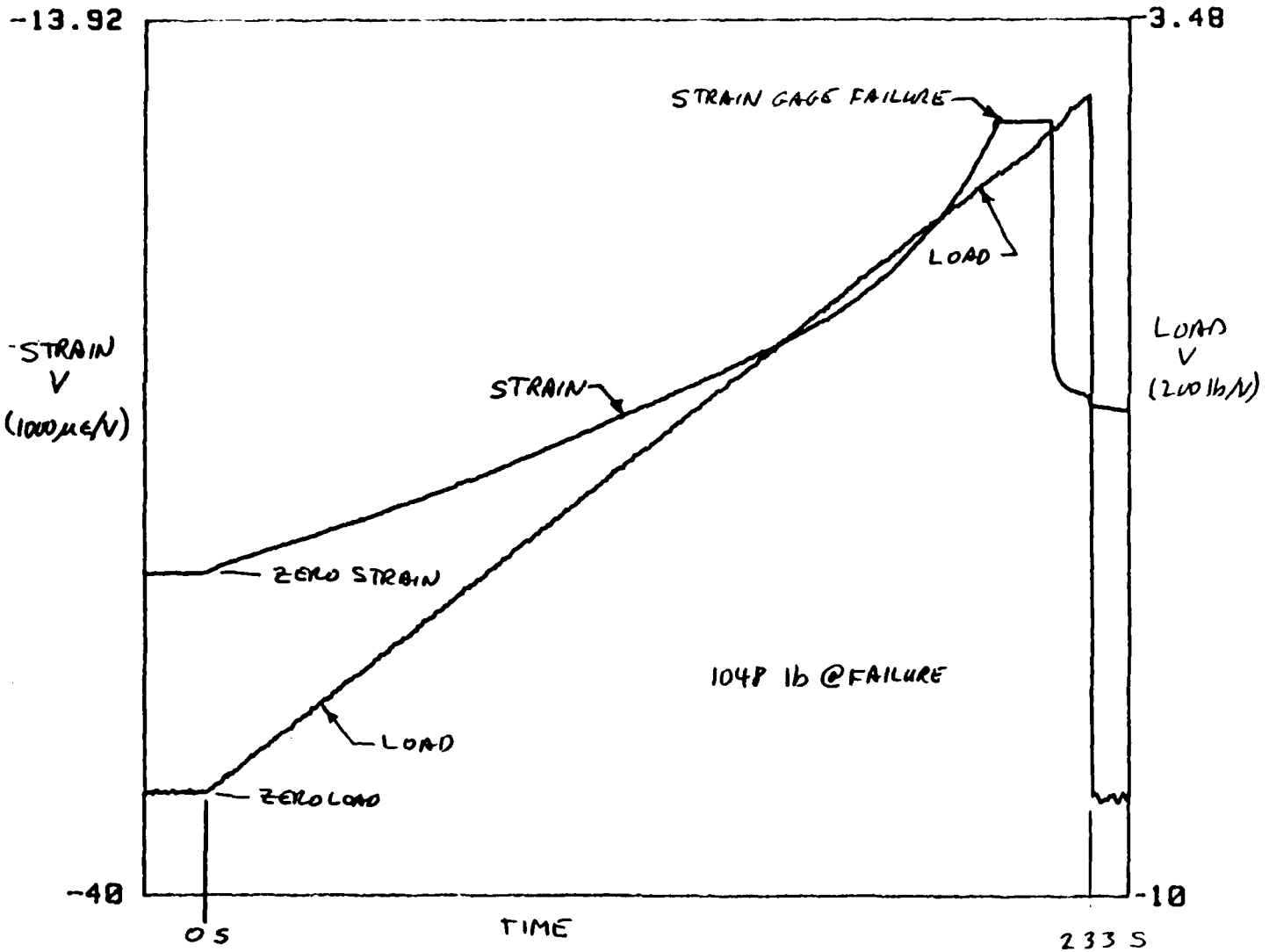

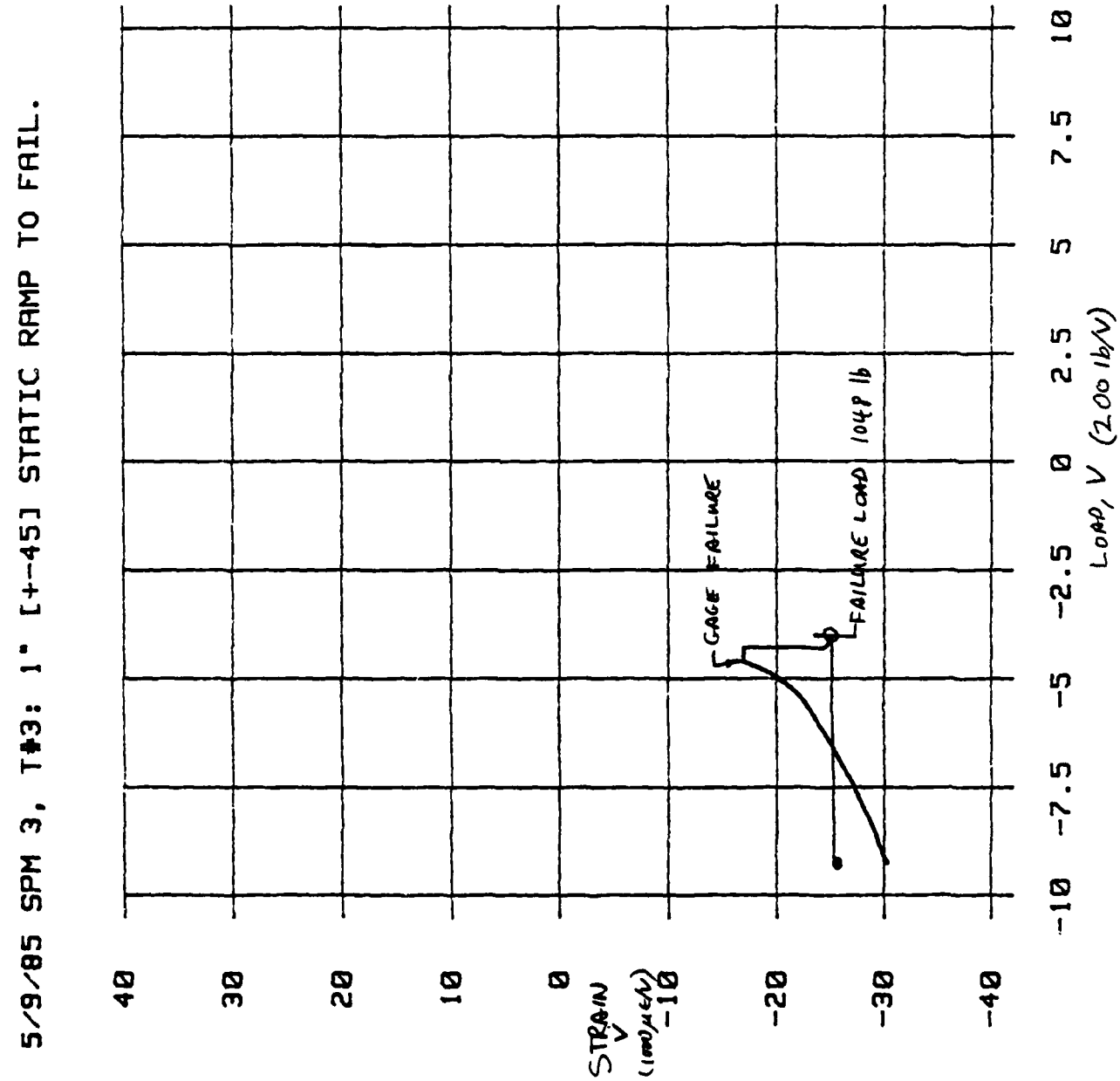
5/9/85 SPM 3, T#3: 1" [+-45] STATIC RAMP TO FAIL.
STRAIN V (1000 μ in/in)
40
30
20
10
0
-10
-20
-30
-40
-10
-7.5
-5
-2.5
0
2.5
5
7.5
10
LOAD, V (2.00 lb/V)
GAGE FAILURE
FAILURE LOAD 1049 lb

APPENDIX B. NONDIMENSIONAL IMPACTOR FORCE p* AND AXIAL BACK-SURFACE STRAIN e* VS. TIME t* FROM FINITE ELEMENT ANALYSIS OF IMPACTED AS-3501 COMPOSITE PLATES

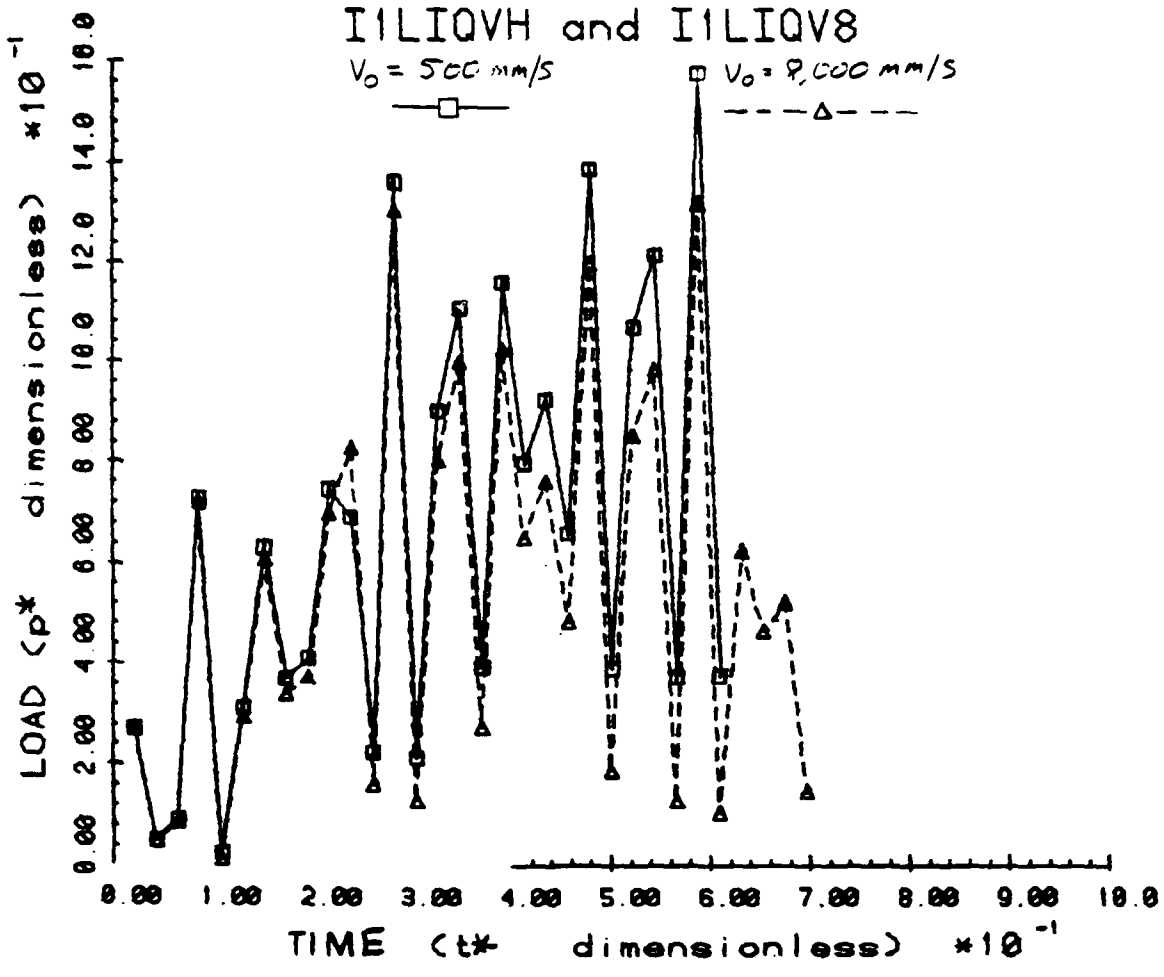
I1LIQVH and I1LIQV8
V_o = 500 mm/s
V_o = 8,000 mm/s
LOAD (p* dimensionless) *10^{-1}
0.00
2.00
4.00
6.00
8.00
10.0
12.0
14.0
16.0
0.00
1.00
2.00
3.00
4.00
5.00
6.00
7.00
8.00
9.00
10.0
TIME (t* dimensionless) *10^{-1}

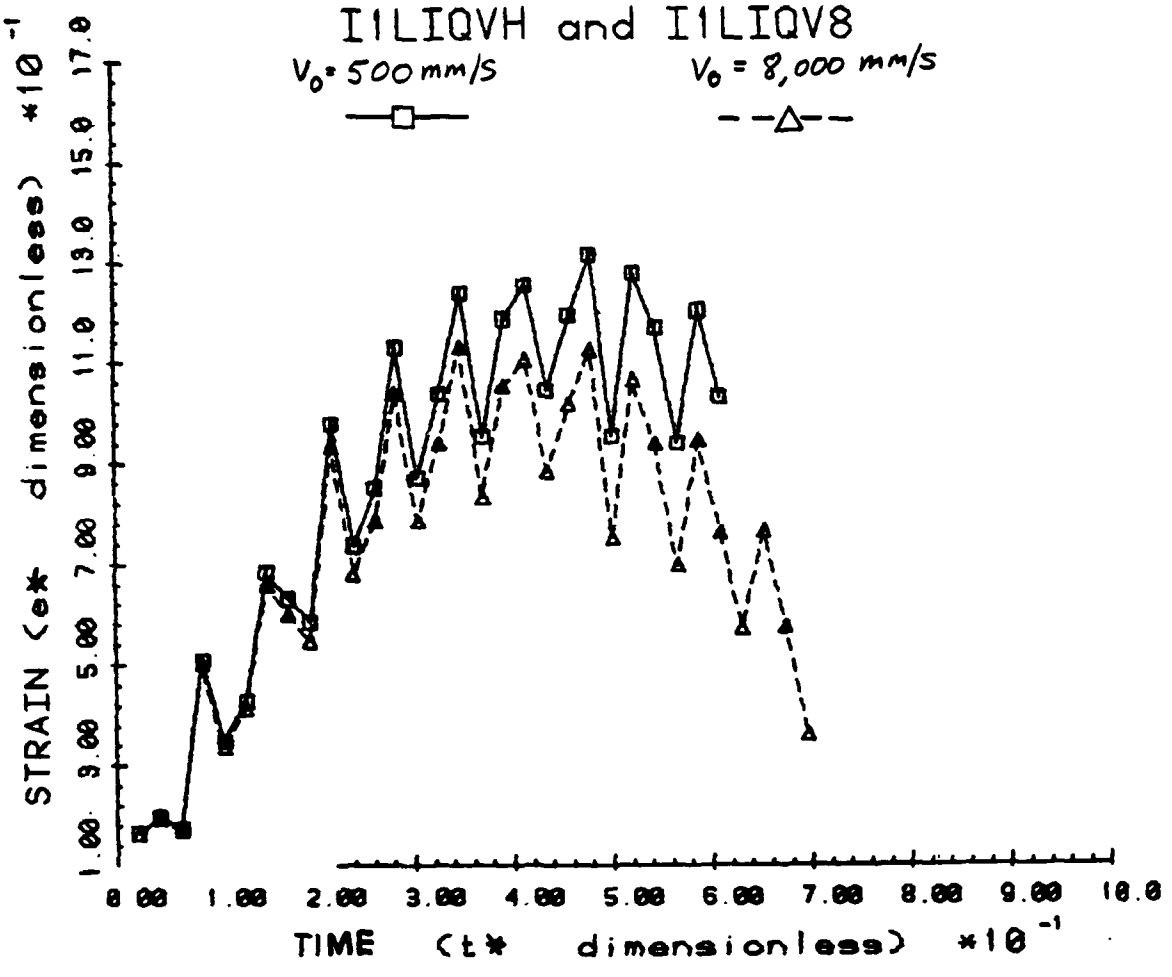
I1LIQVH and I1LIQV8
V_0 = 500 mm/s
V_0 = 8,000 mm/s
STRAIN (e* dimensionless) *10^-1
1.00
3.00
5.00
7.00
9.00
11.0
13.0
15.0
17.0
0.00
1.00
2.00
3.00
4.00
5.00
6.00
7.00
8.00
9.00
10.0
TIME (t* dimensionless) *10^-1

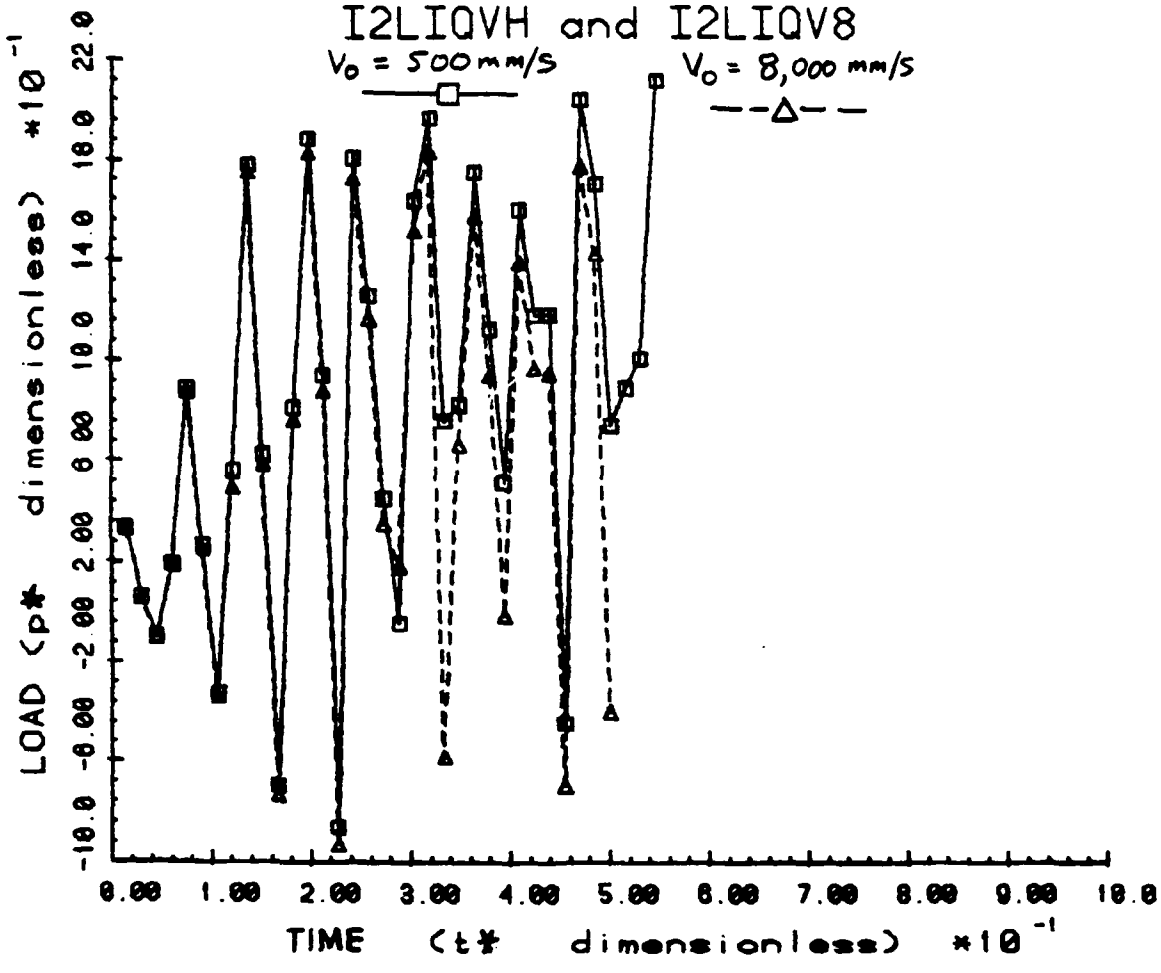
I2LIQVH and I2LIQV8
V_o = 500 mm/s
V_o = 8,000 mm/s
LOAD (p* dimensionless) *10^-1
-10.0
-6.00
-2.00
2.00
6.00
10.0
14.0
18.0
22.0
0.00
1.00
2.00
3.00
4.00
5.00
6.00
7.00
8.00
9.00
10.0
TIME (t* dimensionless) *10^-1

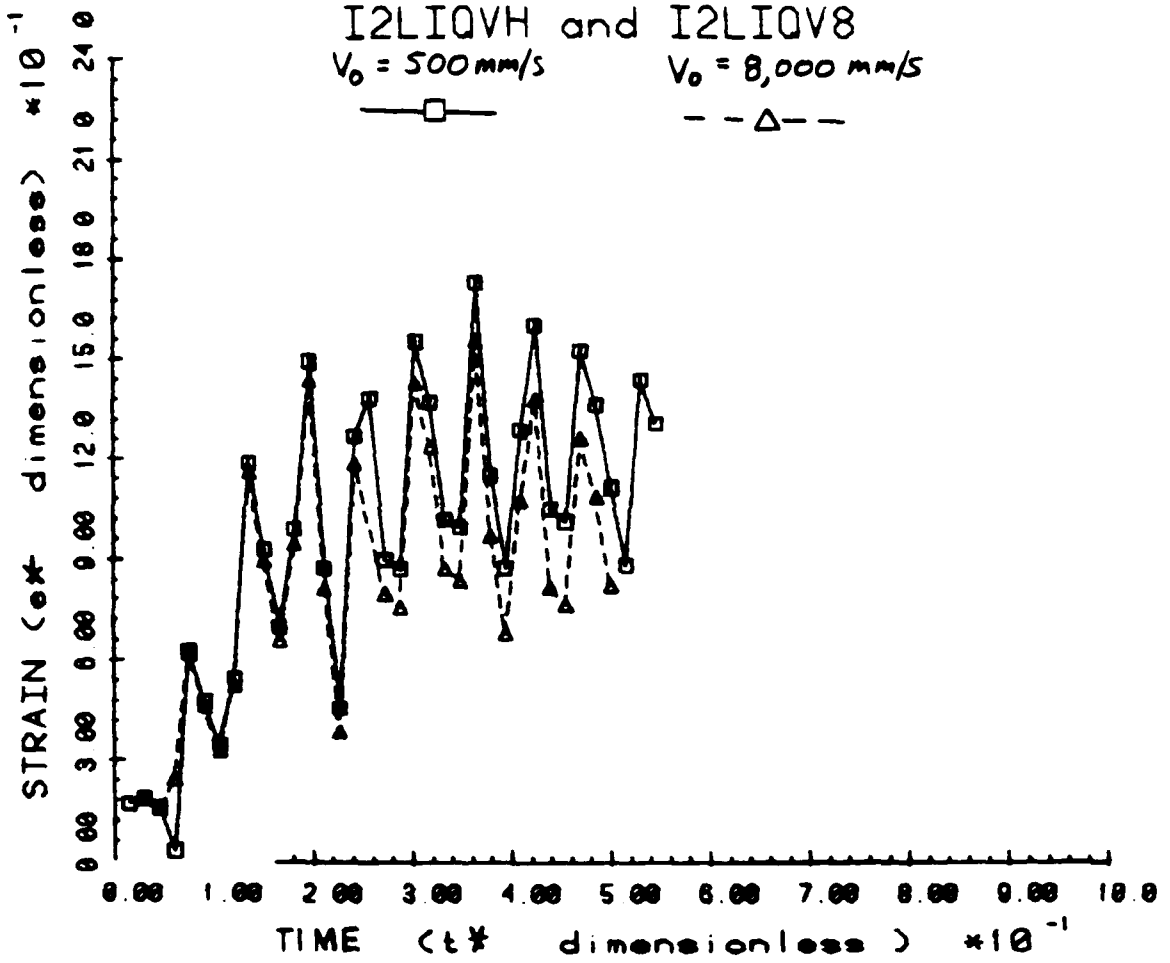
I2LIQVH and I2LIQV8
V_0 = 500 mm/s
V_0 = 8,000 mm/s
STRAIN (ε* dimensionless) *10^-1
0.00 3.00 6.00 9.00 12.0 15.0 18.0 21.0 24.0
0.00 1.00 2.00 3.00 4.00 5.00 6.00 7.00 8.00 9.00 10.0
TIME (t* dimensionless) *10^-1

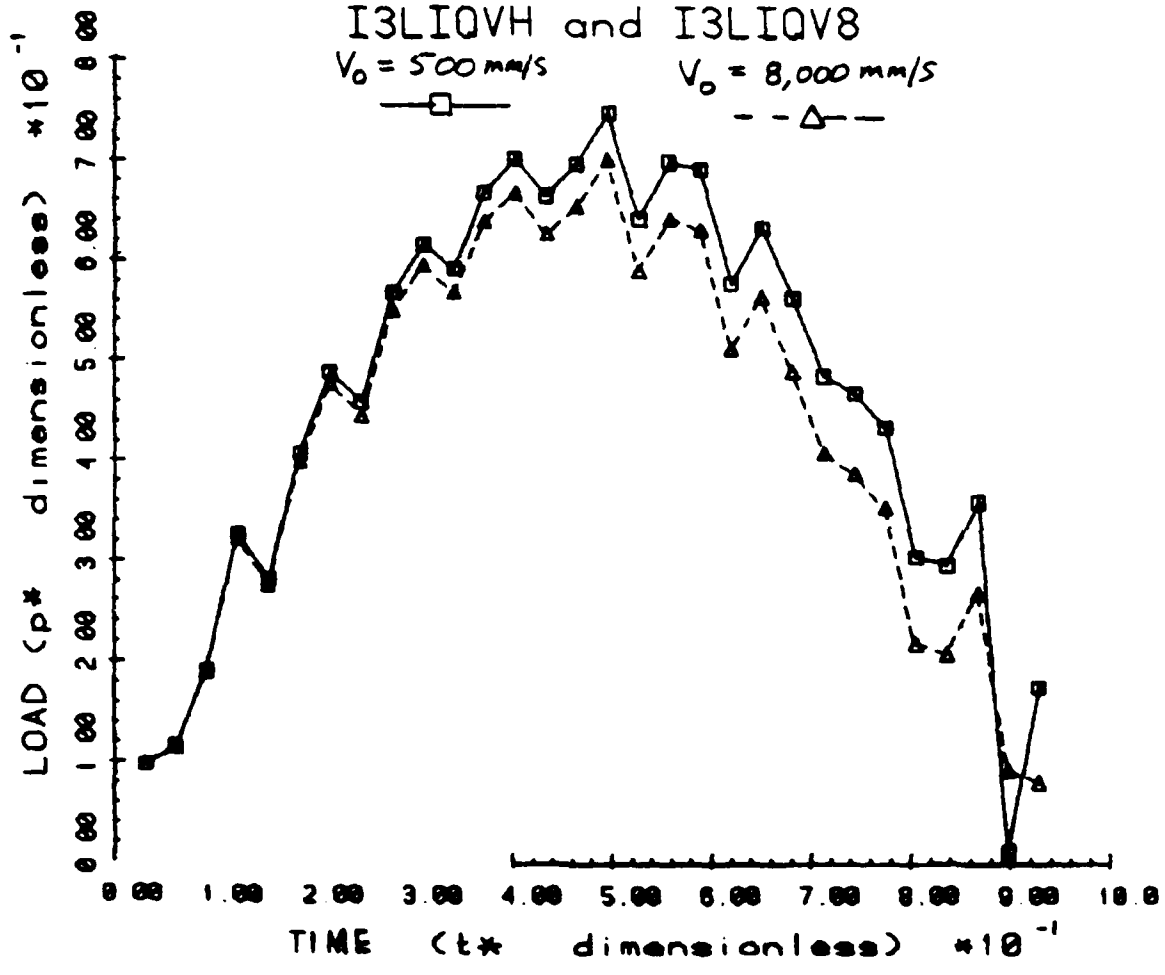
I3LIQVH and I3LIQV8
V_o = 500 mm/s
V_o = 8,000 mm/s
LOAD (p* dimensionless) *10^{-1}
0.00
1.00
2.00
3.00
4.00
5.00
6.00
7.00
8.00
9.00
10.0
TIME (t* dimensionless) *10^{-1}

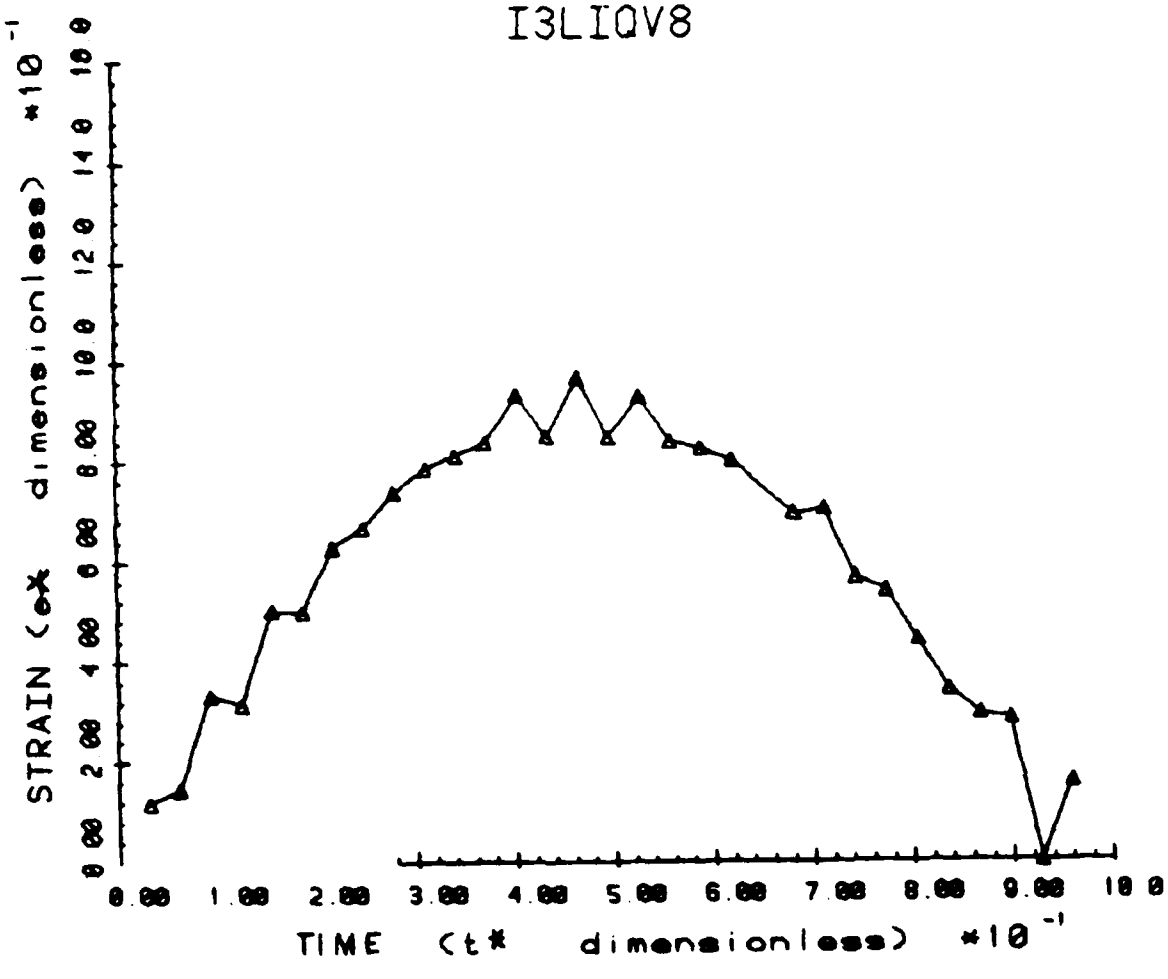
I3LIQV8
STRAIN (ε* dimensionless) *10^-1
0.00 2.00 4.00 6.00 8.00 10.0 12.0 14.0 16.0
0.00 1.00 2.00 3.00 4.00 5.00 6.00 7.00 8.00 9.00 10.0
TIME (t* dimensionless) *10^-1

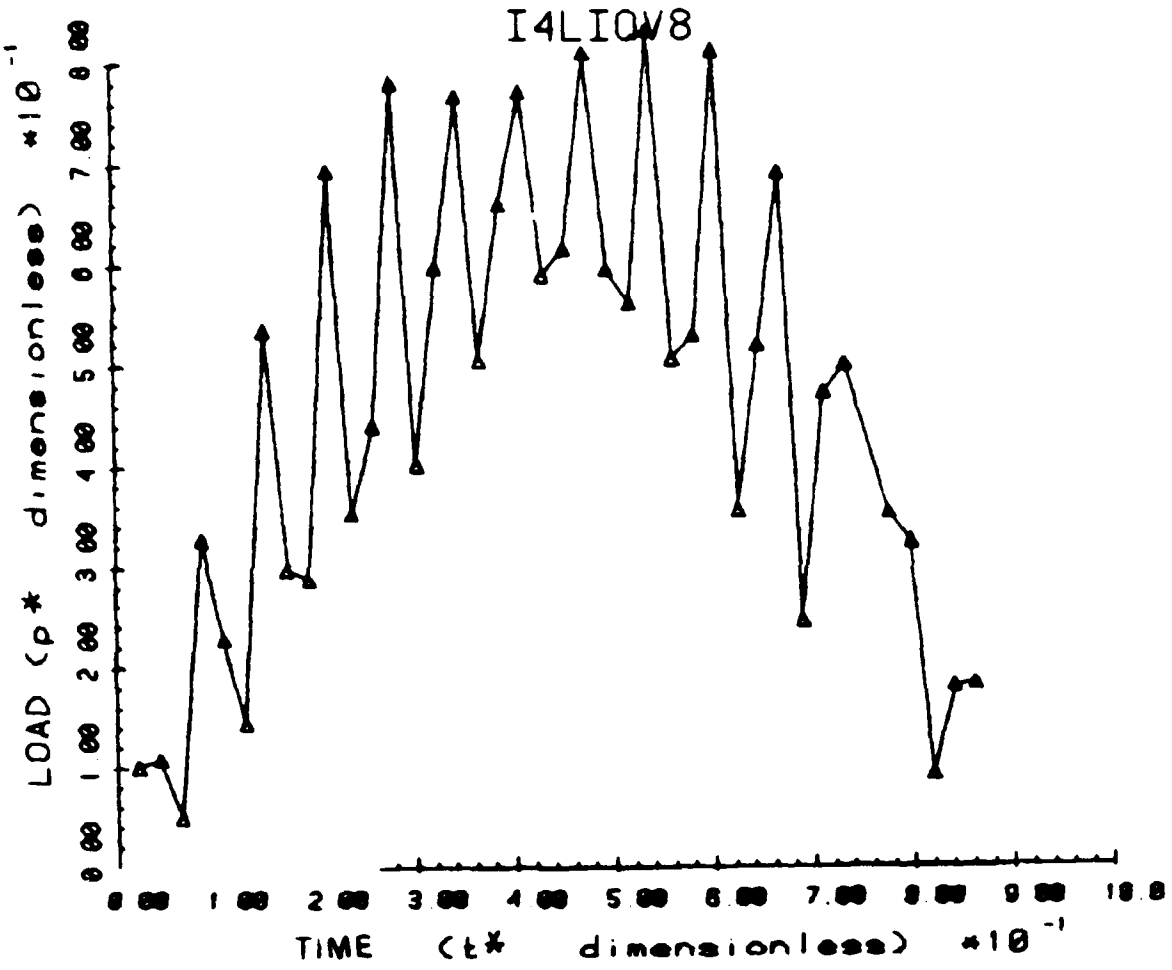
I4LIOV8
LOAD (p* dimensionless) *10^-1
0.00
1.00
2.00
3.00
4.00
5.00
6.00
7.00
8.00
TIME (t* dimensionless) *10^-1
1.00
2.00
3.00
4.00
5.00
6.00
7.00
8.00
9.00
10.0

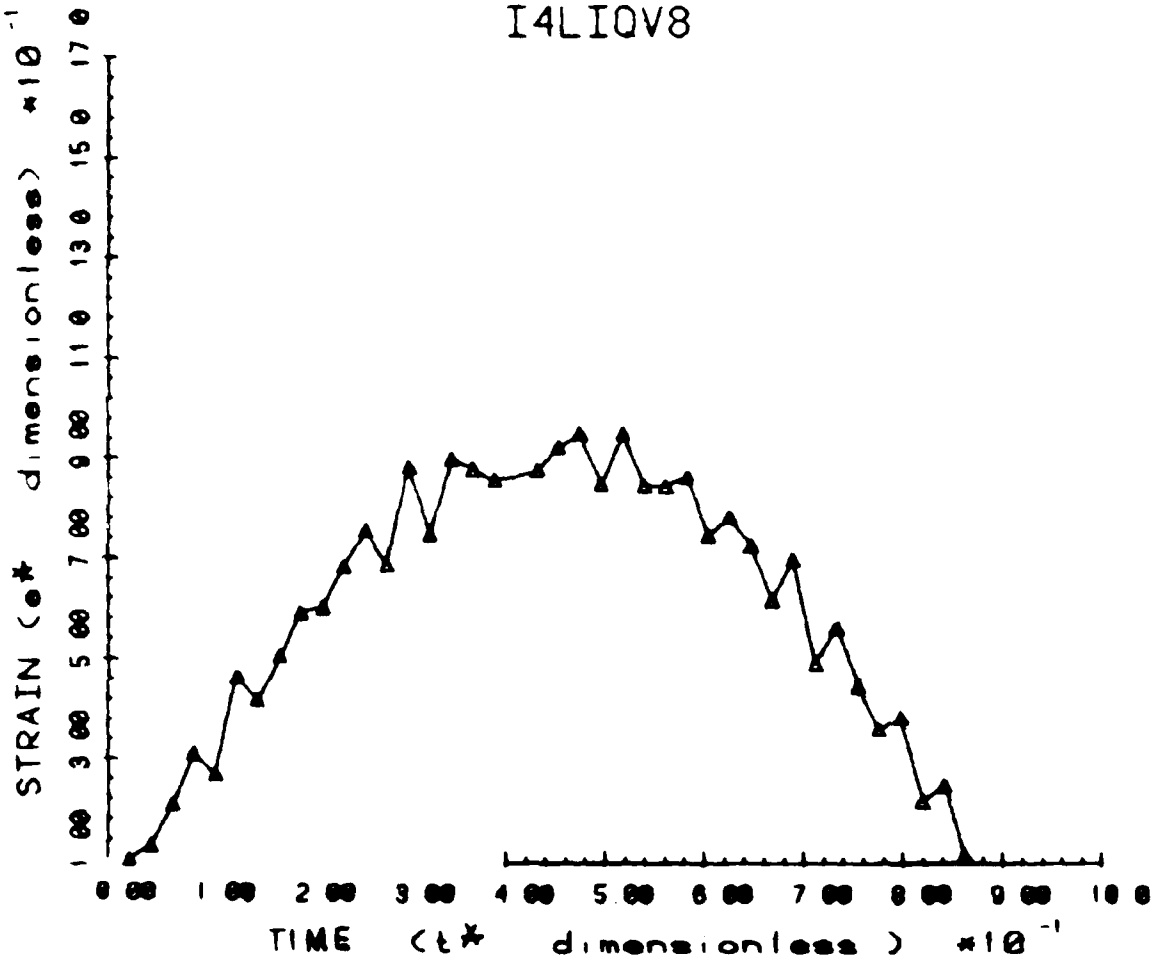
I4LIQV8
STRAIN (e* dimensionless) *10^-1
1.00 3.00 5.00 7.00 9.00 11.0 13.0 15.0 17.0
0.00 1.00 2.00 3.00 4.00 5.00 6.00 7.00 8.00 9.00 10.0
TIME (t* dimensionless) *10^-1

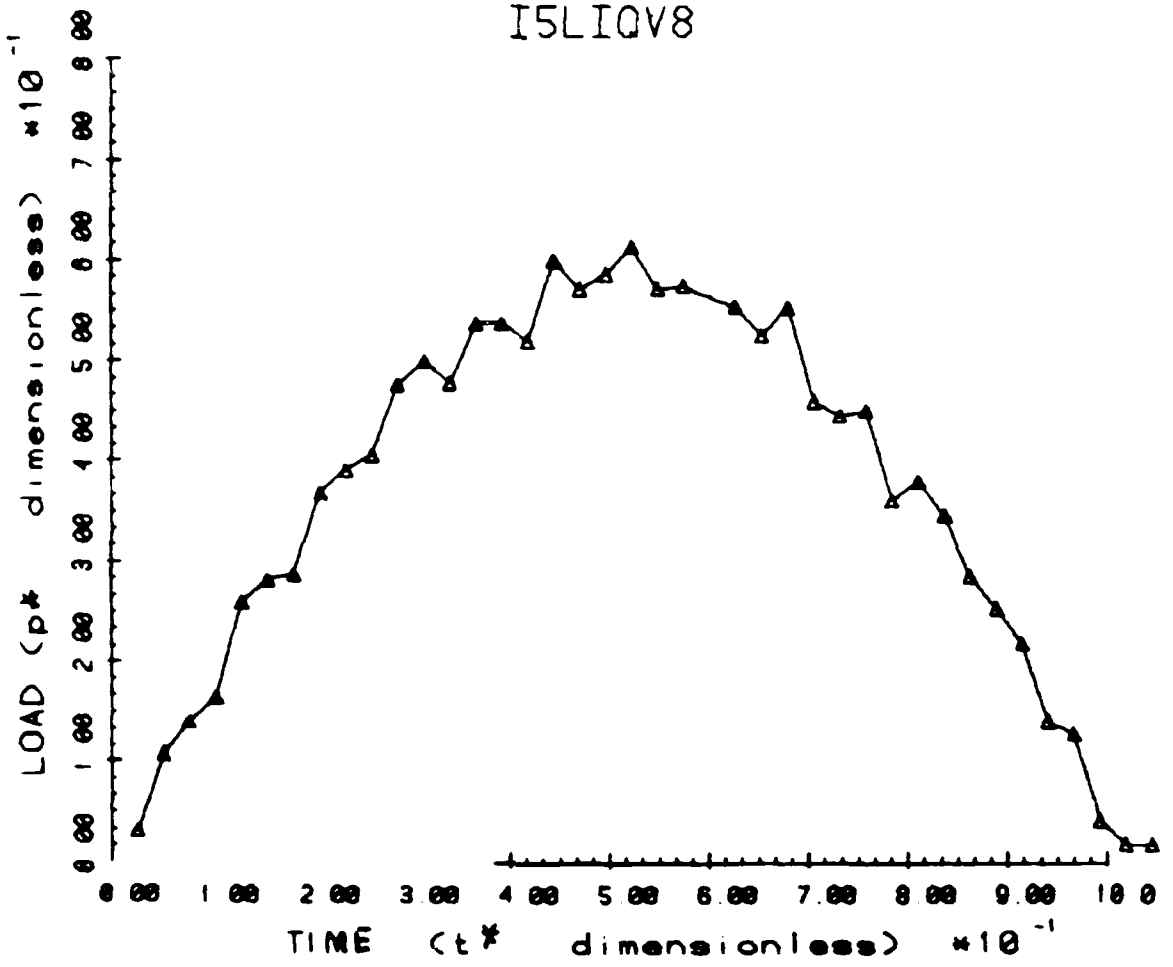
I5LIQV8
LOAD (p* dimensionless) *10^-1
0.00
1.00
2.00
3.00
4.00
5.00
6.00
7.00
8.00
0.00
1.00
2.00
3.00
4.00
5.00
6.00
7.00
8.00
9.00
10.0
TIME (t* dimensionless) *10^-1

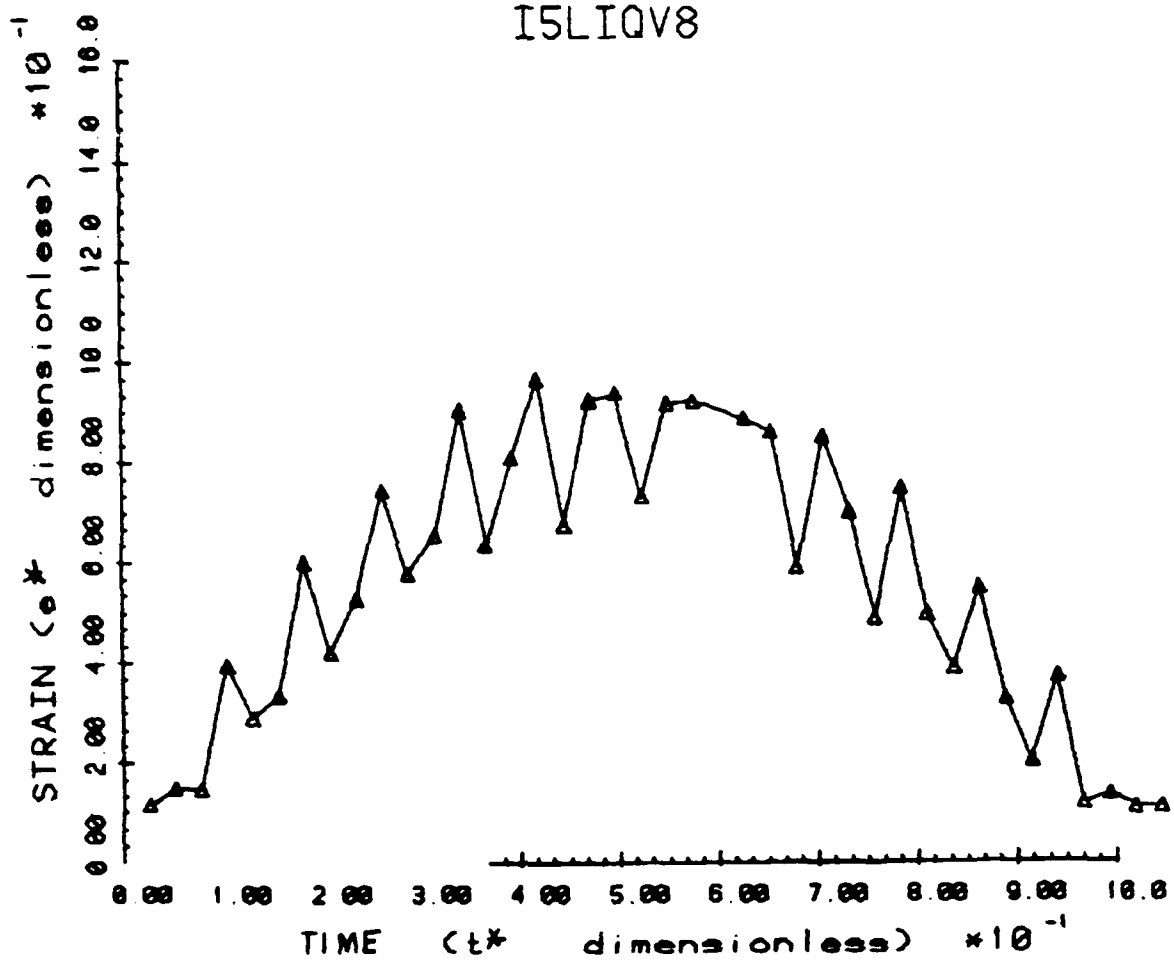
I5LIQV8
STRAIN (e* dimensionless) *10^-1
0.00 2.00 4.00 6.00 8.00 10.0 12.0 14.0 16.0
0.00 1.00 2.00 3.00 4.00 5.00 6.00 7.00 8.00 9.00 10.0
TIME (t* dimensionless) *10^-1

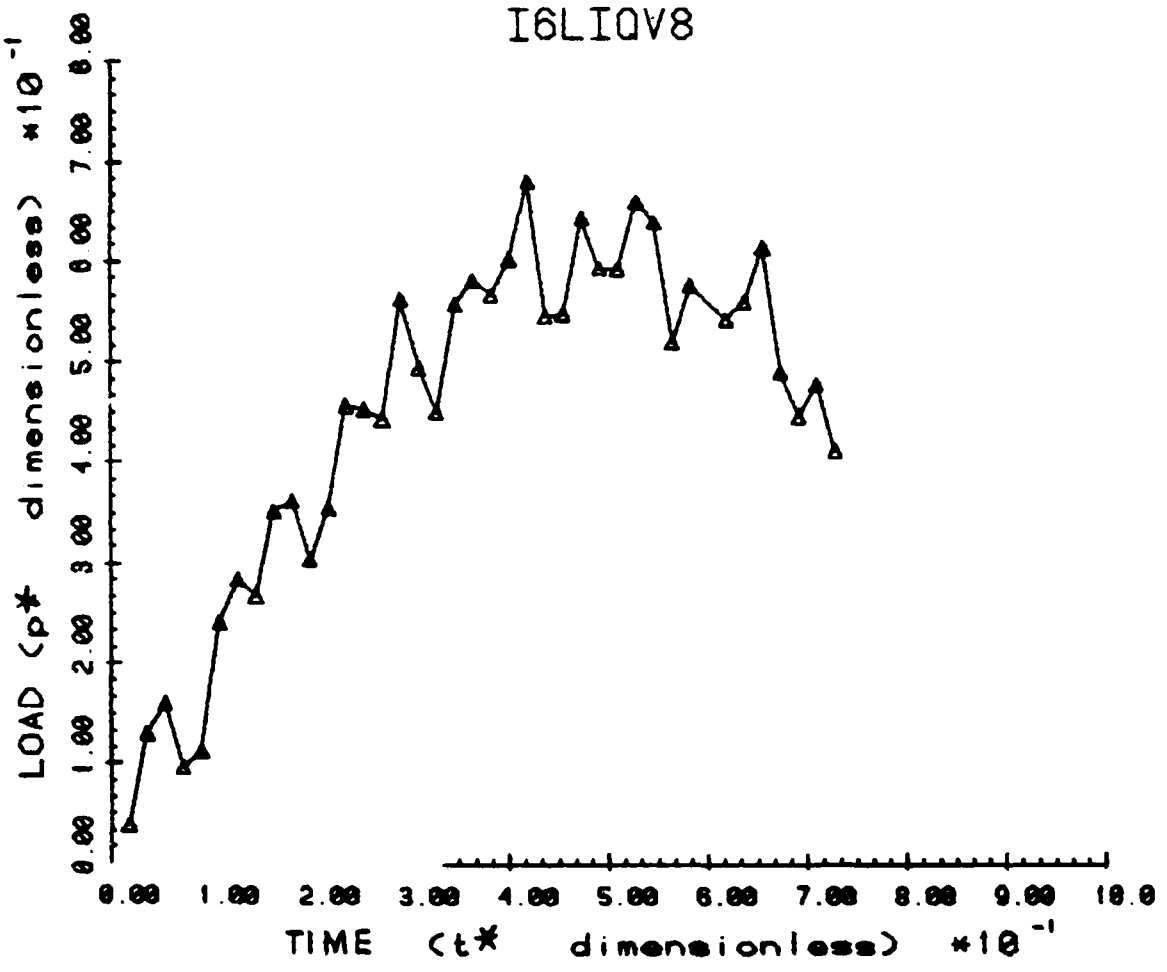
I6LIQV8
LOAD (p* dimensionless) *10^-1
0.00
1.00
2.00
3.00
4.00
5.00
6.00
7.00
8.00
0.00
1.00
2.00
3.00
4.00
5.00
6.00
7.00
8.00
9.00
10.0
TIME (t* dimensionless) *10^-1

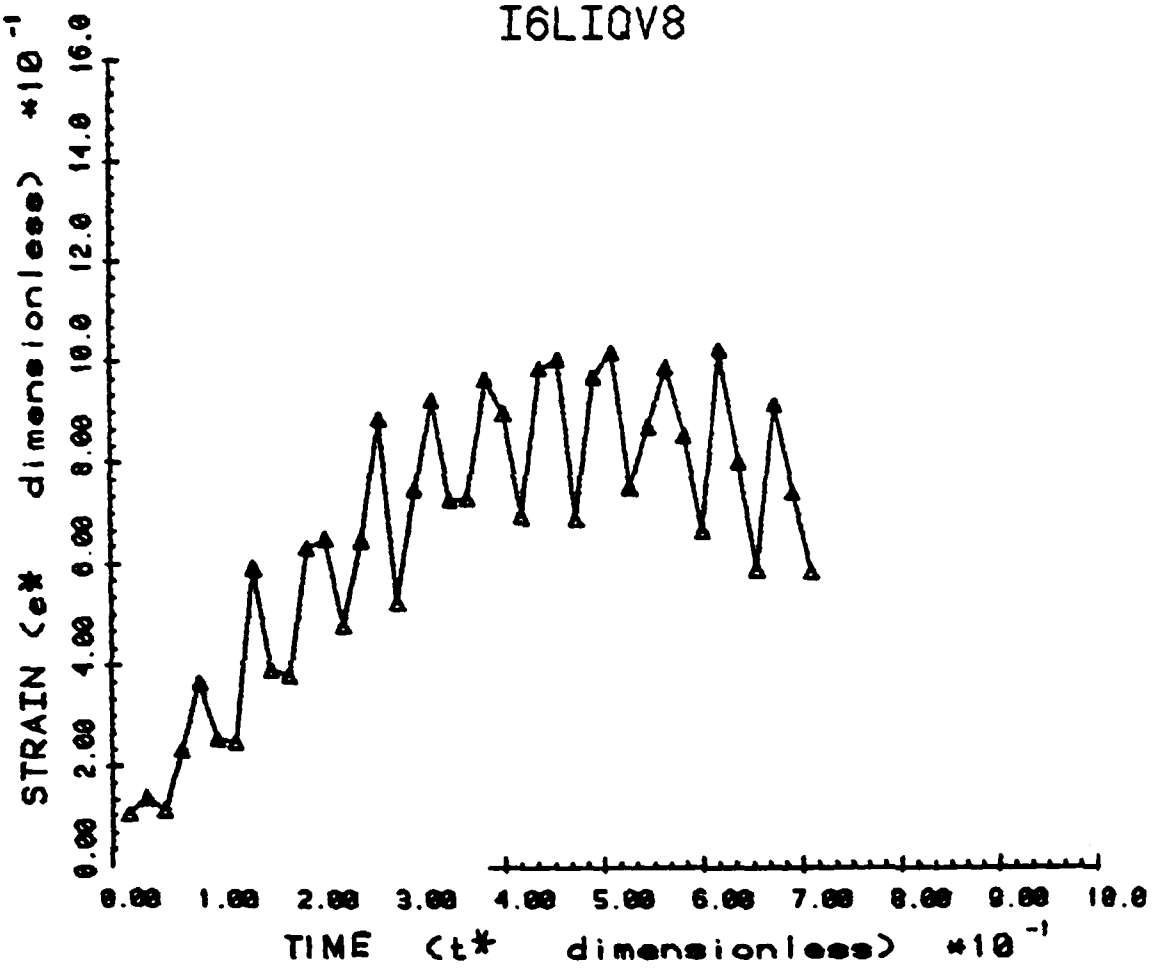
I6LIQV8
STRAIN (e* dimensionless) *10^-1
0.00 2.00 4.00 6.00 8.00 10.0 12.0 14.0 16.0
0.00 1.00 2.00 3.00 4.00 5.00 6.00 7.00 8.00 9.00 10.0
TIME (t* dimensionless) *10^-1

APPENDIX C. LIST OF PLATE IMPACT TESTS, TEST CONDITIONS, AND MAGNETIC DISK STORAGE DATA

TEST NO	DATA TAKEN **	LOAD CALIB (kN/div)	STRAIN CALIB (V/ue)	DROP HEIGHT (in,mm)	DATA DISK MBI*	TRACK NO	COMMENTS
I71	P,e	0.8	6.0	2.0, 51	2	1	
I72	P,e	0.8	6.0	2.0, 51	2	2	Rerun
I73	P,e	0.8	6.0	2.5, 76	2	3	
I74	P,e	0.8	6.0	2.5, 76	2	4	Rerun
I75	P,v	0.8	6.0	2.5, 76	2	5	
I76	P,v	0.8	6.0	5.0,127	2	6	
I77	P,e	0.8	6.0	5.0,127	2	7	
I78	P,e	0.8	6.0	2.0, 51	2	8	Rerun
I79	P,v	0.8	6.0	2.0, 51	3	1	Rerun
I710	P,v	0.8	6.0	2.5, 76	3	2	Rerun
I711	P,e	0.8	6.0	2.5, 76	3	3	Rerun
I712	P,e	0.8	6.0	5.0,127	3	4	Rerun
I713	P,v	0.8	6.0	5.0,127	3	5	Rerun
I81	P,v	0.8	6.0	2.0, 51	3	6	
I82	P,e	0.8	6.0	2.0, 51	3	7	
I83	P,e	0.8	6.0	4.0,102	3	8	
I84	P,v	0.8	6.0	4.0,102	4	1	
I85	P,v	0.8	6.0	4.0,102	4	2	Rerun
I86	P,e	0.8	6.0	4.0,102	4	3	Rerun
I51	P,e	0.8	6.0	2.0, 51	4	4	
I52	P,v	0.8	6.0	2.0, 51	4	5	
I53	P,v	0.8	6.0	3.5, 89	4	6	
I54	P,e	0.8	6.0	3.5, 89	4	7	
I61	P,e	0.8	6.0	1.0, 25	4	8	
I62	P,v	0.2	6.0	1.0, 25	5	1	
I63	P,v	0.2	6.0	1.5, 38	5	2	
I64	P,e	0.2	6.0	1.5, 38	5	3	
I65	P,e	0.2	6.0	2.0, 51	5	4	
I66	P,v	0.2	6.0	2.0, 51	5	5	
I31	P,v	0.2	6.0	1.0, 25	5	6	
I32	P,e	0.2	6.0	1.0, 25	5	7	
I33	P,e	0.2	6.0	1.7, 43	5	8	
I34	P,v	0.2	6.0	1.7, 43	6	1	
I35	P,v	0.2	6.0	2.0, 51	6	2	
I36	P,e	0.2	6.0	2.0, 51	6	3	
I41	P,e	0.2	6.0	0.5, 13	6	4	
I42	P,v	0.2	6.0	0.5, 13	6	5	
I43	P,v	0.2	6.0	1.0, 25	6	6	
I44	P,e	0.2	6.0	1.0, 25	6	7	
I11	P,e	0.2	6.0	2.0, 51	6	8	***
I12	P,v	0.2	6.0	2.0, 51	7	1	***
I13	P,v	0.2	6.0	3.5, 89	7	2	***
I14	P,e	0.2	6.0	3.5, 89	7	3	***
I15	P,e	0.2	6.0	3.5, 89	7	4	Rerun***
I16	P,v	0.2	6.0	3.5, 89	7	5	Rerun***
I17	P,v	0.2	6.0	4.25,108	7	6	***
I18	P,e	0.2	6.0	4.25,108	7	7	***
I19	P,e	0.2	6.0	12.0,305	7	8	Grp
I110	P,e	0.2	6.0	12.0,305	8	1	Rerun,Grp
I111	P,e	0.2	6.0	36.0,914	8	2	Fail,Grp

TEST NO	DATA TAKEN **	LOAD CALIB (kN/div)	STRAIN CALIB (V/ue)	DROP HEIGHT (in,mm)	DATA DISK MBI*	TRACK NO	COMMENTS
I21	P,e	0.2	6.0	1.0, 25	8	3	***
I22	P,e	0.2	6.0	1.0, 25	8	4	Rerun***
I23	P,v	0.2	6.0	1.0, 25	8	5	***
I24	P,v	0.2	6.0	2.0, 51	8	6	***
I25	P,e	0.2	6.0	2.0, 51	8	7	***
I26	P,e	0.2	6.0	4.0,102	8	8	***
I27	P,v	0.2	6.o	4.0,102	9	1	Grp
I28	P,e	0.2	6.0	12.0,305	9	2	Grp

* Data disks are labelled "McLaughlin Beam Impact (disk no.)"

** P,e - impact load and plate strain. P,v - impact load and impactor initial velocity.

*** Data for these specimens suspect due to support slippage.

Grp - Large deflections and support slippage allowed plate to be fully dislodged from grips.

Fail - Flexural failure observed in specimen.

APPENDIX D. DIMENSIONAL PLOTS OF GRAPHITE/EPOXY PLATE IMPACT TEST RESULTS

INSTRUMENTED IMPACT TEST

I71LNG(I5B) 5/29/86 I2.2

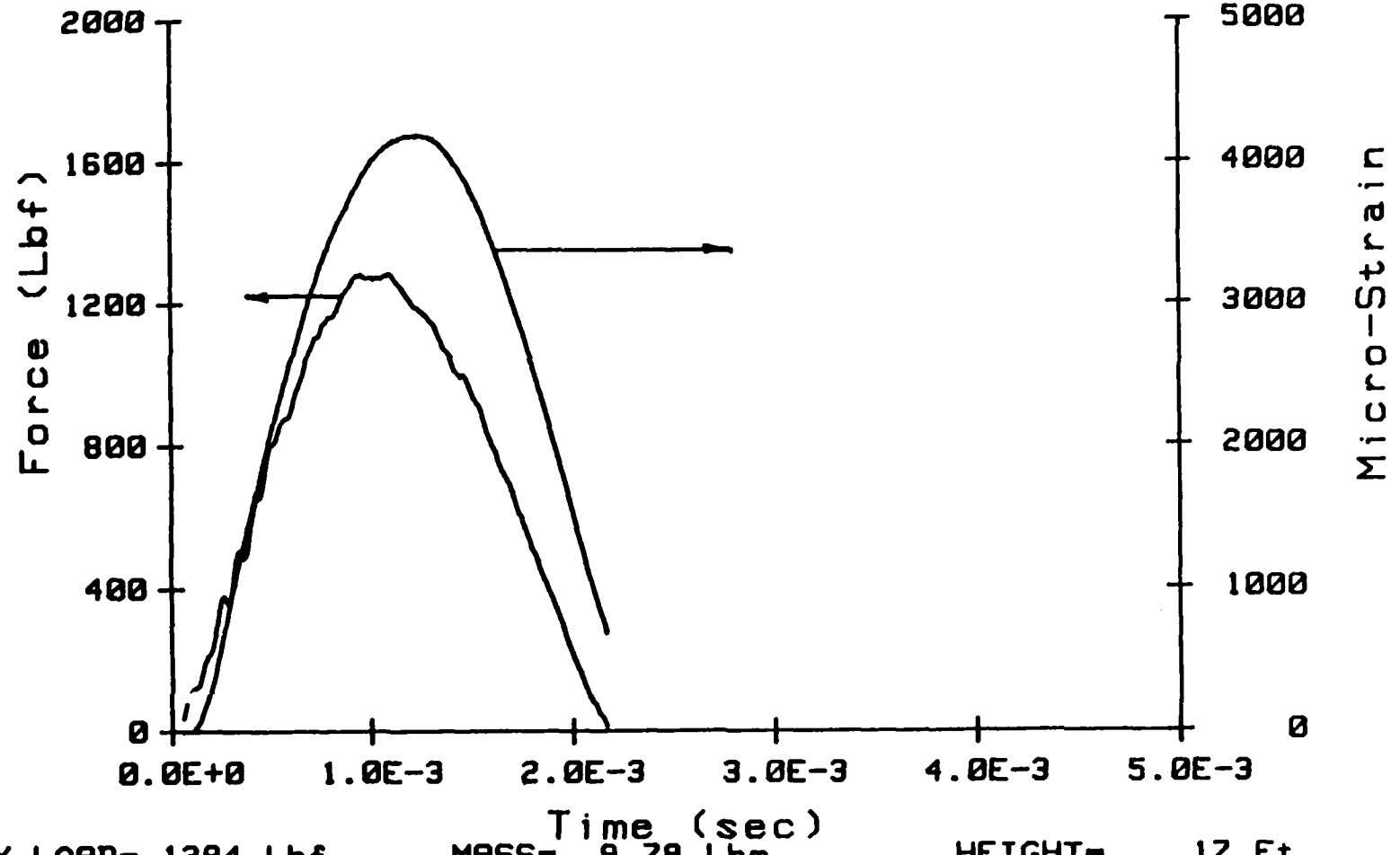

MAX LOAD= 1284 Lbf MASS= 9.78 Lbm HEIGHT= .17 Ft

MAX STRAIN= 4195 Micro inch/inch

RADIUS= .13 inch LOAD SCALE= .8KN/DIV

NADC-87106-60

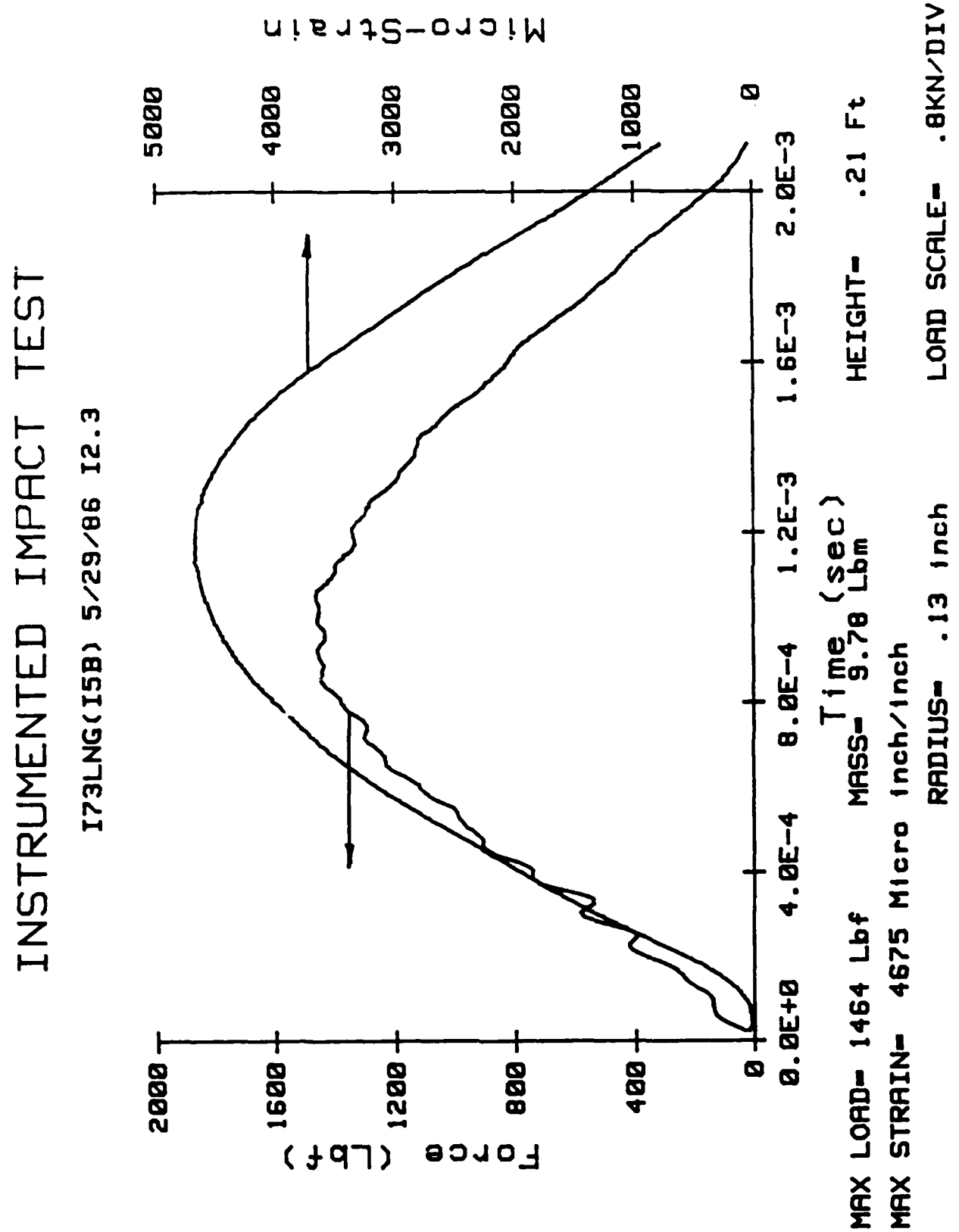
INSTRUMENTED IMPACT TEST
I73LNG(I5B) 5/29/86 I2.3
Force (Lbf)
2000
1600
1200
800
400
0
Micro-Strain
5000
4000
3000
2000
1000
0
0.0E+0
4.0E-4
8.0E-4
1.2E-3
1.6E-3
2.0E-3
Time (sec)
MAX LOAD= 1464 Lbf
MASS= 9.78 Lbm
HEIGHT= .21 Ft
MAX STRAIN= 4675 Micro inch/inch
RADIUS= .13 inch
LOAD SCALE= .8KN/DIV

INSTRUMENTED IMPACT TEST

I74LNG(I5B) 5/29/86 I2.4

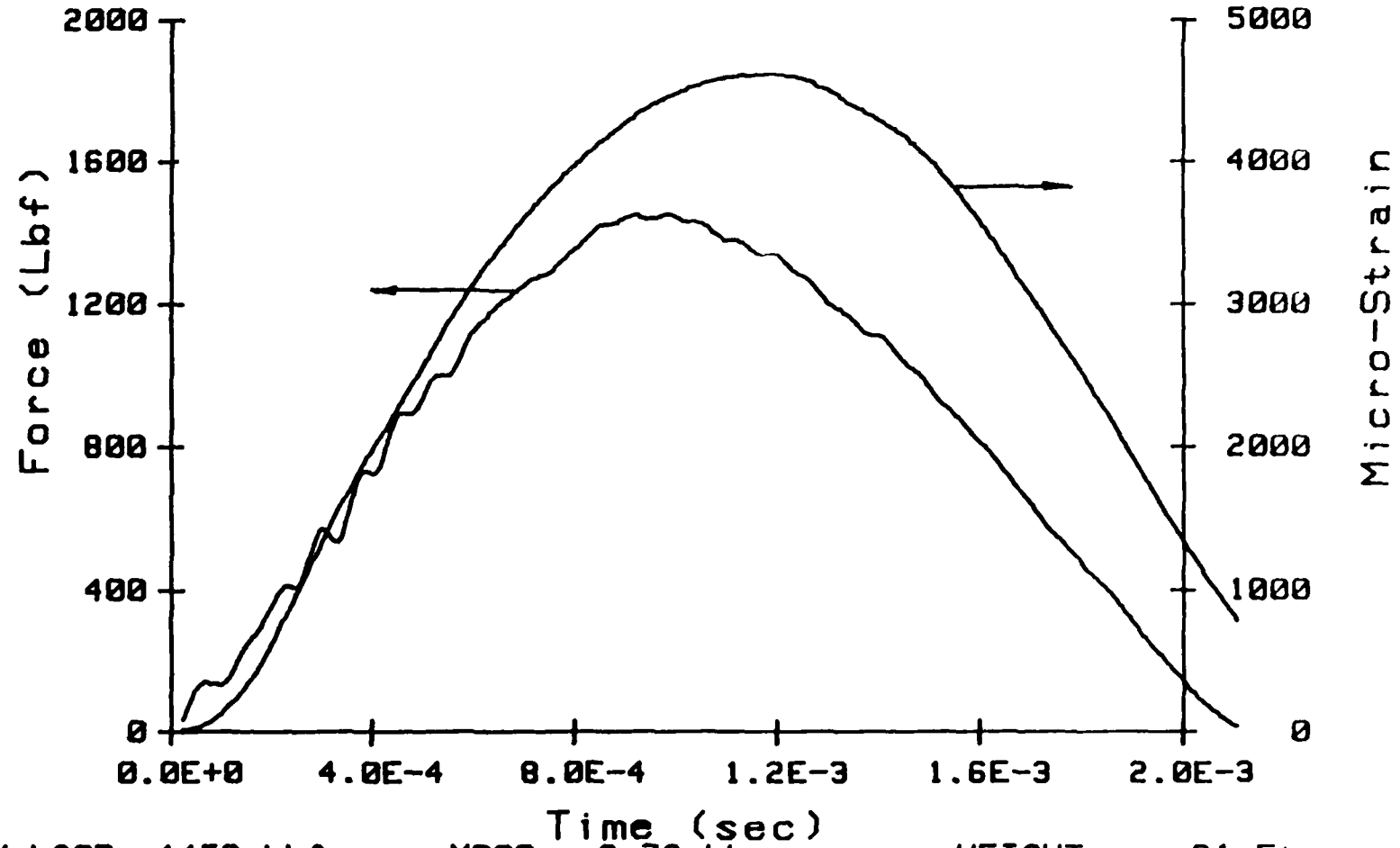

MAX LOAD= 1453 Lbf MASS= 9.78 Lbm HEIGHT= .21 Ft

MAX STRAIN= 4620 Micro inch/inch

RADIUS= .13 inch LOAD SCALE= .8KN/DIV

NADC-87106-60

INSTRUMENTED IMPACT TEST

I75LNG(I5B) 5/29/86

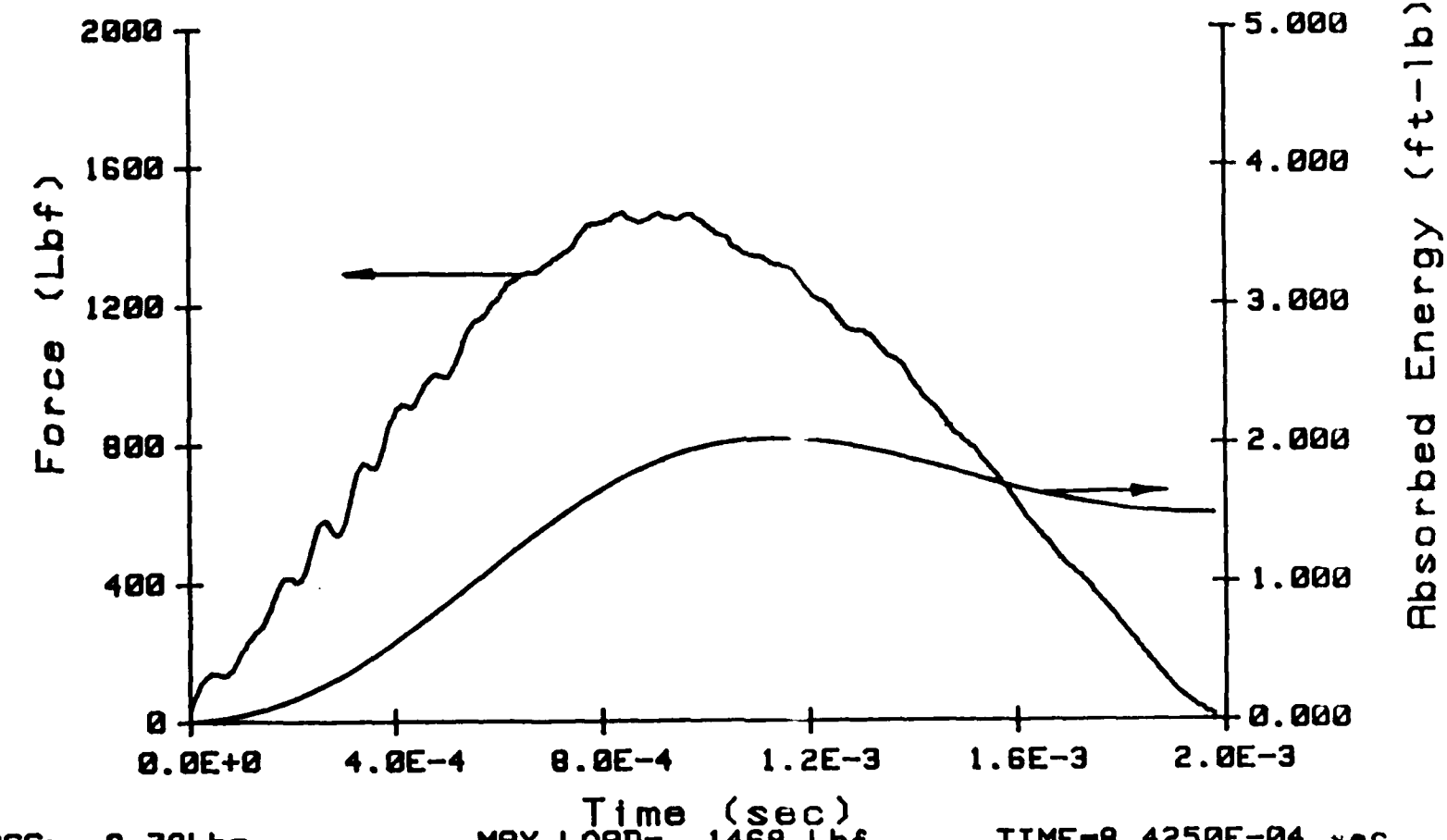

MASS= 9.78Lbm
Vo= 3.64Ft/sec
Eo= 2.02Ft-Lb

MAX LOAD= 1468 Lbf
Displacement= .0291inch
E absorbed= 1.77Ft-Lb

TIME=8.4250E-04 sec

MCBI2.5

INSTRUMENTED IMPACT TEST

I75LNG(I5B) 5/29/86

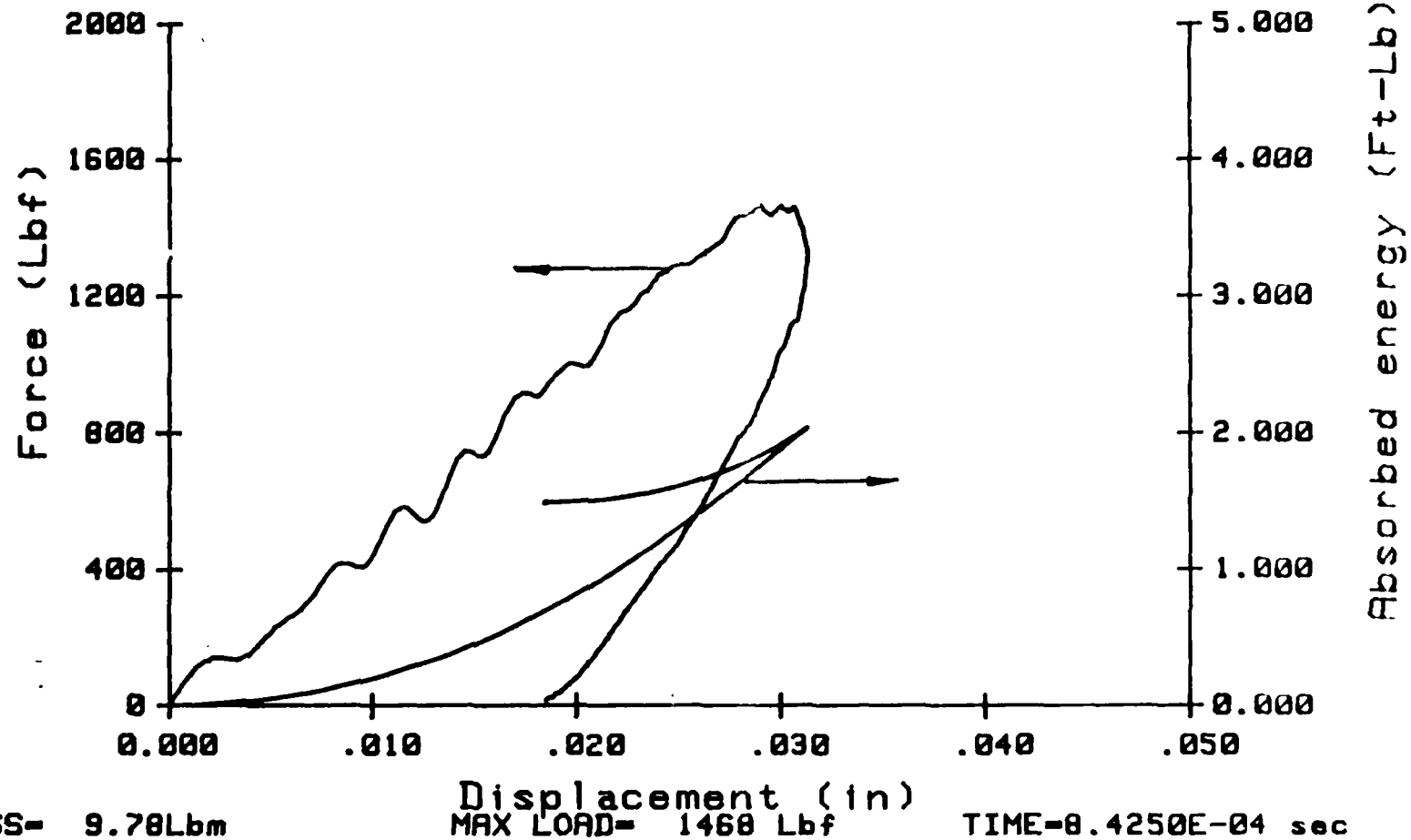

MASS= 9.78Lbm
Vo= 3.64Ft/sec
Eo= 2.02Ft-Lb

MAX LOAD= 1468 Lbf
Displacement= .0291inch
E absorbed= 1.77Ft-Lb

TIME=8.4250E-04 sec

INSTRUMENTED IMPACT TEST

I76LNG(ISB) 5/29/86

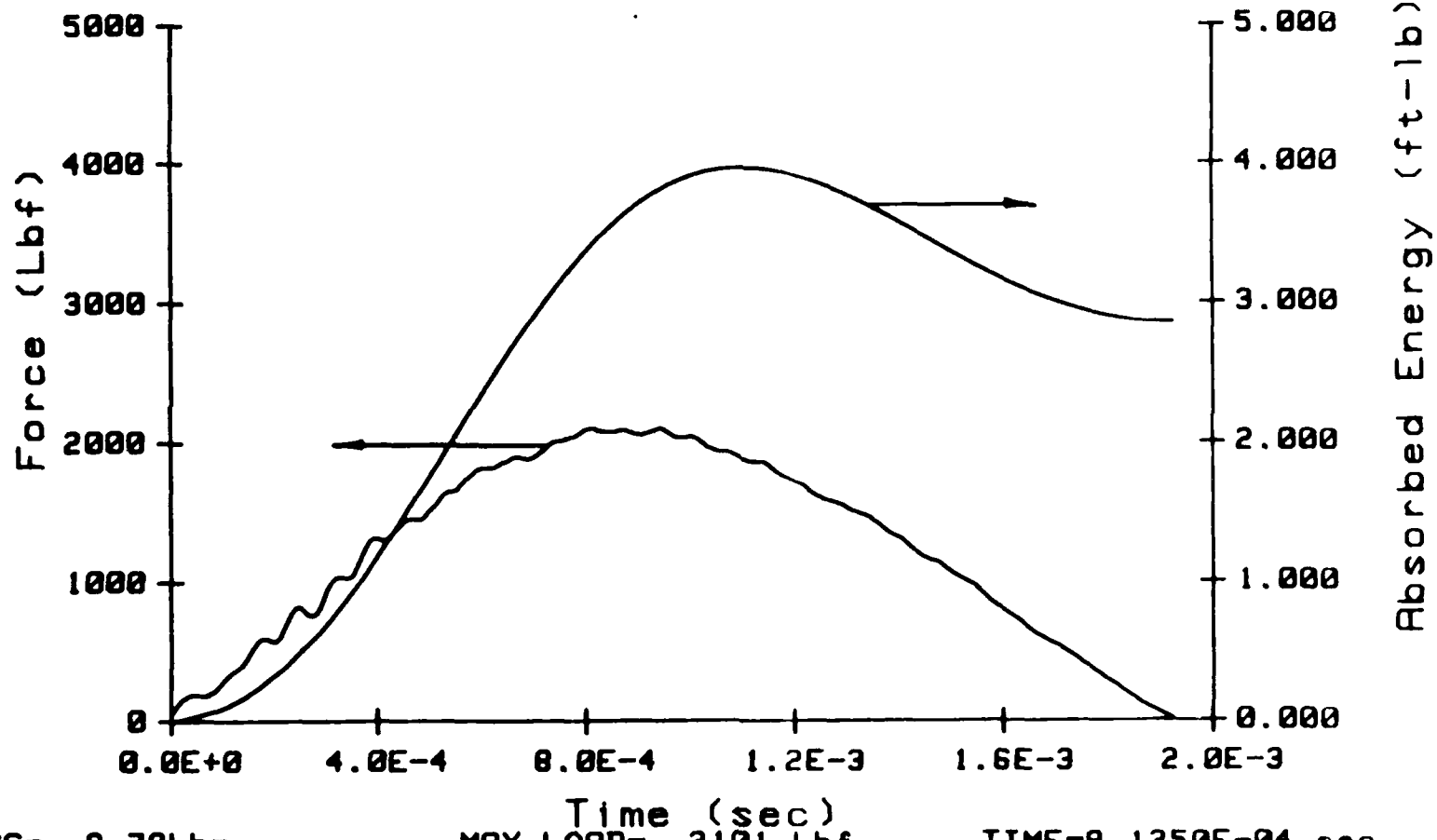

MASS= 9.78Lbm
Vo= 5.09Ft/sec
Eo= 3.93Ft-Lb

MAX LOAD= 2101 Lbf
Displacement= .0392inch
E absorbed= 3.42Ft-Lb

TIME=8.1250E-04 sec

MCB12.6

INSTRUMENTED IMPACT TEST

I76LNG(I5B) 5/29/86

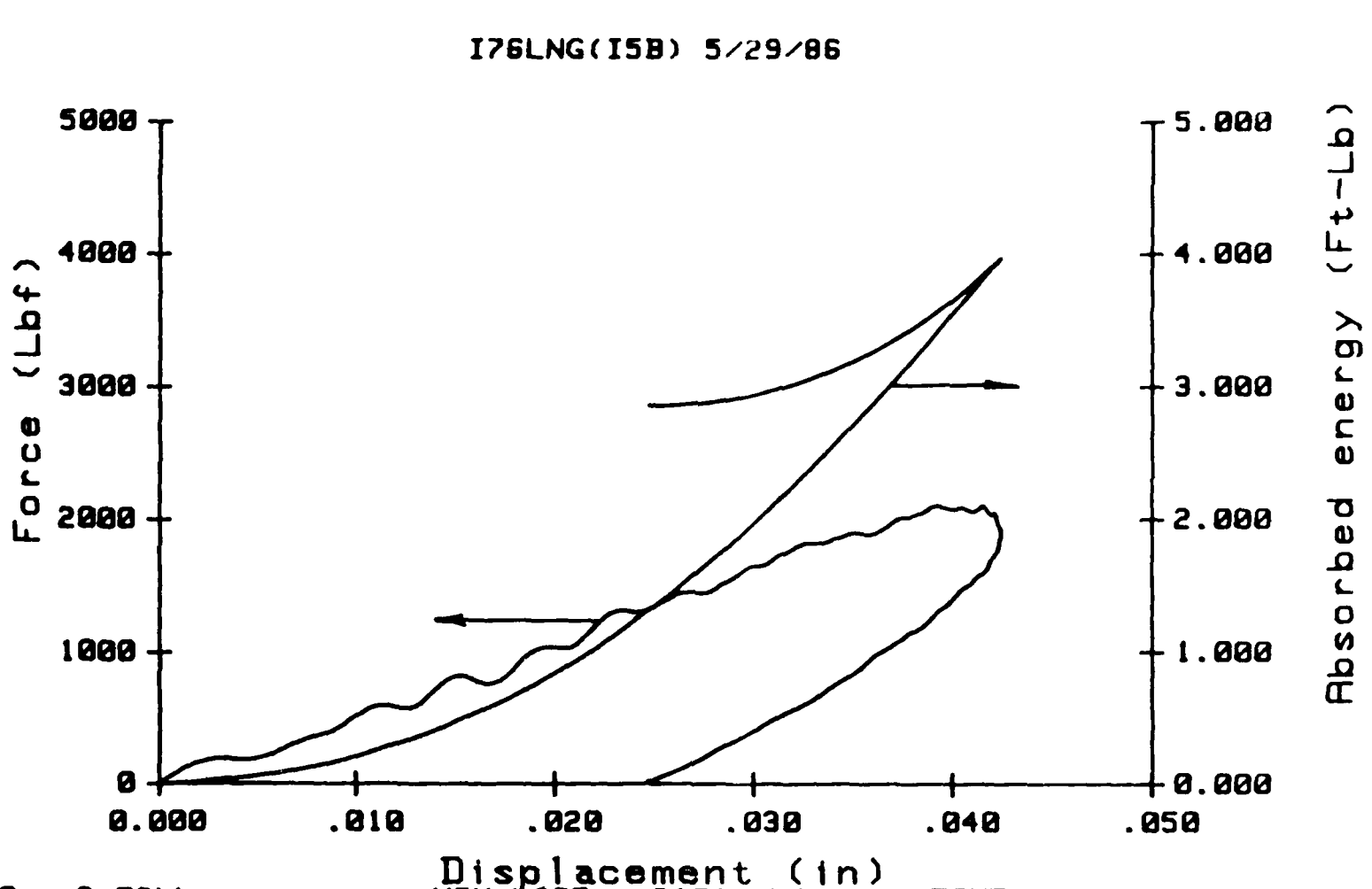

MASS= 9.78Lbm
Vo= 5.09Ft/sec
Eo= 3.93Ft-Lb

MAX LOAD= 2101 Lbf
Displacement= .0392inch
E absorbed= 3.42Ft-Lb

TIME=8.1250E-04 sec

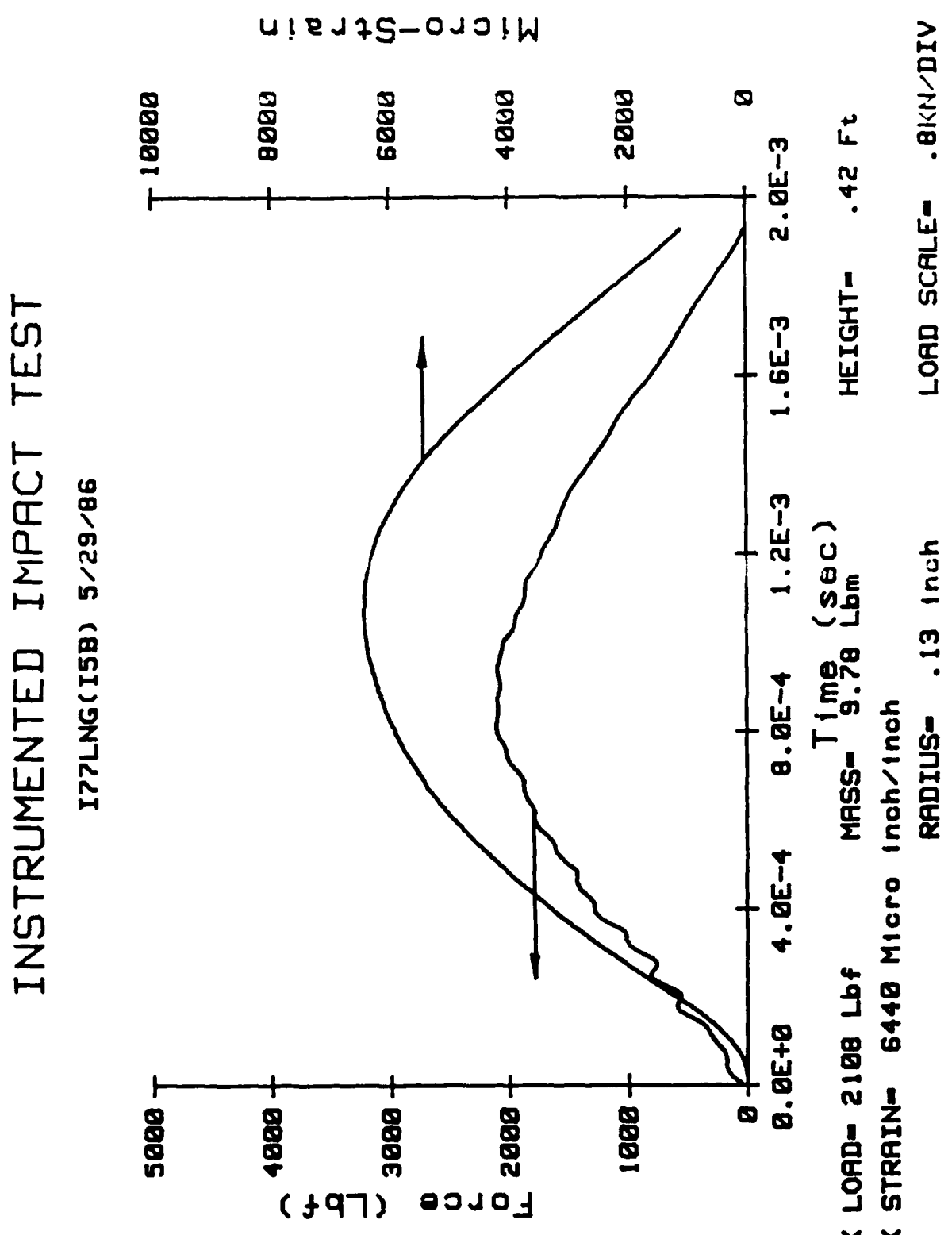
INSTRUMENTED IMPACT TEST
I77LNG(I5B) 5/29/86
Force (Lbf)
5000
4000
3000
2000
1000
0
Micro-Strain
10000
8000
6000
4000
2000
0
0.0E+0
4.0E-4
8.0E-4
1.2E-3
1.6E-3
2.0E-3
Time (sec)
MAX LOAD= 2108 Lbf
MASS= 9.78 Lbm
HEIGHT= .42 Ft
MAX STRAIN= 6440 Micro Inch/Inch
RADIUS= .13 Inch
LOAD SCALE= .8KN/DIV

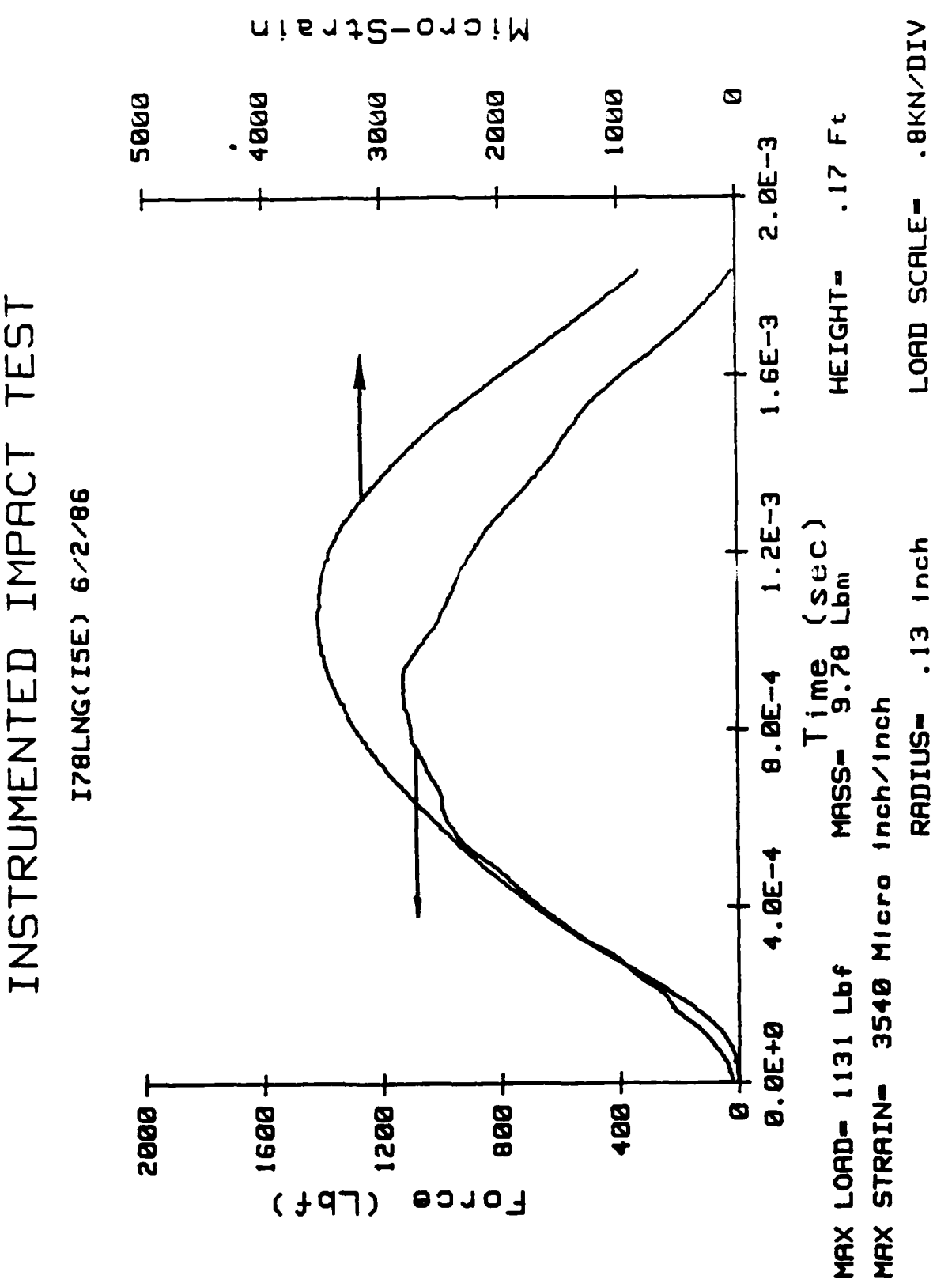
INSTRUMENTED IMPACT TEST
I78LNG(ISE) 6/2/86
Force (Lbf)
2000
1600
1200
800
400
0
Micro-Strain
5000
4000
3000
2000
1000
0
0.0E+0
4.0E-4
8.0E-4
1.2E-3
1.6E-3
2.0E-3
Time (sec)
MAX LOAD= 1131 Lbf
MAX STRAIN= 3540 Micro Inch/Inch
MASS= 9.78 Lbm
RADIUS= .13 Inch
HEIGHT= .17 Ft
LOAD SCALE= .8KN/DIV

MCB13.2

INSTRUMENTED IMPACT TEST

I79LNG(I5E) 6/2/86

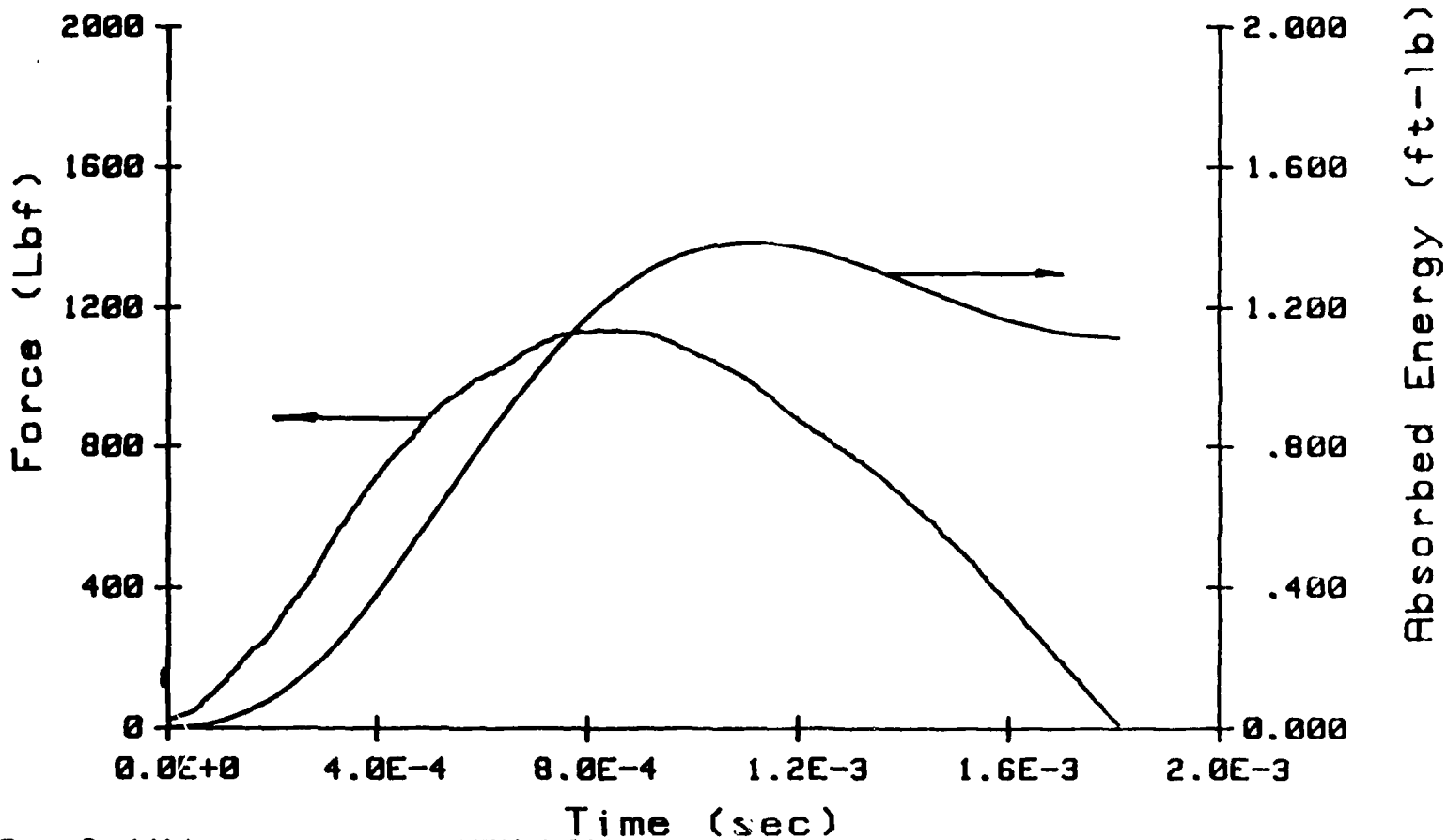

MASS= 8.41Lbm
MAX LOAD= 1138 Lbf
TIME=8.2250E-04 sec
Vo= 3.24Ft/sec
Displacement= .0254inch
Eo= 1.37Ft-Lb
E absorbed= 1.21Ft-Lb

INSTRUMENTED IMPACT TEST

I79LNG(I5E) 6/2/86

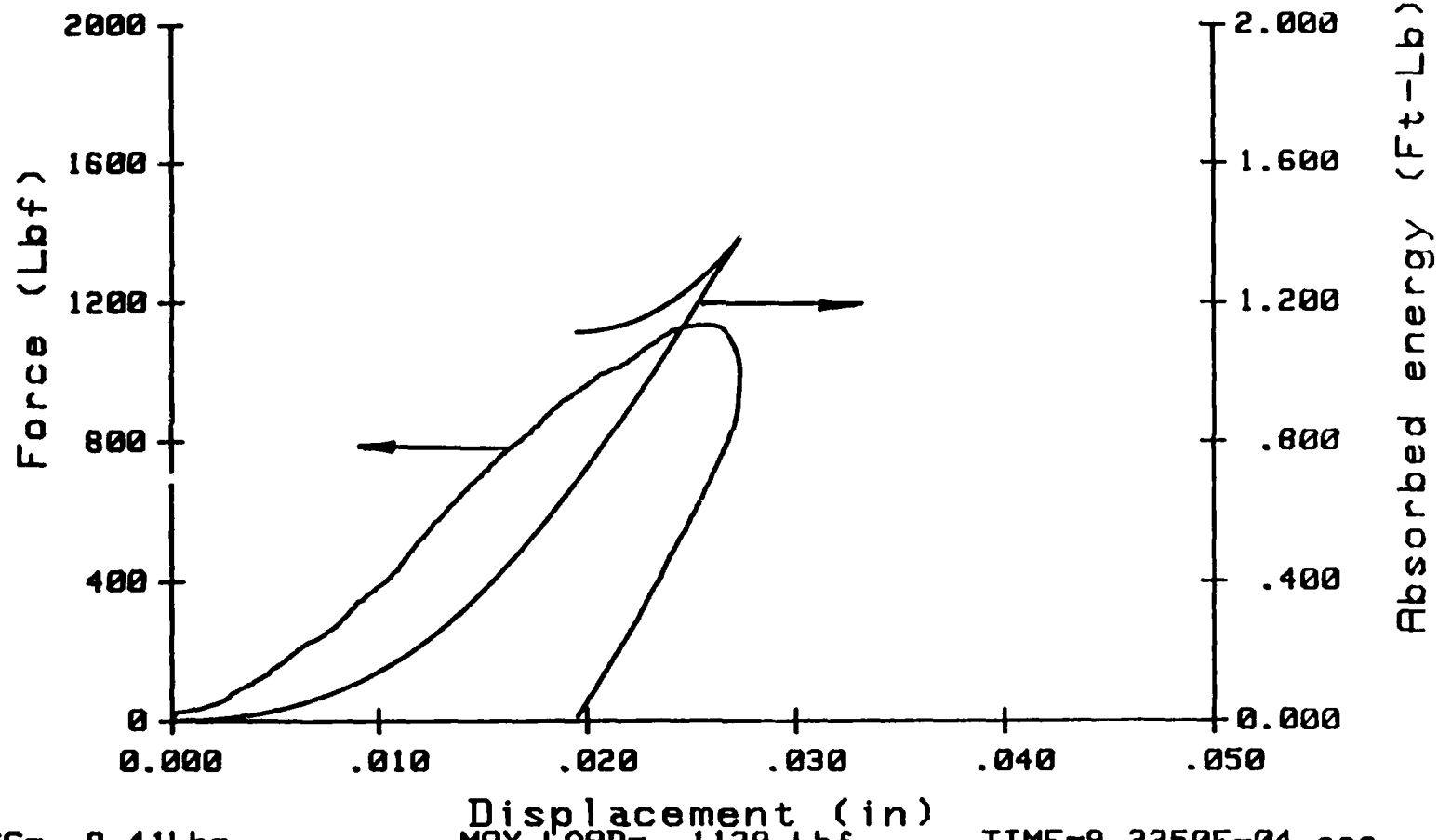

MASS= 8.41Lbm
MAX LOAD= 1138 Lbf
TIME=8.2250E-04 sec
Vo= 3.24Ft/sec
Displacement= .0254inch
Eo= 1.37Ft-Lb
E absorbed= 1.21Ft-Lb

INSTRUMENTED IMPACT TEST

1710LG(I5E) 6/2/86

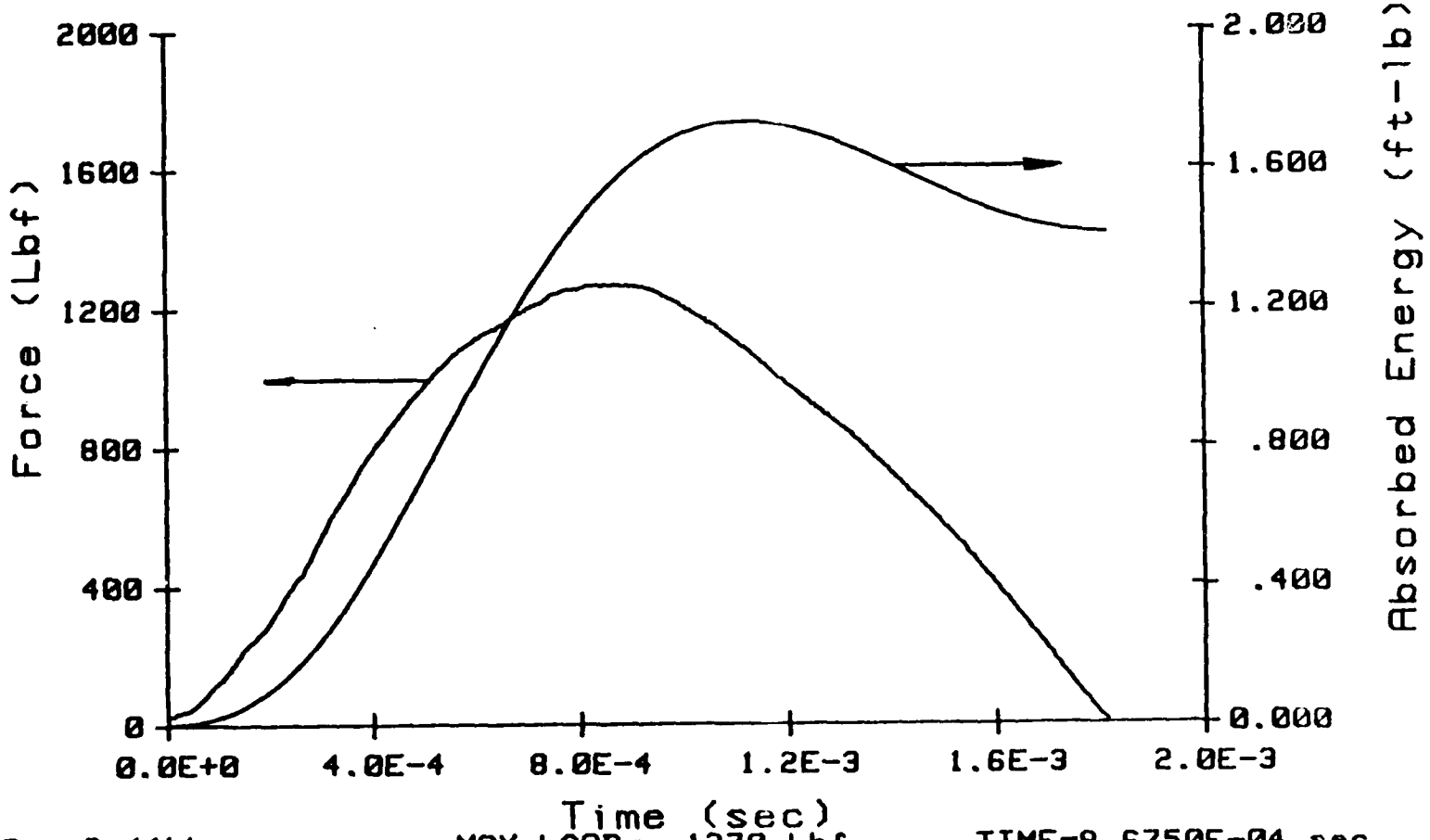

MASS= 8.41Lbm
Vo= 3.62Ft/sec
Eo= 1.71Ft-Lb

MAX LOAD= 1270 Lbf
Displacement= .0292inch
E absorbed= 1.57Ft-Lb

TIME=8.6750E-04 sec

INSTRUMENTED IMPACT TEST

1710LG(I5E) 6/2/86

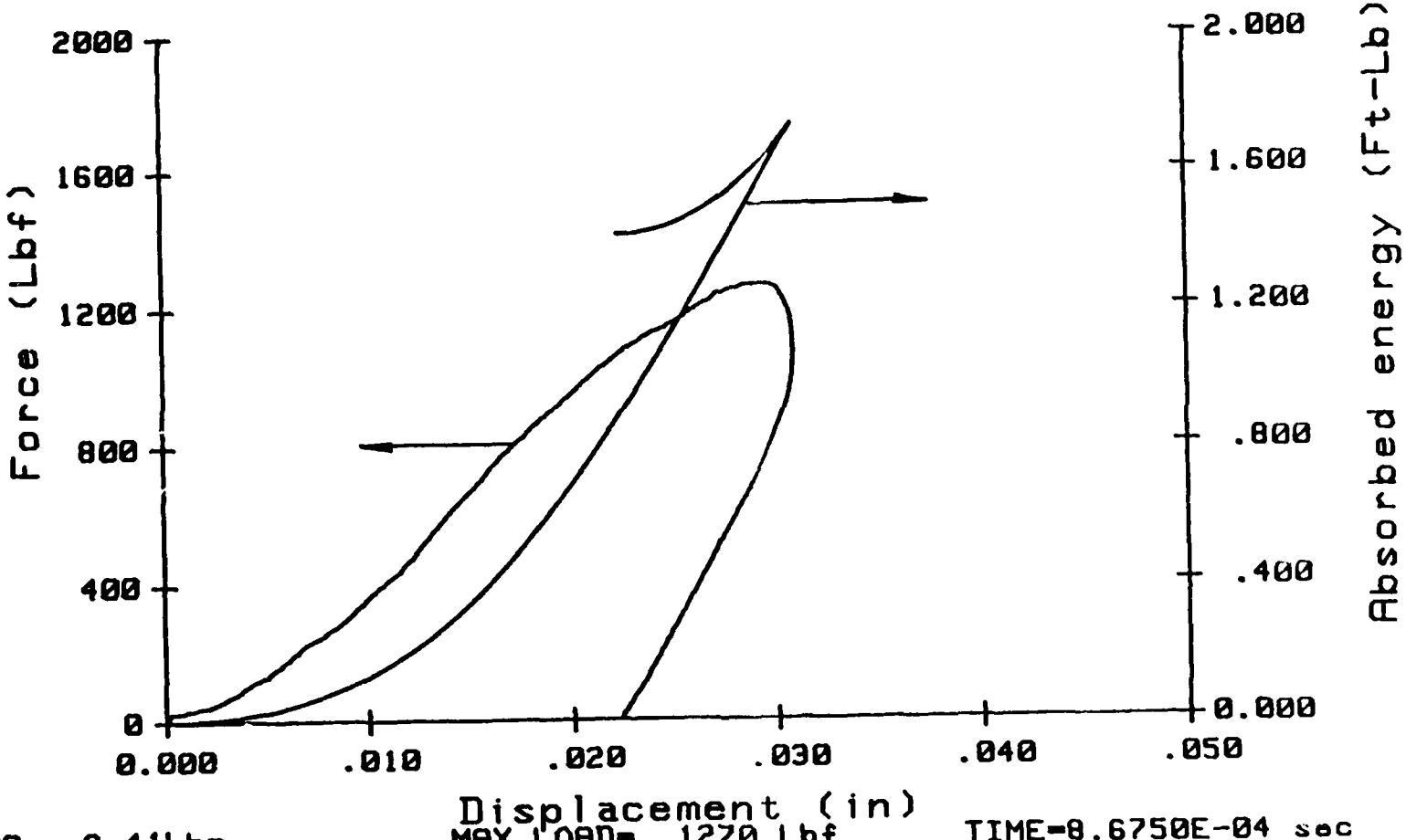

MASS= 8.41Lbm
Vo= 3.62Ft/sec
Eo= 1.71Ft-Lb

MAX LOAD= 1270 Lbf
Displacement= .0292inch
E absorbed= 1.57Ft-Lb

TIME=8.6750E-04 sec

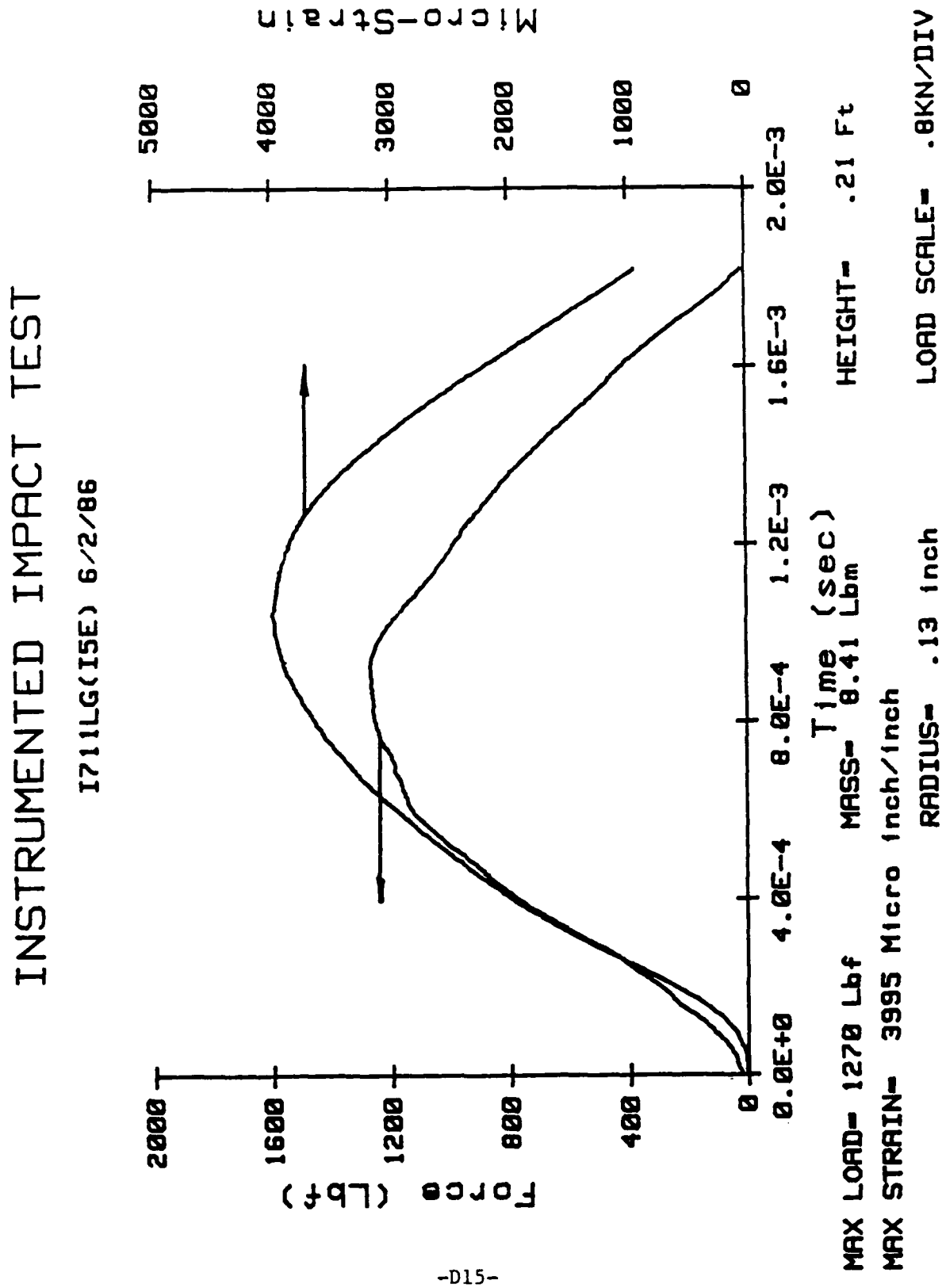
INSTRUMENTED IMPACT TEST
I711LG(ISE) 6/2/86
Force (Lbf)
2000
1600
1200
800
400
0
Micro-Strain
5000
4000
3000
2000
1000
0
0.0E+0
4.0E-4
8.0E-4
1.2E-3
1.6E-3
2.0E-3
Time (sec)
MAX LOAD= 1270 Lbf
MASS= 8.41 Lbm
HEIGHT= .21 Ft
MAX STRAIN= 3995 Micro Inch/Inch
RADIUS= .13 Inch
LOAD SCALE= .8KN/DIV

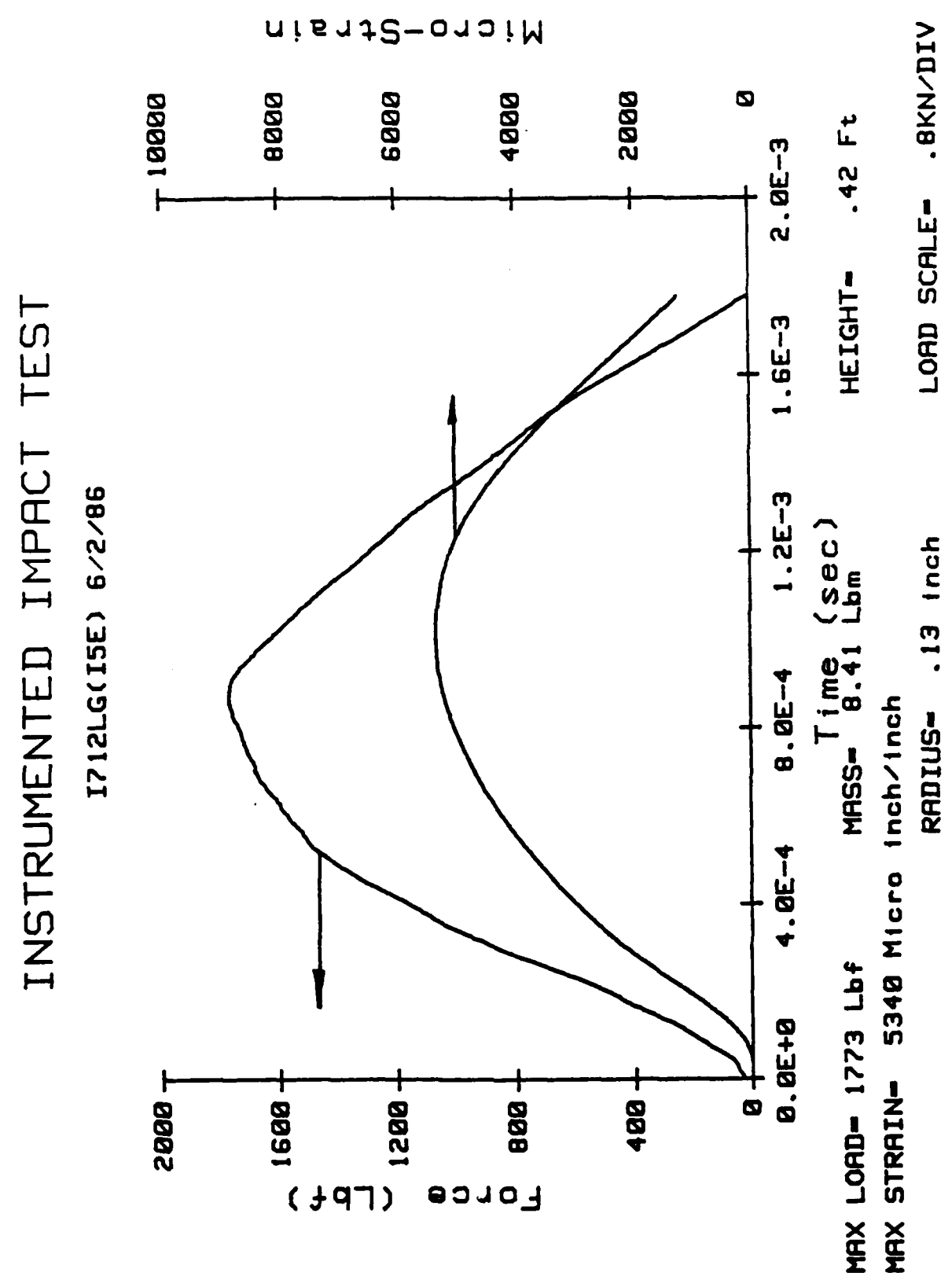
INSTRUMENTED IMPACT TEST
I712LG(ISE) 6/2/86
Force (Lbf)
2000
1600
1200
800
400
0
Micro-Strain
10000
8000
6000
4000
2000
0
0.0E+0
4.0E-4
8.0E-4
1.2E-3
1.6E-3
2.0E-3
Time (sec)
MAX LOAD= 1773 Lbf
MASS= 8.41 Lbm
HEIGHT= .42 Ft
MAX STRAIN= 5340 Micro Inch/Inch
RADIUS= .13 Inch
LOAD SCALE= .8KN/DIV

MCBI3.5

INSTRUMENTED IMPACT TEST

I713LG(I5E) 6/2/86

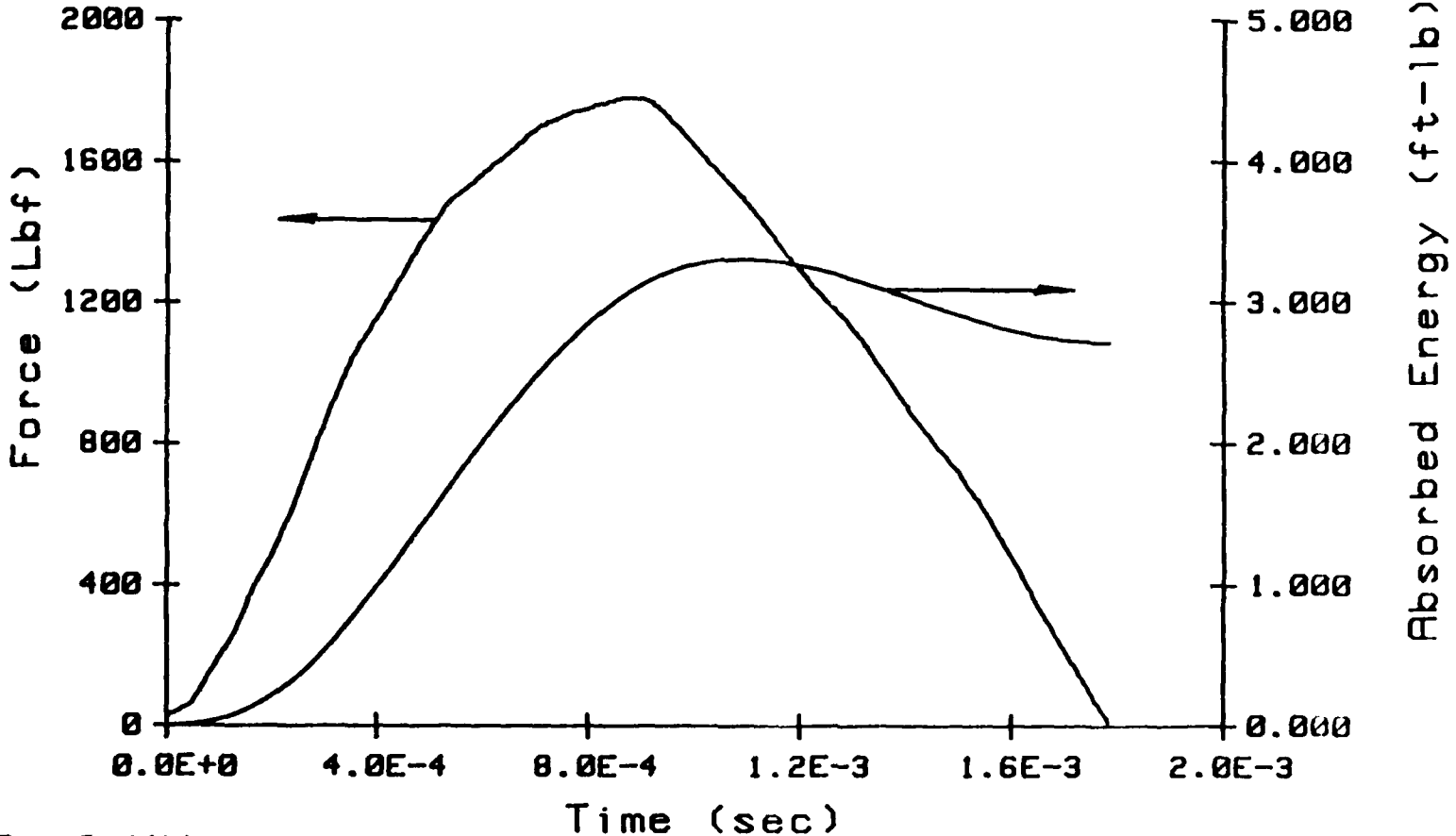

MASS= 8.41Lbm
MAX LOAD= 1782 Lbf
TIME=8.6750E-04 sec
Vo= 5.01Ft/sec
Displacement= .0396inch
Eo= 3.28Ft-Lb
E absorbed= 3.05Ft-Lb

INSTRUMENTED IMPACT TEST

I713LG(I5E) 6/2/86

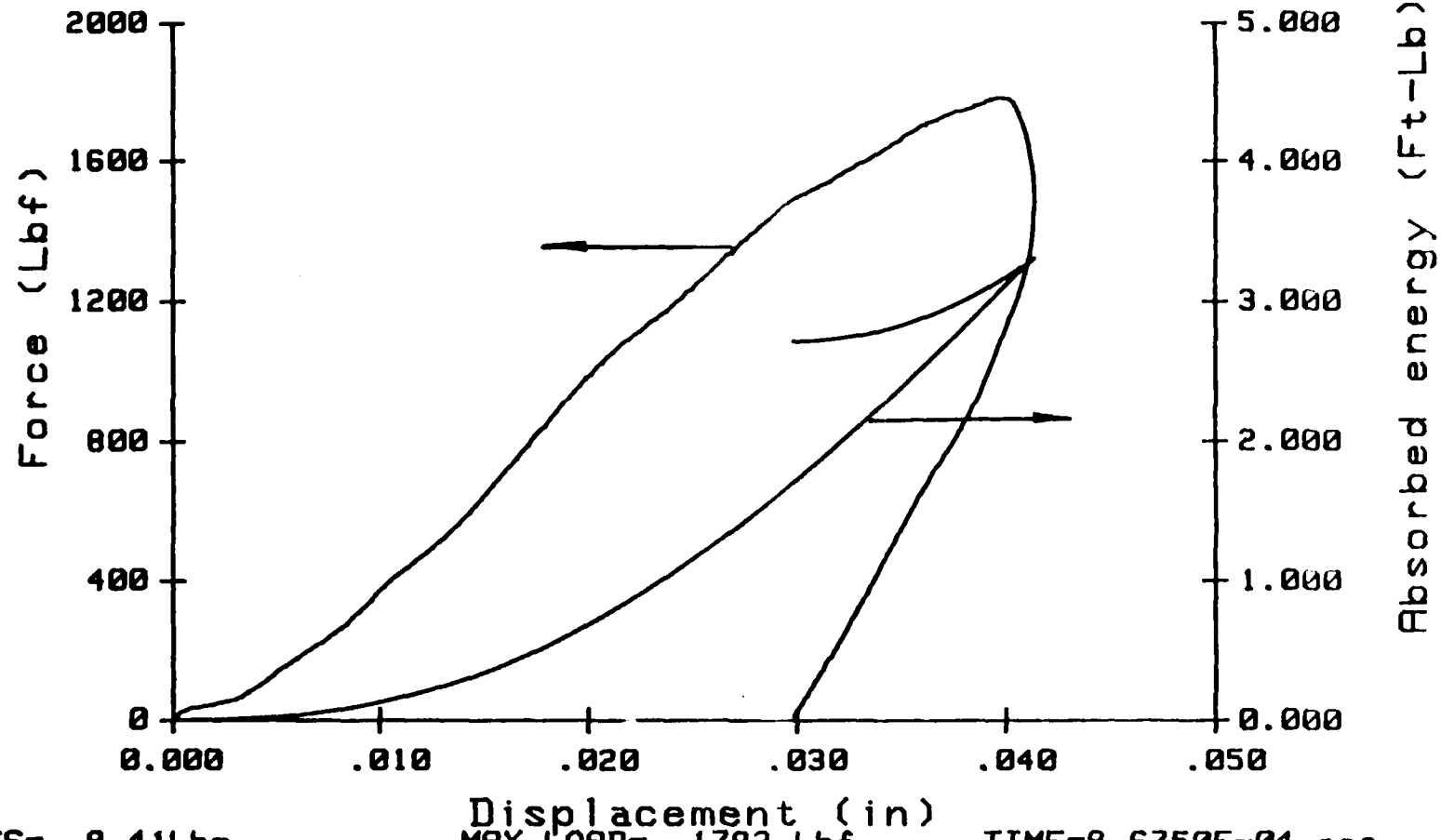

MASS= 8.41Lbm
MAX LOAD= 1782 Lbf
TIME=8.6750E-04 sec
Vo= 5.01Ft/sec
Displacement= .0396inch
Eo= 3.28Ft-Lb
E absorbed= 3.05Ft-Lb

MCBI3.6

INSTRUMENTED IMPACT TEST

I81LNG(I6A) 6/2/86

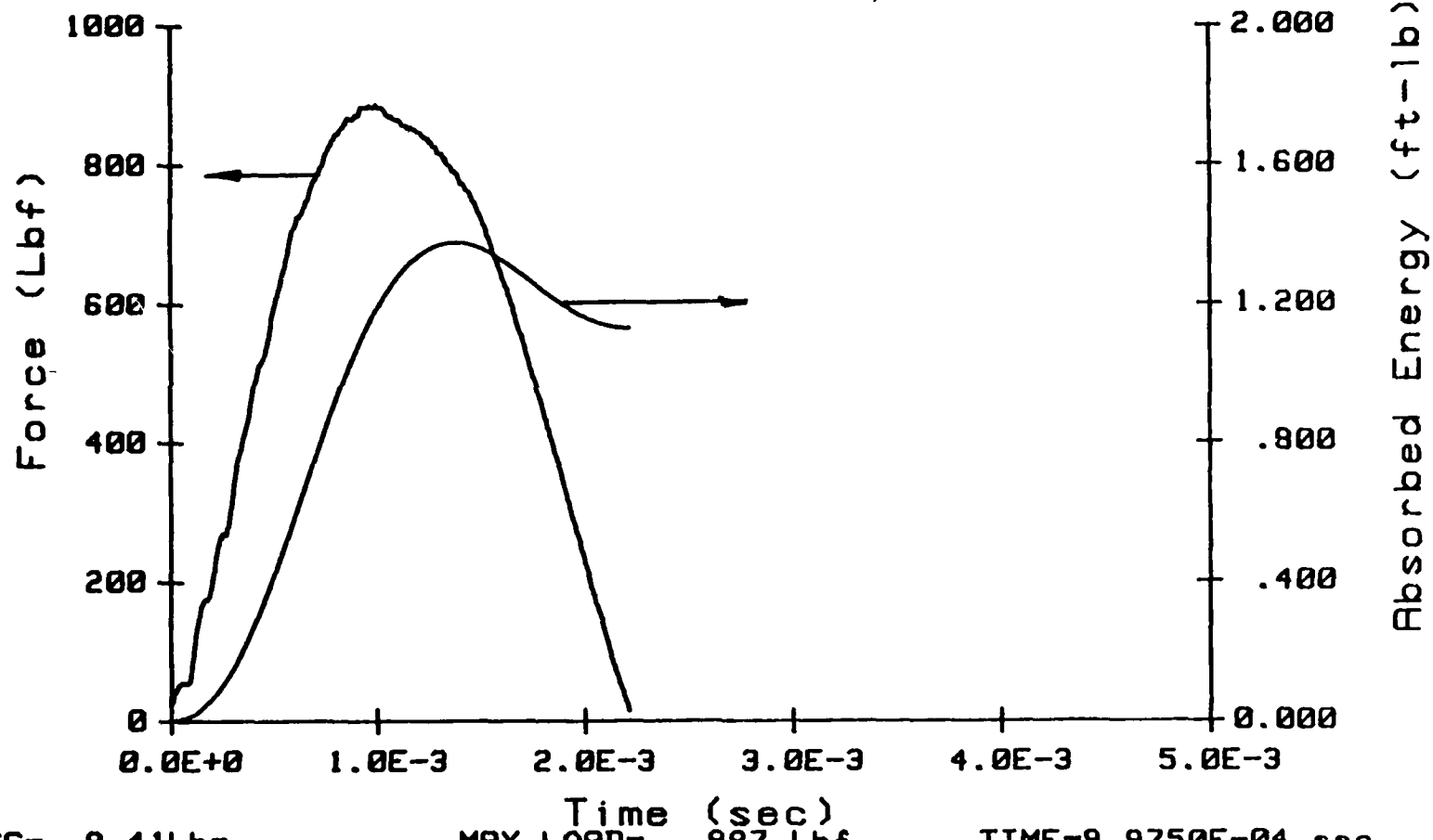

MASS= 8.41Lbm MAX LOAD= 887 Lbf TIME=9.9750E-04 sec

Vo= 3.22Ft/sec Displacement= .0306inch

Eo= 1.35Ft-Lb E absorbed= 1.18Ft-Lb

MCBI3.6

INSTRUMENTED IMPACT TEST

I81LNG(I6A) 6/2/86

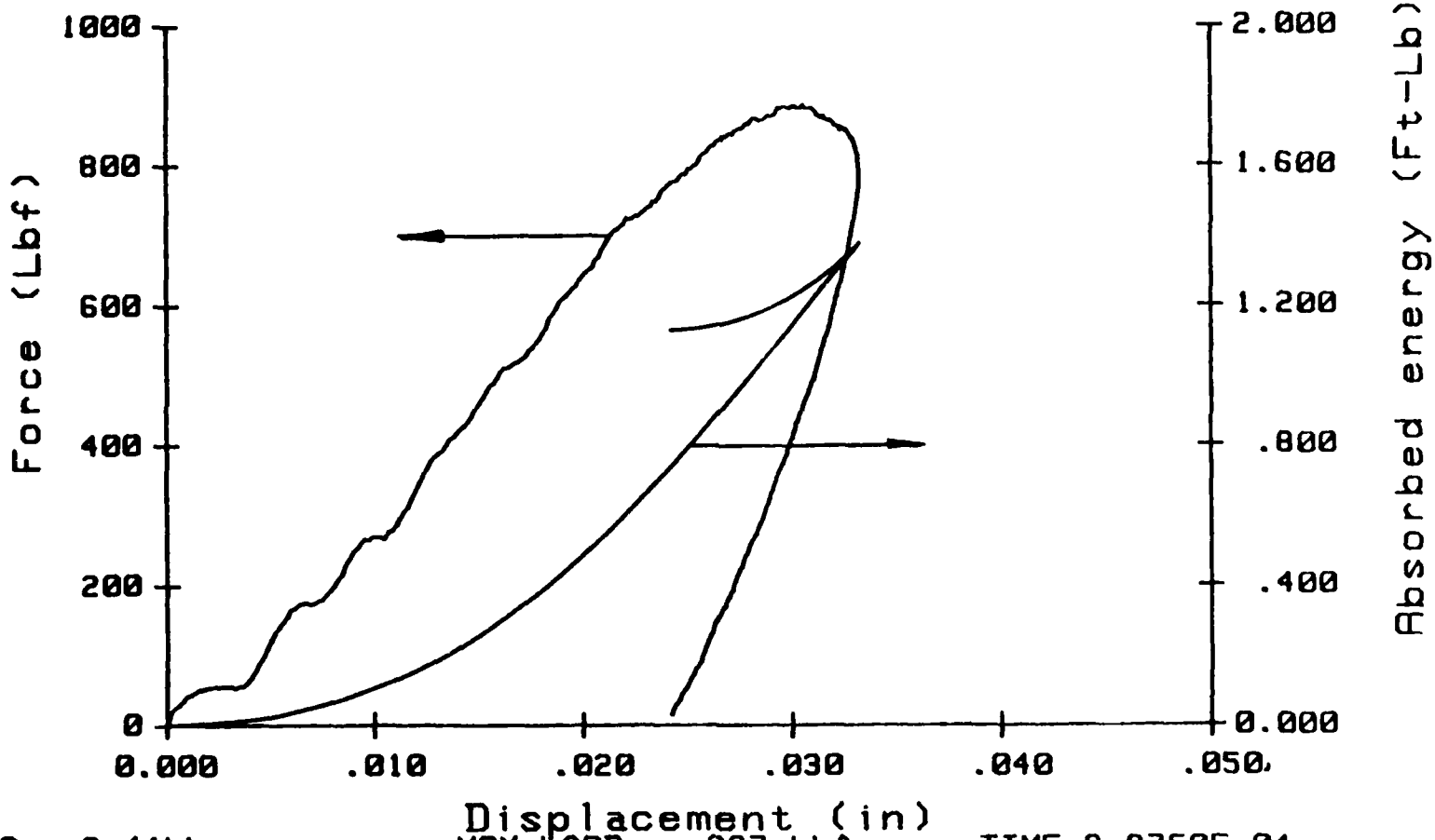

MASS= 8.41Lbm
Vo= 3.22Ft/sec
Eo= 1.35Ft-Lb

MAX LOAD= 887 Lbf
Displacement= .0306inch
E absorbed= 1.18Ft-Lb

TIME=9.9750E-04 sec

NADC-87106-60

INSTRUMENTED IMPACT TEST

I82LNG(I6A) 6/2/86

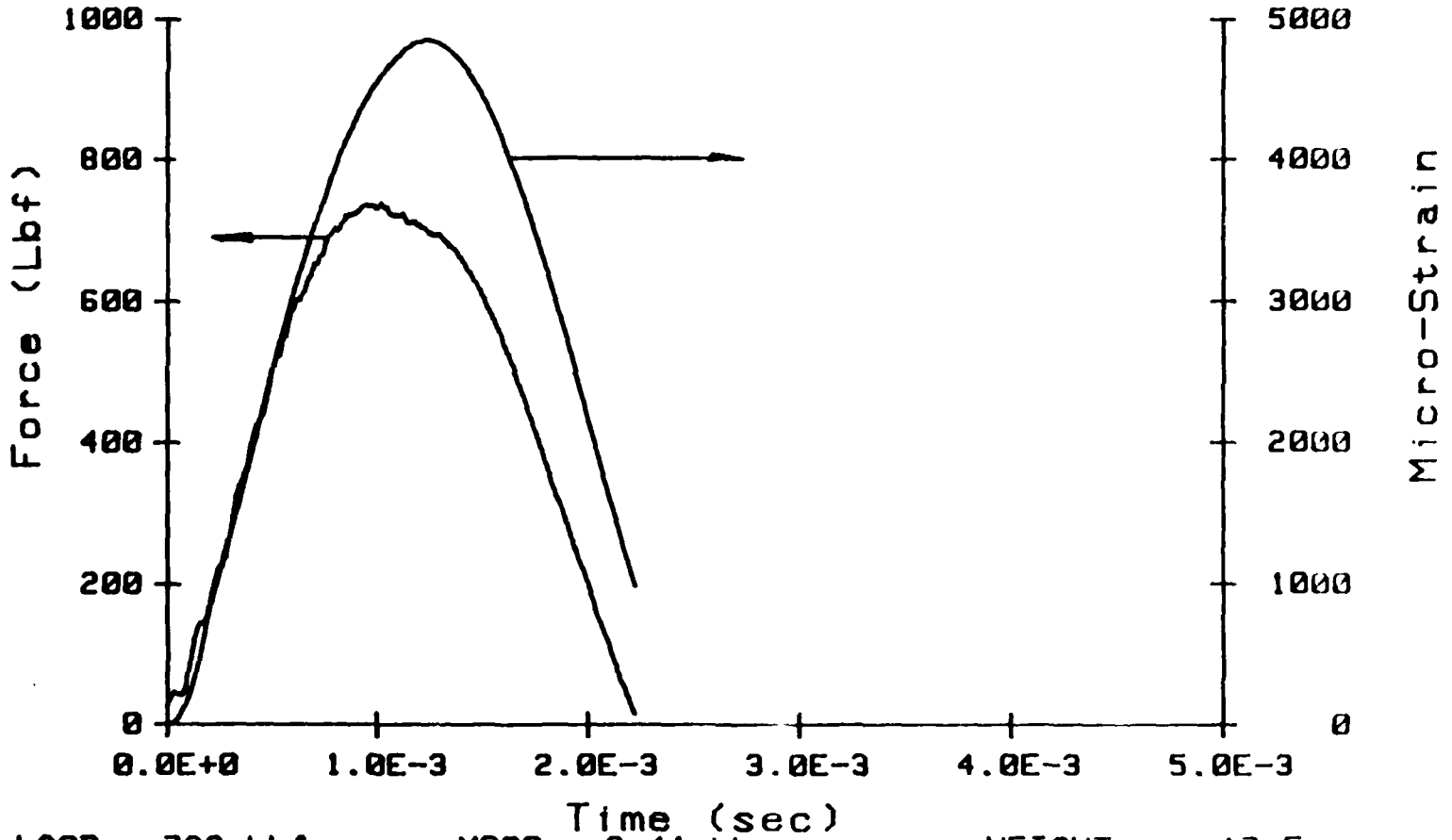

MAX LOAD= 739 Lbf MASS= 8.41 Lbm HEIGHT= .17 Ft

MAX STRAIN= 4855 Micro inch/inch

RADIUS= .13 inch LOAD SCALE= .8KN/DIV

INSTRUMENTED IMPACT TEST

I83LNG(I6A) 6/3/86

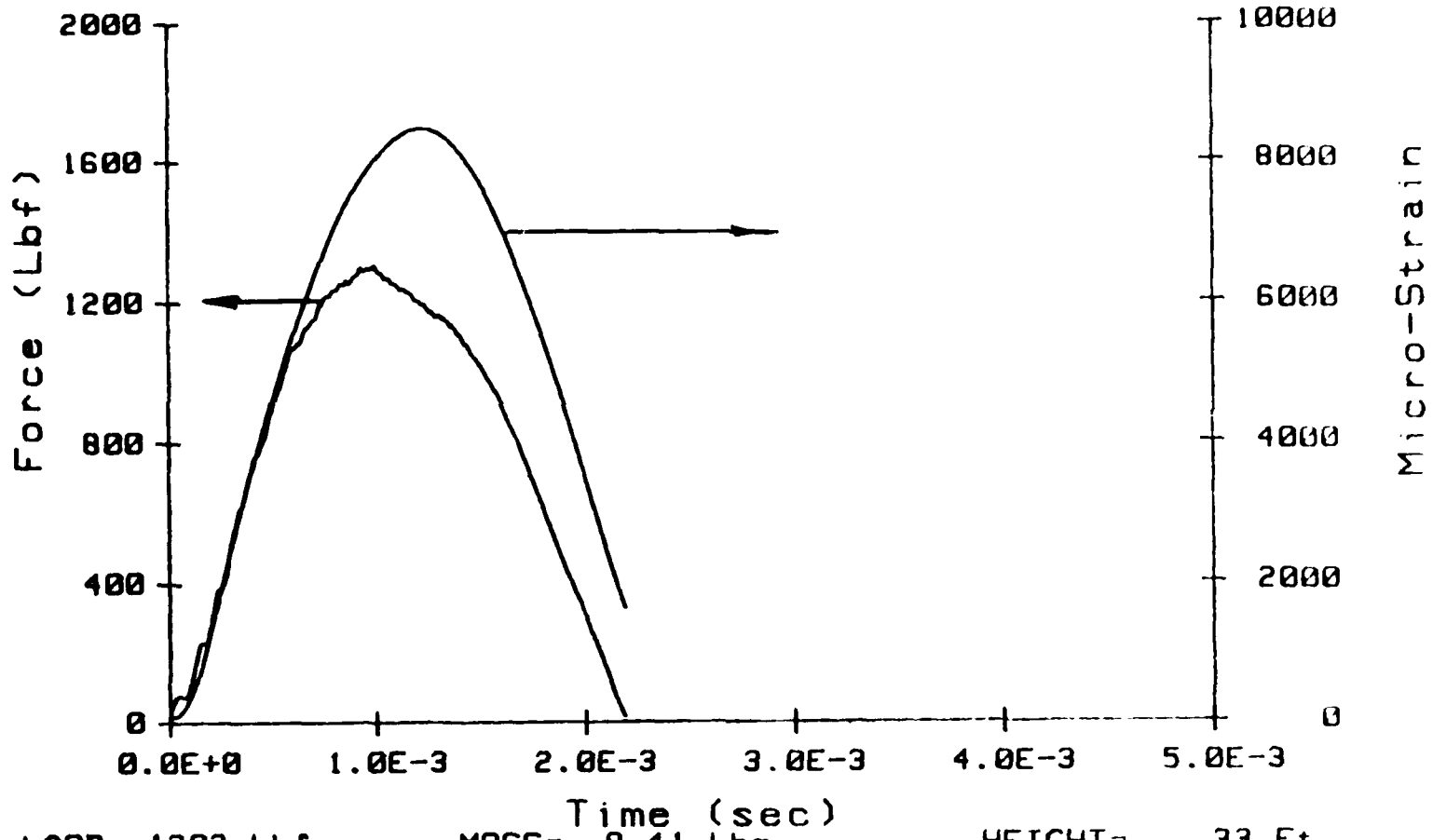

MAX LOAD= 1302 Lbf MASS= 8.41 Lbm HEIGHT= .33 Ft

MAX STRAIN= 8480 Micro inch/inch

RADIUS= .13 inch LOAD SCALE= .8KN/DIV

MCBI4.1

INSTRUMENTED IMPACT TEST

I84LNG(I6A) 6/3/86

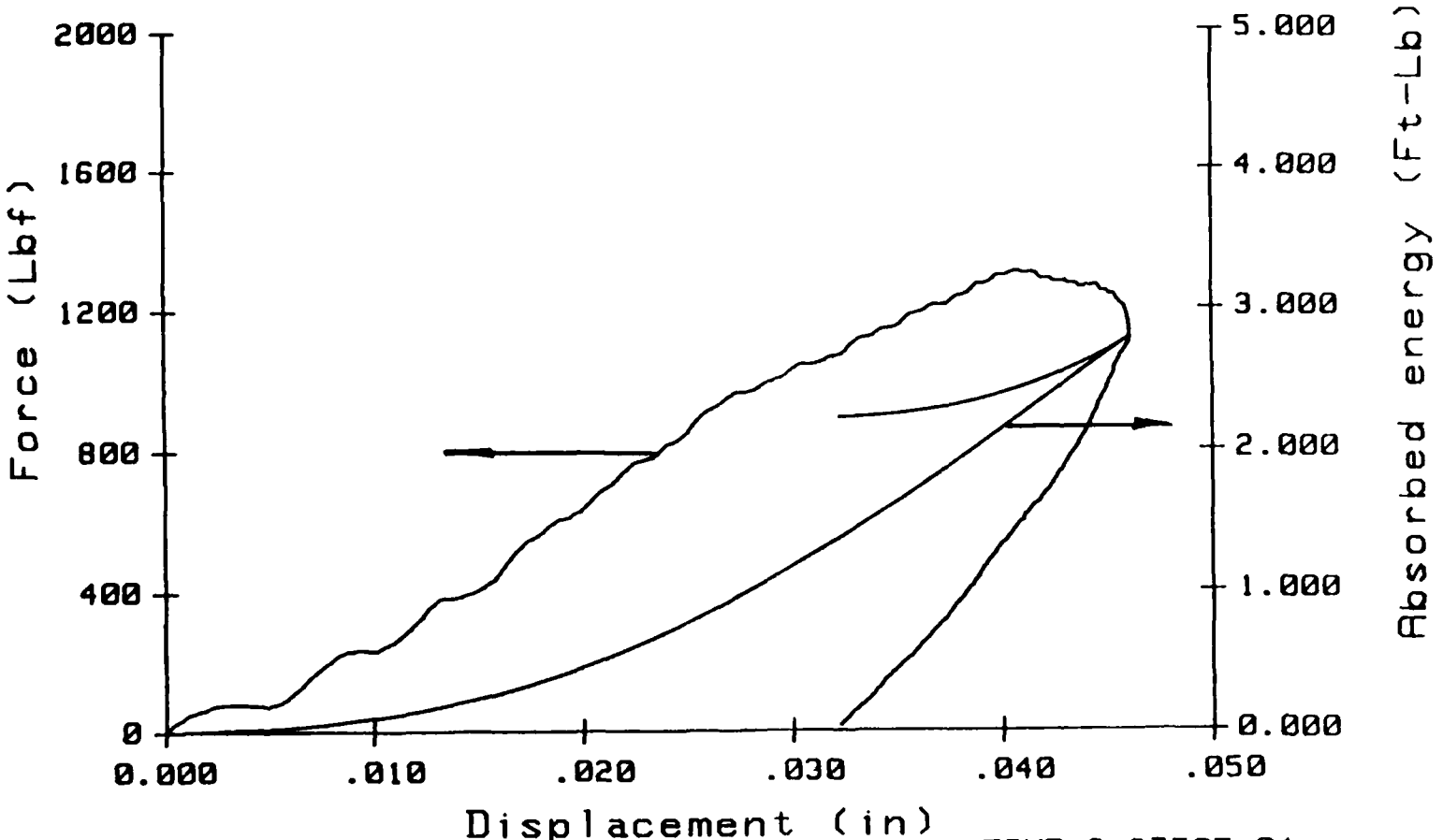

MASS= 8.41Lbm
Vo= 4.60Ft/sec
Eo= 2.76Ft-Lb

MAX LOAD= 1306 Lbf
Displacament= .0408inch
E absorbed= 2.23Ft-Lb

TIME=8.9750E-04 sec

NADC-87106-60

MCBI4.1

INSTRUMENTED IMPACT TEST

I84LNG(I6A) 6/3/86

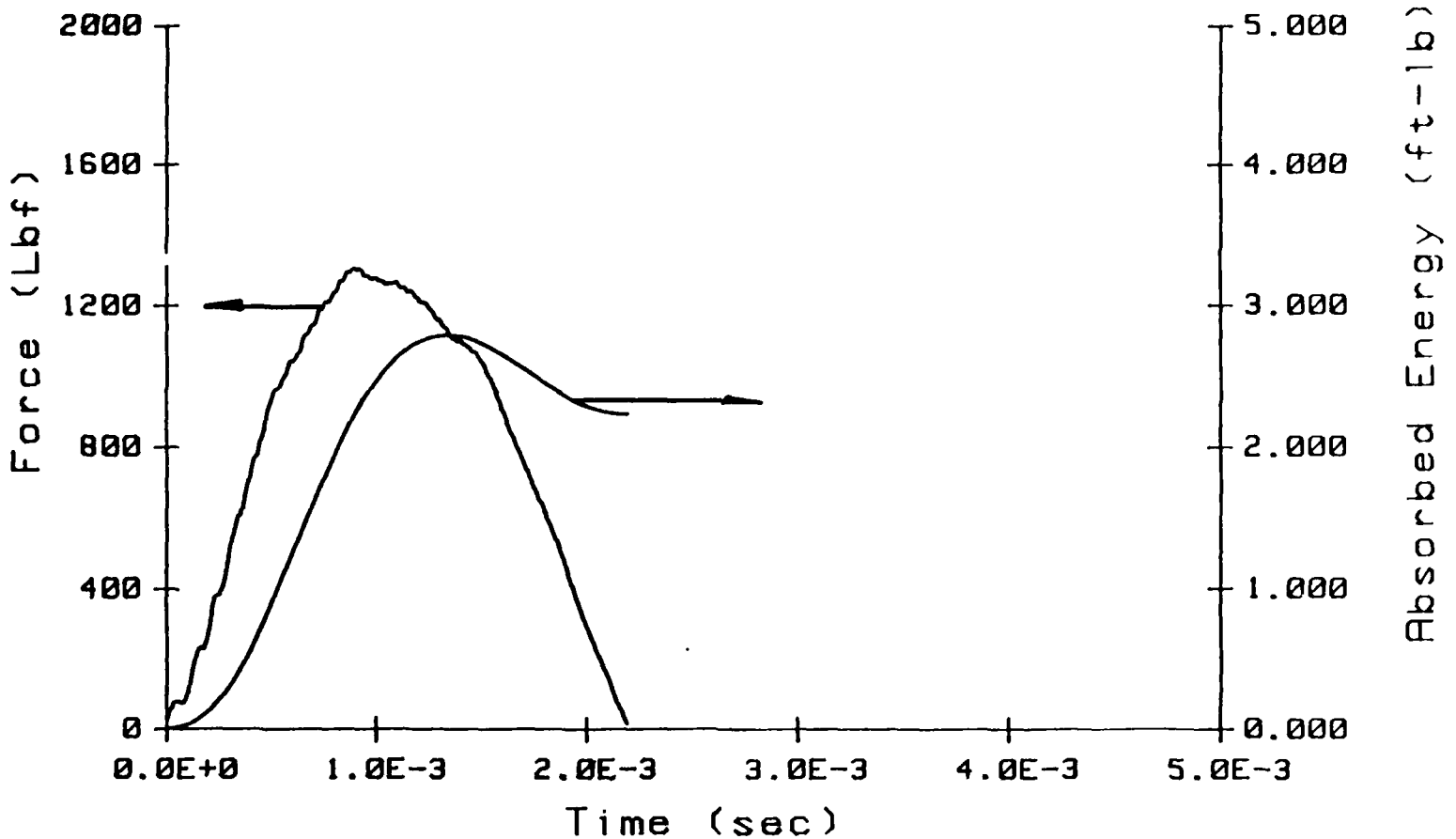

MASS= 8.41Lbm MAX LOAD= 1306 Lbf TIME=8.9750E-04 sec

Vo= 4.60Ft/sec Displacement= .0408inch

Eo= 2.76Ft-Lb E absorbed= 2.23Ft-Lb

MCBI4.2

INSTRUMENTED IMPACT TEST

I85LNG(I6B) 6/3/86

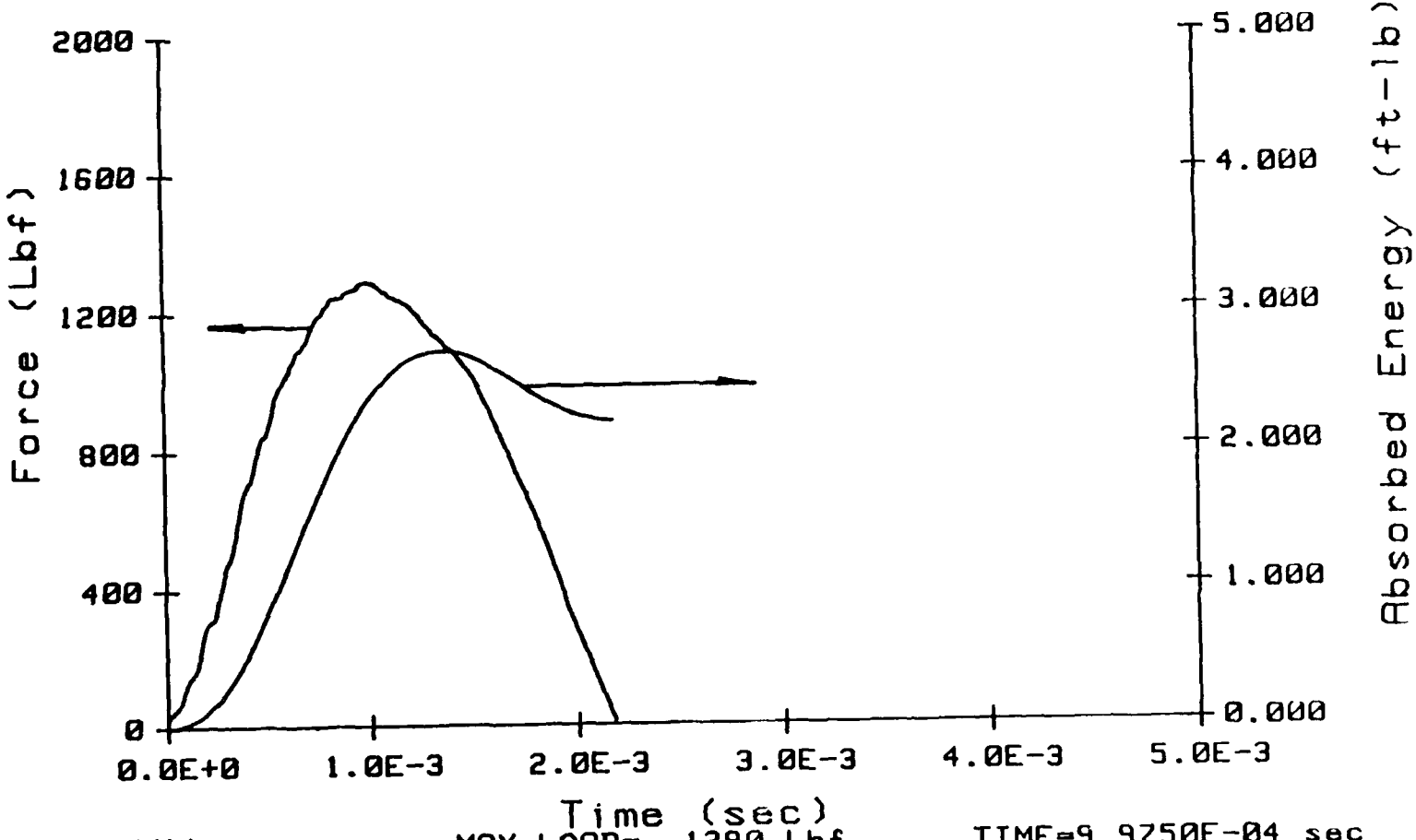

MASS= 8.41Lbm
Vo= 4.54Ft/sec
Eo= 2.69Ft-Lb

MAX LOAD= 1290 Lbf
Displacement= .0427inch
E absorbed= 2.37Ft-Lb

TIME=9.9750E-04 sec

INSTRUMENTED IMPACT TEST

I85LNG(I6B) 6/3/86

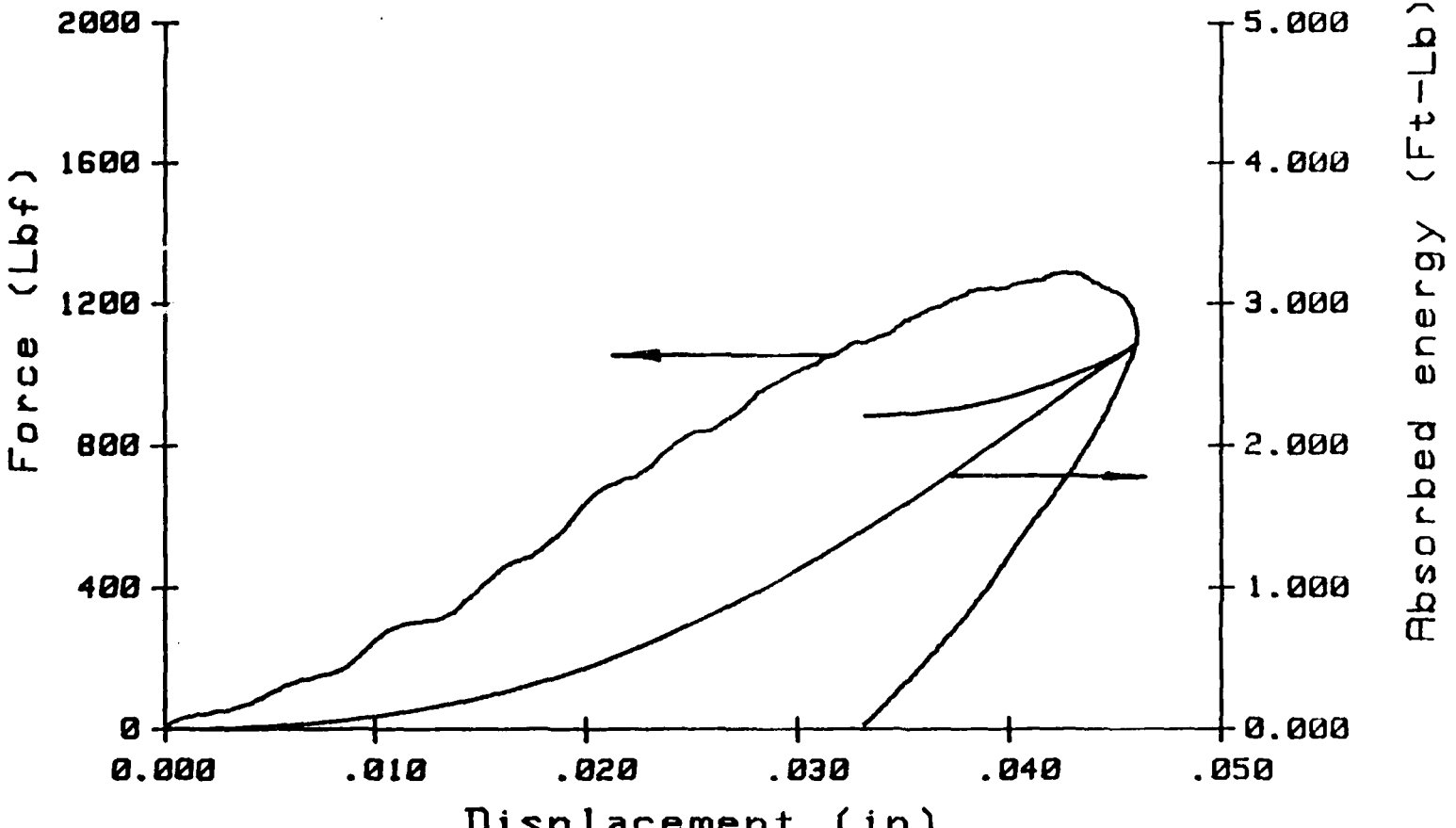

MASS= 8.41Lbm
Vo= 4.54Ft/sec
Eo= 2.69Ft-Lb

MAX LOAD= 1290 Lbf
Displacement= .0427inch
E absorbed= 2.37Ft-Lb

TIME=9.9750E-04 sec

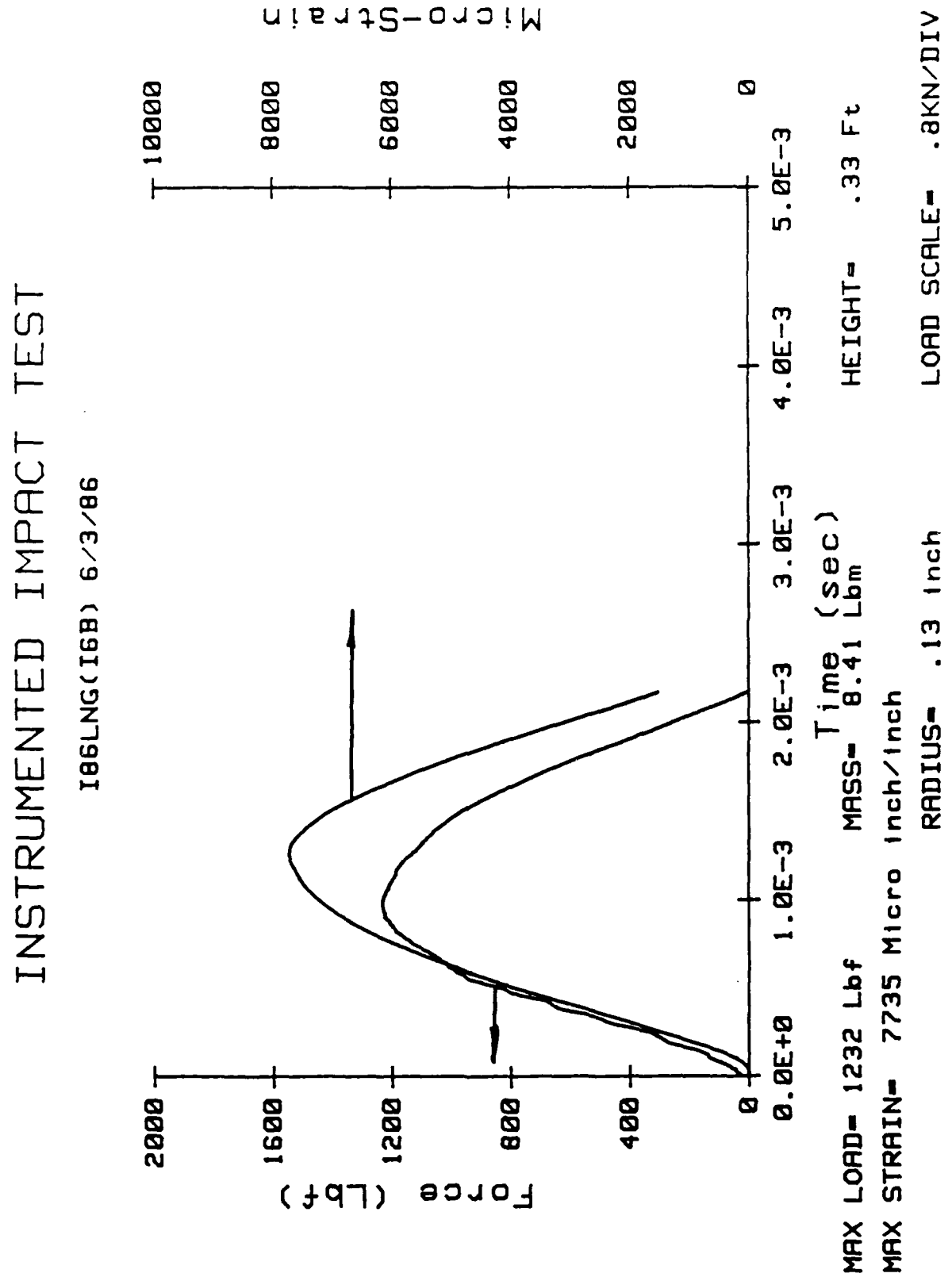
INSTRUMENTED IMPACT TEST
I86LNG(I6B) 6/3/86
Force (Lbf)
2000
1600
1200
800
400
0
Micro-Strain
10000
8000
6000
4000
2000
0
0.0E+0
1.0E-3
2.0E-3
3.0E-3
4.0E-3
5.0E-3
Time (sec)
MAX LOAD= 1232 Lbf
MASS= 8.41 Lbm
HEIGHT= .33 Ft
MAX STRAIN= 7735 Micro Inch/Inch
RADIUS= .13 Inch
LOAD SCALE= .8KN/DIV

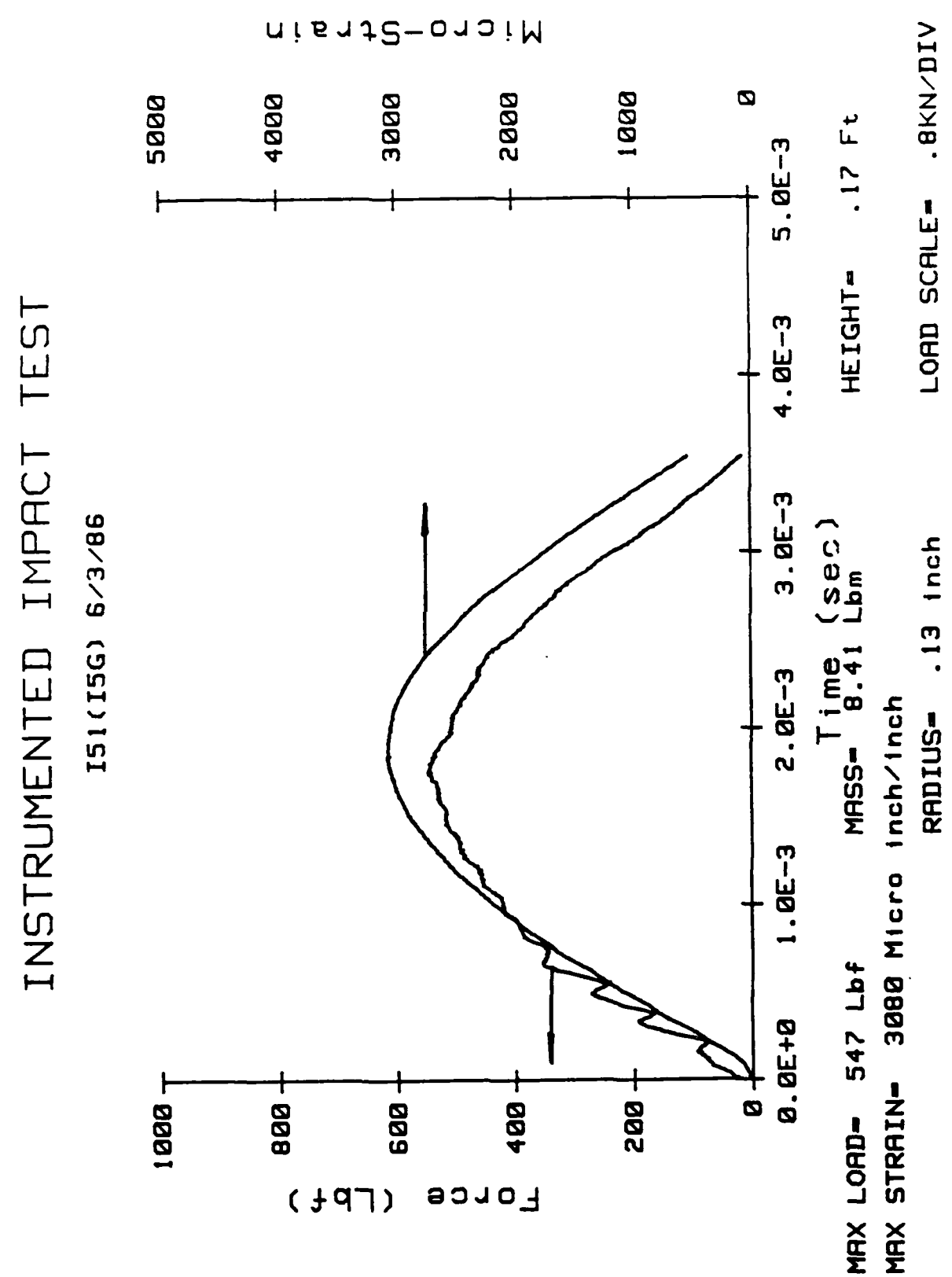
INSTRUMENTED IMPACT TEST
I51(I5G) 6/3/86
Force (Lbf)
1000
800
600
400
200
0
0.0E+0
1.0E-3
2.0E-3
3.0E-3
4.0E-3
5.0E-3
Time (sec)
Micro-Strain
5000
4000
3000
2000
1000
0
MAX LOAD= 547 Lbf
MAX STRAIN= 3080 Micro Inch/Inch
MASS= 8.41 Lbm
RADIUS= .13 Inch
HEIGHT= .17 Ft
LOAD SCALE= .8KN/DIV

MCBI4.5

INSTRUMENTED IMPACT TEST

I52(I5G) 6/3/86

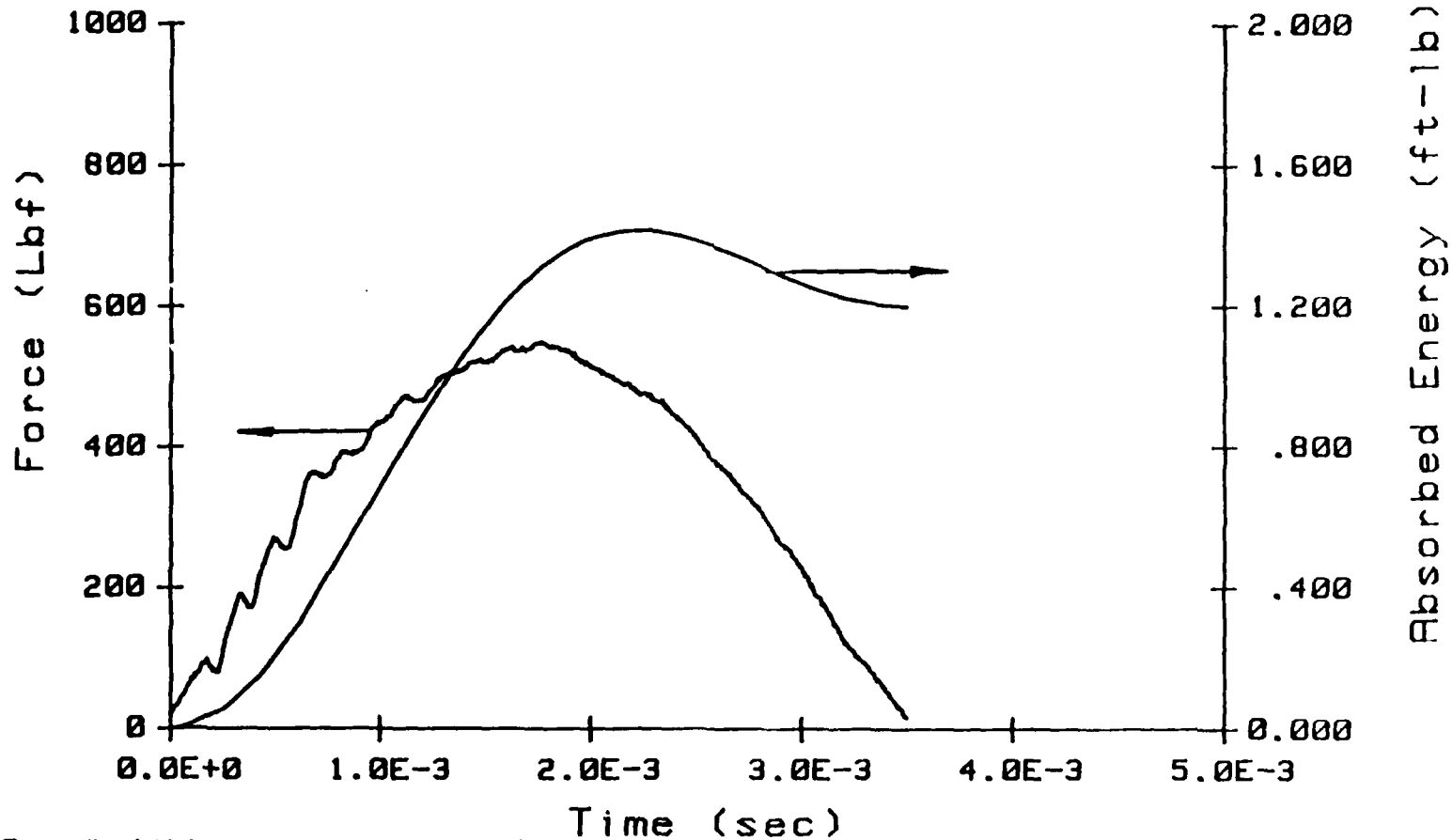

MASS= 8.41Lbm MAX LOAD= 550 Lbf TIME=1.7675E-03 sec

Vo= 3.25Ft/sec Displacement= .0507inch

Eo= 1.38Ft-Lb E absorbed= 1.31Ft-Lb

MCBI4.5

INSTRUMENTED IMPACT TEST

I52(I5G) 6/3/86

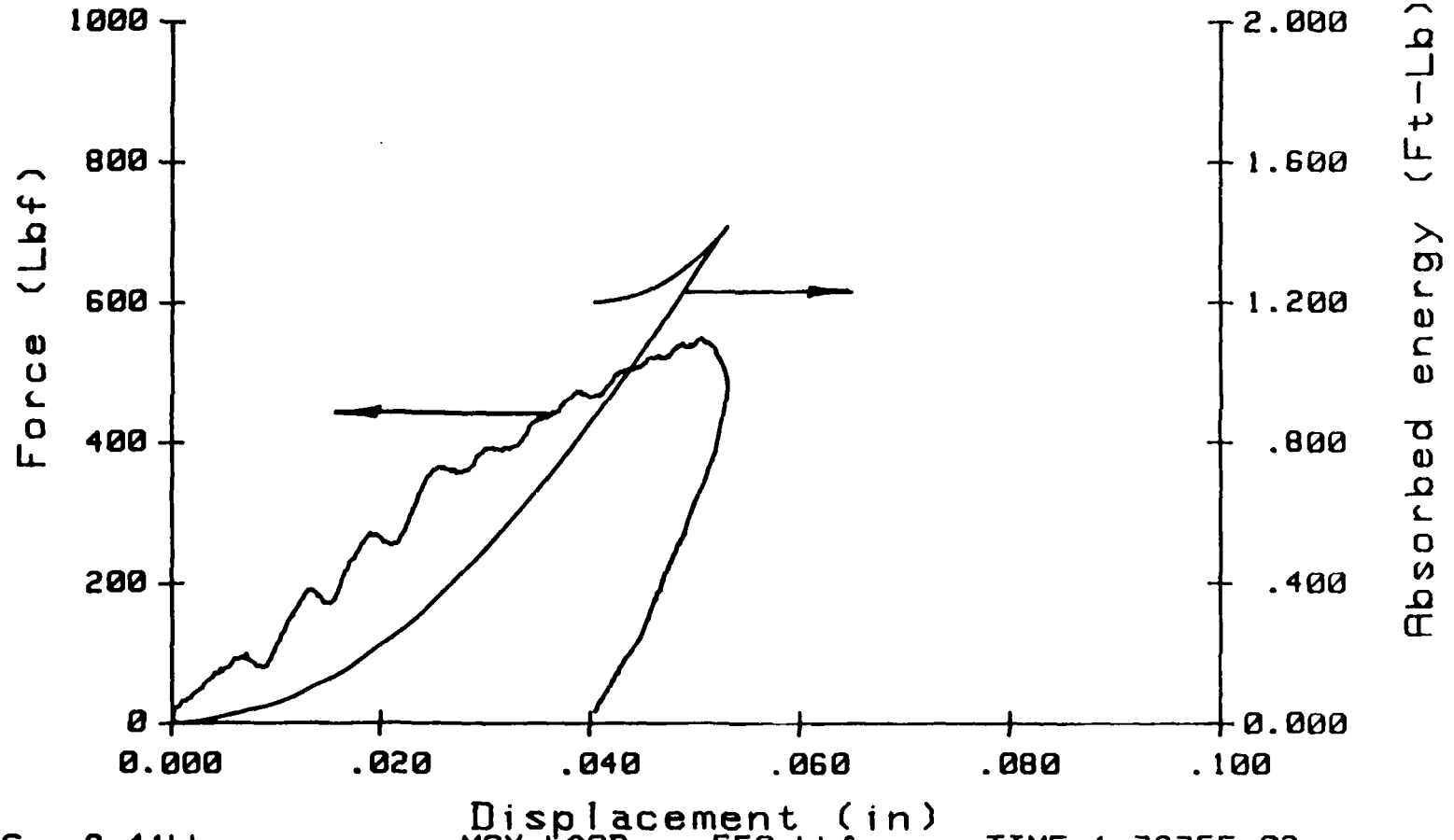

MASS= 8.41Lbm
Vo= 3.25Ft/sec
Eo= 1.38Ft-Lb

MAX LOAD= 550 Lbf
Displacement= .0507inch
E absorbed= 1.31Ft-Lb

TIME=1.7675E-03 sec

INSTRUMENTED IMPACT TEST

I53(I5G) 6/3/86

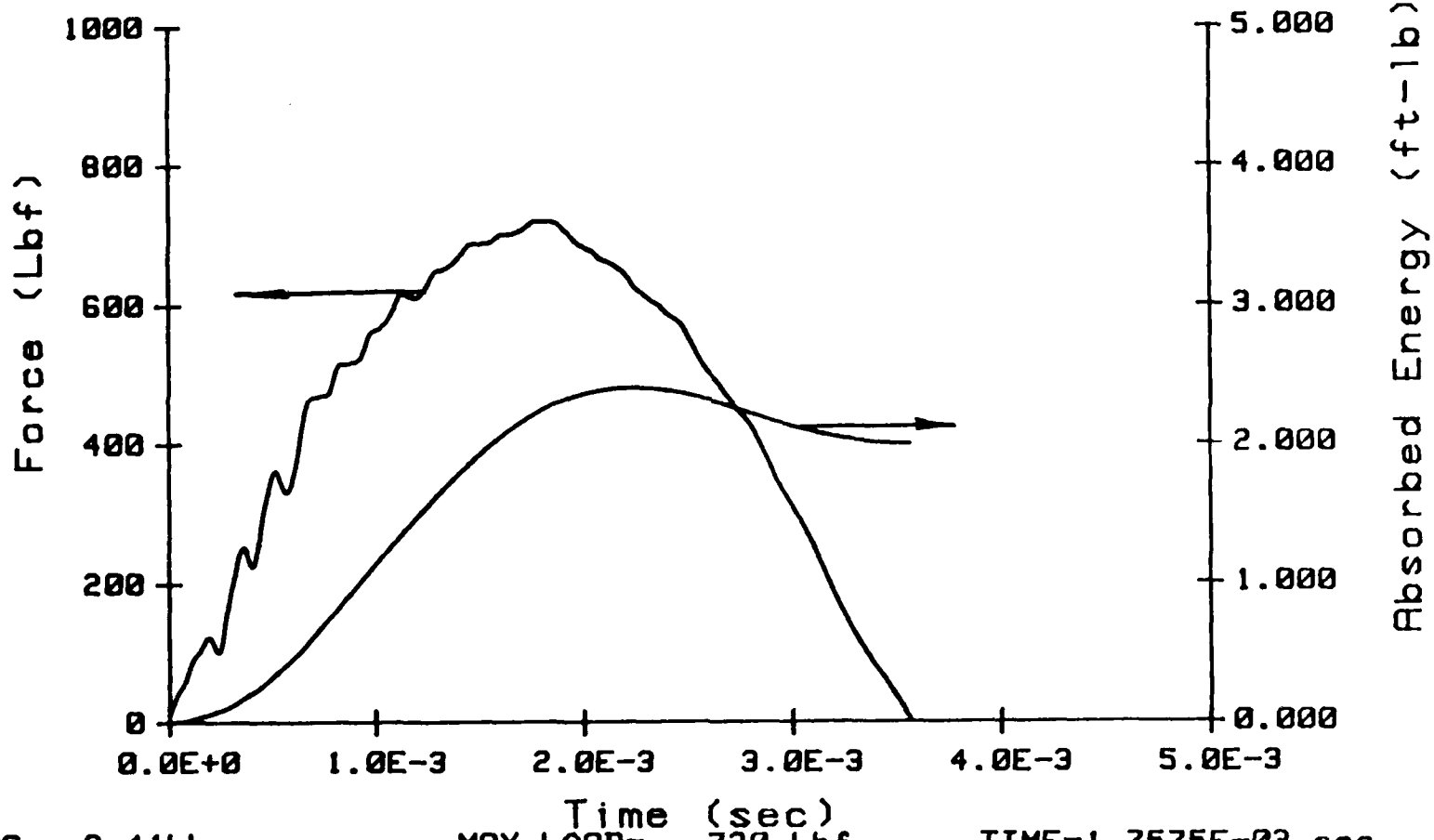

MASS= 8.41Lbm
MAX LOAD= 720 Lbf
TIME=1.7575E-03 sec
Vo= 4.25Ft/sec
Displacement= .0665inch
Eo= 2.35Ft-Lb
E absorbed= 2.21Ft-Lb

MCBI4.6

INSTRUMENTED IMPACT TEST

I53(I5G) 6/3/86

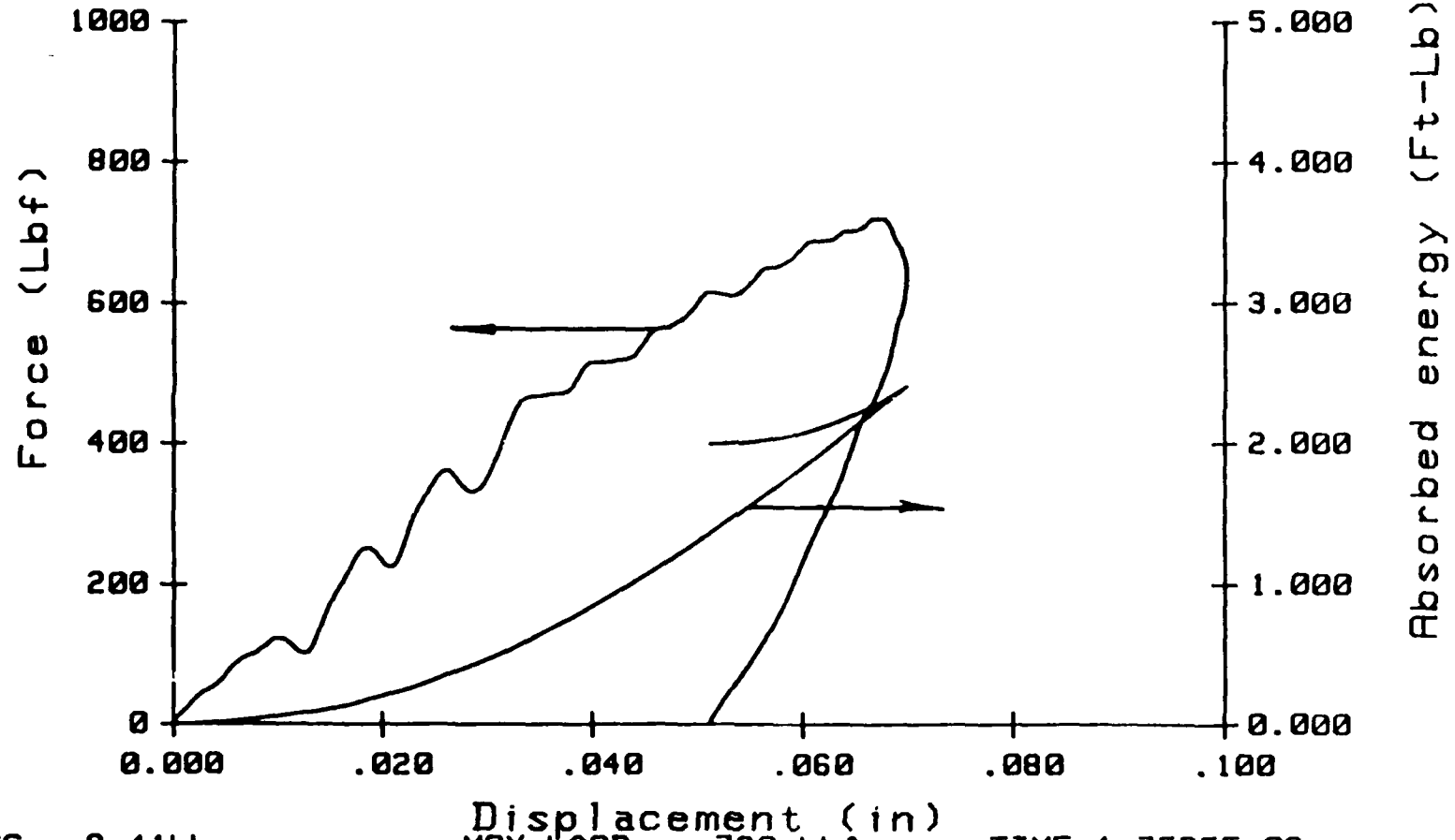

MASS= 8.41Lbm
MAX LOAD= 720 Lbf
TIME=1.7575E-03 sec
Vo= 4.25Ft/sec
Displacement= .0665inch
Eo= 2.35Ft-Lb
E absorbed= 2.21Ft-Lb

INSTRUMENTED IMPACT TEST

I54(I5G) 6/3/86

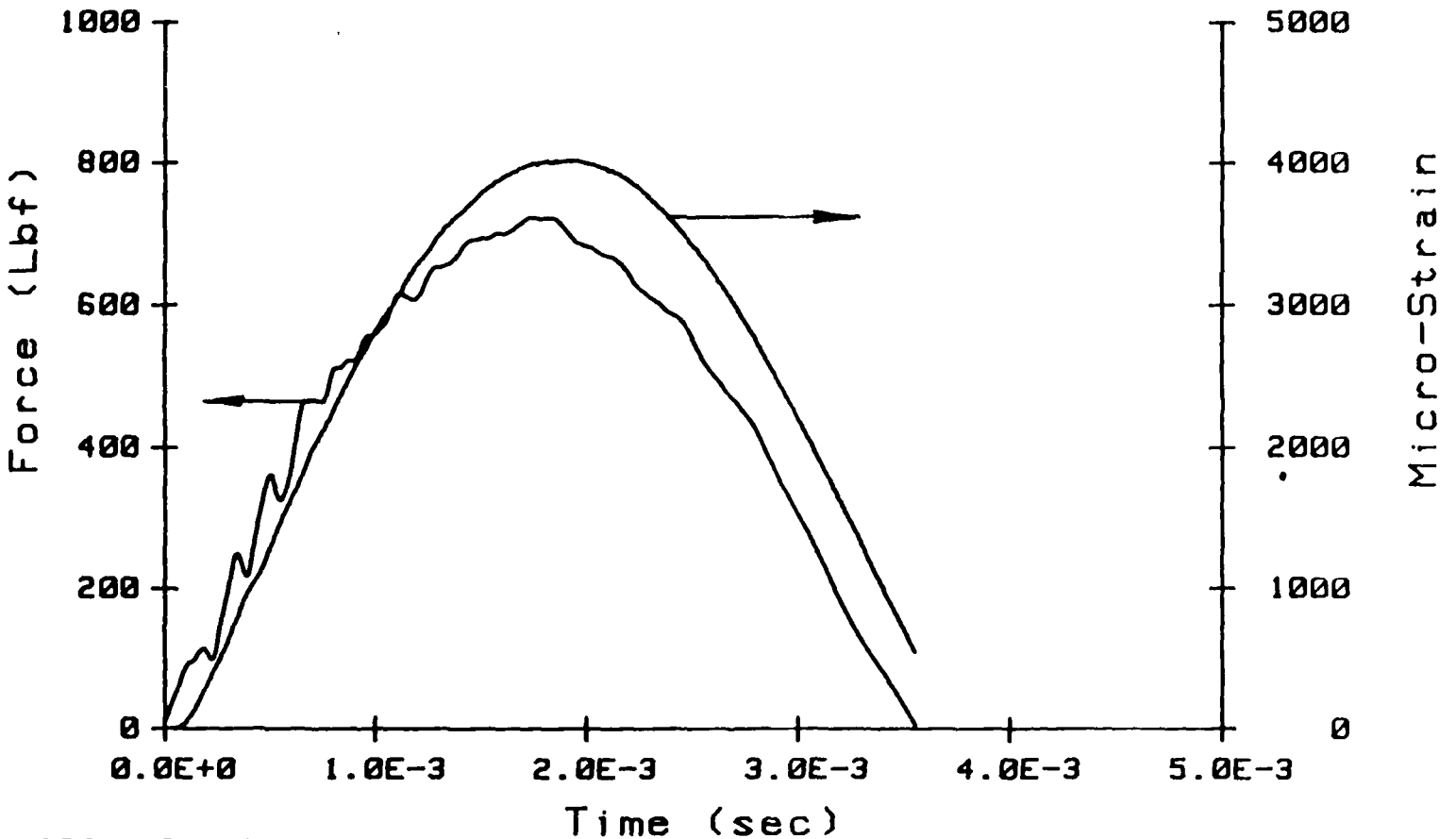

MAX LOAD= 724 Lbf MASS= 8.41 Lbm HEIGHT= .29 Ft

MAX STRAIN= 4020 Micro inch/inch

RADIUS= .13 inch LOAD SCALE= .8KN/DIV

INSTRUMENTED IMPACT TEST

I61(I6C) 6/4/86

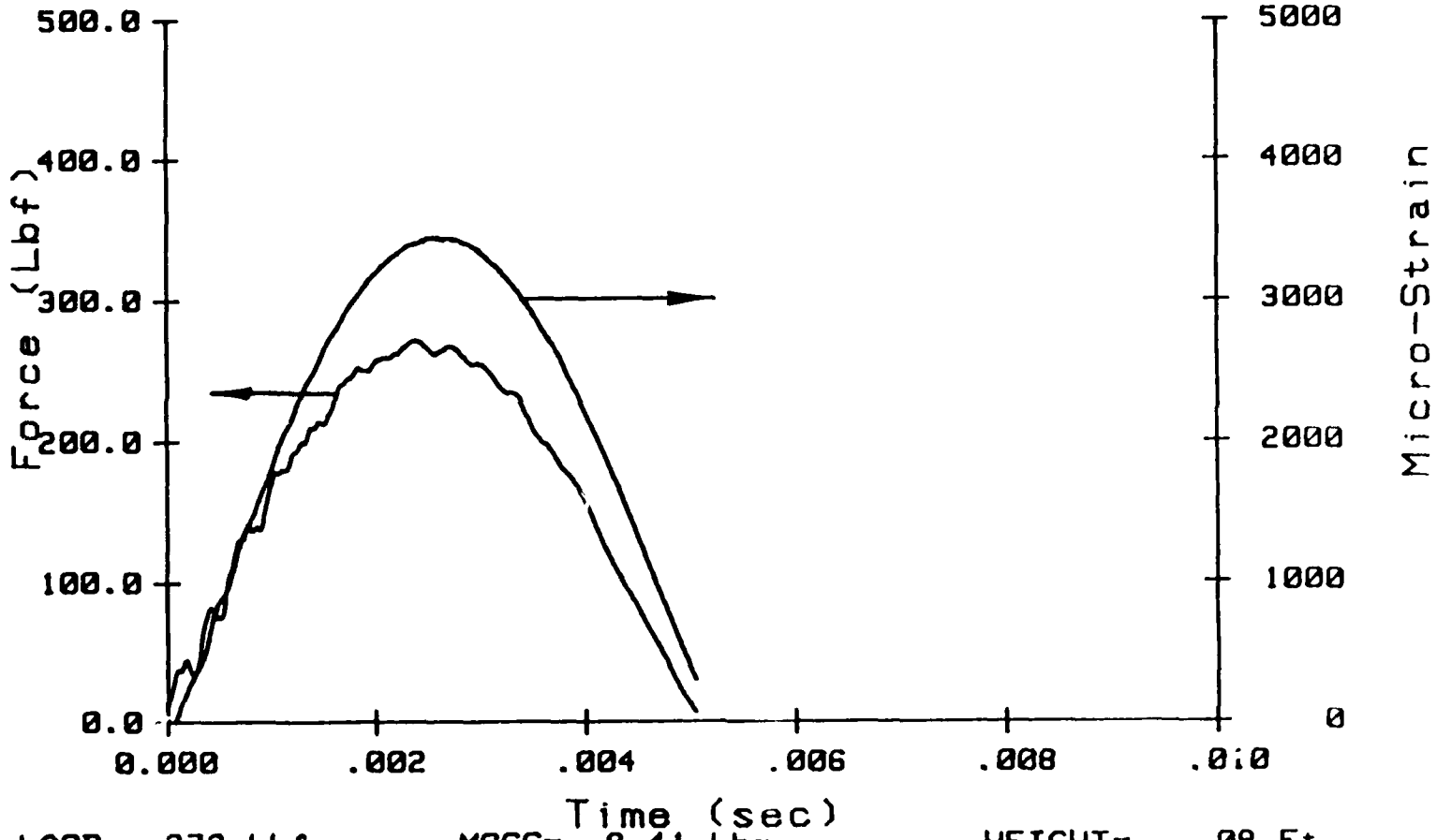

MAX LOAD= 272 Lbf MASS= 8.41 Lbm HEIGHT= .08 Ft

MAX STRAIN= 3450 Micro inch/inch

RADIUS= .13 inch LOAD SCALE= .8KN/DIV

INSTRUMENTED IMPACT TEST

I61 (LOAD CHECK)

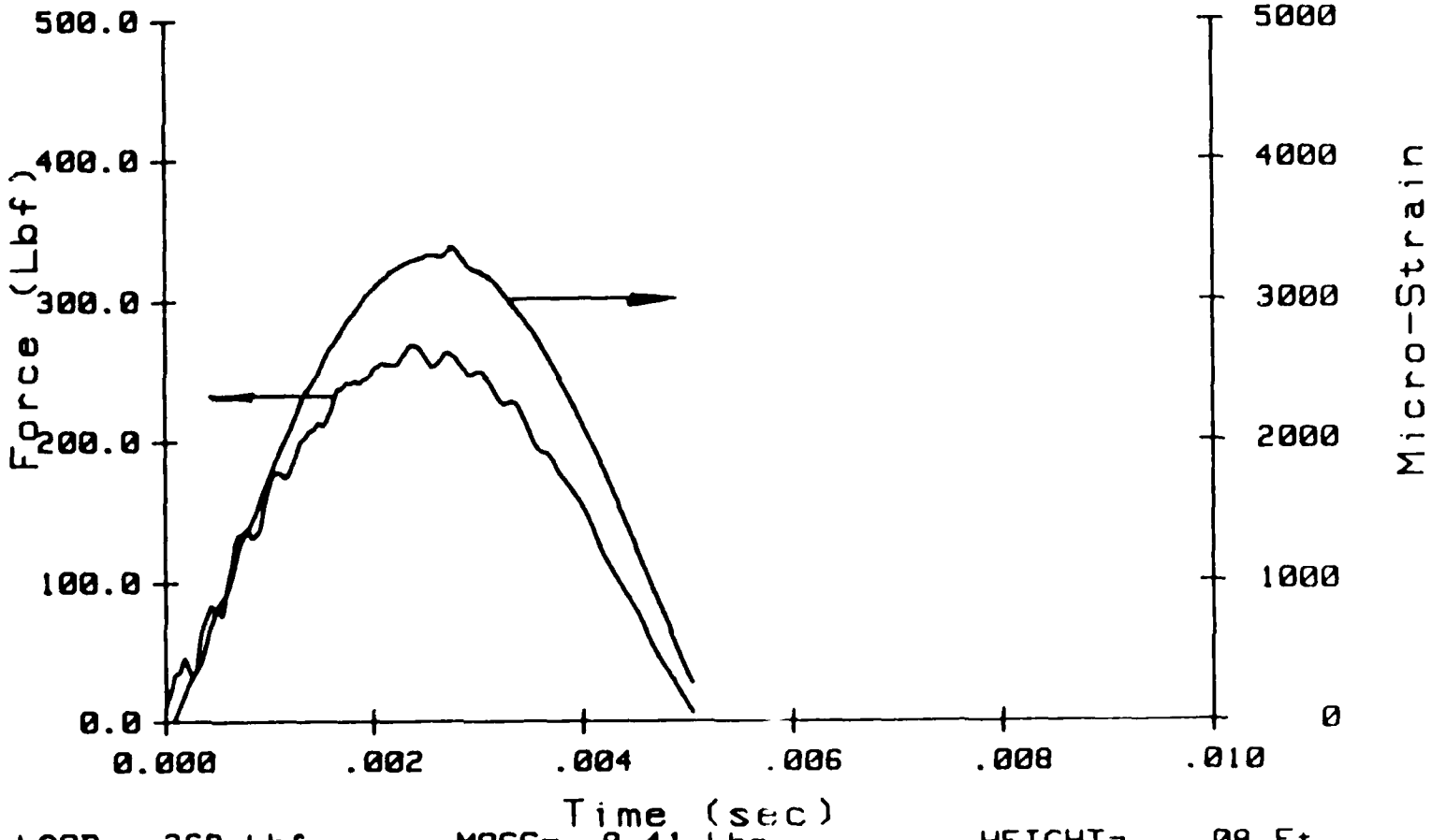

MAX LOAD= 269 Lbf MASS= 8.41 Lbm HEIGHT= .08 Ft

MAX STRAIN= 3390 Micro inch/inch

RADIUS= .13 inch LOAD SCALE= .8KN/DIV

MCBI5.1

INSTRUMENTED IMPACT TEST

I62(I6C) 6/4/86

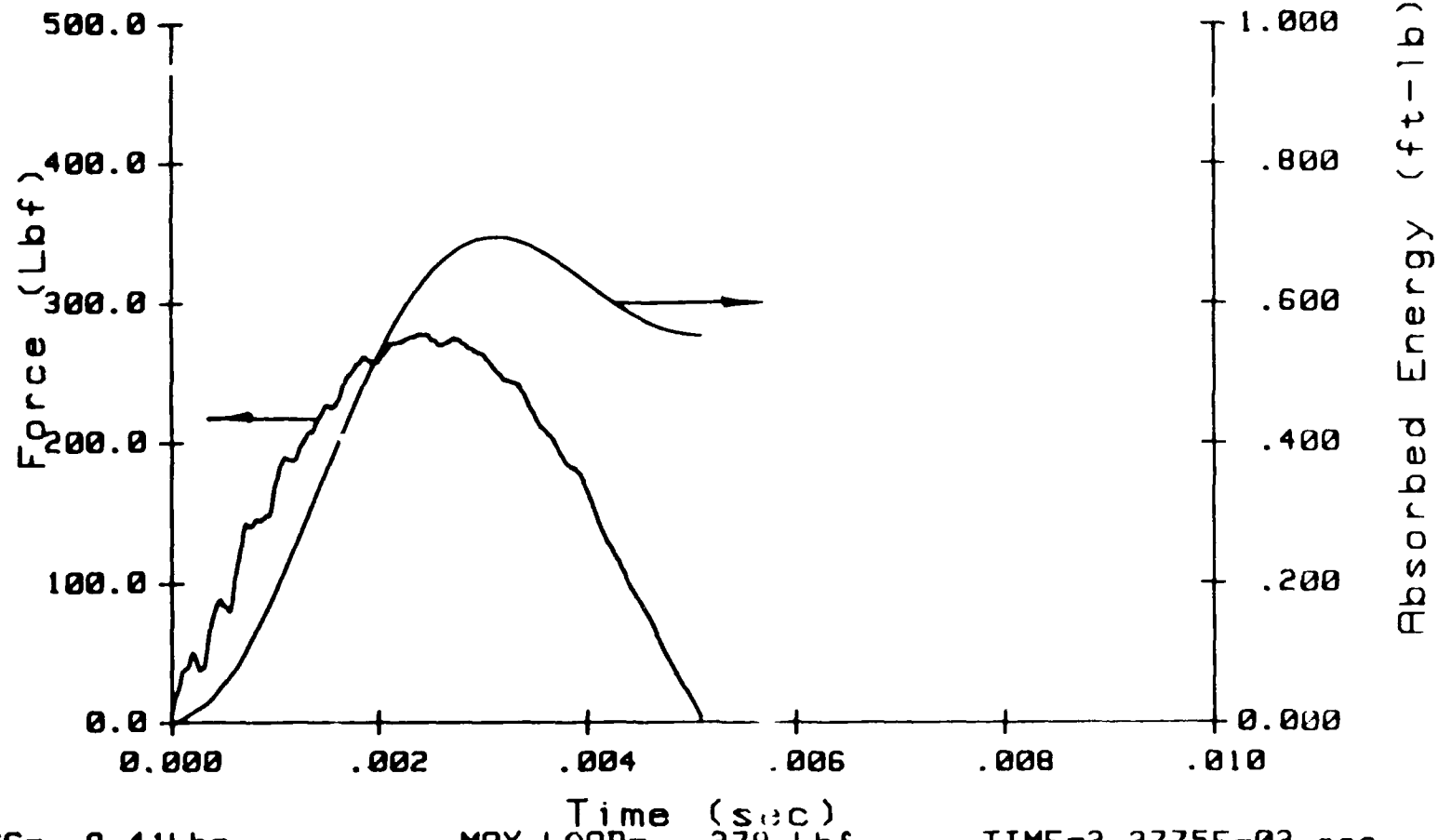

MASS= 8.41Lbm
MAX LOAD= 270 Lbf
TIME=2.3775E-03 sec
Vo= 2.24Ft/sec
Displacement= .0487inch
Eo= .66Ft-Lb
E absorbed= .62Ft-Lb

INSTRUMENTED IMPACT TEST

I62(I6C) 6/4/86

MASS= 8.41Lbm
Vo= 2.24Ft/sec
Eo= .66Ft-Lb

MAX LOAD= 278 Lbf
Displacement= .0487inch
E absorbed= .62Ft-Lb

TIME=2.3775E-03 sec

MCBI5.2

INSTRUMENTED IMPACT TEST

I63(I6C) 6/4/86

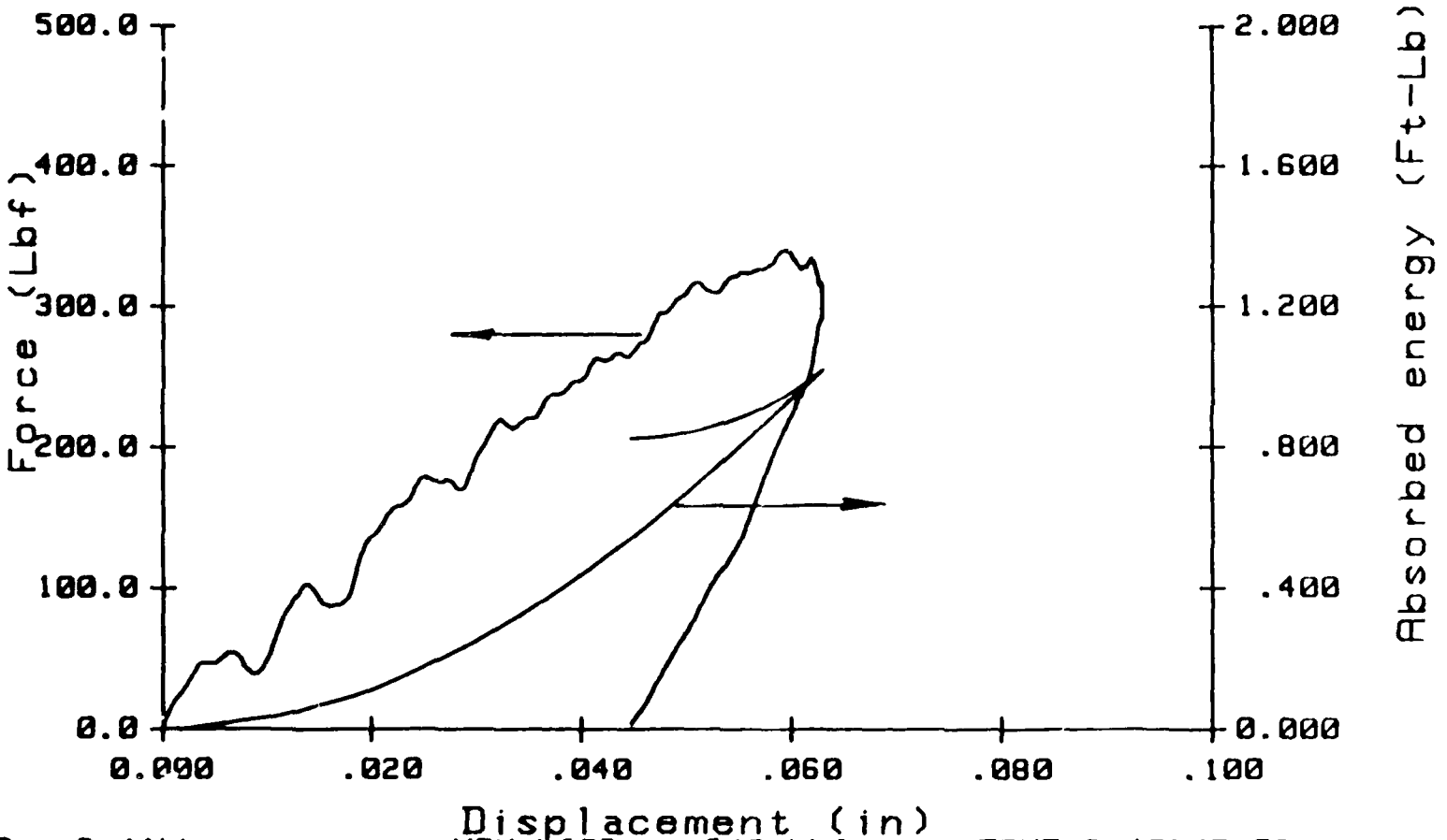

MASS= 8.41Lbm
Vo= 2.73Ft/sec
Eo= .97Ft-Lb

MAX LOAD= 340 Lbf
Displacement= .0594inch
E absorbed= .92Ft-Lb

TIME=2.4025E-03 sec

MCBIS.2

INSTRUMENTED IMPACT TEST

I63(I6C) 6/4/86

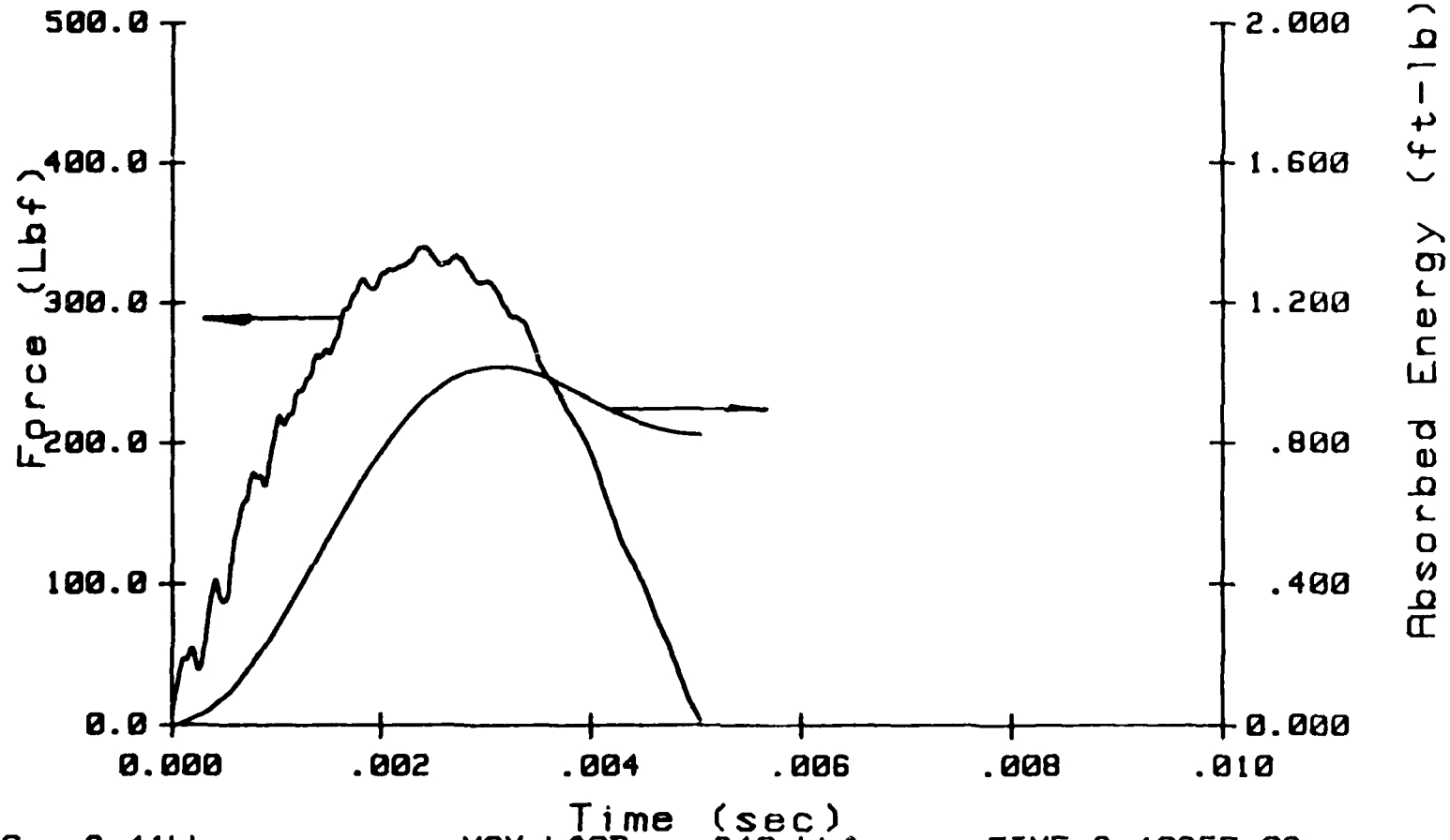

MASS= 8.41Lbm MAX LOAD= 340 Lbf TIME=2.4025E-03 sec

Vo= 2.73Ft/sec Displacement= .0594inch

Eo= .97Ft-Lb E absorbed= .92Ft-Lb

INSTRUMENTED IMPACT TEST

I64(I6C) 6/4/86

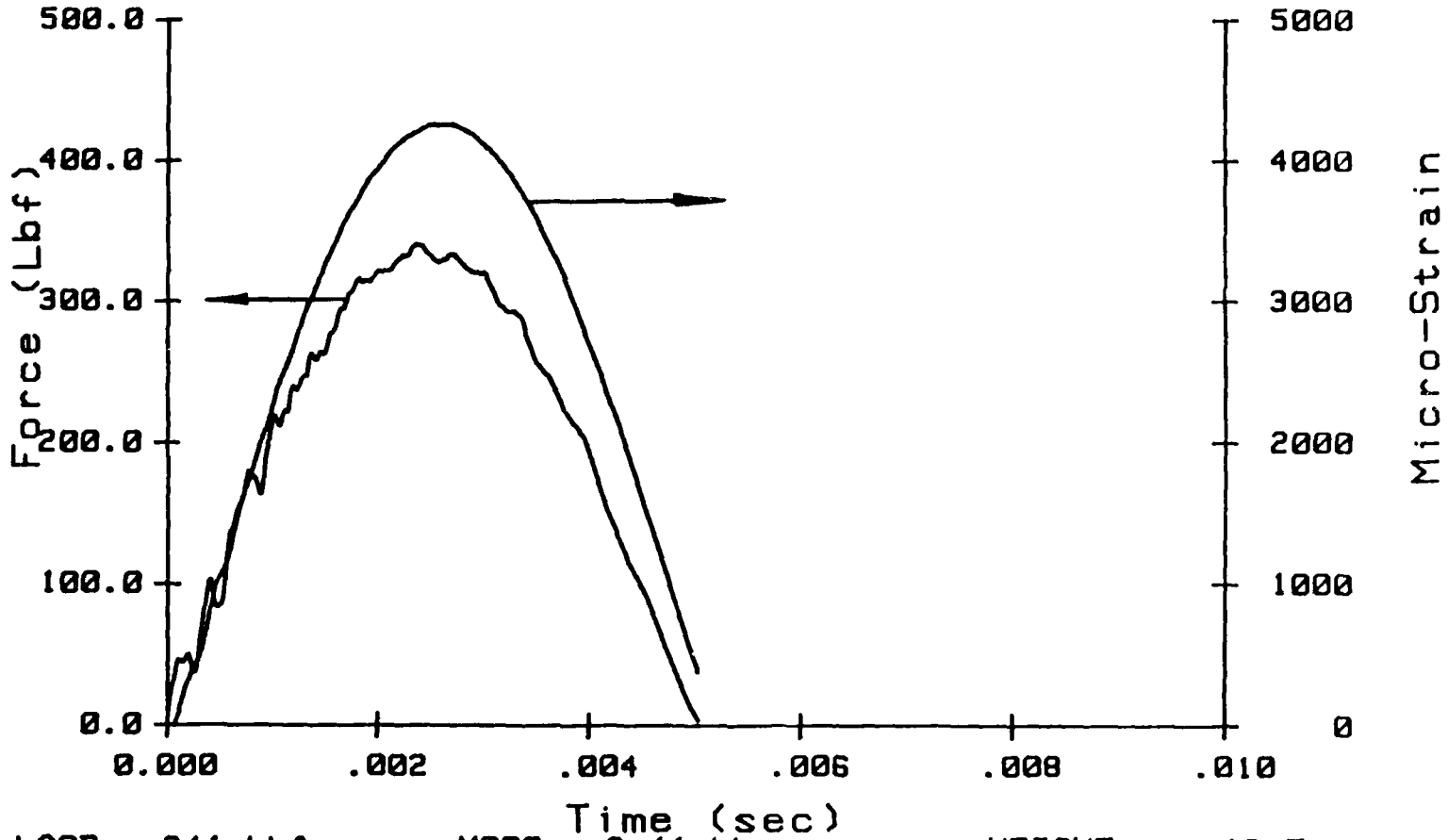

MAX LOAD= 341 Lbf MASS= 8.41 Lbm HEIGHT= .13 Ft

MAX STRAIN= 4265 Micro inch/inch

RADIUS= .13 inch LOAD SCALE= .2KN/DIV

NADC-87106-60

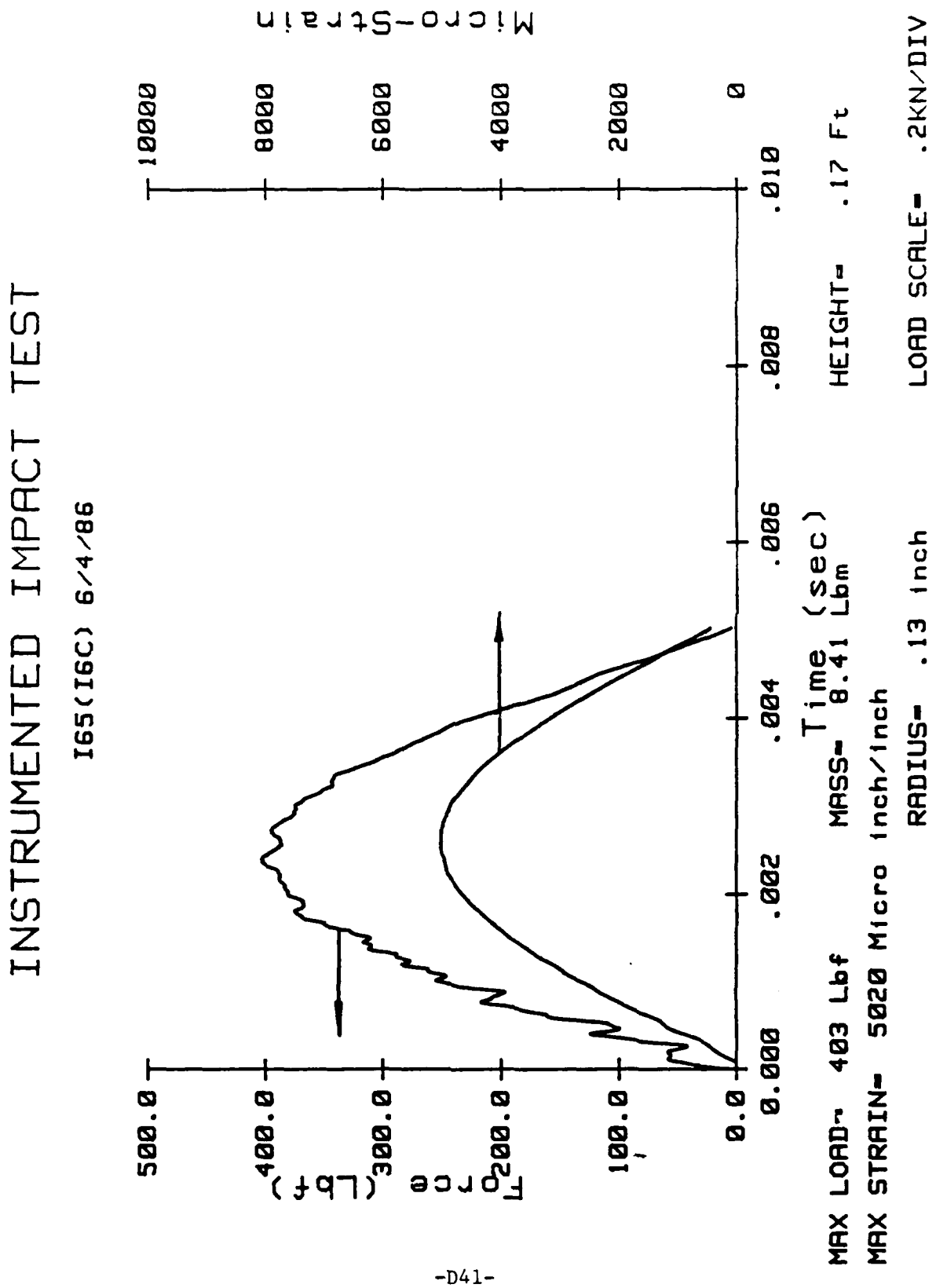
INSTRUMENTED IMPACT TEST
I65(I6C) 6/4/86
Force (Lbf)
500.0
400.0
300.0
200.0
100.0
0.0
0.000
.002
.004
.006
.008
.010
Time (sec)
Micro-Strain
10000
8000
6000
4000
2000
0
MAX LOAD= 403 Lbf
MAX STRAIN= 5020 Micro Inch/Inch
MASS= 8.41 Lbm
RADIUS= .13 Inch
HEIGHT= .17 Ft
LOAD SCALE= .2KN/DIV

MCBI5.5

INSTRUMENTED IMPACT TEST

I66(I6C) 6/4/86

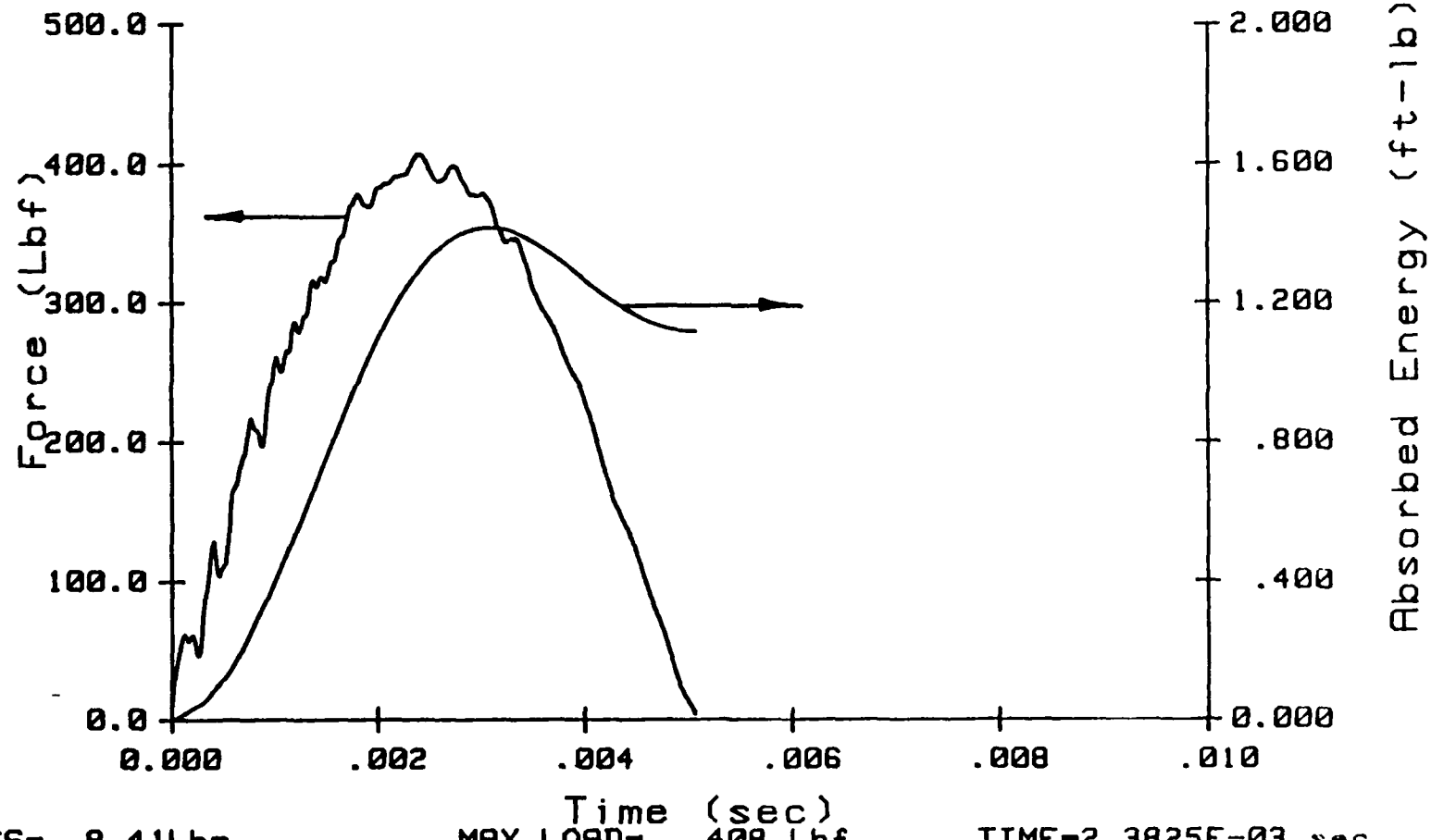

MASS= 8.41Lbm
Vo= 3.24Ft/sec
Eo= 1.37Ft-Lb

MAX LOAD= 408 Lbf
Displacement= .0695inch
E absorbed= 1.29Ft-Lb

TIME=2.3825E-03 sec

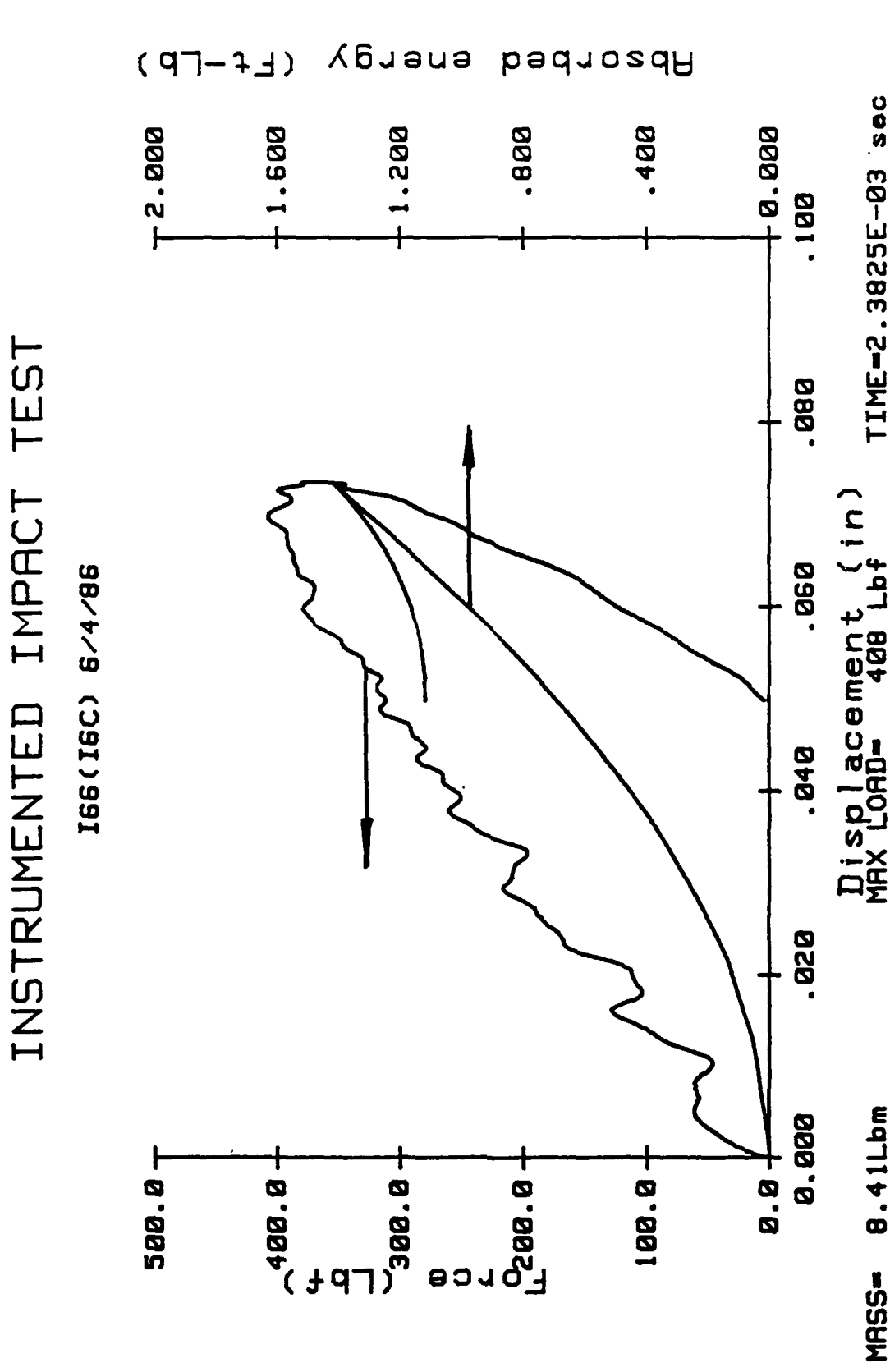
MCBIS.5
INSTRUMENTED IMPACT TEST
I66(I6C) 6/4/86
Absorbed energy (Ft-Lb)
2.000
1.600
1.200
.800
.400
0.000
.100
.080
.060
.040
.020
0.000
Displacement (in)
MAX LOAD= 408 Lbf
TIME=2.3825E-03 sec
Displacement= .0695inch
E absorbed= 1.29Ft-Lb
Force (Lbf)
500.0
400.0
300.0
200.0
100.0
0.0
MASS= 8.41Lbm
Vo= 3.24Ft/sec
Eo= 1.37Ft-Lb

INSTRUMENTED IMPACT TEST

I31(I1A) 6/4/86

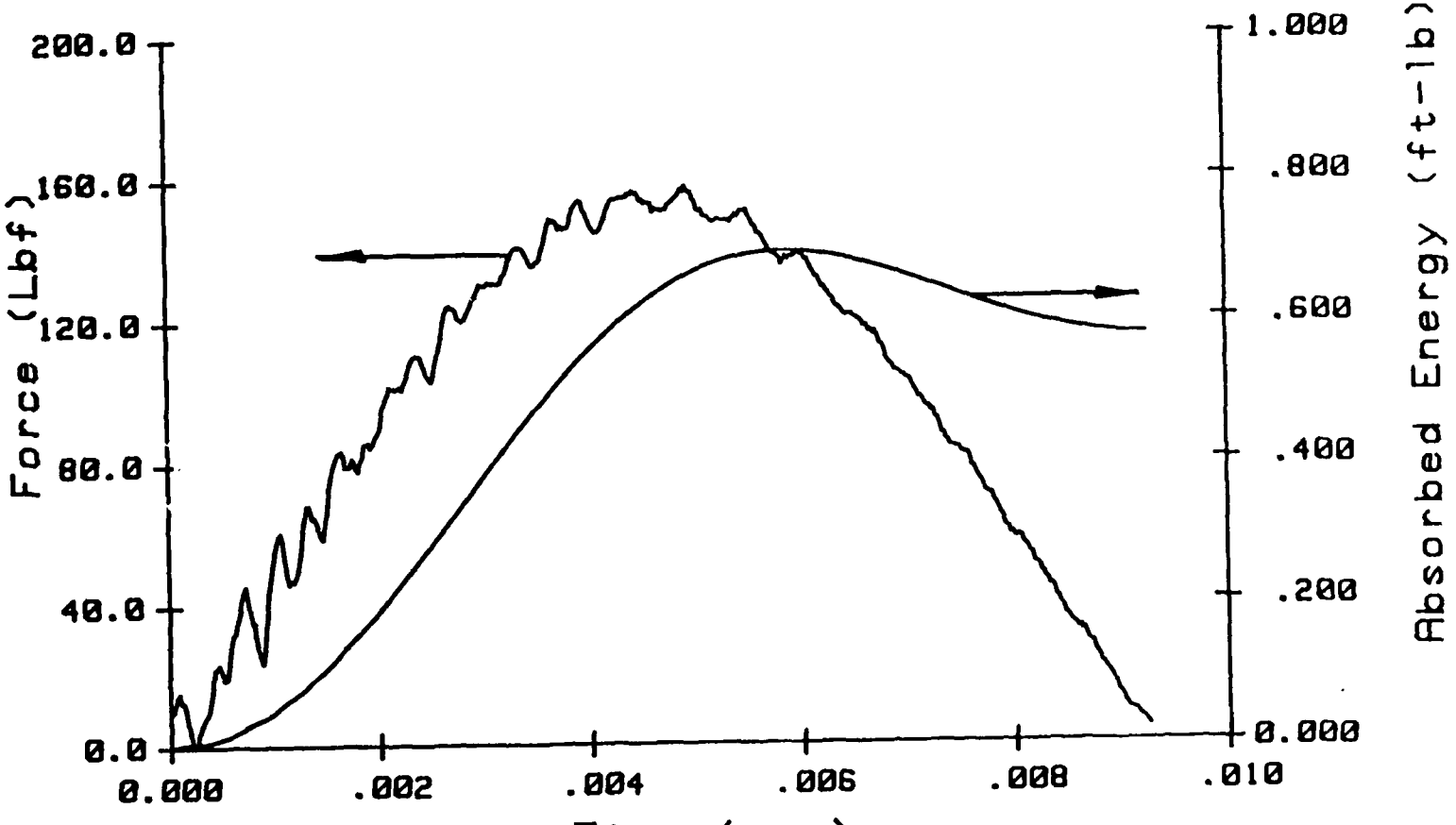

MASS= 8.41Lbm
Vo= 2.19Ft/sec
Eo= .63Ft-Lb

MAX LOAD= 158 Lbf
Displacement= .0953inch
E absorbed= .66Ft-Lb

TIME=4.9300E-03 sec

MCBI5.6

INSTRUMENTED IMPACT TEST

I31(I1A) 6/4/86

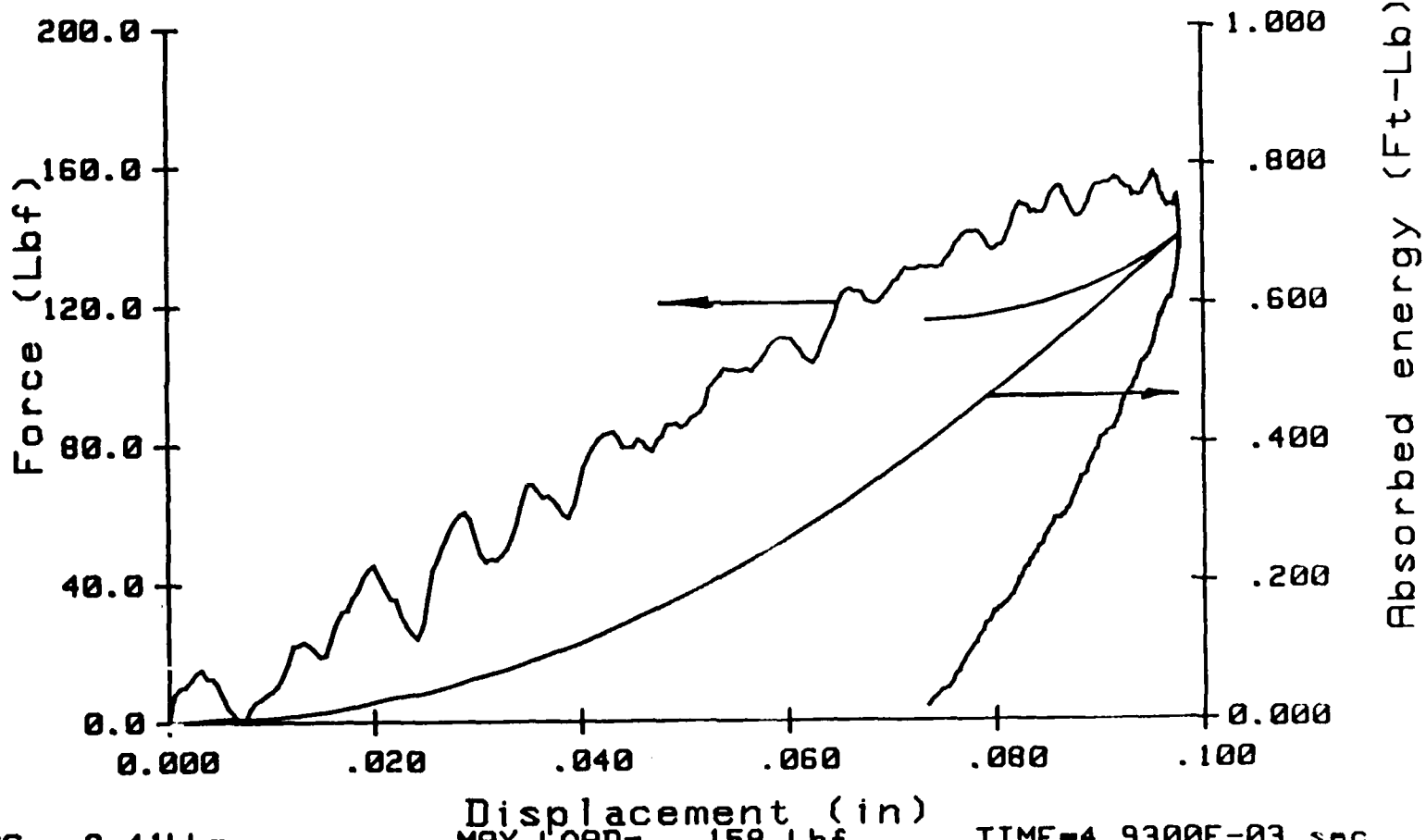

MASS= 8.41Lbm
Vo= 2.19Ft/sec
Eo= .63Ft-Lb

MAX LOAD= 158 Lbf
Displacement= .0953inch
E absorbed= .66Ft-Lb

TIME=4.9300E-03 sec

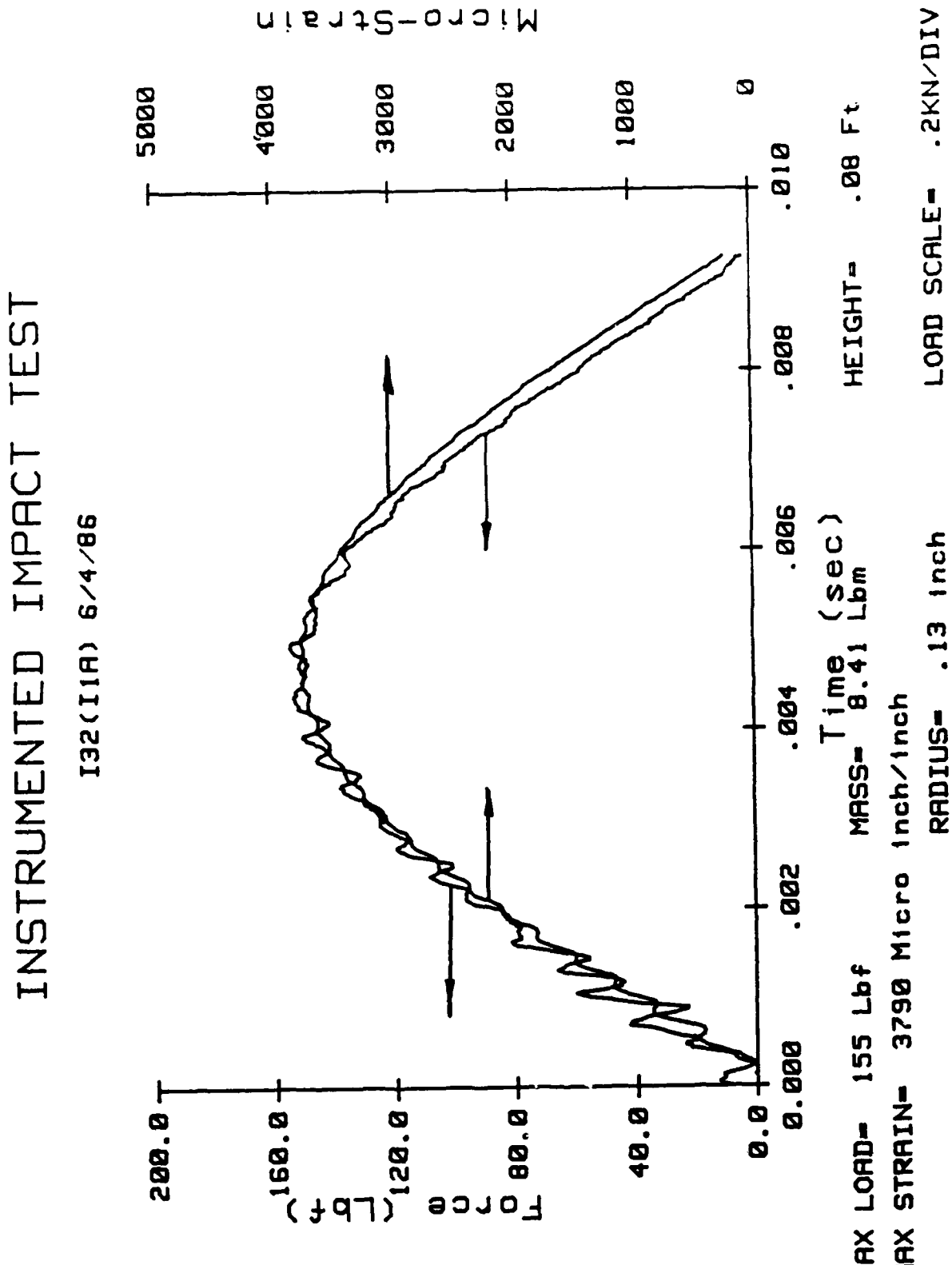
INSTRUMENTED IMPACT TEST
I32(IIA) 6/4/86
Micro-Strain
5000
4000
3000
2000
1000
0
Force (Lbf)
200.0
160.0
120.0
80.0
40.0
0.0
0.000
.002
.004
.006
.008
.010
Time (sec)
MAX LOAD= 155 Lbf
MASS= 8.41 Lbm
HEIGHT= .08 Ft
MAX STRAIN= 3790 Micro Inch/Inch
RADIUS= .13 Inch
LOAD SCALE= .2KN/DIV

INSTRUMENTED IMPACT TEST

I33(I1A) 6/4/86

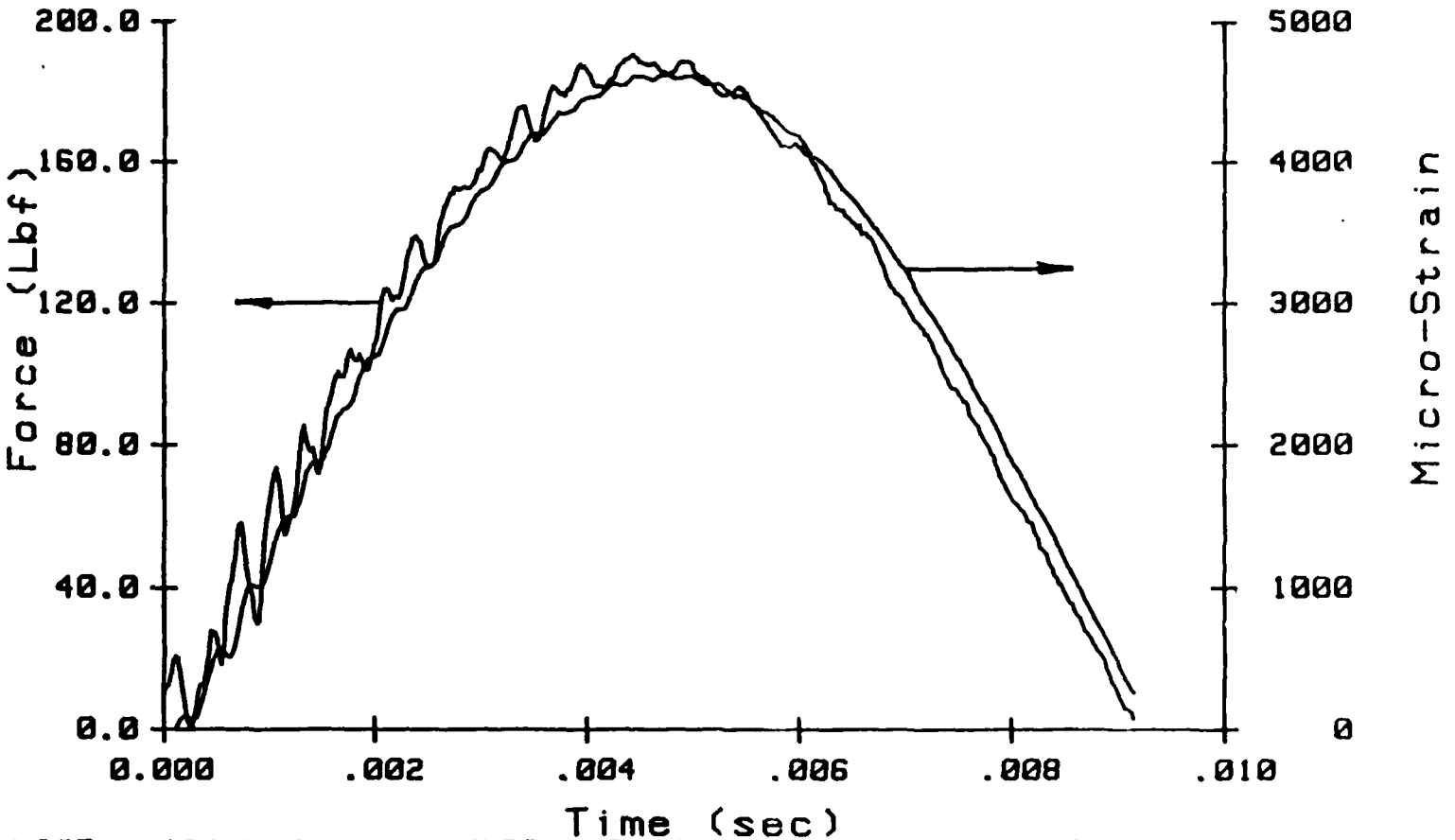

MAX LOAD= 191 Lbf MASS= 8.41 Lbm HEIGHT= .14 Ft

MAX STRAIN= 4620 Micro inch/inch

RADIUS= .13 inch LOAD SCALE= .2KN/DIV

INSTRUMENTED IMPACT TEST

I34(I1A) 6/4/86

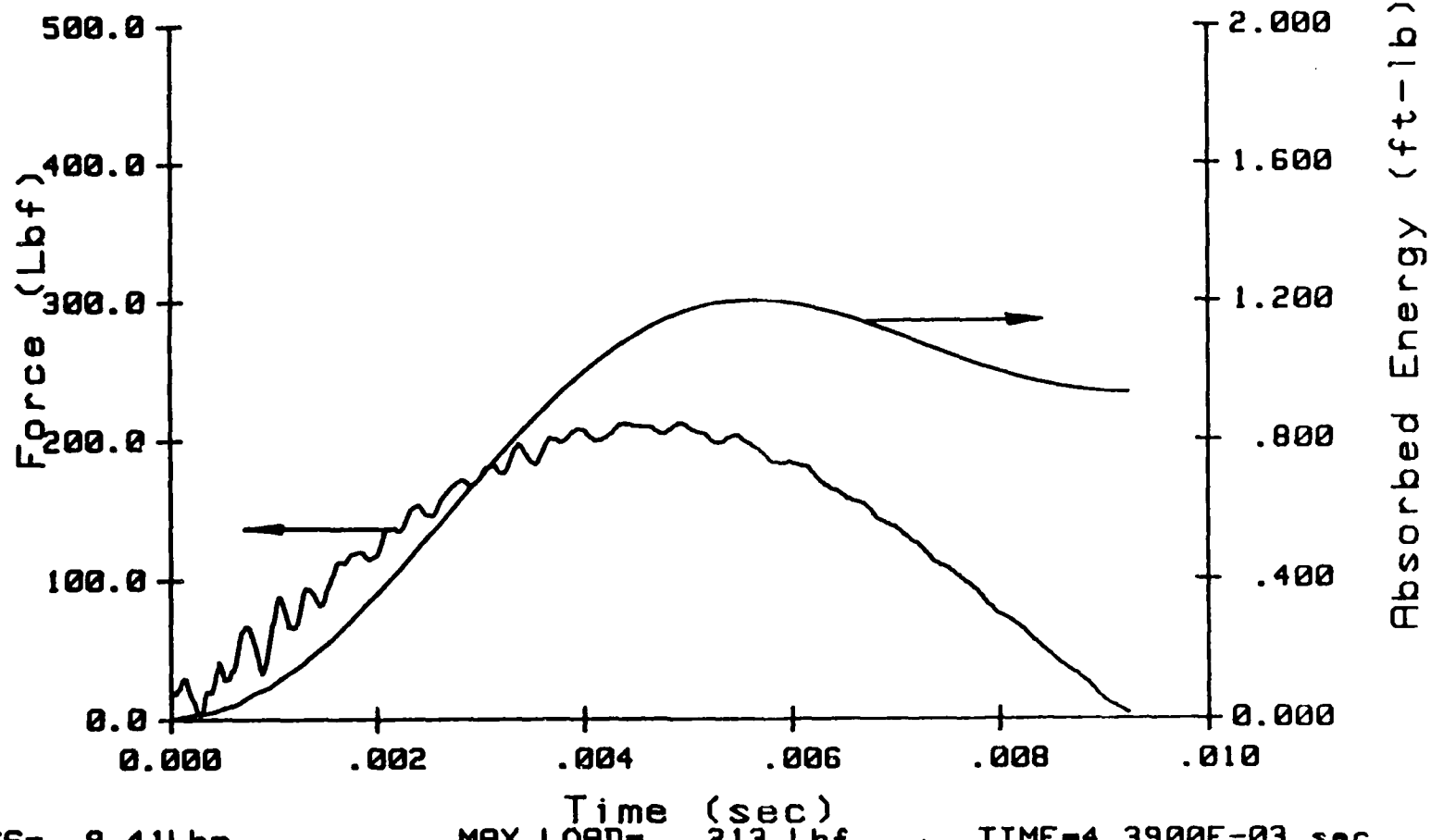

MASS= 8.41Lbm
Vo= 2.92Ft/sec
Eo= 1.12Ft-Lb

MAX LOAD= 213 Lbf
Displacement= .1185inch
E absorbed= 1.09Ft-Lb

TIME=4.3900E-03 sec

MCBI6.1

INSTRUMENTED IMPACT TEST

I34(IIA) 6/4/86

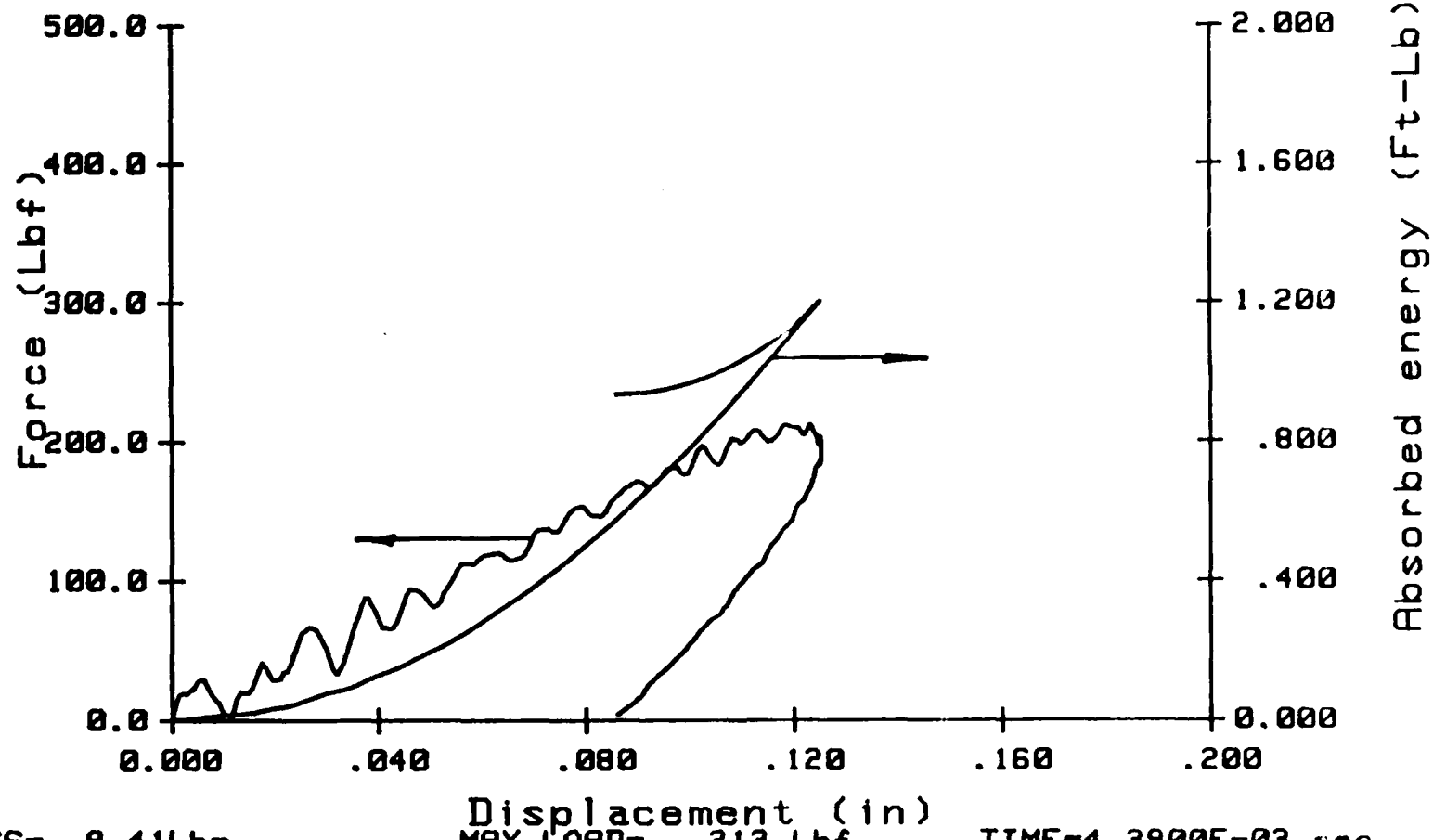

MASS= 8.41Lbm
Vo= 2.92Ft/sec
Eo= 1.12Ft-Lb

MAX LOAD= 213 Lbf
Displacement= .1185inch
E absorbed= 1.09Ft-Lb

TIME=4.3900E-03 sec

MCB16.2

INSTRUMENTED IMPACT TEST

I35(IIA) 6/4/86

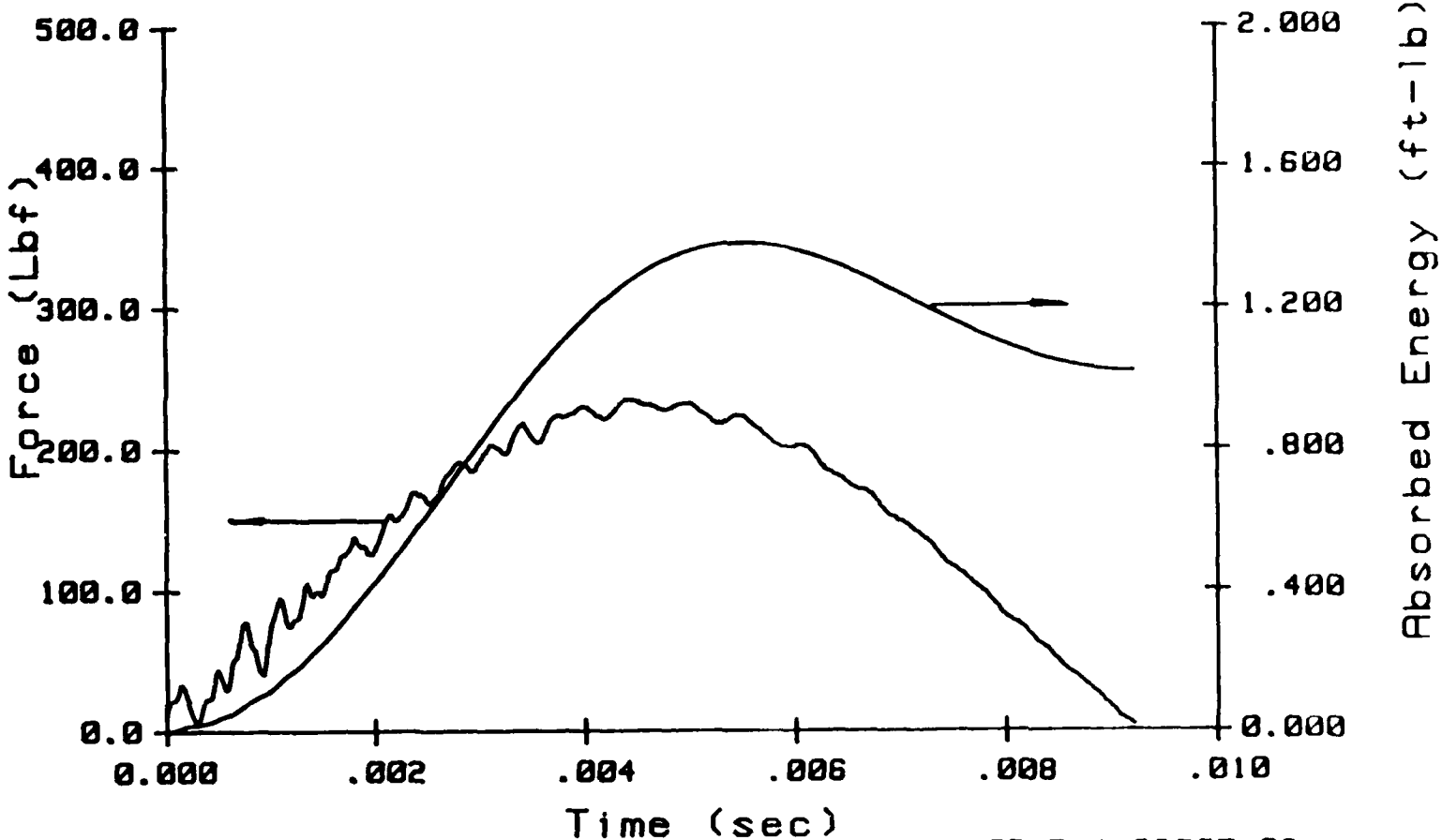

MASS= 8.41Lbm
Vo= 3.14Ft/sec
Eo= 1.29Ft-Lb

MAX LOAD= 235 Lbf
Displacement= .1260inch
E absorbed= 1.27Ft-Lb

TIME=4.3900E-03 sec

INSTRUMENTED IMPACT TEST

I35(I1A) 6/4/86

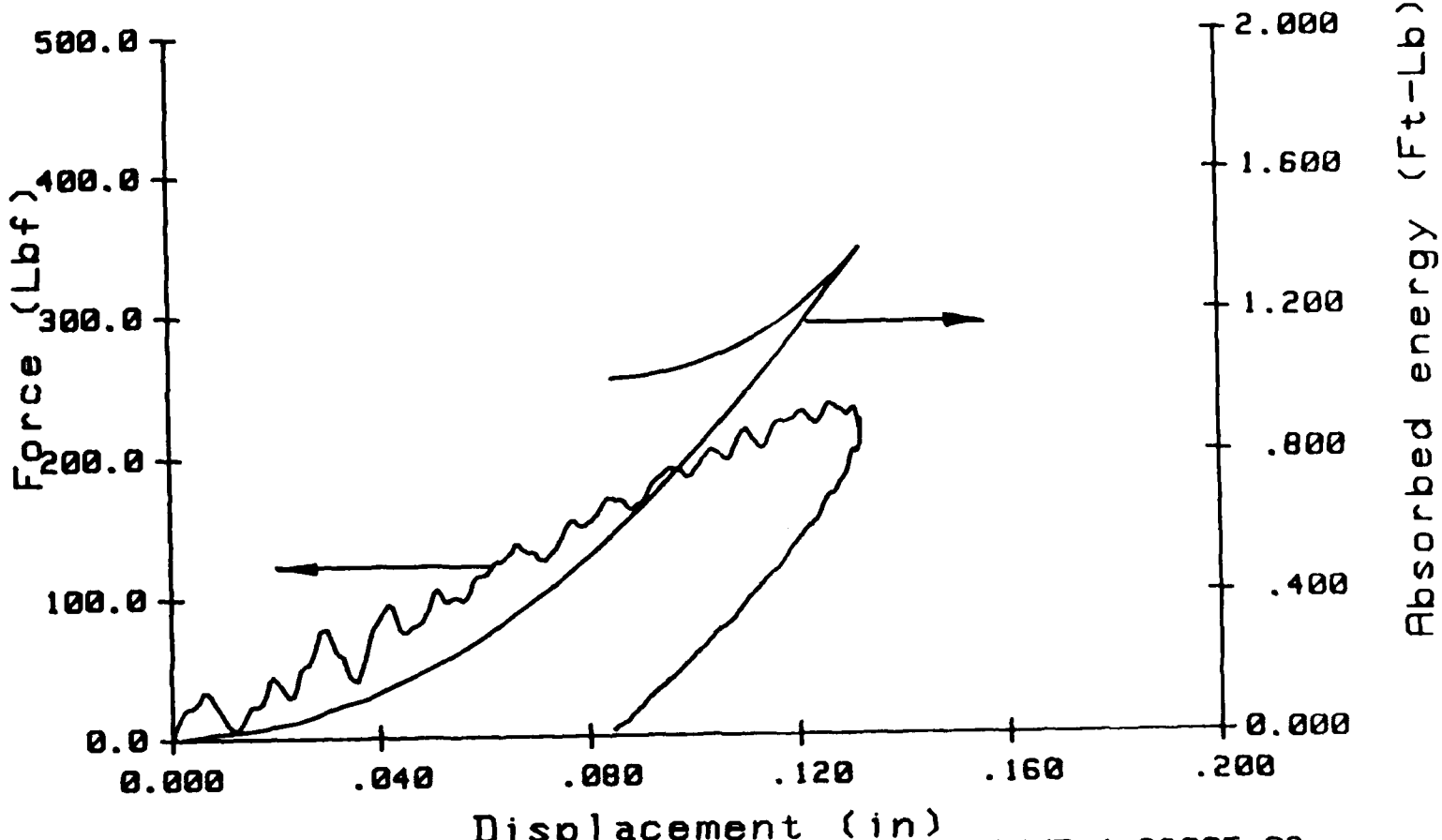

MASS= 8.41Lbm
Vo= 3.14Ft/sec
Eo= 1.29Ft-Lb

MAX LOAD= 235 Lbf
Displacement= .1260inch
E absorbed= 1.27Ft-Lb

TIME=4.3900E-03 sec

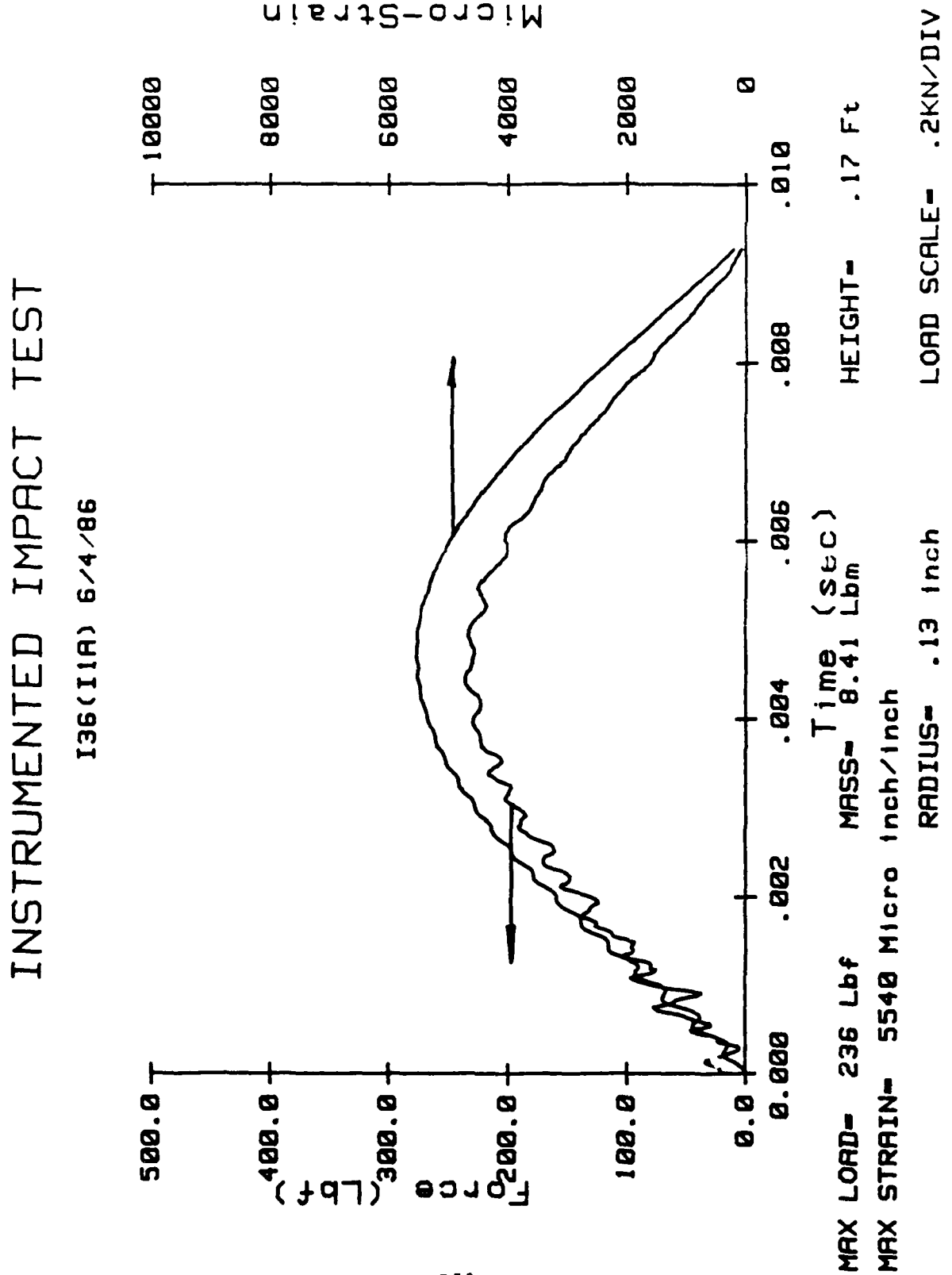
INSTRUMENTED IMPACT TEST
I36(I1A) 6/4/86
Force (Lbf)
500.0
400.0
300.0
200.0
100.0
0.0
Micro-Strain
10000
8000
6000
4000
2000
0
0.000
.002
.004
.006
.008
.010
Time (Sec)
MAX LOAD= 236 Lbf
MAX STRAIN= 5540 Micro Inch/Inch
MASS= 8.41 Lbm
RADIUS= .13 Inch
HEIGHT= .17 Ft
LOAD SCALE= .2KN/DIV

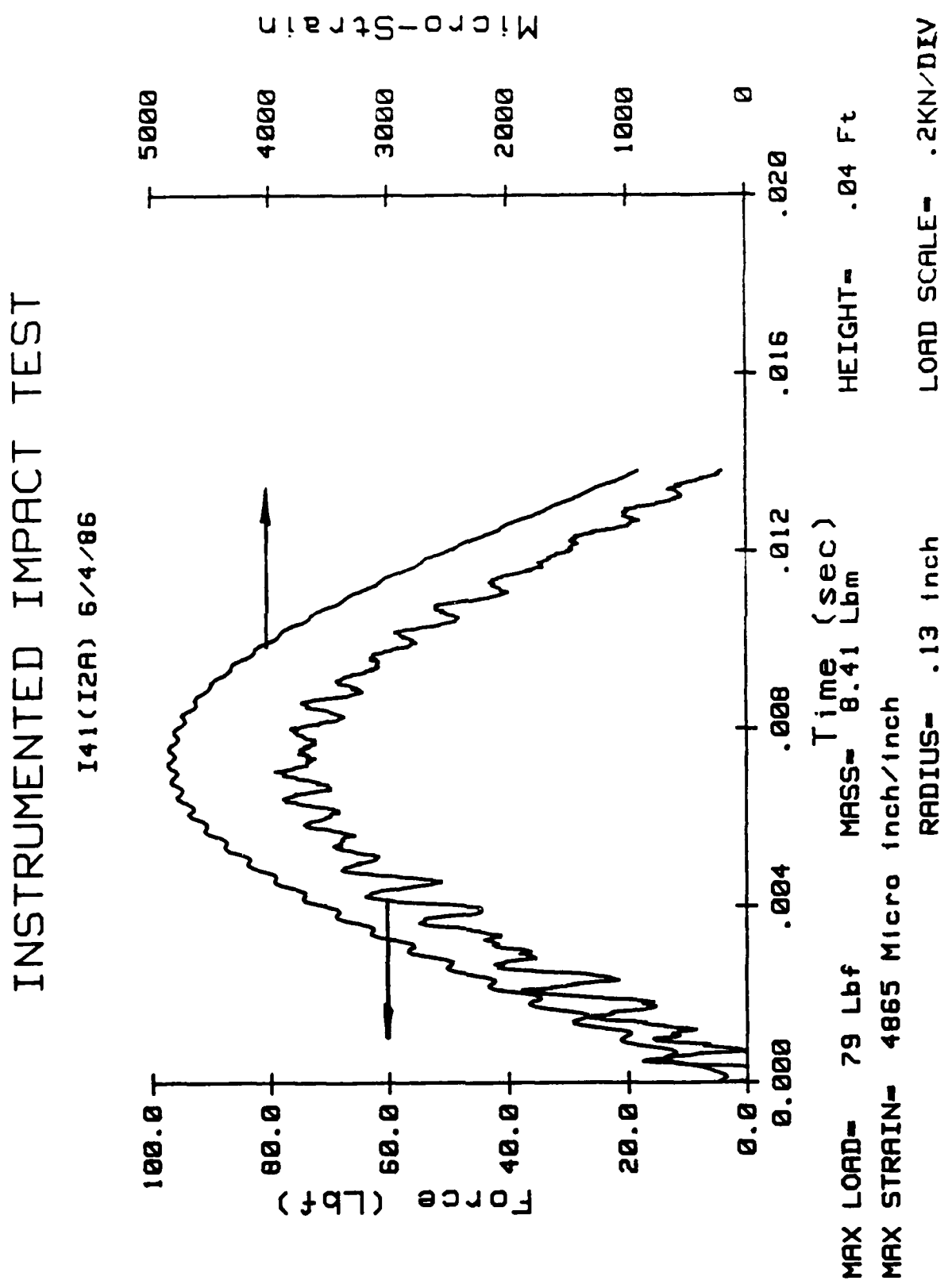
INSTRUMENTED IMPACT TEST
I41(I2A) 6/4/86
Force (Lbf)
100.0
80.0
60.0
40.0
20.0
0.0
0.000
.004
.008
.012
.016
.020
Time (sec)
Micro-Strain
5000
4000
3000
2000
1000
0
MAX LOAD= 79 Lbf
MASS= 8.41 Lbm
HEIGHT= .04 Ft
MAX STRAIN= 4865 Micro inch/inch
RADIUS= .13 inch
LOAD SCALE= .2KN/DIV

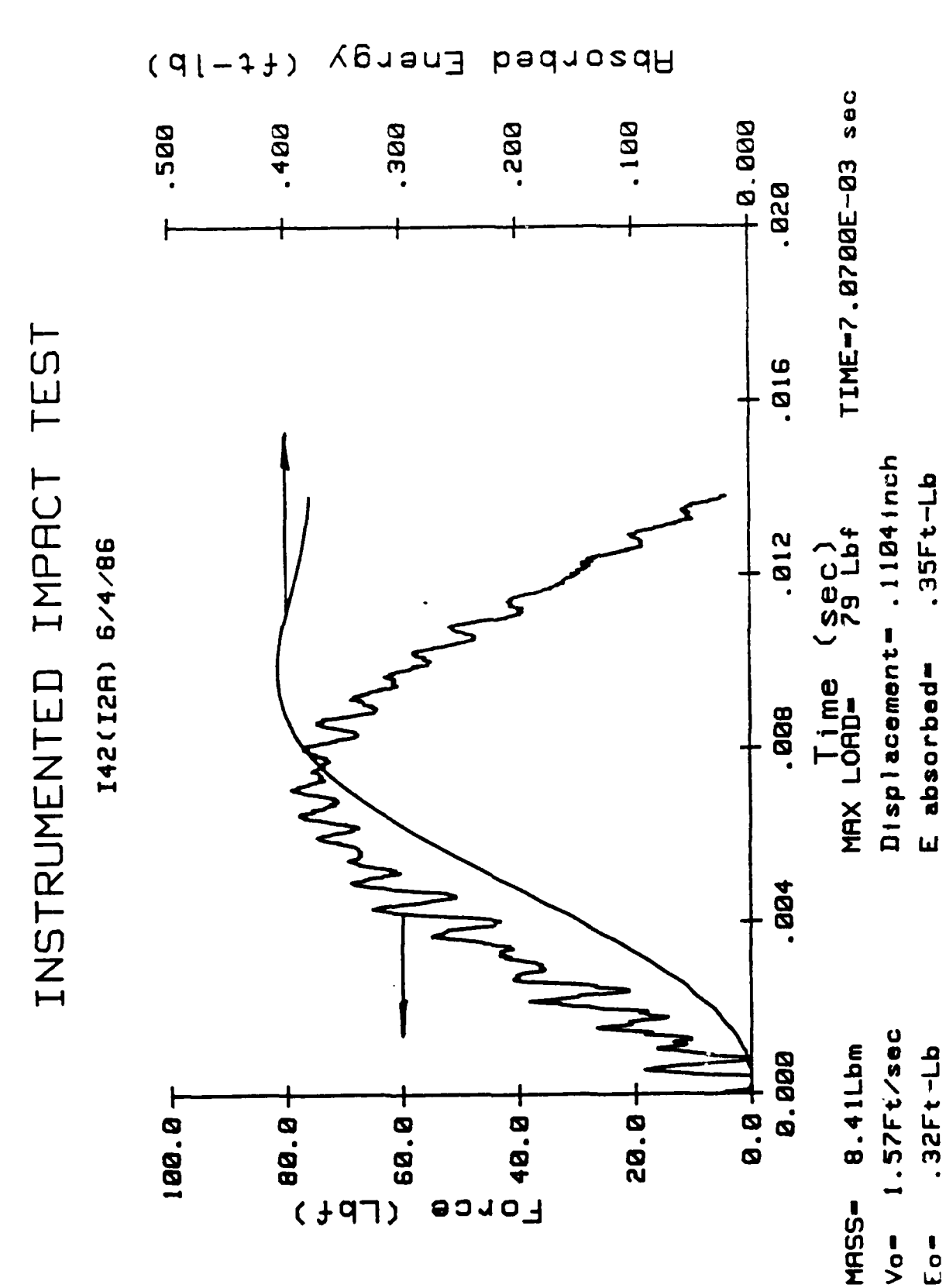
MCBI6.3
INSTRUMENTED IMPACT TEST
I42(I2A) 6/4/86
Force (Lbf)
100.0
80.0
60.0
40.0
20.0
0.0
0.000
.004
.008
.012
.016
.020
Time (sec)
Absorbed Energy (ft-lb)
.500
.400
.300
.200
.100
0.000
MAX LOAD= 79 Lbf
TIME=7.0700E-03 sec
Displacement= .1104inch
E absorbed= .35Ft-Lb
MASS= 8.41Lbm
Vo= 1.57Ft/sec
Eo= .32Ft-Lb

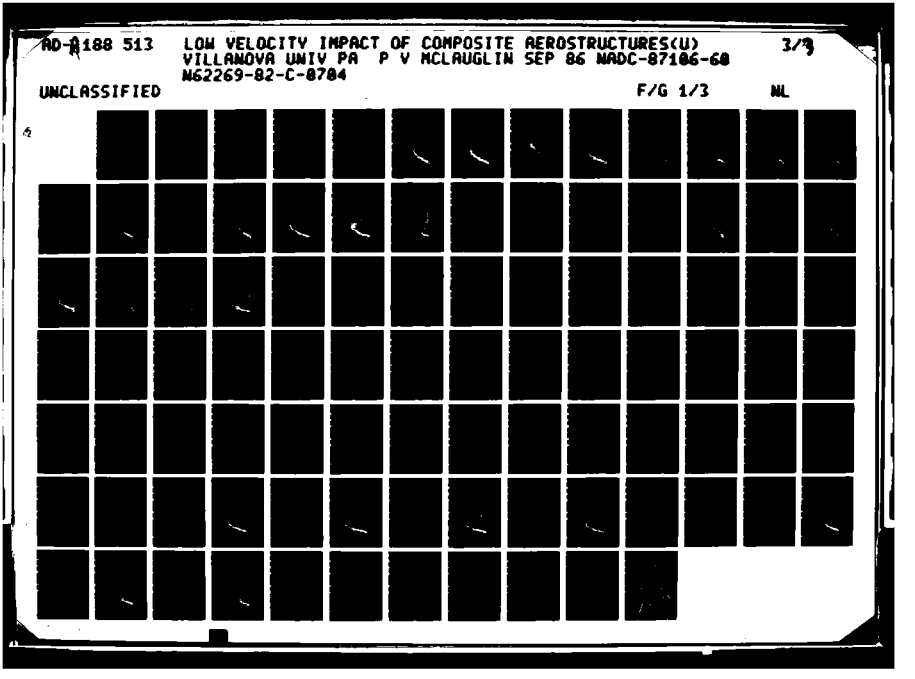
AD-A188 513
LOW VELOCITY IMPACT OF COMPOSITE AEROSTRUCTURES(U)
VILLANOVA UNIV PA P V MCLAUGLIN SEP 86 NADC-87106-68
N62269-82-C-0784
3/3
UNCLASSIFIED
F/G 1/3
NL

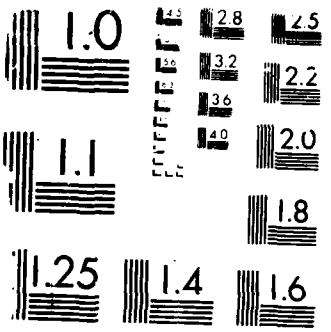

MCBI6.5

INSTRUMENTED IMPACT TEST

I42(I2A) 6/4/86

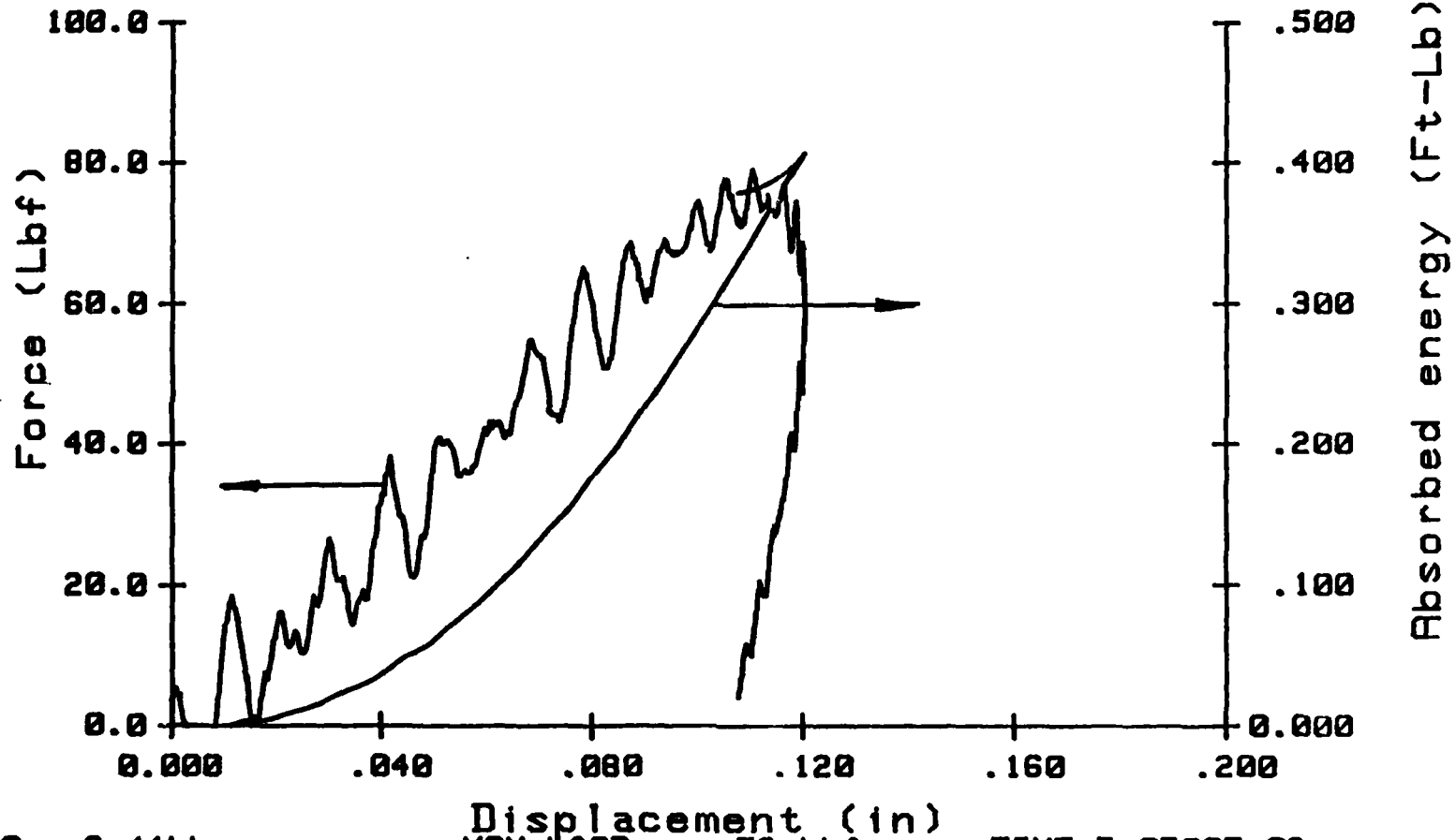

MASS= 8.41Lbm
Vo= 1.57Ft/sec
Eo= .32Ft-Lb

MAX LOAD= 79 Lbf
Displacement= .1104inch
E absorbed= .35Ft-Lb

TIME=7.0700E-03 sec

MCBI6.6

INSTRUMENTED IMPACT TEST

I43(I2A) 6/4/86

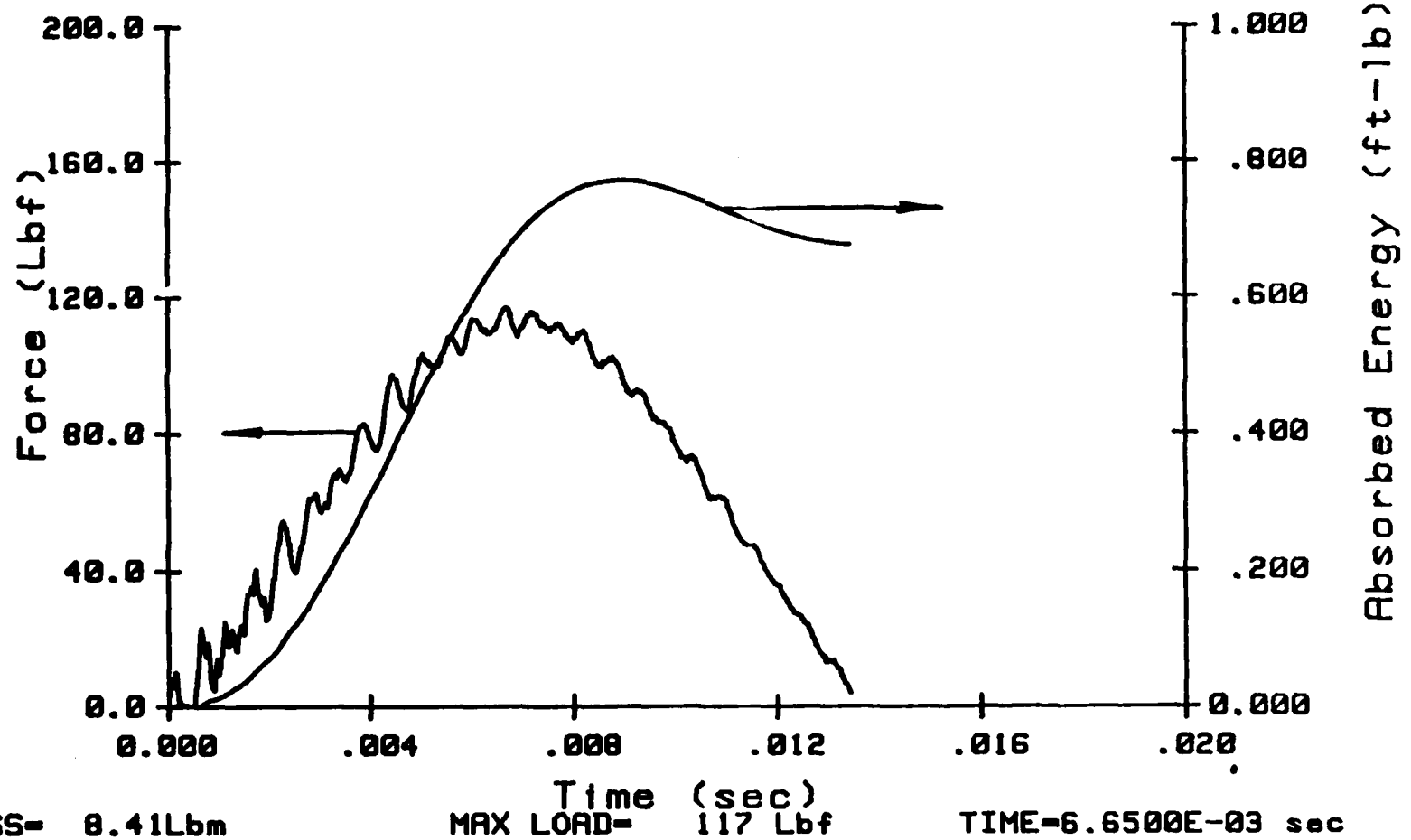

MASS= 8.41Lbm
Vo= 2.25Ft/sec
Eo= .66Ft-Lb

MAX LOAD= 117 Lbf
Displacement= .1466inch
E absorbed= .67Ft-Lb

TIME=6.6500E-03 sec

MCBI6.6

INSTRUMENTED IMPACT TEST

I43(I2A) 6/4/86

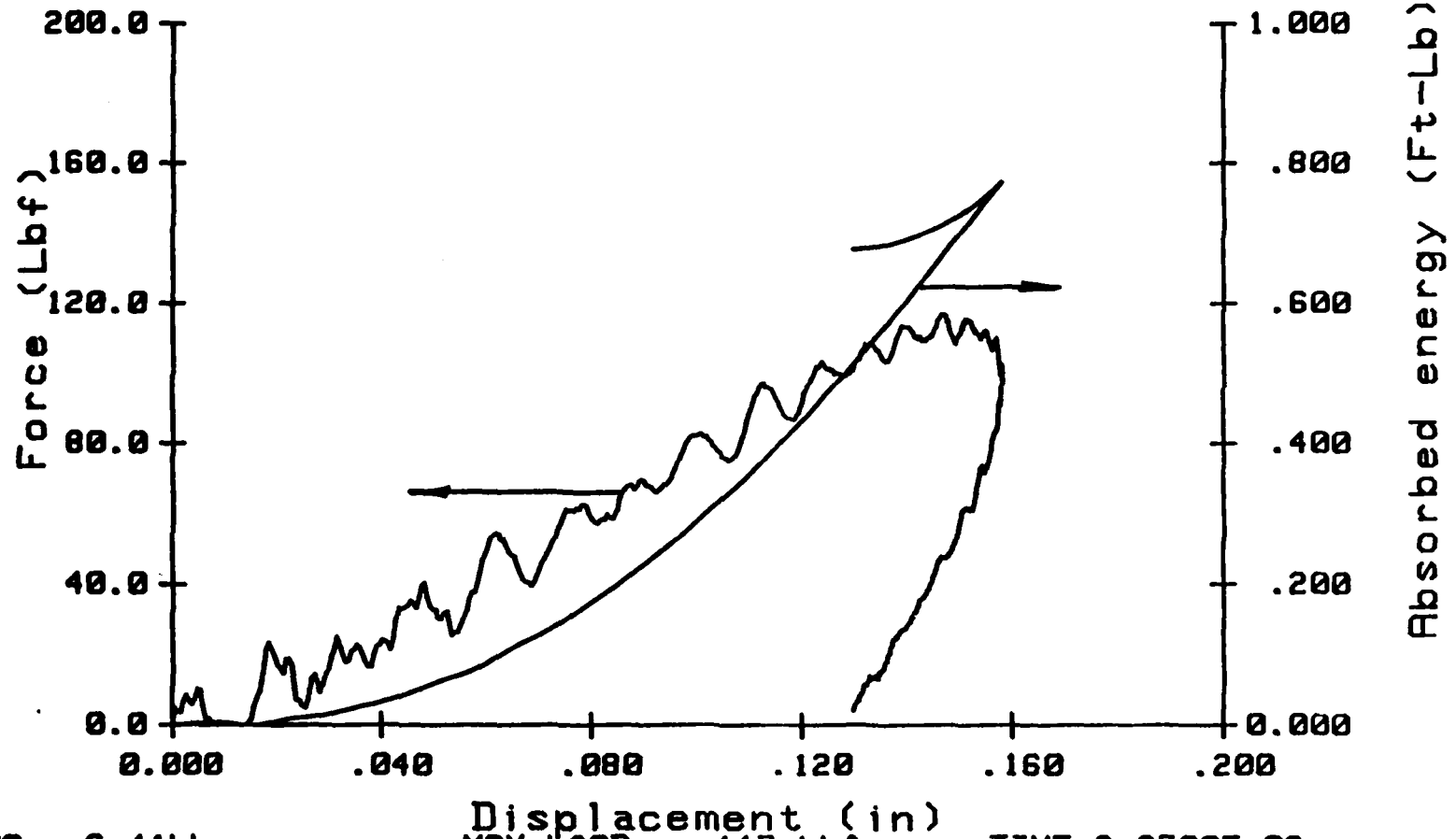

MASS= 8.41Lbm
Vo= 2.25Ft/sec
Eo= .66Ft-Lb

MAX LOAD= 117 Lbf
Displacement= .1466inch
E absorbed= .57Ft-Lb

TIME=6.6500E-03 sec

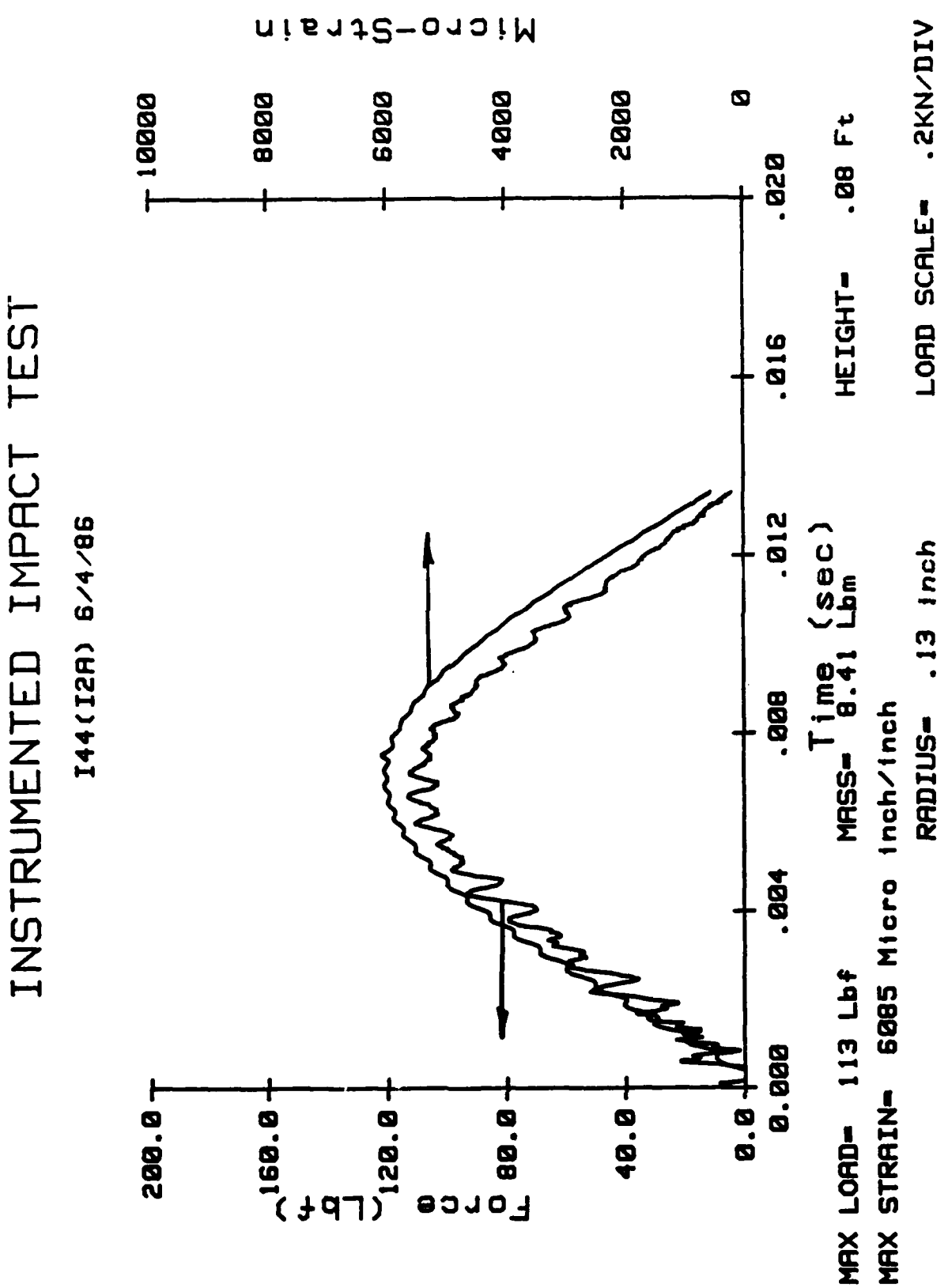
INSTRUMENTED IMPACT TEST
I44(I2A) 6/4/86
Micro-Strain
10000
8000
6000
4000
2000
0
Force (Lbf)
200.0
160.0
120.0
80.0
40.0
0.0
0.000
.004
.008
.012
.016
.020
Time (sec)
MAX LOAD= 113 Lbf
MASS= 8.41 Lbm
HEIGHT= .08 Ft
MAX STRAIN= 6085 Micro Inch/Inch
RADIUS= .13 Inch
LOAD SCALE= .2KN/DIV

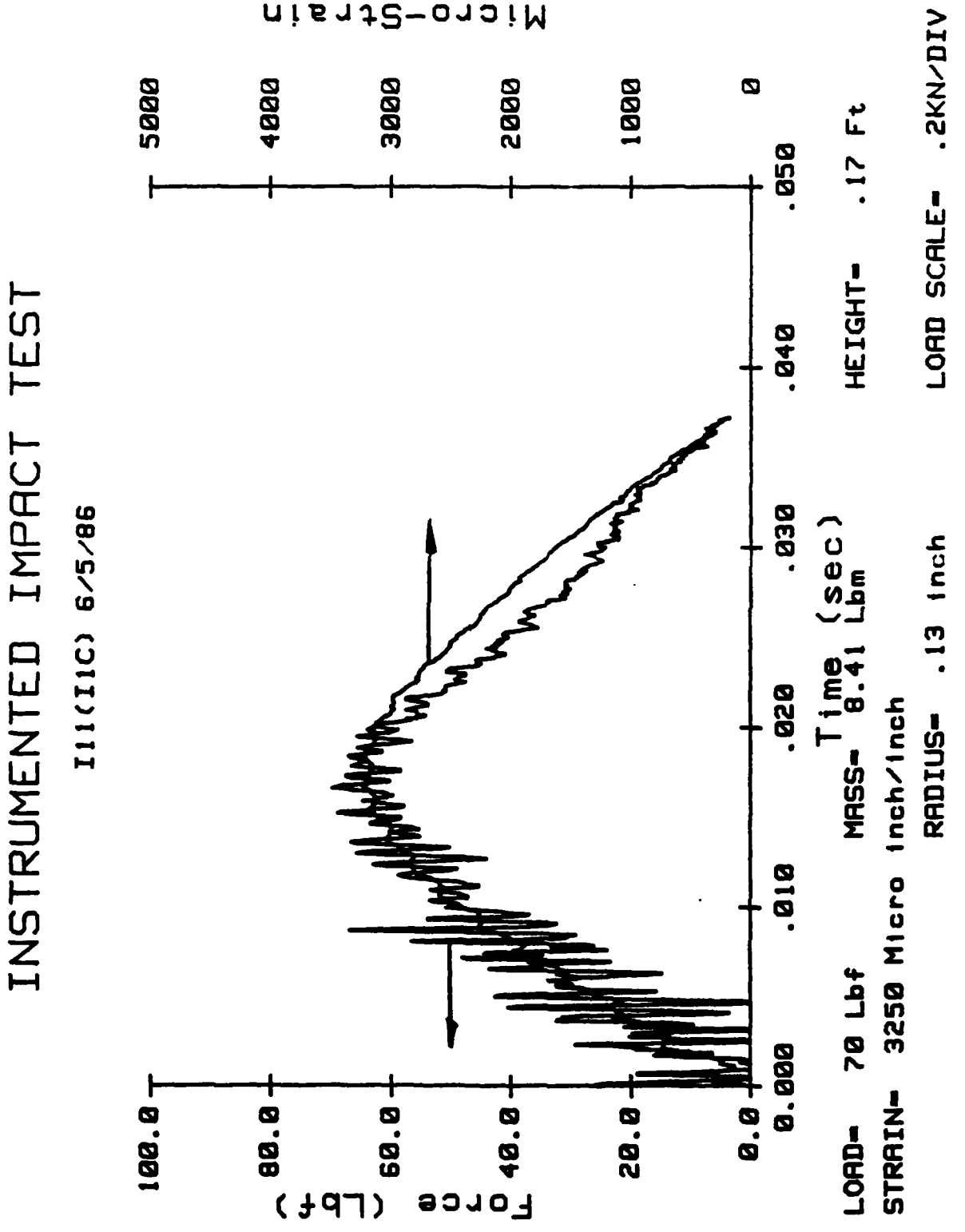
INSTRUMENTED IMPACT TEST
III(IIC) 6/5/86
Force (Lbf)
Micro-Strain
Time (sec)
100.0
80.0
60.0
40.0
20.0
0.0
5000
4000
3000
2000
1000
0
0.000
.010
.020
.030
.040
.050
MAX LOAD= 70 Lbf
MAX STRAIN= 3250 Micro Inch/Inch
MASS= 8.41 Lbm
RADIUS= .13 Inch
HEIGHT= .17 Ft
LOAD SCALE= .2KN/DIV

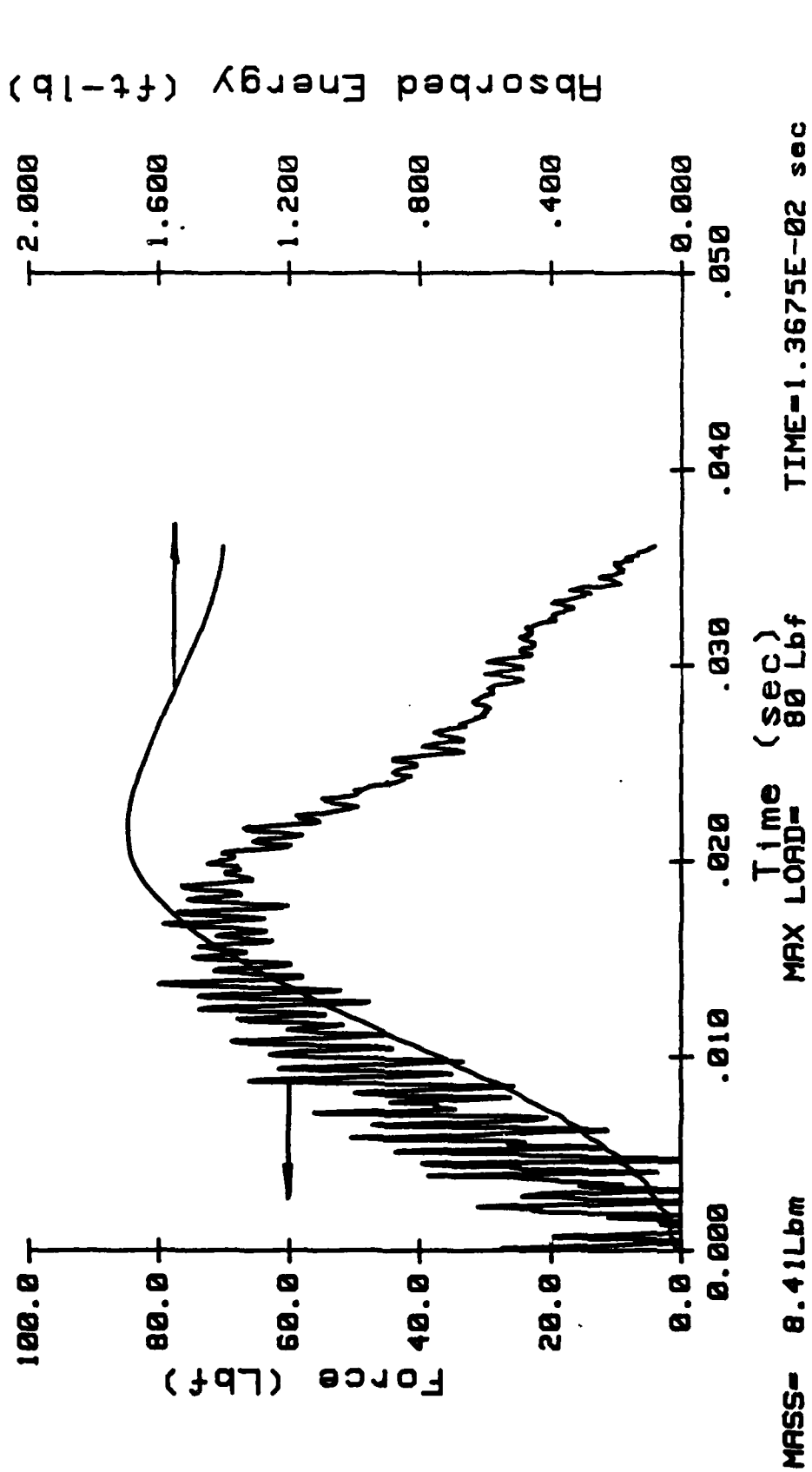
MCBI7. 1
INSTRUMENTED IMPACT TEST
I12(I1C) 6/5/86
Force (Lbf)
100.0
80.0
60.0
40.0
20.0
0.0
Absorbed Energy (ft-lb)
2.000
1.600
1.200
.800
.400
0.000
0.000
.010
.020
.030
.040
.050
Time (sec)
MASS= 8.41Lbm
Vo= 3.17Ft/sec
Eo= 1.32Ft-Lb
MAX LOAD= 80 Lbf
Displacement= .4586Inch
E absorbed= 1.22Ft-Lb
TIME=1.3675E-02 sec

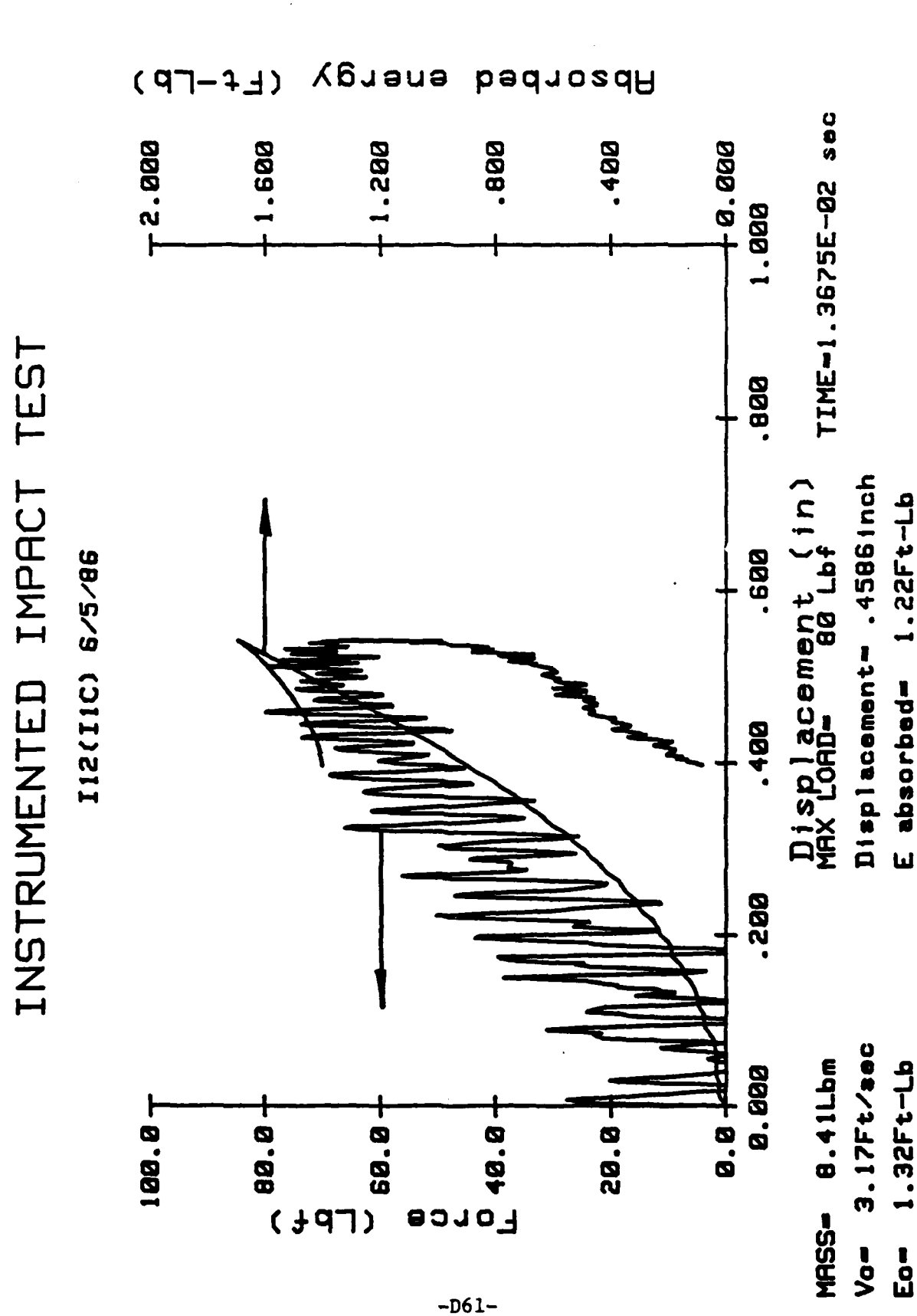
INSTRUMENTED IMPACT TEST
I12(IIC) 6/5/86
Force (Lbf)
100.0
80.0
60.0
40.0
20.0
0.0
0.000
.200
.400
.600
.800
1.000
Displacement (in)
Absorbed energy (Ft-Lb)
2.000
1.600
1.200
.800
.400
0.000
MAX LOAD= 80 Lbf
TIME=1.3675E-02 sec
Displacement= .4586inch
E absorbed= 1.22Ft-Lb
MASS= 8.41Lbm
Vo= 3.17Ft/sec
Eo= 1.32Ft-Lb

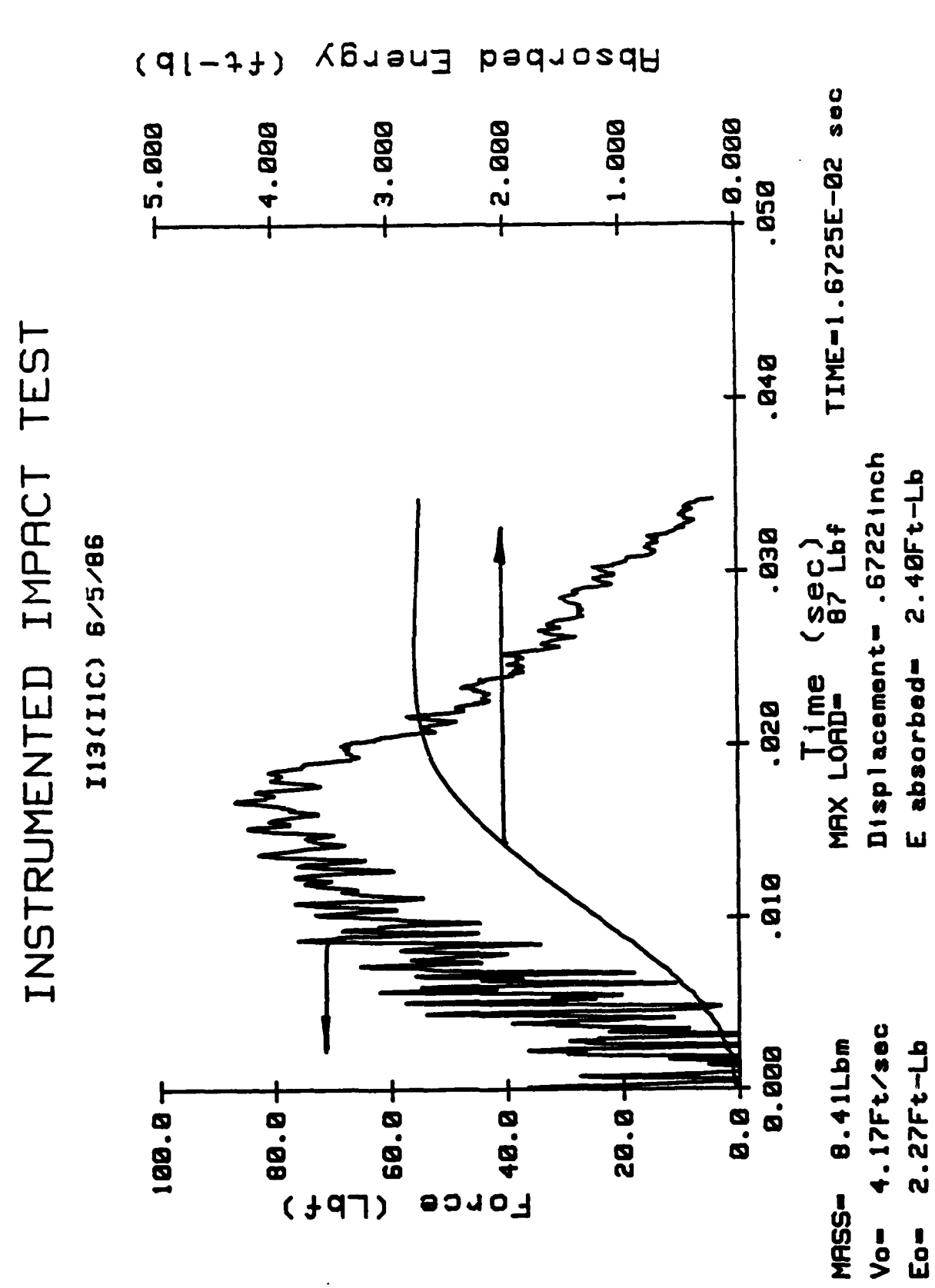
MCBI7.2
INSTRUMENTED IMPACT TEST
I13(IIC) 6/5/86
Force (Lbf)
100.0
80.0
60.0
40.0
20.0
0.0
0.000
.010
.020
.030
.040
.050
Time (sec)
Absorbed Energy (ft-lb)
5.000
4.000
3.000
2.000
1.000
0.000
MAX LOAD= 87 Lbf
TIME=1.6725E-02 sec
Displacement= .6722inch
E absorbed= 2.40Ft-Lb
MASS= 8.41Lbm
Vo= 4.17Ft/sec
Eo= 2.27Ft-Lb

MCBI7.2

INSTRUMENTED IMPACT TEST

I13(I1C) 6/5/86

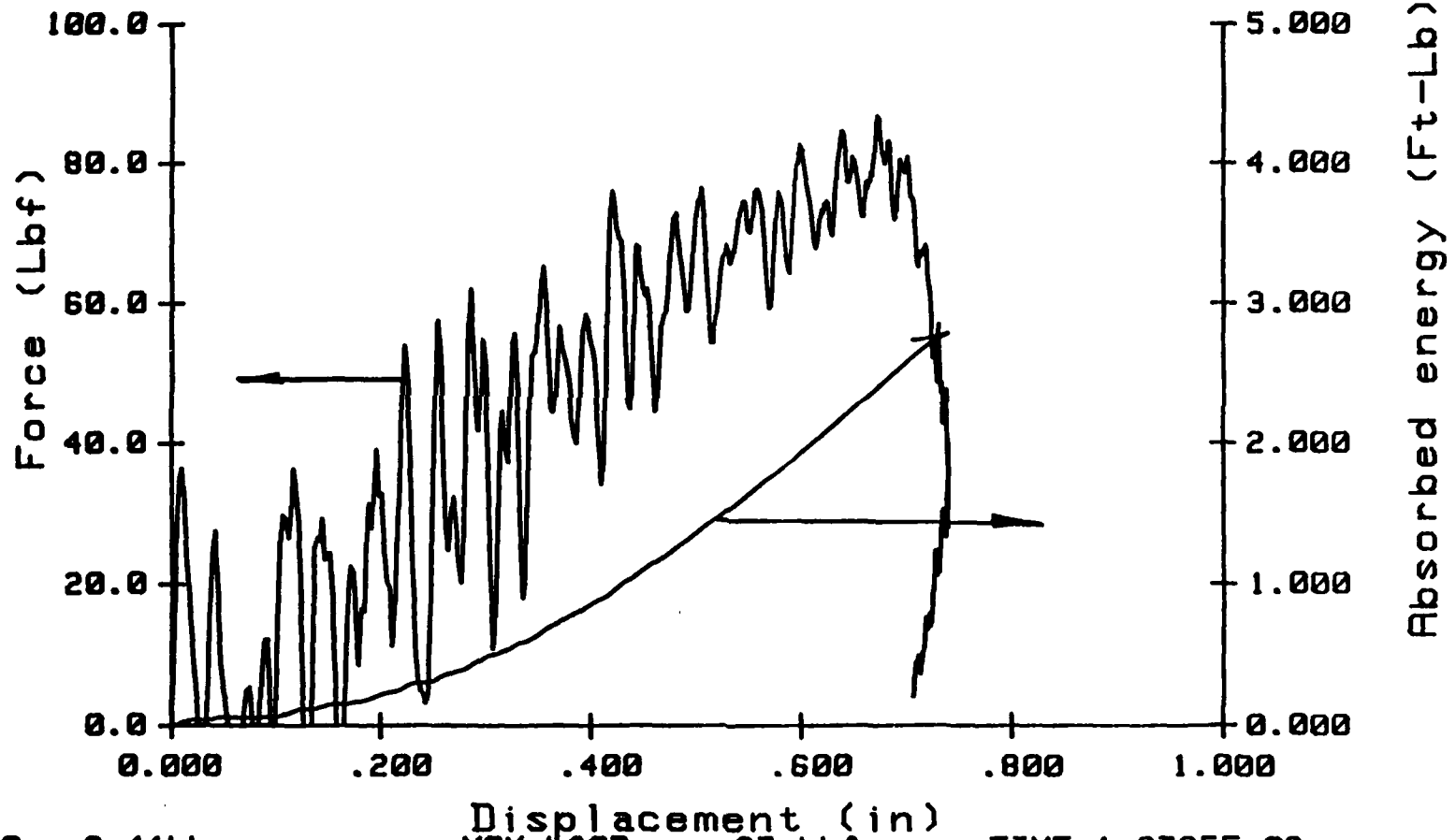

MASS= 8.41Lbm
Vo= 4.17Ft/sec
Eo= 2.27Ft-Lb

MAX LOAD= 87 Lbf
Displacement= .6722inch
E absorbed= 2.40Ft-Lb

TIME=1.6725E-02 sec

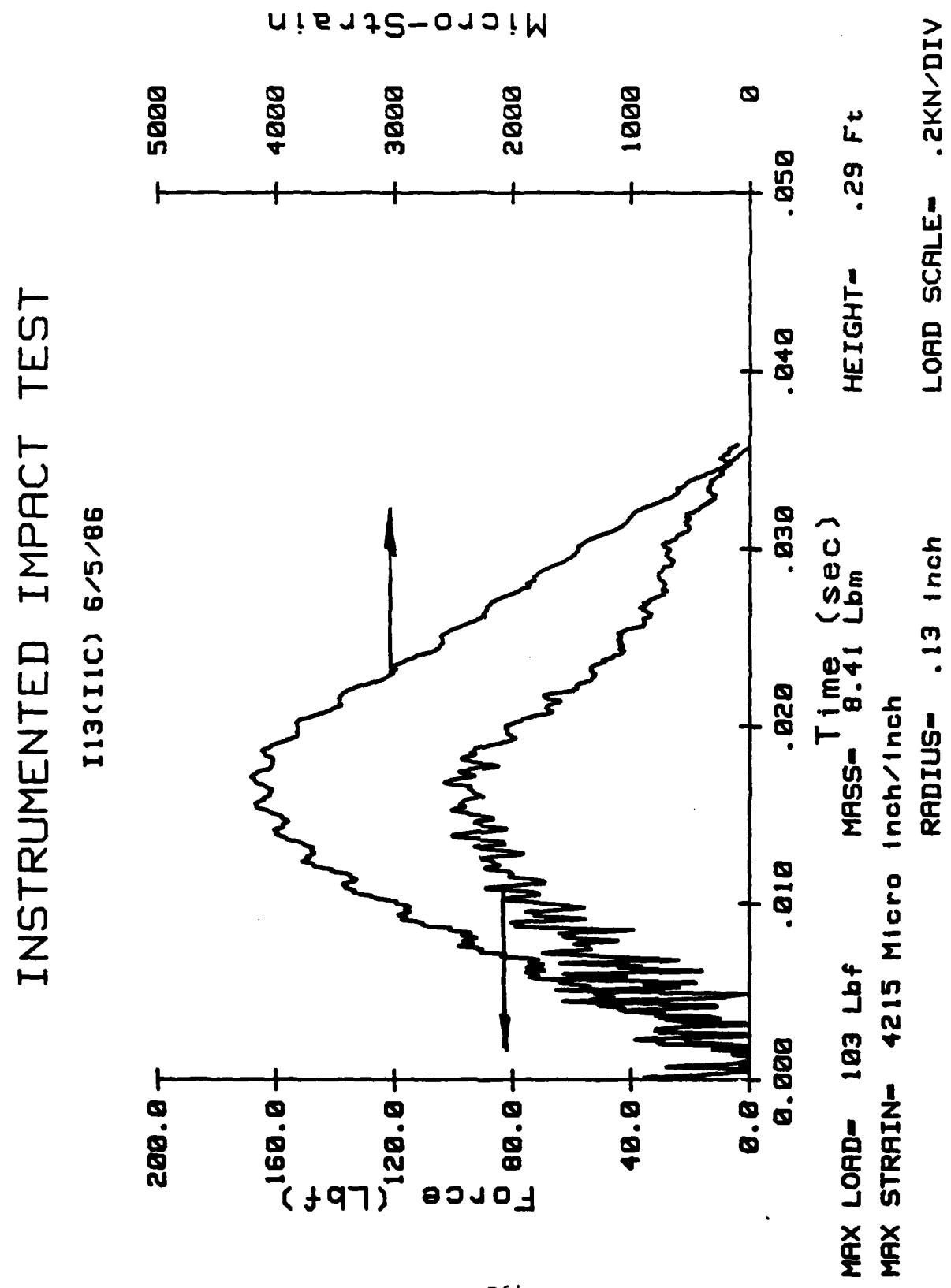
INSTRUMENTED IMPACT TEST
I13(I1C) 6/5/86
Force (Lbf)
200.0
160.0
120.0
80.0
40.0
0.0
Micro-Strain
5000
4000
3000
2000
1000
0
0.000
.010
.020
.030
.040
.050
Time (sec)
MAX LOAD= 103 Lbf
MAX STRAIN= 4215 Micro Inch/Inch
MASS= 8.41 Lbm
RADIUS= .13 Inch
HEIGHT= .29 Ft
LOAD SCALE= .2KN/DIV

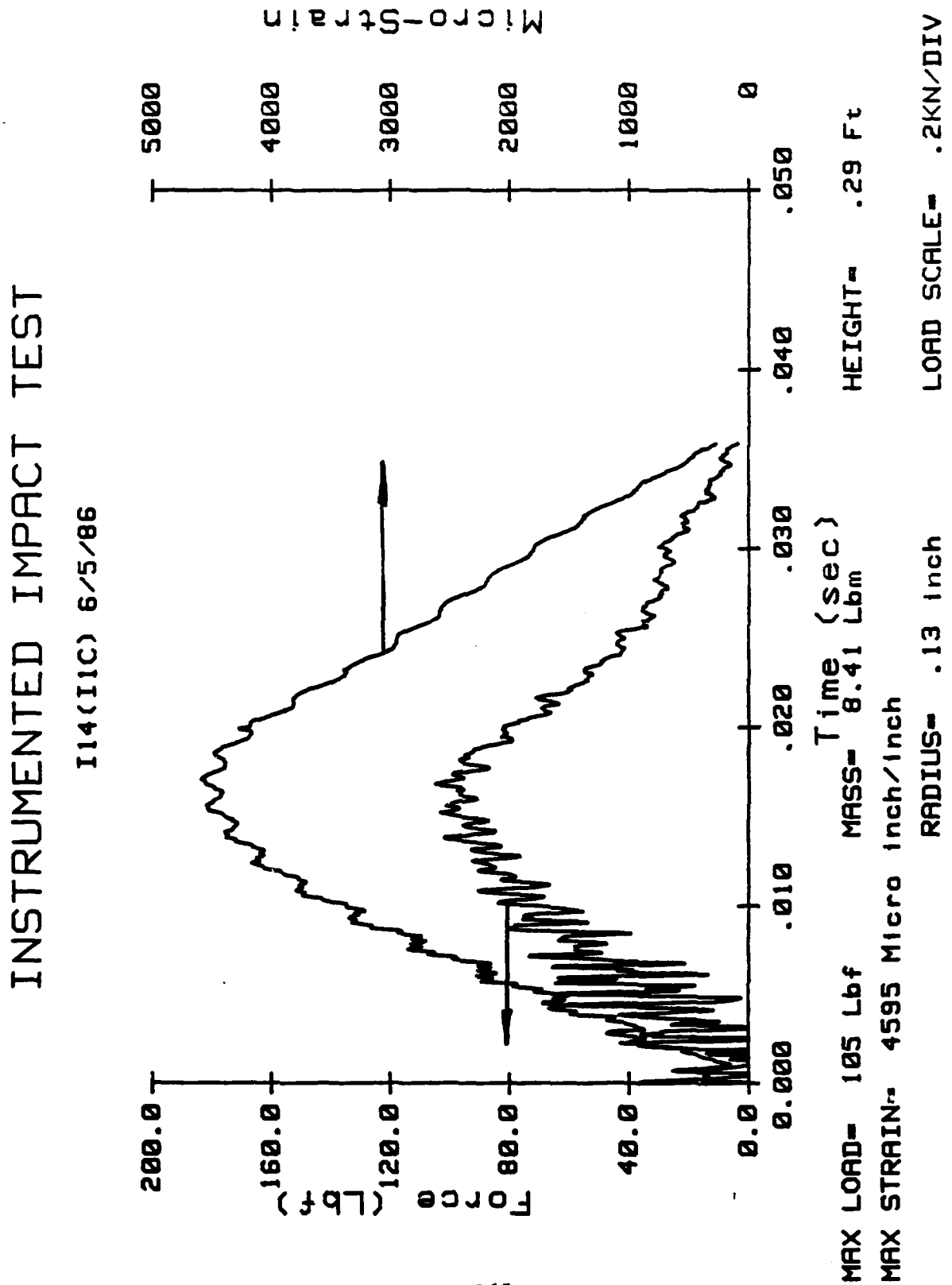
INSTRUMENTED IMPACT TEST
I14(IIC) 6/5/86
Force (Lbf)
200.0
160.0
120.0
80.0
40.0
0.0
Micro-Strain
5000
4000
3000
2000
1000
0
0.000
.010
.020
.030
.040
.050
Time (sec)
MAX LOAD= 105 Lbf
MAX STRAIN= 4595 Micro Inch/Inch
MASS= 8.41 Lbm
RADIUS= .13 Inch
HEIGHT= .29 Ft
LOAD SCALE= .2KN/DIV

MCBI7.5

INSTRUMENTED IMPACT TEST

I16(I1C) 6/5/86

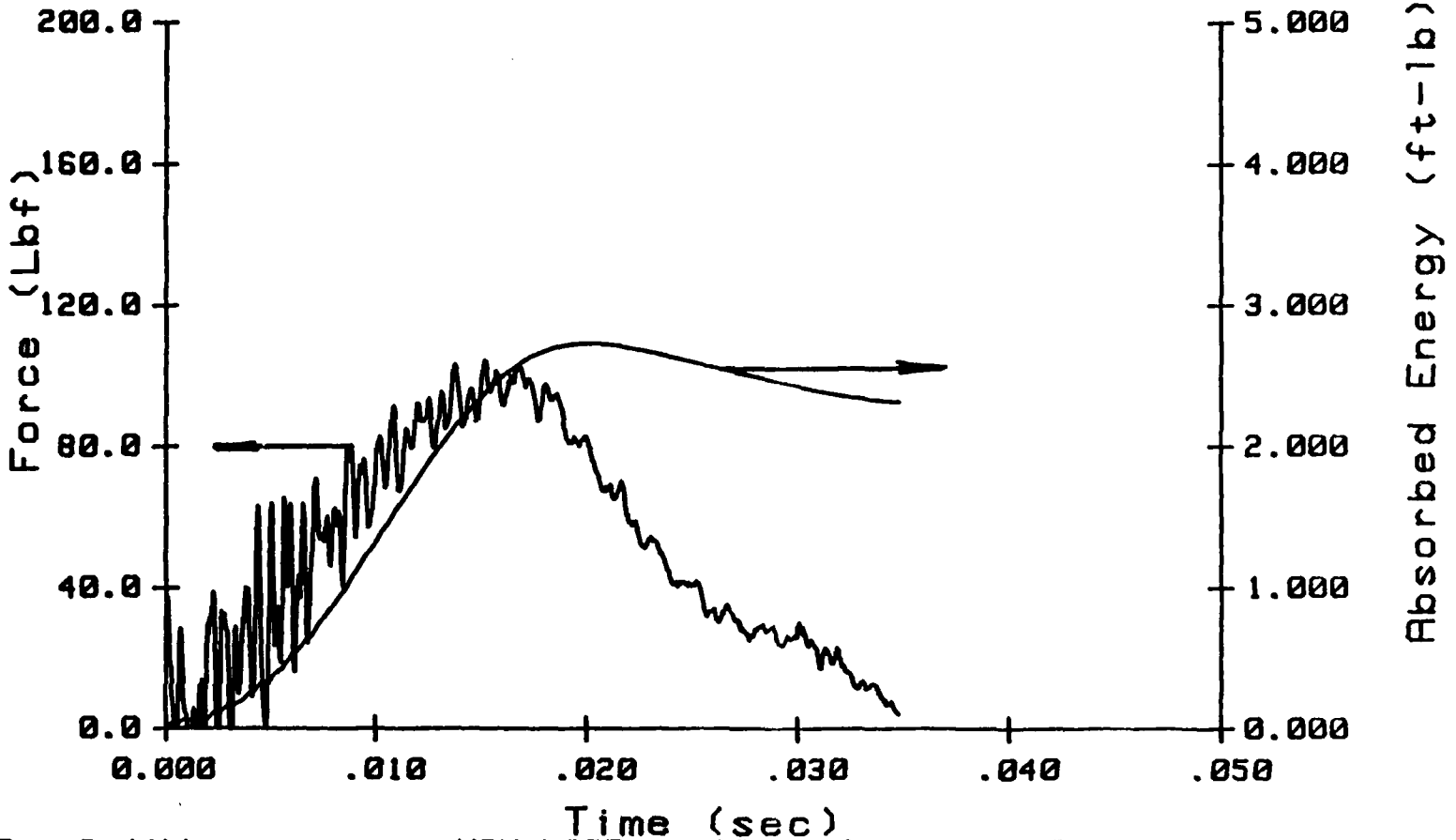

MASS= 8.41Lbm MAX LOAD= 104 Lbf TIME=1.5175E-02 sec

Vo= 4.17Ft/sec Displacement= .6161inch

Eo= 2.27Ft-Lb E absorbed= 2.38Ft-Lb

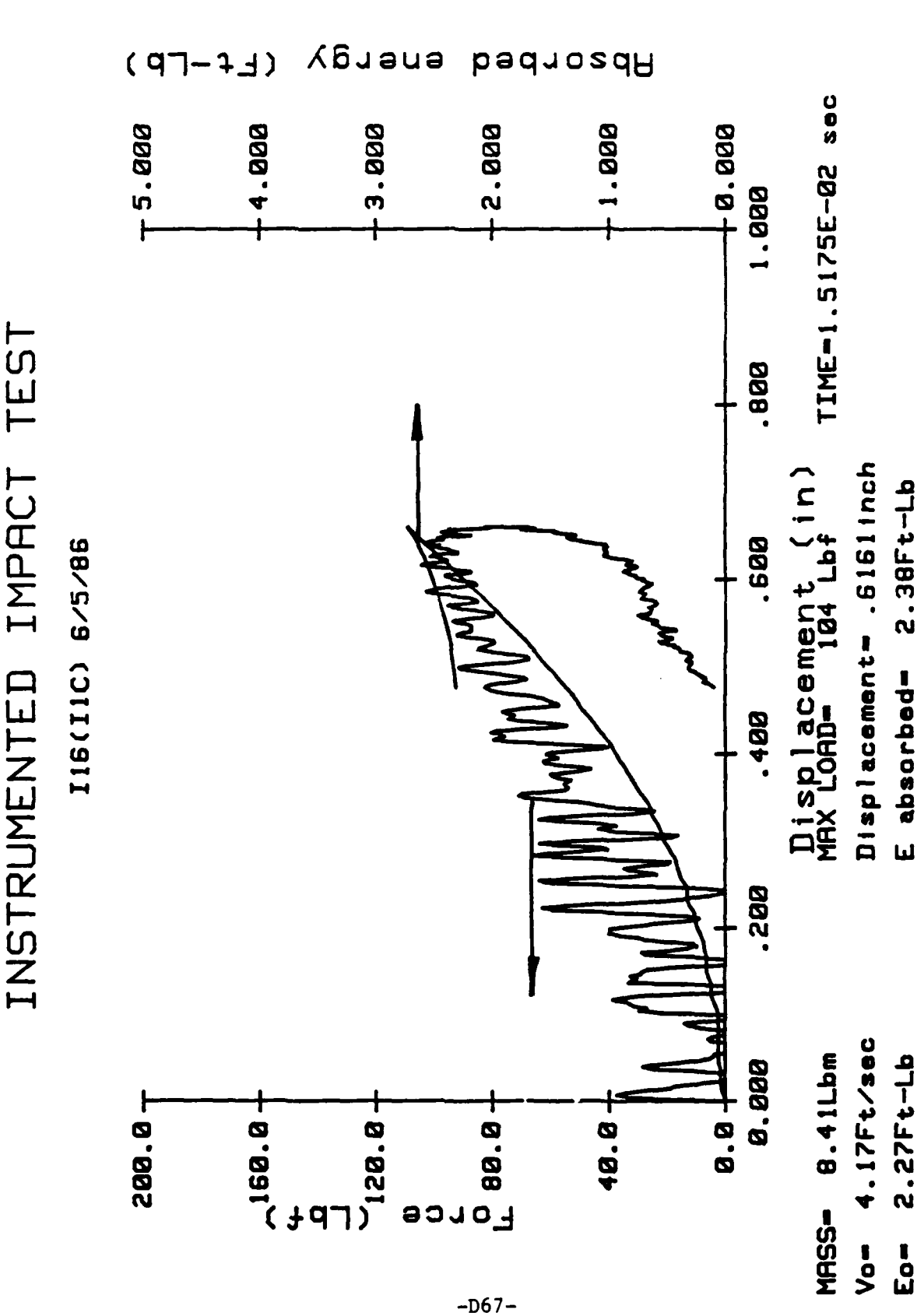
MCBI7.5
INSTRUMENTED IMPACT TEST
I16(I1C) 6/5/86
Absorbed energy (Ft-Lb)
5.000
4.000
3.000
2.000
1.000
0.000
Force (Lbf)
200.0
160.0
120.0
80.0
40.0
0.0
0.000
.200
.400
.600
.800
1.000
Displacement (in)
MAX LOAD= 104 Lbf
TIME=1.5175E-02 sec
Displacement= .6161inch
E absorbed= 2.38Ft-Lb
MASS= 8.41Lbm
Vo= 4.17Ft/sec
Eo= 2.27Ft-Lb

INSTRUMENTED IMPACT TEST

I17(I1C) 6/5/86

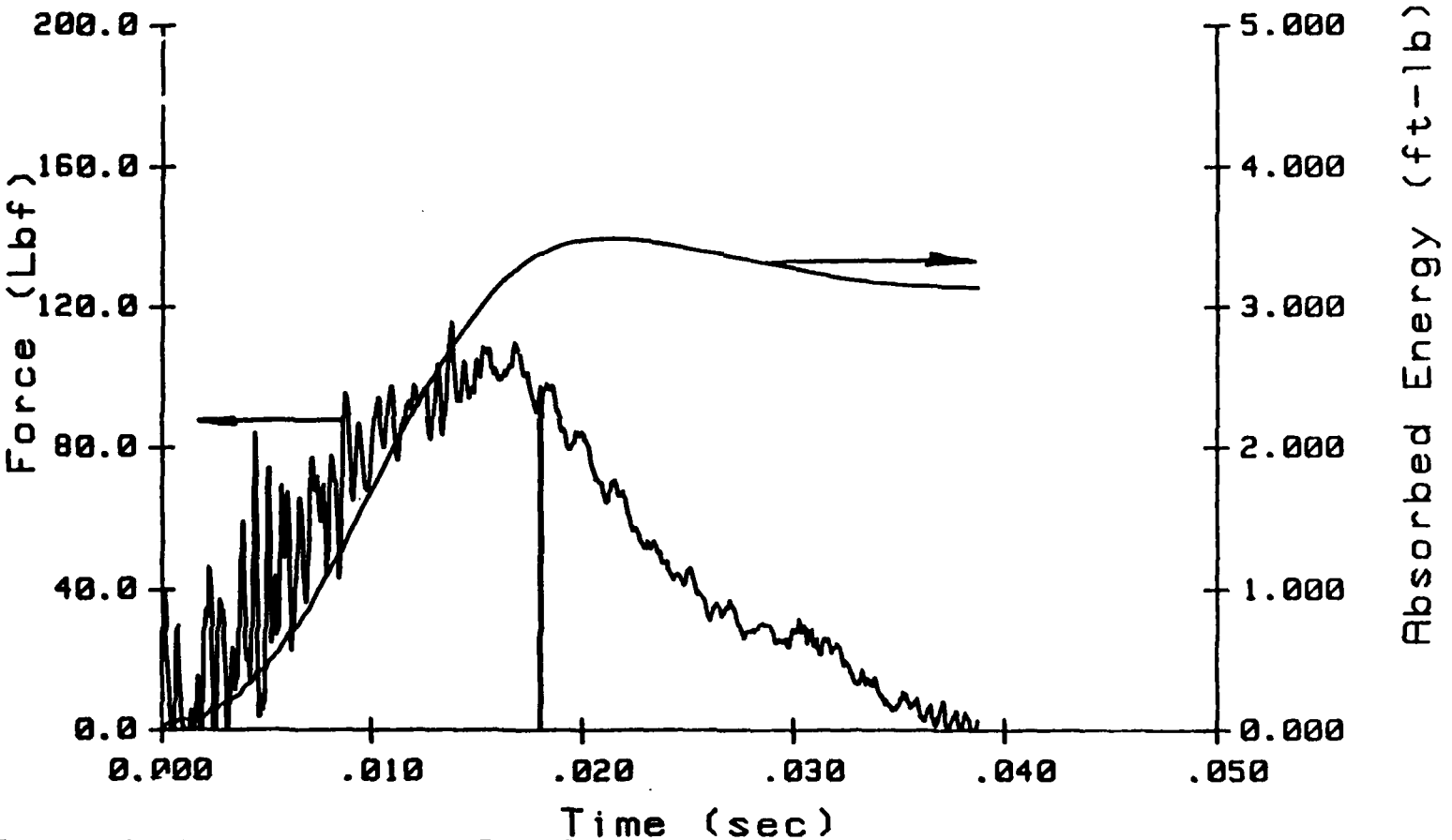

MASS= 8.41Lbm MAX LOAD= 110 Lbf TIME=1.6775E-02 sec

Vo= 4.76Ft/sec Displacement= .7323inch

Eo= 2.96Ft-Lb E absorbed= 3.26Ft-Lb

MCBI7.6

INSTRUMENTED IMPACT TEST

I17(I1C) 6/5/86

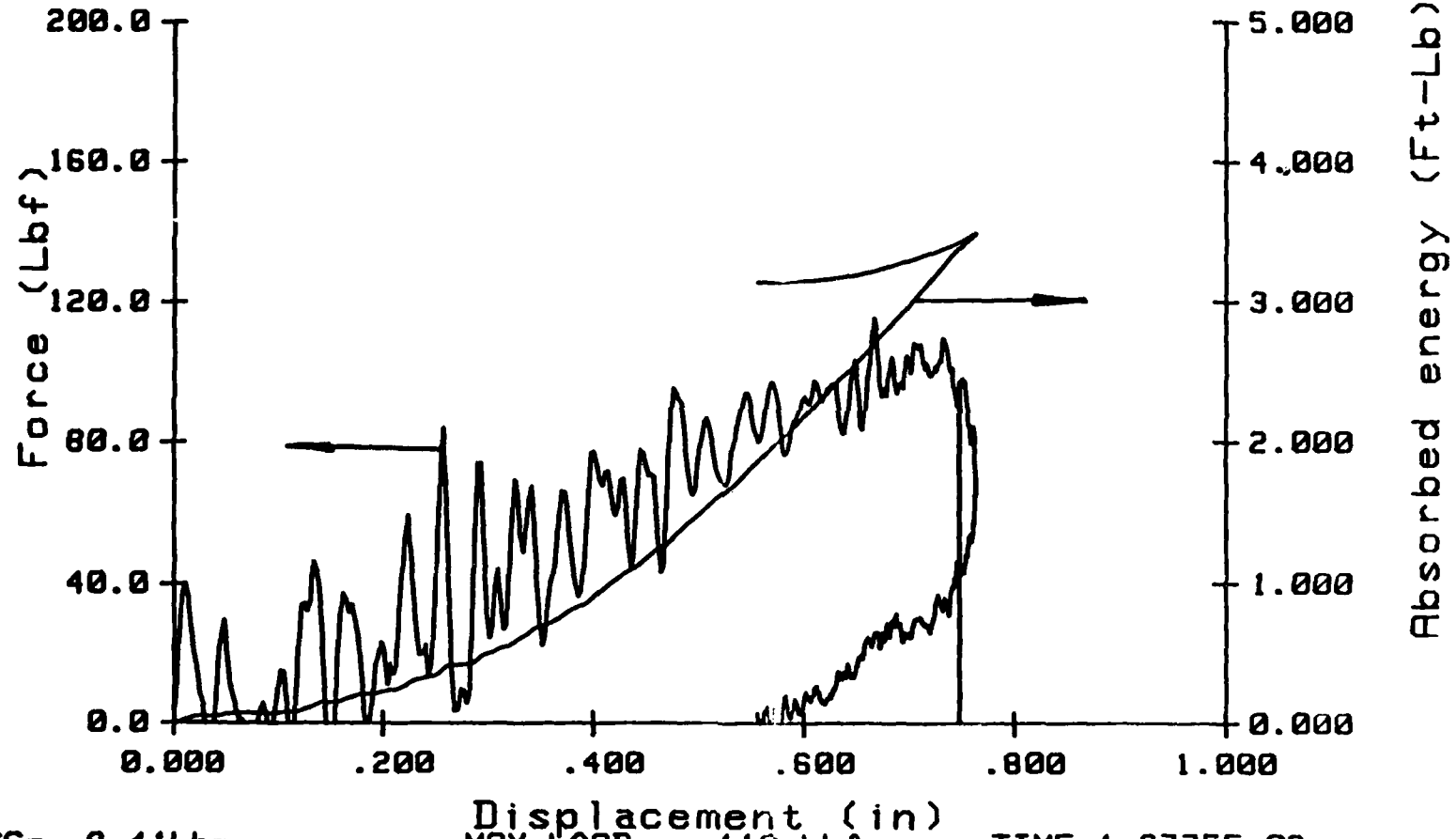

MASS= 8.41Lbm
Vo= 4.76Ft/sec
Eo= 2.96Ft-Lb

MAX LOAD= 110 Lbf
Displacement= .7323inch
E absorbed= 3.26Ft-Lb

TIME=1.6775E-02 sec

NADC-87106-60

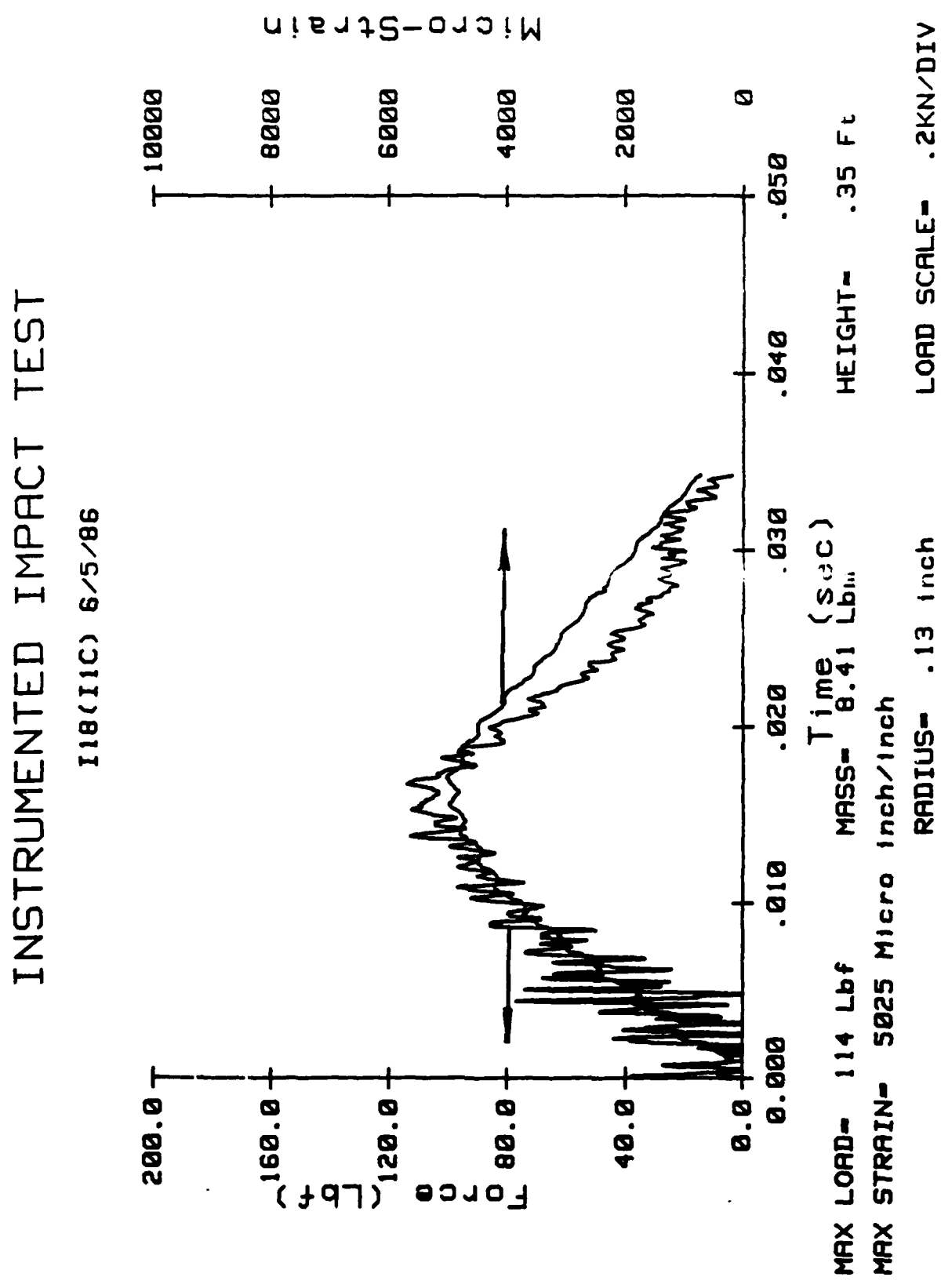
INSTRUMENTED IMPACT TEST
I18(I1C) 6/5/86
Force (Lbf)
200.0
160.0
120.0
80.0
40.0
0.0
Micro-Strain
10000
8000
6000
4000
2000
0
0.000
.010
.020
.030
.040
.050
Time (sec)
MAX LOAD= 114 Lbf
MAX STRAIN= 5025 Micro Inch/Inch
MASS= 8.41 Lbm
RADIUS= .13 Inch
HEIGHT= .35 Ft
LOAD SCALE= .2KN/DIV

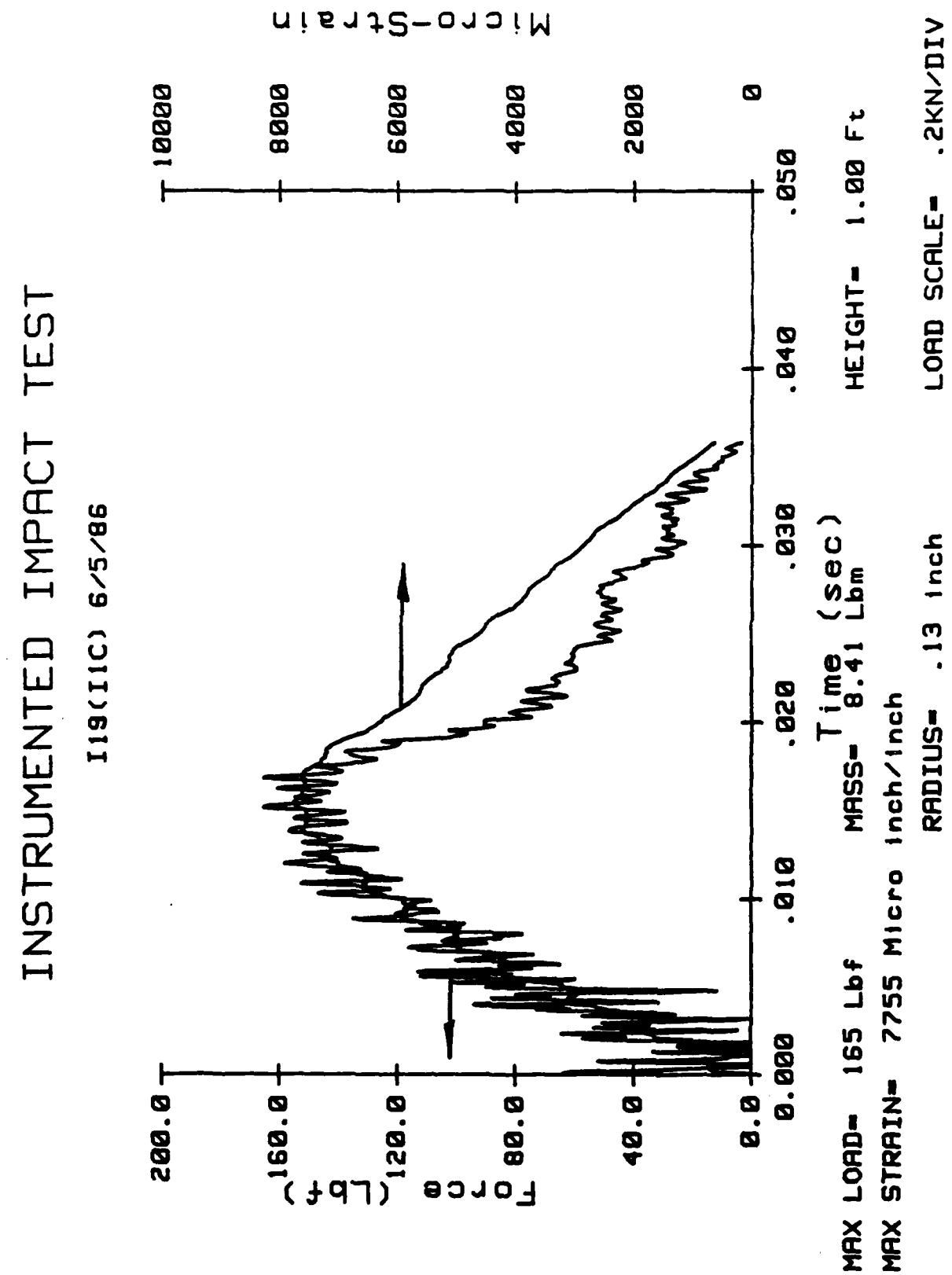
INSTRUMENTED IMPACT TEST
I19(IIC) 6/5/86
Micro-Strain
10000
8000
6000
4000
2000
0
Force (Lbf)
200.0
160.0
120.0
80.0
40.0
0.0
0.000
.010
.020
.030
.040
.050
Time (sec)
MAX LOAD= 165 Lbf
MASS= 8.41 Lbm
HEIGHT= 1.00 Ft
MAX STRAIN= 7755 Micro Inch/Inch
RADIUS= .13 Inch
LOAD SCALE= .2KN/DIV

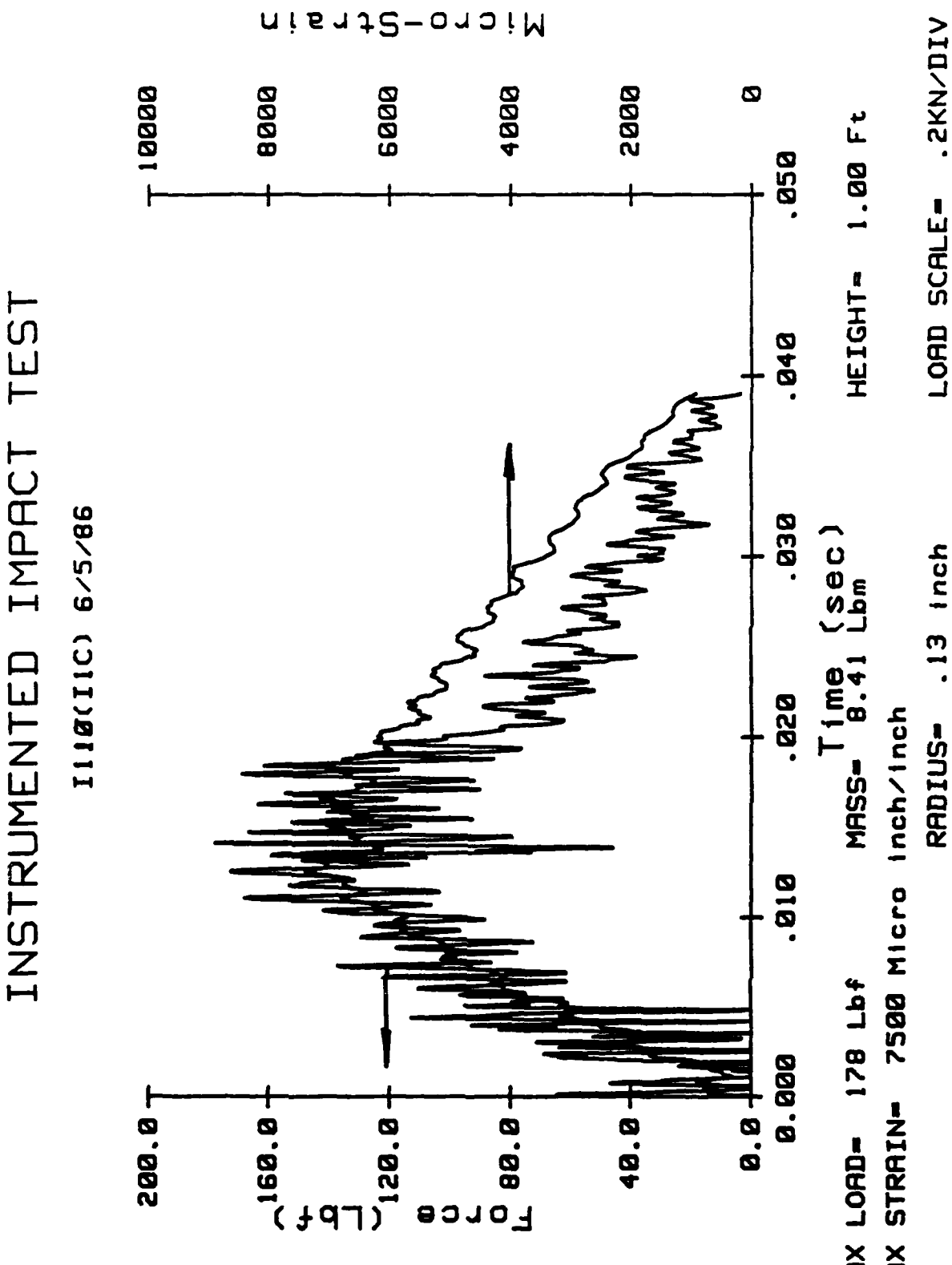
INSTRUMENTED IMPACT TEST
I110(IIC) 6/5/86
Force (Lbf)
200.0
160.0
120.0
80.0
40.0
0.0
Micro-Strain
10000
8000
6000
4000
2000
0
0.000
.010
.020
.030
.040
.050
Time (sec)
MAX LOAD= 178 Lbf
MAX STRAIN= 7500 Micro Inch/Inch
MASS= 8.41 Lbm
RADIUS= .13 inch
HEIGHT= 1.00 Ft
LOAD SCALE= .2KN/DIV

INSTRUMENTED IMPACT TEST

F111(I,C) 6/5/86

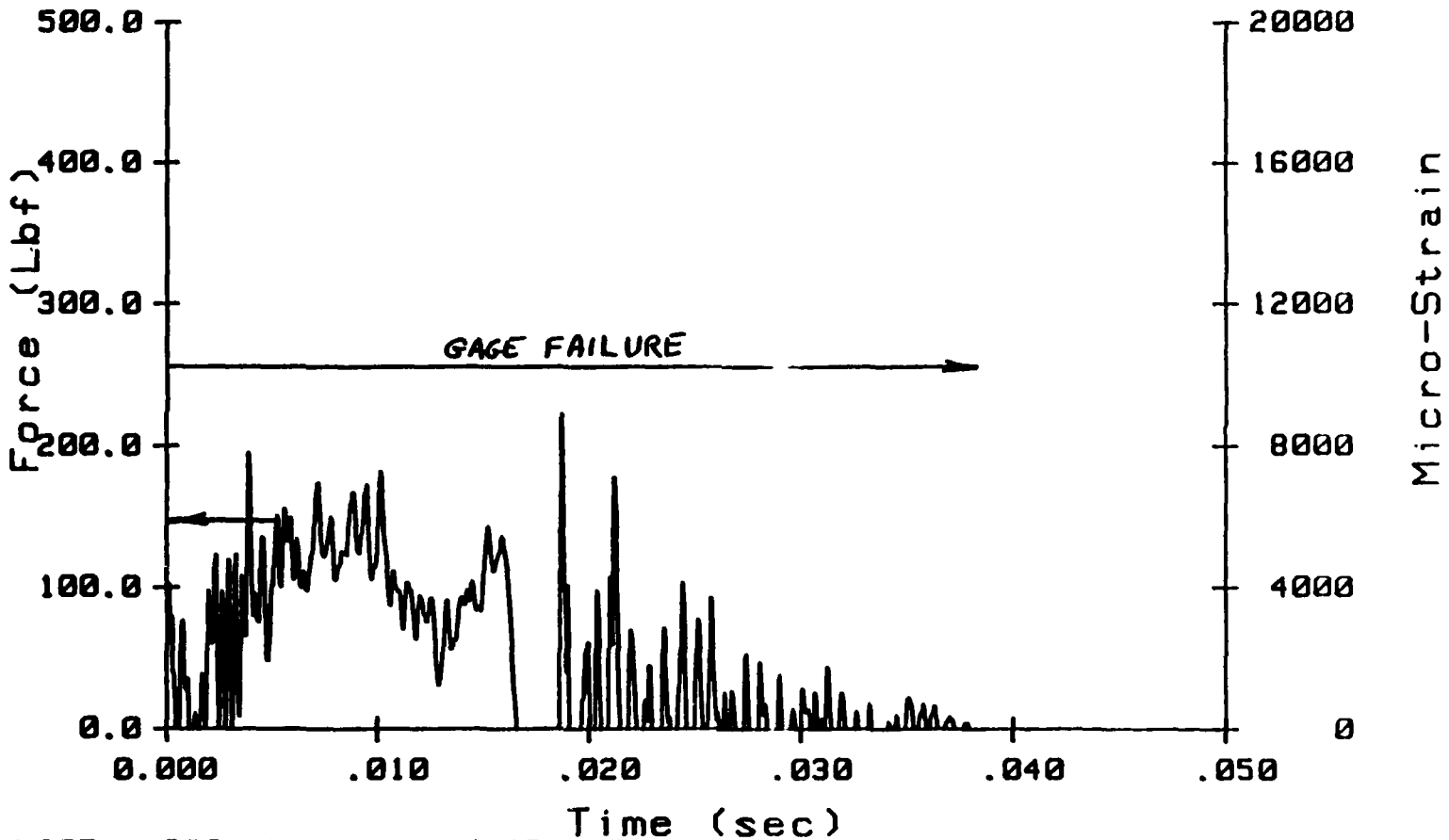

MAX LOAD= 223 Lbf MASS= 8.41 Lbm HEIGHT= 3.00 Ft

MAX STRAIN= 10235 Micro inch/inch

RADIUS= .13 inch LOAD SCALE= .2KN/DIV

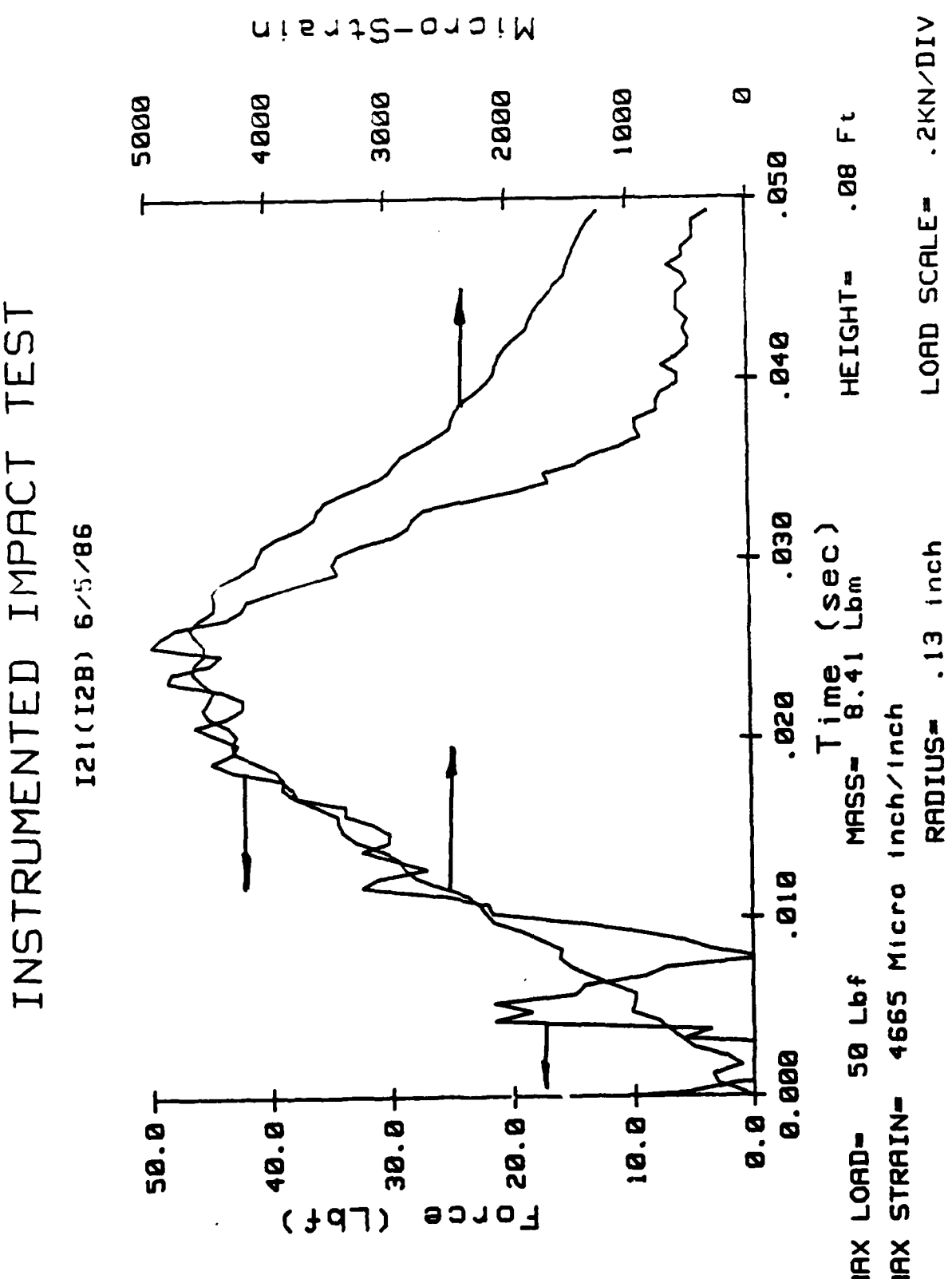
INSTRUMENTED IMPACT TEST
I21(I2B) 6/5/86
Force (Lbf)
50.0
40.0
30.0
20.0
10.0
0.0
0.000
.010
.020
.030
.040
.050
Time (sec)
Micro-Strain
5000
4000
3000
2000
1000
0
MAX LOAD= 50 Lbf
MASS= 8.41 Lbm
HEIGHT= .08 Ft
MAX STRAIN= 4665 Micro inch/inch
RADIUS= .13 inch
LOAD SCALE= .2KN/DIV

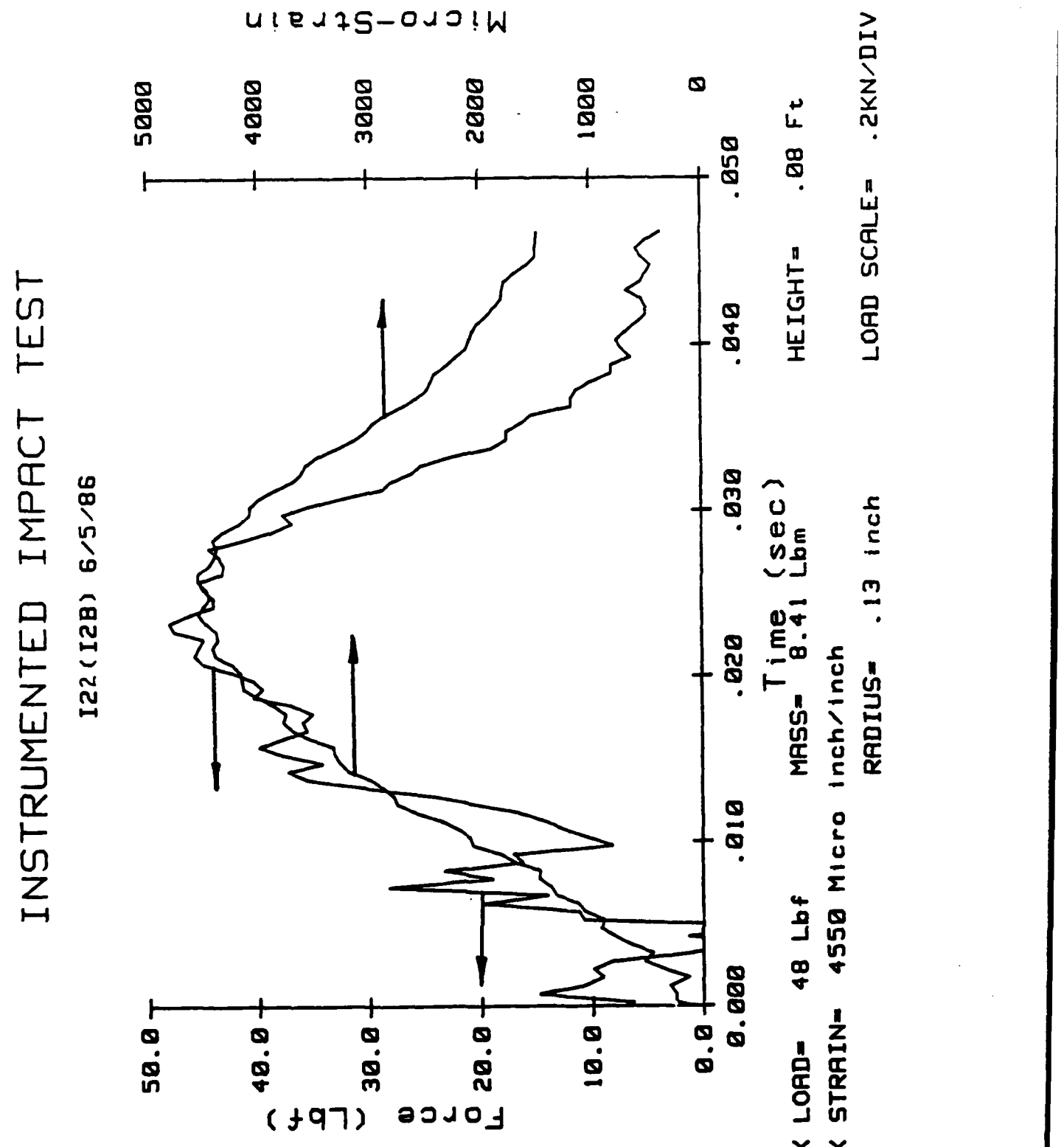
INSTRUMENTED IMPACT TEST
I22(I28) 6/5/86
Force (Lbf)
50.0
40.0
30.0
20.0
10.0
0.0
0.000
.010
.020
.030
.040
.050
Time (sec)
Micro-Strain
5000
4000
3000
2000
1000
0
MAX LOAD= 48 Lbf
MAX STRAIN= 4550 Micro inch/inch
MASS= 8.41 Lbm
RADIUS= .13 inch
HEIGHT= .08 Ft
LOAD SCALE= .2KN/DIV

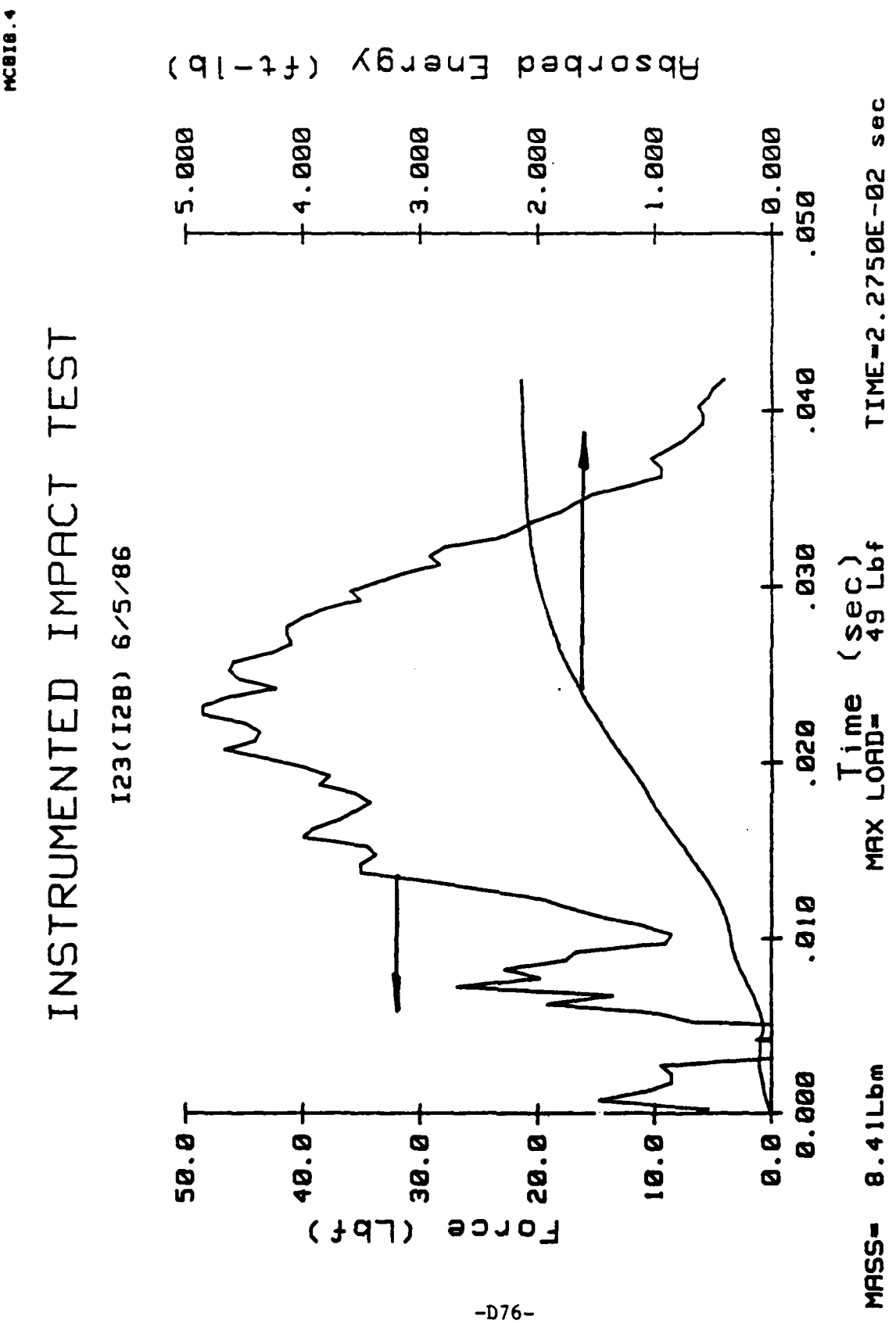
MCB18.4
INSTRUMENTED IMPACT TEST
I23(I28) 6/5/86
Absorbed Energy (ft-lb)
5.000
4.000
3.000
2.000
1.000
0.000
.050
.040
.030
.020
.010
0.000
Time (sec)
Force (Lbf)
50.0
40.0
30.0
20.0
10.0
0.0
MAX LOAD= 49 Lbf
TIME=2.2750E-02 sec
Displacement= .8581inch
E absorbed= 1.52Ft-Lb
MASS= 8.41Lbm
Vo= 2.3 Ft/sec
Eo= 1.45Ft-Lb

INSTRUMENTED IMPACT TEST

I23(I2B) 6/5/86

MASS= 8.41Lbm
MAX LOAD= 49 Lbf
TIME=2.2750E-02 sec
Vo= 2.3 Ft/sec
Displacement= .8581inch
Eo= 1.45Ft-Lb
E absorbed= 1.52Ft-Lb

NADC-87106-60

INSTRUMENTED IMPACT TEST

I24(I2B) 6/5/86

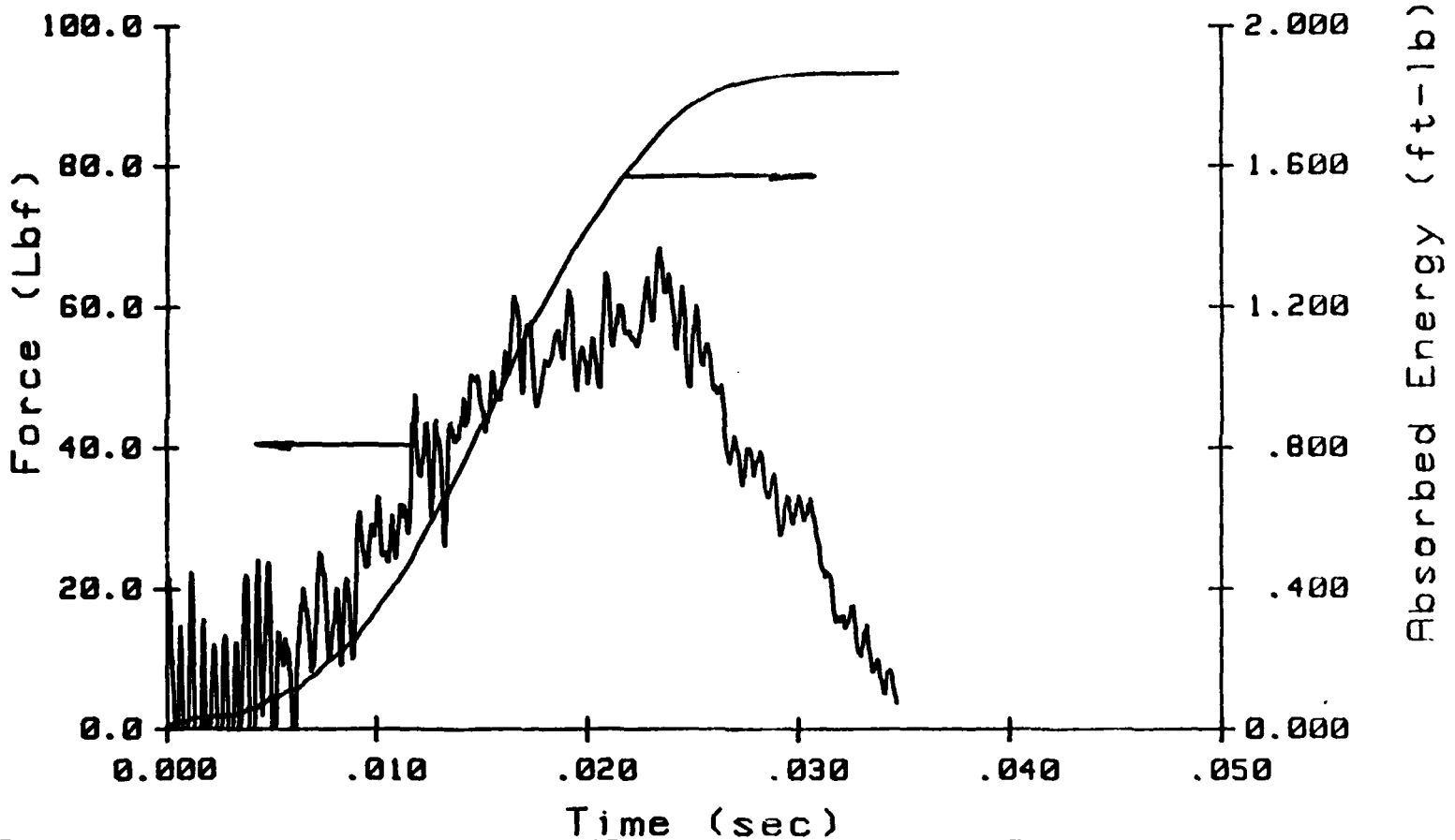

MASS= 8.41Lbm MAX LOAD= 68 Lbf TIME=2.3425E-02 sec

Vo= 3.17Ft/sec Displacement= .7422inch

Eo= 1.32Ft-Lb E absorbed= 1.69Ft-Lb

MCBI8.6

INSTRUMENTED IMPACT TEST

I24(I2B) 6/5/86

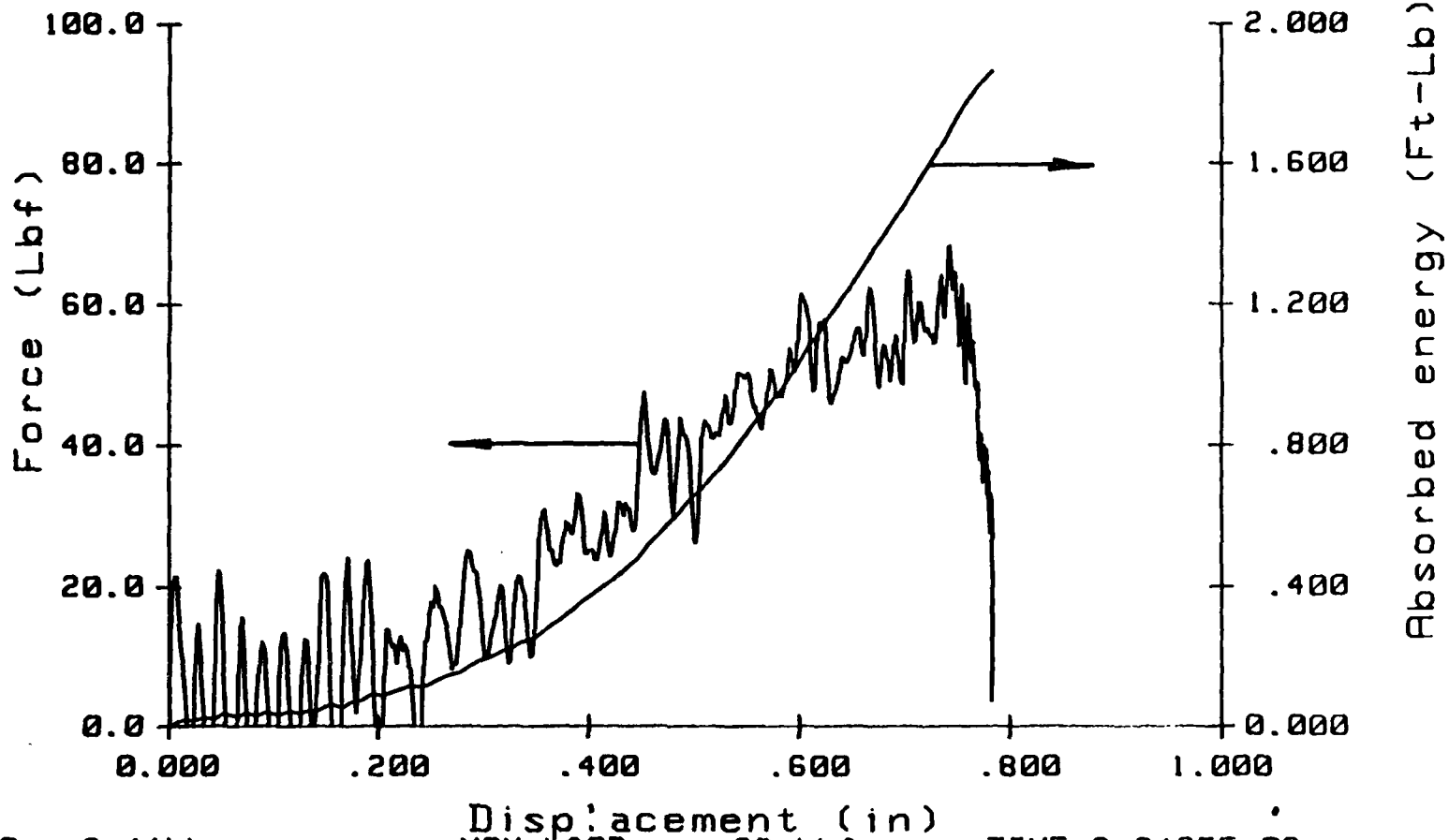

MASS= 8.41Lbm
Vo= 3.17Ft/sec
Eo= 1.32Ft-Lb

MAX LOAD= 68 Lbf
Displacement= .7422inch
E absorbed= 1.69Ft-Lb

TIME=2.3425E-02 sec

NADC-87106-60

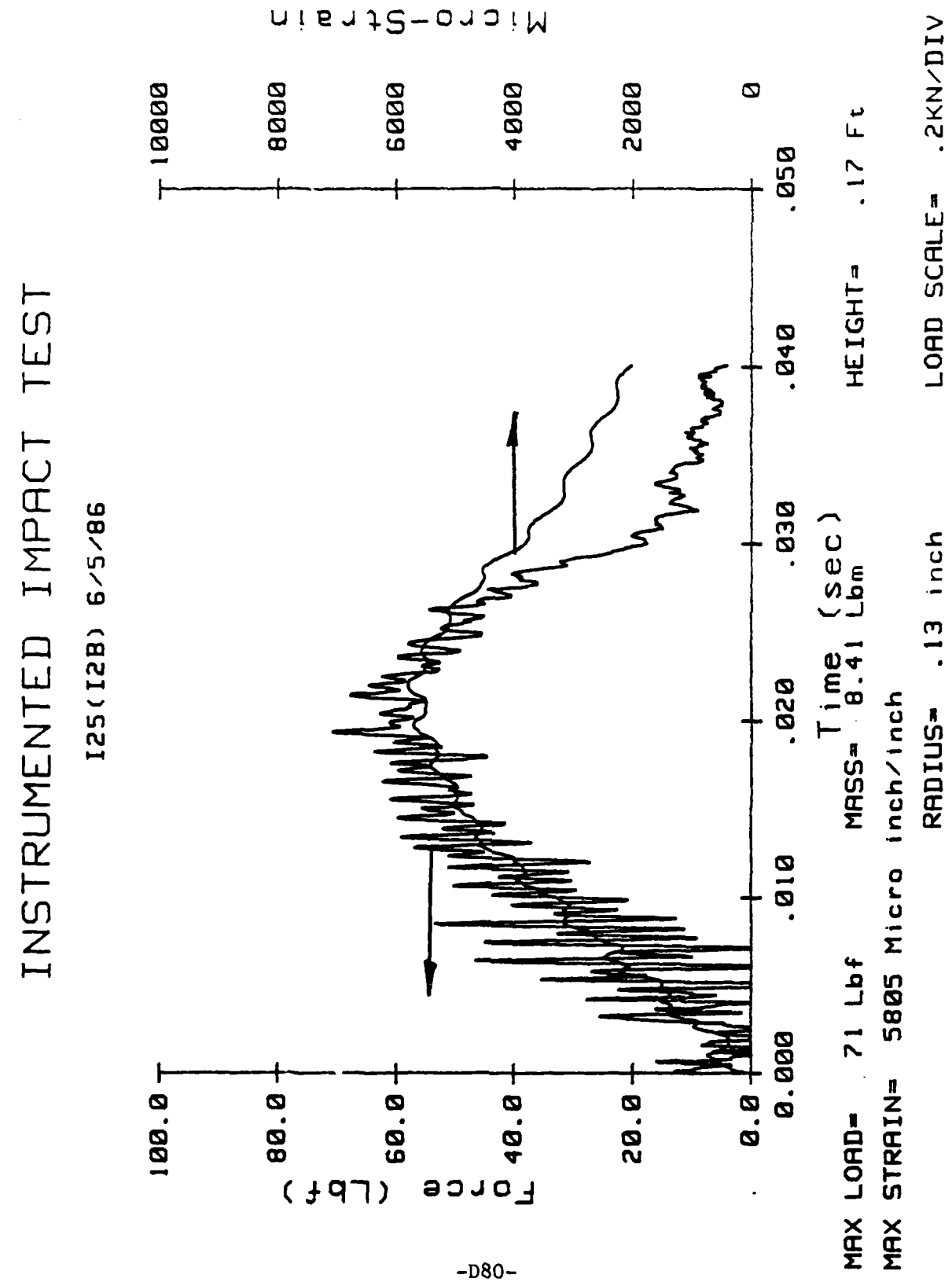
INSTRUMENTED IMPACT TEST
I25(I2B) 6/5/86
Force (Lbf)
Micro-Strain
Time (sec)
100.0
80.0
60.0
40.0
20.0
0.0
10000
8000
6000
4000
2000
0
0.000
.010
.020
.030
.040
.050
MAX LOAD= 71 Lbf
MAX STRAIN= 5805 Micro inch/inch
MASS= 8.41 Lbm
RADIUS= .13 inch
HEIGHT= .17 Ft
LOAD SCALE= .2KN/DIV

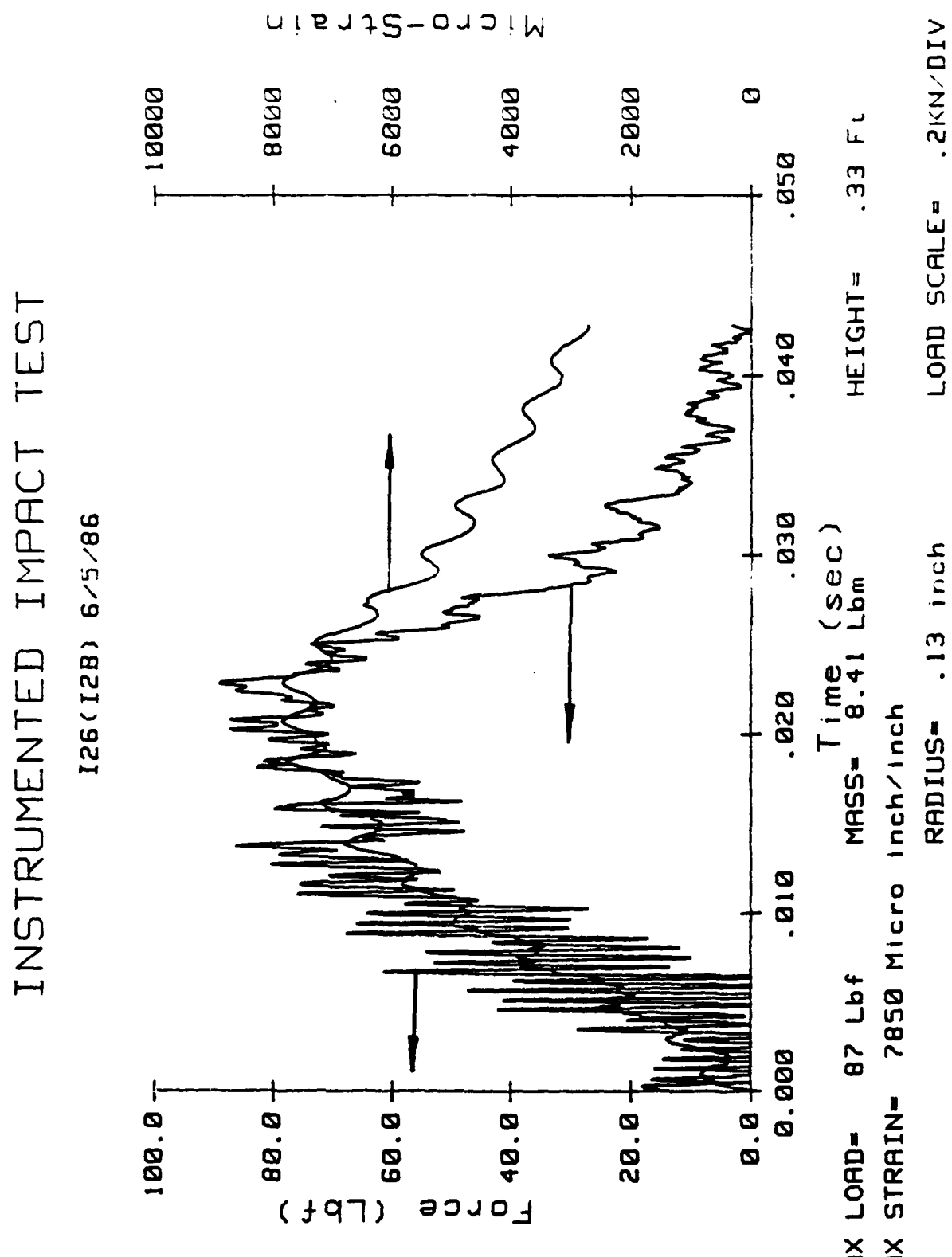
INSTRUMENTED IMPACT TEST
I26(I2B) 6/5/86
Force (Lbf)
100.0
80.0
60.0
40.0
20.0
0.0
Micro-Strain
10000
8000
6000
4000
2000
0
0.000
.010
.020
.030
.040
.050
Time (sec)
MAX LOAD= 87 Lbf
MASS= 8.41 Lbm
HEIGHT= .33 Ft
MAX STRAIN= 7850 Micro Inch/Inch
RADIUS= .13 inch
LOAD SCALE= .2KN/DIV

INSTRUMENTED IMPACT TEST

I27(I2B) 6/5/86

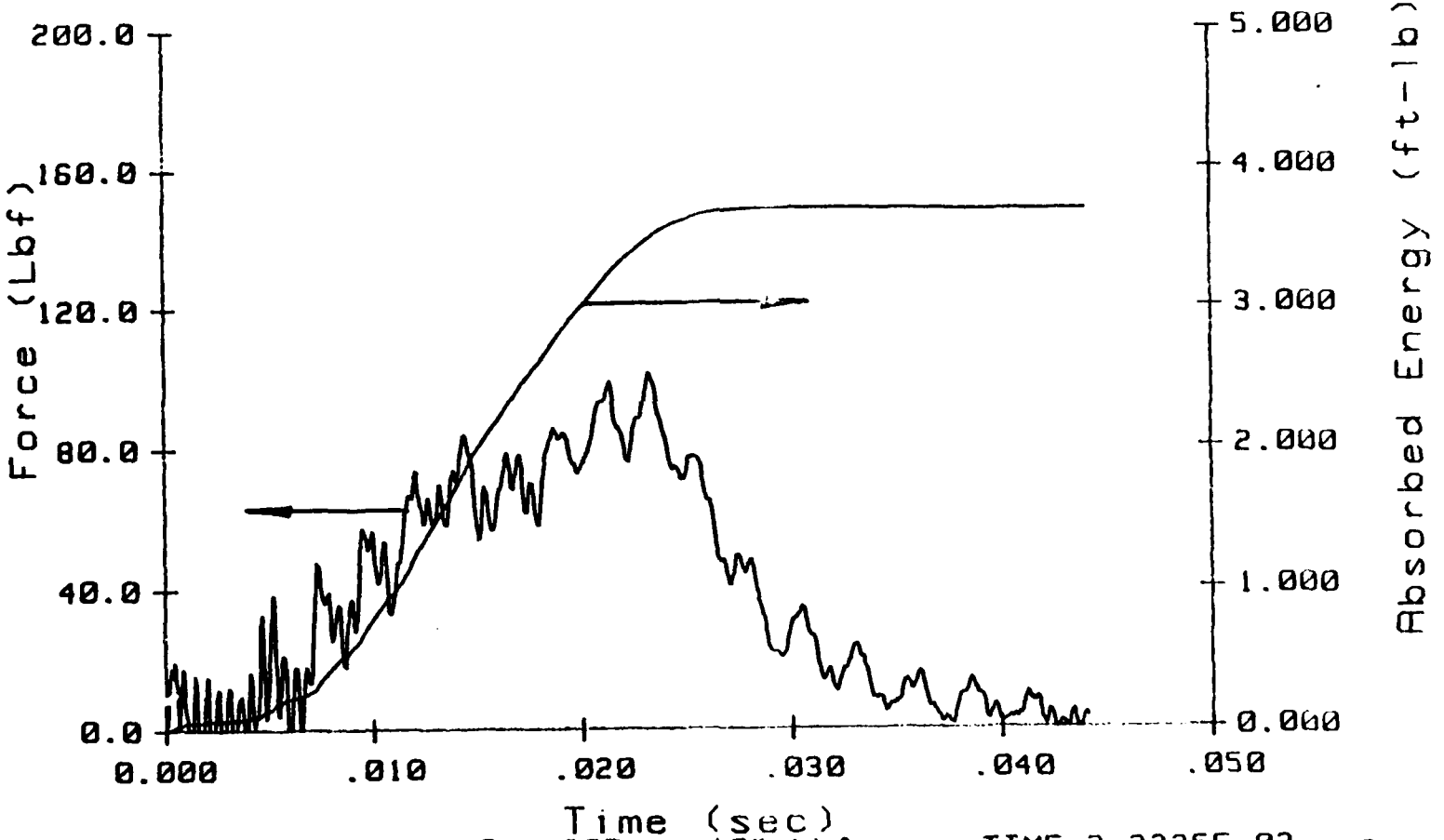

MASS= 8.41Lbm
Vo= 4.76Ft/sec
Eo= 2.96Ft-Lb

MAX LOAD= 102 Lbf
Displacement=1.0491inch
E absorbed= 3.50Ft-Lb

TIME=2.3225E-02 sec

INSTRUMENTED IMPACT TEST

I27(I2B) 6/5/86

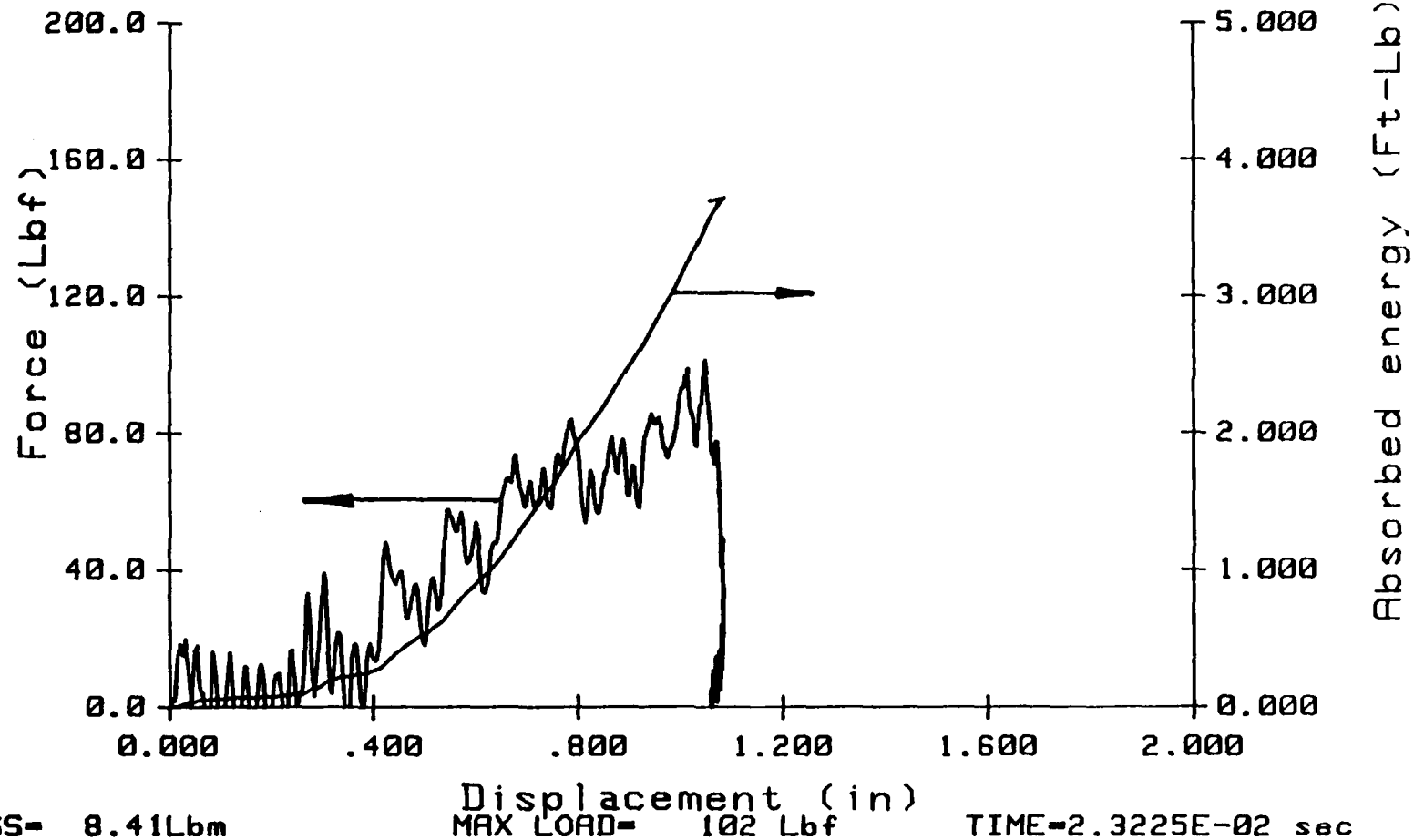

MASS= 8.41Lbm
MAX LOAD= 102 Lbf
TIME=2.3225E-02 sec
Vo= 4.76Ft/sec
Displacement=1.0491inch
Eo= 2.96Ft-Lb
E absorbed= 3.50Ft-Lb

INSTRUMENTED IMPACT TEST

I28(I2B) 6/5/86

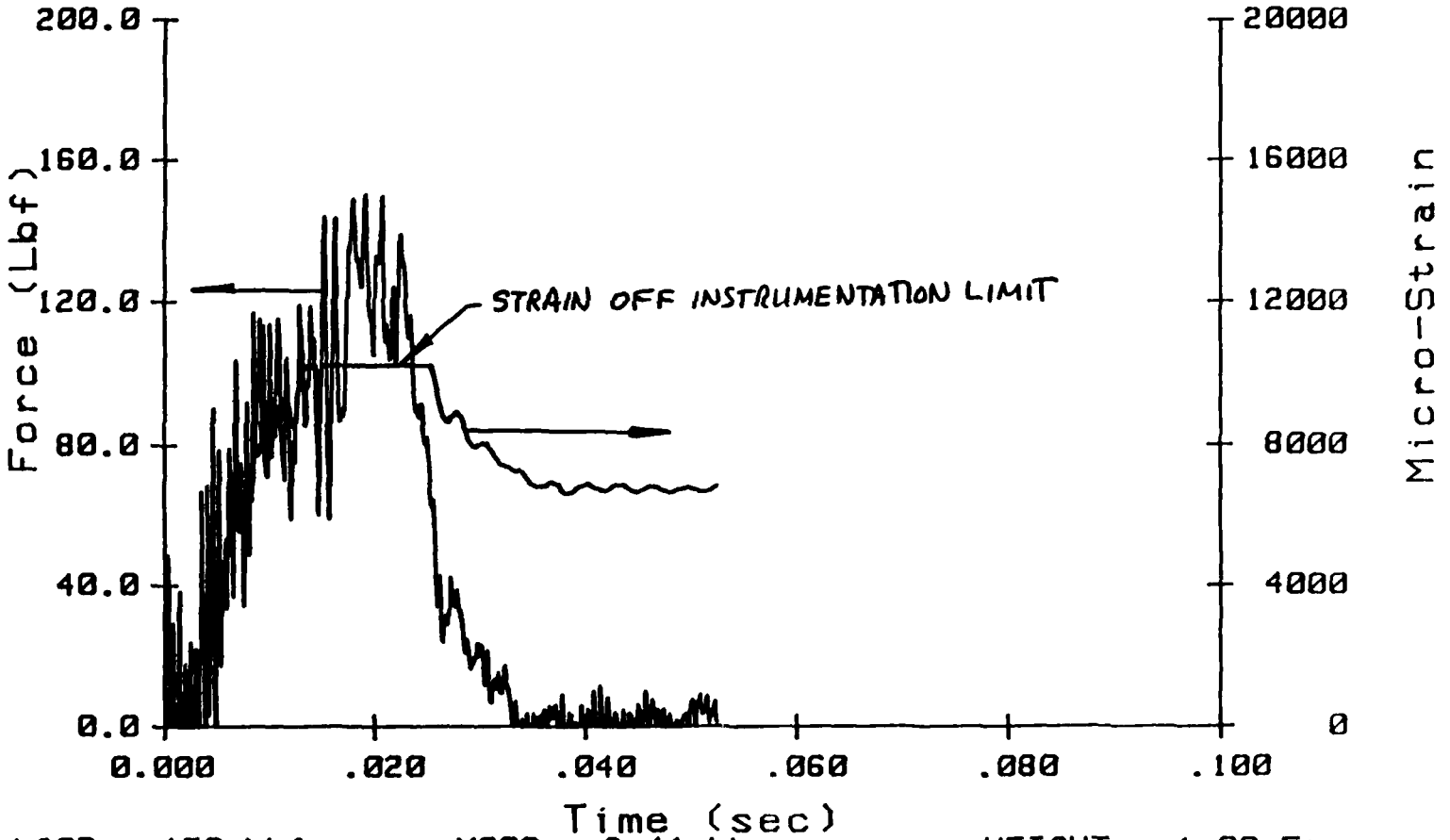

MAX LOAD= 150 Lbf MASS= 8.41 Lbm HEIGHT= 1.00 Ft

MAX STRAIN= 10235 Micro inch/inch

RADIUS= .13 inch LOAD SCALE= .2KN/DIV

NADC-87106-60

APPENDIX E. NONDIMENSIONAL PLOTS OF IMPACTOR FORCE p* AND PLATE AXIAL NORMAL STRAIN e* VERSUS TIME t* DURING GRAPHITE/EPOXY PLATE IMPACT TESTS

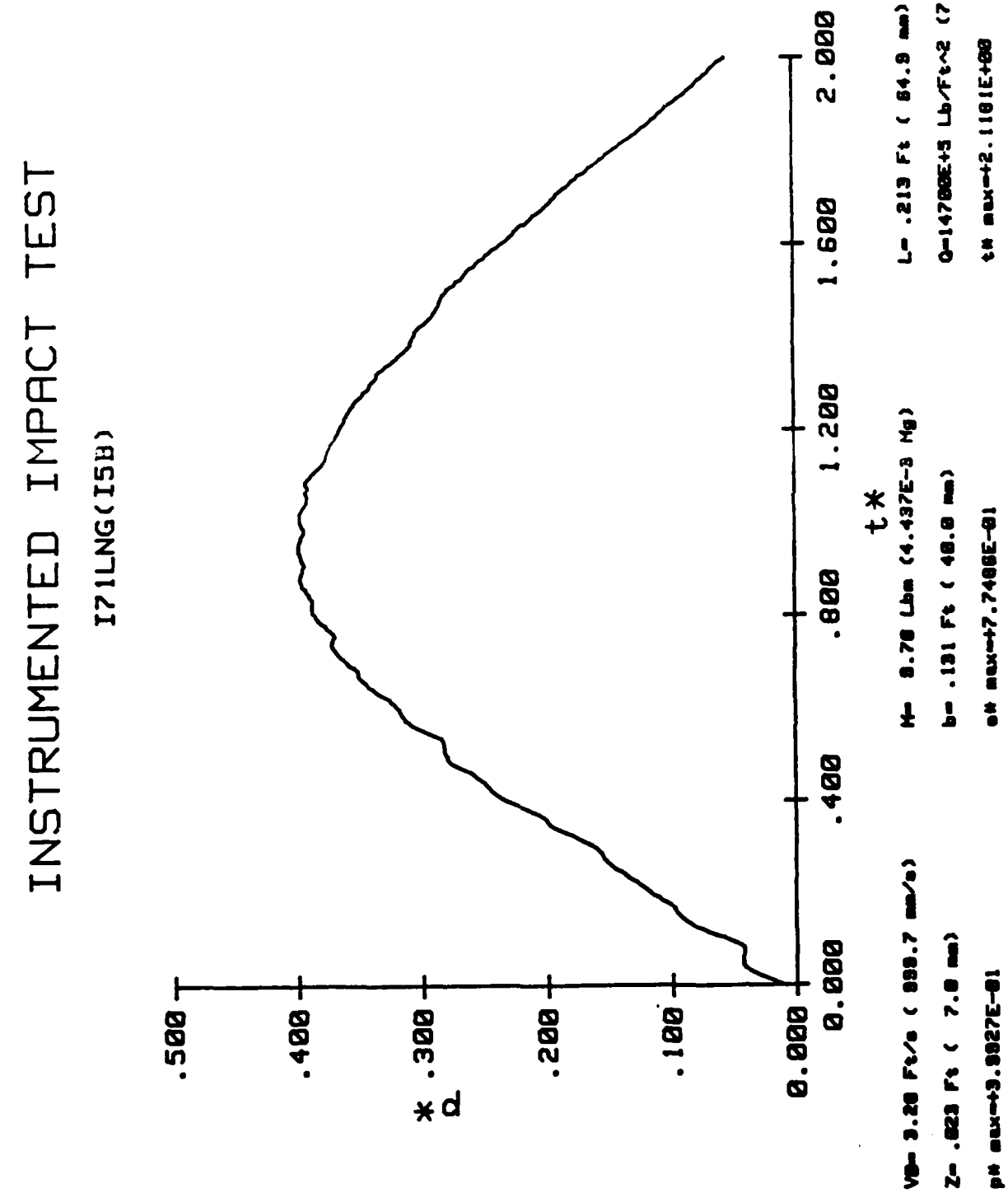
INSTRUMENTED IMPACT TEST
I71LNG(I5B)
.500
.400
.300
.200
.100
0.000
* D
0.000
.400
.800
1.200
1.600
2.000
t*
Vo= 3.20 Ft/s (888.7 mm/s)
M= 8.78 Lbm (4.437E-3 Mg)
L= .213 Ft (84.9 mm)
Z= .023 Ft (7.0 mm)
b= .131 Ft (40.0 mm)
Q=14700E+3 Lb/Ft^2 (7.038E+4 MPa)
p* max=+3.8927E-01
e* max=+7.7488E-01
t* max=+2.1181E+00

INSTRUMENTED IMPACT TEST

I71LNG(I5B)

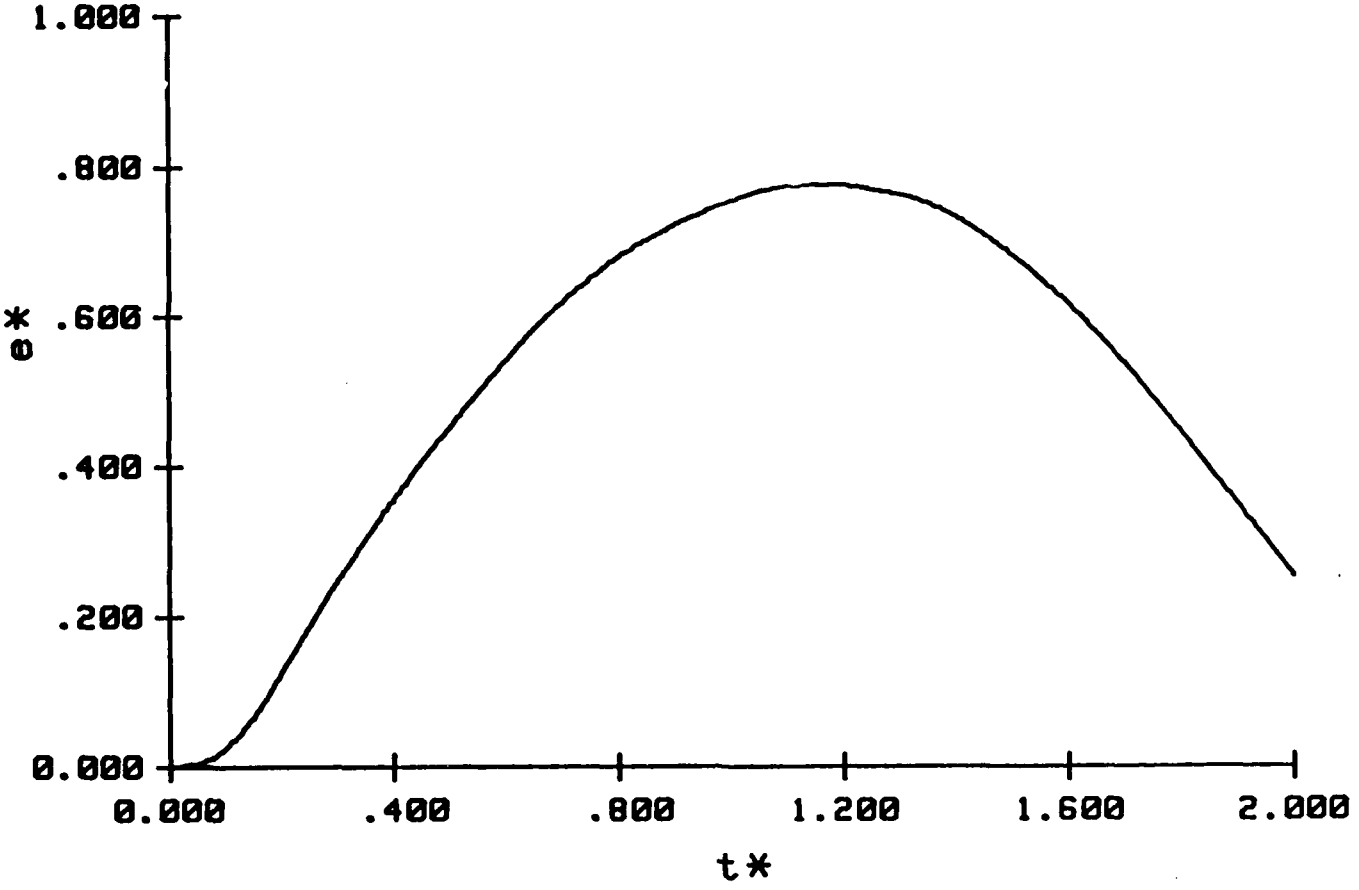

V0= 3.28 Ft/s (999.7 mm/s)
M= 9.78 Lbm (4.437E-3 Mg)
L= .213 Ft (64.9 mm)
Z= .023 Ft (7.0 mm)
b= .131 Ft (40.0 mm)
Q=14700E+5 Lb/Ft^2 (7.038E+4 MPa)
p* max=+3.9927E-01
ω* max=+7.7486E-01
t* max=+2.1181E+00

INSTRUMENTED IMPACT TEST

I74LNG(I5B)

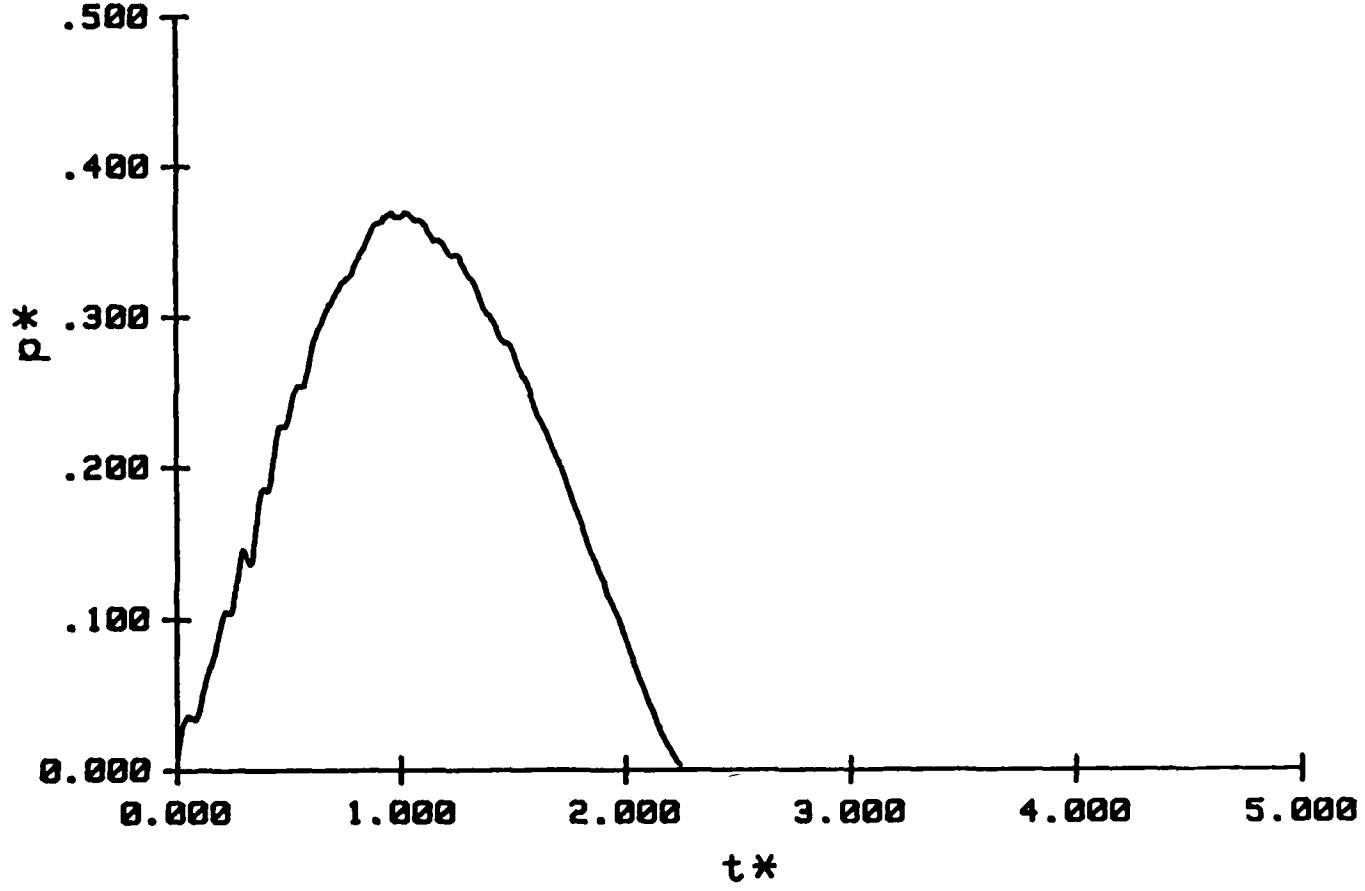

V0= 3.64 Ft/s (1109.5 mm/s)
M= 9.78 Lbm (4.437E-3 Mg)
L= .213 Ft (64.9 mm)
Z= .023 Ft (7.0 mm)
b= .131 Ft (40.0 mm)
Q=14700E+5 Lb/Ft^2 (7.838E+4 MPa)
p* max=+3.8838E-01
σ* max=+7.4419E-01
t* max=+2.2426E+00

INSTRUMENTED IMPACT TEST

I74LNG(I5B)

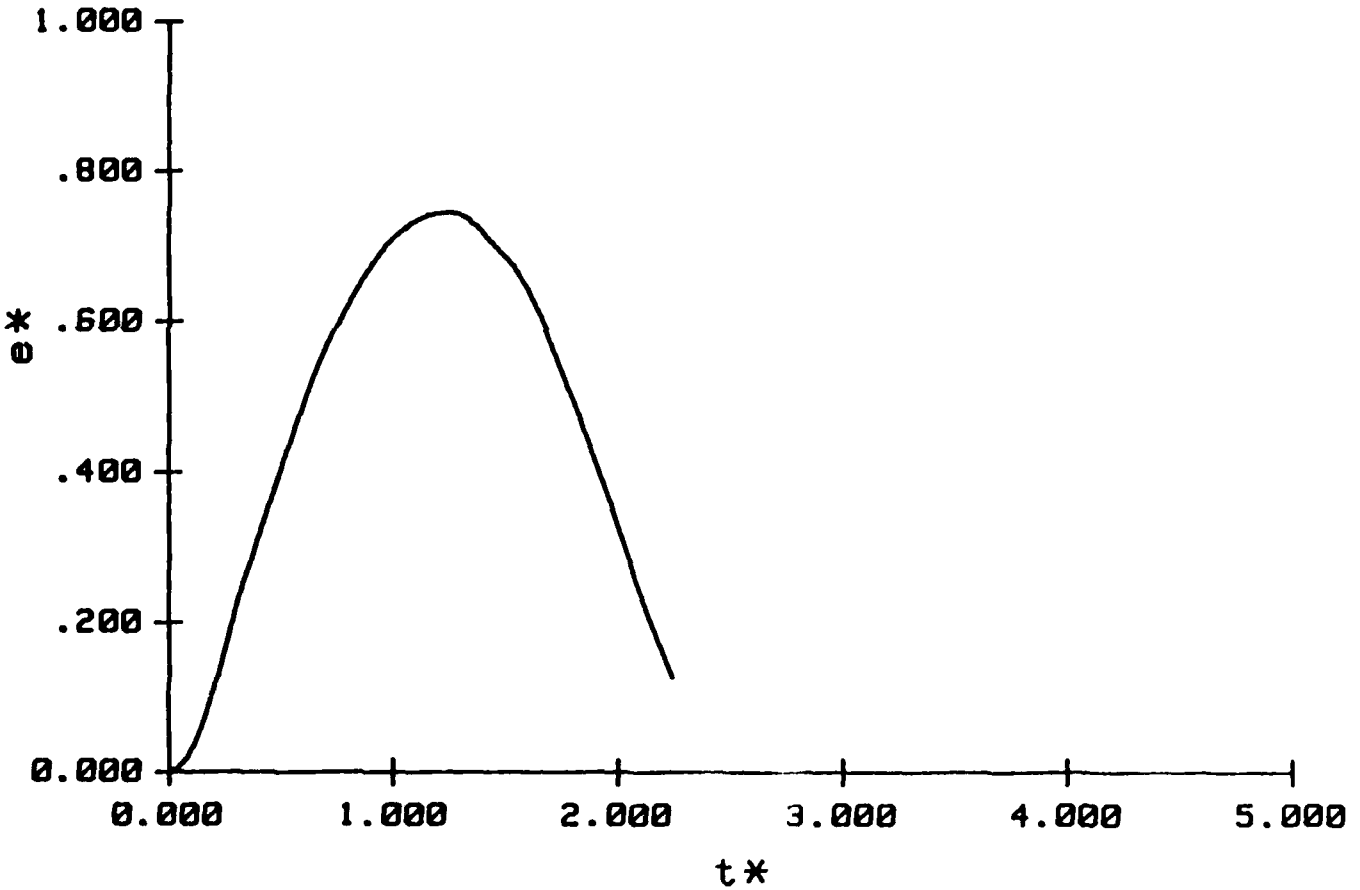

VB= 3.64 Ft/s (1109.5 mm/s)
M= 9.78 Lbm (4.437E-3 Mg)
L= .213 Ft (64.9 mm)
Z= .023 Ft (7.0 mm)
b= .131 Ft (40.0 mm)
Q=14700E+5 Lb/Ft^2 (7.038E+4 MPa)
p* max=+3.6939E-01
e* max=+7.4489E-01
t* max=+2.2426E+00

NADC-87106-60

INSTRUMENTED IMPACT TEST

I74LNG(I5B)

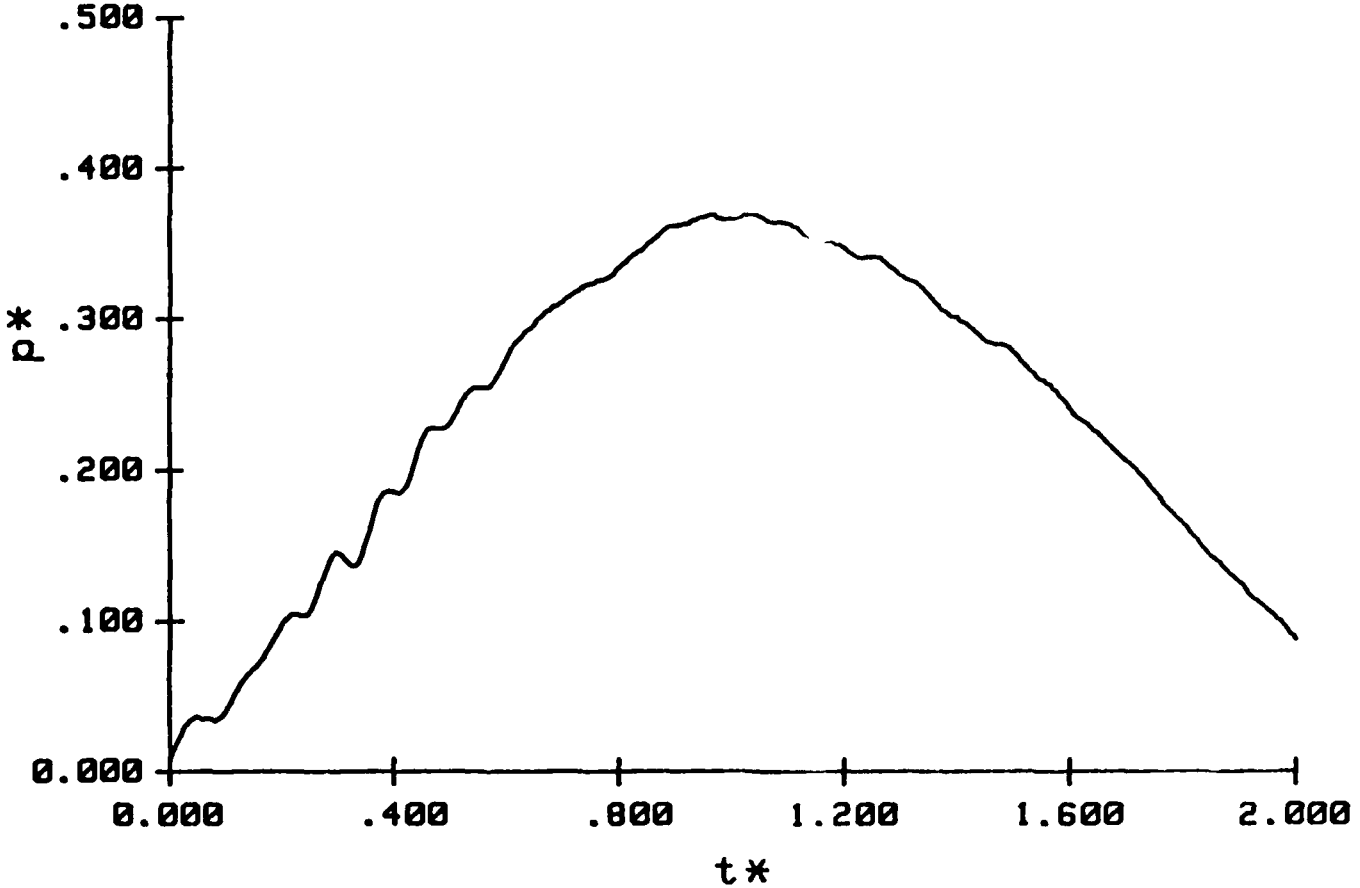

V0= 3.64 Ft/s (1109.5 mm/s)
M= 9.78 Lbm (4.437E-3 Mg)
L= .219 Ft (64.9 mm)
Z= .023 Ft (7.0 mm)
b= .131 Ft (40.0 mm)
Q=14700E+5 Lb/Ft^2 (7.038E+4 MPa)
p* max=+3.6938E-01
e* max=+7.4489E-01
t* max=+2.2426E+00

INSTRUMENTED IMPACT TEST

I74LNG(I5B)

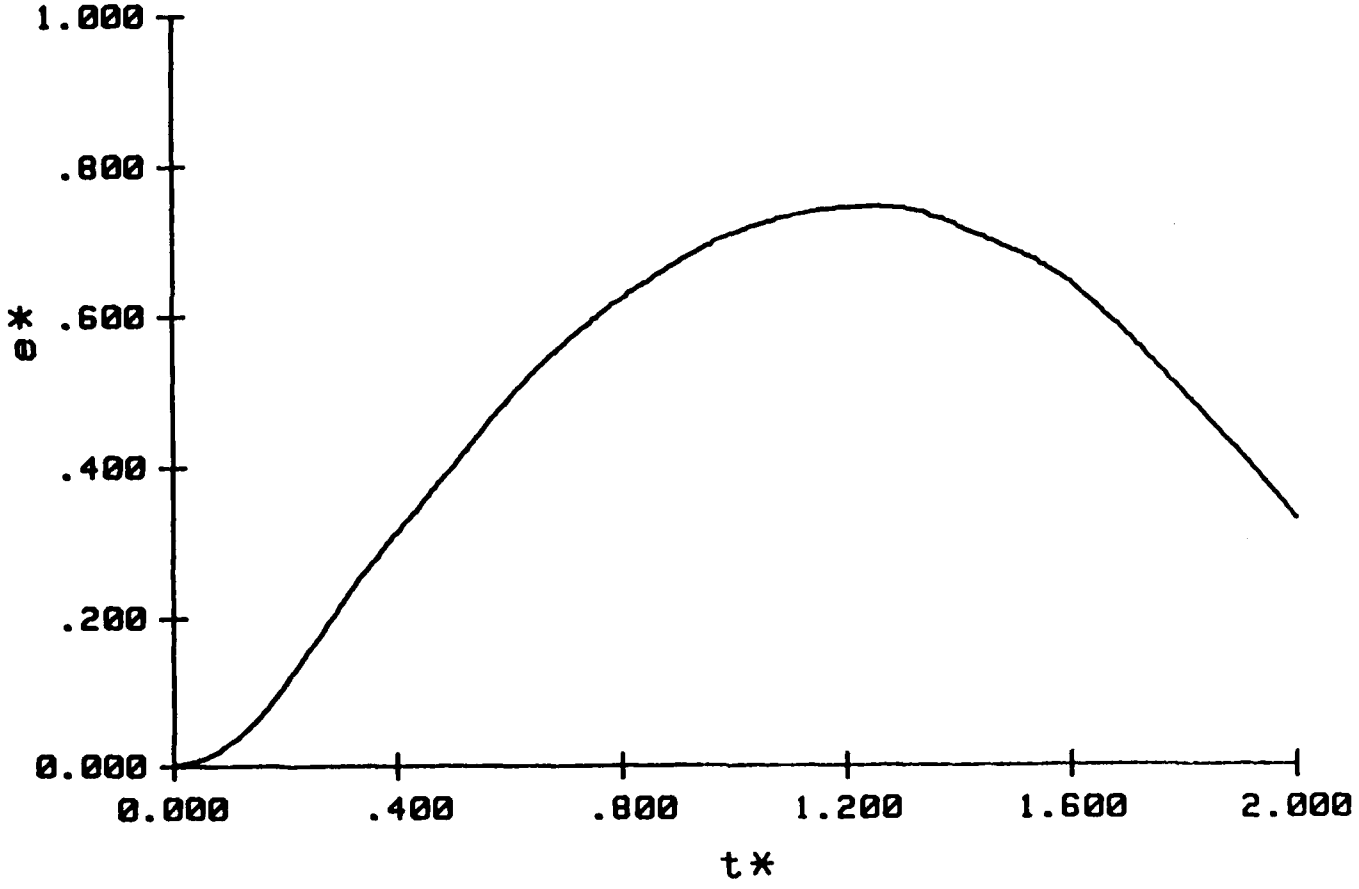

VB= 9.64 Ft/s (1180.5 mm/s)
M= 9.78 Lbm (4.437E-3 Mg)
L= .213 Ft (64.9 mm)
Z= .023 Ft (7.0 mm)
b= .131 Ft (40.0 mm)
Q=14700E+5 Lb/Ft^2 (7.038E+4 MPa)
p* max=+9.6938E-01
ø* max=+7.4489E-01
t* max=+2.2426E+00

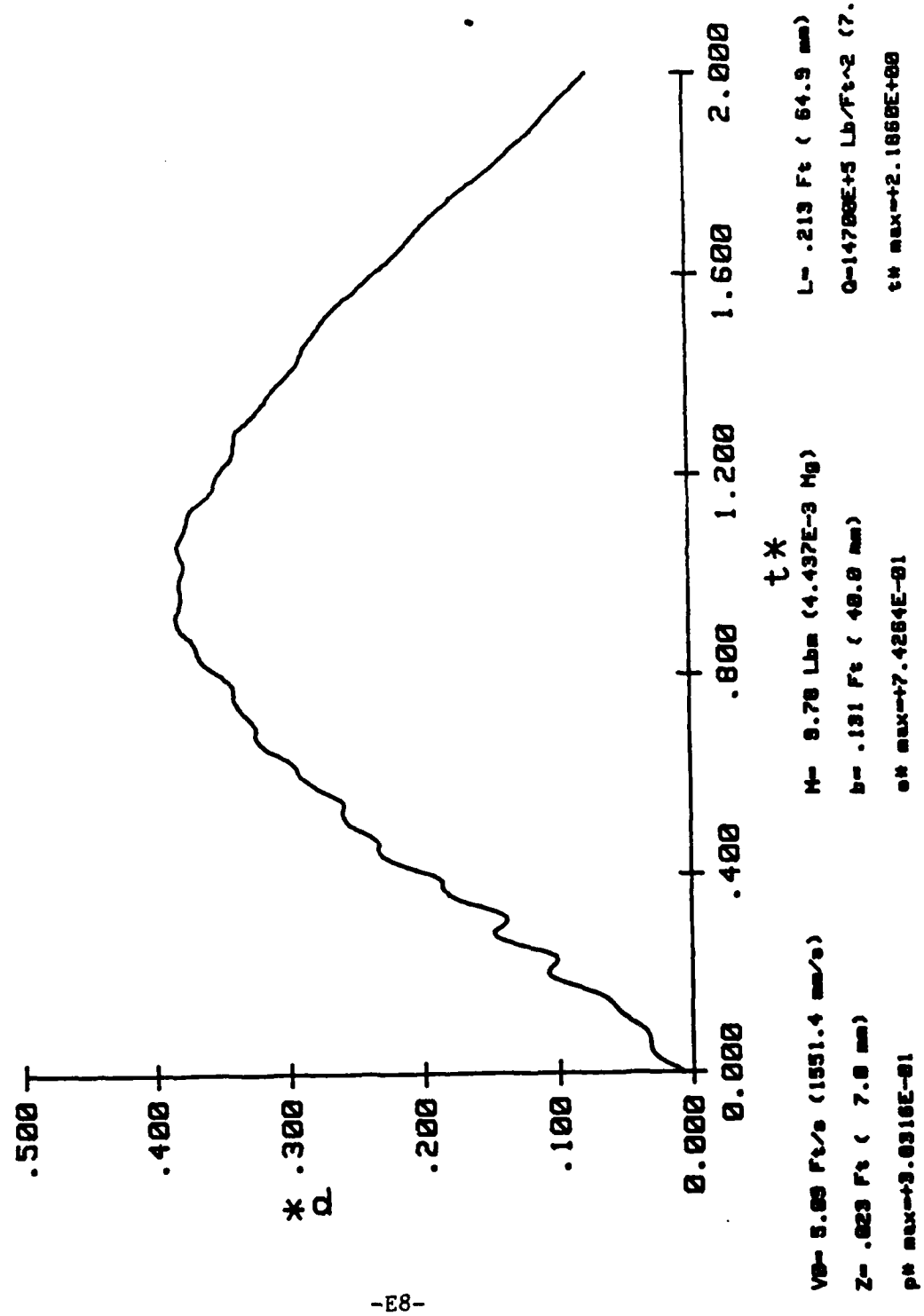
INSTRUMENTED IMPACT TEST
I77LNG(I5B)
.500
.400
.300
.200
.100
0.000
*α
0.000
.400
.800
1.200
1.600
2.000
t*
L= .213 Ft (64.9 mm)
Q=1470E+5 Lb/Ft^2 (7.038E+4 MPa)
t* max=+2.1868E+00
M= 8.78 Lbm (4.437E-3 Hg)
b= .131 Ft (40.0 mm)
α* max=+7.4284E-01
V0= 5.09 Ft/s (1551.4 mm/s)
Z= .023 Ft (7.0 mm)
p* max=+3.8316E-01

INSTRUMENTED IMPACT TEST

I77LNG(I5B)

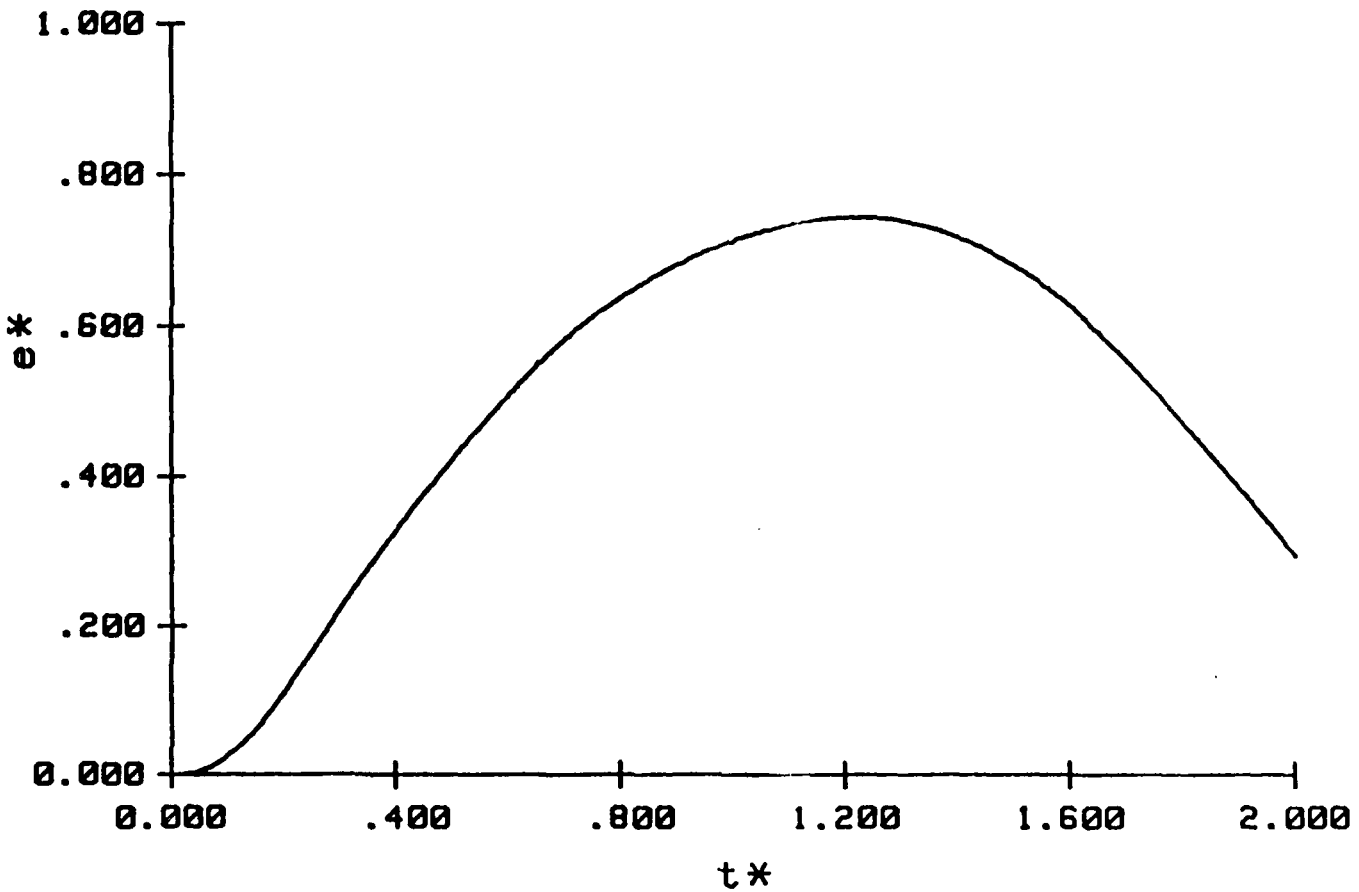

V0= 5.09 Ft/s (1551.4 mm/s)
M= 9.78 Lbm (4.437E 3 Mg)
L= .213 Ft (64.9 mm)
Z= .023 Ft (7.0 mm)
b= .131 Ft (40.0 mm)
Q=14700E+5 Lb/Ft^2 (7.038E+4 MPa)
p* max=+3.8316E-01
e* max=+7.4264E-01
t* max=+2.1868E+00

INSTRUMENTED IMPACT TEST

I78LNG(I5E)

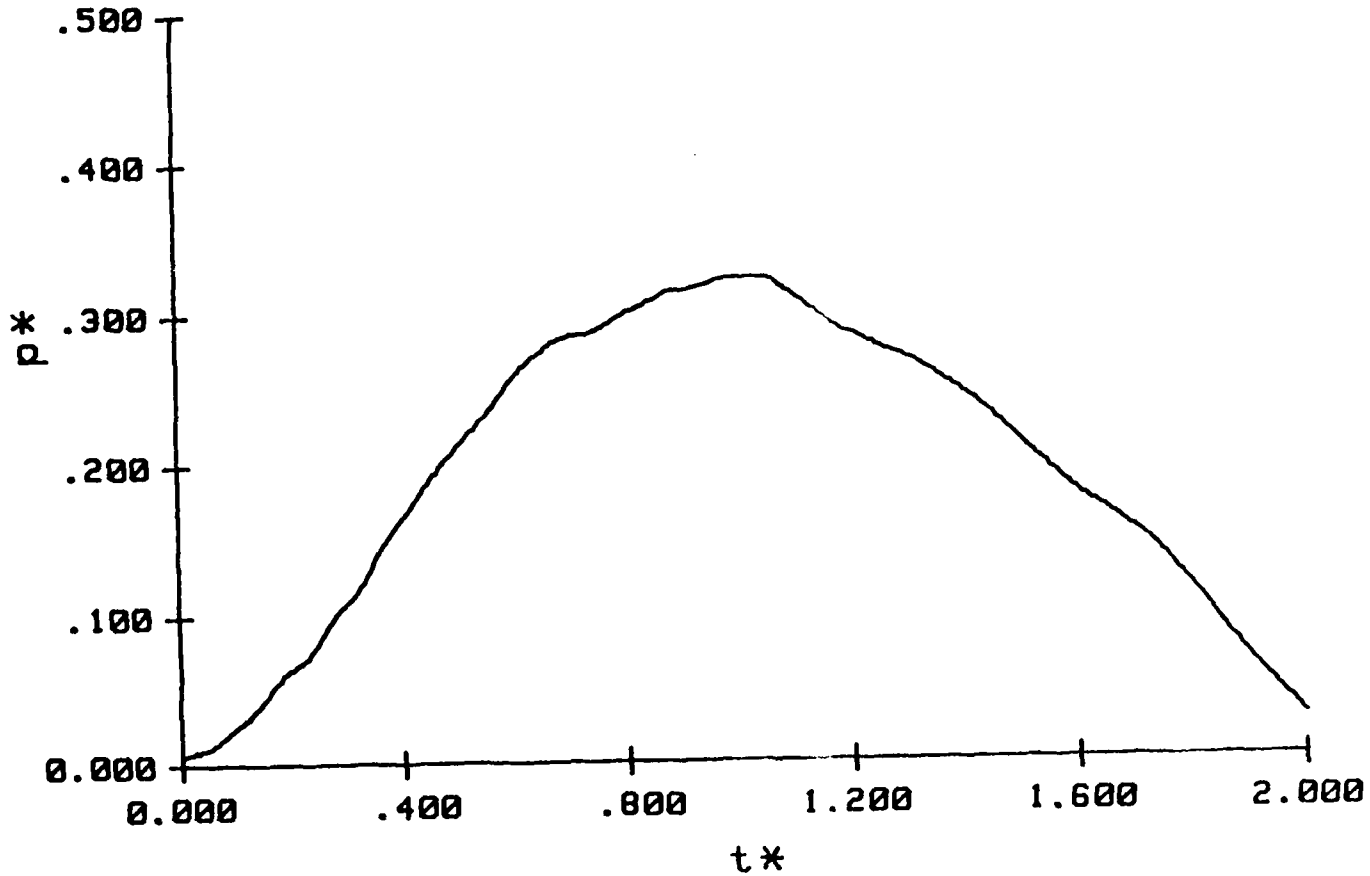

V0= 3.24 Ft/s (987.6 mm/s)

Z= .023 Ft (7.0 mm)

p* max=+9.2305E-01

M= 9.78 Lbm (4.437E-3 Mg)

b= .131 Ft (40.0 mm)

e* max=+6.4131E-01

L= .213 Ft (64.9 mm)

Q=14700E+5 Lb/Ft^2 (7.038E+4 MPa)

t* max=+2.0784E+00

INSTRUMENTED IMPACT TEST

I78LNG(I5E)

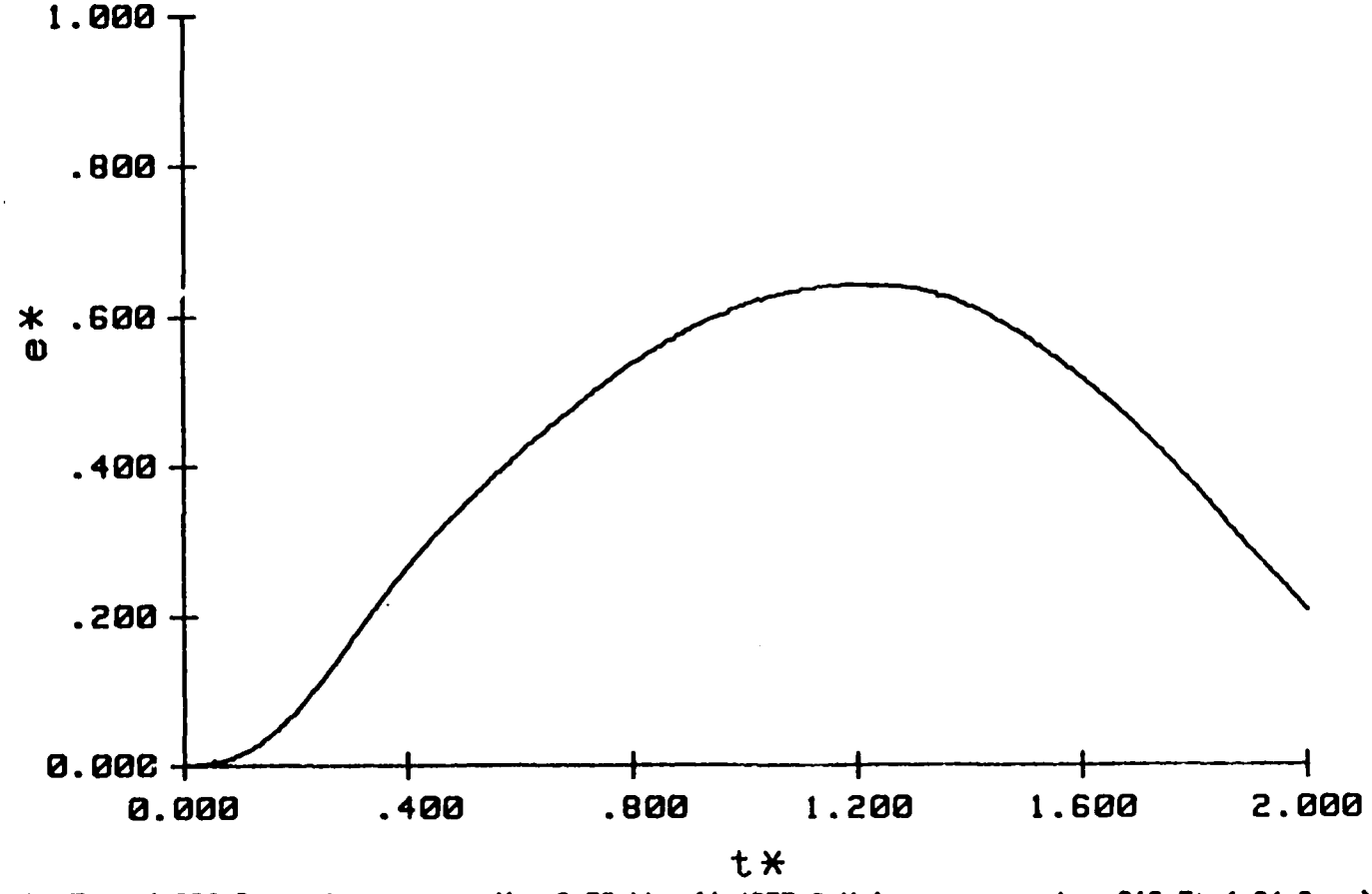

V0= 3.24 Ft/s (987.6 mm/s)
M= 9.78 Lbm (4.437E-3 Mg)
L= .213 Ft (64.9 mm)

Z= .023 Ft (7.0 mm)
b= .131 Ft (40.0 mm)
Q=14700E+5 Lb/Ft^2 (7.038E+4 MPa)

p* max=+3.2305E-01
e* max=+6.4131E-01
t* max=+2.0784E+00

NADC-87106-60

INSTRUMENTED IMPACT TEST

I711LG(I5E)

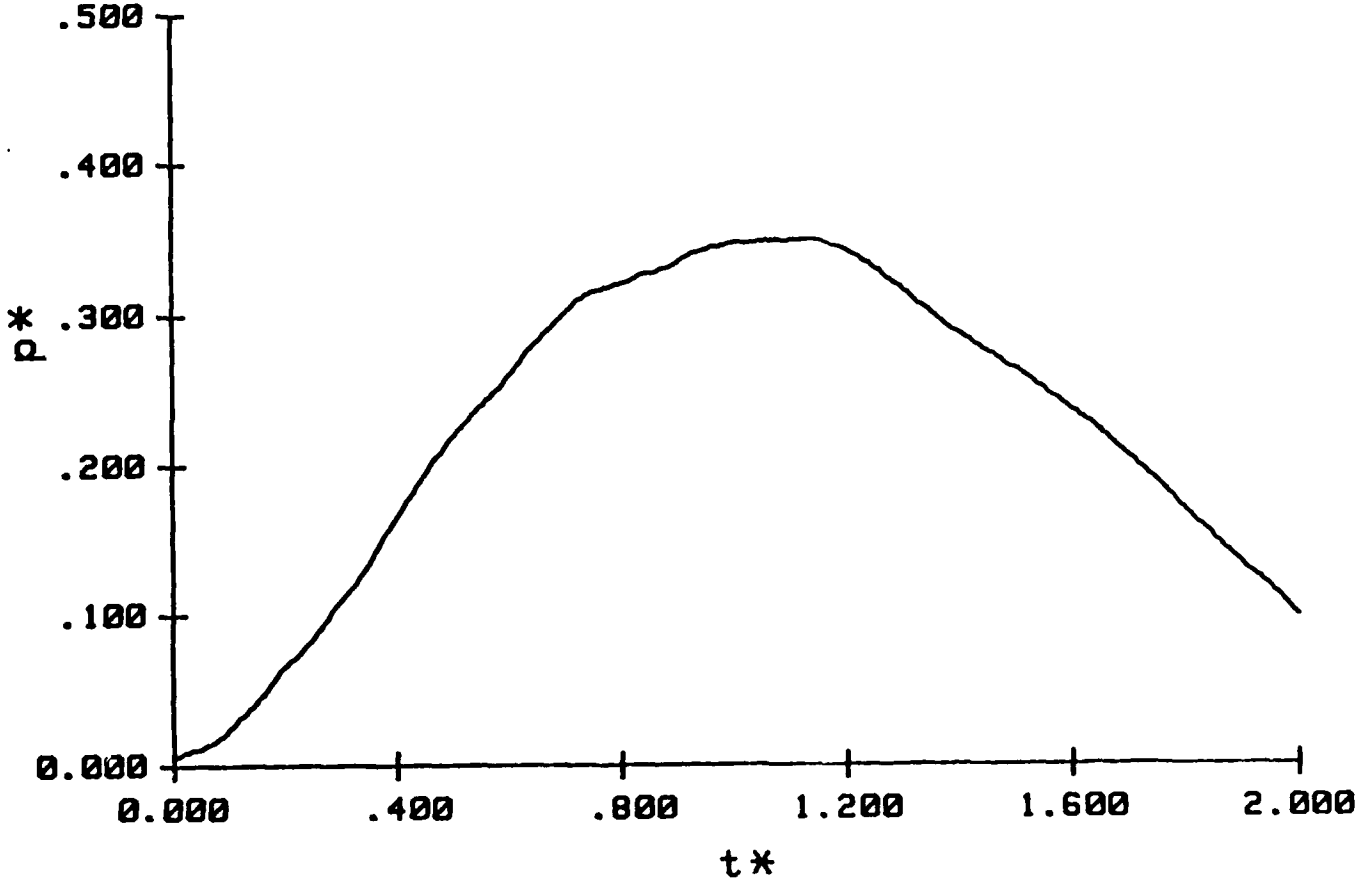

V0= 3.62 Ft/s (1103.4 mm/s)

Z= .023 Ft (7.0 mm)

p* max=+3.4897E-01

M= 8.41 Lbm (3.816E-3 Mg)

b= .131 Ft (40.0 mm)

e* max=+6.8854E-01

L= .213 Ft (64.9 mm)

Q=14700E+5 Lb/Ft^2 (7.038E+4 MPa)

t* max=+2.2238E+00

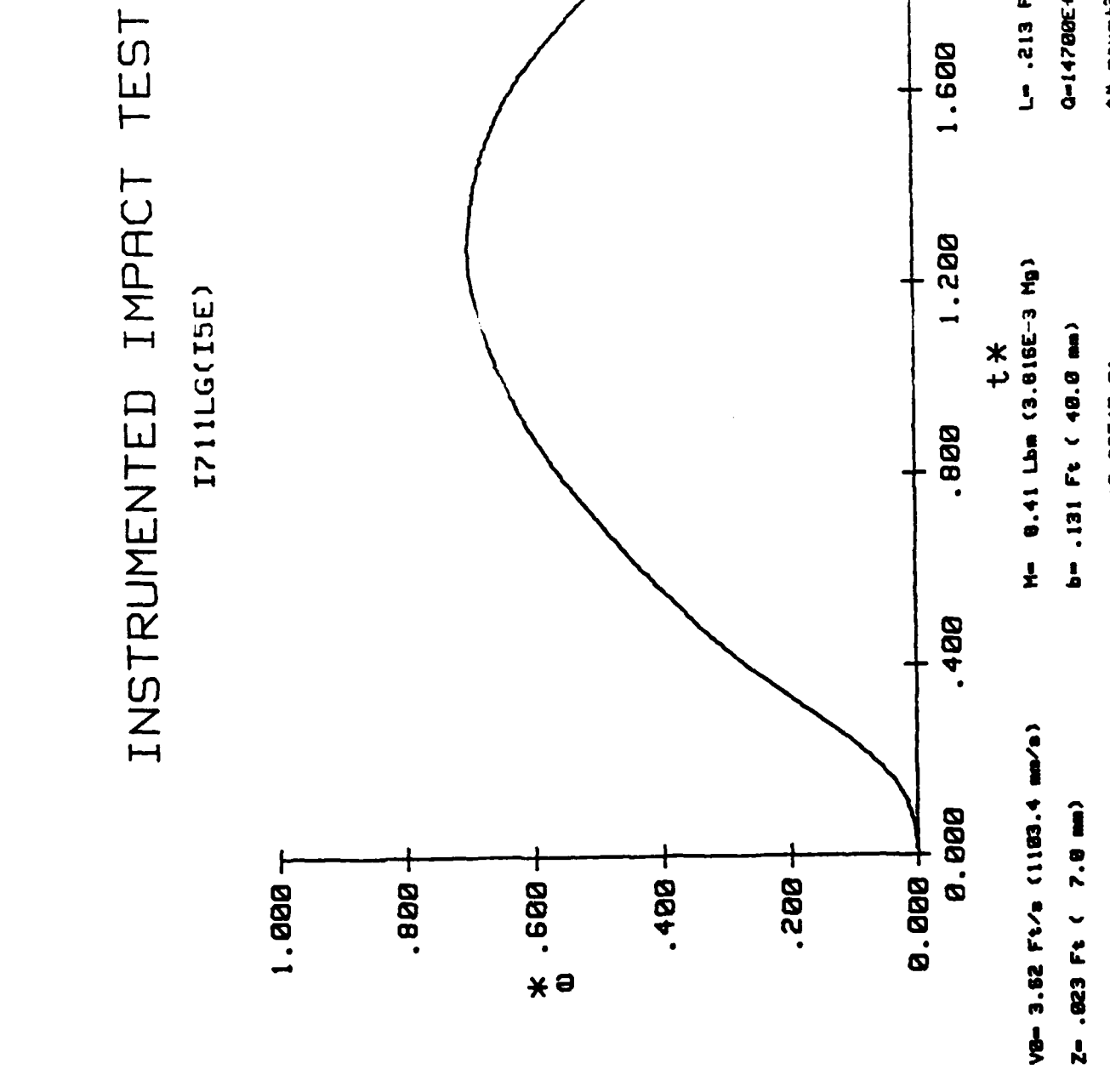
INSTRUMENTED IMPACT TEST
I711LG(I5E)
1.000
.800
.600
.400
.200
0.000
w*
0.000
.400
.800
1.200
1.600
2.000
t*
V0= 3.62 Ft/s (1103.4 mm/s)
M= 8.41 Lbm (3.816E-3 Mg)
L= .213 Ft (64.9 mm)
Z= .023 Ft (7.0 mm)
b= .131 Ft (40.0 mm)
Q=14700E+5 Lb/Ft^2 (7.038E+4 MPa)
p* max=+3.4987E-01
w* max=+8.9854E-01
t* max=+2.2230E+00

INSTRUMENTED IMPACT TEST

I712LG(I5E)

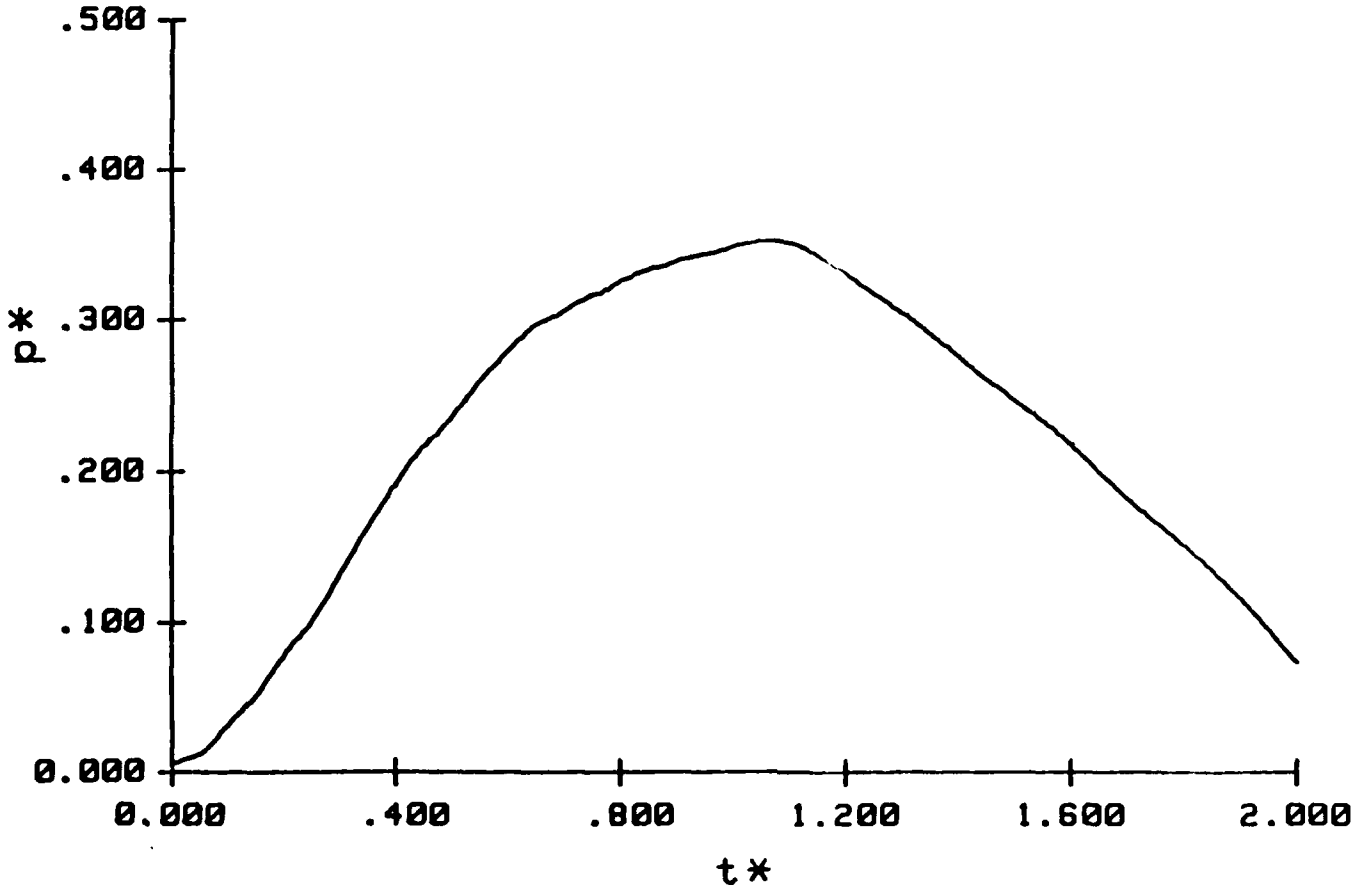

V0= 5.01 Ft/s (1527.8 mm/s)
M= 0.41 Lbm (3.816E-3 Mg)
L= .213 Ft (84.9 mm)
Z= .023 Ft (7.0 mm)
b= .131 Ft (40.0 mm)
Q=14700E+5 Lb/Ft^2 (7.03uE+4 MPa)
p* max=+3.5316E-01
σ* max=+6.7466E-01
t* max=+2.1741E+00

NADC-87106-60

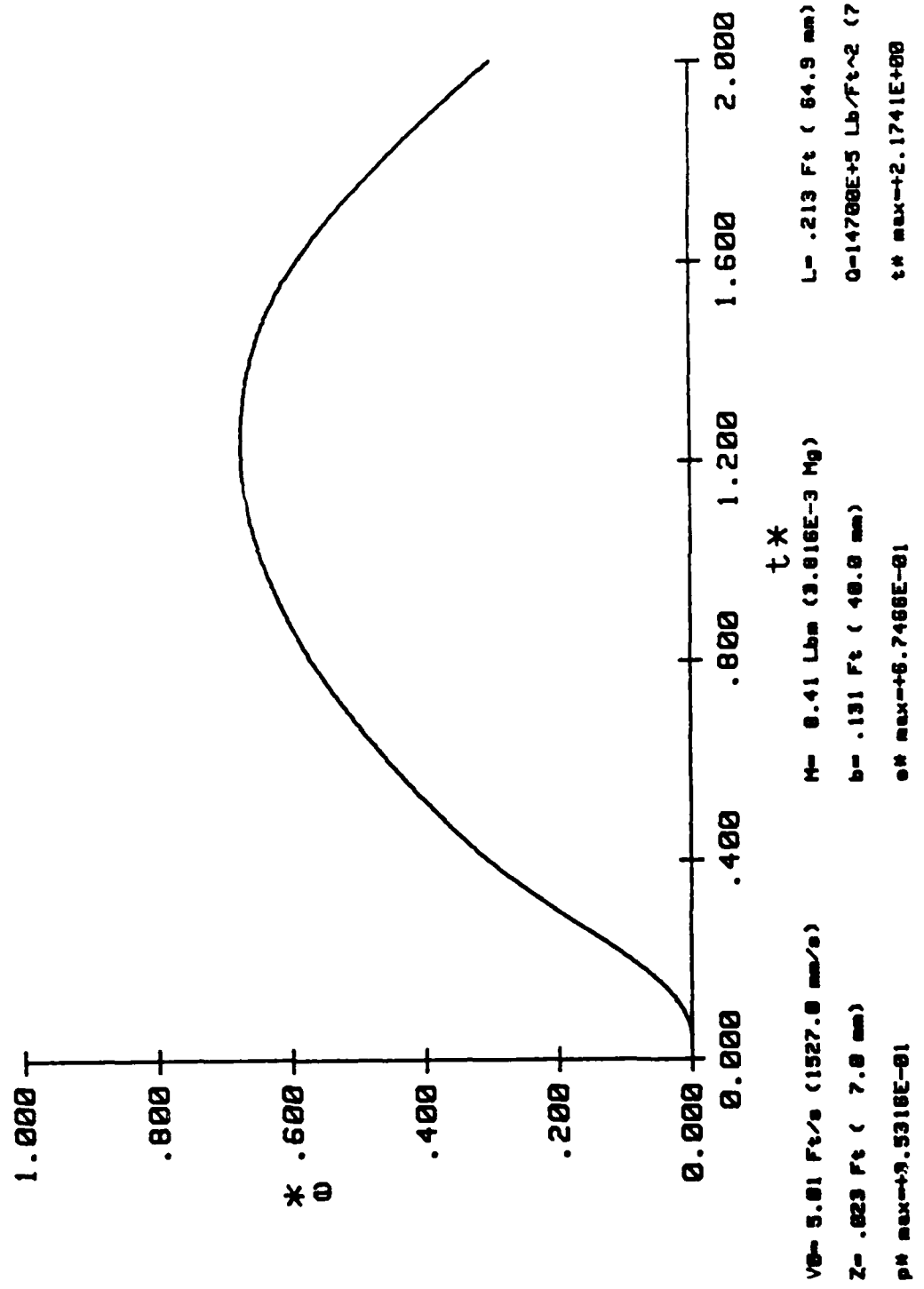
INSTRUMENTED IMPACT TEST
I712LG(I5E)
1.000
.800
.600
.400
.200
0.000
* Ø
0.000
.400
.800
1.200
1.600
2.000
t*
V0= 5.01 Ft/s (1527.0 mm/s)
M= 0.41 Lbm (3.816E-3 Mg)
L= .213 Ft (64.9 mm)
Z= .023 Ft (7.0 mm)
b= .131 Ft (40.0 mm)
Q=14700E+5 Lb/Ft^2 (7.038E+4 MPa)
p* max=+9.5316E-01
ø* max=+6.7466E-01
t* max=+2.1741E+00

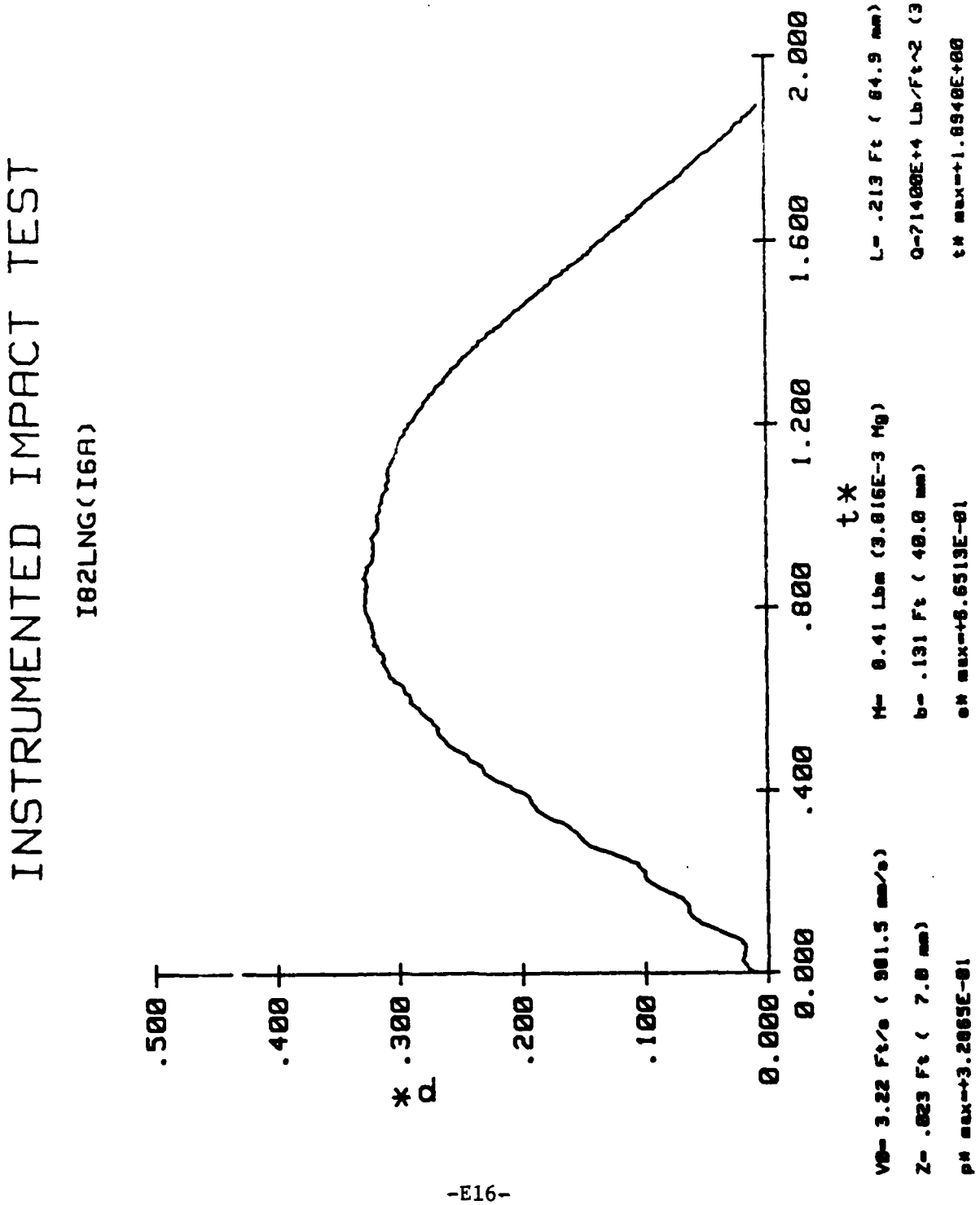
INSTRUMENTED IMPACT TEST
I82LNG(I6A)
.500
.400
.300
.200
.100
0.000
* a
0.000
.400
.800
1.200
1.600
2.000
t*
V0= 3.22 Ft/s (981.5 mm/s)
M= 0.41 Lbm (3.816E-3 Mg)
L= .213 Ft (64.9 mm)
Z= .823 Ft (7.8 mm)
b= .131 Ft (40.0 mm)
Q=71400E+4 Lb/Ft^2 (3.419E+4 MPa)
p# max=+3.2065E-01
a# max=+8.6513E-01
t# max=+1.8940E+00

INSTRUMENTED IMPACT TEST

I82LNG(I6A)

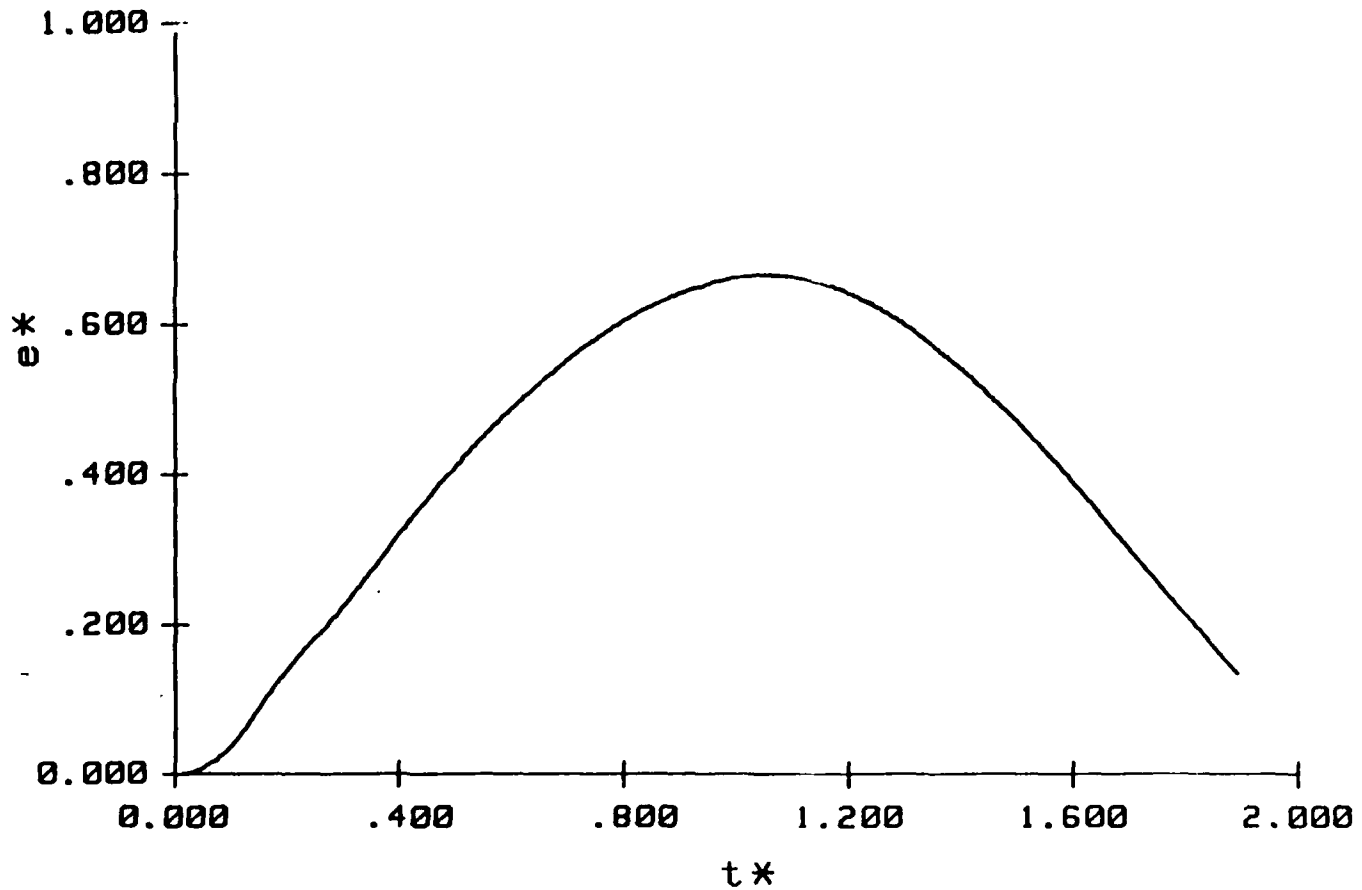

V0= 3.22 Ft/s (981.5 mm/s)
M= 8.41 Lbm (3.816E-3 Mg)
L= .213 Ft (64.9 mm)
Z= .023 Ft (7.0 mm)
b= .131 Ft (40.0 mm)
Q=71400E+4 Lb/Ft^2 (3.419E+4 MPa)
p* max=+3.2865E-01
e* max=+6.6513E-01
t* max=+1.8940E+00

NADC-87106-60

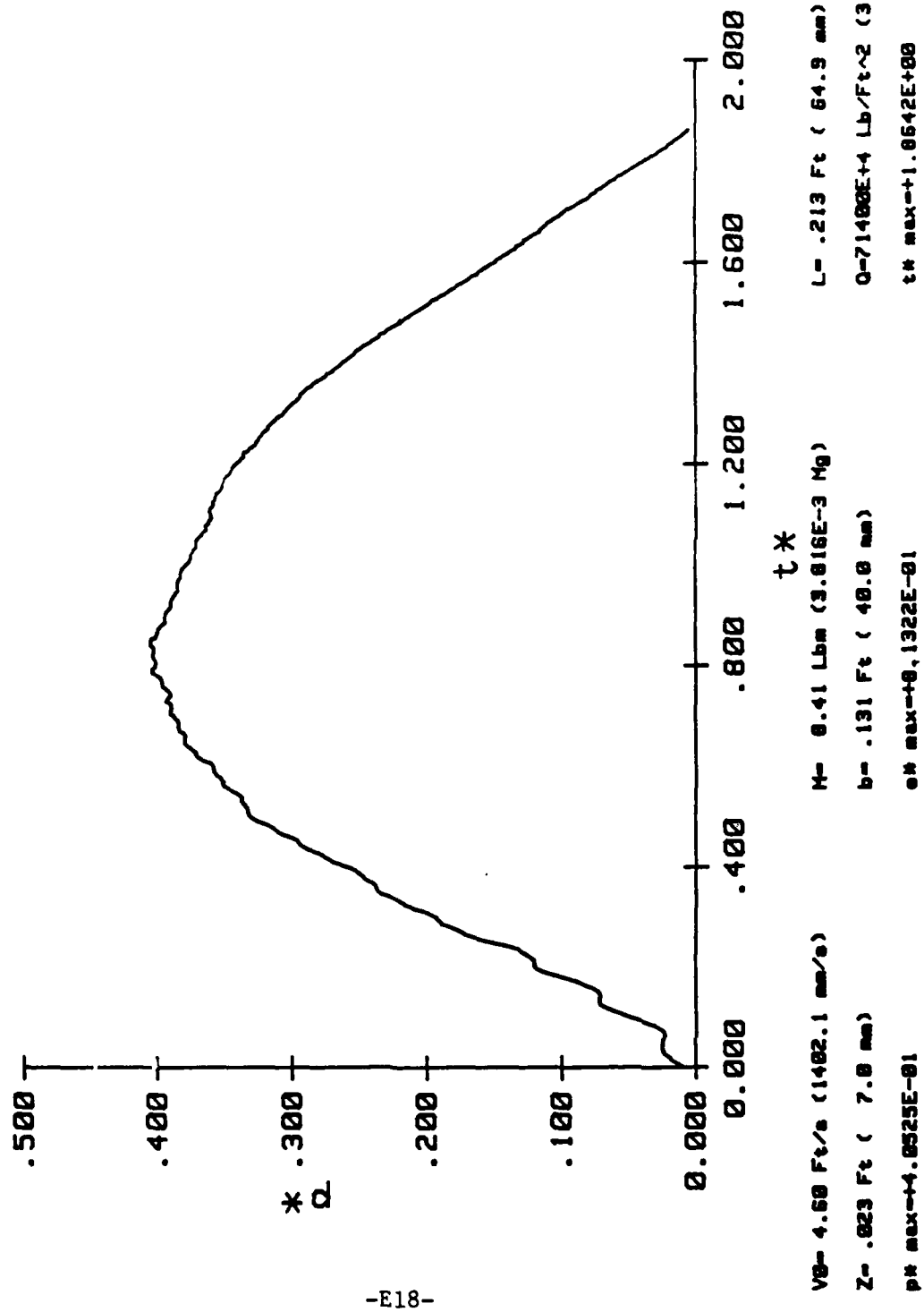
INSTRUMENTED IMPACT TEST
I83LNG(I6A)
.500
.400
.300
.200
.100
0.000
*Ω
0.000
.400
.800
1.200
1.600
2.000
t*
V0= 4.60 Ft/s (1402.1 mm/s)
M= 0.41 Lbm (3.816E-3 Mg)
L= .213 Ft (64.9 mm)
Z= .023 Ft (7.0 mm)
b= .131 Ft (40.0 mm)
Q=71400E+4 Lb/Ft^2 (3.419E+4 MPa)
p* max=+4.8525E-01
e* max=+0.1322E-01
t* max=+1.0642E+00

INSTRUMENTED IMPACT TEST

I83LNG(I6A)

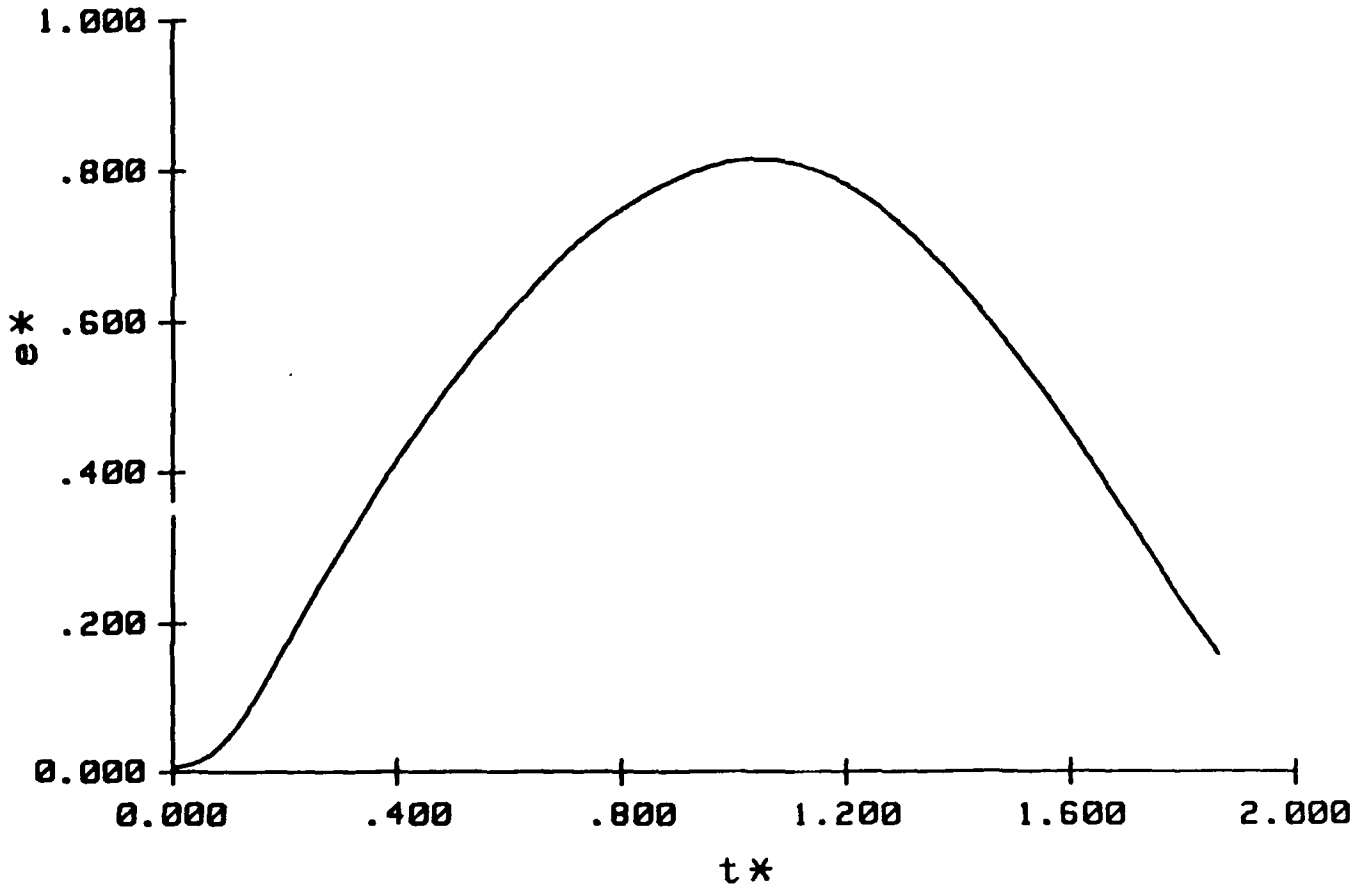

VB= 4.60 Ft/s (1402.1 mm/s)
M= 8.41 Lbm (3.816E-3 Mg)
L= .213 Ft (64.9 mm)
Z= .023 Ft (7.0 mm)
b= .131 Ft (40.0 mm)
Q=71400E+4 Lb/Ft^2 (3.419E+4 MPa)
p* max=+4.0525E-01
e* max=+8.1322E-01
t* max=+1.8642E+00

INSTRUMENTED IMPACT TEST

I86LNG(I6B)

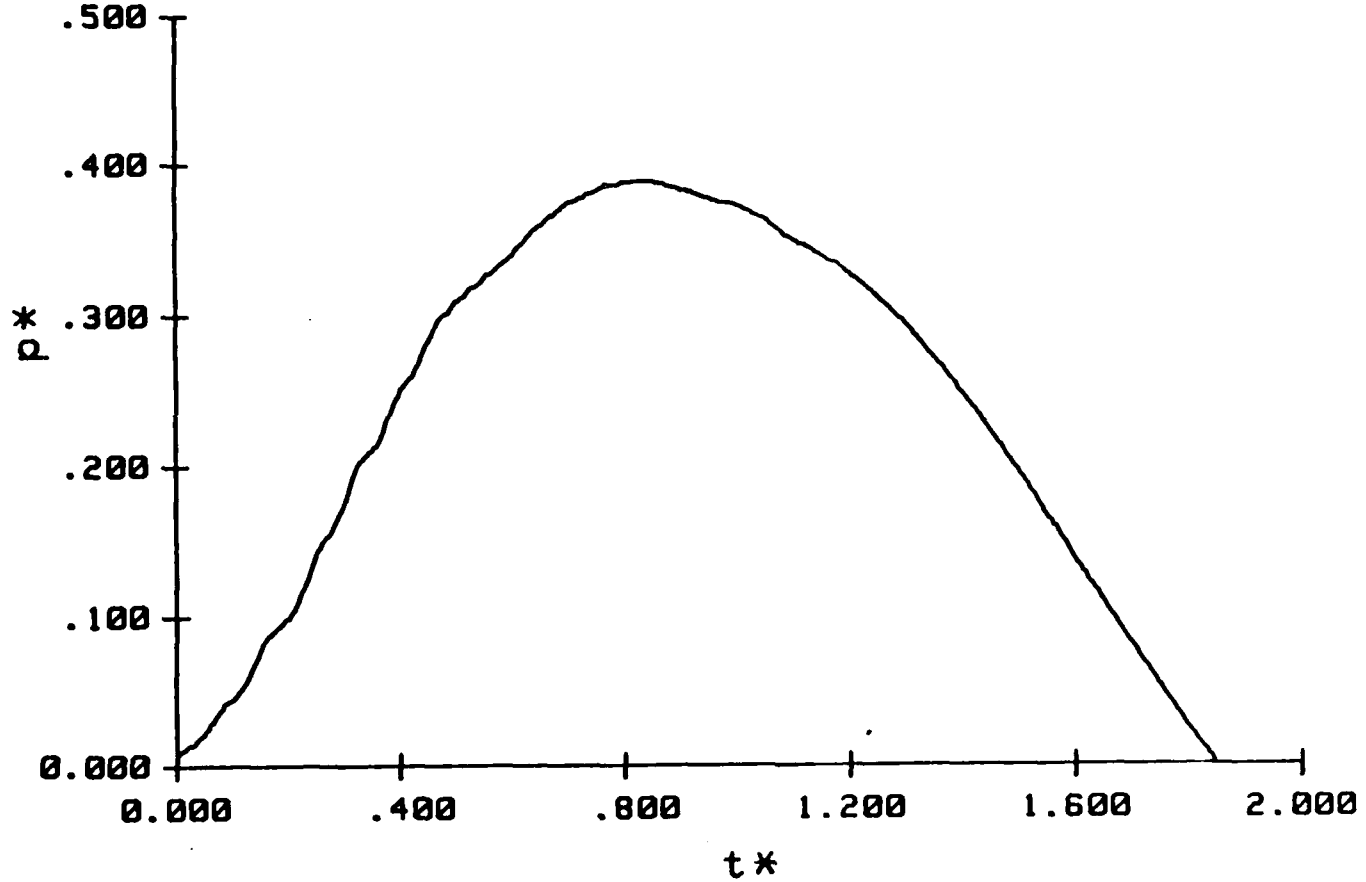

V0= 4.54 Ft/s (1383.6 mm/s)

M= 8.41 Lbm (3.816E-3 Mg)

L= .213 Ft (64.9 mm)

Z= .023 Ft (7.0 mm)

b= .131 Ft (40.0 mm)

Q=71400E+4 Lb/Ft^2 (3.419E+4 MPa)

p* max=+3.8849E-01

e* max=+7.5158E-01

t* max=+1.8472E+00

NADC-87106-60

INSTRUMENTED IMPACT TEST

I86LNG(I6B)

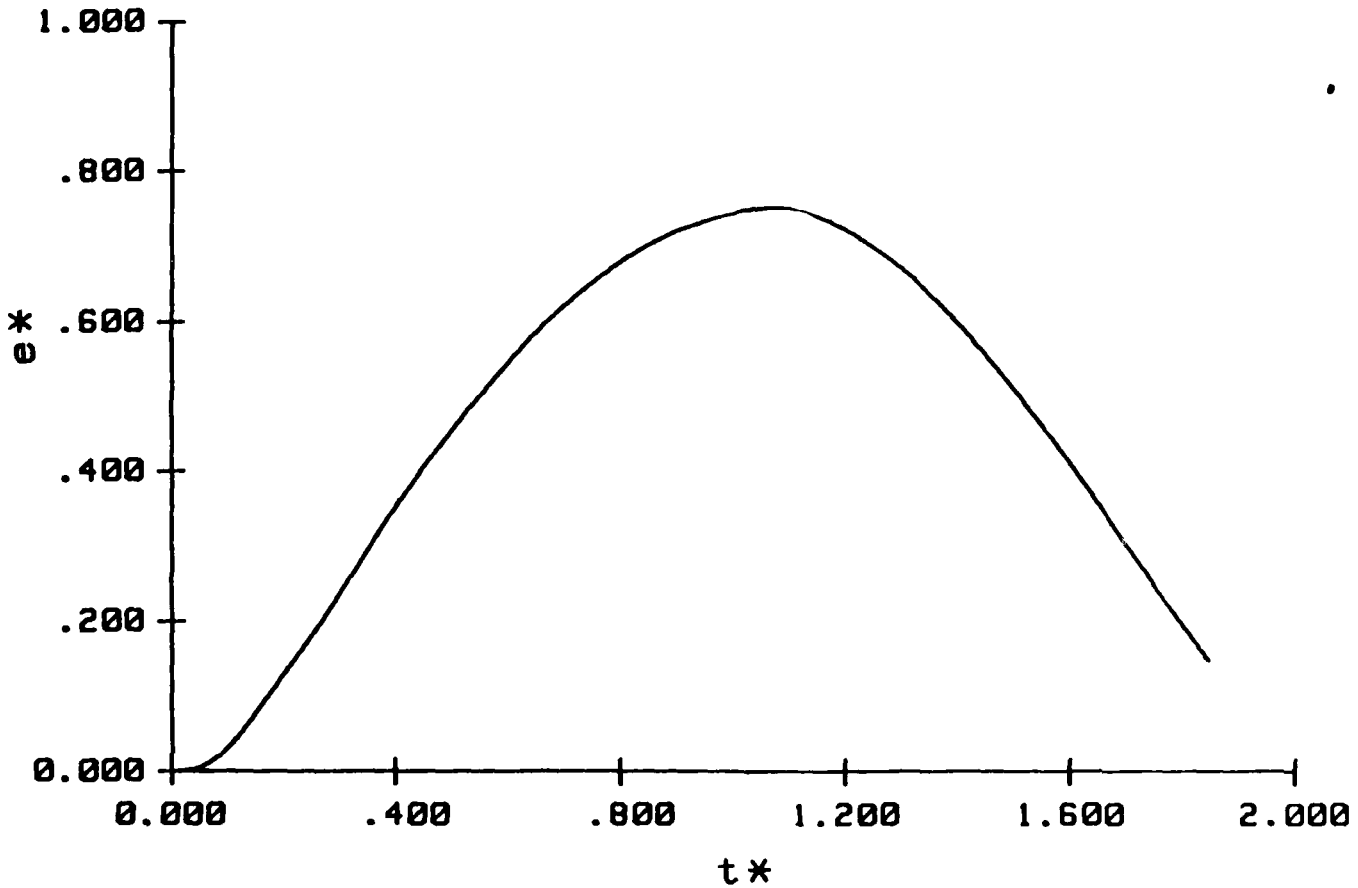

V0= 4.54 Ft/s (1383.8 mm/s)
M= 8.41 Lbm (3.818E-3 Mg)
L= .213 Ft (64.9 mm)
Z= .023 Ft (7.0 mm)
b= .131 Ft (40.0 mm)
Q=71400E+4 Lb/Ft^2 (3.419E+4 MPa)
p* max=+3.0849E 01
e* max=+7.5158E-01
t* max=+1.0472E+00

INSTRUMENTED IMPACT TEST

I51(I5G)

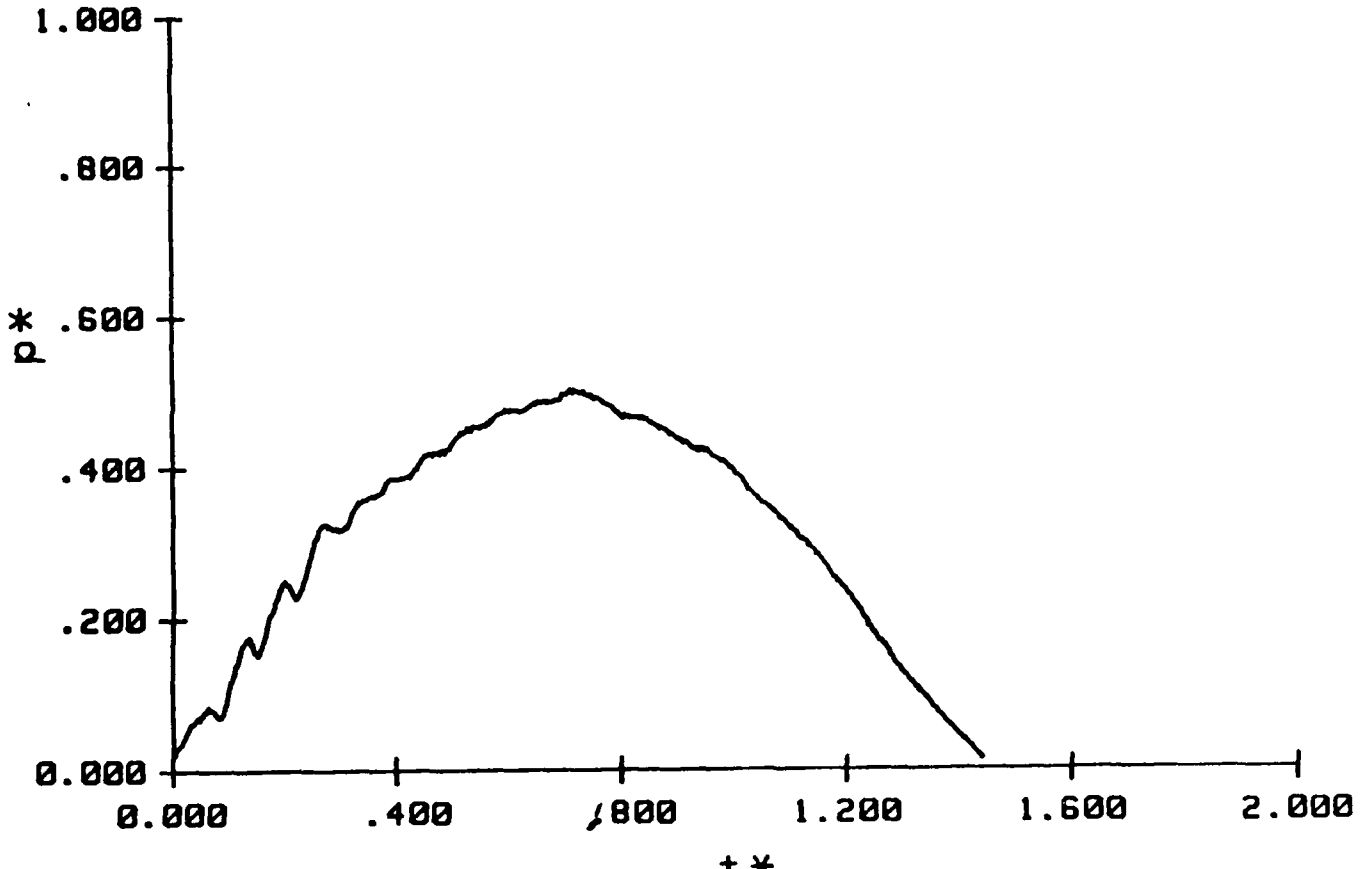

V0= 3.25 Ft/s (990.6 mm/s)

Z= .023 Ft (7.0 mm)

p* max=+5.8346E-01

M= 8.41 Lbm (3.816E-3 Mg)

b= .131 Ft (40.0 mm)

e* max=+8.6589E-01

L= .443 Ft (135.0 mm)

Q=14700E+5 Lb/Ft^2 (7.038E+4 MPa)

t* max=+1.4416E+00

INSTRUMENTED IMPACT TEST

I51(I5G)

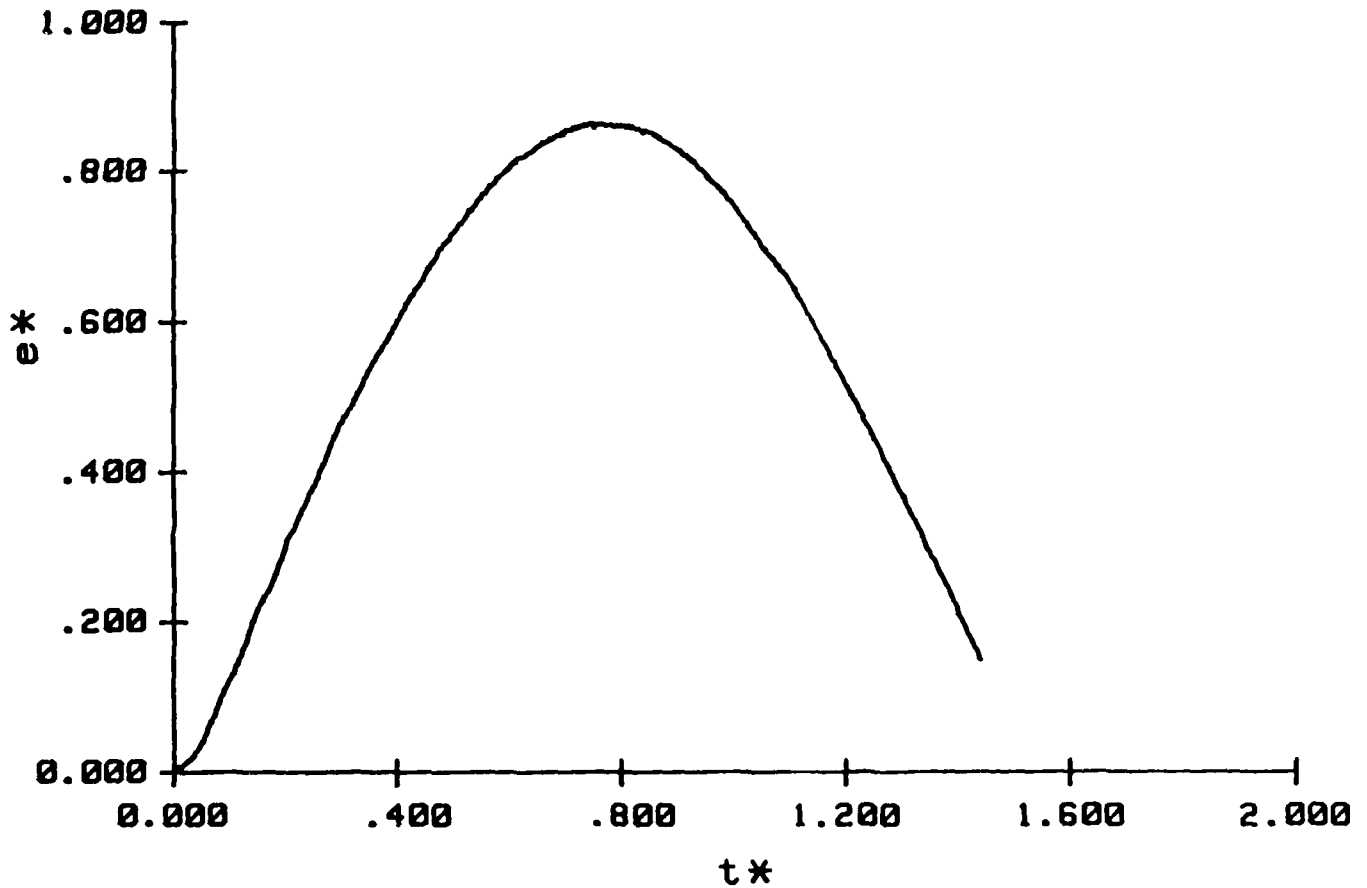

V0= 3.25 Ft/s (990.6 mm/s)
M= 8.41 Lbm (3.816E-3 Mg)
L= .443 Ft (135.0 mm)
Z= .323 Ft (7.8 mm)
b= .131 Ft (40.0 mm)
Q=14700E+5 Lb/Ft^2 (7.038E+4 MPa)
p* max=+5.8346E-01
e* max=+8.6589E-01
t* max=+1.4416E+00

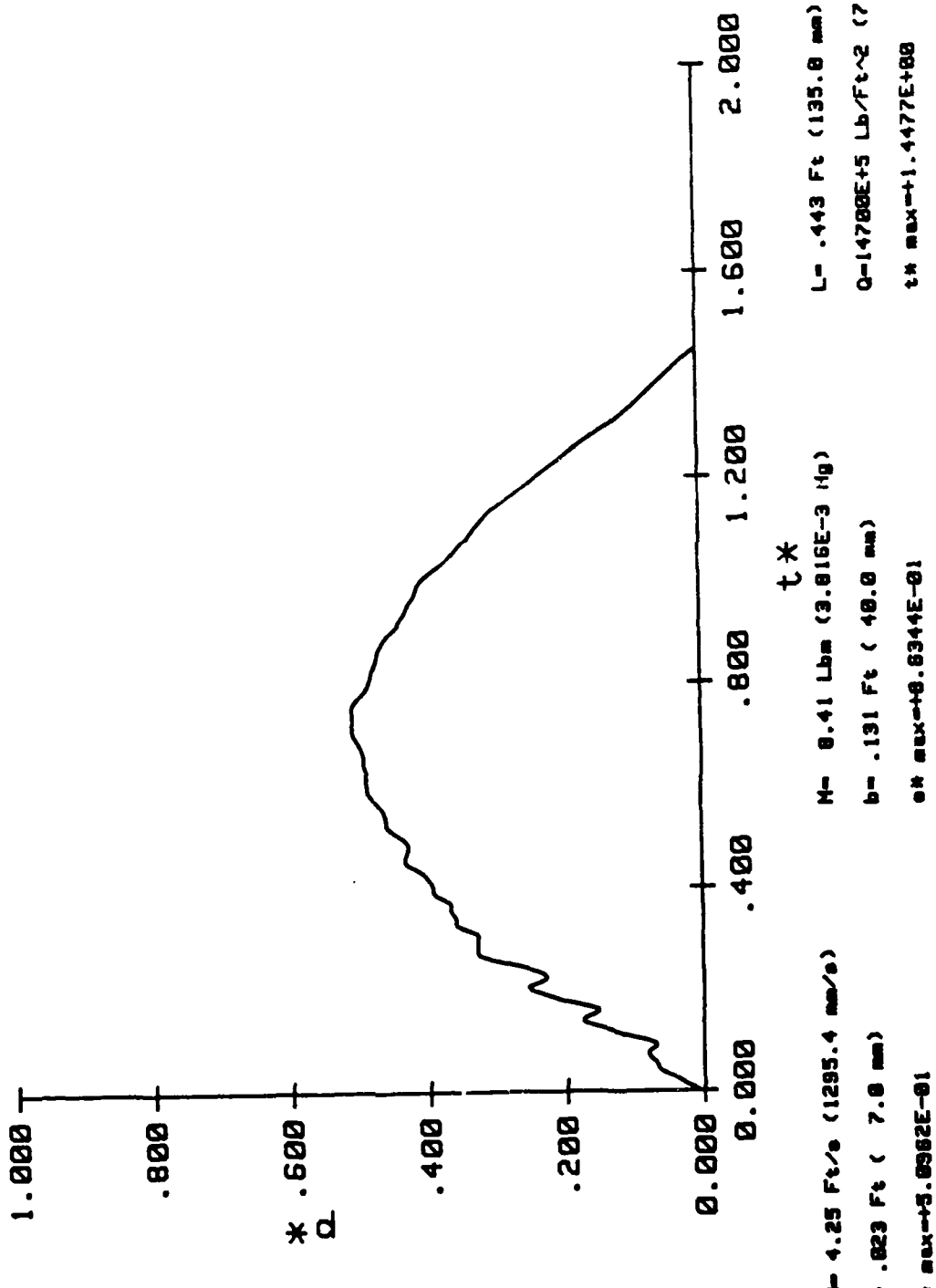
INSTRUMENTED IMPACT TEST
I54(I5G)
1.000
.800
.600
.400
.200
0.000
*d
0.000
.400
.800
1.200
1.600
2.000
t*
L= .443 Ft (135.0 mm)
Q=14700E+5 Lb/Ft^2 (7.038E+4 MPa)
t* max=+1.4477E+00
M= 8.41 Lbm (3.816E-3 Hg)
b= .131 Ft (40.0 mm)
d* max=+8.8344E-01
V0= 4.25 Ft/s (1295.4 mm/s)
Z= .023 Ft (7.0 mm)
p* max=+5.8962E-01

INSTRUMENTED IMPACT TEST

I54(I5G)

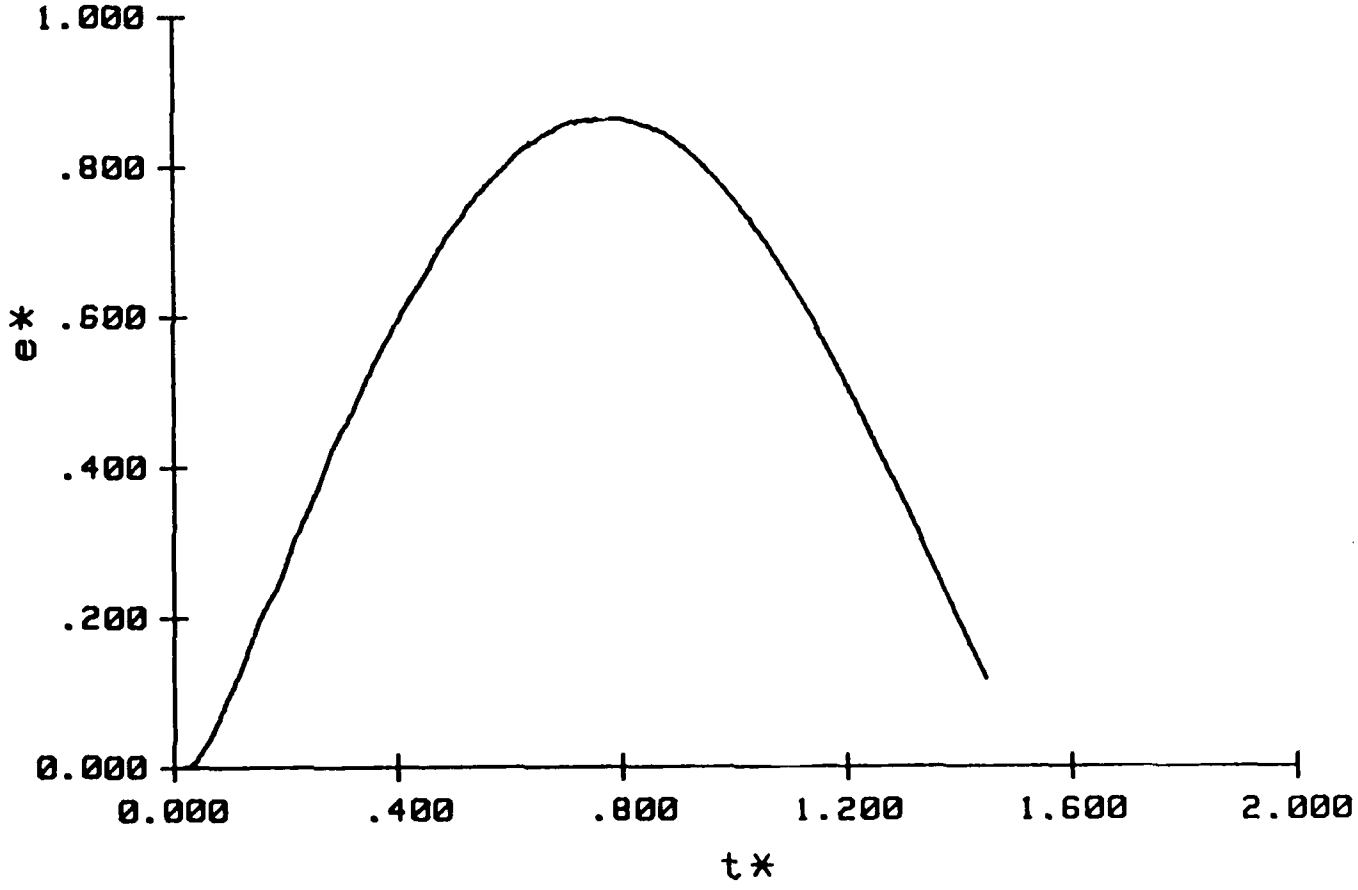

V0= 4.25 Ft/s (1295.4 mm/s)
M= 0.41 Lbm (3.816E-3 Mg)
L= .443 Ft (135.0 mm)

Z= .023 Ft (7.0 mm)
b= .131 Ft (40.0 mm)
Q=14700E+5 Lb/Ft^2 (7.038E+4 MPa)

p* max=+5.0982E-01
e* max=+0.6344E-01
t* max=+1.4477E+00

INSTRUMENTED IMPACT TEST

I61(I6C)

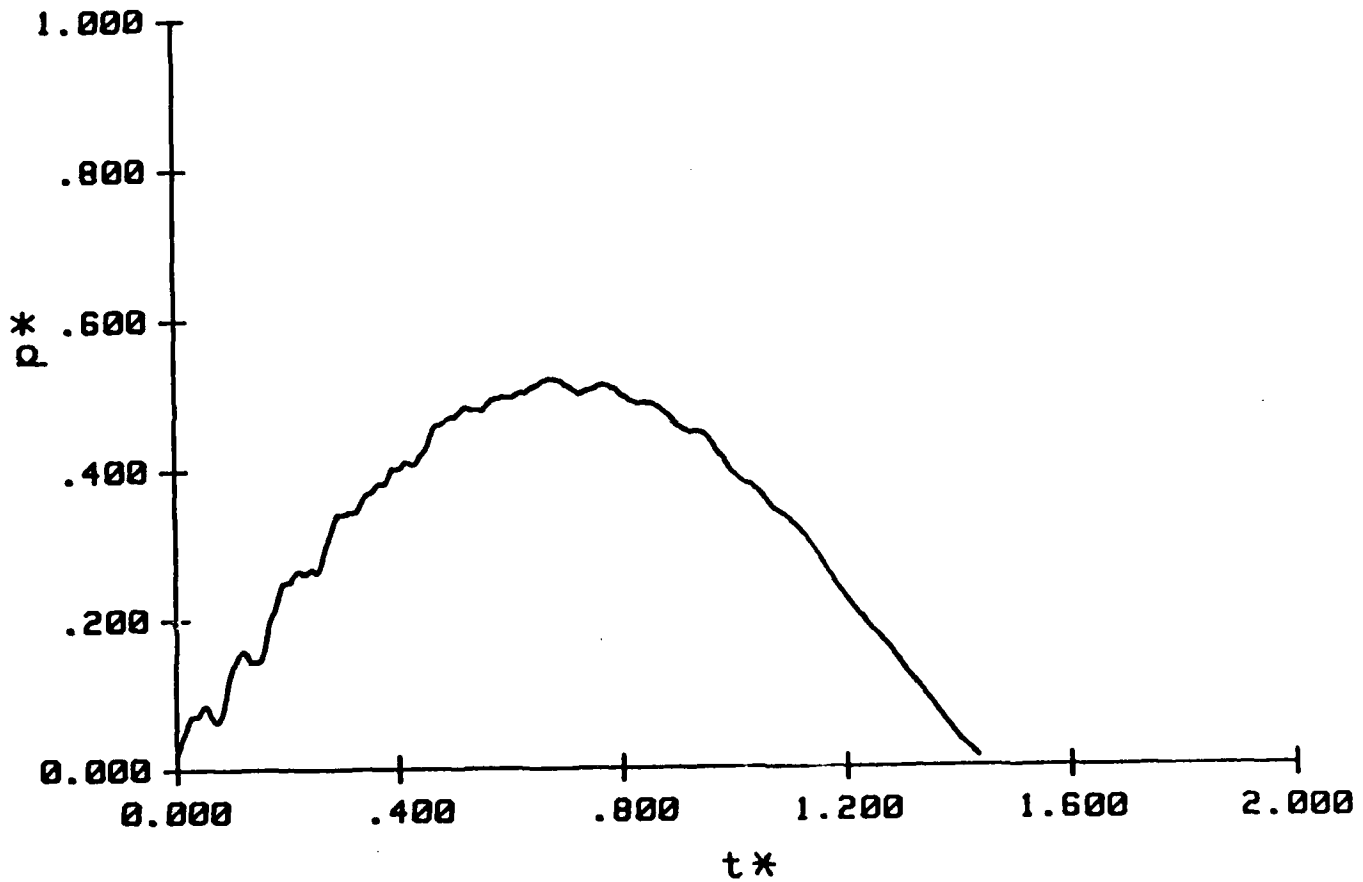

VB= 2.24 Ft/s (682.8 mm/s)

Z= .023 Ft (7.0 mm)

p* max=+8.2138E-01

M= 8.41 Lbm (3.816E-3 Mg)

b= .131 Ft (40.0 mm)

e* max=+8.7984E-01

L= .443 Ft (135.0 mm)

Q=71400E+4 Lb/Ft^2 (3.419E+4 MPa)

t* max=+1.4346E+00

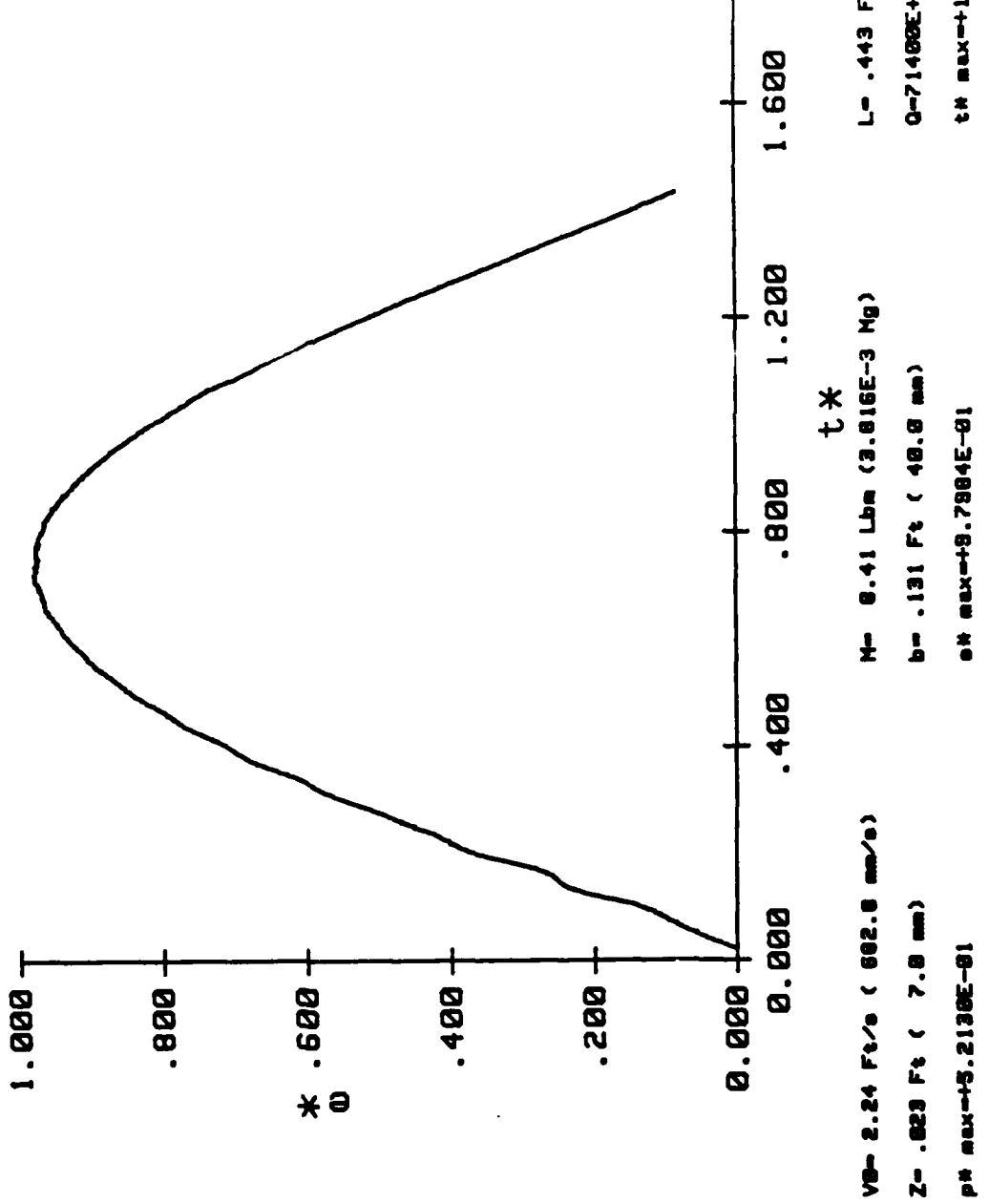
INSTRUMENTED IMPACT TEST
I61(I6C)
1.000
.800
.600
.400
.200
0.000
*0
0.000
.400
.800
1.200
1.600
2.000
t*
V0= 2.24 Ft/s (682.8 mm/s)
M= 0.41 Lbm (3.816E-3 Mg)
L= .443 Ft (135.0 mm)
Z= .023 Ft (7.0 mm)
b= .131 Ft (40.0 mm)
Q=71400E+4 Lb/Ft^2 (3.419E+4 MPa)
p* max=+5.2130E-01
e* max=+8.7804E-01
t* max=+1.4346E+00

INSTRUMENTED IMPACT TEST

I64(I6C)

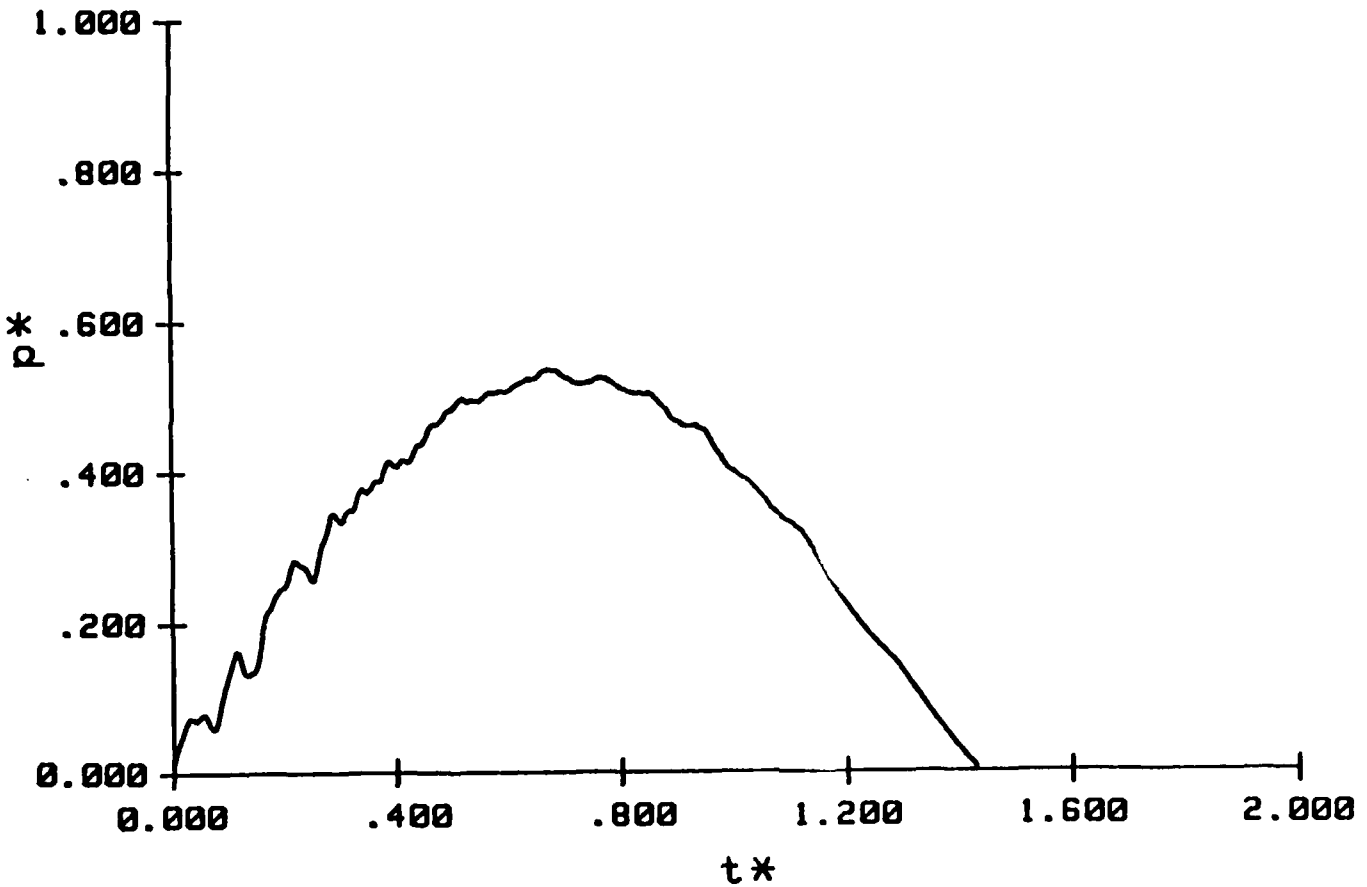

VB= 2.73 Ft/s (832.1 mm/s)

Z= .023 Ft (7.0 mm)

p* max=+5.3600E-01

M= 8.41 Lbm (3.816E-3 Mg)

b= .131 Ft (40.0 mm)

s* max=+8.9300E-01

L= .449 Ft (135.0 mm)

Q=71400E+4 Lb/Ft^2 (3.419E+4 MPa)

t* max=+1.4290E+00

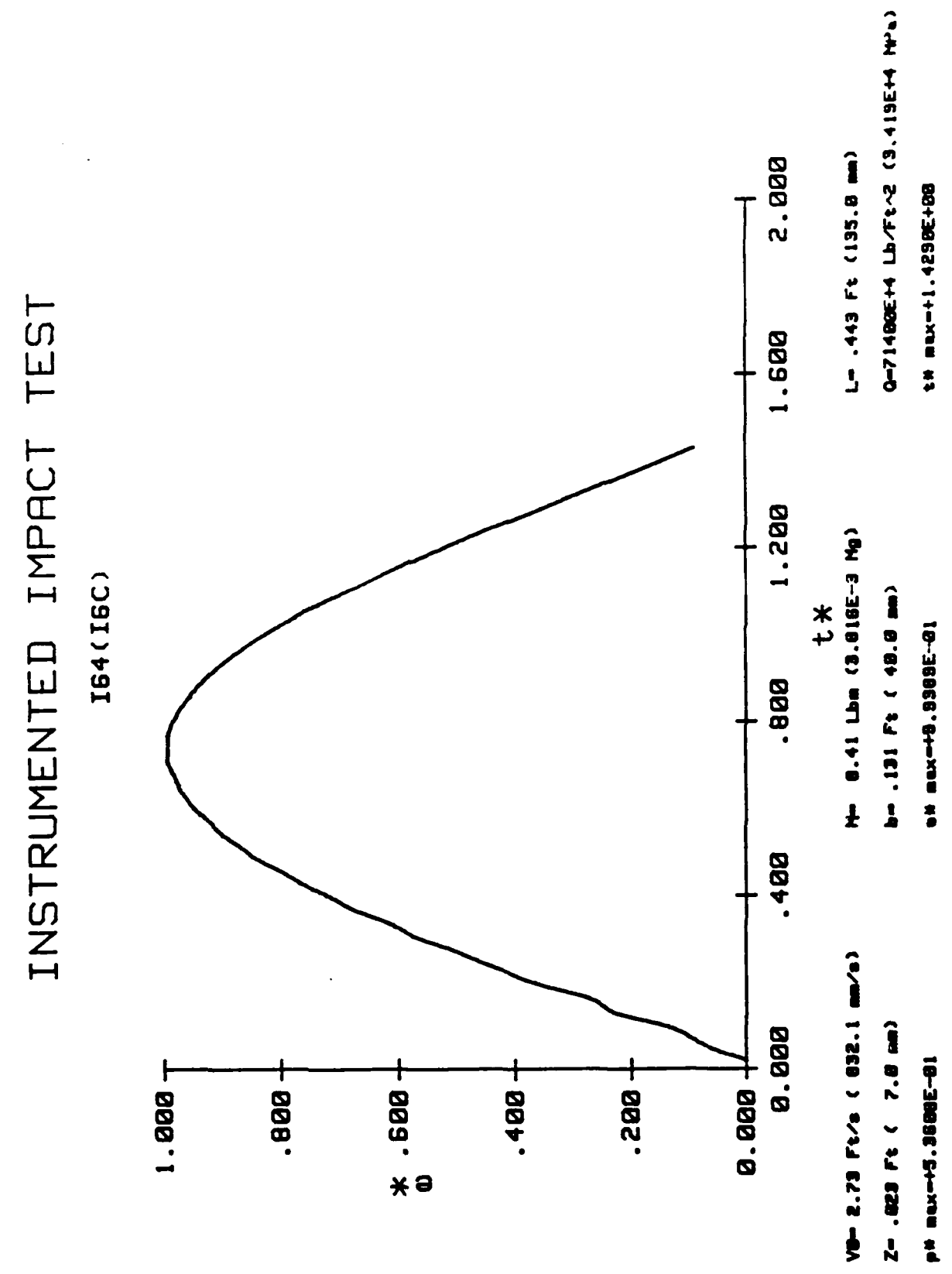
INSTRUMENTED IMPACT TEST
I64(I6C)
1.000
.800
.600
.400
.200
0.000
*
0
0.000
.400
.800
1.200
1.600
2.000
t*
V0= 2.73 Ft/s (832.1 mm/s)
M= 0.41 Lbm (3.816E-3 Mg)
L= .443 Ft (135.8 mm)
Z= .023 Ft (7.0 mm)
b= .131 Ft (40.0 mm)
Q=71480E+4 Lb/Ft^2 (3.419E+4 MPa)
p* max=+5.3688E-01
s* max=+8.8989E-01
t* max=+1.4298E+00

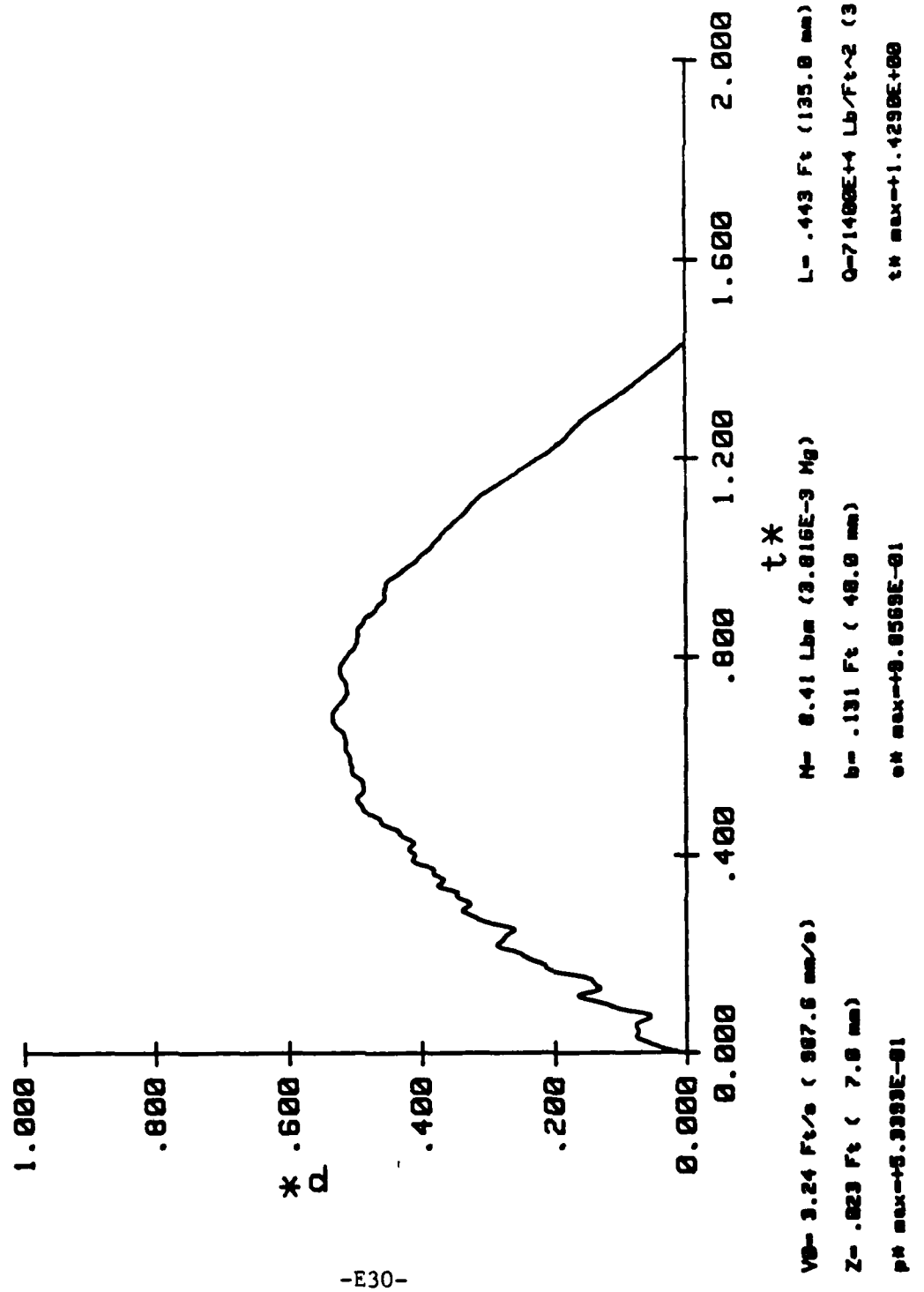
INSTRUMENTED IMPACT TEST
I65(I6C)
1.000
.800
.600
.400
.200
0.000
*a
0.000
.400
.800
1.200
1.600
2.000
t*
L= .443 Ft (135.0 mm)
Q=71400E+4 Lb/Ft^2 (3.419E+4 MPa)
t* max=+1.429E+00
M= 8.41 Lbm (3.816E-3 Mg)
b= .131 Ft (40.0 mm)
a* max=+8.856E-01
V0= 3.24 Ft/s (987.6 mm/s)
Z= .023 Ft (7.0 mm)
p* max=+5.333E-01

INSTRUMENTED IMPACT TEST

I65(I6C)

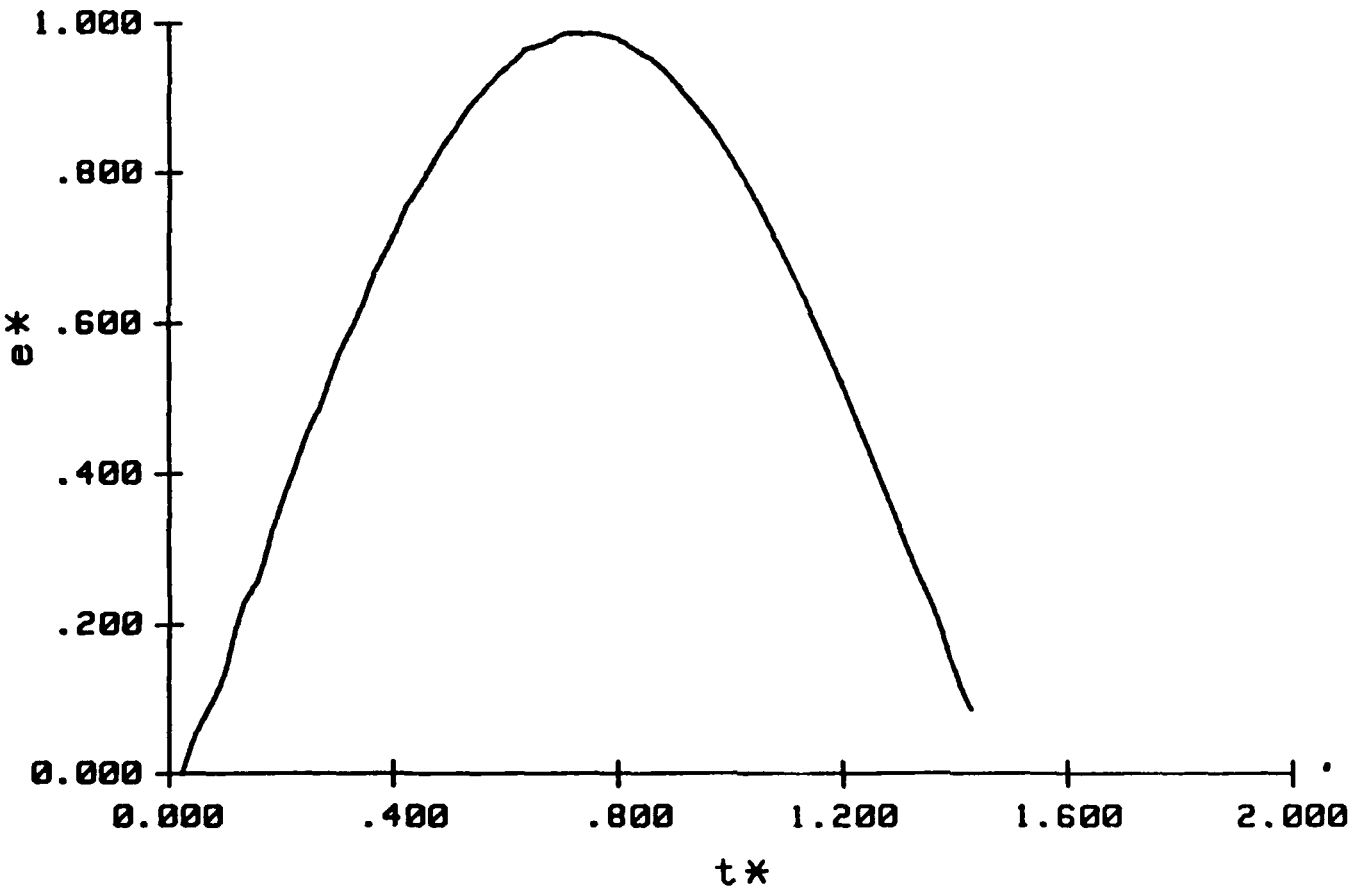

V0= 3.24 Ft/s (987.6 mm/s)
M= 8.41 Lbm (3.816E-3 Mg)
L= .443 Ft (135.0 mm)
Z= .023 Ft (7.0 mm)
b= .131 Ft (40.0 mm)
Q=71400E+4 Lb/Ft^2 (3.419E+4 MPa)
p* max=+5.3393E-01
e* max=+9.6569E-01
t* max=+1.4290E+00

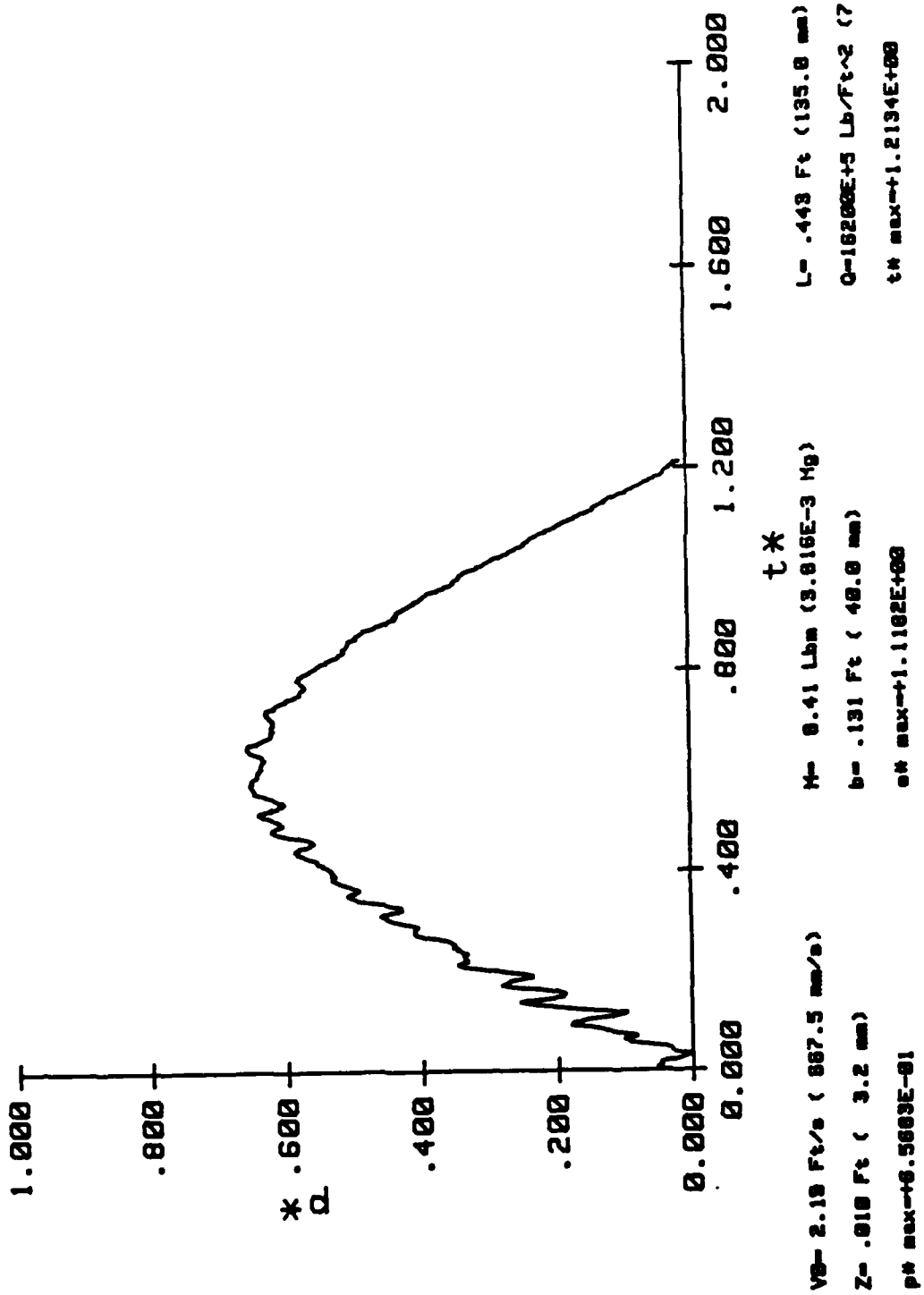
INSTRUMENTED IMPACT TEST
I32(IIA)
1.000
.800
.600
.400
.200
0.000
*D
0.000
.400
.800
1.200
1.600
2.000
t*
VB= 2.19 Ft/s (667.5 mm/s)
Z= .818 Ft (3.2 mm)
p* max=+8.5603E-01
M= 8.41 Lbm (3.816E-3 Mg)
b= .131 Ft (40.0 mm)
σ* max=+1.1182E+00
L= .443 Ft (135.0 mm)
Q=16200E+3 Lb/Ft^2 (7.757E+4 MPa)
t* max=+1.2134E+00

INSTRUMENTED IMPACT TEST

I32(I1A)

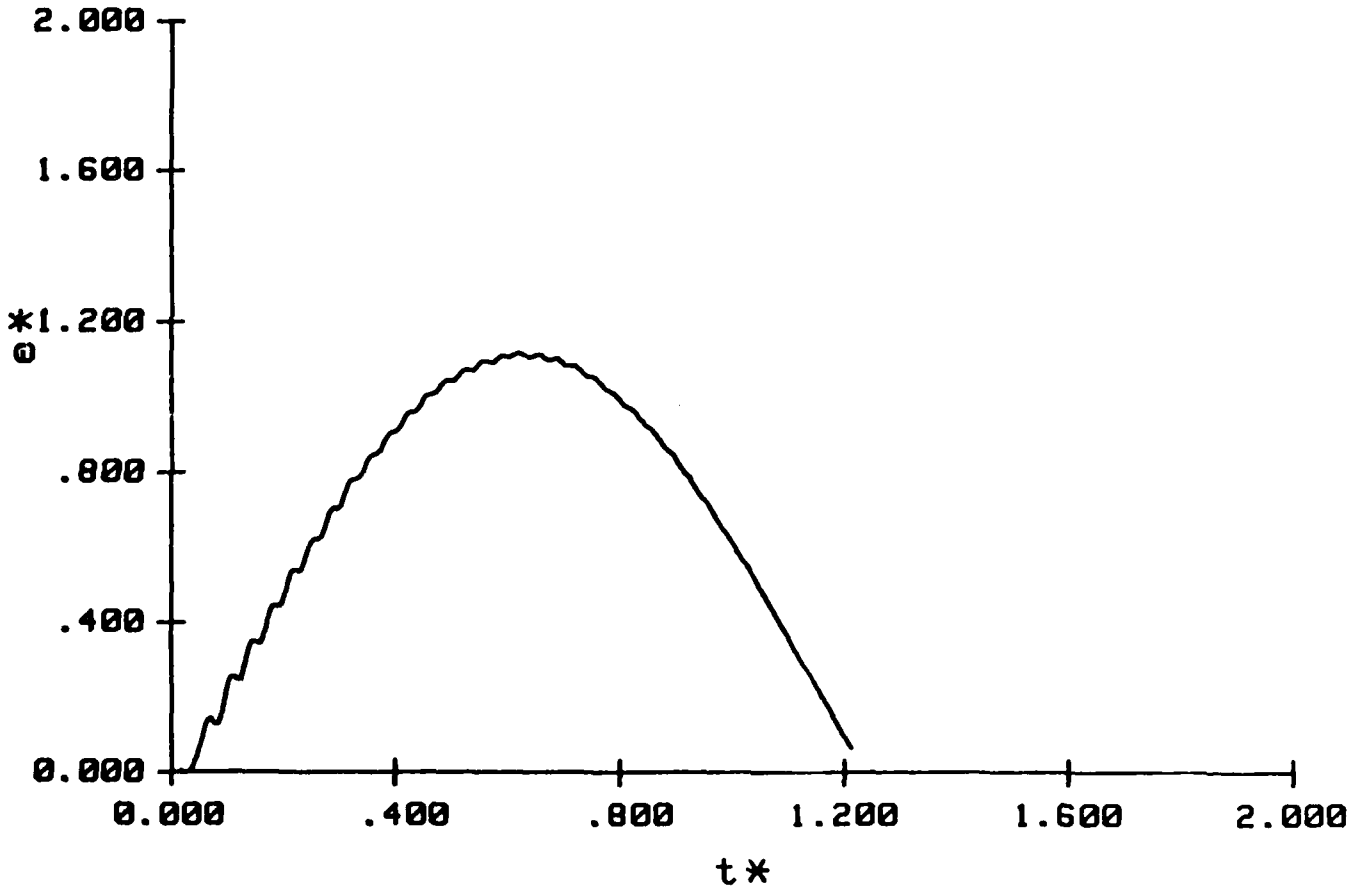

V0= 2.19 Ft/s (667.5 mm/s)
M= 0.41 Lbm (3.816E-3 Mg)
L= .443 Ft (135.0 mm)
Z= .010 Ft (3.2 mm)
b= .131 Ft (40.0 mm)
Q=16200E+5 Lb/Ft^2 (7.757E+4 MPa)
p* max=+6.5603E-01
e* max=+1.1102E+00
t* max=+1.2134E+00

INSTRUMENTED IMPACT TEST

I33(I1A)

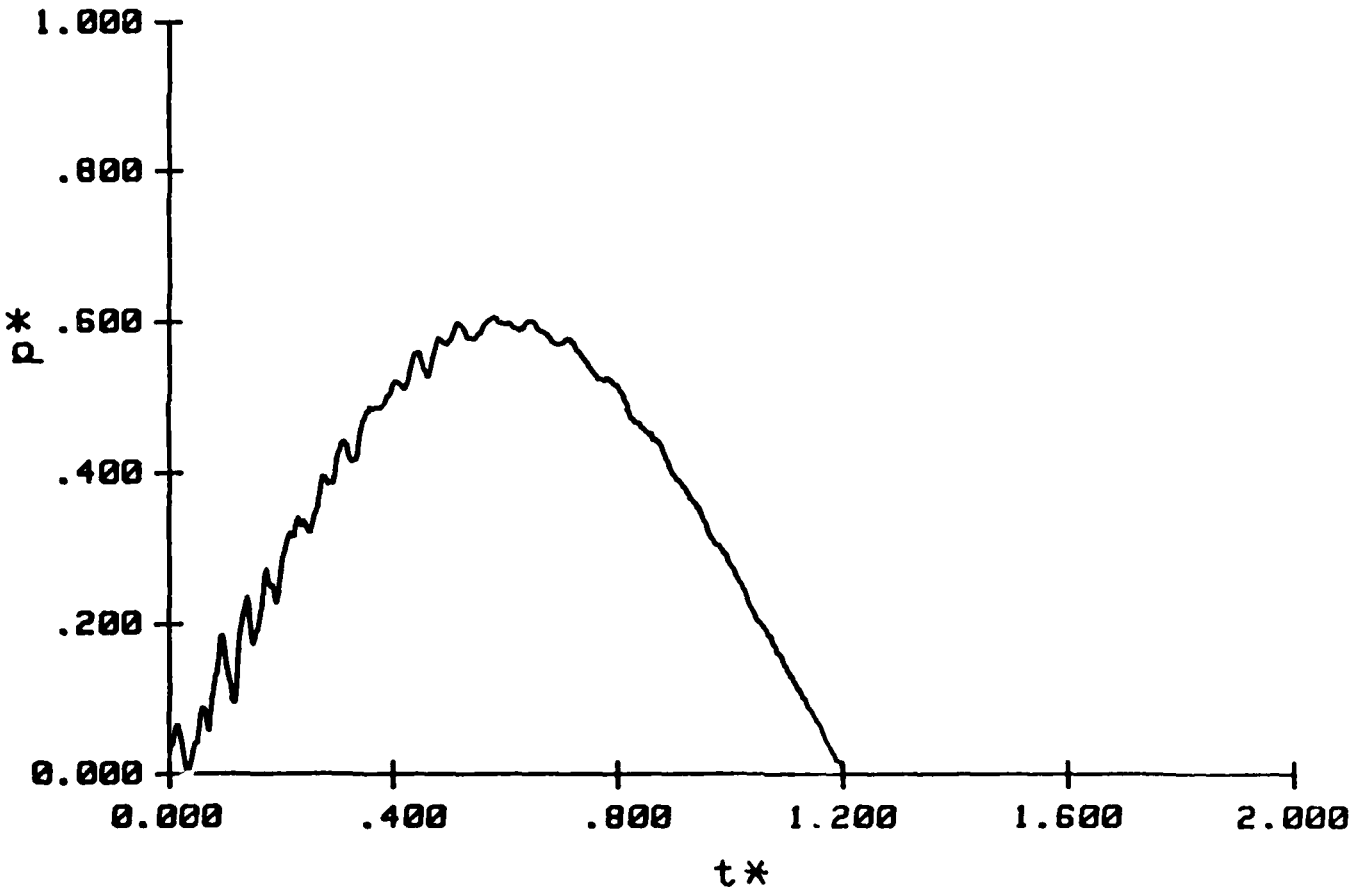

VB= 2.92 Ft/s (890.8 mm/s)
M= 8.41 Lbm (3.816E-3 Mg)
L= .443 Ft (135.0 mm)
Z= .818 Ft (3.2 mm)
b= .131 Ft (40.0 mm)
Q=16200E+5 Lb/Ft^2 (7.757E+4 MPa)
p* max=+6.8718E-01
e* max=+1.0223E+00
t* max=+1.2003E+00

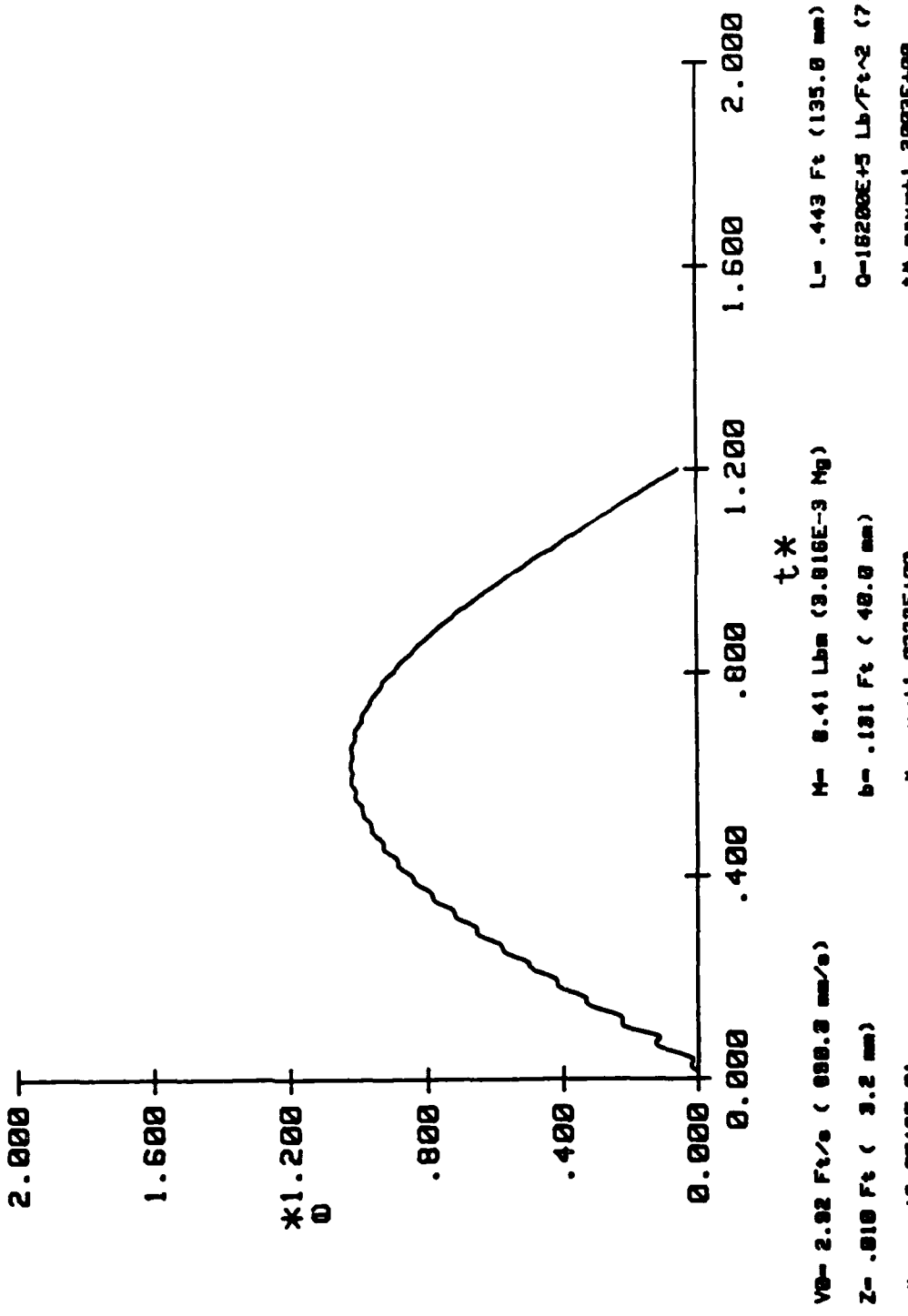
INSTRUMENTED IMPACT TEST
I33(IIA)
2.000
1.600
1.200
.800
.400
0.000
*1.200
Ø
.400
.800
1.200
1.600
2.000
t*
L= .443 Ft (135.0 mm)
Q=18200E+5 Lb/Ft^2 (7.757E+4 MPa)
tM max=+1.2003E+00
M= 8.41 Lbm (3.816E-3 Kg)
b= .181 Ft (48.0 mm)
øM max=+1.8223E+00
V0= 2.92 Ft/s (888.8 mm/s)
Z= .818 Ft (3.2 mm)
pM max=+6.8718E-01

INSTRUMENTED IMPACT TEST

I36(I1A)

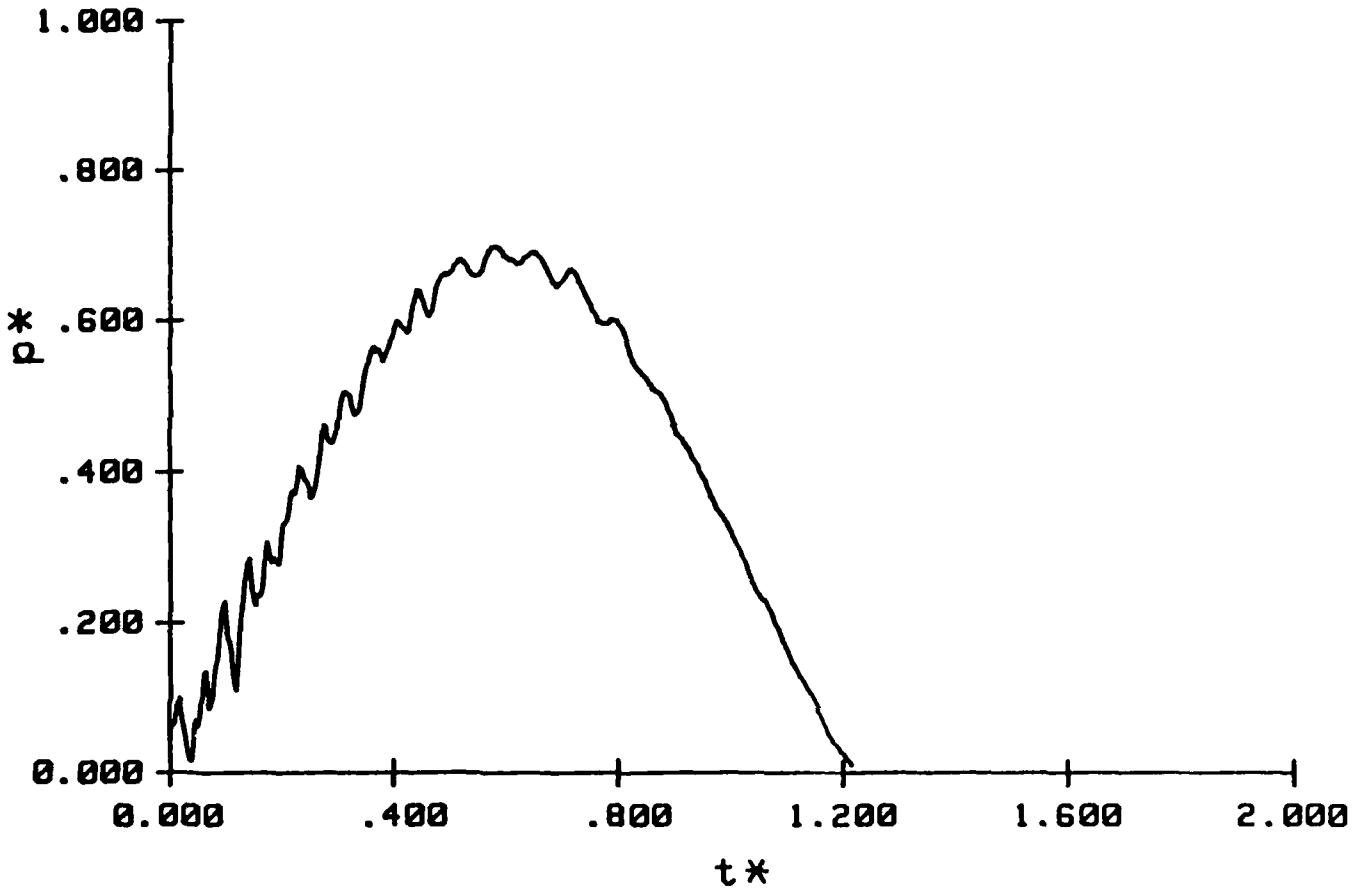

V0= 9.14 Ft/s (957.1 mm/s)
M= 6.41 Lbm (3.816E-3 Mg)
L= .443 Ft (135.0 mm)
Z= .010 Ft (3.2 mm)
b= .131 Ft (40.0 mm)
Q=16200E+5 Lb/Ft^2 (7.757E+4 MPa)
p* max=+6.9814E-01
e* max=+1.1400E+00
t* max=+1.2161E+00

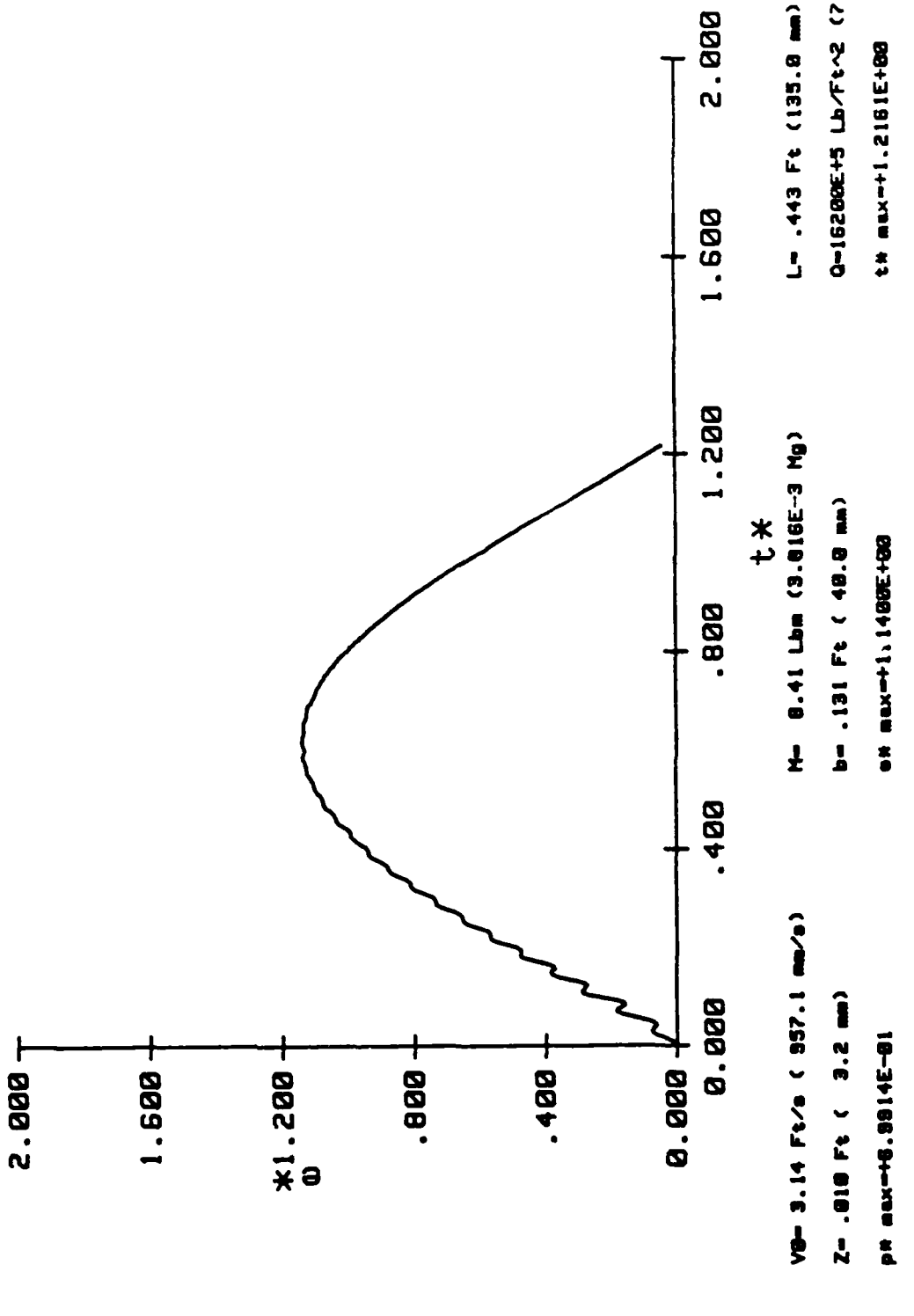
INSTRUMENTED IMPACT TEST
I36(I1A)
2.000
1.600
1.200
.800
.400
0.000
*1.200
Ø
0.000
.400
.800
1.200
1.600
2.000
t*
V0= 3.14 Ft/s (957.1 mm/s)
M= 8.41 Lbm (3.816E-3 Mg)
L= .443 Ft (135.8 mm)
Z= .010 Ft (3.2 mm)
b= .131 Ft (40.0 mm)
Q=16200E+5 Lb/Ft^2 (7.757E+4 MPa)
p* max=+8.9814E-01
e* max=+1.1408E+00
t* max=+1.2161E+00

INSTRUMENTED IMPACT TEST

I41(I2A)

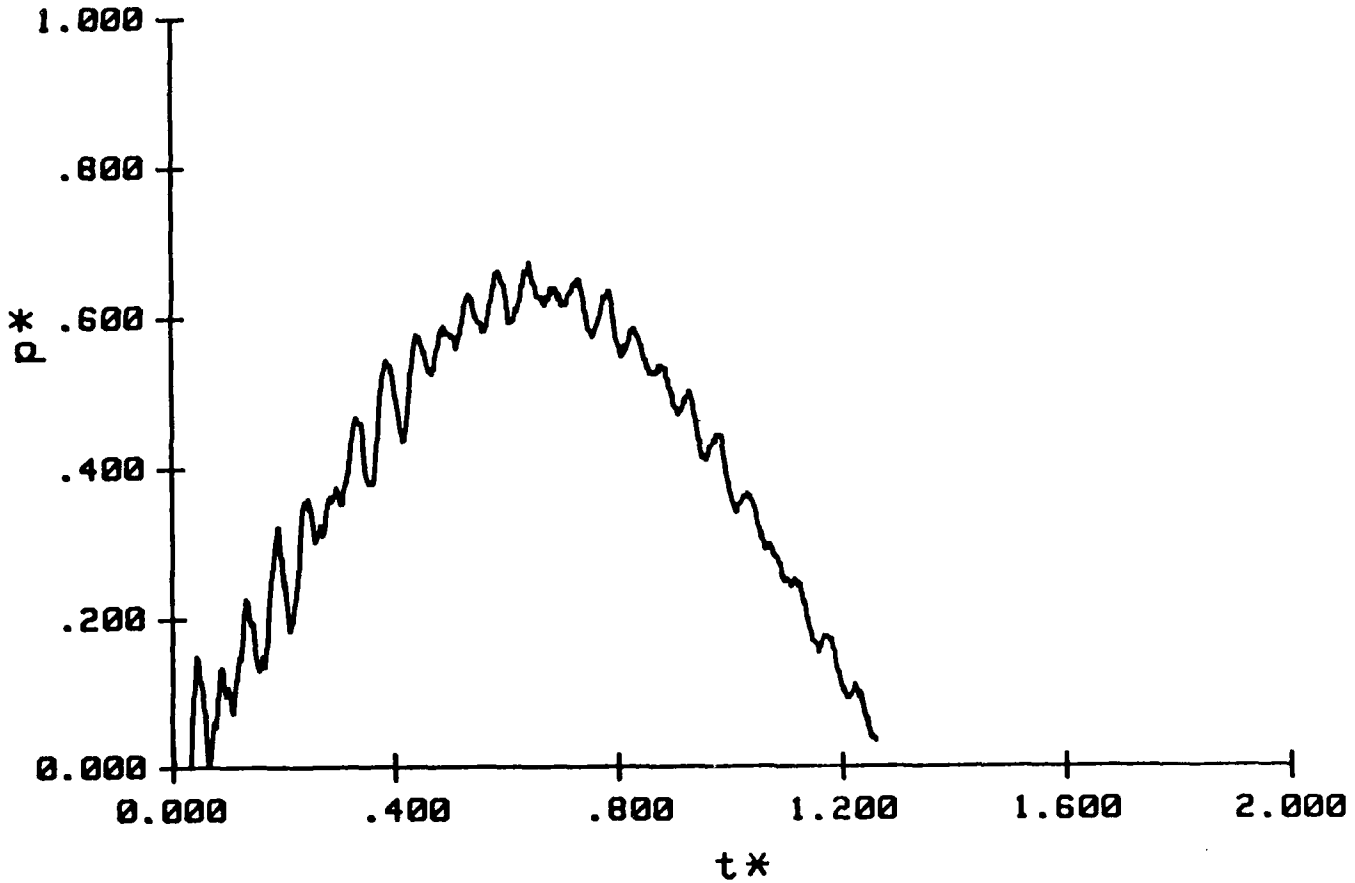

V0= 1.57 Ft/s (478.5 mm/s)
M= 8.41 Lbm (3.816E-3 Mg)
L= .443 Ft (135.0 mm)
Z= .018 Ft (3.2 mm)
b= .131 Ft (40.0 mm)
Q=78500E+4 Lb/Ft^2 (3.759E+4 MPa)
p* max=+6.7348E-01
e* max=+1.3937E+00
t* max=+1.2607E+00

NADC-87106-60

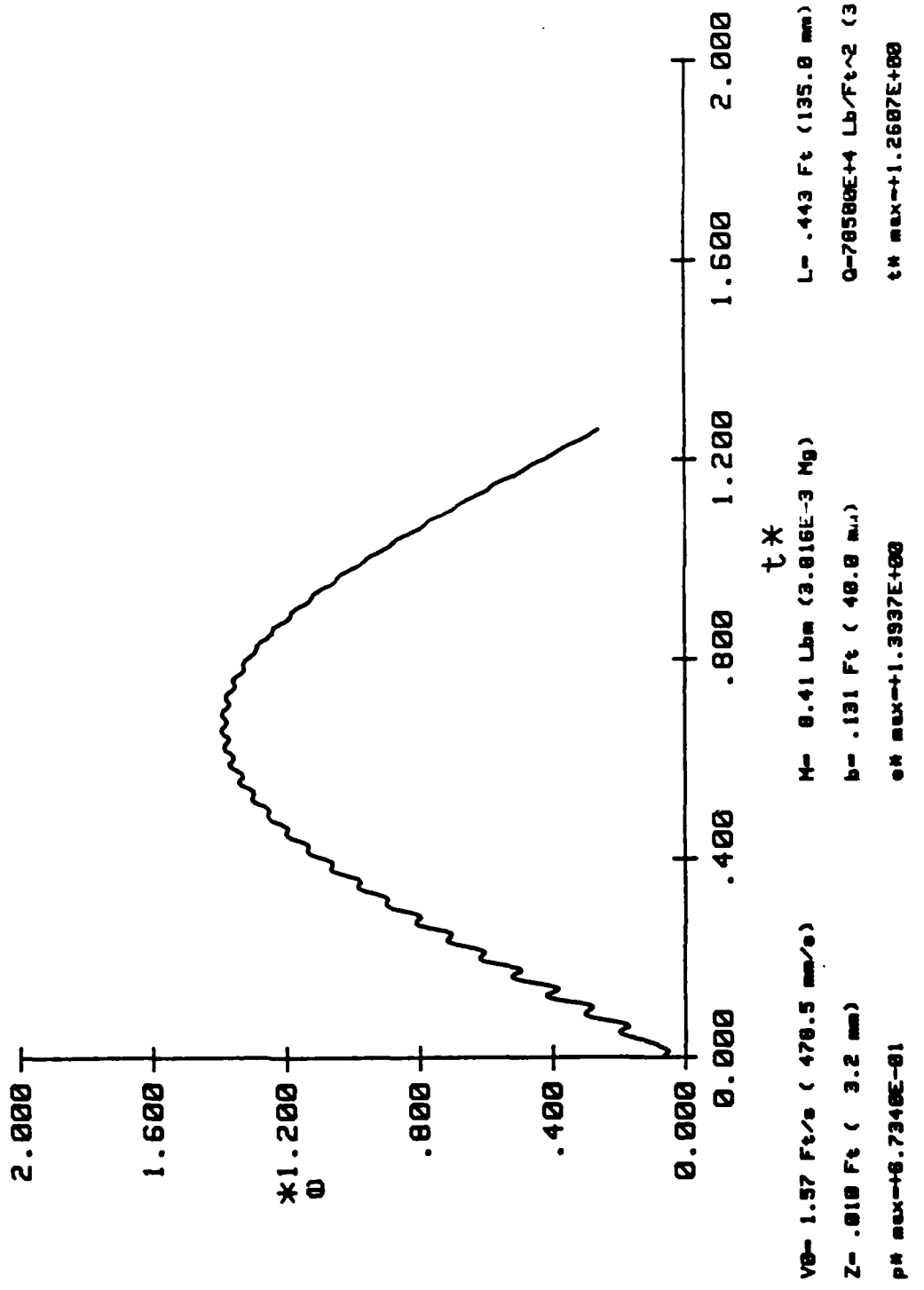
INSTRUMENTED IMPACT TEST
I41(I2A)
2.000
1.600
1.200
.800
.400
0.000
*1.200
Ø
0.000
.400
.800
1.200
1.600
2.000
t*
V0= 1.57 Ft/s (478.5 mm/s)
M= 8.41 Lbm (3.816E-3 Mg)
L= .443 Ft (135.0 mm)
Z= .010 Ft (3.2 mm)
b= .131 Ft (40.0 mm)
Q=78500E+4 Lb/Ft^2 (3.759E+4 MPa)
p* max=+8.7340E-01
σ* max=+1.3937E+00
t* max=+1.2607E+00

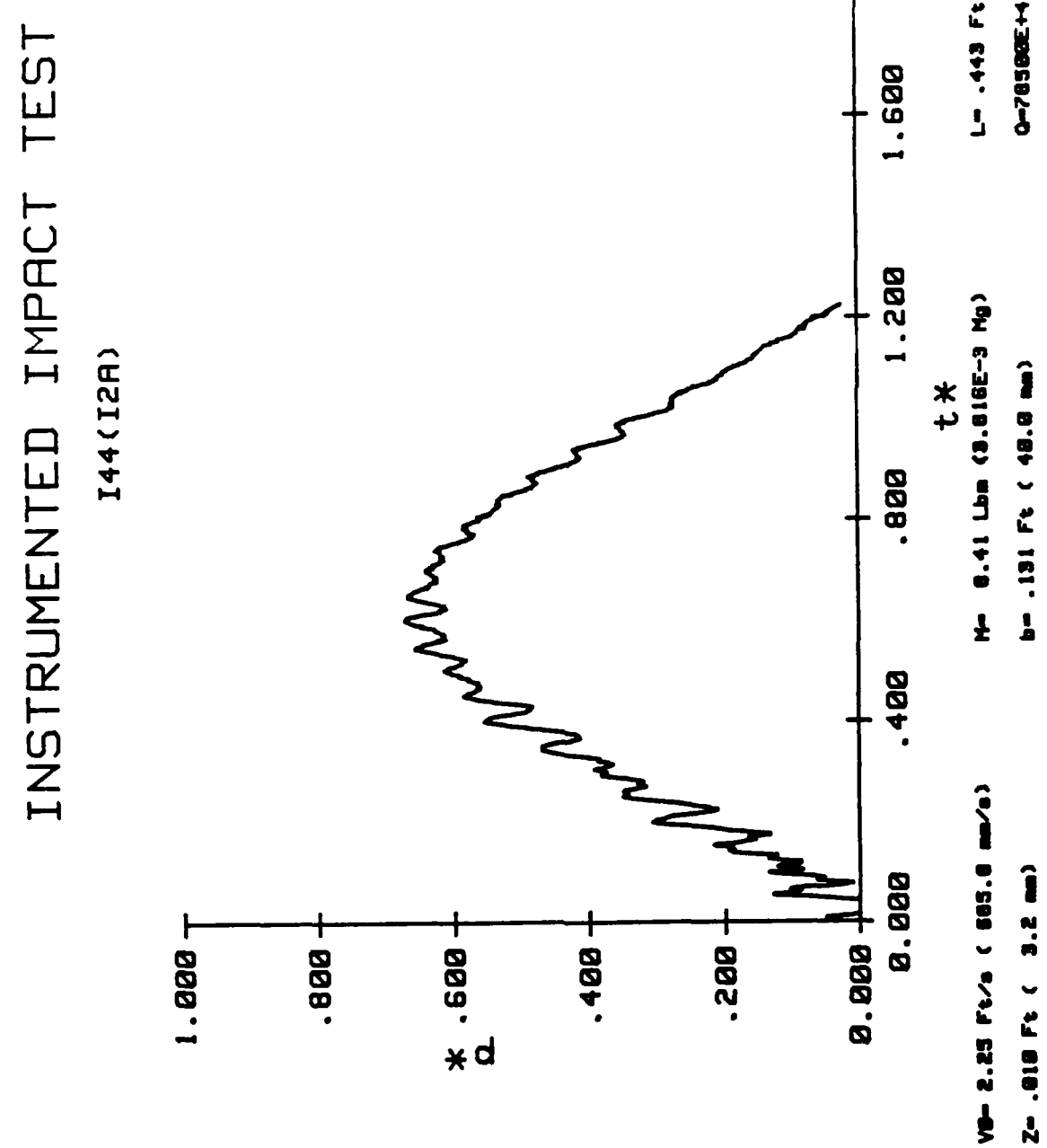
INSTRUMENTED IMPACT TEST
I44(I2A)
1.000
.800
.600
.400
.200
0.000
* a
0.000
.400
.800
1.200
1.600
2.000
t*
Vo= 2.25 Ft/s (685.8 mm/s)
M= 8.41 Lbm (3.816E-3 Mg)
L= .443 Ft (135.8 mm)
Z= .010 Ft (3.2 mm)
b= .131 Ft (40.0 mm)
Q=7850E+4 Lb/Ft^2 (3.759E+4 MPa)
a* max=+6.7276E-01
a* max=+1.2184E+00
t* max=+1.2242E+00

INSTRUMENTED IMPACT TEST

I44(I2A)

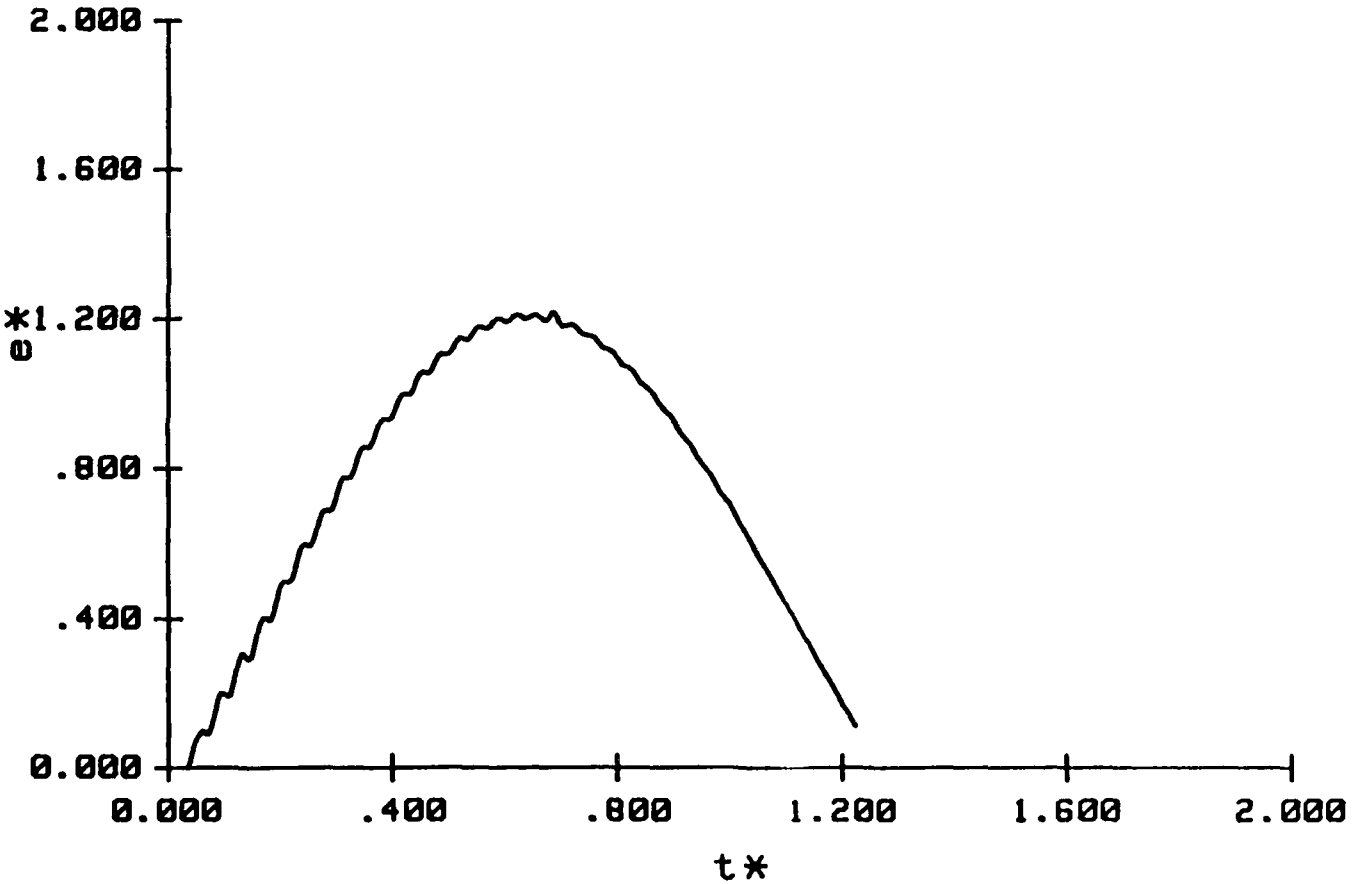

V0= 2.25 Ft/s (685.8 mm/s)
M= 8.41 Lbm (3.816E-3 Mg)
L= .443 Ft (135.0 mm)
Z= .010 Ft (3.2 mm)
b= .131 Ft (40.0 mm)
Q=78500E+4 Lb/Ft^2 (3.759E+4 MPa)
p* max=+6.7278E-01
e* max=+1.2164E+00
t* max=+1.2242E+00

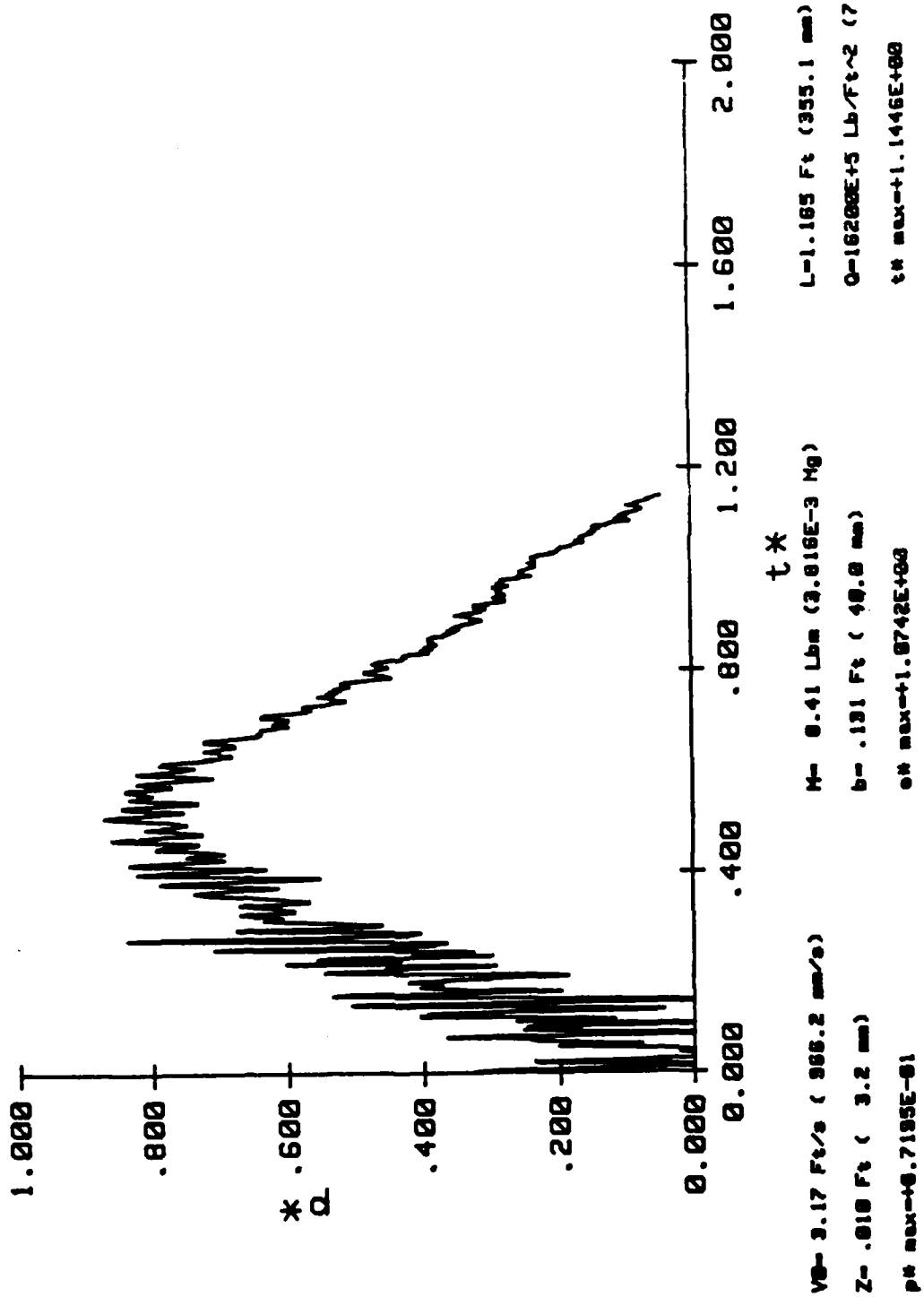
INSTRUMENTED IMPACT TEST
I11(I1C)
1.000
.800
.600
.400
.200
0.000
*d
0.000
.400
.800
1.200
1.600
2.000
t*
L=1.185 Ft (355.1 mm)
Q=16206E+3 Lb/Ft^2 (7.757E+4 MPa)
t* max=+1.1446E+00
M= 8.41 Lbm (3.816E-3 Mg)
b= .131 Ft (40.0 mm)
d* max=+1.8742E+00
Vo= 3.17 Ft/s (966.2 mm/s)
Z= .810 Ft (3.2 mm)
p* max=+8.7195E-01

INSTRUMENTED IMPACT TEST

I11(I1C)

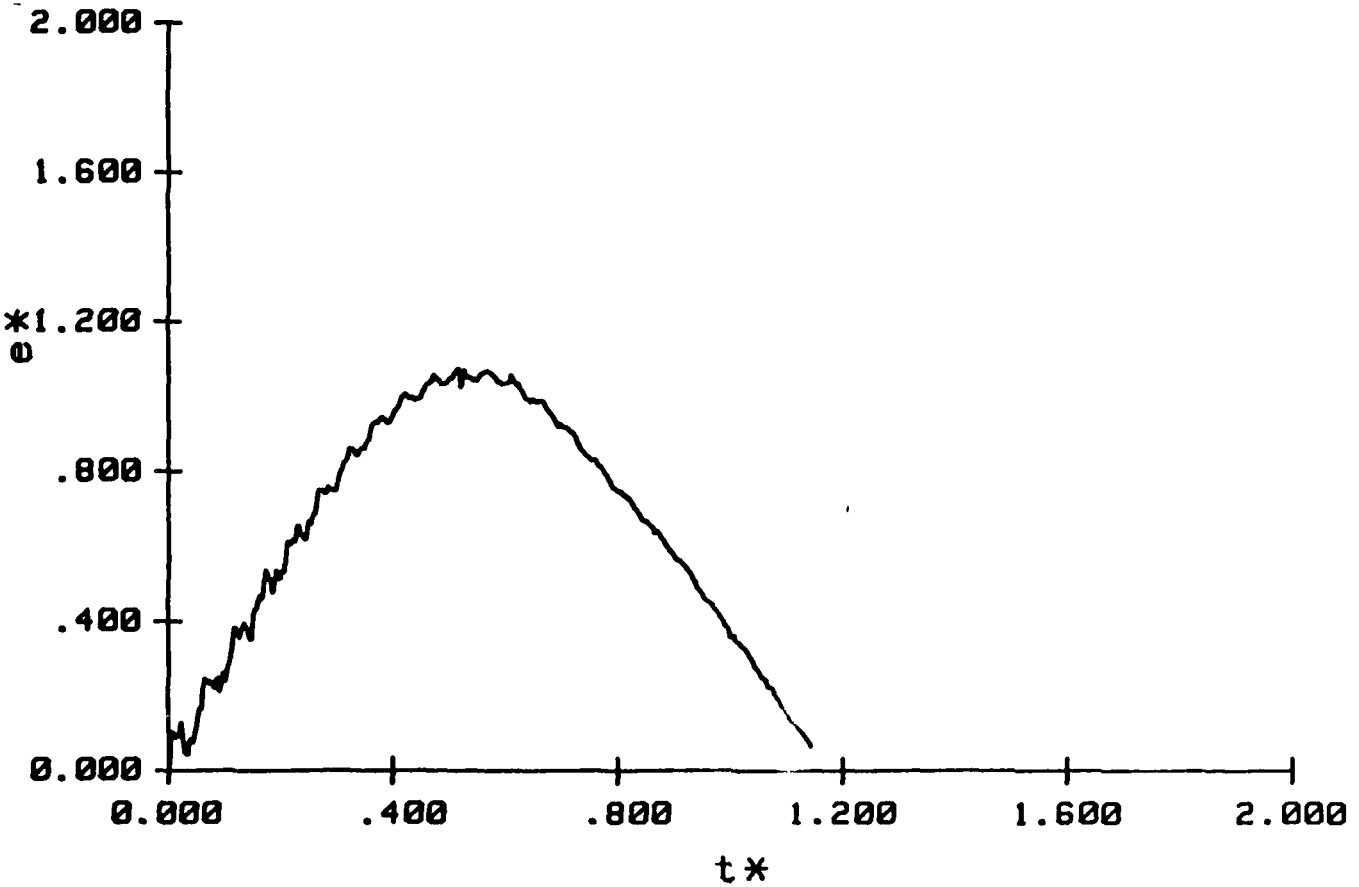

V0= 3.17 Ft/s (966.2 mm/s)
M= 8.41 Lbm (3.816E-3 Mg)
L=1.165 Ft (355.1 mm)
Z= .818 Ft (3.2 mm)
b= .131 Ft (40.0 mm)
Q=16200E+5 Lb/Ft^2 (7.757E+4 MPa)
p* max=+8.7195E-01
e* max=+1.0742E+00
t* max=+1.1446E+00

NADC-87106-60

INSTRUMENTED IMPACT TEST

I14(I1C)

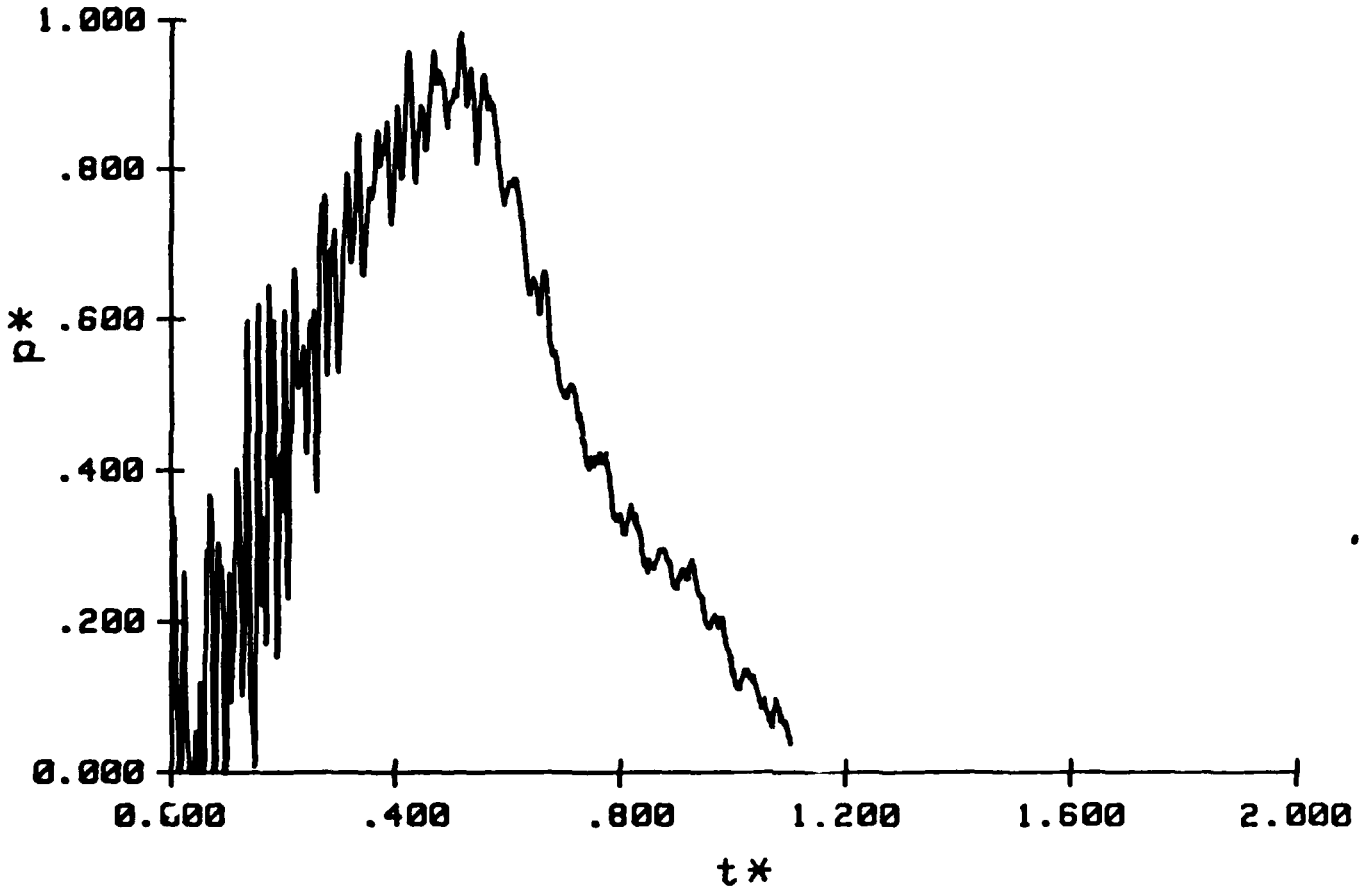

V0= 4.17 Ft/s (1271.8 mm/s)

M= 8.41 Lbm (3.816E-3 Mg)

L=1.185 Ft (355.1 mm)

Z= .818 Ft (3.2 mm)

b= .131 Ft (40.0 mm)

Q=16200E+5 Lb/Ft^2 (7.75/E+4 MPa)

p* max=+0.8350E-01

e* max=+1.0591E+00

t* max=+1.1031E+00

NADC-87106-60

INSTRUMENTED IMPACT TEST

I14(I1C)

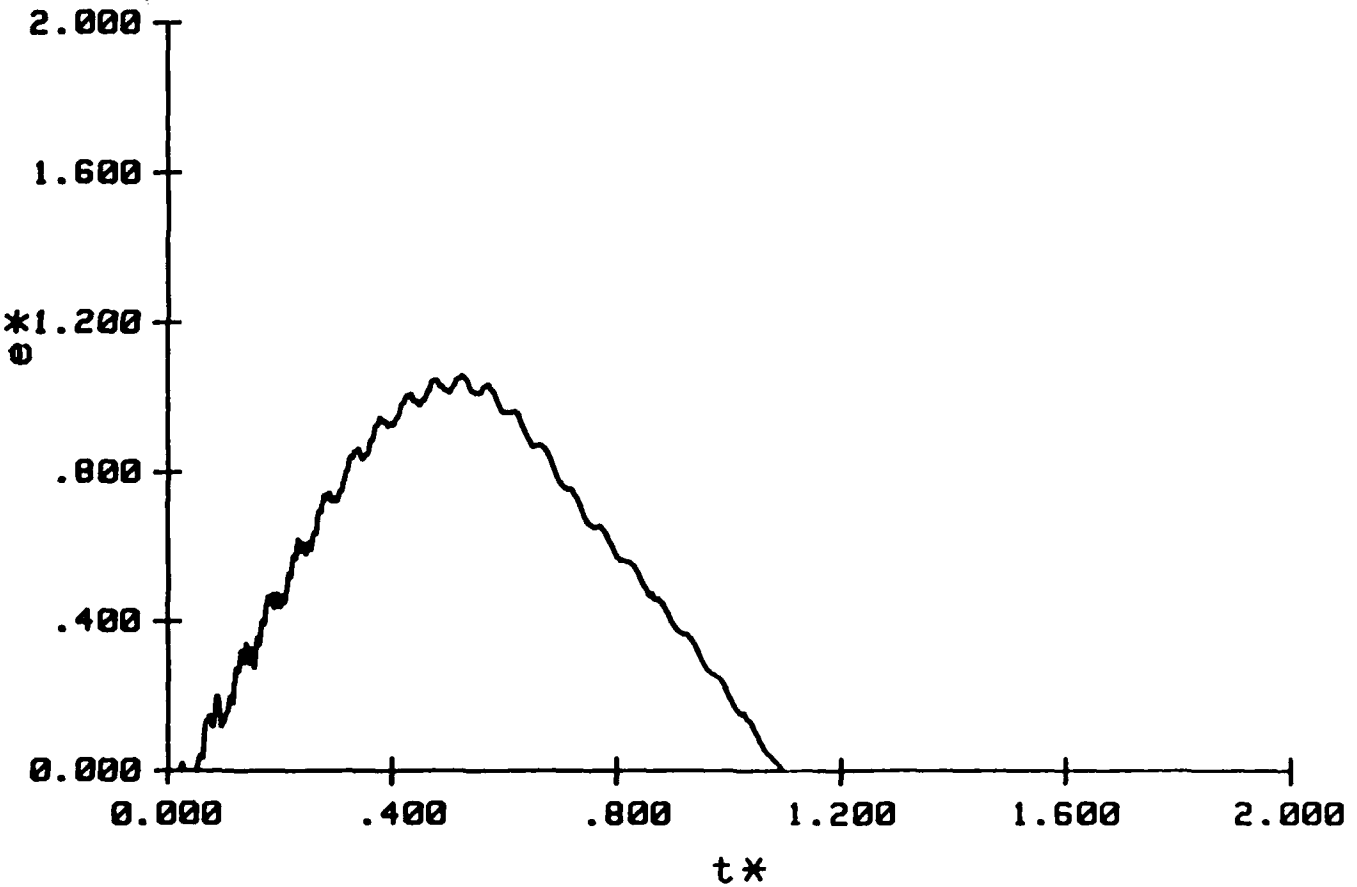

V0= 4.17 Ft/s (1271.8 mm/s)
M= 8.41 Lbm (3.818E-3 Mg)
L=1.165 Ft (355.1 mm)
Z= .818 Ft (3.2 mm)
b= .121 Ft (40.8 mm)
Q=16200E+3 Lb/Ft^2 (7.757E+4 MPa)
p* max=+8.8358E-01
e* max=+1.8591E+00
t* max=+1.1831E+00

NADC-87106-60

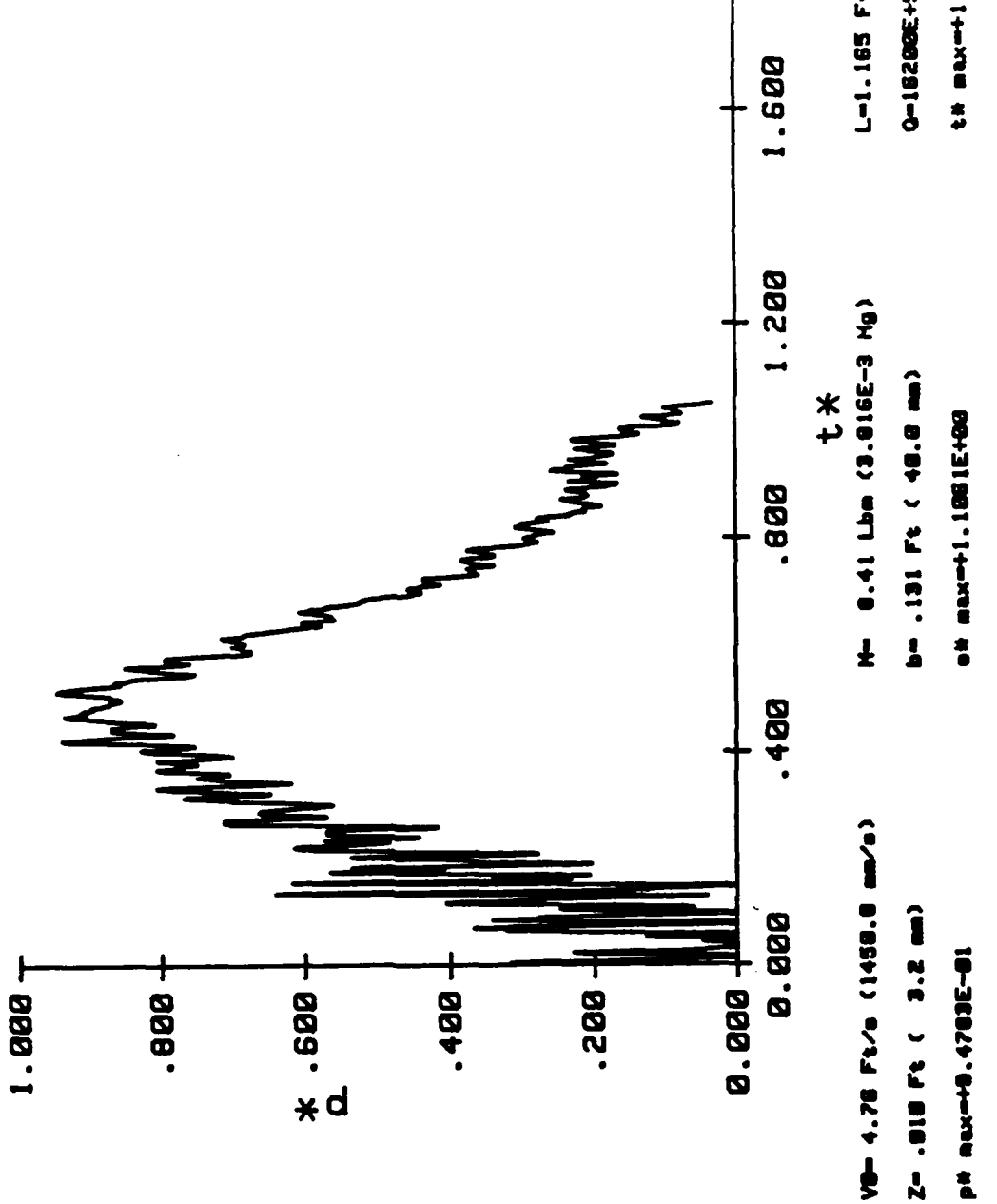
INSTRUMENTED IMPACT TEST
I18(I1C)
1.000
.800
.600
.400
.200
0.000
*d
0.000
.400
.800
1.200
1.600
2.000
t*
V0= 4.78 Ft/s (1458.0 mm/s)
Z= .010 Ft (3.2 mm)
M= 0.41 Lbm (3.016E-3 Hg)
b= .131 Ft (48.0 mm)
L=1.165 Ft (355.1 mm)
Q=18200E+5 Lb/Ft^2 (7.757E+4 MPa)
t* max=+1.0524E+00
d* max=+1.1061E+00
d* max=+0.4703E-01

INSTRUMENTED IMPACT TEST

I18(I1C)

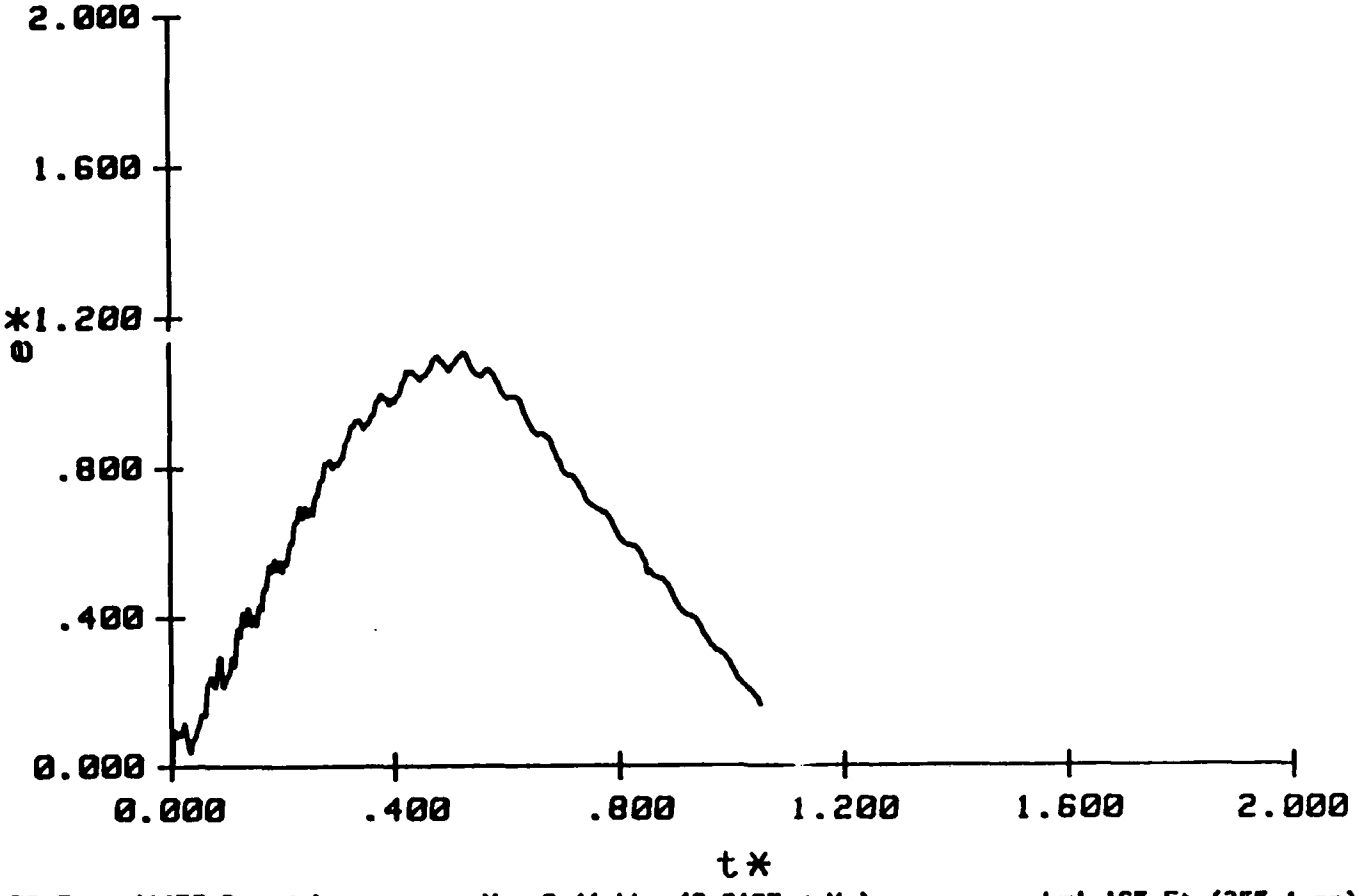

V0= 4.76 Ft/s (1450.8 mm/s)
M= 0.41 Lbm (3.816E-3 Mg)
L=1.165 Ft (355.1 mm)

Z= .810 Ft (8.2 mm)
b= .131 Ft (40.0 mm)
Q=16200E+5 Lb/Ft^2 (7.757E+4 MPa)

p* max=+8.4703E-01
e* max=+1.1061E+00
t* max=+1.0524E+00

INSTRUMENTED IMPACT TEST

I19(I1C)

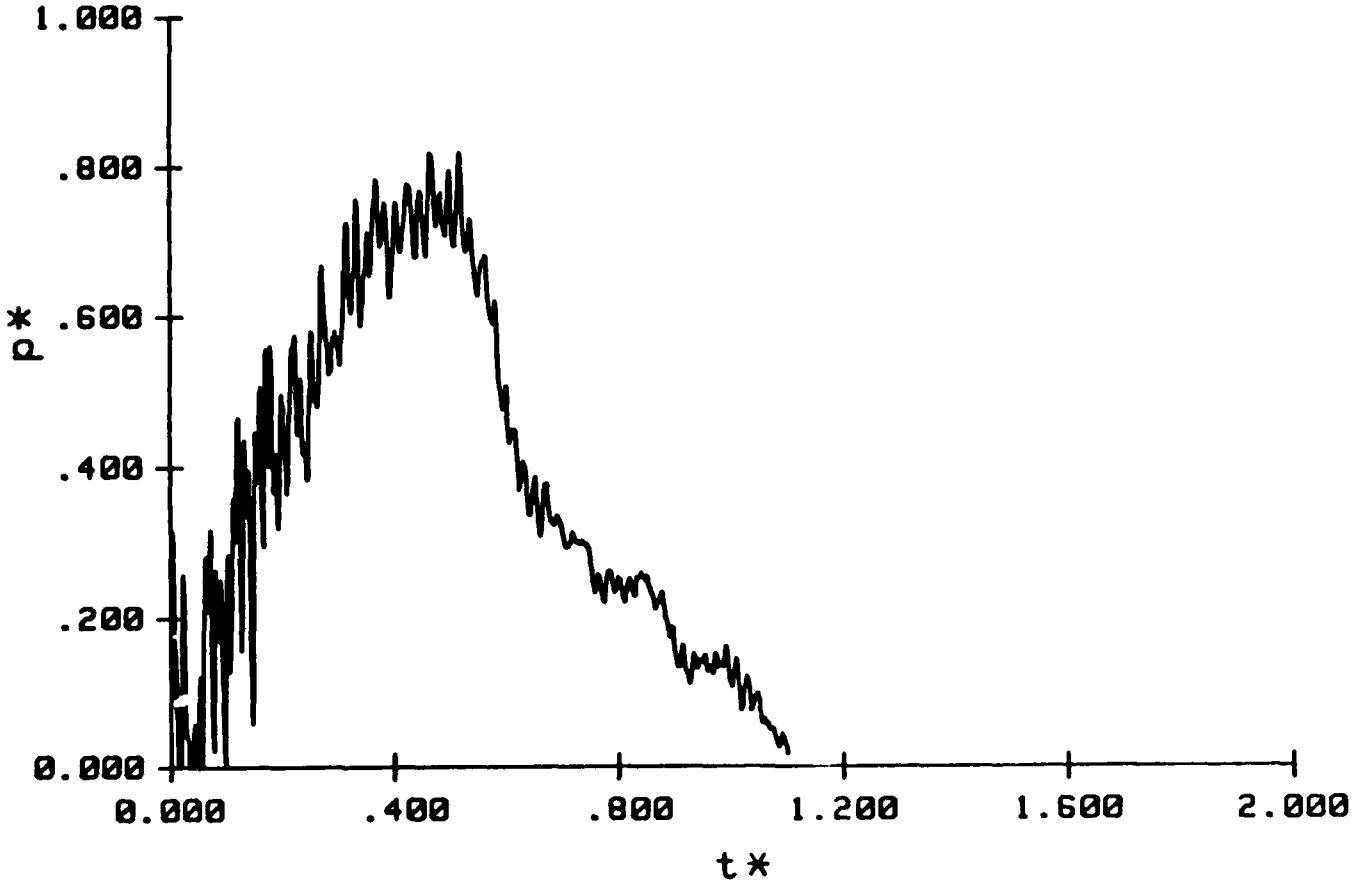

V0= 8.02 Ft/s (2444.5 mm/s)

M= 8.41 Lbm (3.816E-3 Mg)

L=1.165 Ft (355.1 mm)

Z= .818 Ft (3.2 mm)

b= .131 Ft (40.0 mm)

Q=16200E+5 Lb/Ft^2 (7.757E+4 MPa)

p* max=+8.1826E-01

e* max=+1.8132E+00

t* max=+1.1816E+00

NADC-87106-60

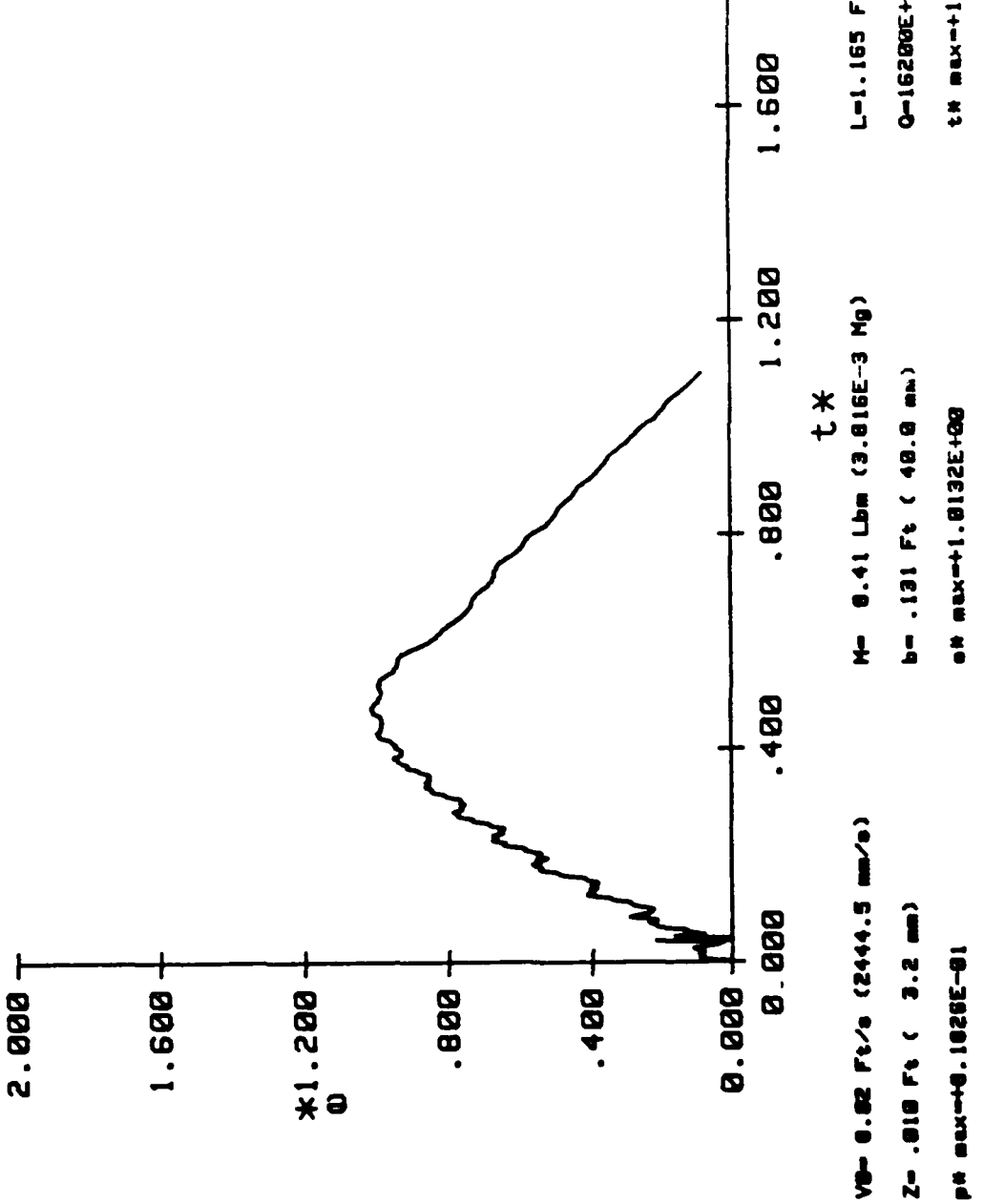
INSTRUMENTED IMPACT TEST
I19(I1C)
2.000
1.600
1.200
.800
.400
0.000
*1.200
ω
0.000
.400
.800
1.200
1.600
2.000
t*
L=1.165 Ft (355.1 mm)
Q=16200E+5 Lb/Ft^2 (7.757E+4 MPa)
t* max=+1.1016E+00
M= 0.41 Lbm (3.816E-3 Mg)
b= .131 Ft (40.0 mm)
ω* max=+1.8132E+00
V0= 8.02 Ft/s (2444.5 mm/s)
Z= .010 Ft (3.2 mm)
p* max=+0.1026E-01

INSTRUMENTED IMPACT TEST

I21(I2B)

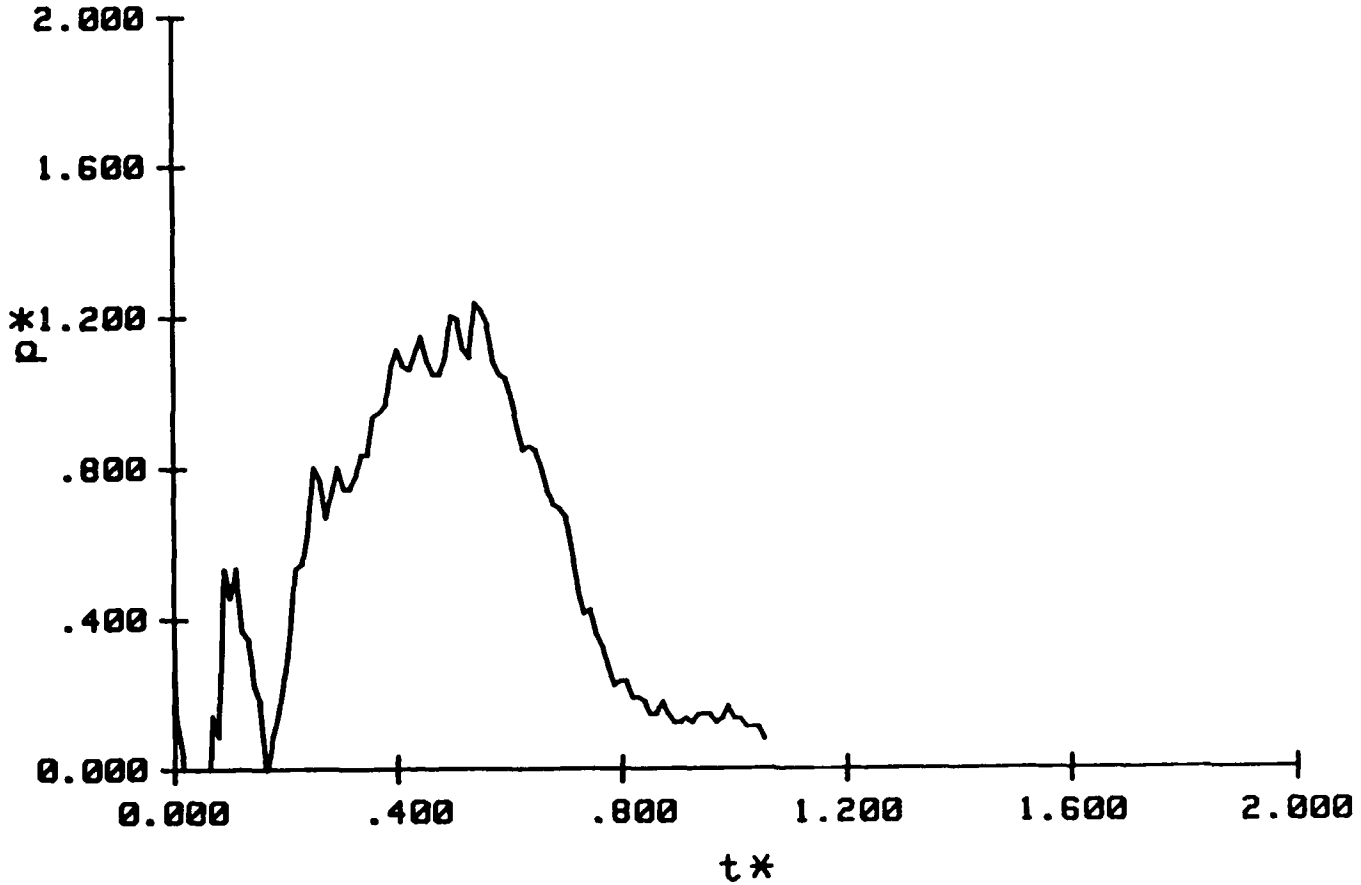

VB= 2.30 Ft/s (701.0 mm/s)
M= 0.41 Lbm (3.816E-3 Mg)
L=1.165 Ft (355.1 mm)

Z= .818 Ft (3.2 mm)
b= .131 Ft (48.0 mm)
Q=78500E+4 Lb/Ft^2 (3.759E+4 MPa)

p* max=+1.2363E+00
e* max=+1.4794E+00
t* max=+1.0588E+00

INSTRUMENTED IMPACT TEST

I21(I2B)

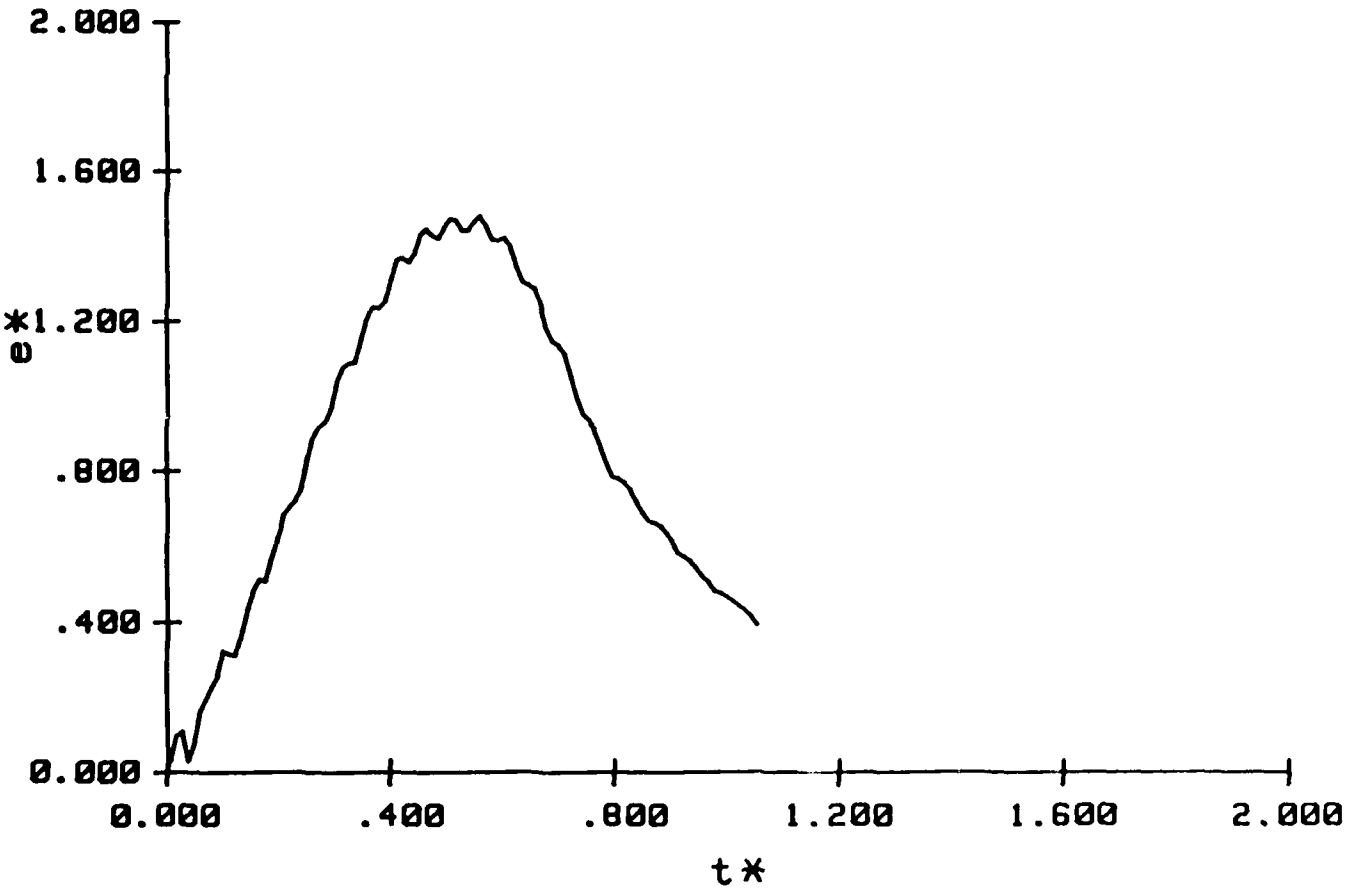

V0= 2.38 Ft/s (781.8 mm/s)
M= 8.41 Lbm (3.816E-3 Mg)
L=1.165 Ft (355.1 mm)
Z= .818 Ft (3.2 mm)
b= .131 Ft (40.0 mm)
Q=70500E+4 Lb/Ft^2 (3.759E+4 MPa)
p* max=+1.2383E+00
e* max=+1.4794E+00
t* max=+1.0588E+00

INSTRUMENTED IMPACT TEST

I25(I2B)

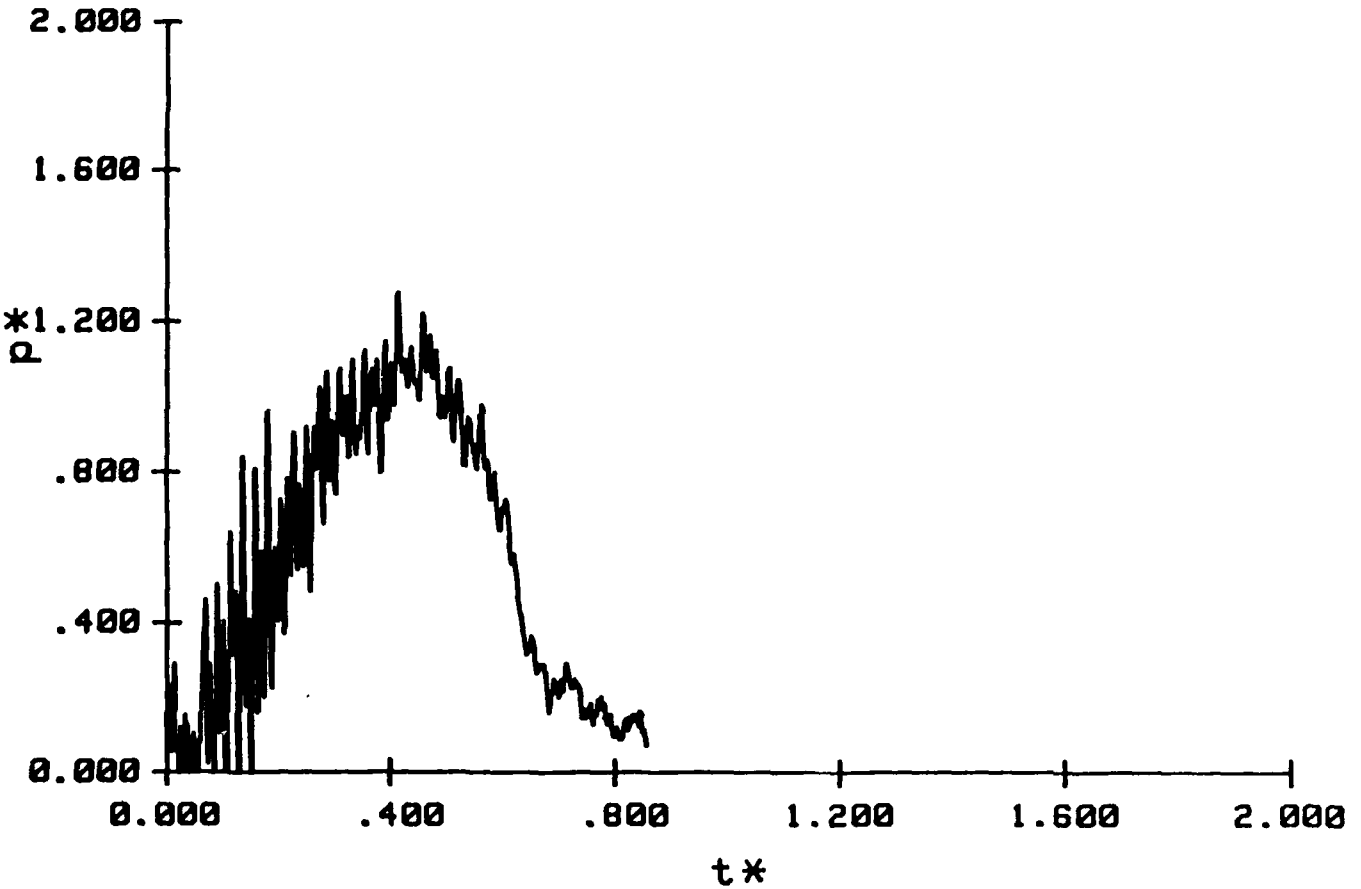

V0= 3.17 Ft/s (966.2 mm/s)
M= 8.41 Lbm (3.816E-3 Mg)
L=1.165 Ft (355.1 mm)
Z= .818 Ft (3.2 mm)
b= .131 Ft (40.0 mm)
Q=78500E+4 Lb/Ft^2 (3.759E+4 MPa)
p* max=+1.2760E+00
e* max=+1.3357E+00
t* max=+8.5773E-01

INSTRUMENTED IMPACT TEST

I25(I2B)

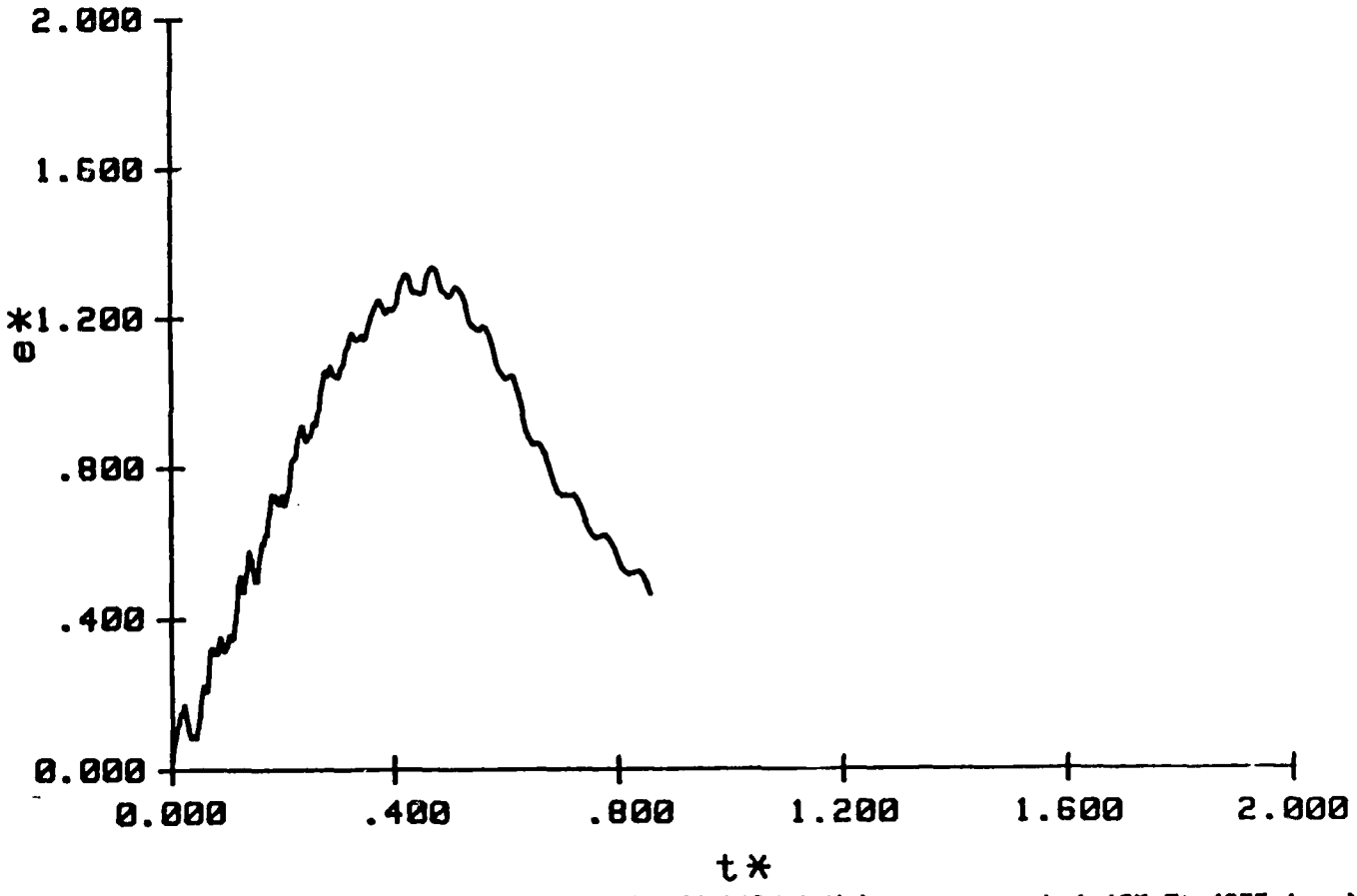

V0= 3.17 Ft/s (966.2 mm/s)
M= 8.41 Lbm (3.816E-3 Mg)
L=1.165 Ft (355.1 mm)
Z= .818 Ft (3.2 mm)
b= .131 Ft (40.0 mm)
Q=78500E+4 Lb/Ft^2 (3.759E+4 MPa)
p* max=+1.2788E+00
e* max=+1.3357E+00
t* max=+8.5773E-01

INSTRUMENTED IMPACT TEST

I26(I2B)

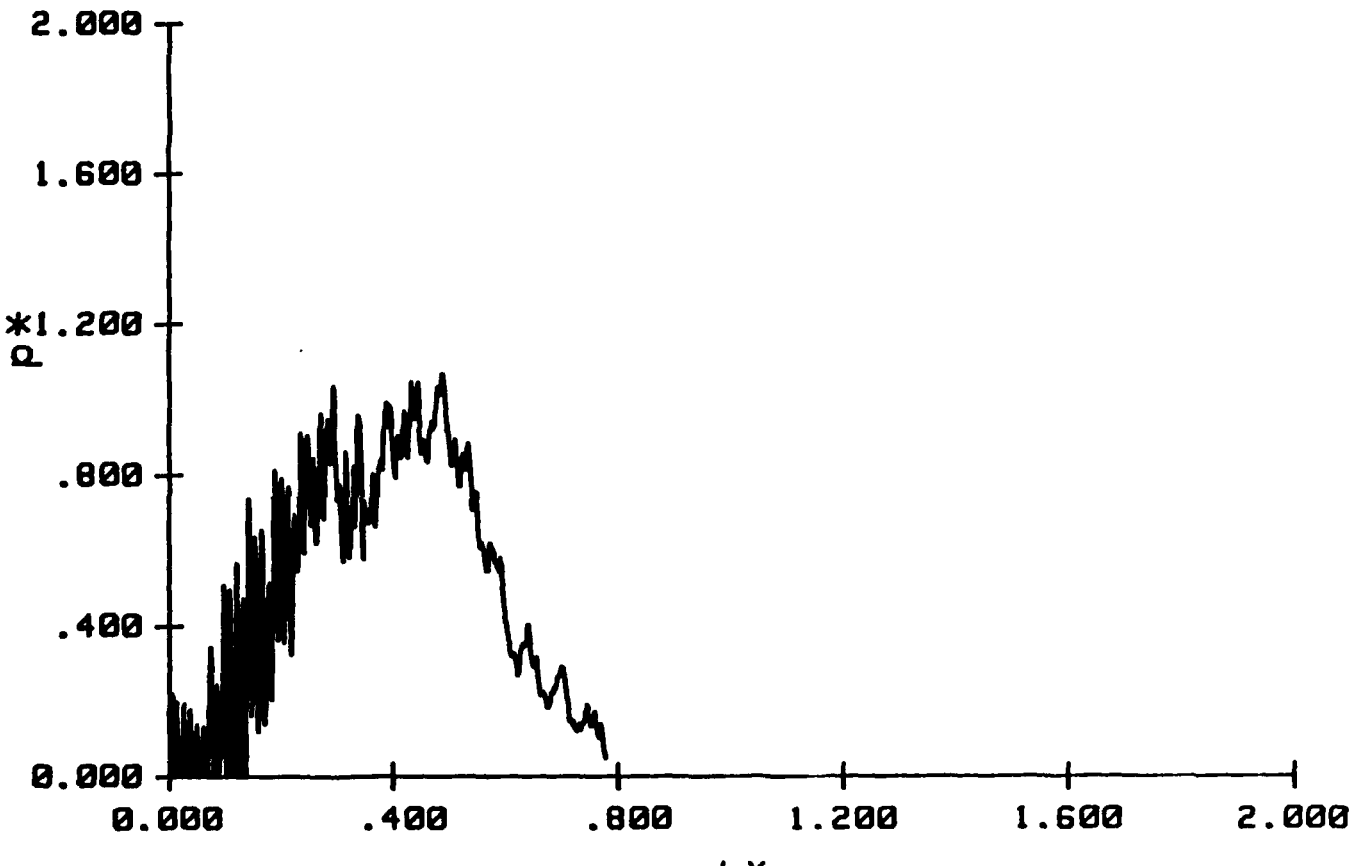

V0= 4.78 Ft/s (1458.8 mm/s)
M= 8.41 Lbm (3.816E-3 Mg)
L=1.165 Ft (355.1 mm)
Z= .018 Ft (5.2 mm)
b= .131 Ft (40.0 mm)
Q=78500E+4 Lb/Ft^2 (3.759E+4 MPa)
p* max=+1.0656E+00
e* max=+1.2029E+00
t* max=+7.7858E-01

NADC-87106-30

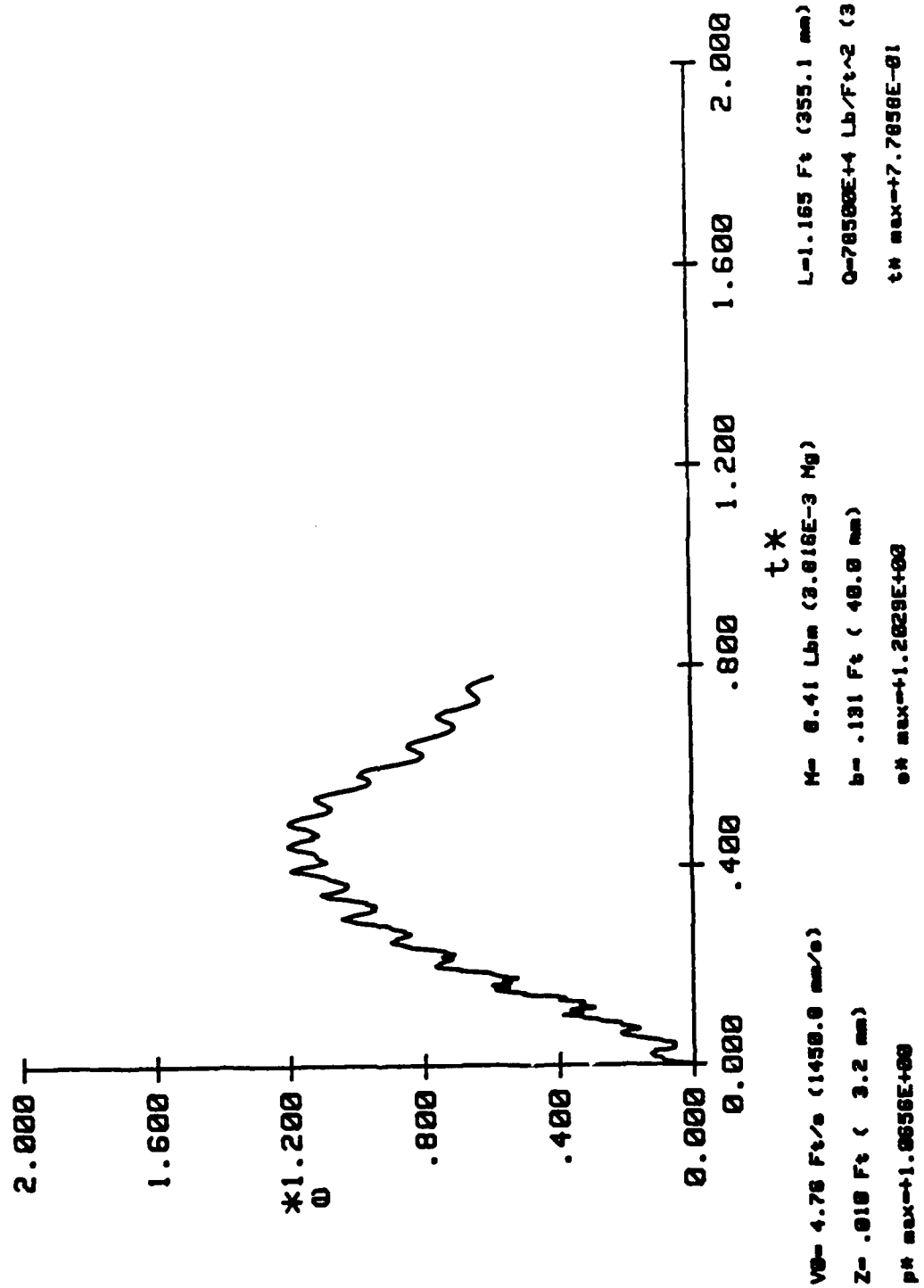
INSTRUMENTED IMPACT TEST
I26(I2B)
2.000
1.600
1.200
.800
.400
0.000
*1.200
0
.800
1.200
1.600
2.000
t*
L=1.165 Ft (355.1 mm)
Q=78500E+4 Lb/Ft^2 (3.759E+4 MPa)
t* max=+7.7858E-01
M= 6.41 Lbm (2.818E-3 Mg)
b= .131 Ft (40.0 mm)
e* max=+1.2829E+00
V0= 4.78 Ft/s (1458.0 mm/s)
Z= .018 Ft (3.2 mm)
p* max=+1.0656E+00

INSTRUMENTED IMPACT TEST

I28(I2B)

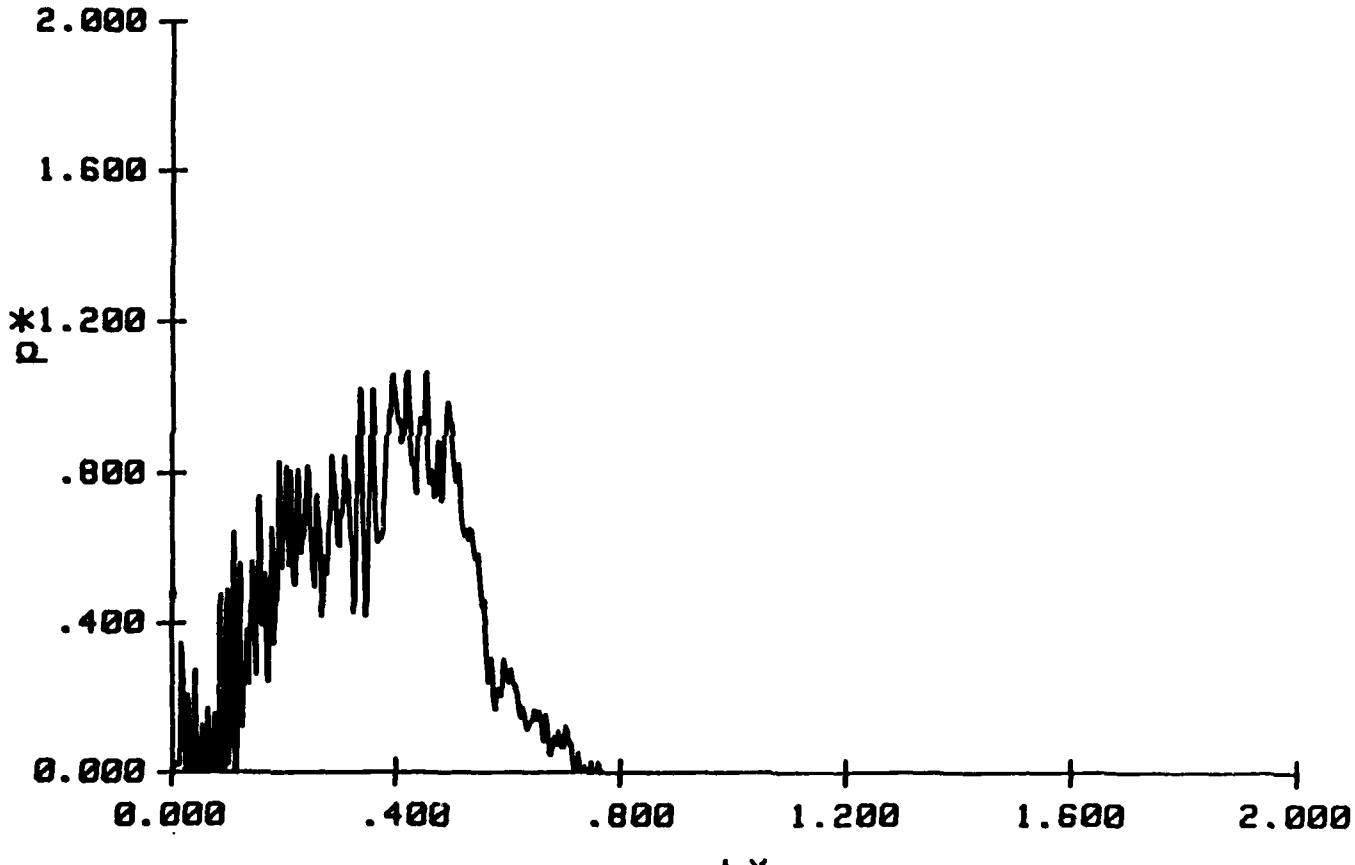

V0= 0.82 Ft/s (24+4.5 mm/s)
M= 0.41 Lbm (3.816E-3 Mg)
L=1.165 Ft (355.1 mm)
Z= .010 Ft (3.2 mm)
b= .131 Ft (40.0 mm)
Q=78500E+4 Lb/Ft^2 (3.759E+4 MPa)
p* max=+1.0669E+00
e* max=+9.3003E-01
t* max=+7.6682E-01

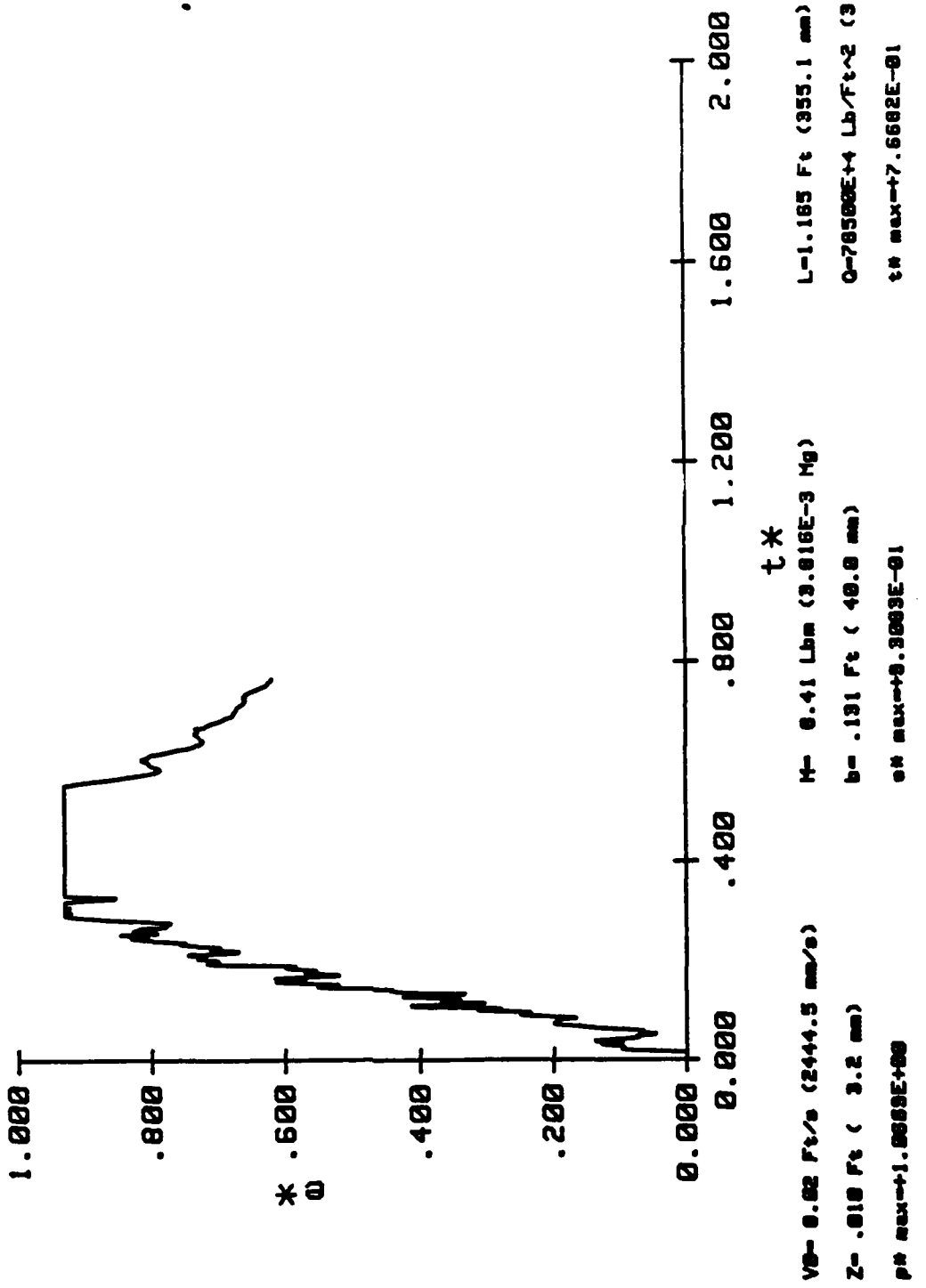
INSTRUMENTED IMPACT TEST
I28(I2B)
1.000
.800
.600
.400
.200
0.000
*
0
.400
.800
1.200
1.600
2.000
t*
V0= 8.02 Ft/s (2444.5 mm/s)
Z= .010 Ft (3.2 mm)
M= 0.41 Lbm (3.816E-3 Mg)
b= .131 Ft (40.0 mm)
L=1.165 Ft (355.1 mm)
Q=78500E+4 Lb/Ft^2 (3.759E+4 MPa)
t* max=+7.6682E-01

DISTRIBUTION LIST

NON-GOVERNMENT ACTIVITIES (continued)

	NO. OF COPIES
NORTHROP AIRCRAFT CORP., One Northrop Avenue, Hawthorne, CA 90250 (Attn: Dr. M. Ratwani, B. Butler and R. Whitehead). . .	3
PURDUE UNIVERSITY, School of Aeronautics and Astronautics, West Lafayette, IN 47907 (Attn: Dr. C. T. Sun).	1
PROTOTYPE DEVELOPMENT ASSOCIATES, INC., 1560 Brookhollow Drive Santa Ana, CA 92705 (Attn: E. L. Stanton).	1
ROCKWELL INTERNATIONAL, Columbus, OH 43216 (Attn: M. Schweiger).	1
ROCKWELL INTERNATIONAL, Los Angeles, CA 90009 (Attn: Dr. Lackman).	1
(Attn: W. O'Brien).	1
ROCKWELL INTERNATIONAL, Tulsa, OK 74151 (Attn: F. Kaufman).	1
ROHR CORP., Riverside, CA 92503 (Attn: Dr. F. Riel).	1
SIKORSKY AIRCRAFT, Stratford, CT 06622 (Attn: S. Garbo).	1
J. P. STEVENS & CO., INC., New York, NY 10036 (Attn: H. I. Shulock).	1
TELEDYNE RYAN AERONAUTICAL CO., San Diego, CA 92138 (Attn: R. Long).	1
UNIVERSITY OF DAYTON RESEARCH INSTITUTE, 300 College Park Avenue, Dayton, OH 45469 (Attn: Dr. J. Gallagher).	1
UNIVERSITY OF DELAWARE, Mechanics & Aerospace Eng. Dept., Evans Hall, Newark, DE 19711 (Attn: Dr. R. B. Pipes, Dr. J. R. Vinson and Dr. D.Wilkins .	3
UNIVERSITY OF OKLAHOMA, Norman, OK 73019 (Attn: Dr. C. W. Bert, School of AMNE).	1
UNIVERSITY OF WYOMING, Laramie, WY 82071 (Attn: Dr. D. Adams).	1
VILLANOVA UNIVERSITY, Villanova, PA 19085 (Attn: Dr. P. V. McLaughlin).	1
VIRGINIA POLYTECHNIC INSTITUTE, Blacksburg, VA 24061 (Attn: Dr. K. Reifsnider).	1
WASHINGTON UNIVERSITY, School of Engineering and Applied Science, Materials Research Laboratory, Campus Box 1087, St. Louis, MO 63130 (Attn: T. Hahn).	1

DISTRIBUTION LIST
NON-GOVERNMENT ACTIVITIES (continued)

	NO. OF COPIES
GENERAL ELECTRIC CO., Philadelphia, PA 19101	
(Attn: A. Garber, C. Zweben).	2
GREAT LAKES CARBON CORPORATION, New York, NY 10017	
(Attn: W. R. Benn, Manager, Market Development). . .	1
GRUMMAN CORPORATION, South Oyster Bay Rd., Bethpage, NY 11714	
(Attn: R. Hadcock).	1
(Attn: S. Dastin).	1
HERCULES AEROSPACE DIVISION, P.O. Box 210, Cumberland, MD 21502	
(Attn: Mr. D. Hug).	1
HITCO, 1600 West 135th Street, Gardena, CA 90249	
(Attn: N. Myers).	1
ITT RESEARCH INSTITUTE, Chicago, IL 60616	
(Attn: K. Hofar).	1
KAMAN AIRCRAFT CORP., Bloomfield, CT 06002	
(Attn: Technical Library).	1
LEHIGH UNIVERSITY, Bethlehem, PA 18015	
(Attn: Dr. G. C. Sih).	1
LEONARD ASSOCIATES, INC., 6 East Avenue, Mt. Carmel, PA 17851	
(Attn: Mr. L. Marchinski).	1
LOCKHEED-CALIFORNIA CO., Burbank, CA 91520	
(Attn: E. K. Walker).	1
(Attn: A. Vaughn).	1
(Attn: A. James).	1
LOCKHEED-MISSILES & SPACE CO., 1111 Lockheed Way, Sunnyvale, CA 94086	
(Attn: J. A. Bailie).	1
LOCKHEED-CALIFORNIA CO., Rye Canyon Research Laboratory, Burbank, CA 91520	
(Attn: D. E. Pettit).	1
LOCKHEED-GEORGIA CO., Marietta, GA 30063	
(Attn: Technical Information Dept., 72-34, Zone 26). . .	1
LTV AEROSPACE & DEFENSE CO., Vought Missile & Advanced Program Division, P.O. Box 225907, Dallas, TX 75265-0003	
(Attn: R. Knight).	1
MASSACHUSETTS INSTITUTE OF TECHNOLOGY, Technology Laboratory for Advanced Composite, 77 Massachuetts Avenue, Cambridge, MA 02139	
(Attn: Dr. P. A. Lagace).	1
MATERIALS SCIENCES CORP., Spring House, PA 19477	
(Attn: Dr. B. W. Rosen).	1
McDONNELL-DOUGLAS CORP., St. Louis, MO 63166	
(Attn: K. Stenberg, R. Garrett, R. Riley, J. Doerr). . .	4
McDONNELL-DOUGLAS CORP. Long Beach, CA 90846	
(Attn: J. Palmer).	1
McDONNELL-DOUGLAS HELICOPTER CO., Culver City, CA 90230	
(Attn: J. K. Sen, Trailer 2002).	1
McDONNELL-DOUGLAS HELICOPTER CO., 5000E. McDowell, M/S B337 Mesa, AZ 85205	
(Attn: Steve Guymon).	1

DISTRIBUTION LIST

NON-GOVERNMENT ACTIVITIES

	NO. OF COPIES
ANAMET LABORATORIES, 100 Industrial Hyw., San Carlos, CA 94070	
(Attn: Dr. R. Arnold).	1
ALCOA DEFENSE SYSTEMS CORP., 16761 Via delCampo Court, San Diego, CA 92127	
(Attn: D. Myers).	1
AVCO, Specialty Materials Div., 2 Industrial Avenue, Lowell, MA 01851	
(Attn: Mr. W. F. Grant).	1
BATTELLE COLUMBUS LABORATORIES, Metals and Ceramics Information Center 505 King Avenue, Columbus, OH 43201.	1
BEECH AIRCRAFT CORP., 4130 Linden Avenue, Dayton, OH 45432	
(Attn: M. B. Goetz).	1
BELL AEROSPACE COMPANY, Buffalo, NY 14240	
(Attn: F. M. Anthony, Zone I-85).	1
BELL HELICOPTER CO., Fort Worth, TX 76101	
(Attn: M. K. Stevenson).	1
BENDIX PRODUCTS, Aerospace Division, South Bend, IN 46619	
(Attn: R. V. Cervelli).	1
BOEING CO., P. O. Box 3707, Seattle, WA 98124	
(Attn: J. McCarty, J. Quinliven, and Dr. R. June). . . .	3
BOEING CO., Vertol Division, P.O. Box 16858, Philadelphia, PA 19143	
(Attn: R. L. Pinckney).	1
(Attn: D. Hart).	1
(Attn: C. Albrecht).	1
BOEING CO., Wichita, KS 67277-7730.	1
(Attn: J. Avery).	1
(Attn: R. Waner).	1
CABOT CORPORATION, Billerica Research Center, Billerica, MA 01821.	1
DEPARTMENT OF TRANSPORTATION, Kendall Square, Cambridge, MA 02142.	1
(Attn: Dr. Ping Tong, DTS 76, TSC).	1
DREXEL UNIVERSITY, Philadelphia, PA 19104	
(Attn: Dr. P. C. Chou).	1
(Attn: Dr. A. S. D. Wang).	1
E. I. DuPONT COMPANY, Textile Fibers Department, Chestnut Run Location CR701, Wilmington, DE 19898	
(Attn: V. L. Bertarelli).	1
FAIRCHILD REPUBLIC CO., Farmingdale, L.I., NY 11735	
(Attn: Mr. Frank Costa).	1
GEORGIA INSTITUTE OF TECHNOLOGY, Atlanta, GA 30332	
(Attn: (L. Rehfield)).	1
GENERAL DYNAMICS/CONVAIR, San Diego, CA 92138	
(Attn: Dr. R. Dunbar).	1
GENERAL DYNAMICS, Fort Worth Division, PO Box 748, Fort Worth, TX 76101	
(Attn: J. A. Fant).	1
(Attn: Composite Structures Eng. Dept.).	1

DISTRIBUTION LIST

GOVERNMENT ACTIVITIES - (continued)

	NO. OF COPIES
NAVSHIPRANDCEN, Annapolis, MD 21403	
(Attn: H. Edlestein, Code 2870).	1
NRL, Washington, D.C. 20375	
(Attn: Dr. I. Wolock, Code 6122; Dr. C. I. Chang, and Dr. R. Badaliance).	3
NSWC, WHITE OAK LABORATORY, Silver Spring, MD 20910	
(Attn: Dr. J. Goff, Materials Evaluation Branch, Code R-34 .	1
(Attn: Dr. J. M. Augl).	2
ONR, 800 N. Quincy St., Arlington, VA 22217	
(Attn: A. Kushner Code 432/A; Y. Rajapakse, Code 1132SM) .	2
ONT, 800 N. Quincy Street, Arlington, VA 22217	
(Attn: Cdr. D. Brown, (OCNR-212).	1
PLASTEC, Picatinny Arsenal, Dover, NJ 07801	
(Attn: H. Pebly).	1
(Attn: Librarian, Code DRDAR-SCM-O, Bldg. 351-N). . .	1
U. S. ARMY MATERIALS RESEARCH LABS, DRXMR-PL, Watertown, MA 02171	
(Attn: D. Oplinger).	1
U. S. ARMY APPLIED TECHNOLOGY LABORATORY, USARTL, (AVRADCOM), Ft. Eustis, VA 23604	
(Attn: J. Waller; T. Mazza).	2
U. S. ARMY AIR MOBILITY R&D LABORATORY, Ft. Eustis, VA 23604	
(Attn. H. Reddick).	1
U. S. ARMY R&T LABORATORY (AVRADCOM), Ames Research Center, Moffet Field, CA 94035	
(Attn: F. Immen, DAVDL-AS-MS 207-5).	1
U. S. NAVAL ACADEMY, Annapolis, MD 21402	
(Attn: Dr. R. D. Jamison, Mechanical Engineering Department).	1
DAVID TAYLOR NAVAL SHIP RESEARCH & DEVELOPMENT CENTER, Annapolis, MD 21402	
(Attn: E. T. Camponeschi, Code 2844; R. Crane, Code 2844). .	2
DAVID TAYLOR NAVAL SHIP R&D CENTER Bethesda, MD 20084	
(Attn: A. Macander, Code 1720).	1
NAVAIRDEVCEN, Warminster, PA 18974	
(Attn: Code 8131).	3
(Attn: Code 09L2).	2

DISTRIBUTION LIST

GOVERNMENT ACTIVITIES

	NO. OF COPIES
AFWAL, WPAFB, OH 45433	
(Attn: FIBEC, Dr. G. Sendeckyj).	1
(Attn: FIB/L. Kelly, W. Goesch, C. Ramsey).	3
(Attn: FIBCA).	1
(Attn: FIBE/Mr. D. Smith).	1
(Attn: MLBM/Dr. J. Whitney, M. Knight).	2
(Attn: MLB/F. Cherry).	1
(Attn: MBC/Reinhart).	1
(Attn: AFWAL/MLSE/S. Fecheck).	1
DEPARTMENT OF THE AIR FORCE, Bldg. 410, Bolling Air Force Base, Washington, D.C. 20332	
(Attn: Dr. M. Salkind, Dr. Amos).	2
DEFENSE TECHNICAL INFORMATION CENTER (DTIC), Bldg.#5, Cameron Station Alexandria, VA 22314	
(Attn: Administrator).	2
FAA, Washington, D.C. 20591	
(Attn: J. R. Soderquist, AW-103).	1
FAA, Technical Center, Atlantic City, NJ 08405	
(Attn: L. Neri, Code ACT-330; M. Caiafa, Code ACT-033).	2
NASA, Washington, D. C. 20546	
(Attn: Airframes Branch, FS-120).	1
(Attn: OAST/RM, Dr. D. Mulville).	1
NASA, George C. Marshall Space Flight Center, Huntsville, AL 35812	
(Attn: E. E. Engler, S&E-ASTN-ES).	1
(Attn: R. Schwinghamer, S&E-ASTN-M).	1
NASA, Langley Research Center, Hampton, VA 23365	
(Attn: Dr. J. R. Davidson, MS 188E; Dr. J. Starnes, MS-190; Dr. M. Mikulus, H. Bohan, and Dr. C. P. Blakenship MS 189M).	5
NASA, Lewis Research Center, Cleveland, OH 44135	
(Attn: Dr. C. Chamis, MS 49-6; M. Hershberg, MS 49-6).	2
NAVAIRSYSCOM, Washington, D.C. 20361	
(Attn: AIR-00D4).	1
(Attn: AIR-530).	1
(Attn: AIR-5302D).	1
(Attn: AIR-5302).	1
(Attn: AIR-5302F).	1
(Attn: AIR-53032D).	1
(Attn: AIR-931B).	1
NAVPGSCHL, Monterey, CA 95940	
(Attn: Prof. R. Ball, Prof. M. H. Bank, Prof. K. Challenger).	3
NAVSEASYSCOM, Washington, D.C. 20360	
(Attn: C. Zannis, SEA-05R25)).	1
NAVSEC, Arlington, VA 20360	
(Attn: NSEC-6101E).	1

END
DATE
FILMD
3-88
DTIC